Nov 3rd, 12:00 AM - Nov 4th, 12:00 AM

20th International Specialty Conference: Recent Research and Developments in Cold-Formed Steel Structures

Wei-Wen Yu Center for Cold-Formed Steel Structures

Continuing Education

Twentieth International Specialty Conference on
Cold-Formed Steel Structures

RECENT RESEARCH AND DEVELOPMENTS IN COLD-FORMED STEEL DESIGN AND CONSTRUCTION

Held in St. Louis, Missouri
November 3 & 4, 2010

Edited by
Roger A. LaBoube and Wei-Wen Yu

Department of Civil, Architectural & Environmental Engineering
Missouri University of Science and Technology
Rolla, Missouri

Presented by

Department of Civil, Architectural & Environmental Engineering
Wei-Wen Yu Center for Cold-Formed Steel Structures
Missouri University of Science and Technology

Sponsored by

American Iron and Steel Institute
Cold-Formed Steel Engineers Institute of the Steel Framing Alliance
Metal Building Manufacturers Association
Rack Manufacturers Institute
Steel Deck Institute
Steel Stud Manufacturers Association
Missouri University of Science and Technology

In Cooperation with

ASCE Committee on Cold-Formed Members
Canadian Sheet Steel Building Institute, Canada
SSRC Task Group on Thin-Walled Metal Construction
Centre for Advanced Structural Engineering
of the University of Sydney, Australia

Conference Directors

Roger A. LaBoube, Director
Wei-Wen Yu, Founding Director
of the Wei-Wen Yu Center for Cold-Formed Steel Structures,
Missouri University of Science and Technology

Planning Committee

D. Allen – Representative of SSMA
R.L. Brockenbrough - R.L. Brockenbrough & Associates, Inc.
H.H. Chen - Representative of AISI
J. Crews – Unarco Material Handling Inc.; Representative of RMI
W.S. Easterling – Virginia Tech
S.R. Fox- Representative of CSSBI, Canada
G.J. Hancock - Representative of the University of Sydney, Australia
R.B. Haws - NUCONSTEEL
D.L. Johnson – Consultant
W.E. Kile – Structuneering Inc.; Representative of ASCE
R.A. LaBoube –Missouri S&T; Conference Director
J.W. Larson – Representative of AISI
J. A. Mattingly – Consultant
T.B. Pekoz - Cornell University
B.W. Schafer – Johns Hopkins University; Representative of
SSRC Task Group on Thin-Walled Metal Construction
W.E. Schultz – Nucor Research and Development;
P.A. Seaburg – Editor, Journal of Architectural Engineering
W.L. Shoemaker - Representative of MBMA
T. Sputo – Representative of SDI
W.W. Yu – Missouri S&T; Conference Co-Director; Representative of
the Wei-Wen Yu Center for Cold-Formed Steel Structures

On the occasion of this 20th International Specialty Conference and the 20th Anniversary of the Wei-Wen Yu Center for Cold-Formed Steel Structures, we recognize the vision of our Founding Director, Dr. Wei-Wen Yu. Dr. Yu served as Director of the Center from 1990 to 2001 and currently serves as Founding Director. He has also served as Director or Co-Director for each of the specialty conferences.

CONTENTS

PREFACE

Cold-formed steel members are used in virtually every area of construction. In order to review the research findings and the design methods developed in this field, 20 International Specialty Conferences on Cold-Formed Steel Structures have been held since 1971. Much has changed since that first conference in 1971, but have things really changed? Following this Preface is the keynote address presented by Dr. George Winter during the first conference. You are encouraged to read Dr. Winter's Perspectives and reflect on the state-of-the-art as we know it today.

In recent years, significant progress has been made in the development of design standards and in research studies of cold-formed steel members and structural systems throughout the world. The Twentieth International Specialty Conference on Cold-Formed Steel Structures was held in St. Louis, Missouri on November 3rd and 4th, 2010. It was sponsored by the American Iron and Steel Institute (AISI), Cold-Formed Steel Engineers Institute of the Steel Framing Alliance (CFSEI), Metal Building Manufacturers Association (MBMA), Rack Manufacturers Institute (RMI), Steel Deck Institute (SDI), Steel Stud Manufacturers Association (SSMA), and the Missouri University of Science & Technology (formerly University of Missouri-Rolla) in cooperation with the American Society of Civil Engineers Committee on Cold-Formed Members, Canadian Sheet Steel Building Institute, Structural Stability Research Council Task Group on Thin-Walled Metal Construction, and the Centre for Advanced Structural Engineering of the University of Sydney in Australia.

This publication contains 42 papers that were presented at the conference. These papers not only report the results of recent research but also discuss the technical developments in cold-formed steel design and construction.

As Directors of the Conference, we are very grateful to all the sponsors and supporting organizations for their financial and technical support and to all authors for their contributions in the field of cold-formed steel structures. Appreciation is also due to members of the Planning Committee (D. Allen. R.L. Brockenbrough, H.H. Chen, J. Crews, W.S. Easterling, S.R. Fox, G.J. Hancock, R.B. Haws, D.L. Johnson, W.E. Kile, R.A. LaBoube, J.W. Larson, J.A. Mattingly, T.B. Pekoz, B.W. Schafer, W.E. Schultz, P.A. Seaburg, W.L. Shoemaker, T. Sputo and W.W. Yu) for review and selection of papers and their advice in preparation of the conference. We would also like to thank all of the session chairpersons listed in the program for their time and effort.

Special thanks are extended to Mrs. Christina Stratman for her assistance in preparing this publication.

Roger A. LaBoube

Wei-Wen Yu

PERSPECTIVES

Keynote Address at the First International Specialty
Conference on Cold-Formed Steel Structures, 1971
by
George Winter, F. ASCE
Professor of Structural Engineering (Class of 1912 Chair), Cornell University

In this year 1971 it may be truly said that cold-formed steel construction has come of age. For it is exactly 25 years since the first design specification has been published in this country, or anywhere in the work for that matter, after six years of intensive research sponsored at Cornell University by the American Iron and Steel Institute. Research has gone on ever since, at Cornell and also elsewhere, and the specification has been repeatedly improved, enlarged, and also translated and followed, in whole or in part, in many other countries. Cold-formed steel construction is being used for the main load-carrying elements from small utility structures to large industrial storage racks, from moderate-size industrial and commercial buildings, schools, and churches, to the largest hangers for jumbo-jets with roofs cantilevering out some 250 ft. Maybe this is the time to take stock on where we are, and to try defining where we should be going.

As always, there is much to be done in research. However, not all research that can be thought of is equally worthwhile. Minor adjustments in effective width equations, in column formulas, in allowable stresses for unbraced beams may be interesting exercises, but they have only limited effect on the economy, and none at all on the versatility of this type of construction. The researcher must be sensitive to the feedback from application, to the needs experienced in practice for new or modified design information. Then one learns that not enough is known regarding connections in thin, cold-formed members, not enough regarding torsional-flexural behavior under all types of loading of the typically asymmetrical or singly-symmetrical cold-formed shapes, not enough regarding the behavior of the unlimited variety of cross-sectional shapes which can be produced by cold-forming, in contrast to almost any other type of construction, be it in metal, concrete, timber or some other material. These and other matters of detail need to be worked on in the traditional path from research to specification to practice.

There are, however, larger issues to be addressed. And none of these affect only cold-formed construction. One of them is the problem of the increasing complexity of design specifications. This increasing complexity is an inevitable consequence of more refined and economical ways of using material structurally, or utilizing the full benefits of higher strength material, and of maximizing the effects of our more sophisticated knowledge of structural mechanics and materials science. It is odd that there should be a problem in this increased complexity at the very time

when ever more efficient computer methods enable one routinely to carry out calculations of previously undreamed of length and complication.

The reason for this is the following: Design codes and specifications are, in effect, legal documents; at the same time they are a set of technical directions to the designer. The manner in which to write these dual-character documents has gradually established itself in the pre-computer era. But this way of writing specifications in relatively simple sets of directions, of closed-form equations, preferably explicit, algebraic and first degree, is the very anti-thesis of the mathematical complexity which can routinely be handled by computer. The result is a bizarre situation in which codified specification provisions, while still written in the accustomed form, have become so complex that they can hardly be used without a computer. The irony in this is that many of these complex provisions are themselves the result of elaborate and highly accurate computer studies. In order to write code provisions, the results of these studies, by a variety of approximations and straight-jacket manipulations (all on the "conservative side") are then cast into excessively simplified code provisions of the accustomed, but by now excessively complex kind. Yet, if computer methods could be directly specified in design codes, not only would much of the present apparent complexity disappear, but the need for many of the present approximations, most of them on the uneconomical side, would also cease. How this can be done I don't know. It is difficult to see how matters which have to stand up in court can be formulated in terms appropriate for computer methods. It is also difficult to see how computer formulations can convey that understanding of structural behavior which is so inescapably necessary and which becomes apparent when matters are formulated in explicit mathematical terms.

Yet, something must be done about this or else the complexity of specifications will get out of hand while at the same time the opportunities of computerization will remain under-exploited. Codes and specifications are mostly written by people like myself, part of a generation older than that which grew up in computer-language, if the term be permitted. Maybe it remains for that generation to develop modified forms of design codes in order to overcome this problem. If so, let them go at it now.

Another problem, again not unique, but particularly pronounced in cold-formed steel structures is this: Structural engineering, especially as formulated in design codes, comes in almost airtight compartments. Cold-formed construction is a particularly relevant example of this because it has suffered under the compartmentalization from its very beginning. In fact, this type of construction was for a long time regarded by the practitioners and specification writers of conventional hot-rolled steel structures as a competing, rather than a complementing way of using steel. Hence research in the two areas was sponsored, and specifications for them were written, by two different organizations hardly

cognizant of each other. It has taken about twenty years, in fact until the latest editions of the two documents, that this separation was at least partially overcome. Yet, in spite of this institutional difficulty, practice has long used the two methods concurrently and inter-mixed, utilizing in otherwise heavy steel framing cold-formed steel for floors, roofs, walls, for bracing against wind and seismic forces, in long-span roofs of truss, shell and folded plate construction, and otherwise. Much more would be done in imaginatively using steel to greater economic advantage if design engineers were made more aware not only of the individual features and merits of the presumably separate methods, but of their mutually supplementary and complementary character.

The same goes for combined use of concrete and steel in construction. Here again practice was ahead of code writing and even of research. Thus, light gage steel deck has been used for some three decades not only as formwork but also as reinforcement of concrete floor and roof slab, in was not recognized by any design code, nor designed by any established method. Parallel to this, concrete slabs have been used to act as a composite with steel girders long before the subsequent recognition and code formulation of composite construction. While such recognition now exists, the two specification writing bodies, in concrete and in steel, are still not really on speaking terms with each other, thus preventing the optimal combined use of the two materials. The next step, the use of composite, deck-reinforced slabs to act compositely with steel girders, is now underway, both in research and in practice. However, the alternative combination of using such composite slabs to act compositely with concrete girders, precast or otherwise, has not even been looked into. These are just examples of the few areas in which the compartmentalization of structural engineering has at least partly been overcome by the designing profession.

To be sure, industry has now come around to a recognition of this structural interactions. Research is being sponsored on various aspects of composite construction of concrete with light-gage and with conventional steel shapes, of interaction of light-gage diaphragms with heavy structural framing, in multi-story building as well as in shell roofs, of combining plastics, gypsum and steel in sandwiches, etc. etc. It is to be hoped that more of this will be undertaken, and that more of it will shortly be reflected in design codes, specifications, manuals and similar documents, so that broader practical use can be made of all these possibilities.

It seems to this writer, presumably an academic person who, however, has been in close touch for most of his professional life with both the steel and concrete industry and also with the designing profession, that what is needed in the context of the urban problem and of the housing problem is radically more economical construction. This cannot be achieved without substantial industrialization of the construction process. Cold-formed steel construction lends itself unusually well to

industrialization. But in order to reap the full benefits of industrialization and of design innovations of all kinds, short-sighted compartmentalization of structural engineering will have to be replaced by positive stimulation toward taking maximum advantage of all promising materials, of all promising combinations of materials and of the widest possible freedom of using new or improved structural shapes and configurations. The increased construction volume which should follow such a development would more than make up for the presumed competitive advantages provide by present compartmentalization.

Tendencies in this direction, while slow, are now clearly discernible and one is justified in hoping that in this direction will lie a real and badly needed renaissance in building.

First International Specialty Conference on Cold-Formed Steel Structures
August 19-20, 1971, Rolla, Missouri

PROGRAM

Tuesday, November 2, 2010

6-9 p.m. Registration

Wednesday, November 3, 2010

7 a.m. – 4 p.m. Registration

8:00 a.m. Welcoming Remarks
R.A. LaBoube, Missouri University of Science and Technology, Rolla, MO, USA

8:10 a.m. Technical Session No. 1
Elements and Cross-Section Behavior

Chairpersons:
D.L. Johnson, Maus Engineering, Wolfeboro, NH, USA
T.B. Pekoz, Cornell University, Ithaca, NY, USA

"Impact of Corner Radius on Cold-Formed Steel Member Strength", V. M. Zeinoddini and B.W. Schafer, Johns Hopkins University, Baltimore, MD, USA

"Buckling Analysis of Cold-Formed Steel Members with General Boundary Conditions using CUFSM: Conventional and Constrained Finite Strip Methods", L. Zhanjie and B.W. Schafer, Johns Hopkins University, Baltimore, MD, USA

8:50 a.m. Technical Session No. 2
Compression Members

Chairpersons:
B.W. Schafer, Johns Hopkins University, Baltimore, MD, USA
W.L. Shoemaker, Metal Building Manufacturers Association, Cleveland, OH, USA

"Evaluating the LRFD Resistance Factor for Cold-Formed Steel Compression Members", K. Ganesan and C.D. Moen, Virginia Tech, Blacksburg, VA, USA

"Experimental Investigation of Optimized Cold-Formed Steel Compression Members", D.J. Klingshirn, NAVFAC Pacific, Honolulu, HI, E.A. Summer, North Carolina State University, Raleigh, NC, and N.A. Rahman, The Steel Network, Durham, NC, USA

"Cyclic Elastoplastic Large Displacement Analysis of Cold-Formed Steel Box Columns under Combined Action of Axial and Bi-Directional Lateral Loading", I.H.P. Mamaghani and S. Montezeri, University of North Dakota, ND, USA

"Test and Finite Element Analysis on Distortional Buckling of Cold-Formed Thin-Walled Steel Lipped Channel Columns", X. Yao, Y. Guo, Tongji University, Shanghai, China, and Z. Huang, University of Architecture and Technology, Xi'an, China

10:10 a.m. **Break**

10:35 a.m. **Technical Session No. 3**
Built-up Compression Members

Chairpersons:
D. Camotim, Technical University of Lisbon, Lisbon, Portugal
W.E. Kile, Structuneering, Inc., Houston, TX, USA

"Load-Carrying Capacity Estimation on Cold-Formed Thin-Walled Steel Columns with Built-up Box Section", Y. Li, X. Yao, Z. Shen, and R. Ma, Tongji University, Shanghai, China

"Comparative Behavior of Built-up Cold-Formed Box Sections Under Rigid and Flexible End Support Conditions", W. Reyes, Acerias de Columbia, Columbia, and A. Guzmán, Universidad del Norte, Barranquilla, Colombia

"Theoretical Analysis of Cold-Formed Steel Battened Double Angle Members under Compression", W.F. Maia, J.M. Neto, and M. Malite, University of Sao Paulo, Brazil

11:35 p.m. **Technical Session No. 4**
Floor Systems

Chairpersons:
R.B. Haws, NUCONSTEEL, Denton, TX, USA
W.S. Easterling, Virginia Tech, Blacksburg, VA, USA

"Improvements to the Fire Performance of Light Gauge Steel Floor Systems", B. Baleshan and M. Mahendran, Queensland University of Technology, Brisbane, Australia

"Feasibility Study for a Repetitive Member Factor for Cold-Formed Steel Framing", S. Clayton and S.F. Stephens, Kansas State University, Manhattan, KS, USA

12:15 p.m. **Lunch**

1:10 p.m. **Technical Session No. 5**
Flexural Members

Chairpersons:
H. Chen, American Iron and Steel Institute, Washington, D.C., USA
R.M. Schuster, University of Waterloo, Ontario, Canada

"Extending Direct Strength Design to Cold-Formed Steel Beams with Holes", C.D. Moen, Virginia Tech, Blacksburg, VA, and B.W. Schafer, Johns Hopkins University, Baltimore, MD, USA

"On the Direct Strength Design of Continuous Cold-Formed Steel Beams", C. Basaglia and D. Camotim, Technical University of Lisbon, Lisbon, Portugal

"Direct Strength Design of Cold-Formed C-Sections for Shear", C.H. Pham and G.J. Hancock, University of Sydney, Sydney, Australia

"Direct Strength Design of Cold-Formed C-Sections in Combined Bending and Shear", C.H. Pham and G.J. Hancock, University of Sydney, Sydney, Australia

"Flexural and Cyclic Behaviour of Hollow and Concrete-Filled Steel Tubes", S. Arivalagan, Dr M.G.R.University, Chennai, TamilNadu, and S. Kandasamy, Anna University-Trichirappali, Ariyallur Campus, Ariyallur, TamilNadu, India

"Lateral Torsional Instability of Single Channels Restrained by Angle Cleats", G. Bukasa and M. Dundu, University of Johannesburg, Auckland Park, South Africa

"Evaluation of the Flexural Strength of Cold-Formed Steel Studs with Embossed Flanges", K.B. Reynolds, S.F. Stephens, Kansas State University, Manhattan, KS, and R.A. LaBoube, Missouri University of Science and Technology, Rolla, MO, USA

3:30 p.m. **Break**

4:00 p.m. **Technical Session No. 6**
Design Standards Development

Chairpersons:
R.L. Brockenbrough, R.L. Brockenbrough and Associates, Pittsburgh, PA, USA
W.W. Yu, Missouri University of Science and Technology, Rolla, MO, USA

"Steel Roof Deck Diaphragms on Cold-Formed Steel Framing", T. Sputo, Steel Deck Institute, Gainesville, FL, USA

"Overview of Recent Changes and Additions to AISI Standards", H. Chen, American Iron and Steel Institute, Washington, D.C., R. Brockenbrough, R.L. Brockenbrough and Associates, Pittsburgh, PA, and R. Haws, NUCONSTEEL, Denton, TX, USA

"Review of AISI Design Guide for Cold-Formed Steel Purlin Roof Framing Systems - Component Stiffness Method", M.W. Seek, East Tennessee State University, Johnson City, TN, USA

5:00 p.m. **AISI Presentation and Adjournment**
Presentation of 2010 AISI Market Development Industry Leadership Award by Robert J. Wills, Vice President, Construction Market Development, American Iron and Steel Institute

6:00-7:00 pm. **Reception**

Sponsored by:
American Iron and Steel Institute
Cold-Formed Steel Engineers Institute of Steel Framing Alliance
Metal Building Manufacturers Association
Rack Manufacturers Institute
Steel Deck Institute
Steel Stud Manufacturers Association

Thursday, November 4, 2010

8:00 a.m. **Technical Session No. 7**
Design Guides Development

Chairpersons:
J.W. Larson, American Iron and Steel Institute, Washington, D.C. USA
B.L. Babich, ITW Building Components Group, Haines City, FL, USA

"The 2008 AISI Cold-Formed Steel Design Manual", R.C. Kaehler, Computerized Structural Design, Milwaukee, WI, and H. Chen, American Iron and Steel Institute, Washington, D.C., USA

"CFSEI: Educating North American Practitioners in Principles of CFS Framing Design", W.D. Allen, Cold-Formed Steel Engineers Institute, Washington, D.C., USA

"Cold-Formed Steel Website for Students", R.A. LaBoube and C.M. Stratman, Missouri University of Science and Technology, Rolla, MO, USA

9:00 a.m. **Technical Session No. 8**
Rack Systems and Panel and Deck Assemblies

Chairpersons:
J. Crews, Unarco Material Handling, Springfield, TN, USA
T. Sputo, Steel Deck Institute, Gainesville, FL, USA

"Frame Analysis and Design of Industrial Cold-Formed Steel Racks", T.B. Pekoz, Cornell University, Ithaca, NY, USA, and A. Karakaplan, A. Koc, LARSA, Inc, Melville, NY, USA

"Cross-Aisle Shear Stiffness Tests on Rack Upright Frames", S.R. Sajja, Amey, Lews, East Sussex, UK, R.G. Beale, and M.H.R. Godley, Oxford Brookes University, Oxford, UK

"Experimental Evaluation of a Vehicular Access Door Subjected to Hurricane Force Winds", T. Gao and C.D. Moen, Virginia Tech, Blacksburg, VA, USA

10:00 a.m. **Break**

10:30 a.m **Technical Session No. 9**
Shear Wall Assemblies

Chairpersons:
S.R. Fox, Canadian Sheet Steel Building Institute, Cambridge, Ontario, Canada
R.C. Kaehler, Computerized Structural Design, Milwaukee, WI, USA

"Shear Behaviours of Light-Gauge Composite Walls under Monotonic and Cyclic Loading", Y. Li, F. Liu, Z. Shen, and X. Yao, Tongji University, Shanghai, China

"Experimental Investigation on 6 Feet Wide Cold-Formed Steel Framed Shear Walls with Steel Sheet Sheathing", C. Yu and Y. Chen, University of North Texas, Denton, TX, USA

"Performance of Knee-Braced Cold-Formed Steel Shear Walls Subjected to Lateral Cyclic Loading", M.Z. Dasterji and H.R. Ronagh, The University of Queensland, Brisbane, Australia

"Innovative Damage Control Systems Using Replaceable Energy Dissipating Steel Fuses for Cold-Formed Steel Structures", F. Ozaki, Y. Kawai, H. Tanaka, T. Okada, and R. Kanno, Nippon Steel Corporation, Japan

11:50 a.m. **Lunch**

1:00 p.m. **Technical Session No. 10**
Wall and Roof Assemblies

Chairpersons:
D. Allen, Steel Stud Manufacturers Association, Washington, D.C., USA
P.A. Seaburg, Consultant, Edwardsville, IL, USA

"A Life-Cycle Assessment of Cold-Formed Steel Enclosures verses Alternative Enclosures in Commercial Buildings", K. J. Van Ooteghem and L. Xu, University of Waterloo, Waterloo, Ontario, Canada

"Behavior and Design of Axially Compressed Sheathed Wall Studs", L.C.M. Vieira, Jr. and B.W. Schafer, Johns Hopkins University, Baltimore, MD, USA

1:40 p.m. **Technical Session No. 11**
Connections

Chairpersons:
J. Mattingly, Consultant, Roselle Park, NJ, USA
C. Rogers, McGill University, Montreal Quebec, Canada

"Shear Behavior of Screw Connections for Cold-Formed Thin-Walled Steel Structures", Y. Li, R. Ma and X. Yao, Tongji University, Shanghai, China

"Single Shear Bolted Connection Tests of G500 1.20mm Thin Sheet Steel at Elevated Temperatures", S. Yan and B. Young, The University of Hong Kong, Hong Kong

"Arc-Spot Welds for Multi-Overlap Roof Deck Panels", N. Guenford, R. Tremblay, and C.A. Rogers, McGill University, Montreal QC, Canada

2:40 p.m. **Break**

3:00 p.m. **Technical Session No. 11 (cont.)**

Chairpersons:
A.J. Harrold, Blue Scope Buildings (Butler), Kansas City, MO, USA
C. Moen, Virginia Tech, Blacksburg, VA, USA

"Strength Prediction Model for Power Actuated Fasteners Connecting Steel Members in Tension and Shear - North American Applications", J.R.U. Mujagic, Structural Engineering Consultant, Atlanta, GA, P.S. Green, Consultant, Myrtle Beach, SC, and W.G. Gould, HILTI, Tulsa, OK, USA

"Cold-Formed Steel Tension Members with Two and Three Staggered Bolts", D.M. Fox, iSPAN Systems, Richmond Hill, Ontario, and R.M. Schuster, University of Waterloo, Waterloo, Ontario, Canada

"Study on the Behavior of Cold-Formed Steel Angle Tension Members", R. PadmaPriya, SRM University, Kattankulathur, Chennai, and S. Kandasamy, Anna University Tiruchirapalli, Ariyalur campus, Ariyalur, India

"Angle Cleat Base Connections," M. Dundu and S. Maphosa, University of Johannesburg, Auckland Park, South Africa

"Some Aspects on Seismic Design of Frames Designed With Cold Formed Steel Shapes", G. Valencia, National University of Colombia, Bogotá, Colombia

"Screw Connections Subject to Tension Pull-Out and Shear Forces", R.M. Francka and R.A. LaBoube, Missouri University of Science and Technology, Rolla, MO, USA

5:00 p.m. **Closing Remarks and Adjournment**

Twentieth International Specialty Conference on Cold-Formed Steel Structures
St. Louis, Missouri, U.S.A, November 3 & 4, 2010

Impact of corner radius on cold-formed steel member strength

V. Zeinoddini[1] and B.W. Schafer[2]

Abstract

The objectives of this paper are to explore (a) how corners of cold-formed steel members are included or ignored in current design methods, and (b) the effectiveness of recent proposals for modifying the strength prediction for local buckling to account for corners. The impact of round corners is examined on the behavior and strength of isolated elements and on full members using material and geometric nonlinear collapse analysis with shell finite elements in ABAQUS. Comparisons between the available methods and the nonlinear finite element analysis are completed to explore the regimes in which the methods are accurate, as well as when they are deficient. The current approach in the main Specification of AISI-S100-07, which applies no reductions regardless of corner size, is demonstrated to be unconservative. Initial recommendations for the design of sections with large corner radius by effective width and direct strength methods are provided.

1 Introduction

The formation of cold-formed steel sections requires cold bending of the sheet steel strip. This bending introduces round corners into the cross-section, along with a relatively complex state of residual stresses and strains: Moen and Schafer 2008, Gao and Moen 2010. The longstanding effective width method of design uses flat plate buckling solutions as its core tool for strength prediction, as a result their have always been questions related to how to handle the round corners in design (e.g., Marsh 1997). This paper addresses the impact of corners in elements, and in members, and provides preliminary recommendations for improving current design methods.

[1] Graduate Research Assistant, Department of Civil Engineering, Johns Hopkins University, Baltimore, MD, USA (vahidzm@jhu.edu)
[2] Professor and Chair, Department of Civil Engineering, Johns Hopkins University, Baltimore, MD, USA (schafer@jhu.edu)

2 Current design

According to the effective width method, as implemented in the main body of the AISI Specification (AISI-S100-07), the strength of a cross section is obtained by finding the effective width of the flat part of each element and then forming the effective area as the sum of the effective flats plus the corners. The corners are always assumed to be fully effective. This creates a false optimal design: sections comprised of all corners are always fully effective. Eurocode uses a modestly different implementation of the effective width method employing a notional flat width that includes the actual flat width plus a portion of the corners (EN-1993-1-3). This approach modestly complicates design.

The direct strength method of Appendix 1 of AISI-S100-07 does not separate the cross-section into flats and corners since full cross-section local buckling analysis is used as the basis, instead of actual or notional flats connected to plate buckling solutions. Reductions are applied to the full section and local buckling may be triggered by the flats, the corners, or any combination thereof. It is worth noting that even this approach has its limits. For extremely large corner radii the behavior may be driven by buckling within the shell-like large corners, instead of the plate-like flats; in this case, the post-buckling may be sharply reduced.

Recently, in support of AISI Specification development, an improved version of the effective width method has been proposed by committee member Robert Glauz. The proposed method continues the AISI main Specification convenience of only reducing the flat portions of the section, but modifies the plate buckling coefficient (k) to account for the reduced capacity due to large rounded corners. The plate buckling stress for any flat of width b, thickness, t, material modulus E, and Poisson's ratio ν, is:

$$f_{cr} = k\frac{\pi^2 E}{12\left(1-\nu^2\right)}\left(\frac{t}{b}\right)^2$$

After studying elastic buckling solutions Robert Glauz proposed that the plate buckling coefficient, k, should be reduced as follows:

$$k_{reduced} = \left(1.08 - 0.02\frac{r_1}{t}\right)\left(1.08 - 0.02\frac{r_2}{t}\right)k$$

where t is the thickness and r_1 and r_2 are the radius of the corners. This approach will be referred to as the "reduced k method" in this paper.

3 Behavior of elements

In this section the effect of corner radius on the strength of isolated elements, both stiffened and unstiffened, is investigated using nonlinear finite element analysis, and compared with available design methods.

3.1 Stiffened elements

Consider a stiffened element (supported on both sides), but with corner radius at its edges, as shown in Figure 1. Here we examine a stiffened element where the centerline out-to-out width, b_o, is held constant as the centerline corner radius, r, is varied (thus in turn varying the flat width, b).

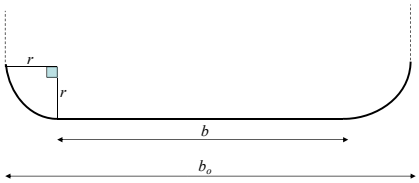

Figure 1: stiffened element in a section

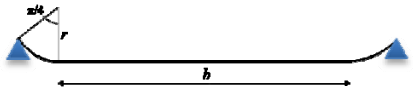

Figure 2: isolated stiffened element

To isolate the stiffened element from the section the selected model, Figure 2, includes half of the corner radius on each edge. The resulting area, A, is:

$$A = \left(b + \tfrac{1}{2} r\pi\right)t = \left(b_o - (2 - \tfrac{1}{2}\pi)r\right)t$$

As can be observed from the equation, the area of the element decreases as the radius increases. (If the full corner is included the area will increase with r).

If the effective width method, as implemented currently in AISI-S100-07, is employed for the strength prediction of this element alone, then:

$$P_{n1} = \left(\rho b + \tfrac{1}{2} r\pi\right)t f_y$$

where f_y is the yield stress and ρ is the effectiveness of the flat portion, defined by Winter's equation as:

$$\rho = \left(1 - 0.22/\lambda\right)/\lambda \text{ for } \lambda > 0.673, \text{ and}$$
$$\rho = 1 \text{ for } \lambda \le 0.673, \text{ and } \lambda = \sqrt{f_y / f_{cr}}$$

where f_{cr} is the buckling stress for the element, defined previously. If the usual k = 4.0 for stiffened elements is employed, then the preceding is the traditional AISI effective width approach. However, if the reduced k equation is employed, f_{cr}, λ, ρ, and finally P_n are modified – thus the reduced k method provides an alternative prediction, P_{n2}, with the same expression as P_{n1} but a revised ρ.

The essential feature of the direct strength method approach is the reduction of the entire member, as opposed to just the flats. Such an approach provides a strength prediction for an isolated element in the following form:

$$P_{n3} = \rho\left(b + \tfrac{1}{2} r\pi\right)t f_y$$

The "effectiveness" may use Winter's equation for ρ, but the f_{cr} as used in λ and in the determination of ρ should be for the full element including corners (a proper section analysis) not just the flats.

3.1.1 Stiffened element comparison with FE

Nonlinear collapse analysis was conducted with ABAQUS to study the ultimate strength of the stiffened element model (Figure 2). The model utilized simply supported boundary conditions (out of plane displacement on the edges were restrained), geometric imperfections in the shape of the first local buckling mode with a maximum magnitude = 0.34t = 0.01in. (Schafer and Peköz 1998), and an elastic perfectly-plastic stress-strain relation with E=29500 ksi, v=*0.3*, and f_y=*33* ksi. A range of elements, 0.03 in. thick, with different width and corner radii: b_o/t =60, 100, 120, 250, and 500*;* and r/t = 0, 4, 7, 10, 15, and 20, are analyzed. The length of the model, a, is four times the total width (a/b_o=*4*).

To compare the effectiveness of strength predictions P_{n1} (traditional effective width ignoring corners) and P_{n3} (direct strength applied to an element including corners) the ρ required for the P_n predictions to match the observed collapse strengths in the ABAQUS analyses were back-calculated and the results plotted in Figure 3. The required reduction for P_{n3} to exactly match the observed ABAQUS results is nearly identical to Winter's equation. For the traditional effective width method modifications are needed in ρ, as at a given slenderness the change in corner radius has a significant impact on the needed ρ.

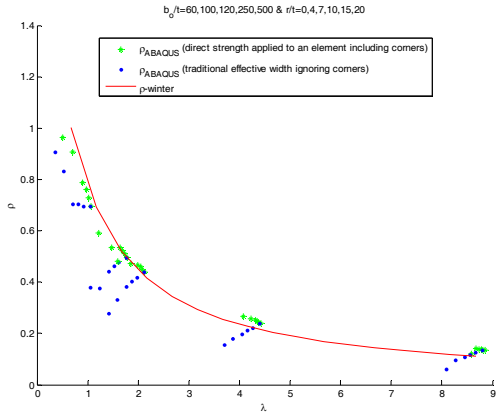

Figure 3: comparison of local reduction factor derived from ABAQUS for whole cross section and for the flat part

A more direct comparison of the finite element collapse strength with the predictions: P_{n1} (traditional effective width ignoring corners) and P_{n3} (direct strength applied to an element including corners) is provided in Figures 4 for P_{n1} and Figures 5 for P_{n3}. In the provided results b_o is set to 3.6 in. (Figures 4a and 5a) and 7.5 in. (Figures 4b and 5b) t = 0.03 in. and r/t is varied from 0 to 20. The traditional effective width prediction, P_{n1}, becomes progressively unconservative for large r/t, and in the studied cases excessively unconservative for r/t in excess of 10. The direct strength style prediction, P_{n3} (applied to just the element and corner) provides a reliable and conservative prediction; though at r/t = 20 in the b_o=3.6 in. case is modestly unconservative.

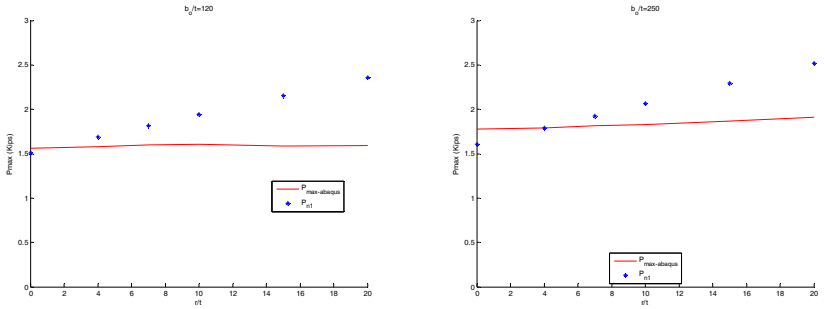

a) b)

Figure 4: comparison between ABAQUS results and P_{n1} (traditional effective width ignoring corners). a) b_o=3.6 in., b) b_o=7.5 in.

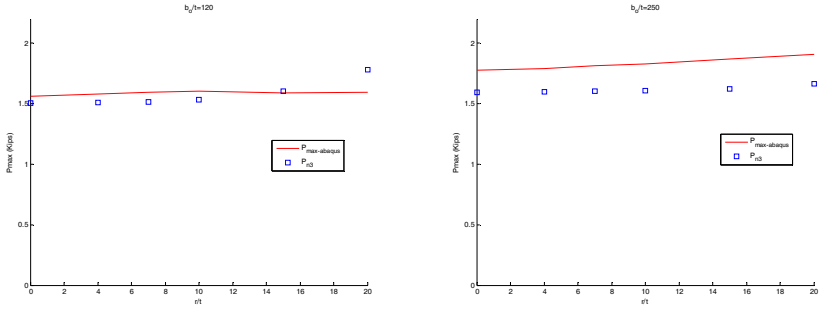

a) b)

Figure 5: comparison between ABAQUS results and P_{n3} (direct strength applied to an element including corners). a) b_o=3.6 in., b) b_o=7.5 in.

3.1.2 Reduced k method for stiffened elements

Consider now the reduced k method, as described in Sections 2 and 3.1, and embodied in the strength prediction, P_{n2}. Figure 6 extends the studies on b_o = 3.6 and 7.5 in. stiffened elements to the reduced k method and compares them with both ABAQUS and the P_{n1} predictions. The trend towards unconservative predictions as r/t increases is decreased using the reduced k method when compared with the P_{n1} predictions. Purely from a strength standpoint, the result is encouraging halving the error (or better) up to r/t of 20.

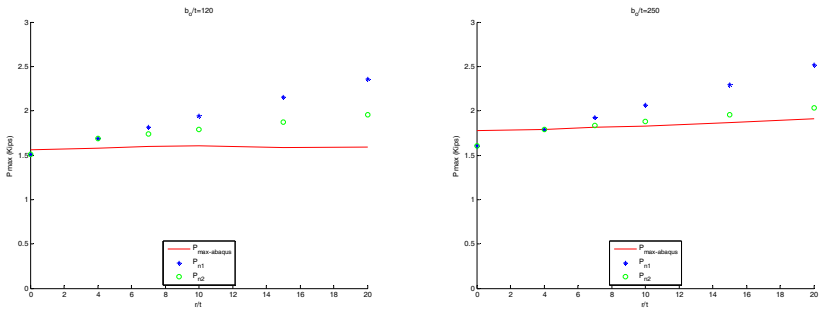

a) b)

Figure 6: Comparison between the results of ABAQUS, reduced k method, and P_{n1}. a) b_o=3.6 in., b) b_o = 7.5 in.

A wider parametric study is also conducted on the reduced k method. ABAQUS predicted collapse strengths for b_o of 1.8, 3 and 7.5 in. are all compared to P_{n2} for increasing r/t in Figure 7. The reduced k method follows the same basic

trend as the expected strength; however, the method becomes more unconservative as radius increases, suggesting limits exist to the strategy.

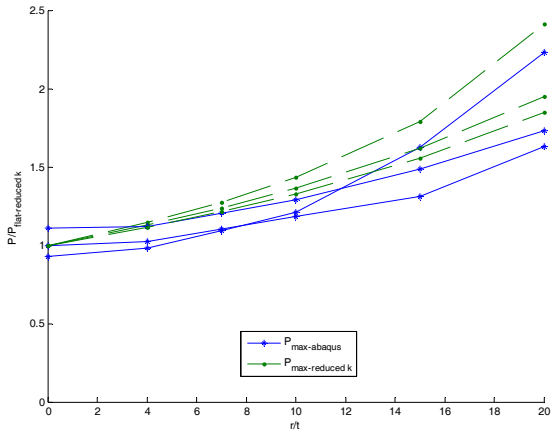

Figure 7: comparison of ABAQUS result with reduced k method (P_{n2})

Given the potential promise of the reduced k method additional analysis is conducted to investigate the $k_{reduced}$ expression directly. Since f_{cr} is defined for the flat width, b, then the plate buckling coefficient, k, may be back-calculated from an elastic buckling ABAQUS analysis and compared with $k_{reduced}$ as provided in Figure 8 for b_o = 1.8, 3 and 7.5 in., t = 0.03 in., and r/t varied from 0 to 20. As Figure 8 shows, $k_{reduced}$ provides an average reduction when compared to *k's* back-calculated from the actual buckling stresses. Dependence of k on both b/t and r/t is observed, but the b/t dependence is ignored in $k_{reduced}$.

Since the ultimate objective of $k_{reduced}$ is to provide an improved strength prediction then a more meaningful comparison may be to the back-calculated k value that would generate a P_{n2} prediction equal to an ABAQUS collapse analysis. This comparison is provided in Figure 9 and in this context $k_{reduced}$ is observed to be an upperbound solution and again missing an observable dependence on b/t.

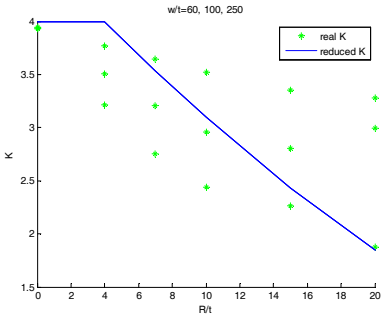

Figure 8: compare k's derived from ABAQUS **buckling** analysis and reduced k method

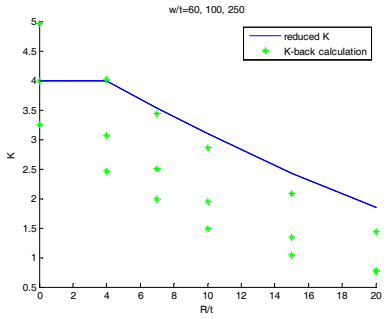

Figure 9: compare k's derived from ABAQUS **collapse** analysis and reduced k method

3.2 Unstiffened elements

In this section finite element studies and comparisons are completed for unstiffened elements similar to those reported on stiffened elements in the previous section. However, in general, the behavior is more complicated and solutions are difficult to generalize. The basic unstiffened element is provided in Figure 10 and the idealized and isolated model with ½ of the corner included is detailed in Figure 11. The traditional effective width strength prediction is:

$$P_{n1} = \left(\rho b + \tfrac{1}{4} r\pi\right) t f_y$$

where ρ follows Winter's equation as previously given in Section 3.1 and f_{cr} is suitably updated with the unstiffened element k = 0.425. A reduced k method strength prediction, P_{n2}, utilizes the same functional form as P_{n1}, but with $k_{reduced}$. replacing k in f_{cr}. The direct strength style expression for an unstiffened element with a corner follows:

$$P_{n3} = \rho\left(b + \tfrac{1}{4} r\pi\right) t f_y$$

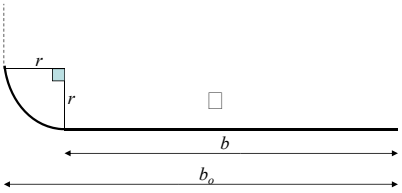

Figure 10: unstiffened element in a section

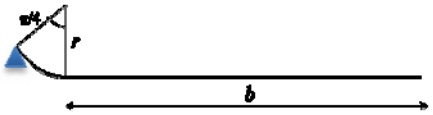

Figure 11: isolated unstiffened element

3.2.1 Unstiffened element comparison with FE

A series of nonlinear finite element models of unstiffened elements are analyzed to collapse using ABAQUS. The models utilize simply supported boundary conditions on the ends and the side that includes the corner, the opposite side has free boundary conditions. Geometric imperfections in the shape of the first local buckling mode with a maximum magnitude of $0.94t = 0.028$ in., where $t = 0.03$ in. (according to [Schafer and Peköz 1998] for type 2 element out-of-straightness imperfections), and an elastic perfectly-plastic stress-strain relation with E=29500 ksi, ν=0.3, and f_y=33 ksi are employed. Models are completed at b_o = 0.9, 1.8, 3.6, and 7.5 in. and for each b_o the r/t is varied from 0 to 20. The length of the models is constant at four times the total width ($a/b_o=4$). Results for the ABAQUS collapse analysis are compared to P_{n1} and P_{n3} in Figures 12.

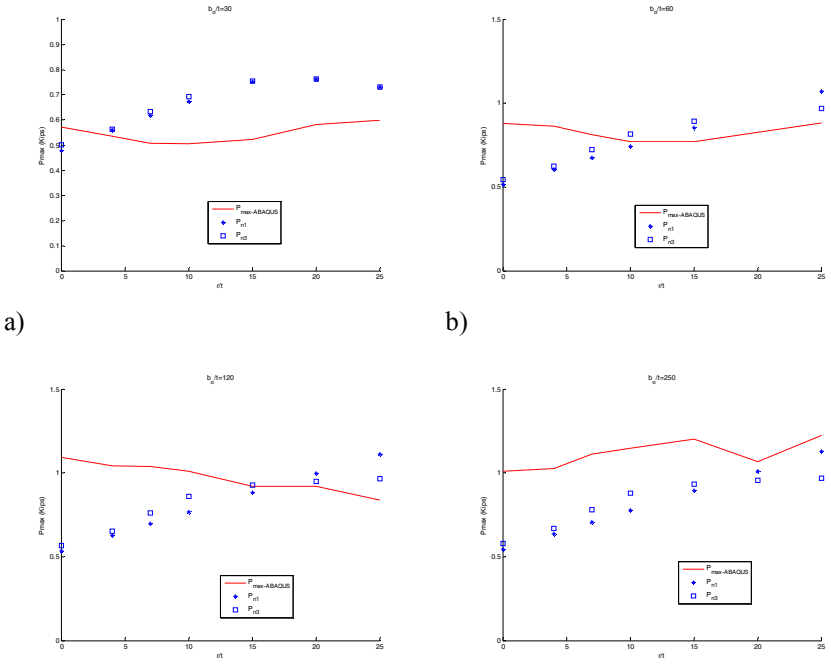

Figure 12: Comparison between the results of ABAQUS, P_{n1} (traditional effective width ignoring corners) and P_{n3} (direct strength applied to an element including corners) for unstiffened elements.:
a) b_o = 0.9 in., b) b_o = 1.8 in., c) b_o = 3.6 in., d) b_o = 7.5 in.

Figure 12 demonstrates that agreement between collapse strength as predicted by ABAQUS and P_{n1} and/or P_{n3} is relatively poor. For stocky unstiffened elements (Figure 12a) P_{n1} and P_{n3} provide generally unconservative predictions, for slender unstiffened elements (Figure 12d) P_{n1} and P_{n3} provide generally conservative predictions and for intermediate slenderness (Figures 12b and 12c) the agreement is better but trends with respect to increasing r/t predicted by P_{n1} and P_{n3} are not generally observed in the ABAQUS collapse analysis. Since the P_{n1} models never reduce the corners it is no surprise that for large corner radius ($\sim r/t > 15$) the P_{n1} models provide strength predictions in excess of P_{n3} and are unconservative compared with the collapse analysis strength from ABAQUS.

As an aside, the plastic strain at collapse for a typical ABAQUS model of an unstiffened element is provided in Figure 13. Ideally, the yielding would be further from the ends of the member. Additional work on the modeling of the unstiffened elements may be beneficial before drawing final conclusions on the adequacy of the design methods.

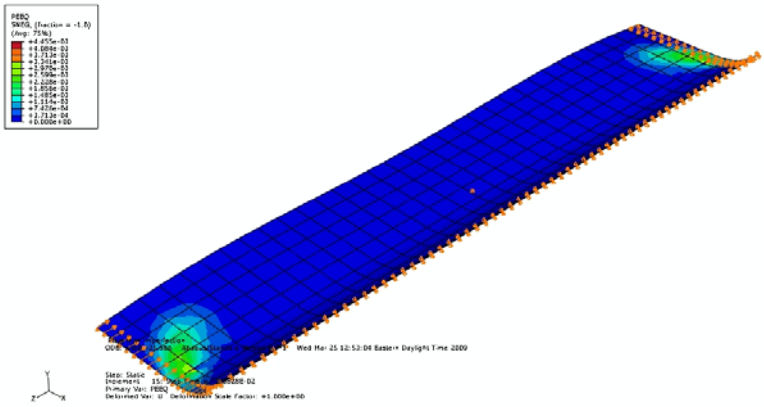

Figure 13: plastic strain at the peak load for an unstiffened element

3.2.2 Reduced k method for unstiffened elements

The reduced k method (and related strength prediction P_{n2}) may also be employed to predict the strength of unstiffened elements. Figures 14 and 15 provide corollaries to the studies of Figures 12a and 12b for the reduced k method. Figure 14 provides comparison to ABAQUS and P_{n3} (direct strength), while Figures 15 provide comparisons to ABAQUS and P_{n3} (effective width). The reduced k method performs largely similar to the direct strength style prediction of P_{n3}. Figure 15b provides the most compelling comparison, indicating the advantage of the reduced k method over the traditional approach (P_{n1}) which is linearly and incorrectly increasing with higher r/t.

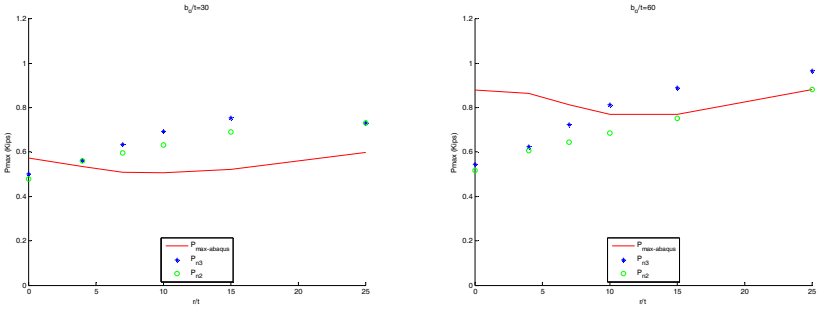

a) b)

Figure14: Comparison between the results of ABAQUS, reduced k method, and P_{n3} for unstiffened elements. a) $b_o = 0.9$ in., b) $b_o = 1.8$ in.

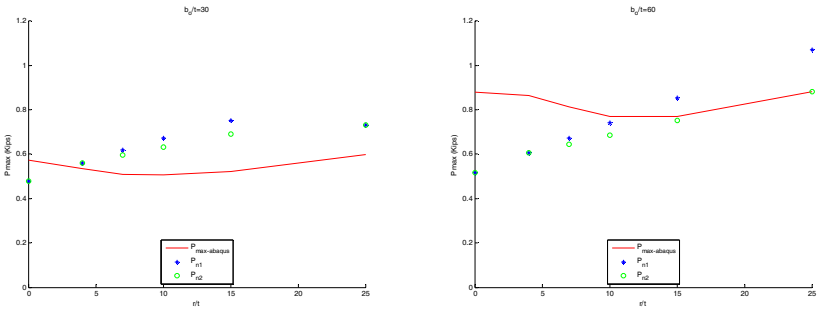

a) b)

Figure15: Comparison between the results of ABAQUS, reduced k method, and P_{n1} for unstiffened elements. a) $b_o = 0.9$ in., b) $b_o = 1.8$ in.

4 Behavior of members

In this section the effect of corner radius on the strength of full cross sections is investigated. Two types of cross sections are considered: square hollow section tubes composed of four stiffened elements, and equal leg angles, composed of two unstiffened elements. Corner radius in the studied sections is varied.

4.1 Members with stiffened elements (i.e. tubes):

Consider a simply supported[3] square hollow section stub column (a/b_o = 2) under compressive loading with centerline out-to-out width, b_o, of 3.6 in. or 7.5

[3] all nodes at the end cross-section of the member are restricted from translation, thus this is a locally simply-supported, warping fixed, boundary condition.

in., t = 0.03 in., and modeled as elastic-perfectly plastic with E = 29500 ksi, v = 0.3, and f_y = 33 ksi. Initial imperfections are considered as the first buckling mode shape with magnitude of 0.34t (Schafer and Peköz 1998). Corner radius is varied from 0 to 25 times the thickness. The strength of these members is obtained using finite element collapse modeling in ABAQUS and compared in Figure 16 with (a) strength prediction from the effective width method in the main Specification of AISI-S100-07, P_{n2}, and (b) strength prediction from the direct strength method in Appendix 1 of AISI-S100-07, P_{n3}.

For the studied square hollow section member both the effective width (P_{n1}) and direct strength (P_{n3}) provide modestly unconservative solutions. However, the direct strength (P_{n3}) predictions follow the same pronounced nonlinear trends observed in the ABAQUS results, while the effective width method essentially assumes a linear change in strength as a function of r/t – a trend not borne out by the ABAQUS results.

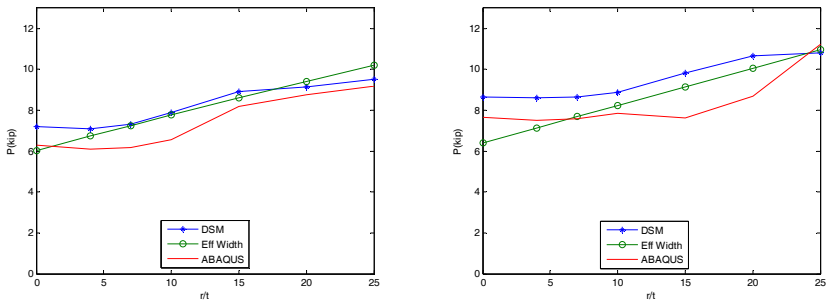

a) b)

Figure16: strength of tube members under axial compression.
a) b_o = 3.6 in. wide, b) b_o = 7.5 in. wide

4.2 Members with unstiffened elements (i.e. angles):

In this section a simply supported[3] angle section stub column (a/b_o = 2) under compressive loading with centerline out-to-out width, b_o, of 0.9 in., 1.8 in., 3.6 in. or 7.5 in., t = 0.03 in., and modeled as elastic-perfectly plastic with E = 29500 ksi, ν = 0.3, f_y = 33 ksi is considered. Initial imperfections are considered in the shape of the first buckling mode with a magnitude of 0.94t (Schafer and Peköz 1998). Corner radius is varied from 0 to 25 times the thickness. The strength of these members is obtained using finite element collapse modeling by ABAQUS and compared in Figure 17 with (a) strength prediction from the effective width method in the main Specification of AISI-S100-07, P_{n2}, and (b)

strength prediction from the direct strength method in Appendix 1 of AISI-S100-07, P_{n3}. For the direct strength (P_{n3}) method the distortional buckling and corresponding load capacity is ignored, further the critical local buckling load for the section is determined at the actual member length.

For the studied angle member both the effective width (P_{n1}) and direct strength (P_{n3}) are modestly unconservative for stocky angles (Figure 17a); however for intermediate and high local slenderness angles (Figure 17b-d) the direct strength (P_{n3}) predictions follow the nonlinear trends observed in the ABAQUS results, while the effective width method again assumes a linear change in strength as a function of r/t – a trend not observed in the ABAQUS results.

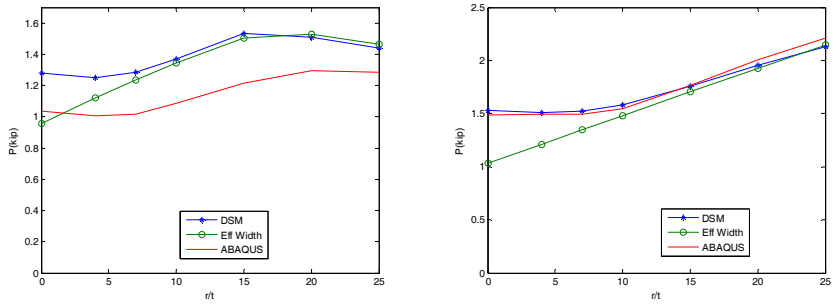

a) b)

c) d)

Figure 17: strength of angle members under axial compression.
a) b_o = 0.9 in. wide, b) b_o = 1.6 in. wide, c) b_o = 3.6 in. wide, d) b_o = 7.5 in. wide

5 Preliminary Recommendations for design

Further study and comparison with testing is warranted, nonetheless the lack of any restriction on corner radius in the effective width method of AISI-S100-07

merits at least preliminary recommendations. It is recognized in the studies herein that the normalized corner radius r/t and the ratio of the area in the corners to the area in the flats, which is proportional to r/b, are both influential in determining when existing methods become systematically unconservative. However, r/t has greater influence (and simplicity) and is thus the focus of the simple recommendations provided herein.

It is recommended that the AISI-S100-07 main specification B1 limits be expanded to include a limit of $r/t < 10$. For $r/t > 10$ this would force the engineer to use rational analysis. If effective width method's are still desired for high r/t, then use of the reduced k method would be appropriate at least up to $r/t = 20$. Thus, it is recommended that $k_{reduced}$ be explicitly added to the AISI-S100 commentary discussion of the new $r/t < 10$ limit.

Based on the results presented here it is recommended that for the AISI-S100-07 Appendix 1 direct strength method that the current pre-qualified limit of $r/t < 10$ be liberalized to $r/t < 20$. At the same time, the commentary should be revised to include commentary consistent with Section 2, discussing why upper limits on r/t must still exist, even in the direct strength method.

6 Conclusions

The formation of cold-formed steel cross-sections requires round corners at the locations of plate bends. The effective width method of member strength determination, as implemented in AISI-S100-07, assumes all corners remain fully effective regardless of their size or slenderness. This approach is demonstrated to be unconservative by comparison to ABAQUS collapse analysis conducted for stiffened elements, unstiffened elements, and members comprised of stiffened elements (tubes) and unstiffened elements (angles); particularly for r/t in excess of approximately 10. A "reduced k method" which provides a simple correction to the plate buckling coefficient employed in the effective width method is demonstrated to improve the accuracy even for r/t as high as ~ 20; however, since it also applies no reduction on the corners it eventually becomes unconservative as well. The direct strength method of member strength determination as implemented in AISI-S100-07 Appendix 1 is also compared to the ABAQUS collapse analysis. The method generally provides good predictions for the corner radius studied. In particular, nonlinear trends in capacity as a function of r/t are replicated in the direct strength method approach. It is recommended that the existing effective width method approach in AISI-S100-07 be limited to $r/t < 10$ and that the pre-qualified limits in the direct strength method (AISI-S100-07 Appendix 1) be liberalized to $r/t < 20$.

Acknowledgments

The input and helpful comments of Robert Glauz in the development of this work is appreciated and gratefully acknowledged.

References

ABAQUS. ABAQUS/Standard Version 6.7-3. Providence, RI: Dassault Systèmes, http://www.simulia.com/, 2007.

AISI-S100-07. North American Specification for the Design of Cold-Formed Steel Structures. American Iron and Steel Institute, Washington, D.C., AISI-S100. 2007.

EN-1993-1-3. Eurocode 3: Design of Steel Structures, Part 1-3: Supplementary rules for cold formed thin gauge members and sheeting. European Committee for Standardization, CEN, Brussels.

Gao, T., Moen, C. D., *The cold work of forming effect in structural steel members.* International Collquium, Stability and Ductility of Steel Structures, Rio de Janeiro, Brazil, 2010.

Marsh, C., *Influence of bend radii on local buckling in cold formed shapes.* ASCE, Journal of Structural Engineering, 1997, 123(12): p. 1686-1689

Moen, C.D., Igusa, T., Schafer, B.W., *Prediction of residual stresses and strains in cold-formed steel members*, Journal of Thin-Walled Structures, 2008

Schafer, B.W. and T. Peköz, *Computational modeling of cold-formed steel: Characterizing geometric imperfections and residual stresses.* Journal of Constructional Steel Research, 1998. 47(3): p. 193-210.

Twentieth International Specialty Conference on Cold-Formed Steel Structures
St. Louis, Missouri, U.S.A., November 3 & 4, 2010

Buckling analysis of cold-formed steel members with general boundary conditions using CUFSM: conventional and constrained finite strip methods

Z. Li[1] and B. W. Schafer[2]

Abstract

The objective of this paper is to provide the theoretical background and illustrative examples for elastic buckling analysis of cold-formed steel members with general boundary conditions as implemented in the forthcoming update to CUFSM. CUFSM is an open source finite strip elastic stability analysis program freely distributed by the senior author. Although the finite strip method presents a general methodology, the conventional implementation (e.g. CUFSM v 3.13 or earlier) employs only simply-supported boundary conditions. In this paper, utilizing specially selected longitudinal shape functions, the conventional finite strip method is extended to general boundary conditions, including the conventional case: simply-simply supported, as well as: clamped-clamped, clamped-simply supported, clamped-free, and clamped-guided. The solution remains semi-analytical as the elastic and geometric stiffness matrices are derived in a general form with only specific integrals depending on the boundary conditions. An example of the stability solution is provided. The selection of longitudinal terms to be included in the analysis is discussed in terms of balancing accuracy with computational efficiency. Also herein, the constrained finite strip method is extended to general boundary conditions. Both modal decomposition and identification can be carried out based on the new bases developed for the constrained finite strip method, and illustrative examples are provided. This extension of CUFSM is intended to aid the implementation of the direct strength method to the case of general boundary conditions.

Keywords: Finite strip method, constrained finite strip method, boundary conditions, elastic buckling analysis, CUFSM

[1] Ph.D. Candidate, Johns Hopkins Univ., Baltimore, MD, lizhanjie@jhu.edu
[2] Professor, Johns Hopkins Univ., Baltimore, MD, schafer@jhu.edu

Introduction

Cold-formed steel members are thin, light and economically efficient. However, this efficiency comes with complication. Engineers must account for cross section instability (i.e., local and distortional) in addition to global buckling (Euler) of the member. Numerical solutions, such as the finite strip method (FSM), are particularly important for addressing this complexity as they take into consideration the inter-element interaction and as a result provide far more accurate solutions for local and distortional buckling than typical hand formulas.

Conventional FSM, e.g., CUFSM [1], freely available from the senior author's website (www.ce.jhu.edu/bschafer/cufsm), provides a method to examine all the instabilities in a cold-formed steel member under uniform longitudinal stresses (axial, bending, warping torsion, or combinations thereof). Additionally, the newly developed constrained finite strip method (*c*FSM) is implemented in CUFSM. When the signature curve of the conventional FSM is not able to provide distinct minima that correspond to local and distortional buckling mode [2], *c*FSM becomes essential for accurately determining the buckling modes and greatly eases and generalizes implementation in new design methods such as the Direct Strength Method (DSM) [3]. However, existing CUFSM and *c*FSM implementations are applicable to only simply supported end boundary conditions.

Recently, extensions of the conventional FSM and *c*FSM to general end boundary conditions, namely: simple-simple (S-S), clamped-clamped (C-C), simple-clamped (S-C), clamped-free (C-F), and clamped-guided (C-G), have been explored by Li and Schafer [4, 5]. Specially selected longitudinal shape functions are employed to represent the specified boundary condition [4, 6] as follows:

simple-simple, $Y_{[m]} = \sin\left(m\pi y / a\right)$ (1)

clamped-clamped, $Y_{[m]} = \sin\left(m\pi y / a\right)\sin\left(\pi y / a\right)$ (2)

simple-clamped, $Y_{[m]} = \sin\left[(m+1)\pi y / a\right] + \left(m+1/m\right)\sin\left(m\pi y / a\right)$ (3)

clamped-free, $Y_{[m]} = 1 - \cos\left[(m-1/2)\pi y / a\right]$ (4)

clamped-guided, $Y_{[m]} = \sin\left[(m-1/2)\pi y / a\right]\sin\left(\pi y / 2 / a\right)$ (5)

where, *m* indicates the longitudinal term to be summed to form the displacement field. These shape functions have been implemented into a new version of CUFSM for both conventional and constrained FSM (*c*FSM). To provide the theoretical basis of this solution the underlying elastic and geometric stiffness matrices are briefly derived and presented. In addition, stability solutions for general boundary conditions are provided against the typical signature curve to

illustrate their coherent relationship. The underlying theory and procedure of *c*FSM for general boundary conditions is provided along with related examples. Finally, FSM and *c*FSM for general end boundary conditions are employed for use with the DSM design procedure. The coupling between longitudinal terms for non-simply supported boundary conditions creates complications and new procedures are suggested.

Conventional Finite Strip Method

A typical strip for a thin-walled member is depicted in Figure 1, along with the degrees of freedom (u_1,v_1,w_1,θ_1, etc., for the m=1 longitudinal term) applied end tractions (T_1, T_2) and the global/member (X, Y, Z) and local/strip (x, y, z) coordinate systems.

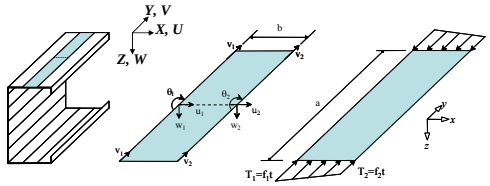

Figure 1 Coordinates, Degree of Freedom, and loads of a typical strip

The u, v and w displacement fields are approximated with shape functions and nodal displacements. These displacement fields are summed for each longitudinal term m, up to q, specifically:

$$u = \sum_{m=1}^{q} \left[(1-\frac{x}{b}) \quad \frac{x}{b} \right] \begin{Bmatrix} u_{1[m]} \\ u_{2[m]} \end{Bmatrix} Y_{[m]}, \quad v = \sum_{m=1}^{q} \left[(1-\frac{x}{b}) \quad \frac{x}{b} \right] \begin{Bmatrix} v_{1[m]} \\ v_{2[m]} \end{Bmatrix} Y'_{[m]} \frac{a}{\mu_{[m]}} \tag{6}$$

$$w = \sum_{m=1}^{q} \left[1 - \frac{3x^2}{b^2} + \frac{2x^3}{b^3} \quad x(1 - \frac{2x}{b} + \frac{x^2}{b^2}) \quad \frac{3x^2}{b^2} - \frac{2x^3}{b^3} \quad x(\frac{x^2}{b^2} - \frac{x}{b}) \right] Y_{[m]} d_{w[m]} \tag{7}$$

where $d_{w[m]} = \left[w_{1[m]} \quad \theta_{1[m]} \quad w_{2[m]} \quad \theta_{2[m]} \right]$ and $\mu_{[m]}=m\pi$. The shape function of the strip in the transverse direction is the same as a classical beam finite element, while in the longitudinal direction, $Y_{[m]}$, is employed with trigonometric functions as shown in Eq.'s (1)-(5).

Elastic and Geometric stiffness matrices

For the elastic stiffness matrices the strain in the strip consists of two portions: membrane and bending. The membrane strains are at the mid-plane of the strip and governed by plane stress assumptions. The bending strains follow Kirchhoff thin plate theory and are zero at the mid-plane, and a function of w alone. For each strip, the elastic stiffness matrix k_e can be formulated through the internal

energy integration, where stress is connected to strain by an orthotropic plane stress constitutive relation. See [1] and [4] for full derivation. Matrix $k_e^{[mn]}$ corresponding to longitudinal terms *m* and *n* is one block elastic stiffness matrix of the full elastic stiffness matrix k_e, which can be separated for membrane ($_M$) and bending ($_B$),

$$k_e^{[mn]} = \begin{bmatrix} k_{eM}^{[mn]} & \cdot \\ \cdot & k_{eB}^{[mn]} \end{bmatrix} \tag{8}$$

The closed-form expressions for the membrane, $k_{eM}^{[mn]}$, and the bending, $k_{eB}^{[mn]}$, elastic stiffness matrices are provided as follows:

$$k_{eM}^{[mn]} = t \begin{bmatrix} \left(\frac{E_1 I_1}{b} + \frac{GbI_5}{3}\right) & \left(-\frac{E_2 v_x I_3}{2c_2} - \frac{GI_5}{2c_2}\right) & \left(-\frac{E_1 I_1}{b} + \frac{GbI_5}{6}\right) & \left(-\frac{E_2 v_x I_3}{2c_2} + \frac{GI_5}{2c_2}\right) \\ \left(-\frac{E_2 v_x I_2}{2c_1} - \frac{GI_5}{2c_1}\right) & \left(\frac{E_2 bI_4}{3c_1 c_2} + \frac{GI_5}{bc_1 c_2}\right) & \left(\frac{E_2 v_x I_2}{2c_1} - \frac{GI_5}{2c_1}\right) & \left(\frac{E_2 bI_4}{6c_1 c_2} - \frac{GI_5}{bc_1 c_2}\right) \\ \left(-\frac{E_1 I_1}{b} + \frac{GbI_5}{6}\right) & \left(\frac{E_2 v_x I_3}{2c_2} - \frac{GI_5}{2c_2}\right) & \left(\frac{E_1 I_1}{b} + \frac{GbI_5}{3}\right) & \left(\frac{E_2 v_x I_3}{2c_2} + \frac{GI_5}{2c_2}\right) \\ \left(-\frac{E_2 v_x I_2}{2c_1} + \frac{GI_5}{2c_1}\right) & \left(\frac{E_2 bI_4}{6c_1 c_2} - \frac{GI_5}{bc_1 c_2}\right) & \left(\frac{E_2 v_x I_2}{2c_1} + \frac{GI_5}{2c_1}\right) & \left(\frac{E_2 bI_4}{3c_1 c_2} + \frac{GI_5}{bc_1 c_2}\right) \end{bmatrix} \tag{9}$$

$$k_{eB}^{[mn]} = \frac{1}{420b^3} \begin{bmatrix} \begin{pmatrix} 5040 D_x I_1 - 504 b^2 D_1 I_2 \\ -504 b^2 D_1 I_3 + 156 b^4 D_y I_4 \\ +2016 b^2 D_{xy} I_5 \end{pmatrix} & \begin{pmatrix} 2520 bD_x I_1 - 462 b^3 D_1 I_2 \\ -42 b^3 D_1 I_3 + 22 b^5 D_y I_4 \\ +168 b^3 D_{xy} I_5 \end{pmatrix} & \begin{pmatrix} -5040 D_x I_1 + 504 b^2 D_1 I_2 \\ +504 b^2 D_1 I_3 + 54 b^4 D_y I_4 \\ -2016 b^2 D_{xy} I_5 \end{pmatrix} & \begin{pmatrix} 2520 bD_x I_1 - 42 b^3 D_1 I_2 \\ -42 b^3 D_1 I_3 - 13 b^5 D_y I_4 \\ +168 b^3 D_{xy} I_5 \end{pmatrix} \\ \begin{pmatrix} 2520 bD_x I_1 - 462 b^3 D_1 I_3 \\ -42 b^3 D_1 I_2 + 22 b^5 D_y I_4 \\ +168 b^3 D_{xy} I_5 \end{pmatrix} & \begin{pmatrix} 1680 b^2 D_x I_1 - 56 b^4 D_1 I_2 \\ -56 b^4 D_1 I_3 + 4 b^6 D_y I_4 \\ +224 b^4 D_{xy} I_5 \end{pmatrix} & \begin{pmatrix} -2520 bD_x I_1 + 42 b^3 D_1 I_2 \\ +42 b^3 D_1 I_3 + 13 b^5 D_y I_4 \\ -168 b^3 D_{xy} I_5 \end{pmatrix} & \begin{pmatrix} 840 b^2 D_x I_1 + 14 b^4 D_1 I_2 \\ +14 b^4 D_1 I_3 - 3 b^6 D_y I_4 \\ -56 b^4 D_{xy} I_5 \end{pmatrix} \\ \begin{pmatrix} -5040 D_x I_1 + 504 b^2 D_1 I_2 \\ +504 b^2 D_1 I_3 + 54 b^4 D_y I_4 \\ -2016 b^2 D_{xy} I_5 \end{pmatrix} & \begin{pmatrix} -2520 bD_x I_1 + 42 b^3 D_1 I_2 \\ +42 b^3 D_1 I_3 + 13 b^5 D_y I_4 \\ -168 b^3 D_{xy} I_5 \end{pmatrix} & \begin{pmatrix} 5040 D_x I_1 - 504 b^2 D_1 I_2 \\ -504 b^2 D_1 I_3 + 156 b^4 D_y I_4 \\ +2016 b^2 D_{xy} I_5 \end{pmatrix} & \begin{pmatrix} -2520 bD_x I_1 + 462 b^3 D_1 I_3 \\ +42 b^3 D_1 I_2 - 22 b^5 D_y I_4 \\ -168 b^3 D_{xy} I_5 \end{pmatrix} \\ \begin{pmatrix} 2520 bD_x I_1 - 42 b^3 D_1 I_2 \\ -42 b^3 D_1 I_3 - 13 b^5 D_y I_4 \\ +168 b^3 D_{xy} I_5 \end{pmatrix} & \begin{pmatrix} 840 b^2 D_x I_1 + 14 b^4 D_1 I_2 \\ +14 b^4 D_1 I_3 - 3 b^6 D_y I_4 \\ -56 b^4 D_{xy} I_5 \end{pmatrix} & \begin{pmatrix} -2520 bD_x I_1 + 462 b^3 D_1 I_3 \\ +42 b^3 D_1 I_2 - 22 b^5 D_y I_4 \\ -168 b^3 D_{xy} I_5 \end{pmatrix} & \begin{pmatrix} 1680 b^2 D_x I_1 - 56 b^4 D_1 I_2 \\ -56 b^4 D_1 I_3 + 4 b^6 D_y I_4 \\ +224 b^4 D_{xy} I_5 \end{pmatrix} \end{bmatrix} \tag{10}$$

where $c_1 = \frac{m\pi}{a}$ $c_2 = \frac{n\pi}{a}$ $I_1 = \int_0^a Y_{[m]} Y_{[n]} dy$ $I_2 = \int_0^a Y''_{[m]} Y_{[n]} dy$ $I_3 = \int_0^a Y_{[m]} Y''_{[n]} dy$ $I_4 = \int_0^a Y''_{[m]} Y''_{[n]} dy$

$I_5 = \int_0^a Y'_{[m]} Y'_{[n]} dy$ $[D_M] = \begin{bmatrix} E_1 & v_x E_2 & 0 \\ v_y E_1 & E_2 & 0 \\ 0 & 0 & G \end{bmatrix}$ $E_1 = \frac{E_x}{1 - v_x v_y}$ $E_2 = \frac{E_y}{1 - v_x v_y}$ $[D_B] = \begin{bmatrix} D_x & D_1 & 0 \\ D_1 & D_y & 0 \\ 0 & 0 & D_{xy} \end{bmatrix}$

$D_x = \frac{E_x t^3}{12(1 - v_x v_y)}$ $D_y = \frac{E_y t^3}{12(1 - v_x v_y)}$ $D_1 = \frac{v_y E_x t^3}{12(1 - v_x v_y)} = \frac{v_x E_y t^3}{12(1 - v_x v_y)}$ $D_{xy} = \frac{Gt^3}{12}$

The geometric stiffness matrix is determined by examining the potential work created as the plate shortens, e.g., due to out-of-plane bending (or the Lagrangian strain terms), allows the geometric stiffness matrix k_g to be formulated as well (see complete derivation in [1, 4]). Similar to the elastic stiffness matrix, $k_g^{[mn]}$ corresponding to longitudinal terms *m* and *n* is broken into membrane, $k_{gM}^{[mn]}$ and bending, $k_{gB}^{[mn]}$:

$$k_g^{[mn]} = \begin{bmatrix} k_{gM}^{[mn]} & \cdot \\ \cdot & k_{gB}^{[mn]} \end{bmatrix} \tag{11}$$

The explicit expressions are given below:

$$k_{gM}^{[mn]} = \begin{bmatrix} \frac{(3T_1+T_2)bI_5}{12} & 0 & \frac{(T_1+T_2)bI_5}{12} & 0 \\ & \frac{(3T_1+T_2)ba^2I_4}{12\mu_m\mu_n} & 0 & \frac{(T_1+T_2)ba^2I_4}{12\mu_m\mu_n} \\ & & \frac{(T_1+3T_2)bI_5}{12} & 0 \\ \textit{symmetric} & & & \frac{(T_1+3T_2)ba^2I_4}{12\mu_m\mu_n} \end{bmatrix} \quad (12)$$

$$k_{gB}^{[mn]} = \begin{bmatrix} \frac{(10T_1+3T_2)bI_5}{35} & \frac{(15T_1+7T_2)b^2I_5}{420} & \frac{9(T_1+T_2)bI_5}{140} & -\frac{(7T_1+6T_2)b^2I_5}{420} \\ & \frac{(5T_1+3T_2)b^3I_5}{840} & \frac{(6T_1+7T_2)b^2I_5}{420} & -\frac{(T_1+T_2)b^3I_5}{280} \\ & & \frac{(3T_1+10T_2)bI_5}{35} & -\frac{(7T_1+15T_2)b^2I_5}{420} \\ \textit{symmetric} & & & \frac{(3T_1+5T_2)b^3I_5}{840} \end{bmatrix} \quad (13)$$

where $\mu_m = m\pi$; $\mu_n = n\pi$; $I_4 = \int_0^a Y''_{[m]} Y''_{[n]} dy$; $I_5 = \int_0^a Y'_{[m]} Y'_{[n]} dy$

The full elastic stiffness matrix k_e and geometric stiffness matrix k_g can be expressed as:

$$k_e = \left[k_e^{[mn]}\right]_{q\times q} \quad \text{and} \quad k_g = \left[k_g^{[mn]}\right]_{q\times q} \quad (14)$$

where each $k_e^{[mn]}$ and $k_g^{[mn]}$ submatrices are 8x8 and q^2 such submatrices exist.

Note, I_1 through I_5 are zero when $m \neq n$ for the simple-simple (*S*-*S*) boundary conditions leaving only a diagonal set of submatrices in k_e and k_g. It is this efficiency that leads to the attractive nature of the classical solution and the universality of the buckling half-wavelength vs. buckling load curve (signature curve) for the *S*-*S* boundary conditions. For all other boundary conditions k_e and k_g have non-zero submatrices off the main diagonal and interaction of buckling modes of different half-wavelengths (or longitudinal terms) occur and the signature curve loses its special significance. In essence, for all boundary conditions other than *S*-*S*, FSM has the same identification problems as finite element method (FEM), unless other tools such as the constrained FSM are implemented.

Assembly and Stability solutions

After necessary transformation from local to global coordinates based on the strip orientation and appropriate assembly over all the strips, the global elastic (K_e) and geometric (K_g) stiffness matrices can be obtained. See complete details in [1] and [4]. For a given distribution of edge tractions on a member the

geometric stiffness matrix scales linearly, resulting in the elastic buckling problem:

$$K_e\Phi = \Lambda K_g\Phi \tag{15}$$

where, Λ is a diagonal matrix containing the eigenvalues (buckling loads) and Φ is a fully populated matrix corresponding to the eigenmodes (buckling modes) in its columns. Validation of the conventional FSM solution may be found in [4].

Signature curve and FSM solution of general boundary conditions

To illustrate the stability solution for general boundary conditions and reveal its relationship with the popularized "signature curve" the stability solutions for a 400S162-68 SSMA stud section [7] under major-axis bending are provided for simple (*S*-*S*) and clamped (*C*-*C*) boundary conditions in Figure 2. Note, the signature curve is a special case of the *S*-*S* FSM solution where only a single longitudinal term (i.e., m=1) is employed. FSM solutions for *S*-*S* boundary conditions for any m are independent due to the resulting orthogonality in K_e and K_g and further the buckling load for any m may be found by performing the solution for m=1 at a length equal to a/m. As a result, it has become conventional to express FSM solutions of *S*-*S* boundary conditions in terms of the first buckling load over a series of lengths as opposed to FEM solutions where typically a model is solved for many buckling loads at a single length by examining higher mode solutions [8].

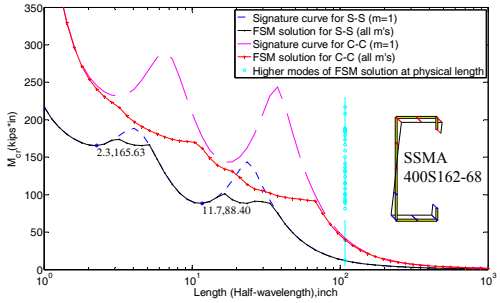

Figure 2 Signature curve and FSM solution for general boundary conditions

For FSM with non simply-supported boundary conditions the orthogonality is lost, and thus the special meaning of the signature curve (an m=1 solution with varying length a) is lost, as shown in Figure 2. Given that many longitudinal (m) terms are used the solution should be interpreted as a function of physical length, as opposed to half-wavelength. In fact, the FSM solution captures the potential interaction of longitudinal terms, and it would be equally valid to use the FEM approach and examine higher mode solutions at a given length (e.g., at L~100in. as shown), instead of varying a as shown in Figure 2.

Longitudinal terms

Although the signature curve is ineffective for non simply-supported boundary conditions, the buckling nature in terms of the inherent half-wavelengths of local, distortional, and global buckling from the signature curve still provide useful information. For problem size and computational efficiency the total number of longitudinal terms included in the analysis should be minimized. Accordingly, longitudinal terms for the physical length (L) to be analyzed should be wisely selected so that higher modes reported from the FSM solution consist of all the three modes (local, distortional and global). Studies in [4] show that given that the simply supported half-wavelengths of local ($L_{cr\ell}$), distortional (L_{crd}), and global (L_{cre}) buckling these represent the three regimes for m of greatest interest, i.e. m near $L/L_{cr\ell}$, L/L_{crd}, and L/L_{cre}. Note, usually, L_{cre} is the physical length, thus 1, 2, and 3 are chosen around L/L_{cre}, and 7 longitudinal terms are chosen around $L/L_{cr\ell}$ and L/L_{crd} to include relevant potential couplings.

The critical buckling moments of the first 10 modes at L=108 in. (see Figure 2) are listed in Table 1 for both *S*-*S* and *C*-*C* boundary conditions using the suggested longitudinal terms. For the *S*-*S* case, modes 1, 4 and 10 are the global, distortional, and local buckling modes, respectively, and match exactly the signature curve. For the *C*-*C* case, critical moments have a negligible difference compared with the solution with all longitudinal terms included, e.g., mode 3 M_{crd} is 0.05% lower with all terms. The difference of the participation of longitudinal terms is illustrated for the 3rd mode in Figure 3.

Table 1 Higher modes of FSM solution for *S*-*S* and *C*-*C* boundary conditions

Higher modes	M_{cr} of FSM solution for S-S	M_{cr} of FSM solution for C-C
1	11.94 G	40.90 G
2	39.47 G	78.63 G
3	81.58 G	89.86 D
4	88.65 D	90.01 D
… Higher order D modes		… Higher order D modes
10	165.53 L	165.58 L

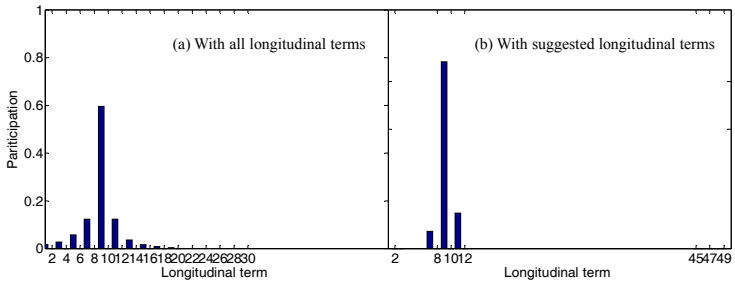

Figure 3 Participations of longitudinal terms for 3rd mode of FSM solution

Constrained Finite Strip Method

The concept and theory of the constrained FSM (*c*FSM) for *S*-*S* boundary conditions is well established [1, 9-11] and at its heart employs the same mechanical assumptions of the deformation modes utilized in Generalized Beam Theory (GBT) [12, 13]. In *c*FSM, the mechanical assumptions provide a means to categorize any deformation, including buckling modes into global (G), distortional (D), local (L), and other (O, or shear and transverse extension--ST) deformation spaces. The key feature of *c*FSM is that the general displacement field *d* may be constrained to any "modal" deformation space, *M*, via:

$$d = R_M d_M \tag{16}$$

where R_M is the constraint matrix for the selected modal space(s) (*G*, *D*, *L*, *O (ST)* or any combination thereof) and d_M is the resulting deformations within that space.

Recently, the authors extended FSM and *c*FSM to the case of general end boundary conditions [4, 5] and this paper summarizes that work as implemented in CUFSM. *c*FSM provides the ability to perform modal decomposition of stability solutions as well as quantitative modal identification. Extension to general boundary conditions is an important step towards *c*FSM's application in general purpose design situations.

Buckling mode definition

The essential feature of *c*FSM is the separation of general deformations into those deformations consistent with *G*, *D*, *L*, and *ST*/O deformation spaces. The deformation spaces are defined by the mechanical assumptions inherent within each space. The criteria are provided below in Table 2 and implemented for each space, as is typical in the *c*FSM literature [1, 4, 5, 9-11].

Table 2 Mechanical criteria of mode definition

Mechanical criteria	G	D	L	ST/O
$\gamma_{xy}=0$, $\varepsilon_x=0$, v is linear (Vlasov's hypothes)	Yes	Yes	Yes	No
$\varepsilon_y \neq 0$ (longitudinal warping)	Yes	Yes	No	-
$\kappa_y=0$ (undistorted section)	Yes	No	-	-

Base definition

Although Table 2 defines the deformation spaces, there are some subtleties in the implementation which do influence the resulting modal decomposition or identification. Full details of the basis definitions are provided in [5] and a summary of the bases utilized in CUFSM's implementation of *c*FSM are provided in Table 3. The simplest application of the Table 3 definitions are embodied in the "Natural basis" which is defined by explicitly following the mechanical criteria (see [4]). The natural basis, which separates the deformations into the G, D, L, O/ST spaces may be transformed to a true "modal" basis (similar to GBT) by performing an auxiliary eigen problem within each space either for a unit axial stress, or for the actual applied stresses. For non-simply supported boundary conditions due to the loss of orthogonality of the stiffness matrices between longitudinal terms, whether the constrained eigenvalue problem is solved inside each longitudinal term or over all the longitudinal terms results in the uncoupled and coupled bases, respectively. Finally, two alternatives exist for defining the O/ST space. Either the O space can be built up as the union of the shear and transverse extensions (generally preferred) or the space may be defined as the null of the GDL subspace, either with respect to elastic stiffness matrix K_e ($^{e}R_O$), geometric stiffness matrix K_g ($^{g}R_O$), or in vector sense ($^{v}R_O$) as detailed in [5].

Table 3 Summary of defined bases

Subspaces	Orthogonalization in the subspace					
	Natural basis (not orthogonal)		Modal basis (orthogonal)			
			Axial uniform force		Applied force	
	Uncoupled basis [c]	Coupled basis	Uncouple basis	Coupled basis	Uncouple basis	Coupled basis
GD	R_{GD}		$[\bar{R}_{GD}]_m$	$\bar{R}_{GD}$	$[\tilde{R}_{GD}]_m$	$\tilde{R}_{GD}$
G	R_G[a]		$[\bar{R}_G]_m$	$\bar{R}_G$	$[\tilde{R}_G]_m$	$\tilde{R}_G$
D	R_D		$[\bar{R}_D]_m$	$\bar{R}_D$	$[\tilde{R}_D]_m$	$\tilde{R}_D$
L	R_L		$[\bar{R}_L]_m$	$\bar{R}_L$	$[\tilde{R}_L]_m$	$\tilde{R}_L$
ST/O	Shear + Transerse extension[b] $R_{ST}=R_S\cup R_T$ Null of GDL $[R_O]_m=[{}^{e}R_O]_m$ or $[{}^{g}R_O]_m$ or $[{}^{v}R_O]_m R_O={}^{e}R_O$ or ${}^{g}R_O$ or ${}^{v}R_O$		$[\bar{R}_S]_m\cup[\bar{R}_T]_m$ or $[{}^{e}\bar{R}_O]_m$ or $[{}^{g}\bar{R}_O]_m$ or $[{}^{v}\bar{R}_O]_m$	$\bar{R}_S\cup\bar{R}_T$ or ${}^{e}\bar{R}_O$ or ${}^{g}\bar{R}_O$ or ${}^{v}\bar{R}_O$	$[\tilde{R}_S]_m\cup[\tilde{R}_T]_m$ or $[{}^{e}\tilde{R}_O]_m$ or $[{}^{g}\tilde{R}_O]_m$ or $[{}^{v}\tilde{R}_O]_m$	$\tilde{R}_S\cup\tilde{R}_T$ or ${}^{e}\tilde{R}_O$ or ${}^{g}\tilde{R}_O$ or ${}^{v}\tilde{R}_O$

(a) G modes may be defined about principle axes or about geometric axes. Also pure torsion mode does not have to be about shear center, though CUFSM (and GBT) does choose to do this.

(b) S and T may be formed from strip-wise shear and transverse extension, e.g. +1,-1 for v in a strip, or +1,0 for v in a strip leading to different S and T spaces.

(c) Uncoupled basis means the null space of GDL space or the orthogonalization is performed inside each longitudinal term m. The resulted basis is a block diagonal matrix.

Also, note, for the purpose of performing modal identification the base vectors in the basis have to be appropriately normalized. Normalization can be done in various ways. Three options are available and each column φ_i in bases must

satisfy the following condition: (1) vector norm $\|\varphi_i\|=1$; (2) strain energy norm $\sqrt{\varphi_i^T K_e \varphi_i}=1$; and (3) work norm $\sqrt{\varphi_i^T K_g \varphi_i}=1$.

Modal decomposition

The constrained eigenvalue problem may be expressed by introducing Eq. (16) into the FSM eigenvalue problem for mode or modes *M* as:

$$K_{e,M}\Phi_M = \Lambda_M K_{g,M}\Phi_M \tag{17}$$

where, $K_{e,M}$ and $K_{g,M}$ are the elastic and geometric stiffness matrix of the constrained FSM problem, respectively, and defined as $K_{e,M}=R_M{}^T K_e R_M$ and $K_{g,M}=R_M{}^T K_g R_M$; Λ_M is a diagonal matrix containing the eigenvalues for the given mode or modes, and Φ_M is the matrix of corresponding eigenmodes (or buckling modes) in its columns.

To illustrate the capability of *c*FSM for general boundary conditions, the *G*, *D*, and *L* modes are decomposed from the FSM solution using the natural basis (ST) of Table 3 and the critical moments are plotted in Figure 4 against the FSM solution for the 400S162-68 SSMA stud section under major-axis bending with *C*-*C* boundary conditions. The longitudinal terms employed are the previously recommended terms. In general, the results are consistent with the observations in previous *c*FSM analyses for *S*-*S* boundary conditions.

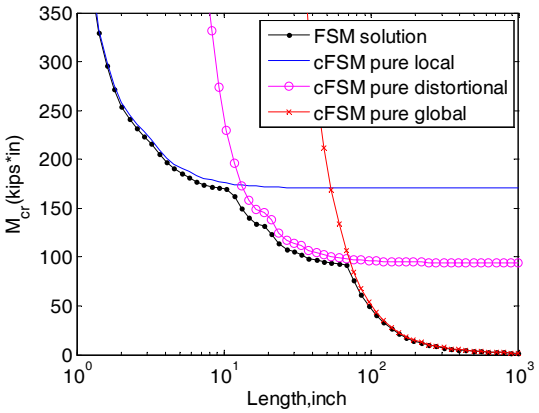

Figure 4 Modal decomposition of *c*FSM

Modal decomposition may also be used to search the participation of longitudinal terms for pure local and distortional buckling, and then use these longitudinal terms to force the member to buckle in local or distortional buckling mode as described in the application with DSM section at the end of this paper.

Modal Identification

Using the defined *c*FSM bases, natural or modal, any nodal displacement vector, *d*, (deformed shape or buckling mode) may be transformed into the basis spanned by the buckling classes, via

$$c = R^{-1}d \tag{18}$$

where the coefficients in *c* represent the contribution to a given column of basis *R*. The participation of each mode class is calculated as:

$$p_M = \|c_M\|_2 \Big/ \sum_{M=G,D,L,ST/O}^{4} \|c_M\|_2 \tag{19}$$

where c_M is column vectors of the contribution coefficients of each mode class (G, D, L, ST/O) in *c*. Eq. (19) uses the L^2 norm to calculate the participation of each mode class other than the absolute sum as previously used. The attraction of formal identification of the buckling modes is not just a theoretical one, as design methods such as the DSM directly utilize this information to select buckling modes and then predict ultimate strength.

To illustrate the capacity of modal identification of *c*FSM, modal participations for the higher modes of Table 1 are provided in Table 4. The basis employed is the uncoupled axial modal basis (ST) with vector normalization. The classification of buckling modes (G, D, L) provide in Table 1 is completed empirically, simply by visualizing the 2D (or 3D) buckling mode. That highly subjective process can be replaced by the quantitative results of Table 4. For example the 9th mode (Figure 5) when using visual identification only may credibly be identified as distortional, but *c*FSM model identification shows it to be dominated by global deformations with only a modest distortional contribution.

Table 4 Modal classification of higher modes of FSM solution

Higher modes	M_{cr}	Participation (%)			
		G	D	L	O
1	40.90	98.3	1.6	0.0	0.0
2	78.63	92.0	7.7	0.2	0.1
3	89.86	4.0	92.4	3.4	0.2
4	90.01	3.8	91.8	4.1	0.2
5	94.60	3.9	90.8	5.1	0.2
6	94.78	5.1	91.4	3.3	0.2
7	102.02	3.6	91.1	5.0	0.3
8	106.17	6.3	90.6	2.9	0.2
9	140.69	82.0	17.5	0.4	0.1
10	165.58	0.8	6.5	91.9	0.8
11	165.58	0.8	6.4	92.0	0.8
12	165.75	0.8	6.4	92.0	0.8

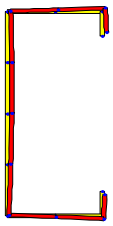

Figure 5 2D buckling shapes of 9th mode of FSM solution

Application with Direct Strength Method

Together with the Direct Strength Method (DSM), an FSM solution can prove to be a powerful tool in member design. FSM application for *S-S* boundary conditions, through the signature curve, has been well studied while the application for non-simply boundary condition is still a work in progress. However, basic ideas for non-simply supported boundary conditions are explored here for the intention of developing consensus.

Application for simply supported boundary condition

Traditionally, the two local minima and the descending branch at longer lengths in the signature curve provide the necessary information for the local, distortional, and global buckling loads for design [1, 14-15]. However, studies on SSMA sections [2] demonstrate that the signature curve often fails to uniquely identify the modes, as illustrated in Figure 6. Although *c*FSM can uniquely identify the buckling modes, two basic issues remain: (1) DSM's strength expressions are calibrated to the conventional FSM minima instead of pure mode solutions from *c*FSM (which are generally a few percent higher), and (2) *c*FSM can not handle rounded corners. To address these issues a two-step procedure has been adopted for determining the elastic buckling loads and moments. First, in step 1, the analyst develops a rounded corner model of the section and runs a conventional FSM model. If unique minima exist the analysis is complete. If not, step 2 is completed where: the analyst develops a straight-line model of the section and runs constrained FSM pure mode solutions for local and distortional, only for the purpose of determining the length (L_{cr}) at which the modes occur. The elastic buckling load (or moment) is determined from the conventional FSM with round corners, Step 1 model, at the L_{cr} identified in the Step 2 model. A shorthand for this solution method is FSM@*c*FSM-L_{cr}, which is detailed in [2], and illustrated for an 550S162-43 stud section under axial compression in Figure 6.

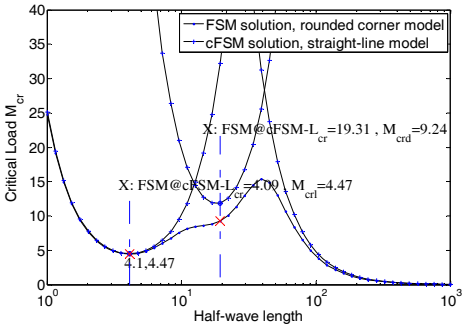

Figure 6 Signature curve augmented with pure mode *c*FSM solution and illustration of the proposed FSM@*c*FSM-L_{cr} solution

Application for general boundary conditions

Modal identification of an FSM solution for general boundary conditions is similar to FEM: at a physical length, L, the higher modes provide the most direct manner for finding the G, D, and L buckling load or moment. The first identified modes (in ascending buckling values) of G, D, and L can be used as the needed inputs in DSM. For example, critical moment of the 1st, 3rd, and 10th modes in Table 1 may be used as M_{cre}, M_{crd}, and $M_{cr\ell}$ respectively, and thus as the DSM inputs to predict the bending strength at L=108 in. Moreover, if *c*FSM is applicable (no round corners), modal identification can be performed by *c*FSM as shown in Table 4. Thus, the engineer can pick the first identified G, D, and L modes, or the modes having the highest individual G, D, and L participation (e.g., the 11th or 12th modes have more L participation than the 10th L mode though the difference in this case is negligible).

Modal decomposition in *c*FSM has the ability to decompose the deformation field into individual mode or combined modes of interest. Though the critical loads of pure modes in *c*FSM can not be used directly with DSM, the longitudinal terms contributing most to the pure modes can be determined and these terms then used in the conventional FSM solution to force the member to buckle in the desired local or distortional buckling mode. These buckling loads may then be used as DSM inputs to predict the ultimate strength in design. To illustrate consider again the 400S162-68 SSMA stud section at L=108 in. and *C*-*C* boundary conditions. The participations for the longitudinal terms in pure local and distortional buckling from *c*FSM are provided in Figure 7.

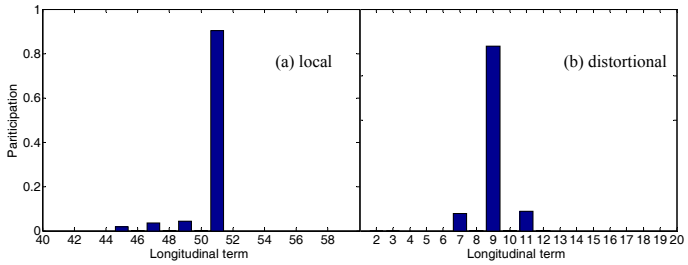

Figure 7 Participation of longitudinal terms of pure local and distortional buckling

Similar to the two step-procedure for simply supported boundary conditions, first, the pure local and distortional buckling modes are solved by *c*FSM (first two columns in Table 5) and the contributed longitudinal terms for each mode are identified (Figure 7). Then, second, the conventional FSM solutions are calculated by using the identified longitudinal terms for each mode (3rd and 4th columns in Table 5). The conventional FSM solution is successfully restrained

to the desired mode by the identified longitudinal terms, and the critical moments show excellent agreement with those by higher modes of the FSM solution (5th and 6th columns in Table 5). Hence, these $M_{cr\ell}$, M_{crd}, together with M_{cre} (critical global buckling moment) can be used as DSM inputs to predict the ultimate strength.

Table 5 Critical moment of pure and FSM solution with *c*FSM suggested longitudinal terms

	*c*FSM solution		FSM solution (1st mode)		FSM solution (higher modes)	
	Local	Dist.	Local	Dist.	Local	Dist.
M_{cr}(kips-in)	170.44	95.90	165.56	89.86	165.58	89.86
Mode shapes						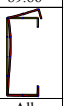
Longitudinal terms	45, 47, 49, 51	7, 9, 11	*c*FSM suggested (45, 47, 49, 51)	*c*FSM suggested (7, 9, 11)	All suggested	All suggested

Conclusion

The conventional finite strip method combined with the constrained finite strip method provides a powerful tool for exploring cross-section stability in cold-formed steel members. Extensions of the conventional and constrained finite strip method to general boundary conditions are important for their application to general purpose design. The elastic and geometric stiffness matrices are formulated based on new shape functions (series) that correspond to general boundary conditions. The constrained finite strip method for general boundary conditions is briefly described with a summary of the bases available. Examples are provided for conventional as well as constrained finite strip method solutions. The discussed algorithms of both conventional and constrained finite strip method are implemented in the open source stability analysis program: CUFSM. The strength of this new extension to general boundary conditions is demonstrated through the application with the direct strength method in member design.

Acknowledgements

This paper is based in part upon work supported by the U.S. National Science Foundation under Grant No. 0448707. Any opinions, findings, and conclusions or recommendations expressed in this material are those of the author(s) and do not necessarily reflect the views of the National Science Foundation. Discussion and collaboration with Sándor Ádány is greatly appreciated.

References

1. Schafer, B.W. and Ádány, S., *Buckling analysis of cold-formed steel members using CUFSM: Conventional and constrained finite strip methods.*, in *18th International Specialty Conference on Cold-Formed Steel Structures: Recent Research and Developments in Cold-Formed Steel Design and Construction*. 2006. p. 39-54.
2. Li, Z. and Schafer, B.W., *Application of the finite strip method in cold-formed steel member design.* Journal of Constructional Steel Research, 2010. 66(8-9): p. 971-980.
3. NAS, *2007 Edition of the North American Specification for the Design of Cold-Formed Steel Structural Members*. 2007, Washington, DC: American Iron and Steel Institute.
4. Li, Z. and Schafer, B.W.. *Finite Strip Stability Solutions for General Boundary Conditions and the Extension of the Constrained Finite Strip Method*. in Trends in Civil and Structural Engineering Computing. 2009. Stirlingshire, UK: Saxe-Coburg Publications.
5. Li, Z. and Schafer, B.W., *The constrained finite strip method for general end boundary conditions*, in Structural Stability Research Council - Proceedings of the 2010 Annual Stability Conference. 2010: Orlando, FL, USA. p. 573-591.
6. Bradford, M.A. and Azhari, M., *Buckling of plates with different end conditions using the finite strip method*. Computers & Structures, 1995. 56(1): p. 75-83.
7. SSMA, *Product Technical Information*, ICBO ER-4943P. 2001, Steel Stud Manufacture Association.
8. Schafer, B.W., Li, Z., and Moen, C.D., *Computational modeling of cold-formed steel*. Thin-Walled Structures, 2010. In Press, Corrected Proof.
9. Ádány, S. and Schafer, B.W., *Buckling mode decomposition of single-branched open cross-section members via finite strip method: Derivation*. Thin-Walled Structures, 2006. 44(5): p. 563-584.
10. Ádány, S. and Schafer, B.W., *Buckling mode decomposition of single-branched open cross-section members via finite strip method: Application and examples*. Thin-Walled Structures, 2006. 44(5): p. 585-600.
11. Ádány, S. and Schafer, B.W., *A full modal decomposition of thin-walled, single-branched open cross-section members via the constrained finite strip method*. Journal of Constructional Steel Research, 2008. 64(1): p. 12-29.
12. Silvestre, N. and Camotim, D., *First-order generalised beam theory for arbitrary orthotropic materials*. Thin-Walled Structures, 2002. 40(9): p. 755-789.
13. Silvestre, N. and Camotim, D., *Second-order generalised beam theory for arbitrary orthotropic materials*. Thin-Walled Structures, 2002. 40(9): p. 791-820.
14. Hancock, G.J., *LOCAL, DISTORTIONAL, AND LATERAL BUCKLING OF I-BEAMS*. ASCE J Struct Div, 1978. 104(11): p. 1787-1798.
15. AISI, *Direct Strength Method Design Guide*. 2006, Washington, DC.

Twentieth International Specialty Conference on Cold-Formed Steel Structures
St. Louis, Missouri, U.S.A., November 3 & 4, 2010

Evaluating the LRFD Resistance Factor for Cold-Formed Steel Compression Members

Karthik Ganesan[1], Cristopher D. Moen[2]

Abstract

This paper summarizes recent work to determine if the LRFD resistance factor for cold-formed steel compression members can be increased above its current value of ϕ_c=0.85. An experimental database of 675 concentrically loaded columns with plain and lipped C-sections, plain and lipped Z-sections, hat sections and angle sections, including members with holes was compiled. The predicted strength of each specimen was calculated with the AISI-S100-07 Main Specification and Direct Strength Method (DSM). Test-to-predicted strength statistics were employed with the first order second moment reliability approach in AISI-S100-07 Chapter F to calculate the resistance factors. The observed trends demonstrate that DSM is a more accurate strength predictor than the current Main Specification, especially for columns with partially effective cross sections. Serious consideration should be given to replacing the Main Specification with DSM, which would provide improved prediction accuracy and a viable rationale for increasing the resistance factor. The test-to-predicted strength ratios for columns with plain and lipped angle cross-sections exhibit a high coefficient of variation and become increasingly conservative with increasing global slenderness. Fundamental research on the mechanics of angle compression members is needed to improve existing design methods.

Introduction

The American Iron and Steel Institute (AISI) implemented the load and resistance factor (LRFD) design approach for cold-formed steel members in 1991 (AISI 1991), with the strength limit state for columns defined as:

$$P_u \leq \phi_c P_n \,. \qquad (1)$$

[1] Graduate Research Assistant, Virginia Tech, Blacksburg, VA, 24061, USA. (gkarthik@vt.edu)
[2] Assistant Professor, Virginia Tech, Blacksburg, VA, 24061, USA. (cmoen@vt.edu)

The required column strength (factored demand) is P_u, and the available strength (resistance) is the nominal capacity, P_n, multiplied by a resistance factor, ϕ_c. The resistance factor reduces nominal capacity based on the likelihood of deleterious variations in column geometry and material properties during fabrication (Nowak 2000). The resistance factor also compensates for bias and variability in a strength prediction approach, and when derived with formal structural reliability theory as in the case of the LRFD approach, can be tuned to produce designs with a uniform probability of failure (Hsiao et al. 1990).

The current AISI LRFD resistance factor of ϕ_c=0.85 was established in 1991, more than 20 years ago, based on a cold-formed steel column database of 264 specimens. Since then, major changes to the AISI Specification have been implemented, including modifications to the column curve predicting global capacity (AISI 1996), the incorporation of a distortional buckling limit state (AISI 2007), and the addition of the Direct Strength Method (AISI 2004; Schafer 2002), which considers cross-section connectivity in the capacity calculation. These changes have improved strength prediction accuracy, however corresponding gains in design efficiency could still be achieved by reevaluating the LRFD resistance factor.

This research takes a fresh look at the AISI LRFD resistance factor, exploring the viability of raising ϕ_c above 0.85, and presents resistance factors by cross-sectional slenderness (i.e., partially or fully effective), by ultimate limit state, and by cross-section type. The research is conducted with an expanded column experiment database containing 675 tests, including C-sections, Z- sections, hat sections and angle sections, as well as columns with and without holes. Resistance factors are calculated for both the AISI Main Specification and Direct Strength Method strength prediction approaches, and code revisions are recommended that have the potential to improve design efficiency and cost competitiveness of cold-formed steel columns.

LRFD resistance factor calculation

Resistance factors in this study are calculated with the first order second moment structural reliability approach described in AISI-S100-07 Chapter F (AISI 2007; Galambos 1998; Hsiao et al. 1990):

$$\phi = C_\phi \left(M_m F_m P_m\right) e^{-\beta_o \sqrt{V_M^2 + V_F^2 + C_P V_P{}^2 + V_Q^2}} \quad . \qquad (2)$$

A detailed derivation of Eq. (2) is provided in Ganesan (2010). The reliability index, β_o, has been established as 2.5 for LRFD cold-formed steel member

design in the United States and Mexico, which corresponds to a probability of failure of approximately 6 in 1000 columns. The coefficient of variation (COV) of the applied loading is assumed as V_Q=0.21 for a dead load to live load ratio of 5 to 1 and the LRFD calibration coefficient C_ϕ=1.52, see Ganesan (2010) for details.

Bias and variability in the predicted column capacity are accounted for with a material factor M (related to steel yield stress), a fabrication factor F (related to column dimensions), and a professional factor P (quantifies the accuracy of capacity predictions relative to tests). For cold-formed steel columns, the steel yield stress is typically higher than the minimum specified, and therefore the mean of the material factor is M_m=1.10 with a COV of V_M=0.10 (Hsiao et al. 1990). The column nominal dimensions are assumed to be unbiased, and therefore F_m=1.00 with a COV of V_F=0.05. The statistics for the professional factor, P_m and V_P, will be calculated with the column test database and prediction methods introduced in the following sections.

Column test database

A cold-formed steel column test database was assembled to facilitate the calculation of the professional factor statistics P_m and V_m in Eq. (2). The database, summarized in Table 1, contains the original 264 columns considered in the 1991, excluding eccentrically loaded columns tests (Loh and Peköz 1985), and including concentrically loaded column data from several experimental programs conducted over the past 30 years, for a total of 675 column tests. Plain and lipped C-sections (with and without holes), Z-sections, plain and lipped angle sections, and hat sections are represented in the database. (Dimension notation for each cross-section type is provided in Figure 1.) Built-up I-sections (DeWolf et al. 1974; Weng and Pekoz 1990) and box sections (DeWolf et al. 1974) have not been considered. Tested boundary condition details and column dimensions for all experimental programs considered is provided in Ganesan (2010).

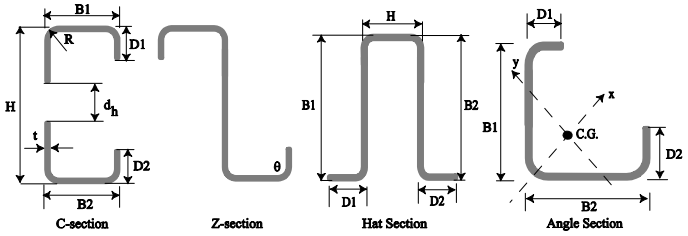

Figure 1 Cross-section dimension notation

Table 1 Cold-formed steel column test database

Reference	Section type	Holes	*n*	B/t		H/t		D/t		D/B		d_h/H		λ_c	
				min	max	min	max	min	max	min	max	min	max	min	max
Thomasson 1978	Lipped C		13	69	159	207	472	14.0	32.4	0.2	0.2	---	---	0.9	1.2
Loughlan 1979	Lipped C		33	30	80	91	226	10.9	32.8	0.4	0.4	---	---	0.6	1.1
Dat 1980	Lipped C		43	19	23	33	41	8.3	10.1	0.4	0.4	---	---	0.4	1.9
Desmond et al. 1981	Lipped C		7	26	30	37	39	2.2	8.9	0.1	0.3	---	---	0.1	0.2
Desmond et al. 1981	Hat		11	51	51	42	42	7.5	29.9	0.2	0.6	---	---	0.2	0.4
Ortiz-Colberg 1981	Lipped C	✓	32	21	33	46	72	6.7	10.4	0.3	0.3	0.1	0.5	0.2	1.4
Ortiz-Colberg 1981	Lipped C		11	21	33	46	72	6.6	10.4	0.3	0.3	---	---	0.2	1.4
Mulligan 1983	Lipped C		37	33	100	64	355	7.4	21.3	0.2	0.2	---	---	0.1	1.1
Wilhoite et al. 1984	Plain Angles		7	23	23	---	---	---	---	---	---	---	---	1.9	2.0
Sivakumaran 1987	Lipped C	✓	42	26	32	58	118	7.9	9.8	0.3	0.3	0.2	0.6	0.2	0.2
Sivakumaran 1987	Lipped C		6	26	32	58	118	7.9	9.8	0.3	0.3	---	---	0.2	0.2
Polyzois et al. 1993	Plain Z		13	30	51	77	137	---	---	---	---	---	---	0.2	0.5
Polyzois et al. 1993	Lipped Z		72	35	56	76	137	2.4	36.2	0.1	0.7	---	---	0.1	0.4
Miller and Peköz 1994	Lipped C		43	17	40	43	175	5.2	9.0	0.2	0.3	---	---	0.2	2.8
Miller and Peköz 1994	Lipped C	✓	37	19	40	47	173	5.7	9.5	0.2	0.3	0.4	0.8	0.1	3.0
Moldovan 1994	Plain C		35	20	35	20	53	---	---	---	---	---	---	0.1	1.2
Moldovan 1994	Lipped C		29	19	46	32	65	6.3	13.7	0.2	0.4	---	---	0.1	1.0
Abdel-Rahman and Sivakumaran 1998	Lipped C	✓	8	22	33	80	108	6.9	10.3	0.3	0.3	0.3	0.4	0.1	0.2
Young and Rasmussen 1998a	Lipped C		12	25	34	66	66	8.0	8.6	0.2	0.3	---	---	0.2	1.7
Young and Rasmussen 1998b	Plain C		14	25	34	64	67	---	---	---	---	---	---	0.2	2.0
Popovic et al. 1999	Plain Angles		12	11	22	---	---	---	---	---	---	---	---	0.9	1.8
Pu et al. 1999	Lipped C	✓	30	43	65	82	122	13.3	20.0	0.3	0.3	0.2	0.4	0.1	0.1
Pu et al. 1999	Lipped C		6	43	65	82	122	13.3	20.0	0.3	0.3	---	---	0.1	0.1
Shanmugam and Dhanalakshmi 2001	Plain Angles		3	20	63	---	---	---	---	---	---	---	---	1.6	4.9
Young and Hancock 2003	Lipped C		42	21	68	41	68	4.7	7.4	0.1	0.2	---	---	0.7	0.9
Young 2004	Plain Angles		24	38	62	---	---	---	---	---	---	---	---	3.0	5.1
Chodraui et al. 2006	Plain Angles		4	25	25	---	---	---	---	---	---	---	---	1.7	2.0
Young and Chen 2008	Lipped Angles		25	44	84	---	---	9.1	17.4	0.2	0.2	---	---	0.4	4.2
Moen and Schafer 2008	Lipped C		12	36	43	92	139	7.8	11.1	0.2	0.3	---	---	0.3	0.7
Moen and Schafer 2008	Lipped C	✓	12	37	42	91	146	8.3	12.2	0.2	0.3	0.2	0.4	0.3	0.8

Strength prediction methods

AISI Main Specification

Column capacity is predicted in the AISI Main Specification (AISI 2007) as the minimum capacity corresponding to three ultimate limit states - global buckling, local-global buckling interaction, and distortional buckling:

$$P_n = min(A_g F_n , A_e F_n , P_{nd}), \quad (3)$$

where A_g is the column gross cross-sectional area, A_e is the column effective cross-sectional area including the local buckling influence, element by element, with the effective width method (Peköz 1987; Von Karman et al. 1932), F_n is the global buckling column strength (stress), and P_{nd} is the distortional buckling column capacity. The original 1991 LRFD development did not consider distortional buckling, however ϕ_c=0.85 was demonstrated to be viable and conservative resistance factor for this limit state (Schafer 2000).

The design expressions for global column strength, F_n, in 1991 were consistent

with the American Institute of Steel Construction (AISC) column curve at that time (AISC 1986):

$$F_e > F_y/2, \quad F_n = \left(1 - F_y/4F_e\right)$$
$$F_e \le F_y/2, \quad F_n = F_e. \qquad (4)$$

The critical elastic global buckling stress, F_e, is the minimum of the critical elastic flexural, torsional, or flexural-torsional column buckling stress and F_y is the steel yield stress. The LRFD resistance factor of ϕ_c=0.85 was established based on Eq. (3).

The global buckling column curve was modified in the 1996 AISI Specification (AISI 1996) to its present form based on research by Peköz (1992) which coincided with updates to the AISC LRFD Specification (AISC 1993):

$$\lambda_c \le 1.5, \quad F_n = \left(0.658^{\lambda_c^2}\right)F_y,$$
$$\lambda_c > 1.5, \quad F_n = \left(0.877F_y\right)/\lambda_c^{\,2}, \qquad (5)$$

where $\lambda_c=(F_y/F_e)^{0.5}$ is the column global slenderness. A comparison of Eq. (4) and Eq. (5) in Figure 1 demonstrates that for the same λ_c, the 1996 AISI column curve (also the current AISI-S100-07 column curve) predicts a lower capacity than the 1991 AISI column curve, with a maximum difference of 10%.

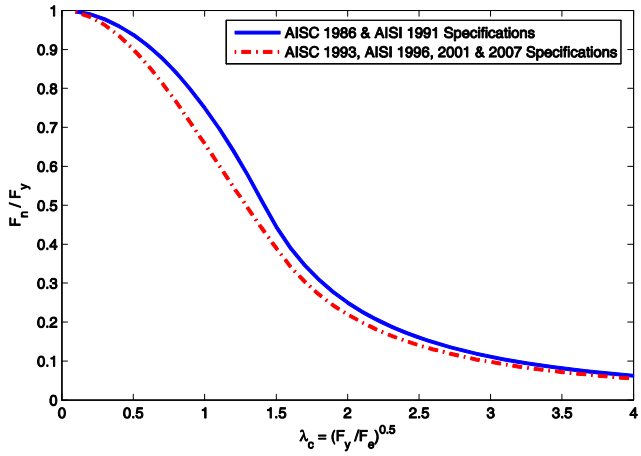

Figure 2 History of AISI and AISC global buckling column curves

AISI Direct Strength Method

Introduced in 2004, the AISI Direct Strength Method (DSM) represents an important advance in cold-formed steel design as it employs elastic buckling

behavior of a general cross-section including cross-section connectivity to predict column strength. The column capacity is calculated in a similar fashion to the AISI Main Specification, considering the minimum of three ultimate limit states – global buckling, local-global buckling interaction, and distortional buckling:

$$P_n = min\left(P_{ne}, P_{n\ell}, P_{nd}\right), \tag{6}$$

where P_{ne}, $P_{n\ell}$, P_{nd} are the nominal capacities for global, local and distortional buckling failures respectively. The global buckling capacity (P_{ne}) and distortional buckling capacity (P_{nd}) are equivalent for the Main Specification and DSM, however the local buckling capacity, $P_{n\ell}$, is calculated including the effects of cross-section connectivity instead of element by element with the effective width method.

AISI capacity prediction for angle columns

AISI-S100-07 states that the axial capacity of partially effective concentrically loaded angle columns should be calculated including a demand moment of $\phi_c P_n L/1000$ from an initial column out-of-straightness imperfection (Peköz 1987; Popovic et al. 1999) applied about the *y*-axis shown in Figure 1. The angle column capacity, P_n, is calculated with an interaction equation (AISI 2007):

$$\frac{\phi_c P_n}{\phi_c P_{no}} + \frac{\phi_c P_n L/1000}{\phi_b M_{ny}} \le 1.0, \tag{7}$$

where P_{no} is the nominal axial capacity and M_{ny} is the flexural strength of the gross cross-section about the *y*-axis (see Figure 1).

Resistance factor results

The tested capacities, P_{test}, from the experimental programs in Table 1 (675 columns in total) and the predicted capacities, P_n, from the AISI Main Specification and Direct Strength Method approaches presented in the previous section, define the professional factor, $P=P_{test}/P_n$. The predicted column specimen strengths (P_n) for the 675 column specimens were computed using custom MATLAB code (Mathworks 2009) validated with the AISI Design Manual (AISI 2008). The mean and COV of the professional factor, P_m and V_P, are input into Eq. (2) to calculate the LRFD resistance factor, ϕ_c. The resistance factor is presented in the following sections considering different groupings of test data: all data, columns with and without holes, columns by cross-section type, columns with partially or fully effective cross-sections, and by predicted

ultimate limit state. Columns inside and outside of the code dimensional limits described in Table 2 for the Main Specification and in Table 3 for DSM are evaluated. The different groupings facilitate comparisons between the Main Specification and DSM and are used to identify trends in prediction accuracy that can be leveraged with future code revisions to improve design efficiency.

Table 2 Main Specification dimensional limits

Cross-section element	Column dimension	Limiting range
Stiffened compression element with longitudinal edge connected to web/flange	Flat-width-to-thickness (w/t)	$w/t \leq 60$
Stiffened compression element with both longitudinal edges connected stiffened elements	Flat-width-to-thickness (w/t)	$w/t \leq 500$
Unstiffened compression element	Flat-width-to-thickness (w/t)	$w/t \leq 60$
Uniformly compressed stiffened element with circular holes	Depth of hole-to-flat width (d_h/w)	$0.5 \geq d_h/w \geq 0$
	Flat-width-to-thickness (w/t)	$w/t \leq 60$
Uniformly compressed stiffened element with non circular holes	Center-to-center hole spacing (s)	$s \geq 24$ in.
	Clear distance from hole at ends (s_{end})	$s_{end} \geq 10$ in.
	Depth of the hole (d_h)	$d_h \leq 2.5$ in.
	Length of the hole (L_h)	$L_h \leq 4.5$ in.
	Depth of hole-to-out-to-out-width(d_h/w_o)	$d_h/w_o \leq 0.5$
Uniformly compressed stiffened element with simple lip edge stiffener	Lip Angle (θ)	$140^o \geq \theta \geq 40^o$

Table 3 DSM prequalified dimensional limits

Cross-section dimension	Lipped C-section	Lipped Z-section	Hat section
Web height-to-thickness (H/t)	H/t < 472	H/t < 137	H/t < 50
Flange width-to-thickness (B/t)	B/t < 159	B/t < 56	B/t < 20
Lip width-to-thickness (D/t)	4 < D/t < 33	0 < D/t < 36	4 < D/t < 6
Web height-to-flange width (H/B)	0.7 < H/B < 5.0	1.5 < H/B < 2.7	1.0 < H/B < 1.2
Lip width-to-flange width (D/B)	0.05 < D/B< 0.41	0.00 < D/B< 0.73	D/B = 0.13
Lip Angle (θ)	θ = 90°	θ = 50°	---

Resistance factors considering all columns in database

The test-to-predicted statistics and resistance factors considering all column data, except angle columns, are summarized in Table 4. (Note that the resistance factor for angle columns is presented in a later section.) The resistance factor calculated considering all data is ϕ_c=0.85 for the Main Specification and ϕ_c=0.87 for DSM, confirming the viability of ϕ_c=0.85 currently established in AISI-S100-07. (Note that the DSM resistance factor does not include specimens with holes as there are currently no DSM provisions to predict the capacity of columns with holes). Both Main Specification and DSM resistance factors are unaffected by column specimens outside their respective dimensional limits (see Table 2 and Table 3). This insensitivity is at least partially attributed to the small number of column specimens exceeding the dimensional limits in this study. An examination of broader applicability for the prediction methods is warranted based on the results though, especially DSM, which currently specifies ϕ_c=0.80 for columns outside prequalified limits.

Table 4 Resistance factors for all columns in the database (except angles)

Prediction method	Classification	Test-to-predicted statistics Mean (P_m)	SD	COV (V_p)	ϕ_c	n
Main Spec	All columns †	1.06	0.18	0.17	0.85	448
	All columns	1.06	0.18	0.17	0.85	600
DSM	All columns*	1.05	0.15	0.14	0.87	390
	All columns	1.04	0.15	0.15	0.87	439

† Within Main Spec dimensional limits, refer toTable 2

* Within DSM prequalified limits, refer to Table 3

Resistance factors for columns with and without holes

Resistance factors for columns with and without holes are provided in Table 5 for the Main Specification. Strength predictions for columns with holes are conservative considering specimens inside and outside AISI dimensional limits (P_m=1.17 and P_m=1.16 respectively, see Table 5). The conservative predictions result in resistance factors that are near or above unity. The Main Specification resistance factor for columns without holes provided in Table 5 facilitates a meaningful comparison to the DSM resistance factor (also for columns without holes) in Table 3. For the Main Specification, ϕ_c=0.83, and for DSM, ϕ_c=0.87. The higher DSM resistance factor results from a lower test-to-predicted COV, demonstrating the improved prediction accuracy of DSM achieved in the local buckling analysis including interaction between connected cross-section elements. (Remember, distortional buckling and global buckling prediction equations are the same for both approaches).

Table 5 Main Specification resistance factors, columns without and with holes

Classification	Test-to-predicted statistics Mean (P_m)	SD	COV (V_p)	ϕ_c	n
Columns without holes†	1.04	0.18	0.17	0.83	397
Columns without holes	1.03	0.18	0.18	0.82	439
Columns with holes †	1.17	0.14	0.12	1.01	51
Columns with holes	1.16	0.15	0.13	0.98	161

† Within Main Spec dimensional limits, refer to Table 2

Resistance factors by cross-section type

Resistance factors calculated per cross-section type for both the Main Specification and DSM are provided in Table 6. The COV increases with the number of specimens for each cross-section, resulting from the statistical variability created by considering multiple experimental programs within each cross-section group. This sensitivity to the number of experimental programs

considered makes it difficult to draw definitive conclusions from the cross-section data representation. For example, the hat section column tests were all performed by one researcher (Desmond et al. 1981) resulting in a conservative test-to-predicted mean (P_m=1.34 for the Main Specification), while the lipped Z-section tests, also performed by one researcher (Polyzois et al. 1993), results in an unconservative test-to-predicted mean (P_m=0.88 for the Main Specification). For both cross-sections groups, the COV is low because there is no statistical influence across experimental programs. For cross-sections with a larger number of tests, for example the lipped C-section, P_m is near unity because experimental bias is averaged across multiple test programs. The results in Table 6 demonstrate that without large quantities of data, it is difficult to specify meaningful resistance factors per cross-section type. It can be concluded that DSM is a more accurate strength predictor of lipped C-section columns than the Main Specification (compare ϕ_c=0.90 versus ϕ_c=0.83 in Table 6). The improved DSM prediction accuracy can be observed in the tighter band of test-to-predicted data around P_{test}/P_n=1 plotted for each cross-section (compare Figure 3a to Figure 3b).

Table 6 Resistance factors by cross-section type

Prediction method	Classification	Test-to-predicted statistics			ϕ_c	n
		Mean (P_m)	SD	COV (V_p)		
Main Spec	Plain C	1.10	0.13	0.12	0.95	49
	Lipped C†	1.06	0.18	0.17	0.85	252
	Lipped C	1.04	0.18	0.17	0.83	294
	Plain Z	1.12	0.07	0.06	1.02	13
	Lipped Z	0.88	0.10	0.11	0.76	72
	Hat Sections	1.34	0.08	0.06	1.21	11
DSM	Plain C	1.03	0.13	0.13	0.88	49
	Lipped C*	1.07	0.15	0.14	0.90	245
	Lipped C	1.06	0.16	0.15	0.88	294
	Plain Z	1.12	0.07	0.06	1.02	13
	Lipped Z	0.94	0.11	0.11	0.81	72
	Hat Sections	1.24	0.05	0.04	1.13	11

† Within Main Spec dimensional limits, refer to Table 2

* Within DSM prequalified limits, refer to Table 3

Resistance factors considering partially and fully effective sections

Resistance factors for columns with partially effective cross-sections (A_e<A_g or $P_{n\ell}$<P_{ne}) and fully effective cross sections (A_e=A_g or $P_{n\ell}$=P_{ne}), excluding columns with holes, are presented in Table 7. The DSM resistance factor is 10% higher than the Main Specification for partially effective cross-sections (compare

ϕ_c=0.89 to ϕ_c=0.81 in Table 7), emphasizing that DSM provides improved strength prediction accuracy over a wide range of cold-formed steel columns sensitive to local buckling. The DSM and Main Specification resistance factors for fully effective sections are consistent (compare ϕ_c=0.83 to ϕ_c=0.81 in Table 7) because the same prediction equations are used in both approaches for global and distortional buckling.

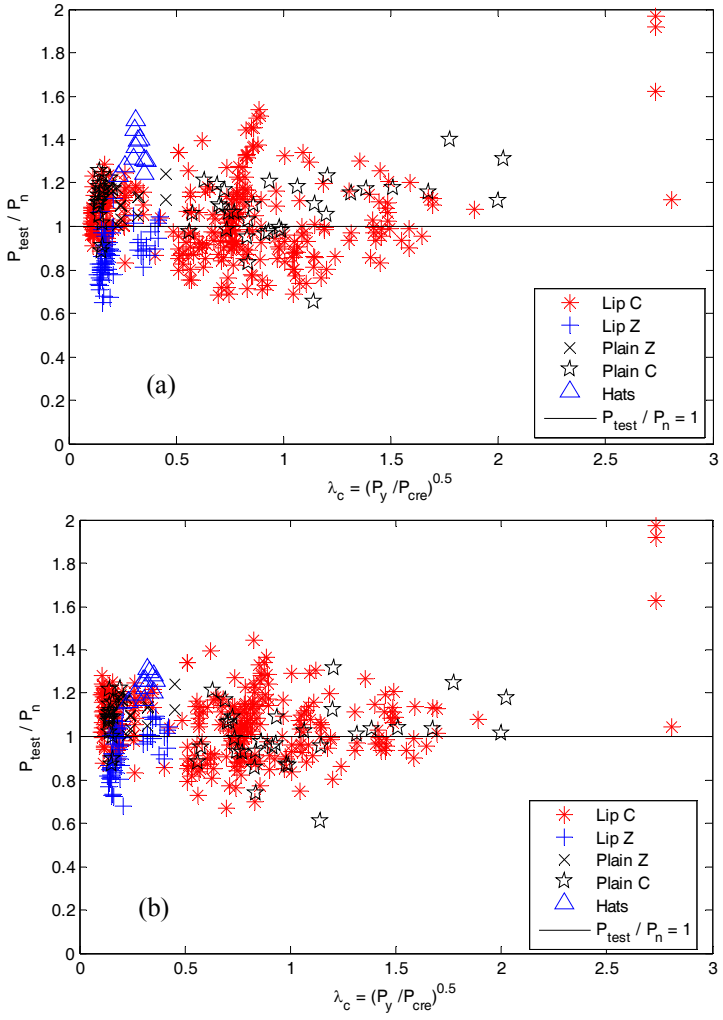

Figure 3 Test-to-predicted ratio as a function of global slenderness for (a) the AISI Main Specification and (b) the AISI Direct Strength Method. Columns with holes are not shown.

Table 7 Resistance factors for partially and fully effective columns

Prediction method	Classification	Test-to-predicted statistics Mean (P_m)	SD	COV (V_p)	ϕ_c	n
Main Spec	Fully effective †	1.04	0.20	0.19	0.81	104
	Fully effective	1.04	0.20	0.19	0.81	104
	Partially effective†	1.00	0.17	0.17	0.81	293
	Partially effective	1.02	0.18	0.17	0.82	335
DSM	Fully effective *	1.07	0.21	0.19	0.83	65
	Fully effective	1.04	0.20	0.19	0.81	109
	Partially effective*	1.04	0.14	0.13	0.89	325
	Partially effective	1.05	0.14	0.13	0.89	330

† Within Main Spec dimensional limits, refer to Table 2

* Within DSM prequalified limits, refer to Table 3

Fully effective: $A_e=A_g$ or $P_{n\ell}=P_{ne}$ Partially effective: $A_e<A_g$ or $P_{n\ell}<P_{ne}$

Resistance factors by limit state

Both the AISI Main Specification and DSM relate column capacity to three limit states: global buckling or yielding of the cross-section, local-global buckling interaction, and distortional buckling as described in Eq. (3) and Eq. (6). Grouping the column data by these limit states, and excluding columns with holes to provide a fair comparison between the Main Specification and DSM, results in the resistance factors provided in Table 8.

Table 8 Resistance factors by ultimate limit state

Prediction method	Limit state	Test-to-predicted statistics Mean (P_m)	SD	COV (V_p)	ϕ_c	n
Main Spec	Global buckling or yielding †	1.04	0.21	0.20	0.81	92
	Global buckling or yielding	1.04	0.21	0.20	0.81	92
	Local-global buckling interaction †	0.98	0.17	0.17	0.78	235
	Local-global buckling interaction	1.00	0.19	0.19	0.79	265
	Distortional buckling †	1.09	0.11	0.10	0.96	70
	Distortional buckling	1.09	0.10	0.10	0.96	82
DSM	Global buckling or yielding*	1.06	0.22	0.20	0.81	59
	Global buckling or yielding	1.03	0.20	0.19	0.80	103
	Local-global buckling interaction *	1.03	0.15	0.14	0.87	235
	Local-global buckling interaction	1.03	0.15	0.14	0.87	236
	Distortional buckling*	1.07	0.10	0.09	0.94	96
	Distortional buckling	1.08	0.10	0.09	0.95	100

† Within Main Spec dimensional limits, refer to Table 2

* Within DSM prequalified limits, refer to Table 3

The most accurate strength predictor is distortional buckling, with ϕ_c=0.96 for the Main Specification and ϕ_c=0.94 for DSM. Local-global buckling interaction

is predicted much more accurately by DSM (compare ϕ_c=0.87 versus ϕ_c=0.78 in Table 8) which is consistent with the results in Table 7 for columns with partially effective cross-sections. The global buckling resistance factor is the same for DSM and the Main Specification (ϕ_c=0.81). An increase in the resistance factor for the distortional buckling limit state to ϕ_c=0.95 is a valid consideration for a future code revision, as is the replacement of the current Main Specification approach with DSM, which could lead to better prediction accuracy and a higher resistance factor.

Resistance factors for angle columns

Angle columns have been treated separately from the other columns in this study because of their highly variable test-to-predicted statistics summarized in Table 9. Figure 4 demonstrates that the Main Specification and DSM strength predictions become overly conservative as global slenderness, λ_c, increases for both plain angles and lipped angles. The additional PL/1000 moment required by AISI-S100-07 for partially effective angle cross-sections (Popovic et al. 1999) causes the prediction to be even more conservative.

Table 9 LRFD resistance factors for angle columns

		Test-to-predicted statistics				
Prediction method	Classification	Mean (P_m)	SD	COV (V_p)	ϕ_c	n
Main Spec	Plain Angles	3.13	2.42	0.77	0.69	50
	Lipped Angles	2.00	0.91	0.46	0.93	25
	All Angles	2.76	2.11	0.76	0.62	75
	Angles with $\lambda c \leq 2$	1.35	0.36	0.26	0.93	38
DSM	Plain Angles	3.02	2.09	0.69	0.81	50
	Lipped Angles	1.97	0.97	0.49	0.84	25
	All Angles	2.67	1.86	0.69	0.71	75

The low resistance factors indicate that fundamental research on angle columns is needed, with a concerted effort to identify the source of post-buckling capacity currently neglected by the global buckling column curve for slender angle columns. Prediction accuracy improves when $\lambda_c \leq 2$ (ϕ_c=0.93, see Table 9), potentially supporting a higher resistance factor for stockier angle columns, however even for this case, the high test-to-predicted variability (V_p=0.26) is shrouded by conservative predictions (P_m=1.35).

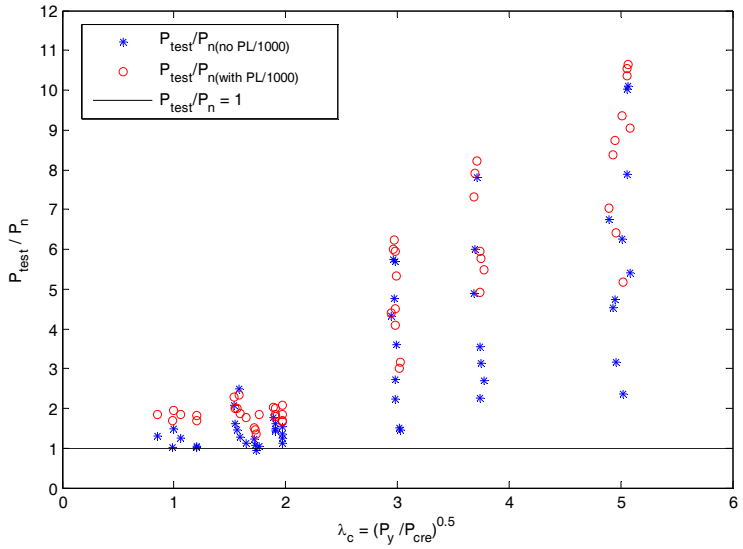

Figure 4 Comparison of angle column predicted strengths with and without PL/1000

Conclusions

LRFD resistance factors for cold-formed steel columns were calculated with a first order second moment reliability approach to identify potential AISI code modifications that could improve design efficiency and cost competitiveness. A test database of 675 cold-formed steel columns was assembled, and test-to-predicted statistics were obtained for the AISI Main Specification and Direct Strength Method. Different groups of test-to-predicted data were considered to evaluate trends in the resistance factors based on prediction method, columns with and without holes, columns with partially or fully effective cross-sections, and columns failing in global buckling, local-global buckling interaction, or distortional buckling.

The AISI Direct Strength Method is a more accurate predictor of local buckling capacity, and a replacement of the current Main Specification with DSM should be seriously considered, as well as an expansion of the DSM prequalified dimensional limits. Distortional buckling is the most accurately predicted strength limit state, and consideration of an increased resistance factor to ϕ_c=0.95 is warranted. Main Specification and DSM capacity predictions for angles columns were found to be overly conservative and highly variable relative to tested values. Research is needed to identify the source of angle column post-buckling strength.

References

Abdel-Rahman, N., and Sivakumaran, K. S. (1998). "Effective design width for perforated cold formed steel compression members." *Canadian Journal of Civil Engineering*, 25, 315-330.

AISC. (1986). *Load and resistance factor design specification for structural steel buildings.*, Chicago, IL.

AISC. (1993). "Load and Resistance Factor Design Specification for Structural Steel Buildings." American Institute of Steel Construction, Chicago, IL.

AISI. (1986). "Cold-Formed Steel Design Manual." American Iron and Steel Institute, Washington, DC.

AISI. (1991). "LRFD Cold-Formed Steel Design Manual." American Iron and Steel Institute, Washington, DC.

AISI. (1996). "Cold-Formed Steel Design Manual." American Iron and Steel Institute, Washington, DC.

AISI. (2001). *North American Specification for the Design of Cold-Formed Steel Structural Members and Commentary*, American Iron and Steel Institute, Washington, D.C.

AISI. (2004). *Supplement to the North American Specification for the Design of Cold-Formed Steel Structural Members, Appendix 1*, American Iron and Steel Institute, Washington, D.C.

AISI. (2007). *AISI-S100-07, North American Specification for the Design of Cold-Formed Steel Structural Members*, American Iron and Steel Institute, Washington, D.C.

AISI. (2008). "Cold-Formed Steel Design Manual." American Iron and Steel Institute, Wash., DC.

Chodraui, G. M. B., Shifferaw, Y., Malite, M., and Schafer, B. W. "Cold-formed steel angles under axial compression." *Eighteenth International Specialty Conference on Cold-Formed Steel Structures: Recent Research and Developments in Cold-Formed Steel Design and Construction*, Orlando, FL, United States, 285-300.Dat, D. T. (1980). "The Strength of Cold-Formed Steel Columns." Cornell University Department of Structural Engineering Report No. 80-4, Ithaca, NY.

Desmond, T. P., Pekoz, T., and Winter, G. (1981). "EDGE STIFFENERS FOR THIN-WALLED MEMBERS." *ASCE Journal of Structural Division*, 107(2), 329-353.

DeWolf, J. T., Peköz, T., and Winter, T. (1974). "LOCAL AND OVERALL BUCKLING OF COLD-FORMED MEMBERS." *ASCE Journal of Structural Division* , 100(10), 2017-2036.

Galambos, T. (1998). *Guide to Stability Design Criteria for Metal Structures, 5th Edition*, John Wiley & Sons, New York, NY.

Ganesan, K. (2010). "Resistance Factor for Cold-Formed Steel Compression Members," M.S. Thesis, Virginia Tech, Blacksburg.

Hsiao, L.-E., Yu, W.-W., and Galambos, T. V. (1990). "AISI LRFD method for cold-formed steel structural members." *ASCE Journal of Structural Engineering New York, N.Y.*, 116(2), 500-517.

Loh, T. S., and Peköz, T. (1985). "Combined Axial Load and Bending in Cold-Formed Steel Members." Cornell University Department of Structural Engineering Report, Ithaca, NY.

Loughlan, J. (1979). "Mode Interaction in Lipped Channel Columns under Concentric or Eccentric Loading," Ph.D. Thesis, University of Strathclyde, Glasgow.

Mathworks. (2009). "Matlab 7.8.0 (R2009a)." Mathworks, Inc., www.mathworks.com.

Miller, T. H., and Peköz, T. (1994). "Unstiffened strip approach for perforated wall studs." *ASCE Journal of Structural Engineering*, 120(2), 410-421.

Moen, C. D., and Schafer, B. W. (2008). "Experiments on cold-formed steel columns with holes." *Thin-Walled Structures*, 46, 1164-1182.

Moldovan, A. (1994). "Compression tests on cold-formed steel columns with monosymmetrical section." *Thin-Walled Structures*, 20(1-4 pt 2), 241-252.

Mulligan, G. P. (1983). "The Influence of Local Buckling on the Structural Behavior of Singly-Symmetric Cold- Formed Steel Columns," Ph.D. Thesis, Cornell University, Ithaca, NY.

Nowak, A. S., Collins, Kevin R. (2000). *Reliability of Structures*, McGraw Hill, NY.

Ortiz-Colberg, R. A. (1981). "The Load Carrying Capacity of Perforated Cold-Formed Steel Columns," M.S. Thesis, Cornell University, Ithaca, NY.

Peköz, T. B. (1987). "Development of a Unified Approach to the Design of Cold-Formed Steel Members." American Iron and Steel Institute, Washington, D.C.

Peköz, T., and Sümer Ö. (1992). "Design provisions for cold-formed steel columns and beam columns." American Iron and Steel Institute, Washington, DC.

Polyzois, D., and Charnvarnichborikarn, P. (1993). "Web-flange interaction in cold-formed steel z-section columns." *Journal of Structural Engineering*, 119(9), 2607-2628.

Popovic, D., Hancock, G. J., and Rasmussen, K. J. R. (1999). "Axial compression tests on cold-formed angles." *ASCE Journal of Structural Engineering*, 125(5), 515-523.

Pu, Y., Godley, M. H. R., Beale, R. G., and Lau, H. H. (1999). "Prediction of ultimate capacity of perforated lipped channels." *ASCE Journal of Structural Engineering*, 125(5), 510-514.

Schafer, B. W. (2000). "Distortional buckling of cold-formed steel columns." American Iron and Steel Institute, Washington, D.C.

Schafer, B. W. (2002). "Local, distortional, and Euler buckling of thin-walled columns." *ASCE Journal of Structural Engineering*, 128(3), 289-299.

Schafer, B. W., and Ádány, S. (2006). "Buckling analysis of cold-formed steel members using CUFSM: conventional and constrained finite strip methods." *Eighteenth International Specialty Conference on Cold-Formed Steel Structures*, Orlando, FL.

Shanmugam, N. E., and Dhanalakshmi, M. (2001). "Design for openings in cold-formed steel channel stub columns." *Thin-Walled Structures*, 39, 961-981.

Sivakumaran, K. S. (1987). "Load capacity of uniformly compressed cold-formed steel section with punched web." *Canadian Journal of Civil Engineering*, 14, 550-558.

Thomasson, P. O. (1978). "Thin-Walled C-Shaped Panels in Axial Compression." Swedish Council for Building Research, Report: ISBN-91-540-2820-5 Sweden.

Weng, C. C., and Pekoz, T. (1990). "Compression tests of cold-formed steel columns." *ASCE Journal of Structural Engineering*, 116(5), 1230-1246.

Young, B. (2004). "Tests and Design of Fixed-Ended Cold-Formed Steel Plain Angle Columns." *ASCE Journal of Structural Engineering*, 130(12), 1931-1940.

Young, B., and Chen, J. (2008). "Column tests of cold-formed steel non-symmetric lipped angle sections." *Journal of Constructional Steel Research*, 64(7-8), 808-815.

Young, B., and Hancock, G. J. (2003). "Compression tests of channels with inclined simple edge stiffeners." *Journal of Structural Engineering*, 129(10), 1403-1411.

Young, B., and Rasmussen, K. J. R. (1998a). "Design of lipped channel columns." *Journal of structural engineering New York, N.Y.*, 124(2), 140-148.

Young, B., and Rasmussen, K. J. R. (1998b). "Tests of fixed-ended plain channel columns." *ASCE Journal of Structural Engineering*, 124(2), 131-139.

Von Karman, T., Sechler, E. F., and Donnell, L. H. (1932). "Strength of thin plates in compression." *American Society of Mechanical Engineers -- Transactions -- Applied Mechanics*, 54(2), 53-56.

Twentieth International Specialty Conference on Cold-Formed Steel Structures
St. Louis, Missouri, U.S.A., November 3 & 4, 2010

Experimental Investigation of Optimized Cold-Formed Steel Compression Members

D.J. Klingshirn[1], E.A. Sumner[2], and N.A. Rahman[3]

Abstract

In the past, standard C-shaped metal studs have been the only option for designers and contractors when selecting a cross section for load bearing compression members. The sigma shaped section has recently emerged as an alternative to the C-section. The sigma shaped section is very similar to the C-shape, with the exception of having an intermediate web return and complex stiffeners. The experimental results of concentric axial compression tests of fifty-eight sigma shaped members are reported. Specimens were tested at various lengths to force global, distortional, and local buckling failure modes. Additionally, the test program contained members with and without web holes. Comparisons of experimental results with the American Iron and Steel Institute (AISI) design methods, Effective Width Method (EWM) and Direct Strength Method (DSM), are discussed.

Introduction

Over the years, extensive research on cold-formed steel (CFS) has proven that the slender nature of these members makes them susceptible to several failure major modes: overall buckling at long unbraced lengths, distortional buckling at medium to long unbraced lengths, and local buckling, which can occur over a wide range of unbraced length. Local buckling has been widely observed and, in many cases, controls the design strength of a CFS compression member. Often, there is interaction between several buckling modes. The complex behavior of these members can induce significant variability in desired (and observed) behavior.

The sigma shaped CFS member has recently been introduced to the US construction market as a compression member. This shape has typically been used in Europe, mainly as a roof purlin. Other research programs [1, 2] have evaluated some aspect of the sigma shape in compression, but this study [3] is the first comprehensive study of sigma shaped compression

[1] EIT, Civil Engineer, NAVFAC Pacific, Honolulu, HI
[2] Ph.D., P.E., Assistant Professor, North Carolina State University, Raleigh, NC
[3] Ph.D., P.E., Research & Development, The Steel Network, Durham, NC

members that are known to the authors. Utilizing this optimized shape as a compression member can provide significant strength advantages when compared to the conventional C-section. The intermediate web return serves to decrease the web slenderness, thereby increasing its resistance to local bucking. Additionally, recent research [4-6] has shown that the complex stiffeners attached to the flange can boost the compression and flexural strengths of the member.

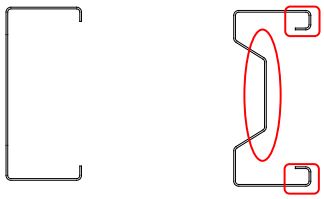

a. b.

Figure 1. a. C-section and b. sigma section

The results reported in this paper are part of a research program to add the sigma shape to the pre-qualified column set of the DSM design specification. These results are only for the sigma shape described in this paper; additional testing was undertaken with conventional C-sections. Full details are contained in [3]. The specimens follow a labeling pattern similar to the SSMA convention:

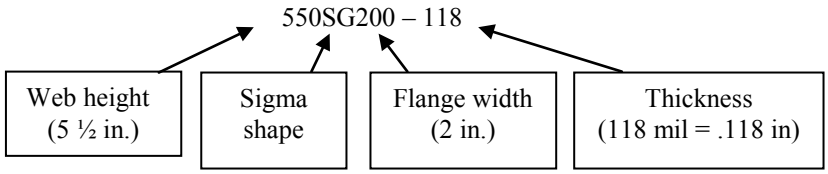

In this test program, specimen ID labels were generated using the following designation process:

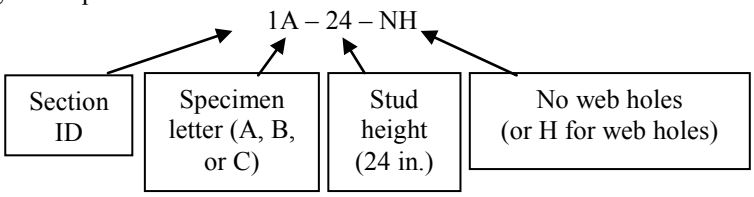

Sigma sections were selected based on geometric ratios, and test lengths were determined by modeling the chosen section in the finite strip software

CUFSM [7]. Table 1 contains the ID labels for the sections reported in this paper.

Table 1. Section ID Labeling

Section	Shape	Section ID
550SG200-118	Sigma	1
550SG300-118	Sigma	2
600SG250-54	Sigma	3
800SG200-33	Sigma	4
800SG300-43	Sigma	5

Experimental Setup

The experimental investigation consisted of both short studs and long studs. The short studs were tested at short (8 or 10 in.) lengths and intermediate (15 or 24 in.) lengths, while long studs were tested at 120 in. lengths.

Short specimen preparation consisted of measuring the actual dimensions, strain gauging the corners at mid-height, and filing the ends to ensure flatness as required by [8]. The specimens were tested in a 220 kips universal hydraulic MTS machine with calibrated displacement accuracy of 0.0001 inches shown in Figure 1. Flange and web displacements were measured with linear potentiometers, and the specimen ends bore directly on steel platens. A scholarly discussion of this end condition is contained in [9], and the boost in strength resulting from this friction bearing condition is calculated as recommended in [10].

Long specimen preparation was very similar to the short specimens. In addition to cross section measurements, long axis imperfection (sweep) was recorded. The studs were tested using an oversized steel frame with hydraulic jack. Strong and weak axis displacements were recorded, as well as mid-height strain on each corner. In an attempt to replicate pinned boundary conditions, a 3 in. diameter saddle (Figure 2) was sandwiched between steel platens, on which the stud bore directly. Post-test analysis revealed that these boundary conditions, coupled with the complex behavior of CFS members, did not result in a pinned configuration. Figure 3 shows the long specimen setup. Both short and long studs were loaded at 3 ksi/minute as prescribed by [8].

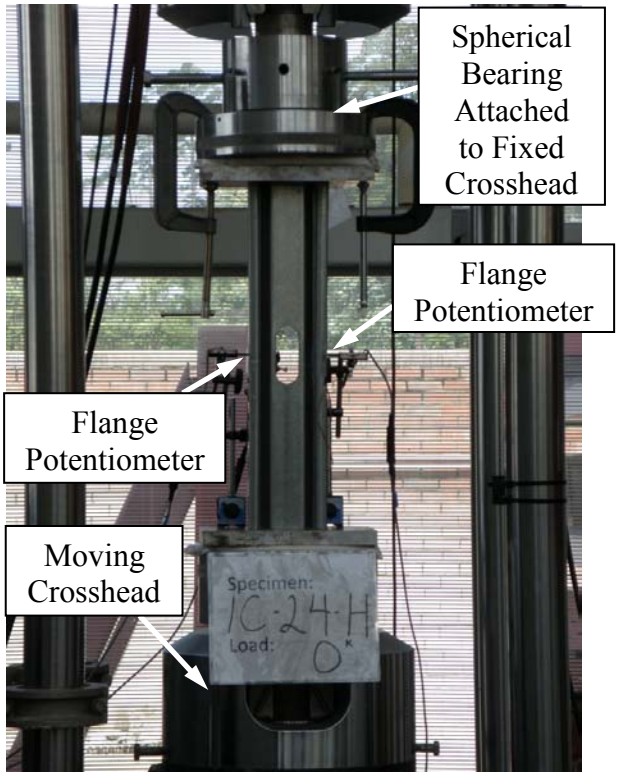

Figure 1. Short test setup

Experimental Results

Multiple buckling modes were observed throughout the test program and in some cases, interaction between buckling modes occurred in the same specimen. In thinner sections, local buckling would develop first, followed by another buckling mode (distortional or global). In thicker sections, distortional or global buckling would control but local buckling could develop as instability increased in the cross section approaching and after failure.

Figure 2. Spherical bearing boundary condition

The results of the test program are displayed in three tables: Table 2 and Table 3 (sigma section without holes), and Table 4 (sigma section with holes). The column of "buckling mode" describes the buckling modes which were observed during each individual test, in the order in which they developed. The terms F, FT, D, and L stand for flexural, flexural-torsional, distortional, and local buckling, respectively. If tests of 8 in. or 10 in. sigma columns revealed no significant difference in strength or behavior compared to the same 24 in. section, only one test was conducted of that series. The exception to this was the 550SG300-118 series, in which 3 tests were conducted to determine the behavior. This was the first 10 in. test series, so three tests were performed. The "DSM" column shows the DSM predicted strength for fixed boundary conditions.

Table 3 contains the results for six 120 in. tests of the 800SG200-33 section. This is because the first test specimen failed prematurely. There was intermediate weak axis displacement prior to the final failure, but there were no defects in the specimen or test setup to explain the early failure. Consequently, six tests were carried out to determine the section strength.

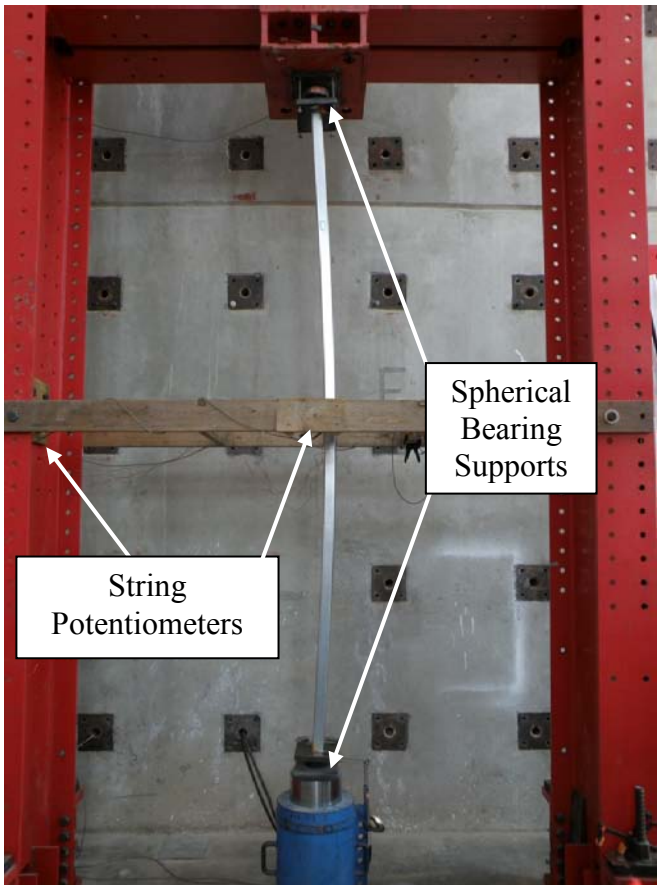

Figure 3. Long test setup

Supplemental Testing

Material property tests were conducted on samples of steel in order to determine the actual properties. Tensile coupon tests were conducted in accordance with [11]. Individual steel samples were provided by the manufacturer for the sigma sections. Actual material properties (yield strength and Young's modulus), along with nominal dimensions, were used to determine the predicted section strengths by the EWM and DSM. Tables 5 and 6 contain results of tensile coupon tests.

Table 2. Sigma section test results (no holes)

Section	Test ID	Buckling mode	Ult. Load (kips)	Avg. (kips)	DSM (kips)
550SG200-118	1A-15-NH	D	86.0	86.0	91.7
	1A-24-NH	D	91.3	91.3	91.7
	1B-24-NH	D	91.0		
	1C-24-NH	D	91.7		
	1A-120-NH	F	32.1	34.3	51.9
	1B-120-NH	F	33.4		
	1C-120-NH	F	37.2		
550SG300-118	2A-10-NH	D	109.7	108.7	103.9
	2B-10-NH	D, L	107.2		
	2C-10-NH	D	109.2		
	2A-24-NH	D	97.4	96.9	103.5
	2B-24-NH	D, L	97.5		
	2C-24-NH	D	95.7		
	2A-120-NH	F	61.2	61.2	78.6
	2B-120-NH	F	52.6		
	2C-120-NH	F	69.8		
600SG250-54	3A-8-NH	D, L	41.7	41.7	38.7
	3A-24-NH	D	40.4	39.8	37.5
	3B-24-NH	D, L	38.9		
	3C-24-NH	D	40.0		
	3A-120-NH	F	18.6	20.0	27.7
	3B-120-NH	F	21.9		
	3C-120-NH	F	21.1		

Strength Predictions

A summary of the strength predictions for the short sigma sections are contained in Table 7. The evaluated predictions, P_{exp} / P_{EWM} and P_{exp} / P_{EWM} as well as the statistical analysis, are computed for fixed boundary conditions and account for the boost in strength for this test setup as

recommended in [10]. Results indicate that both methods are good predictors of strength and are consistent with other CFS research programs.

The DSM strength predictions for the short 800SG300-43 section were unconservative and therefore reduced the overall accuracy. If this section is omitted from the accuracy calculation in Table 7, P_{exp}/P_{DSM} becomes 0.99.

Table 3. Sigma section test results (no holes) continued

Section	Test ID	Buckling mode	Ult. Load (kips)	Avg. (kips)	DSM (kips)
800SG200-33	4A-10-NH	L, D	18.7	18.7	19.5
	4A-24-NH	L, D	17.7	17.9	19.5
	4B-24-NH	L, D	17.8		
	4C-24-NH	L, D	18.2		
	4A-120-NH	D, F	6.8	9.0	16.2
	4B-120-NH	D, F	9.1		
	4C-120-NH	D, F	9.7		
	4D-120-NH	D, F	10.3		
	4E-120-NH	D, F	8.9		
	4F-120-NH	D, F	9.4		
800SG300-43	5A-10-NH	L, D	28.0	28.0	35.6
	5A-24-NH	D	25.9	27.3	35.9
	5B-24-NH	L, D	28.2		
	5C-24-NH	L, D	27.7		
	5A-120-NH	D, FT, L	25.5	24.4	37.2
	5B-120-NH	D, FT	22.9		
	5C-120-NH	D, FT, L	24.9		

Table 4. Sigma section test results (holes)

Section	Test ID	Buckling mode	Ult. Load (kips)	Avg. (kips)
550SG200-118	1A-24-H	D	75.2	75.2
	1B-24-H	D	76.3	
	1C-24-H	D	74.2	
	1A-120-H	F	26.5	24.9
	1B-120-H	F	24.3	
	1C-120-H	F	23.8	
600SG250-54	3A-24-H	L, D	34.9	35.5
	3B-24-H	L, D	35.2	
	3C-24-H	L, D	36.3	
	3A-120-H	FT	24.1	23.7
	3B-120-H	FT	22.1	
	3C-120-H	FT	25.0	
800SG200-33	4A-24-H	L, D	15.4	15.5
	4B-24-H	L, D	15.4	
	4C-24-H	L, D	15.6	
	4A-120-H	D, F	7.8	8.2
	4B-120-H	D, F	7.8	
	4C-120-H	D, F	9.0	

Table 5. Sigma section coupon results (no holes)

Profile	ID	F_y (ksi)	F_u (ksi)	E (10^3 ksi)
550SG200-118	A	56.4	75.0	35.7
	B	57.0	76.6	28.8
	C	56.7	74.1	34.0
	Avg.	**56.7**	**75.2**	**32.8**
550SG300-118	A	55.5	67.5	29.9
	B	55.3	67.7	29.9
	C	56.4	70.4	25.7
	Avg.	**55.7**	**68.5**	**28.5**
600SG250-54	A	48.6	77.3	29.9
	B	50.2	80.1	27.8
	C	50.2	79.1	24.5
	Avg.	**49.7**	**78.8**	**27.4**
800SG200-33	A	53.6	66.2	33.3
	B	52.9	64.8	29.9
	C	52.4	65.6	31.4
	Avg.	**53.0**	**65.5**	**31.5**
800SG300-43	A	56.8	82.0	31.8
	B	60.8	87.2	34.8
	C	61.1	86.1	31.6
	Avg.	**59.6**	**85.1**	**32.7**

Table 6. Sigma section coupon results (holes)

Profile	ID	F_y (ksi)	F_u (ksi)	E (10^3 ksi)
550SG200-118	A	58.8	72.6	22.8
	B	59.3	72.6	34.1
	C	58.5	71.3	25.6
	Avg.	**58.9**	**72.2**	**27.5**
600SG250-54	A	55.3	66.6	28.8
	B	56.3	60.0	27.4
	C	55.2	66.4	28.2
	Avg.	**55.6**	**64.3**	**28.1**
800SG200-33	A	59.0	67.5	26.0
	B	58.0	67.0	28.8
	C	58.5	67.5	27.1
	Avg.	**58.5**	**67.3**	**27.3**

Table 7. Design method accuracy

	P_{exp} / P_{EWM}	P_{exp} / P_{DSM}
Avg.	0.966	0.948
COV	0.159	0.114
n	22	

Conclusions

The results of an experimental program to evaluate the strength of sigma shaped CFS columns in concentric axial compression are reported. Both AISI design methods (effective width and direct strength) are good predictors of ultimate strength for these sections. These results are part of an effort to pre-qualify the sigma shape as a column in the DSM. Further details and recommendations can be found in [3].

References

[1] Boylan, M., Sumner, E., Rahman, N. and di Girolamo, E. (2006) "Web Crippling of Sigma-Shaped Metal Studs in a Wall Assembly",

Eighteenth International Specialty Conference on Cold-Formed Steel Structures, Orlando, FL.

[2] Neville, K.L. (2006) "Buckling Behavior of Cold-Formed Sigma Shaped Columns: Testing of the SigmaStud", In partial fulfillment of MCE. North Carolina State University, Raleigh, NC.

[3] Klingshirn, D.J. (2009) "Experimental and Analytical Investigation of Optimized Cold-Formed Steel Compression Members", MS Thesis. North Carolina State University, Raleigh, NC.

[4] Schafer, B.W., Sarawit, A., and Pekoz, T. (2006) "Complex Edge Stiffeners for Thin Walled Members", *Journal of Structural Engineering*, 132(2), 212-226.

[5] Yan, J., and Young, B. (2002) "Column Tests of Cold-Formed Steel Channels with Complex Stiffeners", *Journal of Structural Engineering,* 128(6), 737-745.

[6] Young, B., and Yan, J. (2004) "Design of Cold-Formed Steel Channel Columns with Complex Edge Stiffeners by Direct Strength Method", *Journal of Structural Engineering*, 130(11), 1756-1763.

[7] Schafer, B.W., and Ádány, S. (2006) "Buckling Analysis of Cold-Formed Steel Members using CUFSM: Conventional and Constrained Finite Strip Methods", *Eighteenth International Specialty Conference on Cold-Formed Steel Structures*, Orlando, FL.

[8] AISI TS-2-02. (2002) "Stub-Column Test Method for Effective Area of Cold-Formed Steel Column", American Iron and Steel Institute, Washington DC.

[9] Moen, C.D., and Schafer, B.W. (2008) "Experiments on Cold-Formed Steel Columns with Holes", *Thin Walled Structures*, 46(10), 1164-1182.

[10] Moen, C.D. (2008) "Direct Strength Design of Cold-Formed Steel Members with Perforations", Ph.D. thesis, Johns Hopkins University, Baltimore, MD.

[11] ASTM A370-07. (2007) "Standard Test Methods and Definitions for Mechanical Testing of Steel Products", ASTM International, West Conshohocken, PA.

Twentieth International Specialty Conference on Cold-Formed Steel Structures
St. Louis, Missouri, U.S.A., November 3 & 4, 2010

Cyclic Elastoplastic Large Displacement Analysis of Cold-formed Steel Box Columns under Combined Action of Axial and Bidirectional Lateral Loading

Iraj H.P. Mamaghani [1]
Saman Montazeri [2]

ABSTRACT

This paper deals with the cyclic elastoplastic large displacement analysis of cold-formed steel box columns under combined action of axial and bidirectional lateral loading. Cold-formed steel box columns are very useful in highway bridge pier construction as they offer flexible space requirement and provide speedy construction. Behavior of cold-formed steel box columns under earthquake-induced loads is rather complicated as earthquakes occur in an oblique direction. However, modern seismic design philosophies have been based on the behavior of structures under independent actions of uni-directional loading in orthogonal directions. In this study, inelastic cyclic behavior of steel columns subjected to constant axial force together with simultaneous bi-directional cyclic lateral loads is investigated using an advanced finite element analyses procedure. Several types of linear and non-linear idealized loading patterns are employed to check the strength and ductility. The effects of important structural parameters

[1]Associate Professor, Department of Civil Engineering, University of North Dakota, 243 Centennial Dr., Grand Forks, ND, 58202-8115
Email: irajmamaghani@mail.und.edu
[2]Graduate Student, Department of Civil Engineering, University of North Dakota, 243 Centennial Dr., Grand Forks, ND, 58202-8115

and loading history on the behavior of cold-formed thin-walled steel box columns are examined using the proposed procedure.

INTRODUCTION

Cold-formed thin-walled steel box columns used as steel bridge piers have found wide application in highway bridge systems in Japan compared with other countries, where such structures are much less adopted. Steel tubular bridge piers, compared with concrete ones, are light and ductile. They can be built under severe constructional restrictions, such as in limited spaces at urban areas like New York and Tokyo, where the effective use of the limited spaces are strictly desired. They are also applied to locations where heavy superstructures are unfavorable, such as on soft ground, reclaimed land and bay areas.

In general, because of these restrictions, steel bridge piers are designed as single columns of the cantilever type, or one to three-story frames, and they are commonly composed of relatively thin-walled members of closed cross-sections, either box or circular in shape because of their high strength and torsional rigidity (Mamaghani, 1996). These make them vulnerable to damage caused by the coupled instability, i.e., the interaction of local and overall buckling, in the event of a major earthquake. For example, Figure 1 shows cold-formed thin-walled steel tubular columns of circular and box sections supporting elevated highway bridge in Nagoya, Japan. When structural members are composed of thin-walled steel plate elements, the local buckling of the component plates may influence the strength and ductility of those members. As is well known, the earthquake waves consist of three-dimensional components. Specifically, the coupling of the two horizontal components is expected to have an unfavorable effect on the ultimate behavior of columns. Therefore, it is important to examine the ultimate behavior of thin-walled columns under cyclic axial and bidirectional lateral loading.

Figure 1. Cold-formed thin-walled steel tubular columns of circular (front column) and box (rare columns) sections supporting elevated highway bridge in Nagoya, Japan.

.

Present seismic design guidelines for steel columns have been based on numerous analytical and experimental investigations conducted under constant axial load plus uni-directional lateral loads. The superposition of independent action of uni-directional design seismic motion in orthogonal directions or the behavior in the most critical direction is being considered in the present seismic capacity checks. However, it is important to incorporate the bi-axial effects in seismic designs. Several experimental studies have been so far carried out to investigate the effect of bi-directional cyclic loads on the behavior of steel and concrete columns (Saatcioglu and Ozcebe, 1989; Ohnishi et al., 2003).

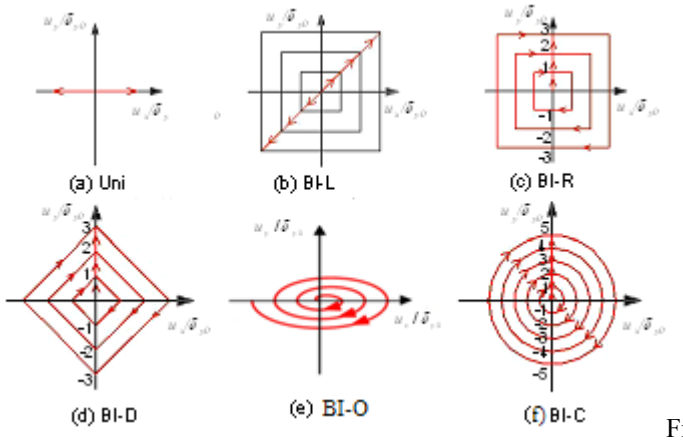

Figure 2. Cyclic loading patterns: (a) Unidirectional (Uni), (b) Bidirectional-linear (BI-L), (c) Bidirectional rectangular (BI-R), (d) Bidirectional-diamond (BI-D), (e) Bidirectional-Oval (BI-O), and (f) Bidirectional-circular (BI-C).

Nevertheless, those tests were found to be very costly and the results were inadequate to make firm conclusions. This strongly suggests the importance of having a reliable analytical procedure.

In this study, while keeping the vertical compressive load constant, the behavior of thin-walled steel tubular columns under the cyclic bidirectional lateral loads is examined in comparison with that under the cyclic unidirectional lateral loads shown in Figures 2 and 3. The advanced general purpose finite element program ABAQUS (2008) was employed in the analysis. The results obtained from the cyclic bidirectional loading experiment are used to substantiate the validity of geometrically and materially nonlinear finite element analysis.

COLD-FORMED THIN-WALLED STEEL TUBULAR COLUMNS

Cold-formed steel tubular columns in highway bridge systems are commonly composed of relatively thin-walled members of closed cross-sections, either box or circular in shape because of their high strength and torsional rigidity, see Figure 1. Such structures are considerably different from columns in buildings. The former are characterized by: failure attributed to local buckling in the thin-walled members; irregular distribution of the story mass and stiffness; strong beams and weak columns; low rise (1-3 stories); and a need for the

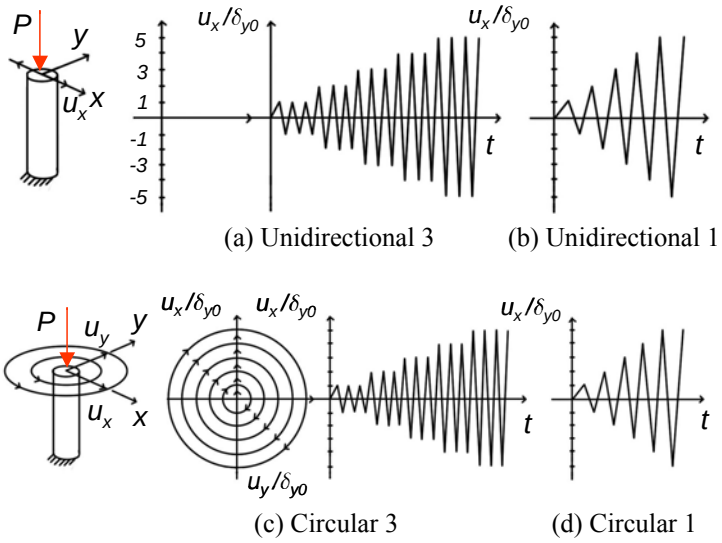

Figure 3. Loading programs.

evaluation of the residual displacement. These make the columns vulnerable to damage caused by interaction of local and overall buckling in the event of a severe earthquake.

The most important parameters considered in the practical design and ductility evaluation of thin-walled steel hollow box sections are the width-to-thickness ratio parameter of the flange plate R_f for box section, radius-to-thickness ratio parameter of the circular section R_t, and the slenderness ratio parameter of the column λ (Mamaghani, 2008). While R_f and R_t influence local buckling of the section, λ controls the global stability. They are given by:

$$R_f = \frac{b}{t}\frac{1}{n\pi}\sqrt{3(1-\nu^2)\frac{\sigma_y}{E}} \quad \text{(for box section)} \tag{1}$$

$$R_t = \frac{r}{t}\sqrt{3(1-\nu^2)}\,\frac{\sigma_y}{E} \quad \text{(for circular section)} \tag{2}$$

$$\lambda = \frac{2h}{r_g}\frac{1}{\pi}\sqrt{\frac{\sigma_y}{E}} \tag{3}$$

in which, b = flange width; t = plate thickness; σ_y = yield stress; E = Young's modulus; ν = Poisson's ratio; n = number of subpanels divided by longtudinal stiffeners in each plate panel ($n = 1$ for unstiffened sections); r = radius of the circular section; h = column height; r_g = radius of gyration of the cross section.

The elastic strength and deformation capacity of the column are expressed by the yield strength H_{y0}, and the yield deformation (neglecting shear deformations) δ_{y0}, respectively, corresponding to zero axial load. They are given by:

$$H_{y0} = \frac{M_y}{h} \tag{4}$$

$$\delta_{y0} = \frac{H_{y0}h^3}{3EI} \tag{5}$$

where M_y = yield moment and I = moment of inertia of the cross section. Under the combined action of buckling caused by constant axial and monotonically increasing lateral loads, the yield strength is reduced from H_{y0} to a value denoted by H_y. The corresponding

yield deformation is denoted by δ_y. The value H_y is the minimum of yield, local buckling, and instability loads evaluated by the following equations:

$$\frac{P}{P_u}+\frac{0.85H_y h}{M_y(1-P/P_E)}=1 \tag{6}$$

$$\frac{P}{P_u}+\frac{H_y h}{M_y}=1 \tag{7}$$

in which $P=$ the axial load; $P_y=$ the yield load; $P_u=$ the ultimate axial load; and $P_E=$ the Euler load.

NUMERICAL ANALYSIS

Finite element analysis procedure is very effective in determining the seismic resisting capacity of structures. The reliability of such an analysis mainly depends on the modeling technique and the type of elements, boundary condition, type of material model, etc. In this section, analytical procedure is explained in view of geometrical details of column, element mesh, loading procedure including loading patterns and the material model.

Analytical Model

The cantilever steel columns with box and circular cross-section subjected to a constant axial force and cyclic lateral loadings are accounted for in the present analysis. The test specimens available in the literature are numerically analyzed following an elastoplastic large displacement finite element analysis procedure. For such thin-walled steel columns, local buckling always occurs near the base of the columns. Therefore, the beam-column element is employed for the upper part of the column; while the shell element that can consider the

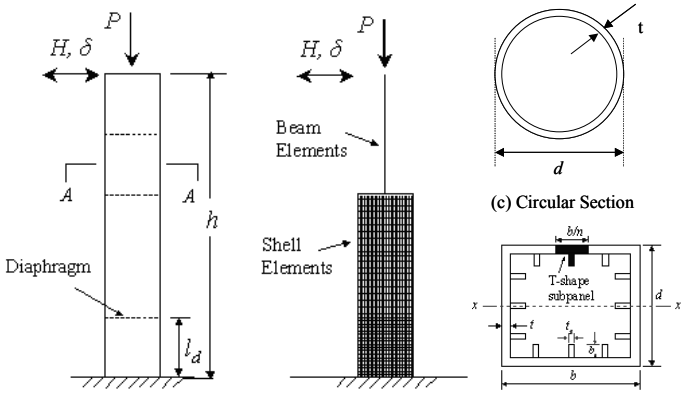

(a) Steel tubular column (b) Analytical model (d) Cross section

Figure 4. Finite element modeling of steel tubular columns.

effect of local buckling is employed for the lower part of the column, see Figure 4b. The interface between the shell elements and the beam-column element is modeled using rigid beams, Figure 4b. The column is stiffened by both longitudinal stiffeners and diaphragms, see Figures 4a and 4d. The longitudinal stiffeners and each subpanel between longitudinal stiffeners are modeled by using a four-node doubly curved shell element (S4R) available in the general purpose finite element program ABAQUS (2008). The diaphragm is also modeled using the same type of shell element. Shell elements are used only up to the height of the third diaphragm, see Figure 4b. The length between the base and the first diaphragm is divided into 18 segments, while the subsequent same lengths are divided into 9 segments along the column length. In the width and depth directions 24 elements are used. Each subpanel consists of eight columns of shell elements. Five columns of shell elements are assigned in longitudinal stiffeners. For shell elements five layers are assumed across the thickness, and the spread of the plasticity is considered both through the thickness and along the element plane. The portion of the column beyond the third diaphragm

Table 1. Dimensions of analytical models.

Specimens	h	$b = d$	b_s	t	R_f	λ	γ/γ^*
Uni, BI-L27, BI-L45	2420	450	53	5.8	0.61	0.39	2.4
C35-35	5551	1043	179	6.0	0.35	0.35	3.0
C35-50	8160	1043	105	6.0	0.35	0.50	3.0
C46-35	7559	1364	113	6.0	0.46	0.35	3.0
Unit : millimeters (mm) Uni, BI-L27, and BI-L45 are test specimens. C35-35, C35-50, and C46-35 are numerical specimens. Uni = Unidirectional, BI = Bidirectional							

is modeled using a beam-column element (B31). The sectional dimension of this element is chosen in such a way that the moment of inertia and the cross-sectional area of the element section are identical to those of the actual specimen. Ten beam-column elements are adopted to model the upper part of the specimen. The above stated mesh divisions are determined by trial and error method. It is found that such mesh divisions can give an accurate result. The residual stresses due to welding and the initial deflections of the flange and web plates are not considered in the analysis because their effect is insignificant on the cyclic behavior (Mamaghani 1996; Banno et al. 1998).

In what follows, first analysis of specimen tested by Ohnishi et al. (2003) under linear loading paths will be presented. Then the results of parametric study using non-linear loading paths will be presented and discussed. The finite element modeling of the steel column used in the analysis is shown in Figure 4b. The dimensions of the column used in the analysis are listed in Table 1. The analyzed test specimens (*Uni*, *BI-L27*, and *BI-L45*) have height of h = 2420 mm; cross section size of b = d = 450 mm; thickness of t = 5.8mm; and stiffener width of b_s= 53 mm. The cross sectional area *A,* and the second moment of inertia *I,* of the section are 1.28×104 mm^2 and 3.92×108 mm^4, respectively.

Table 2. Material properties.

Specimens	σ_y (MPa)	E (GPa)	ν
Uni, BI-L27, BI-L45	412	206	0.28
C35-35, C35-50, C46-35	315	200	0.30

The structural parameters that play important roles in earthquake resisting performance of stiffened steel columns are the width to thickness ratio R_t and R_f, slenderness ratio λ, and the stiffness rigidity ratio γ/γ* (Chen and Duan, 2000). The values of R_f , λ, and γ/γ* of the test column are 0.61, 0.39, and 2.4, respectively. In the parametric study, three numerical specimens namely C35-35 (R_f = 0.35, λ= 0.35), C35-50 (R_f = 0.35, λ= 0.50), and C46-35 (R_f = 0.46, λ=0.35) were considered. The value of γ/γ* of all three specimens was 3.0, see Table 1.

Modern seismic design specifications allow steel structures to deform up to a certain displacement level in inelastic range, which involves both material and geometrical non-linearity. In non-linear analysis, the accuracy of the material model has a large effect on the reliability of predictions. The modified two-surface plasticity model (2SM) developed by Mamaghani et al. (1995), which has been proved to be very accurate in simulating cyclic behavior of steel structures (Mamaghani, 1996; Shen et al., 1995) is introduced into the commercial computer program ABAQUS (2008) used in the analysis. The material properties of steel such as yield stress σ_y, Young's modulus E, and Poisson's ratio ν are listed in Table 2.

ANALYTICAL RESULTS

Comparison with test

The analyses were carried out using three loading patterns described in Figures 2a and 2b to check the effect of bi-axial cyclic bending. In loading pattern Uni, incremental cyclic lateral displacements were applied along the X-direction only. For comparison purposes, the same

Table 3. Comparison of test and analytical results.

Loading Paterns		$H_{l,m}/H_y$	$\partial_{l,m}/\partial_y$	$\partial_{l,95}/\partial_y$
Uni	Test	1.23	2.23	2.87
	Analysis	1.35	1.89	2.50
BI-L27	Test	1.15	3.35	3.76
	Analysis	1.32	2.35	2.70
BI-L45	Test	1.11	2.46	3.37
	Analysis	1.29	1.89	2.95

Uni = Unidirectional, BI = Bidirectional

loading history as used in the test was employed in the analysis. Figure 5a shows the comparison of test and the analytical results of the loading type Uni. The envelope curves are plotted in Figure 5b. The comparison of analytical and test results for loading pattern BI-L27 is shown in Figure 6. These results indicate that the analytical and test results match very well in all the cases, hence the proposed procedure can be considered to be accurate enough for reliable predictions.

The resultant lateral displacement δ_l and lateral load H_l for the cases BI-L27 and BI-L45 are calculated using the following two equations.

$$H_l = H_x \cos\theta + H_y \sin\theta \tag{8}$$

$$\delta_l = \delta_x \cos\theta + \delta_y \sin\theta \tag{9}$$

Where, θ is the angle between the loading direction and the major axis of the section (i.e., *X*-axis). The values of strength and ductility indices H_m/H_y, δ_m/δ_y, and δ_{95}/δ_y are calculated in terms of resultant load H_l *and* resultant displacements δ_l using the test and analytical results and are given in Table 3. It is seen here that the $H_{l,m}/H_y$, of uni-directional loading case (Uni) is higher than those of the BI-L27 and BI-L45 cases. On the other hand, values of $\delta_{l,m}/\delta_y$ and $\delta_{l,95}/\delta_y$ of the unidirectional loading case are quite lower than the other two cases. This means that bi-directional loading will result in lower strength while the ductility will be increased. The results clearly prove that the bi-directional loads

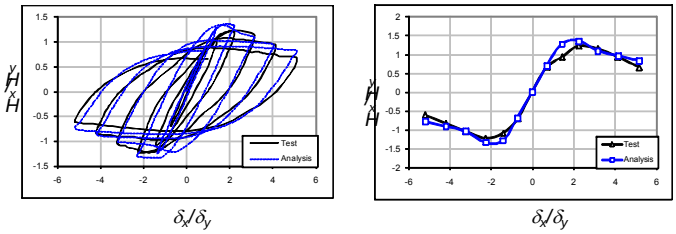

(a) *X*- direction (b) *X*- direction

Figure 5. Comparison of test and analytical results for loading type Uni: (a) Lateral load versus lateral displacement hysteretic behavior, in *X*- direction, (b) Envelope curves in *X*- direction.

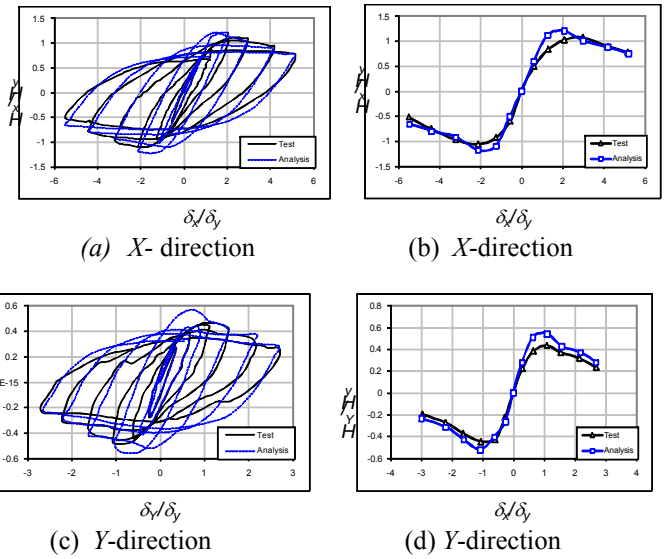

(a) *X*- direction (b) *X*-direction

(c) *Y*-direction (d) *Y*-direction

Figure 6. Comparison of test and analytical results for loading type BI-L27: (a) Lateral load versus lateral displacement hysteretic behavior in *X*-direction, (b) Envelope curves in *X*-direction, (c) Lateral load versus lateral displacement hysteretic behavior in *Y*-direction, (d) Envelope curves in *Y*- direction.

considerably affect the seismic behavior of columns. As a result, investigating the effects of parameters such as width to thickness ratio (R_t and R_f) and slenderness ratio λ, on the strength and ductility

Table 4. Comparison of strength and ductility performance for various loading patterns.

Specimen	Loading	$H_{l,m}/H_y$	$\partial_{l,m}/\partial_y$	$\partial_{l,95}/\partial_y$
C35-35	UNI	1.65	6.00	6.40
	BI-O	1.55	2.67	4.27
	BI-C	1.42	2.43	2.87
	BI-R	1.61	4.00	4.36
C35-50	UNI	1.55	4.00	4.50
	BI-O	1.57	3.24	4.77
	BI-C	1.48	2.43	3.13
	BI-R	1.47	3.00	3.22
C46-35	UNI	1.47	3.01	3.40
	BI-O	1.47	2.67	3.14
	BI-C	1.30	1.81	2.03
	BI-R	1.36	2.00	2.36

performance of columns has significant practical importance when they are subjected to multi-directional cyclic loads.

Parametric Study

The columns for parametric study specifically designed in order to check the effects of parameters R_t, R_f and λ were analyzed using three types of non-linear loading patterns as shown in Figure 2. The corresponding strength and ductility indices obtained in the *X*-direction are given in Table 4.

It has been revealed from these results that the strength and ductility of columns having the same width to thickness ratio and slenderness ratio are different when they are subjected to different loading patterns. Also, as expected, the results were different for different width to thickness and slenderness ratio for a particular loading pattern. The minimum strength and ductility were found to occur under circular (BI-C) loading pattern and the maximum were under uni-directional loading. It is understood from results in Table 4 that the values of H_m/H_y, of C35-35 (1.42) and C35-50 (1.48) under loading type BI-C do not differ much. The corresponding values under loading type BI-O (1.55 and 1.57) are very close. This means that the effect of λ on the strength is not significant when circular loading type is concerned. On the other hand under the loading type BI-R the values of H_m/H_y of C35-35 (1.61) and C35-50 (1.47) differ about 8 percent. Thus, it seems that the effect of λ on the strength varies with the loading type. Moreover,

similar comparisons revealed that the effects of parameters R_t and R_f on the strength are different with different loading types. Similar to the strength, effects of parameters on the ductility also significantly varie with the type of loading.

CONCLUSIONS

The finite element modeling procedure for analyzing steel columns subjected to constant axial loads and bi-directional cyclic loads are presented in this paper. The analytical procedure was verified by analyzing previous test specimens. Several columns were designed in view of identifying the effects of structural parameters such as width to thickness ratio and slenderness ratio on the behavior when columns undergo different bi-directional loading paths. The obtained results from this study confirm the importance of considering behavior of steel columns under multidirectional loading. The multidirectional tests and finite element analysis results showed that the behavior of a tubular column under multidirectional loading becomes complex and exhibits a circular trajectory once local buckling occurs. The local buckling bulge in the multidirectional loading case tends to develop monotonically due to the circular trajectory. As a result, the residual deformation becomes larger. On the contrary, the unidirectional loading test and analysis are likely to underestimate the damage and the residual displacements caused by an earthquake. It is concluded that the effects of multidirectional loading should be considered in ductility evaluation and seismic resistance design of steel structures.

REFERENCES

ABAQUS/STANDARD user's manual, Version 6.7. 2008. HKS Inc., Pawtucket, R.I.

Banno, S., I. H.P. Mamaghani, T. Usami, E. Mizuno, 1998. Cyclic elastoplastic large deflection analysis of thin steel plates. *Journal of Engineering Mechanics, ASCE*, 124(4), 363-370.

Chen, W. F., Duan, L., 2000. *Bridge Engineering Handbook*, CRC Press, Boca Raton, FL.

Mamaghani, I.H.P. 2008. Seismic design and ductility evaluation of thin-walled steel bridge piers of box sections, *Transportation Research Record: Journal of the Transportation Research Board,* Volume 2050, pp. 137-142.

Mamaghani, I.H.P., 1996. Cyclic elastoplastic behavior of steel structures: theory and experiment, *Ph.D. Thesis*, Nagoya University, Nagoya, Japan.

Mamaghani, I. H. P., C. Shen, E. Mizuno, and T. Usami, 1995. Cyclic behavior of structural steels. I: experiments, *J. Engrg. Mech.*, ASCE, 121(11), 1158-1164.

Ohnishi, A., Susantha, K.A.S., Mizuno, T., Okazaki, S., Takahara, H., Aoki, T., Usami, T., 2003. Experimental study on strength and ductility of steel bridge piers subjected to 2-directional seismic loading. *Proceedings of the Annuals of JSCE*, No. 58, pp. 7-10.

Saatcioglu, M., Ozcebe, G., 1989. Response of reinforced concrete columns to simulated seismic loading." *ACI Structural Journal*, pp. 3-12.

Shen, C., Mamaghani, I.H.P., Mizuno, E. and Usami, T. 1995. Cyclic behavior of structural steels. II: theory. *Journal of Engineering Mechanics*, ASCE, USA, Vol.121, No.11, 1165-1172.

Twentieth International Specialty Conference on Cold-Formed Steel Structures
St. Louis, Missouri, U.S.A., November 3 & 4, 2010

Test and Finite Element Analysis on Distortional Buckling of Cold-formed Thin-walled Steel Lipped Channel Columns

Xingyou YAO[1], Yanli GUO[2], Zhiguang HUANG[3]

Abstract

High-strength cold-formed thin-walled steel sections have been widely used in the recent several years. However, distortional buckling or interaction between it and local buckling can occur for high strength cold-formed thin-walled steel members. This paper describes a series of compression tests performed on lipped channel section columns with V-shape intermediate stiffener in the web and flanges fabricated from cold-formed high strength steel of thickness 0.48 and 0.6mm with nominal yield stress 550MPa. The lipped channel sections were tested to failure with both ends of the columns fixed. The test results of 16 specimens show that the local buckling usually appears before distortional buckling of the specimens and it makes the distortional buckling occur in advance. This interaction of local and distortional buckling may have the effect of reducing the stiffness and bearing capacity of the columns. The comparison on ultimate strength and buckling mode between test results and results of finite element analysis considering geometric and material nonlinear show that finite element method (FEM) can simulate the distortional buckling of cold-formed steel channel columns effectively. The calculative results using Direct Strength Method (DSM) of the North American Specification show that this design method couldn't consider the reverse effect of interaction between local and distortional buckling on ultimate strength. Direct Strength Method (DSM) considering interaction between local and distortional buckling should be developed.

[1] Doctoral candidates, Tongji University, Shanghai, China

[2]Lecturer, Guangdong Ocean University, Zhanjiang, China

[3] Doctoral Candidates,Xi'an University of Architecture and Technology, Xi'an, China

Introduction

High strength cold-formed thin-walled steel sections with nominal yield stress 550MPa have been widely used in low-rise and multi-story residential buildings and portal steel frame structures in developed countries, especially in Australia. High strength steel members usually have low ductility and thinner and more complicated sections (see Fig.1). So those high strength cold-formed thin-walled sections may undergo local, distortional and overall buckling or mixed buckling modes. Meanwhile, geometry of section, mode of distortional buckling, load type, end supported condition, and stiffeners all effect on the ultimate strength of distortional buckling of cold-formed steel members, the accurate prediction on the member strength of thin-walled cold-formed steel sections becomes more complex.

Research into the distortional buckling mode of thin-walled cold-formed open sections has attracted considerable attention in recent years since the first discussion by Hancock (1985), Lau and Hancock (1987, 1990) tested a range of channel and rack sections columns and proposed a set of design chart and curve. Kwon and Hancock((1992,2004,2009) conducted compression tests of high strength cold-formed channel columns, which showed a substantial post-distortional buckling strength, and proposed a distortional buckling strength equation for the columns considered the interaction of buckling modes. Meanwhile, the Direct Strength Method (DSM), a new design method considering interaction of local or distortional and overall buckling modes, was developed by Shafer and Pekoz (1998) and was studied further by Hancock et al.(2001). North American Specification Supplement 1(NAS2004) and Australian/New Zealand Standard for Cold-formed Steel Structures Standard (AS/NZS 4600:2005) recently adopted the Direct Strength Method as an alternative to the conventional Effective Width Method to predict the member strength. However, extensive research into the interaction between local and distortional buckling has not been conducted yet.

Test investigations

Test specimens

As shown in Fig.1, a lipped channel section which has a V shaped stiffener in each flange as well as in the web was selected as specimens' section in order to ensure distortional buckling occur. The nominal dimensions of h, b, and d are 110, 80, and 12mm respectively for all sections. Meanwhile, sections have four kind of length for two kinds of thickness of 0.48 and 0.6mm respectively, including 500, 1000, 1500 and 2000mm. the width (S_{w1},S_{w2}) and height(S_{d1},S_{d2}) of V-shape intermediate stiffener of web and flange are 20 and 10 mm. the radius of corner(r) is 0.48 and 0.6mm for

columns of two different thickness. The nominal section geometric properties are shown in table 1.

Specimen labeling

The test specimens were labeled such that the type section, the nominal length and thickness of specimen and specimen number were expressed by the label. For example, the label “LCC2060-AC-2”defines the following specimen: 1. The first three letters indicate the specimen is a lipped channel section columns. 2. The “2060”indicate that nominal length and thickness of specimen is 2000 and 0.6mm. 3. The sequence number of same specimens was appended at the label end.

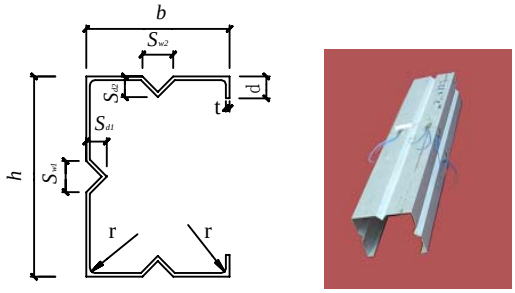

(a) Section dimensions （b）The specimen

Fig.1 Section of the specimens

Table 1 Nominal section properties of columns

specimen	*t*/ mm	Width-thickness ratio			*L*/mm	Slenderness ratio		Half-wavelength/ mm
		web	flange	lip		Strong axis	Weak axis	
LCC0548-1	0.48	229	167	25	500	10.9	17.4	1130
LCC0548-2	0.48	229	167	25	500	10.9	17.4	1130
LCC1048-1	0.48	229	167	25	1000	21.8	34.9	1130
LCC1048-2	0.48	229	167	25	1000	21.8	34.9	1130
LCC1548-1	0.48	229	167	25	1500	32.6	52.3	1130
LCC1548-2	0.48	229	167	25	1500	32.6	52.3	1130
LCC2048-1	0.48	229	167	25	2000	43.5	69.8	1130
LCC2048-2	0.48	229	167	25	2000	43.5	69.8	1130
LCC0560-1	0.60	183	133	20	500	10.9	17.4	995
LCC0560-2	0.60	183	133	20	500	10.9	17.4	995
LCC1060-1	0.60	183	133	20	1000	21.8	34.9	995
LCC1060-2	0.60	183	133	20	1000	21.8	34.9	995
LCC1560-1	0.60	183	133	20	1500	32.6	52.3	995
LCC1560-2	0.60	183	133	20	1500	32.6	52.3	995
LCC2060-1	0.60	183	133	20	2000	43.5	69.8	995
LCC2060-2	0.60	183	133	20	2000	43.5	69.8	995

Material properties

The structural steel grade of the test sections of thickness 0.48 and 0.60 mm was G550. The minimum specified yield stresses of the test sections of thickness 0.48 and 0.6mm is all 550MPa. Tensile coupons tested were

previously conducted for flat coupons cut from the fabricated sections. All coupons were tested in a 20kN capacity displacement controlled testing machine. The coupon test results were shown in table 2. The table 2 contains the experimental yield stress($f_{0.2}$), the ultimate stresses(f_u), and the initial Young's modulus(E). The experimental yield stress (2% offset) was higher than the nominal yield stress.

Test rig and gauge arrangement

Specimens were placed between the top and bottom end plates which is thick and flat enough to ensure fixed end boundary conditions. The 300kN capacity servo-controlled hydraulic testing machine system was used to apply compressive axial force for the specimens as shown in Fig.2. Load, strain, and displacement were recorded automatically by a date acquisition instrument and showed directly on the screen of the computer in this system. After geometric and physical alignment completed, axial loads can be subjected onto specimens by increments until the failure of them.

Table2 Material properties of columns

t/mm	*fu / MPa*	*f0.2/ MPa*	*E/ MPa*
0.48	727	695	216000
0.60	730	710	216000

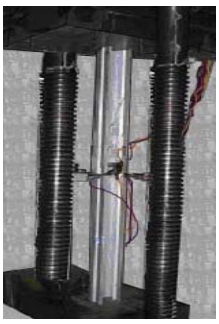

Fig.2 Set-up of the specimens

Lateral displacement transducers and strain gauges were commonly placed at mid-height of the columns, as shown in Fig.3 and Fig.4 for axially compressive specimens respectively. These strain gauges were used for alignment and to confirm buckling stress and experimental loading eccentricity.

Stud column test results

For shorter specimens of length 500mm, local buckling appeared first in the lip and then in the web (see Fig.5), distortion of flanges occurred nearly before the failure of specimens. These behaviors indicate that the failure of these shorter specimens resulted mainly from local buckling and significant distortional buckling only occurred when the ultimate load for local buckling was approached. Overall bucking wasn't obvious.

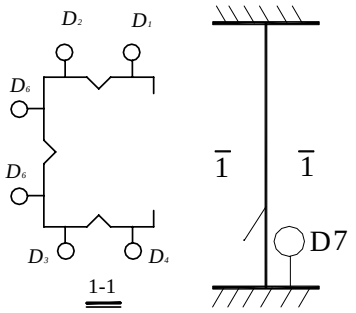

Fig.3 Displacement transducer

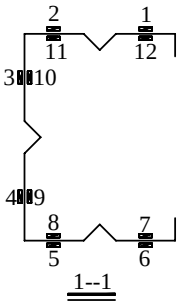

Fig.4 Strain gauges

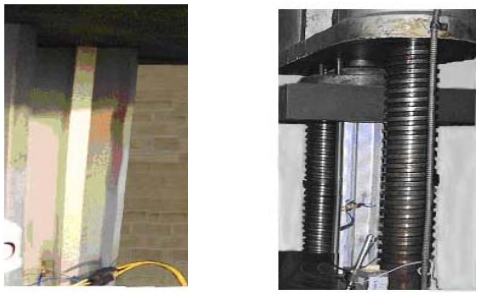

Fig. 5 Local buckling of stud column

Intermediate column test results

For specimens of intermediate lengths 1000mm and 1500mm, local buckling occurred in the web first and the obvious distortion of flanges occurred soon. The load of local buckling and distortional buckling was approximately same. Then the phenomena shows that local and distortional buckling almost existed simultaneously as shown in Fig.6. The member was failure with load and deflection increased. These specimens displayed a significant post-buckling strength reverse. These specimens were distortional buckling failure mode. Overall buckling wasn't obvious.

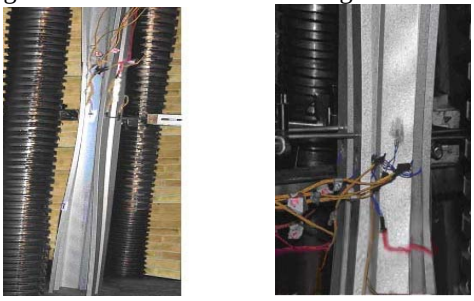

Fig.6 Buckling mode of medium-length specimens

Long column

For longer specimens of length 2000mm, the distortion of flanges appeared as soon as specimens were subjected to load as shown in Fig.7. With the load increasing, the distortional deformation of flanges got so significant that two flanges contact together. Local buckling in the web occurred nearly before the failure of specimen. These specimens were failure for large deflection of flange. So the main reason for the failure of longer specimens is distortional buckling. Interaction of local and distortional only occurred when the ultimate load was approached. Distortional buckling was obvious and the specimens occurred torsional-flexual deformation before the specimens were failure.

Fig.7 Buckling mode of longer specimens

Effect of buckling modes on ultimate load-carrying capacity

Three kinds of flange buckling mode shape were observed during tests. The specimens buckled inwards (I-I mode), outwards (O-O mode) for two flanges and one flange inward and one flange outward (I-O mode) respectively. The three buckling modes are shown in Fig.8.

(a) *I-I* mode (b)*O-O* mode (c) *O-I* mode

Fig.8 Three types of flange distortional buckling modes

The detailed reason is summarized as following: If the web (with intermediate stiffeners) occur local bucking firstly and local bucking deformed shape is symmetrical about inter-mediate stiffeners, I-I mode can occur; otherwise O-I mode can occur, O-O mode can occur if local buckling doesn't occur before distortional buckling occur. Test results

show that O-O mode bears the load highest, I-O mode takes second place, I-I mode is the lowest.

The test results show that the failure modes of all the specimens are distortional buckling. The ultimate load-carrying capacity and distortional buckling mode are shown in table 3.

Finite element analysis

The finite element method ANSYS8.1 considering the material non-linear and geometry large deformation was used to simulate the experimental behavior and ultimate strength of the compressive specimens. The FEM contain two stages. An eigenvalue elastic buckling analysis was performed to solve the probable buckling modes first, and then, the non-linear buckling analysis was carried out to predict the ultimate strength, deformation, and failure mode of the test specimens using arc-length method, which can follow the post-buckling range.

Element type and mesh

A four-node three-dimensional quadrilateral shell element with six degrees of freedom at each node was used in FEM. The elastic shell element, shell63, was used to obtain the critical elastic local buckling and distortional buckling mode and the assumed initial geometric imperfection shape, and the plastic shell element, shell181, was used in the non-linear analysis. The mesh element size of 10x10mm is best to simulate the behavior and ultimate strength of the specimens. The Finite element medal meshed is shown as Fig.9.

Boundary condition

The tested members were fixed at each end supported with plate, so the end plates were modeled in the FEM. All nodes of the top end are constrained on displacement in the X, Y-direction and rotation in all X, Y, and Z-direction, and the below end are constrained on displacement and rotation in all direction. In order to simulate the rigid loading plates, the CERIG command was used at both ends to create rigid regions. The loading point and reaction point were defined as the master nodes (see Fig. 10).

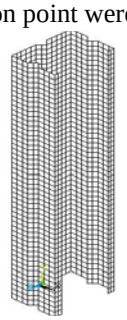

Fig.9 Finite element medal

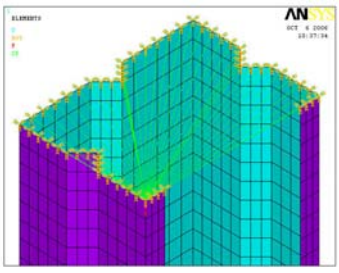

Fig. 10 Constrain on the reaction end

Geometric imperfection, material behavior

The geometric imperfection for the non-linear analysis was obtained by the eigenmode 1 multiplied a factor, which was specified by the maximum amplitude of the geometric imperfection measured for every specimen.

The material behavior was approximately described by a bilinear stress-strain curve, and the elastic modulus and the yield stress of the material were specified by the average of the material properties in Table1.

Failure mode and ultimate load prediction

The failure modes obtained from FEM were compared with the experimental failure modes as shown in Fig.11. Table3 summoned the ultimate strength analyzed by FEM. All results show that the failure mode and ultimate strength obtained from the FEM closed to the experimental failure modes and ultimate strength. So FEM can simulate the experimental buckling modes and calculate the ultimate loads closely.

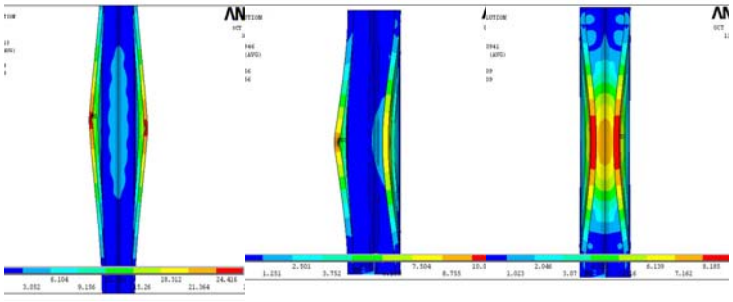

（a) *I-I* mode (b)*O-O* mode (c) *O-I* mode

Fig.11 distortional buckling modes of finite element analysis

Results compared with design methods

The supplement of North America Specification (NAS2004) provides the Direct Strength Method (DSM) to determinate the ultimate strength of axially compressive columns. The nominal member capacity of a member in compression shall be the minimum of the nominal member capacity of a member for flexural, torsional or flexural-torsional buckling, the nominal member capacity of a member in compression for local buckling and the nominal member capacity of a member in compression for distortional buckling. There are only the equations of the capacity for distortional buckling in this paper. These equations are

For $\lambda_d \le 0.561$ $\quad P_{nd} = P_y$ (1a)

For $\lambda_d > 0.561$ $\quad P_{nd} = P_y[1-0.25(P_{crd}/P_y)^{0.6}](P_{crd}/P_y)^{0.6}$ (1b)

Where $\lambda_d = \sqrt{P_y / P_{crd}}$; P_{crd} is the elastic distortional buckling strength; $P_{crd} = f_d \times A$; f_d is the elastic distortional bucking stress, which was obtained using the CUFSM, but the specimens all are fixed, so the elastic distortional buckling was obtained by the FEM; $P_y = AF_y$, A is the cross-sectional area, F_{y} is the yield strength.

The curve of member ultimate strength using Direct Strength Method (DSM) considering the minimum of the nominal member capacity of overall, local and distortional buckling against the length is shown in fig.11. Meanwhile, the average values of test results and the average values of finite element analytical results also are shown in fig.11. These results are also shown in table 3. As shown in table 3 and fig. 11, FEM can simulate the experimental buckling modes and calculate the ultimate loads closely. For the intermediate and long columns, the calculated results(P_{nd}) using NAS are higher than the test results(P_{t}), but the test results are close to the calculated results(P_{a}) using NAS for stud columns and long columns, because result from the intermediate columns display a significant interaction between local buckling and distortional buckling, which decrease the ultimate strength.

Table3 Comparison of experimental, FEA and NAS results

specimen	Test		Finite element method			North American specification	
	P_t/kN	buckling mode	P_a / kN	P_a/ P_{nd}	buckling mode	P_{nd} / kN	P_{nd}/ P_t
LCC0548-1	40.6	O-I	41.40	1.020	O-I	31.82	0.78
LCC0548-2	37.83	I-I	38.54	1.019	I-I	31.82	0.84
LCC1048-1	23.56	I-I	23.89	1.014	I-I	29.13	1.24
LCC1048-2	22.53	I-I	23.29	1.034	I-I	29.13	1.29
LCC1548-1	20.79	O-I	21.34	1.026	O-I	24.41	1.17
LCC1548-2	21.34	I-I	21.79	1.021	I-I	24.41	1.14
LCC2048-1	18.44	I-I	20.65	1.120	I-I	20.18	1.09
LCC2048-2	20.58	O-I	21.43	1.041	O-I	20.18	0.98
LCC0560-1	47.54	I-I	49.93	1.050	I-I	50.96	1.07
LCC0560-2	50.95	I-I	51.95	1.020	I-I	50.96	1.00
LCC1060-1	46.44	O-O	45.21	0.974	O-O	45.92	0.99
LCC1060-2	45.38	O-O	44.75	0.986	O-O	45.92	1.01
LCC1560-1	33.19	I-I	35.9	1.082	I-I	40.13	1.21
LCC1560-2	35.38	O-I	35.93	1.016	O-I	40.13	1.13
LCC2060-1	32.56	I-I	33.12	1.017	I-I	28.39	0.87
LCC2060-2	30.39	I-I	32.65	1.074	I-I	28.39	0.93

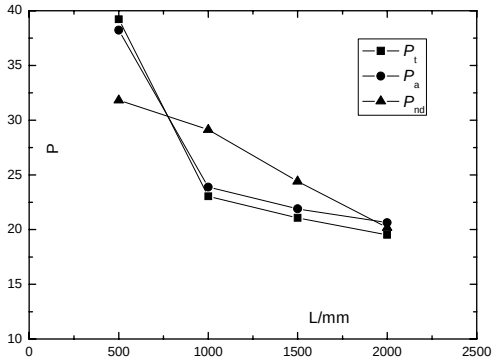

(a) t=0.48mm

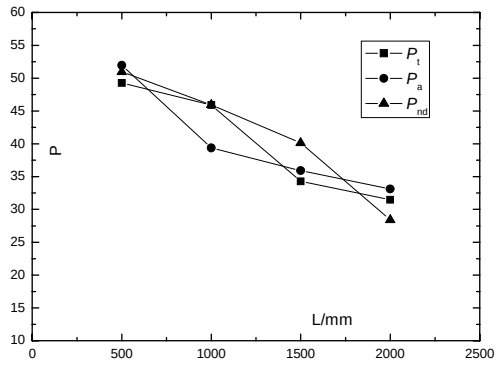

(b) t=0.6mm

Fig.10 flange distortional buckling modes of finite element analysis

Conclusion

The distortional buckling behavior of 16 high strength steel cold-formed thin-wall lipped channel specimens under axial compression loads have been tested in this paper. According to comparisons of test results and calculated results based on DSM and analytical results using FEM, the following conclusions can be drawn:

(1)Distortional buckling can occur in singly-symmetric sections of high strength cold-formed thin-walled steel columns if given certain section dimensions, and boundary conditions. Distortional buckling may control

member ultimate load-carrying capacity. So it should be considered in design.

(2)The behaviors of distortional buckling are much different from local or overall buckling of members. Therefore the design method for distortional buckling should be analysis.

(3)The stud columns display a significant post- local-buckling strength reverse and the distortional buckling just observe in the stage of failure, so the ultimate load-carrying capacity of the stud columns is relatively high. The intermediate and long columns display the distortional buckling early and interaction with local buckling which decrease the ultimate strength.

(4) FEM can simulate the experimental buckling modes and calculate the ultimate loads closely.

(5)The design formulas for the compressive column in DSM can be used to predict the ultimate strength for columns subjected to local and overall buckling, but can't be used to predict the ultimate strength for columns subjected to interaction between local and distortional buckling.

Notation

The following symbols are used in this paper:

A = cross-sectional area (mm^2);
b = flange width (mm);
d = lip width (mm);
E = initial Young's modulus (MPa);
$f_{0.2}$ = experimental yield stress (MPa);
f_d = elastic distortional bucking stress(MPa);
f_u = the ultimate stresses(MPa);
F_y = yield stress (MPa);
h = web height (mm);
L = length of column (mm);
P_a = FEM analytical ultimate strength (kN);
P_{crd} = elastic distortional buckling stength (kN);
P_{nd} = distortional buckling strength (kN);
P_t = ultimate test load (kN);
P_y = yield stength (kN);
R = the radius of corner(mm);
S_{w1},S_{w2} = width of V-shape intermediate stiffener of web and flange(mm);
S_{d1},S_{d2} = height of V-shape intermediate stiffener of web and flange (mm);
t = thickness of base metal (mm);

References

AS/NZS. (2005). “Cold-formed steel structures” *AS/NZS 4600: 2005*, Australian/New Zealand Standard, Sydney, Australia.

Hancock G. J. (1985), “Distortional buckling of steel storage rack columns”. *Journal of structural engineering*, 111(12):2770-2783.

Hancock G. J., Murray T.M. (2001), Cold-formed steel structures to the AISI specifications. Marcel Dekker, Inc..

Kwon Y.B., Kim B. S., Hancock G. J. (2009). “Compression tests of high strength cold-formed steel channels with buckling interaction”. *Journal of constructional steel research*. 65(2):278-289.

Kwon Y. B., Hancock G. J. (1992). “Test of cold-formed channels with local and distortional buckling”. *Journal of structural engineering*, 117(7):1786-1803.

Lau S.C.W., Hancock G. J. (1987), “Distortional buckling formulas for channel columns”. *Journal of structural engineering*, 113(5):1063-1078.

Lau S.C.W., Hancock G. J. (1990), “Inelastic buckling of channel columns in the distortional mode”. *Thin-Walled structures*, 10(2):59-84.

NAS.(2004). *Supplement 2004 to the North American specifications for the design of cold-formed steel structural members*, American Iron and Steel Institute, Washington D.C..

Schafer B. W., “Elastic buckling analysis of thin-walled members by finite strip analysis”, *CUFSM* v2.6.

Schafer B.W., Pekoz T. (1998) “Direct strength prediction of cold-formed steel members using numerical elastic buckling solutions”. In: Shanmugan NE, Liew JYR, Thevendran V, editors. *Thin-walled structures, research and development* Elsevier; 137-144.

Yang D.M., Hancock G. J.(2004). “Compression tests of high strength steel channel columns with interaction between local and distortional buckling”. *Journal of structural engineering*.2004, 130(12):1954-1963.

Twentieth International Specialty Conference on Cold-Formed Steel Structures
St. Louis, Missouri, U.S.A., November 3 & 4, 2010

Load-Carrying Capacity Estimation on Cold-Formed Thin-Walled Steel Columns with Built-up Box Section

Yuanqi LI[1], Xingyou YAO[2], Zuyan SHEN[1], Rongkui MA[2]

Abstract

The use of cold-formed thin-walled steel structural members has increased in recent years, and most of their sections are open section with only one symmetrical axis, which would likely fail by twisting and interaction with the others buckling mode, such as local buckling and distortional buckling. To improve the ultimate strength of columns, built-up box section can be used. In this paper, a series of loading capacity tests on high-strength cold-formed steel columns with built-up box section are presented, including 21 axially-compressed columns and 19 eccentrically-compressed columns subjected to bending moments about weak axis as well as strong axis. The test specimens are built up by two channel sections with two intermediate stiffeners in the web, and they connect at their flanges using self-drilling screws. It was shown that distortional buckling and twisting do not occur and the ultimate load-carrying capacity is 10 to 20 percent higher than the sum of the ultimate load-carrying capacity of each lipped channel section columns. According to the test results and theoretical analysis, an improved method based on the suggestion of current China code 'Technical code of cold-formed thin-walled steel structures' (GB50018-2002) considering the plate-coupling effect was proposed to estimate the ultimate load-carrying capacity of built-up box section column. With the proposed method, the calculated results are close and conservative to the test results.

Introduction

The use of high-strength cold-formed thin-walled steel structural members has increased in re-cent years, especially in low-rise and multi-story residential buildings and portal steel frame structures. High strength steel sections have higher strength, lower ductility, and larger width-to-thickness

[1] Professor, Tongji University, Shanghai, China
[2] Doctoral candidates, Tongji University, Shanghai, China

ratio, which are different from the ordinarily used cold-formed thin-walled steel. The national design code for cold-formed thin-walled steel structures, 'Technical code of cold-formed thin-wall steel structures'(GB50018-2002), have no provision to estimate the ultimate load-carrying capacity of high-strength cold-formed thin-walled members with thickness less than 2mm. Meanwhile, cold-formed steel section are usually formed in singly-,point-,or non-symmetric open sections as shown in Fig.1. These open sections have a relatively small torsional stiffness compared to closed sections. So open sections would likely fail by twisting and interaction with the others buckling mode, such as local buckling and distortional buckling, depending on the dimension of the cross sections and the length of the members. Box-shaped sections made by connecting two channel sections tip to tip are often found in using in cold-formed steel structures due to their relatively large torsional stiffness and their favorable radius of gyration about both principal axes (1977). But when the width-to-thickness ratio of the built-up sections is relatively large, local buckling will decrease the full section strength of the member. Therefore, the cold-formed steel built-up closed sections with two intermediate stiffeners in the web are investigated in this paper.

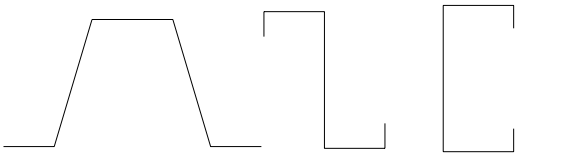

(a) Hat section (b) Z-section (c) Channel section

Fig.1 Cold-formed steel section

In the past decades, there are many test data on cold-formed thin-walled steel open section columns performed by researchers all over the world, such as Rhodes and Harvey(1977), Thomasson(1978), Mulligan and Peköz(1984), Lau and Hancock(1988), Weng and Peköz(1990), Kwon and Hancock(1992),Young and Rasmussen(1998), Young(2005), and some other researchers as summarized by Yu(2000). Meanwhile, the high strength cold-formed thin-walled channel sections columns with two inter-mediate stiffeners in the web were researched by SHEN and LI (2008). However, not many test data have been reported on cold-formed thin-walled steel built-up closed section columns. De Wolf et al.(1974) conducted column tests on cold-formed steel box-shaped sections built up by two plain channel sections connected at their flanges. The webs of the box-shaped sections were flat and local buckling occurred during the tests. The column strengths were influenced by local buckling. However, the use of intermediate stiffeners could improve the situation. Ben Young et al(2008) proposed the design methods of cold-formed thin-walled steel built-up closed sections with one intermediate stiffener. The web of build-up closed sections displayed the distortional buckling which can reduce the ultimate strength of members. Therefore, the behavior and design of cold-formed thin-walled

steel built-up sections with two intermediate stiffeners in the webs are investigated in this paper.

Experimental investigation

Material properties

The structural steel grade of the test sections is G550 (AS1397-2001). The minimum specified yield stresses of the test sections is 550MPa. Tensile coupons tested were previously conducted for flat coupons cut from the fabricated sections. The coupons were prepared and tested according to the Chinese Standard, 'Metallic materials—Tensile testing—Method of test at ambient temperature' (GB/T228-2002). All coupons were tested in a 20kN capacity displacement controlled testing machine. The coupon test results are shown in table 1 and the typical stress-strain relations are shown in Fig.2. The 0.2% proof stress was used as the corresponding yield stress in calculating the design strength of columns. The table 1 contains the experimental yield stress($f_{0.2}$), ultimate tensile strength(f_u), initial Young's modulus(E), and elongation after fracture(δ). The experimental yield stress (2% offset) were higher than the nominal yield stress. The elongation ranged from 10.7%-11.7% with the average being 11.2%, which is significantly lower than that of mild steel.

Table1 Material properties of columns

Specimen	t (mm)	$f_{0.2}$ (MPa)	f_u (MPa)	E (MPa)	Elongation Ratio δ
S1001	1.00	613	623	2.02	11.70%
S1002	1.00	617	619	2.14	10.70%
S1003	1.00	615	618	1.98	11.10%

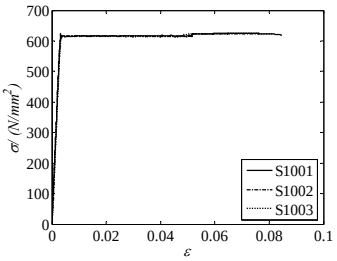

Fig. 2 Typical stress versus strain relation

Specimen tests

The test specimens of built-up sections were first brake pressed from structural steel sheets to form the channel sections with two intermediate stiffeners in the web, then two of the channel sections were connected at their flanges using self-drilling screws to form the built-up sections, as

shown in Fig.3. The space of screws was 300 or 600mm. The sections selected are used as the main members in low-rise and multi-story residential buildings in Chinese. The section geometry of lipped channel sections and the built-up section are given in Fig.3. The detailed actual cross-sectional dimensions are summarized in table 2 and table 3 for axially-compressed and eccentrically-compressed columns respectively. The internal radii of the corners and intermediate stiffeners are 4.0, 5.0, and 2.5mm for r_1, r_2, and r_3 respectively. The nominal widths of the flange, web, and lip of the test sections are 50, 100, and 12mm respectively. The nominal section properties are shown in table 4. The nominal length of the test members are from 200mm to 3000mm. The test specimens were labeled so that the thickness of specimens, the height of web, approximate slenderness ratio of specimens, load patters, axial of instability and sequence number of same specimens could be included. DS means build-up sections. The first four numbers of the specimen label indicates the height and thickness of specimens, the second two numbers refers to the approximate slenderness ratio, the third letters indicates the load patters, the next last letter displays the instability axial, the sequence number of same specimens is appended at the label end, such as DS1010-30-AC-Y-1 as showed in Fig.4.

Table 2 Geometries of axially compressed specimens

specimen	Nominal length(mm)	Actual length(mm)	web(mm)		flange(mm)		lip(mm)	
			h_1	h_2	b_1	b_2	a_1	a_2
DS1010-10-	200	197.5	100.09	98.82	53.07	49.56	13.22	12.20
AC-Y-1	200	197.5	101.23	103.62	53.31	50.21	12.77	13.03
DS1010-10-	200	197.9	100.65	100.01	53.00	49.93	13.38	12.21
AC-Y-2	200	197.9	100.78	99.74	53.08	49.89	13.58	11.68
DS1010-30-	600	596.8	99.89	99.27	53.44	49.83	13.37	12.08
AC-Y-1	600	596.8	100.13	98.85	53.41	49.92	12.89	12.10
DS1010-30-	600	596.8	100.07	98.80	53.56	49.59	12.80	11.98
AC-Y-2	600	596.8	99.97	98.49	53.36	49.86	13.25	12.32
DS1010-30-	600	598.9	100.53	100.11	53.59	49.81	12.82	12.26
AC-Y-3	600	598.9	99.91	99.60	53.62	49.95	13.31	11.93
DS1010-50-	1000	997.5	99.97	98.97	53.44	49.62	13.07	12.03
AC-Y-1	1000	997.5	100.25	99.55	53.39	49.76	13.10	12.49
DS1010-50-	1000	997.0	100.18	99.24	53.38	50.00	13.60	11.60
AC-Y-2	1000	997.0	100.16	99.37	53.46	49.74	13.12	12.02
DS1010-75-	1500	1497.0	99.81	98.27	53.39	49.10	12.80	11.64
AC-Y-1	1500	1497.0	99.77	98.41	36.27	49.53	12.66	11.66
DS1010-75-	1500	1497.0	99.81	98.27	53.39	49.10	12.80	11.64
AC-Y-2	1500	1497.0	99.77	98.41	52.94	49.53	12.66	11.66
DS1010-75-	1500	1500.0	101.62	102.58	52.89	49.24	12.12	13.27
AC-Y-3	1500	1500.0	101.43	103.27	52.62	49.27	12.04	12.70
DS1010-100-	2000	2000.0	99.79	98.63	53.27	49.34	12.89	11.46
AC-Y-1	2000	2000.0	99.82	99.39	52.91	49.28	13.21	11.29
DS1010-100-	2000	2000.0	99.81	98.27	53.39	49.10	12.80	11.64
AC-Y-2	2000	2000.0	99.77	98.41	52.94	49.53	12.66	11.66
DS1010-100-	2000	2000.0	100.93	100.03	52.20	49.10	11.85	13.20
AC-Y-3	2000	2000.0	100.74	99.81	52.31	48.71	11.13	13.21
DS1010-120-	2500	2500.0	100.96	100.19	53.06	49.75	12.08	13.61

AC-Y-1	2500	2500.0	100.92	100.04	53.00	49.55	12.51	13.53
DS1010-120-	2500	2500.0	100.78	100.05	53.07	49.55	11.82	13.85
AC-Y-2	2500	2500.0	100.92	100.24	53.00	49.52	12.14	13.57
DS1010-150-	3000	3000.0	99.78	98.45	53.46	49.79	13.67	11.55
AC-Y-1	3000	3000.0	100.89	100.27	53.61	49.47	11.73	13.27
DS1010-150-	3000	3000.0	100.71	99.85	53.19	49.37	11.87	12.91
AC-Y-2	3000	3000.0	100.57	99.09	53.27	49.25	11.93	13.25
DS1010-50-	2000	1997.0	99.85	98.63	52.96	49.49	12.71	11.39
AC-X-1	2000	1997.0	99.80	98.67	53.25	49.31	12.67	11.82
DS1010-50-	2000	2000.0	99.75	97.91	52.85	49.58	12.96	11.82
AC-X-2	2000	2000.0	99.74	98.39	53.13	49.43	12.40	11.88
DS1010-75-	3000	3000.0	100.63	99.78	53.45	49.37	11.97	13.07
AC-X-1	3000	3000.0	99.84	98.98	53.90	49.96	11.64	12.92
DS1010-75-	3000	3000.0	99.92	98.46	53.53	49.83	12.76	11.62
AC-X-2	3000	3000.0	100.86	100.46	53.66	49.48	11.45	13.23

Table 3 Geometries of eccentrically compressed specimens

specimen	Nominal length (mm)	Actual length (mm)	web(mm)		flange(mm)		lip(mm)	
			h_1	h_2	b_1	b_2	a_1	a_2
DS1010-50-	1000	996.8	100.02	98.85	53.53	49.79	12.61	11.76
EC1-Y-1	1000	996.8	100.09	98.08	53.36	49.83	13.14	12.17
DS1010-50-	1000	997.0	100.67	99.63	53.64	49.82	13.11	12.13
EC1-Y-2	1000	997.0	100.12	99.67	53.64	49.82	13.11	12.13
DS1010-100-	2000	2000.0	100.74	99.96	52.49	48.80	11.54	13.40
EC1-Y-1	2000	2000.0	100.78	100.08	52.37	49.32	11.94	13.36
DS1010-100-	2000	2000.0	100.93	100.03	52.20	49.10	11.85	13.20
EC1-Y-2	2000	2000.0	70.74	99.81	52.31	48.71	11.13	13.21
DS1010-150-	3000	3000.0	99.72	99.00	53.09	49.45	12.82	11.48
EC1-Y-1	3000	3000.0	99.75	98.53	52.97	49.33	12.76	11.46
DS1010-150-	3000	3000.0	99.76	98.42	52.97	49.47	12.35	11.79
EC1-Y-2	3000	3000.0	99.75	98.28	53.36	49.49	12.71	11.45
DS1010-15-	600	598.0	100.97	101.55	52.21	49.30	11.43	13.51
EC1-X-1	600	598.0	102.14	101.23	52.26	49.87	11.60	13.23
DS1010-15-	600	603.0	100.96	101.43	52.57	49.44	11.54	13.40
EC1-X-2	600	603.0	100.97	101.39	52.81	49.64	11.58	13.27
DS1010-25-	1000	1000.0	101.25	101.59	53.56	50.13	11.54	13.37
EC1-X-1	1000	1000.0	101.07	101.71	53.43	50.27	11.29	13.51
DS1010-25-	1000	1000.0	100.96	101.46	52.09	49.78	11.42	13.69
EC1-X-2	1000	1000.0	101.03	101.56	51.98	49.41	11.47	13.58
DS1010-35-	1400	1396.0	99.75	98.63	52.80	49.64	12.88	11.54
EC1-X-1	1400	1396.0	99.80	98.74	53.04	49.14	12.63	11.38
DS1010-35-	1400	1400.0	101.17	101.93	52.86	49.35	11.54	13.29
EC1-X-2	1400	1400.0	100.63	101.38	52.21	49.15	11.67	13.47
DS1010-50-	2000	2000.0	100.77	100.11	52.36	49.24	11.66	13.26
EC1-X-1	2000	2000.0	101.05	99.89	51.96	49.56	11.97	13.33
DS1010-50-	2000	2000.0	100.74	99.75	52.45	49.08	11.41	13.31
EC1-X-2	2000	2000.0	100.00	98.78	51.44	48.66	11.50	12.74
DS1010-65-	2500	2500.0	100.73	100.04	53.14	49.58	12.28	13.28
EC1-X-1	2500	2500.0	100.78	100.00	52.88	49.50	12.42	13.62
DS1010-65-	2500	2498.0	99.90	98.71	53.37	49.36	12.78	11.36
EC1-X-2	2500	2498.0	99.83	98.44	53.30	49.62	12.43	11.33
DS1010-65-	2500	2498.0	99.90	98.71	53.37	49.36	12.78	11.36
EC1-X-3	2500	2498.0	99.83	98.44	53.30	49.62	12.43	11.33
DS1010-75-	3000	3000.0	99.70	98.51	53.83	49.42	12.75	11.47
EC1-X-1	3000	3000.0	100.81	100.44	53.59	49.68	11.69	13.50

DS1010-75-EC1-X-2	3000	3000.0	100.75	100.06	53.77	49.53	11.78	13.14
	3000	3000.0	101.11	100.76	53.60	49.62	12.04	13.18

Table4 Property of nominal section

Size of specimen	A/mm^2	i_x/mm	i_y/mm	I_x/mm^4	I_y/mm^4
SS1010	218	41.01	18.26	366725	72708
DS1010	436	41.02	20.34	733856	180378

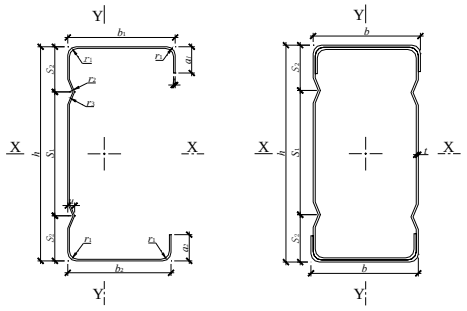

(a) channel section (b) build-up section

Fig.3 Sectional geometries

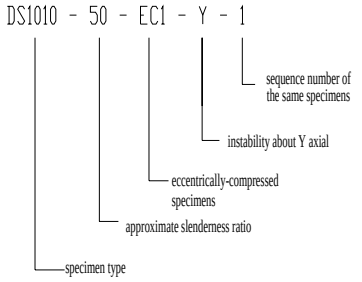

Fig.4 Specimen labeling rule

The 300kN capacity servo-controlled hydraulic testing machine system was used to apply compressive force for the stud specimens with length of 200mm. Hydraulic jack and support frame were used to apply compressive force for the other specimens. Load, strain, and displacement were recorded automatically by a date acquisition instrument and showed directly on the screen of the computer in this system. After geometric and physical alignment completed, compressive loads can be subjected onto specimens by increments until the failure of them. Loading modes include three types, axial compression and eccentrical compression about strong and weak axial. Eccentrical value equals to half of the radius of gyration.

The braces were fixed to prevent the member from bending along Y axis and rotation about X axial for the members bending about the strong axis(X axial).

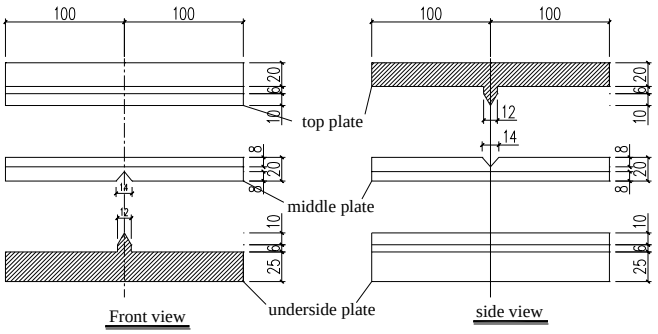

Fig.5 The bidirectional-hinged support

(a)Top support seat (b) below support seat
Fig.6 The actual bidirectional-hinged support

The tested members were bidirectional-hinged at each end supported with three plates, as shown in Fig.5 and Fig.6. A hoop-plate was applied in the test in order to avoid crush occurring at the end of these too thin members as shown in Fig.7.

Strain gauges and lateral displacement transducers were placed at mid-height of the columns, as shown in Fig.8. Furthermore, four axial displacement transducers were employed to measure axial shortening and rotation of support seat. These strain gauges were used for alignment and to confirm buckling stress and experimental loading eccentricity.

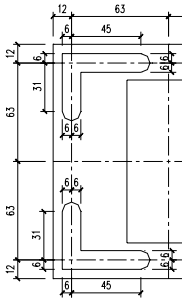

Fig.7 hoop-plate of specimens

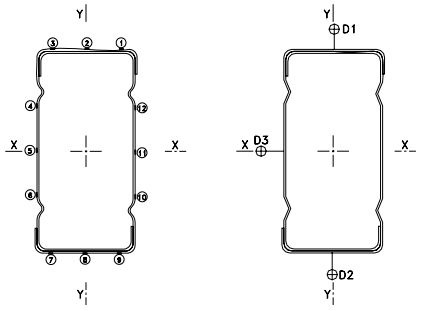

(a)Strain gauges (b) displacement transducer
Fig.8 Gauges arrangement

Test results

Axially compressive columns

(1)The specimens with the length being less than 500mm are considered as stud columns. Load and deformation were linear when load was applied, and the magnitude of the deformation was low. As the load was increased, one single channel column yielded firstly, and another single channel column also yielded subsequently. Then the built-up columns failed.

The cooperative ability of the two single channel columns was weak. The failure mode of stud columns is shown in Fig9a.

(2)The load and deformation of the intermediate columns whose slenderness ratio are less than 50 were linear when load was applied, and the magnitude of the deformation was low. As the load increased gradually to the ultimate load, crippling failure occurred abruptly. The failure mode of intermediate columns is shown in Fig9b.

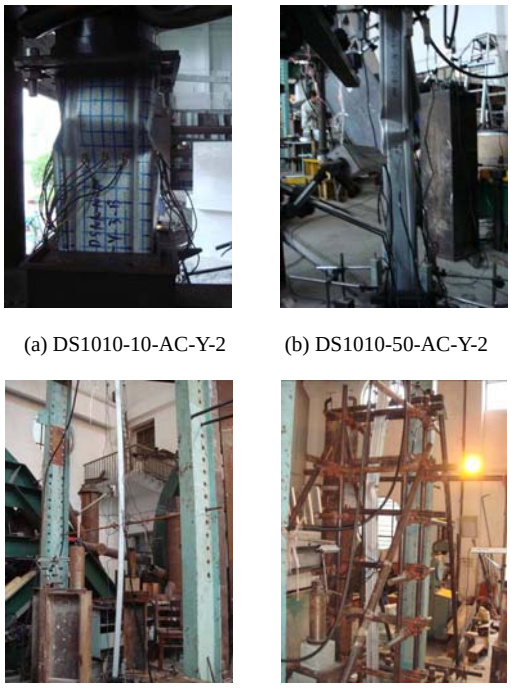

(a) DS1010-10-AC-Y-2 (b) DS1010-50-AC-Y-2

(c) DS1010-150-AC-Y-1 (d) DS1010-75-AC-X-2

Fig.9 Buckling mode of axially compressed specimens

(3)The final failure shapes of the long columns whose slenderness ratio are more than 50 were mainly the overall flexural buckling mode about the weak axial. The load and deformation of the long columns were linear when load was applied. As the load was increased, local buckling occurred in the lips and the larger deformation occurred in the middle of the specimens. And then, the loads were up to the maximum, the flanges and the webs failed. The specimens displayed a significant post-buckling strength reserve. The failure mode of long columns is shown in Fig9c.

(4)Load and deformation of the specimen of instability about the strong axis were linear when load was applied. As the load was increased, local buckling occurred in the web and flange in the middle of the specimens firstly. The deformation increased gradually due to elastic local buckling.

Then the transverse displacement along the Y axial increased, instability about strong axial occurred. The failure mode of columns instability about the strong axis is shown in Fig9d.

(5)The ultimate strength have little different for specimens with different space of connecting screw. The ultimate strength with 300mm in the space of connecting screw were little higher than that of 600mm.

(a)DS1010-50-EC1-Y-1 (b) DS1010-50-EC1-Y-2

Fig.10 Buckling of eccentrically compressed specimens

Eccentrically compressive columns

(1)The failure modes of all specimens were flexural buckling as shown in Fig. 10. The load and deformation of columns were linear when load was applied. As the load increased gradually to the ultimate load, crippling failure occurred abruptly.

(2)As the load was increased, one single channel column yielded firstly, and another single channel column also yielded subsequently for the stud columns. Then the built-up columns failed. The cooperative ability of the two single channel columns is weak.

(3)Local buckling occurred for most of the specimens with eccentricity about weak axial because of the larger width-to-thickness.

(4)The space of connecting screw had nothing to do with the ultimate strength of the specimens.

Comparison of test strengths with design strengths

Introduction of design methods

Three different design methods are used to estimate the ultimate strength of the build-up sections specimens and all use the Chinese current code 'Technical Code of Cold-formed Thin-Walled steel structures' (GB50018-2002) considering the plate-coupling effect: 1) The ultimate strength of the built-up section is equal to the total of the ultimate strength of two single channel sections, 2) The load-carrying capacity is the ultimate strength of built-up section with flange considered as stiffened element, and the thickness of flange of built-up section is equal to the total of thickness of

flange of two single channel sections, 3) The load-carrying capacity is the ultimate strength of built-up section with flange considered as partially stiffened element, and the thickness of flange of built-up section is equal to the total of thickness of flange of two single channel sections.

Design methods compared with test results

The design ultimate load-carrying capacity P_{Cr1}, P_{Cr2}, and P_{Cr3} of the total 21 axially compressive and 19 eccentrically compressive specimens were shown in Table 5 and Table 6, where P_{Cr1} is the total of the ultimate strength of two single channel sections and P_{Cr2}, and P_{Cr3} are the ultimate strength of built-up sections considering the flanges as stiffened element and partially stiffened element based on Chinese current code 'Technical Code of Cold-formed Thin-Walled steel structures' (GB50018-2002) considering the plate-coupling effect respectively. Meanwhile, the ultimate load-carrying capacities of tests are shown in Table 5 and Table 6. The test strengths of the cold-formed steel built-up section axially and eccentrically compressive columns are compared with the nominal design strengths obtained using the Chinese code in different methods, as shown in Fig. 11 and Fig.12 respectively.

Table 5 Comparison of axially compressive columns between test results and calculated values

Specimen	λ	P_t/kN	P_{cr1}/kN	P_{cr2}/kN	P_{cr3}/kN
DS1010-10-AC-Y-1	9.71	118.00	144.73	225.61	183.34
DS1010-10-AC-Y-3	9.73	127.50	144.51	225.27	183.21
DS1010-30-AC-Y-1	33.77	128.78	129.96	198.74	165.61
DS1010-30-AC-Y-2	33.77	137.25	129.92	198.59	165.40
DS1010-30-AC-Y-3	33.87	130.60	129.85	198.85	165.43
DS1010-50-AC-Y-1	53.47	133.58	107.22	165.04	142.15
DS1010-50-AC-Y-2	53.44	121.84	107.14	165.11	142.20
DS1010-75-AC-Y-1	78.02	96.46	71.39	101.25	95.87
DS1010-75-AC-Y-2	78.02	87.25	72.18	105.09	97.46
DS1010-75-AC-Y-3	78.17	87.20	72.66	105.57	98.00
DS1010-100-AC-Y-2	102.75	71.50	49.25	67.81	66.72
DS1010-100-AC-Y-3	102.75	65.46	49.24	67.81	66.73
DS1010-100-AC-Y-4	102.75	65.89	49.38	67.83	66.61
DS1010-120-AC-Y-2	127.34	58.61	35.02	46.17	46.17
DS1010-120-AC-Y-3	127.34	52.88	34.97	46.09	46.09
DS1010-150-AC-Y-1	151.92	39.99	25.78	32.74	32.74
DS1010-150-AC-Y-2	151.92	36.96	25.77	32.67	32.67
DS1010-50-AC-X-1	50.88	136.55	117.52	169.66	145.38
DS1010-50-AC-X-2	50.95	139.30	117.62	169.67	145.57
DS1010-75-AC-X-2	75.33	120.74	85.71	111.96	102.59
DS1010-75-AC-X-3	75.33	130.40	85.59	111.82	102.48

As shown in Table 5 and Fig. 11, the specimens with slenderness ratio less than 50 have less cooperative ability to work together, and the ultimate load-carrying capacity of the specimens with length being 200mm are even lower than that of total of two single channel sections. But the ultimate load-carrying capacity of the specimens with slenderness ratio more than 50 are agreement with the ultimate strength estimated using the Chinese code

considering flange as partially stiffened element and higher 20 percent than the total ultimate strength of two single channel sections.

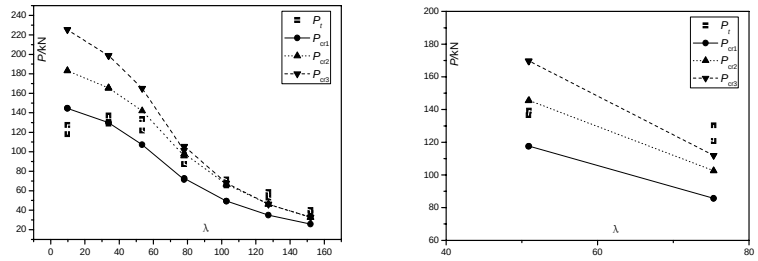

(a) Instability about weak axial (b) Instability about strong axial

Fig.11 Comparison of axially compressed columns between test results and calculated values

Table 6 Comparison of eccentrically compressive columns between test and calculated values

specimen	λ	P_t/kN	P_{cr1}/kN	P_{cr2}/kN	P_{cr3}/kN
DS1010-50-EC1-Y-1	53.6	91.0	82.1	103.0	103.0
DS1010-50-EC1-Y-2	53.6	90.6	82.1	102.8	102.8
DS1010-100-EC1-Y-1	102.8	46.2	36.7	52.3	52.3
DS1010-100-EC1-Y-2	102.8	51.0	36.7	52.2	52.2
DS1010-150-EC1-Y-1	151.9	30.4	18.2	27.6	27.6
DS1010-150-EC1-Y-2	151.9	30.6	18.2	27.6	27.6
DS1010-15-EC1-X-1	16.8	113.8	105.6	144.8	129.6
DS1010-15-EC1-X-2	16.8	108.0	105.6	144.7	129.3
DS1010-25-EC1-X-1	26.6	102.6	99.3	136.0	121.2
DS1010-25-EC1-X-2	26.6	120.0	99.3	136.3	122.5
DS1010-35-EC1-X-1	36.3	94.8	93.4	128.0	115.3
DS1010-35-EC1-X-2	36.3	106.8	93.4	127.0	114.0
DS1010-50-EC1-X-1	51.0	94.0	82.5	111.0	100.4
DS1010-50-EC1-X-2	51.0	90.3	82.5	111.0	100.4
DS1010-65-EC1-X-1	63.1	73.1	71.4	95.5	86.3
DS1010-65-EC1-X-2	63.1	82.6	71.4	95.9	86.7
DS1010-65-EC1-X-3	63.1	83.2	71.4	95.9	86.7
DS1010-75-EC1-X-1	75.3	74.6	59.8	80.3	72.4
DS1010-75-EC1-X-2	75.3	73.8	59.8	79.9	72.0

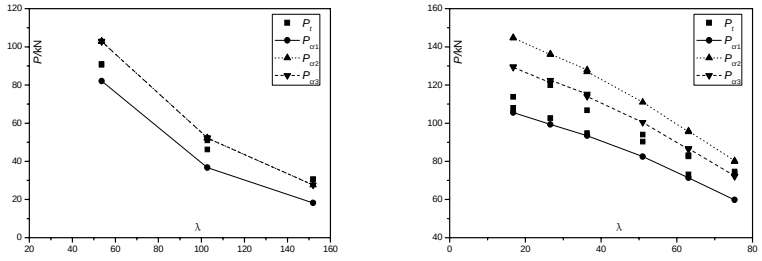

(a) Instability about weak axial (b) Instability about strong axial

Fig.12 Comparison of eccentrically compressive columns between test results and values

As shown in Table 6 and Fig. 12, the test results of the eccentrically compressive specimens are intermediate between that of total of two single channel sections and that predicted using the Chinese code considering flange as stiffened element and higher 10 to 20 percent than the total ultimate strength of two single channel sections.

Proposed design methods

For built-up section column formed with two channel sections with two intermediate stiffeners in the web, a purposed design method is presented to estimate its ultimate strength based on comparison with ultimate strength between test results and results predicted using three different design methods.

For the axially compressed built-up columns, ultimate load-carrying capacity equal to the total of ultimate strength of single open section if the column is instability about strong axial or weak axial with slenderness ratio being less than 50, and the ultimate load-carrying capacity equal to 1.2 times the total of ultimate strength of single open section if the column is instability about weak axial with slenderness ratio being more than 50.

For the eccentrically compressed built-up columns，ultimate load-carrying capacity equal to the total of ultimate strength of single open section if the column is instability about strong axial, and the ultimate load-carrying capacity equal to 1 or 1.2 times the total of ultimate strength of two single columns (eccentricity prone to the web and lip) if the column is instability about weak axial with the slenderness ratio being less or more than 50 respectively.

The comparison with ultimate strength between test results and results predicted using the proposed design method are shown in Fig.13, Fig.14 and Table 7, Table 8 for the axially and eccentrically compressive columns respectively. P_t is test results and P is obtained with proposed design methods.

Table 7 Comparison of axially compressed columns between test results and calculated values by proposed method

specimen	λ	P_t/kN	P/kN	P_t/P	specimen	λ	P_t/kN	P/kN	P_t/P
DS1010-10-AC-Y-1	9.7	118.00	144.73	0.82	DS1010-100-AC-Y-3	102.7	65.46	59.09	1.11
DS1010-10-AC-Y-3	9.7	127.50	144.51	0.88	DS1010-100-AC-Y-4	102.7	65.89	59.26	1.11
DS1010-30-AC-Y-1	33.7	128.78	129.96	0.99	DS1010-120-AC-Y-2	127.3	58.61	42.02	1.39
DS1010-30-AC-Y-2	33.7	137.25	129.92	1.06	DS1010-120-AC-Y-3	127.3	52.88	41.96	1.26
DS1010-30-AC-Y-3	33.8	130.60	129.85	1.01	DS1010-150-AC-Y-1	151.9	39.99	30.94	1.29
DS1010-50-AC-Y-1	53.5	133.58	128.66	1.04	DS1010-150-AC-Y-2	151.9	36.96	30.92	1.20
DS1010-50-AC-Y-2	53.4	121.84	128.57	0.95	DS1010-50-AC-X-1	50.9	136.55	141.02	0.97
DS1010-75-AC-Y-1	78.0	96.46	85.67	1.13	DS1010-50-AC-X-2	50.9	139.30	141.14	0.99
DS1010-75-AC-Y-2	78.0	87.25	86.62	1.01	DS1010-75-AC-X-2	75.3	120.74	102.85	1.17
DS1010-75-AC-Y-3	78.2	87.20	87.19	1.00	DS1010-75-AC-X-3	75.3	130.40	102.71	1.27
DS1010-100-AC-Y-2	102.7	71.50	59.10	1.21	DS1010-100-AC-Y-3	102.7	65.46	59.09	1.11

Table 8 Comparison of eccentrically compressed columns between test results and calculated values by suggested method

specimen	λ	P_t/kN	P/kN	P_t/P	specimen	λ	P_t/kN	P/kN	P_t/P
DS1010-50-EC1-Y-1	53.6	91.0	98.52	0.92	DS1010-35-EC1-X-1	36.3	94.8	93.4	1.01
DS1010-50-EC1-Y-2	53.6	90.6	98.52	0.92	DS1010-35-EC1-X-2	36.3	106.8	93.4	1.14
DS1010-100-EC1-Y-1	102.8	46.2	44.04	1.05	DS1010-50-EC1-X-1	51.0	94.0	82.5	1.14
DS1010-100-EC1-Y-2	102.8	51.0	44.04	1.16	DS1010-50-EC1-X-2	51.0	90.3	82.5	1.09
DS1010-150-EC1-Y-1	151.9	30.4	21.84	1.39	DS1010-65-EC1-X-1	63.1	73.1	71.4	1.02
DS1010-150-EC1-Y-2	151.9	30.6	21.84	1.40	DS1010-65-EC1-X-2	63.1	82.6	71.4	1.16
DS1010-15-EC1-X-1	16.8	113.8	105.6	1.08	DS1010-65-EC1-X-3	63.1	83.2	71.4	1.16
DS1010-15-EC1-X-2	16.8	108.0	105.6	1.02	DS1010-75-EC1-X-1	75.3	74.6	59.8	1.24
DS1010-25-EC1-X-1	26.6	102.6	99.3	1.03	DS1010-75-EC1-X-2	75.3	73.8	59.8	1.23
DS1010-25-EC1-X-2	26.6	120.0	99.3	1.21					

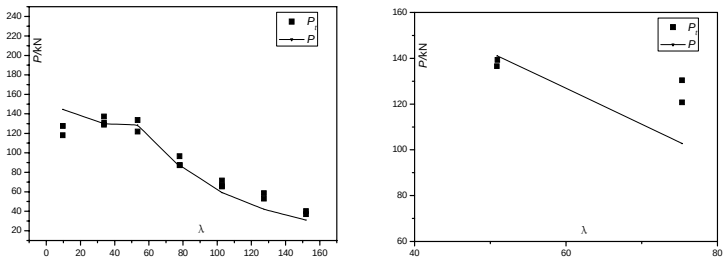

(a) Instability about weak axial (b) Instability about strong axial

Fig.13 Comparison of axially compressed columns between test results and calculated values by suggested method

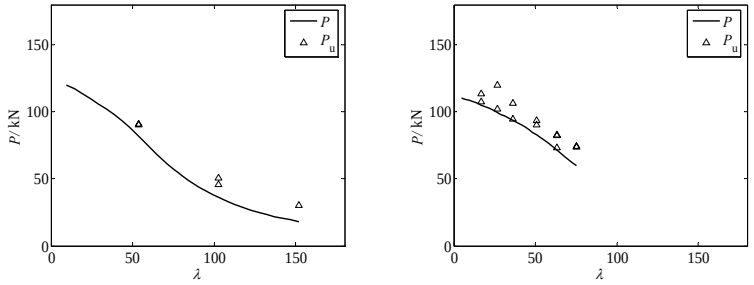

(a) Instability about weak axial (b) Instability about strong axial

Fig.14 Comparison of eccentrically compressed columns between test results and calculated values by suggested method

As shown in Fig.13, Fig.14 and Table 7, Table 8, the ultimate strength estimated using proposed methods are close to the test results for the axially and eccentrically compressed columns respectively. So the proposed methods could be used to calculate the ultimate strength of high strength cold-formed thin-walled built-up section columns safety.

Conclusion

A total 21 axially and 19 eccentrically compressed built-up columns were experimental and theoretical studied in this paper. On the base of comparison with ultimate strength between test results and results calculated using proposed design methods, the follow conclusions can be presented.

(1) The cold-formed thin-walled steel built-up sections column made by connecting two channel sections with two intermediate stiffeners in the web at their flanges using self-drilling screws are found having higher ultimate capacities due to their relatively large torsional rigidity and their favorable radius of gyration about both principal axes.

(2) The cold-formed thin-walled steel built-up sections column with larger slenderness ratio has great cooperative ability to work together. The ultimate strength of built-up section columns can increase 20 percent than the total of ultimate load-carrying capacity of single open section members.

(3) For the axially compressed built-up columns, ultimate load-carrying capacity equal to the total of ultimate strength of single open section if the column is instability about strong axial or weak axial with slenderness ratio being less than 50, and the ultimate load-carrying capacity equal to 1.2 times the total of ultimate strength of single open section if the column is instability about weak axial with slenderness ratio being more than 50.

(4)For the eccentrically compressed built-up columns，ultimate load-carrying capacity equal to the total of ultimate strength of single open section if the column is instability about strong axial, and the ultimate load-carrying capacity equal to 1or 1.2 times the total of ultimate strength of two single columns (eccentricity prone to the web and lip) if the column is instability about weak axial with the slenderness ratio being less or more than 50 respectively.

Notation

a_1, a_2 = width of lip (mm);
A = cross-sectional area (mm^2);
b_1,b_2 = width of flange(mm);
E = initial Young's modulus (MPa);
$f_{0.2}$ = experimental yield stress (MPa);
f_u = ultimate tensile strength(MPa);
h_1, h_2 = width of web (mm);
i_x, i_y = radius of gyration(mm);
I_x, I_y = inertia moment about x and y axial (mm^4);
P_{Cr1}, P_{Cr2}, P_{Cr3}= ultimate strength (kN) calculated by three different method;

P_t = ultimate test load (kN);
P = ultimate strength (kN) calculated by the proposed method;
t = thickness of base metal (mm);
λ = slenderness ratio;
δ = elongation after fracture.

Reference

AS1397 (2001), "Steel sheet and strip-Hot-dip zinc-coated or aluminium/ zinc-coated" *AS1397-2001* Australian Standard, Sydney, Australia.

Dewolf J. T., Peköz, T., Winter, G(1974). "Local and overall buckling of cold-formed members". *Journal of structural engineering,* 100(10):2017–2036.

GB50018 (2002), "Technical code of cold-formed thin-wall steel structures" *GB50018-2002* Chinese Standard, Beijing, China.

GB/T 228(2002), "Metallic materials—Tensile testing—Method of test at ambient temperature" *GB/T 228-2002* Chinese Standard, Beijing, China.

Kwon Y. B., Hancock G. J. (1992), "Tests of cold-formed channels with local and distortional buckling". *Journal of structural engineering*, 118(7):1786–1803.

Lau S. C.W., and Hancock G. J. (1988), "Strength tests and design methods for cold-formed channel columns undergoing distortional buckling", No. R579, School of Civil and Mining Engineering, Univ. of Sydney, Australia.

Mulligan G. P., Peköz T.(1984), " Locally buckled thin-walled columns". *Journal of structural engineering*, 110(11):2635–2654.

Rhodes J., Harvey J. M.(1977), Interaction behaviour of plain channel col-umns under concentric or eccentric loading. Proc. 2nd Int. Colloquium on the Stability of Steel Structures, ECCS, Liege, Belgium, 439–444.

SHEN Z.Y., LI Y.Q. (2008), "Experimental research on load-carrying capac-ity of axially compressed high strength cold-formed thin-walled steel channel columns". Report, Tongji university, BlueScope Steel （Shanghai） Co. Ltd. Shanghai, China.

SHEN Z.Y., LI Y.Q. (2008), "Experimental research on load-carrying capacity of eccentrically compressed high strength cold-formed thin-walled steel channel columns", Report, Tongji university, BlueScope Steel （Shanghai） Co. Ltd. Shanghai, China.

Thomasson P.O. (1978). "Thin-walled C-shaped panels in axial compression", *Journal of structural engineering*, 116(5):1230-1246.

Weng C. C., and Peköz T.(1990). "Compression tests of cold-formed steel columns", *Journal of structural engineering*, 116(5):1230–1246.

Young B., Rasmussen K. J. R.(1998), "Design of lipped channel columns", *Journal of structural engineering*,124(2):140–148.

Young B. (2005), "Experimental investigation of cold-formed steel lipped angle concentrically loaded compression members". *Journal of structural engineering*, 131(9):1390–1396.

Young B., ASCE M., Chen J. (2008), "Design of cold-formed steel built-up closed sections with intermediate stiffeners", *Journal of structural engineering* ,134(5):727-737.

Yu W. W. (2000). "Cold-formed steel design" (3rd Edition), Wiley, New York.

Twentieth International Specialty Conference on Cold-Formed Steel Structures
St. Louis, Missouri, U.S.A., November 3 & 4, 2010

COMPARATIVE BEHAVIOR OF BUILT-UP COLD-FORMED BOX SECTIONS UNDER RIGID AND FLEXIBLE END SUPPORT CONDITIONS

W. Reyes[1] and F.A. Guzman[2]

Abstract:

According to section D1.2 of AISI S100-2007 for compression members composed of two sections in contact whose buckling mode involves shear forces in the connectors, a reduction must be made, KL/r must be replaced by $(KL/r)_m$. This new modified slenderness ratio takes into account the connection weld spacing and the minimum radius of gyration of an individual shape in the built-up member. Under the provisions of section D1.2 a reduction in load capacity must be made for built-up welded box members, which are the subject of this study. An experimental investigation on 48 samples was done addressed to determine the comparative behavior under compression load of box sections composed of two C-section members in contact by seam welds with different weld spacings. The weld spacings in connections in the samples are 100 mm, 300 mm, 600 mm and 900 mm. The first set of 24 studs was tested under a rigid end support condition and the second set of 24 studs was tested using a flexible end support. The length of the samples was 900 mm with a cross-section of 100 mm x 100 mm. This configuration to form box members is widely used for columns or beams as frame and truss members. The base material thickness was 1.5 mm (gauge 16) for 24 samples and 2.0 mm (gauge 14) for the rest. The weld seams were 50 mm long in all cases except on the member ends; where they were 25 mm long. The testing done on the samples did not show a statistical reduction in the ultimate compression load capacity for these members except with a weld spacing of 900 mm and a flexible end support condition. The results of the investigation showed the reduction considered in section D1.2 section of

[1] C.E., M. Sc. Candidate, Research Coordinator, ACERIAS DE COLOMBIA, ACESCO. wreyes@acesco.com

[2] C.E., Ph.D., Associated Professor of the Department of Civil Engineering, Universidad del Norte, Barranquilla, Colombia. faguzman@uninorte.edu.co

AISI S100-2007 not applicable to determine the ultimate load capacity for the rest of the members.

Keywords: Built-up section, modified slenderness ratio, axial strength

1. Introduction

It is a common practice to attach two or more cold-formed single sections in order to obtain greater cross-section properties. The advantages of using cold-formed steel assembled members are well known by the building construction industry. The closed box sections allow spanning greater distances between supports and carrying heavier loads than single C-sections. This connection to conform a box is usually made by seam welds, being an easy and affordable way to do so. It is especially true in countries where the hourly wage rate for welders is low compared to others. In these countries the use of seam welds applied in-situ is widely used as a good means of coupling two single C-sections in order to make up box sections to be used for structural members as columns and beams.
Usually the spacing for these seam-weld connectors ranges from 200 mm through 600 mm for sections no wider than 300 mm. There are no certain specifications to set limits in this regard, however a good criteria supported on experimental studies will lead to an optimum process of attaching two C-sections.

2. Normative

In accordance with section C4.1 of AISI S100-2007 the nominal axial strength shall be calculated by the following equation:

$$P_n = A_e F_n \qquad Eq.1$$

where

A_e = Effective area calculated at stress F_n

F_n shall be calculated as follows:

For $\lambda_c \leq 1.5$ (Inelastic buckling mode)

$$F_n = \left(0.658^{\lambda_c^2}\right) F_y \qquad Eq.2$$

For $\lambda_c > 1.5$ (Elastic buckling mode)

$$F_n = \left[\frac{0.877}{\lambda_c^2}\right] F_y \qquad Eq.3$$

where

$$\lambda_c = \sqrt{\frac{F_y}{F_e}} \qquad Eq.4$$

$F_e =$ The least of the applicable elastic flexural, torsional and flexural-torsional buckling stress

For sections not subject to torsional or flexural-torsional buckling as doubly-symmetric sections or closed cross-sections:

$$F_e = \frac{\pi^2 E}{(KL/r)^2} \qquad Eq.5$$

where

$E =$ Modulus of Elasticity
$K =$ Effective Length factor
$L =$ Laterally unbraced length of member
$r =$ Radius of gyration of full unreduced cross section about axis of buckling

The design specifications for assembled members under compression loads described in the section D1.2 of the AISI S100-2007 modify the overall slenderness ratio of the built-up member according to the spacing between connection seam welds in individual shapes. If shear forces are present in the weld connector due to deformations related to the buckling mode of the member, KL/r, in the $Eq.5$, shall be replaced by $(KL/r)_m$ as follows:

$$\left(\frac{KL}{r}\right)_m = \sqrt{\left(\frac{KL}{r}\right)_o^2 + \left(\frac{a}{r_i}\right)_o^2} \qquad Eq.6$$

Where

$(KL/r)_o =$Overall slenderness of the entire section about built-up member axis
$a =$ Seam weld spacing

r_i = Minimum radius of gyration of full unreduced cross-sectional area of an individual shape in a built-up member

Other studies take a different approach to determine the modified slenderness ratio of a built-up member. The AISC *Specification for Structural Steel Buildings* presents a different expression based on the work of Zahn and Haaijer (1987) to predict the behavior of built-up sections with welded connectors:

For $a/r_i > 50$

$$\left(\frac{KL}{r}\right)_m = \sqrt{\left(\frac{KL}{r}\right)_o^2 + \left(\frac{a}{r_i} - 50\right)^2} \qquad Eq.7$$

For $a/r_i \leq 50$

$$\left(\frac{KL}{r}\right)_m = \left(\frac{KL}{r}\right)_o \qquad Eq.8$$

The work of Zahn and Haaijer concludes that reduction shall be applicable when the value of a/r_i is greater than 50.

3. Experimental Investigation

The study performed by Stone and LaBoube on the behavior of built-up cold-formed steel I-sections (2005) provided the basic guidance to develop all the research on assembled box members.

Figure 1 presents both the typical stud sample for the first set rigidly supported (left) and the typical sample for the second set under a flexible end supporting condition (right). For the flexible support neoprene plates 12 mm thick at each end were used (figure 5). The experimentation focused on ultimate axial strength was performed at Universidad del Norte, Barranquilla (Colombia).

The purpose of this research was to determine the variation of the ultimate load capacity for the built-up member evaluating how it is affected by the variability in the weld spacing (distance “a” in figure 1) taking into consideration different end supporting conditions and also shedding light on determining whether current AISI provisions are applicable for cold-formed box section members.

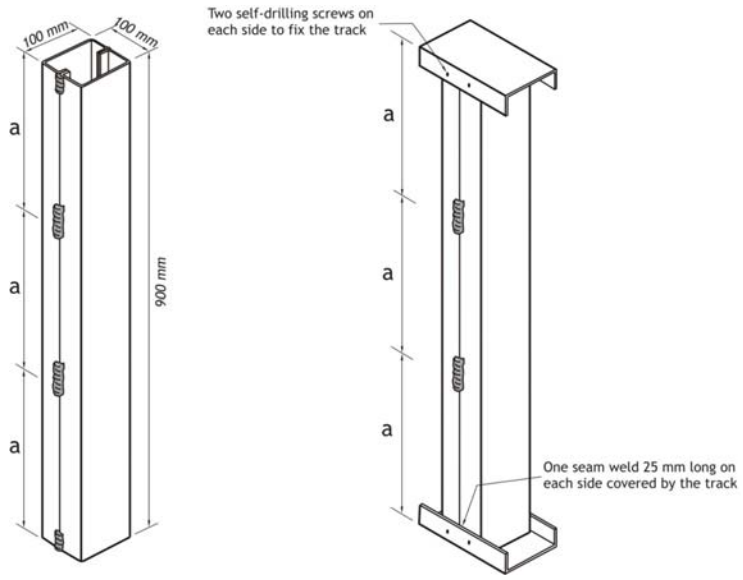

Figure 1 Typical tested sample for rigid end supports (left) and for flexible end supports (right)

The figure 2 shows the dimensions of the cross-section:

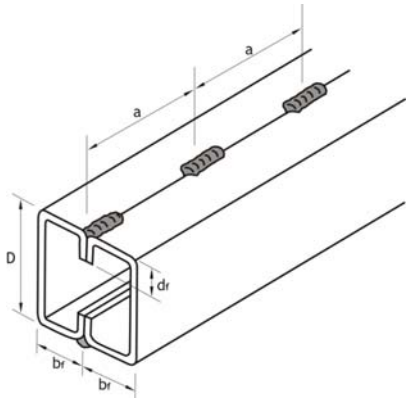

Figure 2 Typical box section

3.1 Section parameters:

The parameters of the typical section are shown in Figure 2 and their magnitudes are shown in table 1.

Table 1 Parameter magnitudes of the cross-section

Parameter	***Magnitude***
Stud Thickness, t	1.5 mm, 2.0 mm
Depth, D	100 mm
Flange, b_f	50 mm
Edge stiffener, d_f	15 mm
Weld seam spacing, a	100 mm, 300 mm, 600 mm, 900 mm

All the samples were 900 mm long and the tracks were made of material 1.5 mm thick. An inelastic buckling mode was expected during the test.

3.2 Test setup

The single C-sections were attached by seam welds of 50 mm long except for the seam welds on the member ends; there they were 25 mm long. The weld spacing of 300 mm is the one commonly used to attach two single C-sections. The welding work was done using electrodes E6011 meeting the specifications of the AWS *(American welding society)*. A complete penetration of the seam welds was guaranteed. Figure 3 shows the work of attaching the two single C-sections.

The first set of 24 samples was directly supported on the plates of the Universal Testing Machine. This condition simulates a rigid support for the structural members. No additional plates were used to test the samples during the first set. The second set of 24 samples was similar to the first but the end support conditions were changed. In this case neoprene plates 15 mm thick were used to simulate a flexible supporting condition (figure 5). Short tracks were fixed by self-drilling screws to the member ends to consider the real support handled in construction.

Figure 3 Attachment of two single sections

Figure 4 Test setup for the rigid support condition

Figure 5 Test setup for the flexible support condition

All the specimens were tested under compression load in the Universal Testing Machine. The criterion to stop the testing was determined by the point where failure load was reached (ultimate load capacity). The test was stopped shortly after reaching that point, at which point the force-deformation curve started decreasing.

3.3 Test procedure

The failure load, P_{test}, is the largest load that a built-up member sustained during a test. The load application was done through the centroid of the section after adjusting the samples on the bearing supports of the machine according to Figures 4 and 5. All the samples were tested under compression loads.

4. Test results

Almost all the specimens with rigid support showed local buckling near the connection welds during the test. Nevertheless they still were able to continue carrying load. The set of samples supported on the neoprene plate mainly showed local buckling at the member ends and several of them showed local buckling near the connection seam welds. Most of the specimens reached failure load after presenting notorious lateral deformations on the walls of the cross-section. At the end of the testing for the first set almost all the specimens presented a smooth curvature as shown in figure 6.

Figure 6 Typical failure mode for rigidly supported specimens

Some of the rigidly supported specimens showed a curvature different from figure 6 before reaching the failure load. Each single C-section curved smoothly in opposite directions one from another following the pattern shown in figure 7. It was mainly presented in samples with weld spacings of 600 mm and 900 mm.

Figure 7 Other failure modes for rigidly supported specimens

On the other hand the second set of specimens on flexible supports showed a local buckling at the ends. The typical curvature is described in Figure 8.

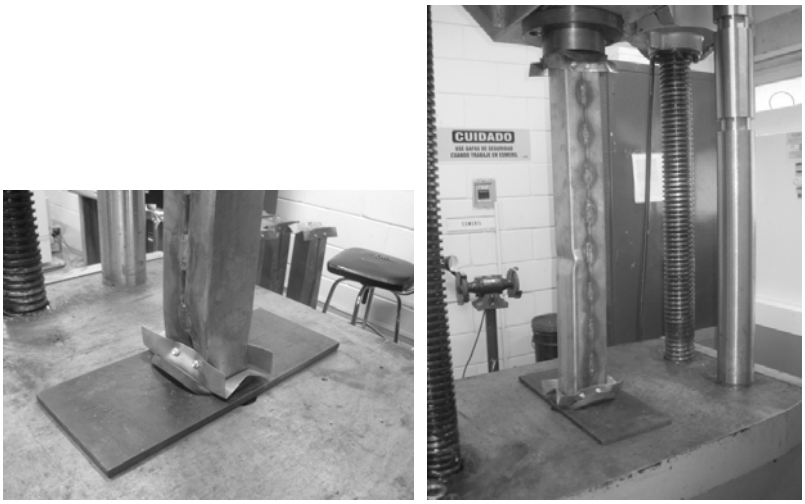

Figure 8 Local buckling at ends for samples with flexible supports (left) and buckling close to seam welds along the specimen (right).

The specimens with seam weld spacing of 900 mm on flexible supports presented a deformation as shown in figure 9. Each C-section member curved in

opposite direction one from another limiting the maximum load capacity of the member. There was a significant statistical reduction in the maximum load capacity for these samples.

Figure 9 Failure curvature mode typical on samples with flexible supports and welds spaced 900 mm (there was a reduction in the maximum load capacity under this configuration)

Table 2 Built-Up Compression-Member Test Results for rigid supports

Reference	Weld spacing (mm)	P_{test1}, Failure load (kN)		
		1st test	2nd test	3rd test
Box 100x100-1.5 mm	100	131.4	141.6	133.2
Box 100x100-1.5 mm	300	133.1	134.0	129.8
Box 100x100-1.5 mm	600	131.0	123.6	121.1
Box 100x100-1.5 mm	900	141.9	130.2	144.3
Box 100x100-2.0 mm	100	240.1	265.4	256.9
Box 100x100-2.0 mm	300	264.0	267.9	264.1
Box 100x100-2.0 mm	600	263.8	246.2	263.9
Box 100x100-2.0 mm	900	257.5	269.6	263.9

Table 3 Built-Up Compression-Member Test Results for flexible supports

Reference	Weld spacing (mm)	P_{test2}, Failure load (kN)		
		1st test	2nd test	3rd test
Box 100x100-1.5 mm	100	131.2	125.8	129.7
Box 100x100-1.5 mm	300	120.9	128.2	121.4
Box 100x100-1.5 mm	600	124.8	121.8	129.7
Box 100x100-1.5 mm	900*	115.8	119.5	118.2
Box 100x100-2.0 mm	100	239.4	247.8	251.8
Box 100x100-2.0 mm	300	250.8	262.9	259.5
Box 100x100-2.0 mm	600	243.6	253.3	254.9
Box 100x100-2.0 mm	900*	238.3	235.8	240.0

*These samples presented a significant statistical reduction in the average of the maximum load capacity

Table 2 and Table 3 summarize the failure loads for each specimen. These tables collect all the maximum loads obtained from the tests for rigid and flexible supports. The results of the first set of samples, under a rigid support condition, are summarized in table 2 (P_{test1}). Table 3 presents the results obtained from the second set of samples according to a flexible support condition (P_{test2}). In figures 10 and 11 several load-deformation curves obtained from tests present combined results from both sets of samples as a comparison of the top loads sustained during tests.

Figure 10 and Figure 11 show the difference presented between the results for samples under flexible versus rigid support conditions. These curves describe the behavior presented during the test for specimens with weld spacing of 900 mm before reaching the failure load (maximum load capacity). For this spacing there was a significant statistical difference between the failure load obtained from rigid and flexible supports for both 1.5 mm and 2.0 mm thicknesses.

5. Data Analysis

The results of failure load from the first set, P_{test1}, and the second test, P_{test2}, were compared one to another. Figure 12 and Figure 13 show separately the difference presented due to the different seam weld spacings in the cold-formed samples from material 1.5 mm and 2.0 mm thick. The P_{test2}/P_{test1} ratio establishes the variation of the maximum load capacity between the second and the first test.

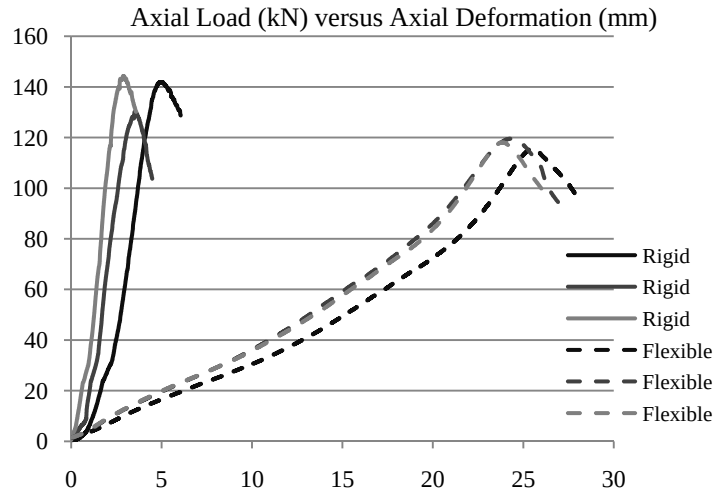

Figure 10 Comparative behavior of samples under Rigid versus Flexible support conditions for box members 100 x 100 – 1.5 mm and weld spacing of 900 mm.

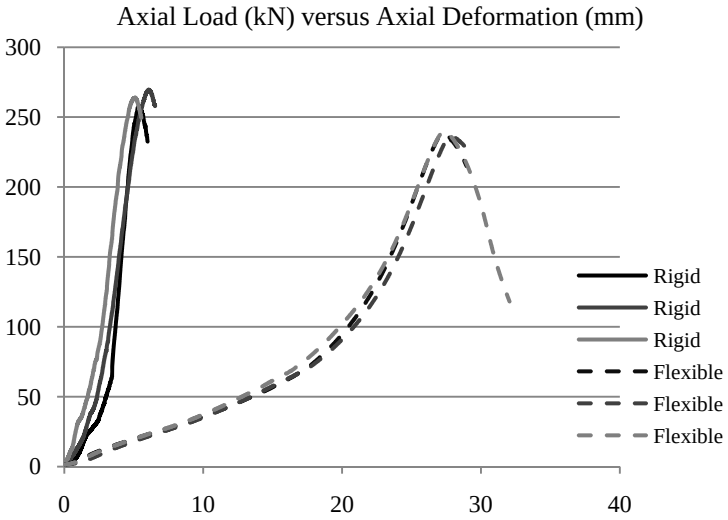

Figure 11 Comparative behavior of samples under Rigid versus Flexible support conditions for box members 100 x 100 - 2.0 mm and weld spacing of 900 mm.

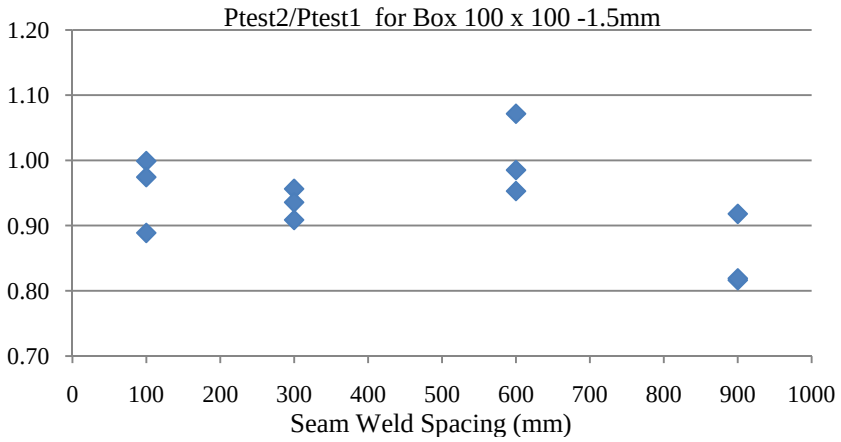

Figure 12 Comparison between the maximum load capacity (failure load) under a flexible and a rigid support condition. Cold-formed box section of 100 mm x 100 mm and thickness material 1.5 mm.

According to the values presented in Figure 12 and a statistical analysis there is no noticeable reduction in the maximum load capacity due to the greater spacing between the seam welds. For both end support conditions the statistical values of failure load are about the same magnitude except for the 900 mm spacing with a flexible end support. This latter spacing showed a reduced capacity with a flexible support compared to that with an end rigid support. The reduction considered in the section D1.2 of the North American Specification (AISI S100-2007) due to the weld spacing would not be applicable to predict the failure load up to a weld spacing of 600 mm no matter the type of support. In other words, the actual overall slenderness ratio of the entire section might not be modified due to the weld spacing as it is less than or equal to 600 mm.

For the seam weld spacing of 900 mm the results obtained from the second set of samples with flexible supports are, by an average of 15%, below the values obtained with rigid supports for the material 1.5 mm thick. This indicates that it may be necessary to use a reduction in the load capacity, using the same weld spacing or greater, following the provisions of section D1.2 of the American Specification.

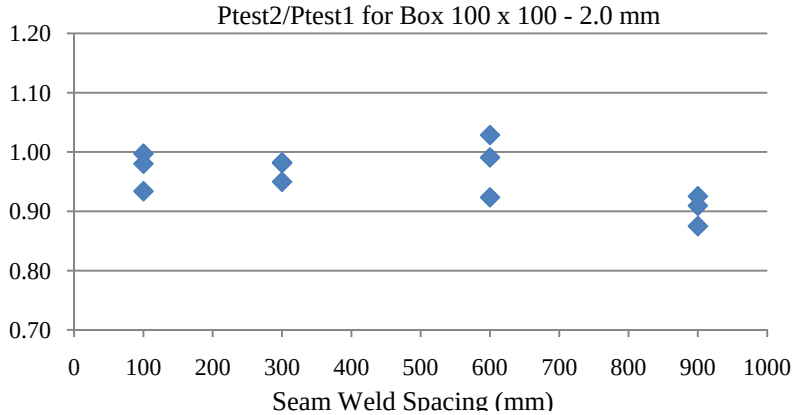

Figure 13 Comparison between the maximum load capacity (failure load) under a flexible and a rigid support condition. Cold-formed box section of 100 mm x 100 mm and thickness material 2.0 mm.

According to the values presented in Figure 13 and a statistical analysis there is no noticeable reduction in the maximum load capacity due to the greater spacing between the seam welds. For both end support conditions the statistical values of failure load are about the same magnitude except for the 900 mm spacing with a flexible end support. This latter spacing showed a reduced capacity with a flexible support compared to that with an end rigid support. The reduction considered in section D1.2 of the North American Specification (AISI S100-2007) due to the weld spacing would not be applicable to predict the failure load up to a weld spacing of 600 mm no matter the type of support. In other words, the actual overall slenderness ratio of the entire section might not be modified due to the weld spacing as it is less than or equal to 600 mm.

For the seam weld spacing of 900 mm the results obtained from the second set of samples with flexible supports are, by an average of 10%, below the values obtained with rigid supports for the material 2.0 mm thick. This indicates that it may be necessary to use a reduction in the load capacity, using the same weld spacing or greater, following the provisions of section D1.2 of the American Specification.

6. Conclusions

The analysis of the results obtained from the 48 specimens shows that the modified slenderness ratio is not always necessary for material 1.5 mm and 2.0

mm thick and therefore the actual slenderness ratio could be used to compute the ultimate load capacity for these structural members if the seam weld spacing is less than or equal to 600 mm since there is not a significant statistical reduction in the failure load in laboratory tests.

The values were slightly affected by the type of support but this reduction did not represent a significant statistical difference except for the samples on flexible supports with a seam weld spacing of 900 mm. Disregarding this latter spacing there is no need to use the modified slenderness ratio to determine the maximum load capacity of the members under consideration no matter the type of support.

7. Acknowledgments

ACERIAS DE COLOMBIA, ACESCO & CIA S.C.A., PIMSA Parque Industrial Malambo, Malambo, Atlántico, Colombia, www.acesco.com .
Garza, Luis, M. Sc., Associated Professor of the Department of Civil Engineering, Universidad Nacional de Medellín, Colombia, lgarza@unal.edu.co
LaBoube, Roger, Ph. D, Department of Civil Engineering, University of Missouri-Rolla, Rolla, MO, USA, laboube@mst.edu
Tests and Materials Laboratory of the Universidad del Norte, Department of Mechanical Engineering, Barranquilla, Colombia, www.uninorte.edu.co

8. References

American Institute of Steel Construction, Inc., AISC (2005) “Manual of Steel Construction, Load and Resistance Factor Design” Chicago, IL.
American Iron and Steel Institute, AISI (2007). “North American Specification for the Design of Cold-Formed Steel Structural Members”. Washington, D.C.
American Standard of Testing and Materials A370-97, ASTM (1997) “Standard Test Methods and Definitions for Mechanical Testing of Steel Products”
Duan et al (2002) “Effect of Compound Buckling on Compression Strength of Built-Up Members” Engineering Journal/First Quarter, Pages 30-37
Sato, A. and Uang, C. (2007) “Modified Slenderness Ratio for Built-Up Members” Engineering Journal/Third Quarter, Pages 267-80.
Stone, T.A. and LaBoube, R.A. (2005) “Thin-Walled Structures, 43 (2005), Elsevier Ltd.”

Twentieth International Specialty Conference on Cold-Formed Steel Structures
St. Louis, Missouri, U.S.A., November 3 & 4, 2010

THEORETICAL ANALYSIS OF COLD-FORMED STEEL BATTENED DOUBLE ANGLE MEMBERS UNDER COMPRESSION

W. F. Maia[1], J. Munaiar Neto[2], and M. Malite[2]

Abstract

In Brazil, battened double angle system is one of the systems most used in light truss, however, there are not any specific studies on its behavior, resulting in the fact that the standard procedures do not provide subsidies for the design of this section. Moreover, cold-formed steel simple angles under compression, mostly with slender legs, have an interesting structural behavior compared to other cold-formed steel shapes. Two critical modes are observed in the elastic stability analysis: (i) global flexural mode in the case of longer members and (ii) a coincident local-plate/global flexural-torsional mode, which is critical for shorter members. Studying the behavior of double angle members is interesting, because in this case, besides the critical modes of the single angle, they also show critical modes, due to the presence of the batten plates that sometimes interfere with the behavior of the system. In this work, a nonlinear numerical analysis on the behavior of double angle in battened system is presented. The number of batten plates was varied studying their effectiveness in the nominal axial strength. The sensitivity of the members to initial geometric imperfections was also analyzed. Except for the thin angle specimen (t = 1.5 mm) the results obtained from the nonlinear analysis showed that the presence of the batten plates significantly increased the nominal axial strength of the members. However for an increased number of batten plates the nominal axial strength of the members remained almost constant. It was observed that the members were more sensitive to initial geometric imperfections increasing that to the number of batten plates.

[1]Graduate Student, [2]Professor, Department of Structural Engineering – School of Engineering of Sao Carlos – University of Sao Paulo – Av. Trabalhador Sao-Carlense, 400 – CEP 13566-590 – Sao Carlos, SP, Brazil – Tel.: +55 16 3373 9468
e-mails: wfmaia@sc.usp.br; jmunaiar@sc.usp.br; mamalite@sc.usp.br

1. Introduction

Members made of double angles within a battened system, consist of two identical sections which are placed parallely. They are slightly separated and linked with each other just in some points by batten plates. The here shown system is often used, mainly in light trusses, however, it is difficult to find specific studies about their behavior. Consequently the existing standard procedures do not offer subsidies for the project of this structural component. Besides, simple angles which are exposed to compression show a particular behavior if compared to other sections. Analysing the elastic stability one can observe two critical modes, (i) the flexural mode in longer members and (ii) the coincident local-plate/global flexural-torsional mode (in the following called local/torsional mode), which is seen in shorter members (Maia et.al. (2008)). It is highly relevant to study the behavior of members made of double angles, as there can be seen buckling in the members, caused by the batten plates, which tend to modify the behavior of the system.

This paper deals with a numerical analysis about the behavior of members of double angles with batten plates, using either simple or lipped angles. The analyses were done using Ansys (1997). We varied the number of batten plates in order to study their efficiency in the nominal axial strength of the members. The results from this analysis show that it could be interesting to carry out deeper studies for a better understanding of member-associated phenomena, especially for eccentric compression.

In order to compare the results, two design procedures based on ANSI/AISI S100 (2007) were used, considering axial compression. First each angle was considered as a single member, independently from batten plates, considering local, flexural-torsional and flexural buckling. In the second procedure the double angle was analysed based only on local and flexural buckling in relation to the minor main axis (x-axis – see figure 1).

2. Numerical analysis

The numerical simulations were carried out with FEM, using the program Ansys v9.0. The element SHELL 181 was used to model the sections, batten plates and the application device of the load. The element is ideal for the non-linear analysis of thin shells exposed to large strains and rotations.

There are results for two sections of the simple double angle and one section of the lipped double angle with load applied to the legs. Initially simulations were carried out where centred load was applied. After that the applied load was

moved to the legs, which actually happens in reality. The analyses did not indicate significant differences concerning the models where load was applied to the centre or to the legs that is why in this article the latter was chosen to represent the results.

In all simulations it was paid attention to the fact that the nodes of the batten plates coincided with the nodes of the sections, guaranteeing the compatibilization of their displacement. The same procedure was adopted at the extremities, i.e. the nodes of the channel section agreed with the nodes of the angles. All the elements were kind of square, with sides of approximately 1cm, except for the edges and the lips which each had been divided in two equal parts. All the sections were built with the dimensions of the midline and using round edges with a radius of 1.5 times thickness. The batten plates were adapted to the width and thickness of the angles, using the same material. The simulations were carried out with fixed extremities, only allowing the rotation in relation to the minor axis (x-axis). In order to apply load a line through the centroid was created in the double angle (x-axis). The longitudinal displacement of the nodes in that line was the same in all nodes.

In the present analyses we evaluated the sensibility of the members in relation to the initial geometric imperfections. Furthermore the number of batten plates was varied during the studies in order to reflect on their efficiency in the nominal axial strength towards the member compression. Regarding the initial geometric imperfections for the simple double angles we adopted imperfections type 2 associated to the coincident local/torsional mode, whereas for the lipped double angle imperfections type 1 associated to the local mode and type 2 associated to the flexural-torsional mode, according to Schafer & Peköz (1998). For the imperfection associated to the flexural mode one adopted $L_c/1500$. In the simulations where one did not use the imperfection associated to the coincident local/torsional, local and flexural-torsional mode, there was also not associated any flexural mode.

Figure 1 shows an overview of the system with batten plates and the position of the angles. In Table 1 the analysed angles and the geometric properties are presented.

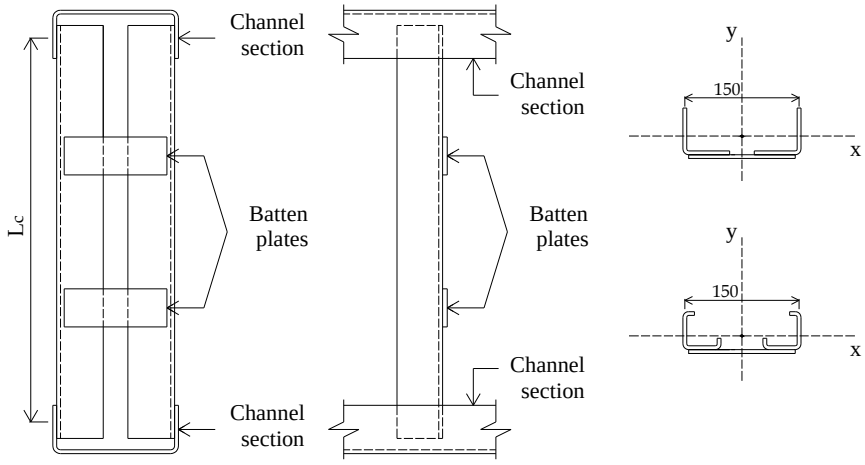

Front view **Side view** **Double angle section**

Figure 1 – Overview member in battened system

Table 1 – Sections and geometric properties

Section	Leg (mm)	Lip (mm)	Thickness (mm)	Area (cm^2)	I_x (cm^4)
2L 60x1.50	60	-	1.50	3.53	12.93
2L 60x3.00	60	-	3.00	6.90	24.75
2Le 50x15x1.50	50	15	1.50	3.68	12.02

3. Results

In the Tables 2 to 4 and the Figures 2 to 12 the results are shown, regarding the analyses of the sensibility towards the initial geometric imperfections compared to theoretical procedures.

Table 2 – Sensibility analysis of initial geometric imperfections: section 2L 60x1.50

L_c (mm)	Batten plates	Imperfections (local/torsional and flexural)	P_{FE} (kN)	Failure mode	P_{FE}/P_y
600 (λ_x=31)	0	0 and 0	41.7	LT+F*	0.43
		0.64t and L_c/1500	39.8	LT+F*	0.41
		1.55t and L_c/1500	34.5	LT+F*	0.36
	2	0 and 0	34.8	LT	0.36
		0.64t and L_c/1500	33.0	LT	0.34
		1.55t and L_c/1500	31.6	LT	0.33
	4	0 and 0	35.3	LT	0.37
		0.64t and L_c/1500	32.5	LT	0.34
		1.55t and L_c/1500	30.3	LT	0.31
1200 (λ_x=63)	0	0 and 0	29.4	LT+F*	0.30
		0.64t and L_c/1500	29.3	LT+F*	0.30
		1.55t and L_c/1500	NC	-	-
	2	0 and 0	30.2	LT+F	0.31
		0.64t and L_c/1500	27.9	LT+F	0.29
		1.55t and L_c/1500	26.9	LT+F	0.28
	5	0 and 0	30.0	LT+F	0.31
		0.64t and L_c/1500	26.8	LT+F	0.28
		1.55t and L_c/1500	24.4	LT+F	0.25
	7	0 and 0	31.1	LT+F	0.32
		0.64t and L_c/1500	25.4	LT+F	0.26
		1.55t and L_c/1500	22.3	LT+F	0.23
1800 (λ_x=94)	0	0 and 0	19.8	LT+F*	0.21
		0.64t and L_c/1500	NC	-	-
		1.55t and L_c/1500	NC	-	-
	1	0 and 0	23.9	LT+F	0.25
		0.64t and L_c/1500	23.2	LT+F	0.24
		1.55t and L_c/1500	22.6	LT+F	0.23
	2	0 and 0	25.0	LT+F	0.26
		0.64t and L_c/1500	22.7	LT+F	0.24
		1.55t and L_c/1500	21.9	LT+F	0.23
	6	0 and 0	26.0	LT+F	0.27
		0.64t and L_c/1500	22.4	LT+F	0.23
		1.55t and L_c/1500	20.0	LT+F	0.21
	11	0 and 0	27.1	LT+F	0.28
		0.64t and L_c/1500	20.5	LT+F	0.21
		1.55t and L_c/1500	16.9	LT+F	0.18

$P_y = A \cdot F_y$ = 96.4 kN – Squash load (F_y = 273 MPa)
P_{FE} = ultimate load from finite element analysis
L_c = member length ($\lambda_x = L_c/r_x$)
LT = coincident local/torsional mode (single angle), F* = flexural mode (single angle), F = flexural mode (double angle), NC = FE analysis did not converge

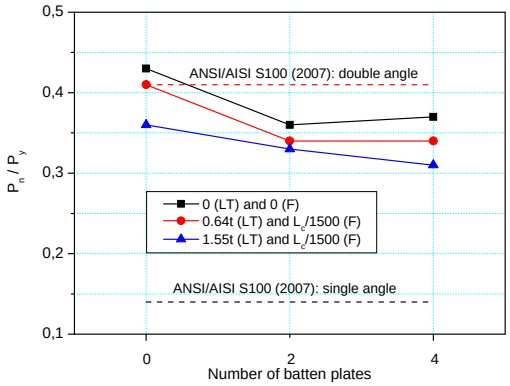

Figure 2 – Sensibility analysis of imperfections: section 2L 60x1.50 (L_c = 600 mm)

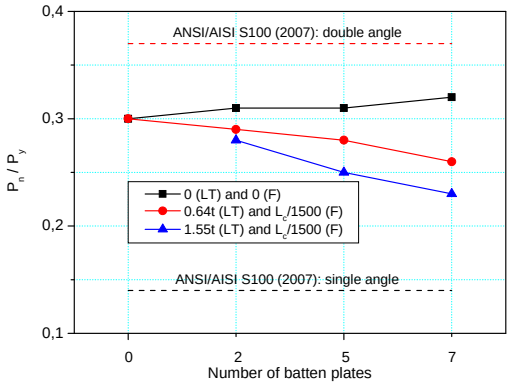

Figure 3 – Sensibility analysis of imperfections: section 2L 60x1.50 (L_c = 1200 mm)

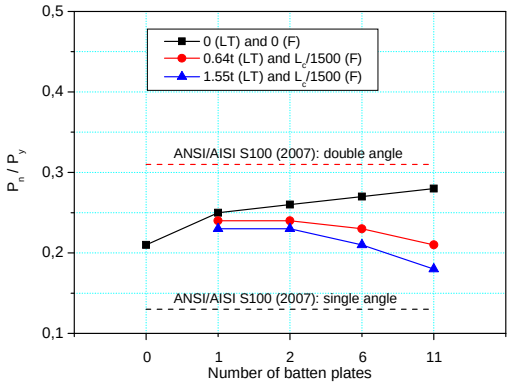

Figure 4 – Sensibility analysis of imperfections: section 2L 60x1.50 (L_c = 1800 mm)

Table 3 – Sensibility analysis of initial geometric imperfections: section 2L 60x3.00

L_c (mm)	Batten plates	Imperfections (local/torsional and flexural)	P_{FE} (kN)	Failure mode	P_{FE}/P_y
600 (λ_x=32)	0	0 and 0	94.6	LT+F*	0.50
		0.64t and L_c/1500	NC	-	-
		1.55t and L_c/1500	NC	-	-
	1	0 and 0	133.1	LT+F	0.71
		0.64t and L_c/1500	111.6	LT+F	0.59
		1.55t and L_c/1500	96.8	LT+F	0.51
	2	0 and 0	143.5	LT+F	0.76
		0.64t and L_c/1500	126.4	LT	0.67
		1.55t and L_c/1500	108.8	LT+F	0.58
	4	0 and 0	150.9	LT+F	0.80
		0.64t and L_c/1500	122.0	LT+F	0.65
		1.55t and L_c/1500	96.9	LT+F	0.51
1200 (λ_x=63)	0	0 and 0	67.8	LT+F*	0.36
		0.64t and L_c/1500	NC	-	-
		1.55t and L_c/1500	NC	-	-
	1	0 and 0	118.2	LT+F	0.63
		0.64t and L_c/1500	102.2	LT+F	0.54
		1.55t and L_c/1500	92.9	LT+F	0.49
	2	0 and 0	127.5	LT+F	0.68
		0.64t and L_c/1500	112.5	LT+F	0.60
		1.55t and L_c/1500	99.9	LT+F	0.53
	5	0 and 0	142.6	F	0.76
		0.64t and L_c/1500	103.5	LT+F	0.55
		1.55t and L_c/1500	81.4	LT+F	0.43
	7	0 and 0	145.4	F	0.77
		0.64t and L_c/1500	97.0	LT+F	0.51
		1.55t and L_c/1500	71.9	LT+F	0.38
1800 (λ_x=95)	0	0 and 0	47.1	LT+F*	0.25
		0.64t and L_c/1500	NC	-	-
		1.55t and L_c/1500	NC	-	-
	1	0 and 0	97.4	LT+F	0.52
		0.64t and L_c/1500	88.8	LT+F	0.47
		1.55t and L_c/1500	83.9	LT+F	0.45
	2	0 and 0	111.0	LT+F	0.59
		0.64t and L_c/1500	94.3	LT+F	0.50
		1.55t and L_c/1500	85.9	LT+F	0.46

See next page…

… continuing Table 3

L_c (mm)	Batten plates	Imperfections (local/torsional and flexural)	P_{FE} (kN)	Failure mode	P_{FE}/P_y
1800 (λ_x=95)	4	0 and 0	112.9	F	0.60
		0.64t and L_c/1500	91.7	LT+F	0.49
		1.55t and L_c/1500	81.8	LT+F	0.43
	6	0 and 0	108.8	F	0.58
		0.64t and L_c/1500	84.1	LT+F	0.45
		1.55t and L_c/1500	67.9	LT+F	0.36
	11	0 and 0	102.4	F	0.54
		0.64t and L_c/1500	74.4	LT+F	0.39
		1.55t and L_c/1500	53.0	LT+F	0.28
2400 (λ_x=127)	0	0 and 0	33.1	F*	0.18
		0.64t and L_c/1500	NC	-	-
		1.55t and L_c/1500	NC	-	-
	1	0 and 0	68.0	LT+F	0.36
		0.64t and L_c/1500	61.8	LT+F	0.33
		1.55t and L_c/1500	61.9	LT+F	0.33
	2	0 and 0	76.5	LT+F	0.41
		0.64t and L_c/1500	67.2	LT+F	0.36
		1.55t and L_c/1500	65.6	LT+F	0.35
	4	0 and 0	75.1	F	0.40
		0.64t and L_c/1500	63.8	LT+F	0.34
		1.55t and L_c/1500	57.3	LT+F	0.30
	8	0 and 0	72.9	F	0.39
		0.64t and L_c/1500	60.7	LT+F	0.32
		1.55t and L_c/1500	50.8	LT+F	0.27

$P_y = A \cdot F_y$ = 188.4 kN – Squash load (F_y = 273 MPa)
P_{FE} = ultimate load from finite element analysis
L_c = member length ($\lambda_x = L_c/r_x$)
LT = coincident local/torsional mode (single angle)
F* = flexural mode (single angle)
F = flexural mode (double angle)
NC = FE analysis did not converge

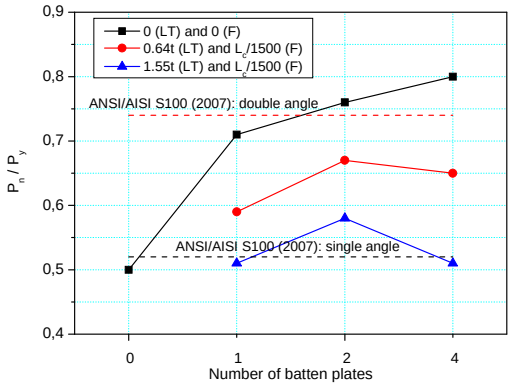

Figure 5 – Sensibility analysis of imperfections: section 2L 60x3.00 (L_c = 600 mm)

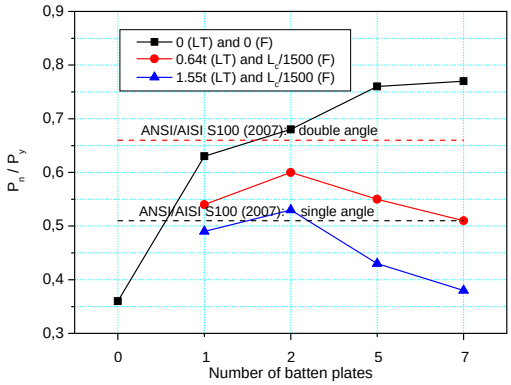

Figure 6 – Sensibility analysis of imperfections: section 2L 60x3.00 (L_c = 1200 mm)

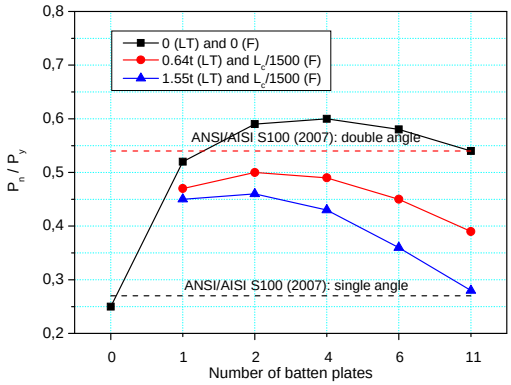

Figure 7 – Sensibility analysis of imperfections: section 2L 60x3.00 (L_c = 1800 mm)

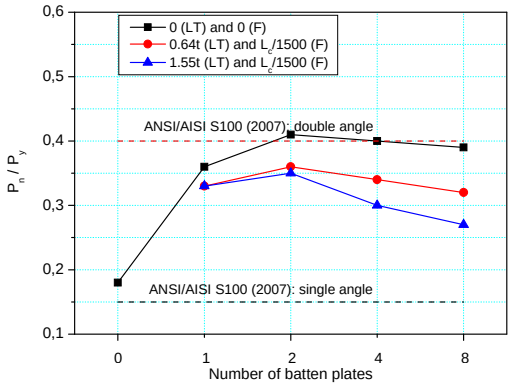

Figure 8 – Sensibility analysis of imperfections: section 2L 60x3.00 (L_c = 2400 mm)

Table 4 – Sensibility analysis of initial geometric imperfections: section 2Le 50x15x1.50

L_c (mm)	Batten plates	Imperfections (local; flexural-torsional and flexural)	P_{FE} (kN)	Failure mode	P_{FE}/P_y
600 (λ_x=33)	0	0; 0 and 0	47.7	FT+F*	0.47
		0.14t; 0.64t and L_c/1500	NC	-	-
	1	0; 0 and 0	62.0	FT+F	0.62
		0.14t; 0.64t and L_c/1500	58.5	FT+F	0.58
	2	0; 0 and 0	64.0	FT+F	0.64
		0.14t; 0.64t and L_c/1500	61.1	FT+F	0.61
	4	0; 0 and 0	65.3	FT+F	0.65
		0.14t; 0.64t and L_c/1500	62.4	FT+F	0.62
1200 (λ_x=66)	0	0; 0 and 0	34.3	FT+F*	0.34
		0.14t; 0.64t and L_c/1500	NC	-	-
	1	0; 0 and 0	46.5	FT+F	0.46
		0.14t; 0.64t and L_c/1500	44.5	FT+F	0.44
	2	0; 0 and 0	54.7	FT+F	0.54
		0.14t; 0.64t and L_c/1500	48.4	FT+F	0.48
	4	0; 0 and 0	62.6	FT+F	0.62
		0.14t; 0.64t and L_c/1500	59.7	FT+F	0.59
	6	0; 0 and 0	64.0	FT+F	0.64
		0.14t; 0.64t and L_c/1500	62.4	FT+F	0.62
1800 (λ_x=100)	0	0; 0 and 0	23.8	FT+F*	0.24
		0.14t; 0.64t and L_c/1500	NC	-	-
	1	0; 0 and 0	38.2	FT+F	0.38
		0.14t; 0.64t and L_c/1500	30.1	FT+F	0.30
	2	0; 0 and 0	45.3	FT+F	0.45
		0.14t; 0.64t and L_c/1500	36.3	FT+F	0.36

See next page…

… continuing Table 4

L_c (mm)	Batten plates	Imperfections (local; flexural-torsional and flexural)	P_{FE} (kN)	Failure mode	P_{FE}/P_y
1800 (λ_x=100)	4	0; 0 and 0	56.4	FT+F	0.56
		0.14t; 0.64t and L_c/1500	47.6	FT+F	0.47
	6	0; 0 and 0	54.5	F	0.54
		0.14t; 0.64t and L_c/1500	47.1	F	0.47
	8	0; 0 and 0	53.4	F	0.53
		0.14t; 0.64t and L_c/1500	46.7	F	0.46
2400 (λ_x=133)	0	0; 0 and 0	16.6	FT+F*	0.17
		0.14t; 0.64t and L_c/1500	NC	-	-
	1	0; 0 and 0	29.4	FT+F	0.29
		0.14t; 0.64t and L_c/1500	26.7	FT+F	0.27
	2	0; 0 and 0	32.8	FT+F	0.33
		0.14t; 0.64t and L_c/1500	29.7	FT+F	0.30
	4	0; 0 and 0	36.1	F	0.36
		0.14t; 0.64t and L_c/1500	31.0	F	0.31
	6	0; 0 and 0	36.0	F	0.36
		0.14t; 0.64t and L_c/1500	32.7	F	0.33
	8	0; 0 and 0	35.8	F	0.36
		0.14t; 0.64t and L_c/1500	32.7	F	0.33

$P_y = A \cdot F_y$ = 100.5 kN – Squash load (F_y = 273 MPa)
P_{FE} = ultimate load from finite element analysis
L_c = member length ($\lambda_x = L_c/r_x$)
FT = flexural-torsional mode (single angle)
F* = flexural mode (single angle)
F = flexural mode (double angle)
NC = FE analysis did not converge

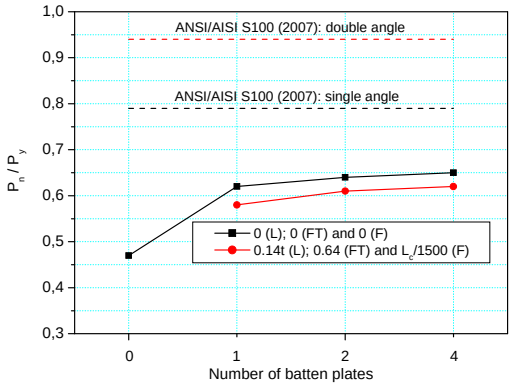

Figure 9 – Sensibility analysis of imperfections: section 2Le 50x15x1.50 (L_c = 600 mm)

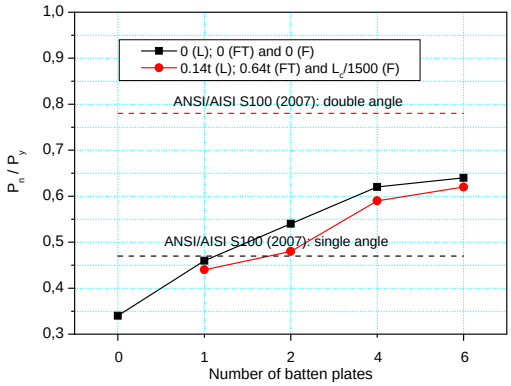

Figure 10 – Sensibility analysis of imperfections: section 2Le 50x15x1.50 (L_c = 1200 mm)

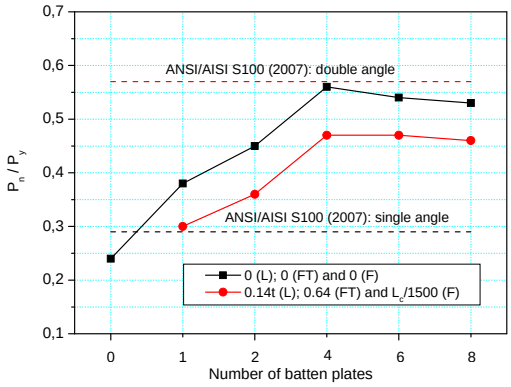

Figure 11 – Sensibility analysis of imperfections: section 2Le 50x15x1.50 (L_c = 1800 mm)

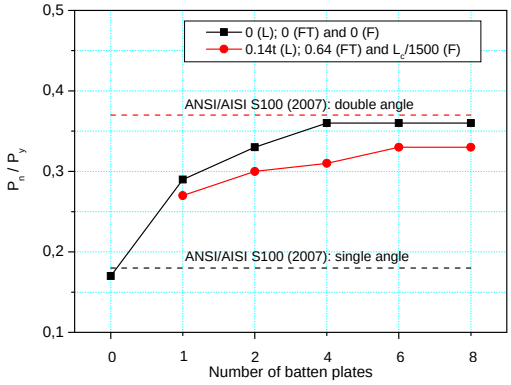

Figure 12 – Sensibility analysis of imperfections: section 2Le 50x15x1.50 (L_c = 2400 mm)

Figure 13 shows buckling modes obseved in the analyses of the simple or the lipped double angles for different numbers of batten plates.

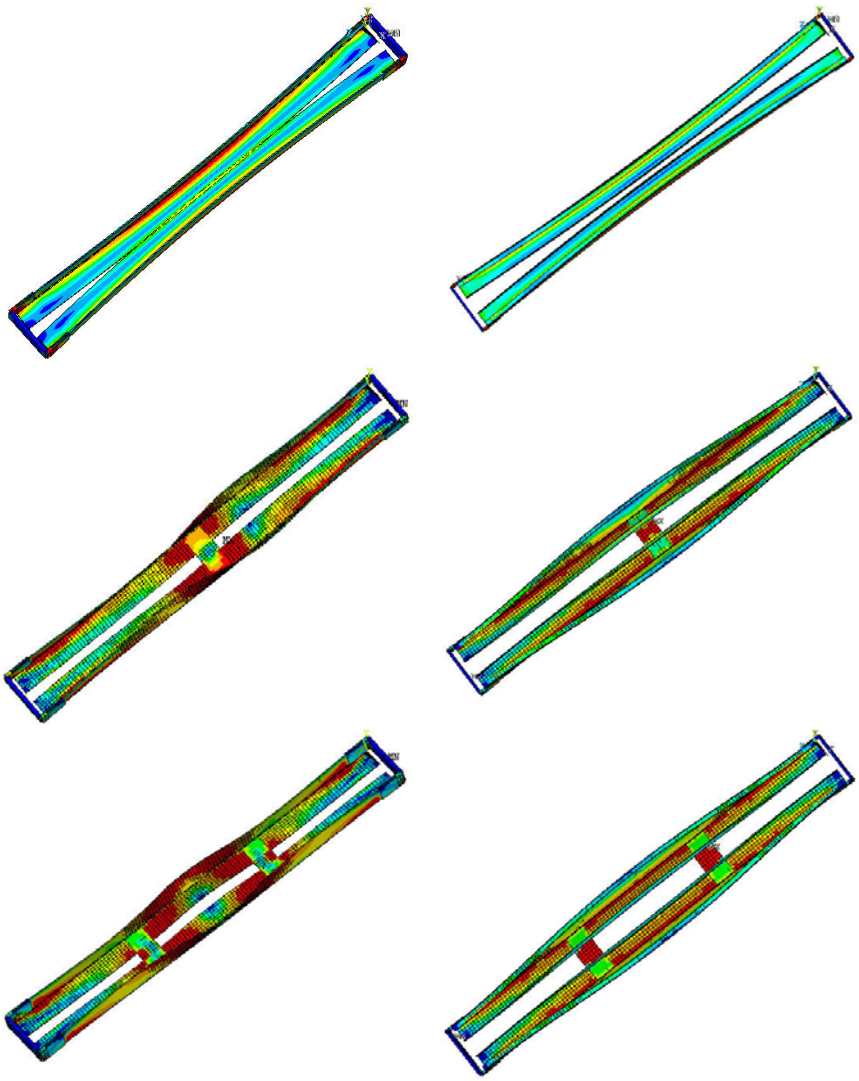

(a) **(b)**

Figure 13 – Buckling modes observed in the numerical analysis
(a) simple double angle (b) lipped double angle

The results of the analysis of the members in simple double angles (2L 60x1.50) shows that the insertion of batten plates did generally not improve the behavior of the members. On the contrary, in some cases it even worsened it, mainly in members with high imperfections of the local/torsional type (LT). This behavior can be explained by the fact that here we deal with a section of an elevated width-thickness ratio. The most dominant mode of buckling was the local/torsional one, and because of this the increase of the local/torsional imperfection can have induced the early buckling. Moreover, with the increasing number of batten plates there was a greater shift of the effective centroid of the section, a fact that was not taken into consideration in the analysis, and created a number of effects, i.e. the initial geometric imperfection and the shift of the centroid of the section. During the analyses the most critical combination was considered.

For the 2L 60x3.00 section the insertion of batten plates raised the nominal axial strength significantly, however, from a certain number on one could observe that the nominal axial strength stayed practically the same for the members with a low rate of imperfections. In the case of members with a high rate of imperfections one observed a tendency of reduction in the nominal axial strength. It is of importance that this fact occurs mostly in short members, i.e. where there is seen some predominance of local/torsional buckling.

For the lipped double angle (2Le 50x15x1.50) one can observe that the insertion of the batten plates also increased significantly the nominal axial strength, however, like in the case of the simple double angles, there was a certain number of plates from which on the nominal axial strength almost remained the same. It is important to observe that in this case the members do not tend to reduce their nominal axial strength.

4. Conclusions

The numeric analysis generally shows intermediate results among the ones obtained by the theoretical procedures. It was observed that for the members with a predominance of flexural buckling the results tended to look like the ones for the double angle, however, in the case of the members with a predominance of local/torsional (in simple double angles) or flexural-torsional (in lipped double angles) buckling the results showed the need for a procedure that evaluates more adequately the influence of the local and flexural-torsional modes.

The influence of the number of batten plates deserves a closer and more detailed investigation, considering that from a certain number on the nominal axial

strength of the member remains practically constant for a low rate of imperfections and tends to decrease for the ones with a high rate of imperfections. Thus, one can deduct that it is necessary to deepen the knowledge of a numeric analysis as well as a realization of an experimental program which allows the evaluation and gives some consistency to the here obtained results.

Acknowledgments

Research conducted in this paper was supported by CNPq.

References

ANSI/AISI S100. North American Specification for the Design of Cold-Formed Steel Structural Members. American Iron and Steel Institute, Washington, DC, 2007.

Ansys. Structural nonlinearities: user's guide for revision 5.5, Houston. v.1, 1997.

Maia, W. F.; Munaiar Neto, J.; Malite, M. Stability of cold-formed steel simple and lipped angles under compression. In: LaBoube, R.A.; Yu, W.W. (Ed). Recent research and developments in cold-formed steel design and construction (19th International Specialty Conference on Cold-Formed Steel Structures, St. Louis, USA, Oct. 14 & 15, 2008). Missouri University of Science & Technology, Rolla, Missouri, USA, 2008.

Schafer, B.W.; Peköz, T. Computational modeling of cold-formed steel: characterizing geometric imperfections and residual stresses. Journal of Constructional Steel Research, v.47, 193-210, 1998.

Twentieth International Specialty Conference on Cold-Formed Steel Structures
St. Louis, Missouri, U.S.A., November 3 & 4, 2010

IMPROVEMENTS TO THE FIRE PERFORMANCE OF LIGHT GAUGE STEEL FLOOR SYSTEMS

B.Baleshan[1] and M. Mahendran[2]

Abstract

Light gauge steel frame (LSF) structures are increasingly used in commercial and residential buildings because of their non-combustibility, dimensional stability and ease of installation. A common application is in floor-ceiling systems. The LSF floor-ceiling systems must be designed to serve as fire compartment boundaries and provide adequate fire resistance. Fire-rated floor-ceiling assemblies have been increasingly used in buildings. However, limited research has been undertaken in the past and hence a thorough understanding of their fire resistance behaviour is not available. Recently a new composite floor-ceiling system has been developed to provide higher fire rating. But its increased fire rating could not be determined using the currently available design methods. Therefore a research project was conducted to investigate its structural and fire resistance behaviour under standard fire conditions. This paper presents the results of full scale experimental investigations into the structural and fire behaviour of the new LSF floor system protected by the composite ceiling unit. Both the conventional and the new floor systems were tested under structural and fire loads. It demonstrates the improvements provided by the new composite panel system in comparison to conventional floor systems. Numerical studies were also undertaken using the finite element program ABAQUS. Measured temperature profiles of floors were used in the numerical analyses and their results were compared with fire test results. Tests and numerical studies provided a good understanding of the fire behaviour of the LSF floor-ceiling systems and confirmed the superior performance of the new composite system.

Keywords: *Cold-formed steel, LSF Floors, Gypsum plaster board, Fire test, Insulation, Fire rating, Finite element analysis*

[1]PhD researcher, [2]Professor, School of Urban Development, Faculty of Built Environment & Engineering, Queensland University of Technology, Australia.

1.0 Introduction

Cold-formed and thin-walled steel members can be assembled in various combinations to provide cost-efficient and safe light gauge floor systems for buildings. Such Light gauge Steel Framing (LSF) systems are widely accepted in industrial and commercial building construction. Light gauge cold-formed steel joist sections are commonly used in planer structural floor systems with plasterboard on both sides as fire protection. Under fire conditions, thin cold-formed steel sections heat up quickly resulting in rapid reduction to their strength and stiffness. The use of plasterboards provides protection to steel joists during building fires, delaying the temperature rise in the cavity. Fire rating of LSF floor systems is increased simply by adding more plasterboard sheets to the steel joists (the traditional method). Innovative fire protection systems are therefore essential without simply adding on more plasterboard sheets, which is inefficient. According to Sakumoto et al. (2003), the interior (cavity) insulation was found to be increasing the fire resistance of LSF floor panels. However, in the studies of Sultan et al. (1998) and Alfawickhari (2001), floor assemblies without cavity insulation provided higher fire resistance compared to cavity insulated assemblies. Hence the past researches were unable to conclude the effects of traditional approach of using cavity insulation. Recently a new composite LSF wall system was proposed by Kolarkar and Mahendran (2008) at the Queensland University of Technology (QUT) to provide higher fire rating under standard fire conditions**.** They developed a new composite panel system in which insulation was used externally between plasterboards instead of the traditional cavity insulation located within the stud space and investigated its application for LSF wall systems. Such innovations in the plasterboard and insulation systems, steel joist configurations and construction methods have the potential of increasing the fire resistance rating of LSF floor systems. This research therefore proposes that the new composite system is used in ceilings as part of the LSF floor assemblies.

Compared with full-scale fire tests, numerical or finite element analyses (FEA) provide a relatively inexpensive and time efficient alternative. Therefore it can be used to expand the investigation into the behaviour of LSF floor joists under fire conditions without using excessive resources. The numerical analyses of the steel joists were undertaken using the finite element program ABAQUS standard version 6.9 (HKS, 2009) based on the measured temperature profiles obtained from fire tests. Numerical models were calibrated using the full scale test results and were used to further provide a detailed understanding of the structural fire behaviour of LSF floor-ceiling systems. This paper presents the details of the experimental and numerical studies into the thermal and structural performance

of three LSF floor assemblies chosen in this research. Experimental results are presented along with joist failure times and modes and temperatures. Details of the development and validation of a suitable finite element model of LSF floor joists are also presented in this paper.

2.0 Experimental Study

2.1 General

Full-scale fire tests were conducted to investigate the structural and thermal performance of LSF floor systems under fire conditions. Table 1 gives the details of the three full scale floor specimens used in this study. Test specimens were built using four joists, two tracks, two layers of plasterboard and one layer of plywood. The floor area was more than 5 m^2 (2.4m x 2.1m) with a span of 2400 mm, and the floor specimen was simply supported along its two short sides. All the joists and tracks used were fabricated from 1.15 mm G500 galvanized steel sheets. The frames consisted of four joists made of 180 mm deep lipped channel sections as shown in Figure 1. Test frames were made by attaching the joists at the ends to tracks made of unlipped channel sections using 12 mm long self-drilling wafer head screws. Test steel frames were lined on the ceiling side (fire side) by two layers of gypsum plasterboards (16mm) manufactured by Boral Plasterboard under the product name Fire-stop. The face layer of fire side plasterboard was fixed in the same manner as the first layer, but its joints were staggered by 200 mm.

Table1: Details of test specimen configurations

Test	Configuration	Insulation
1		None
2	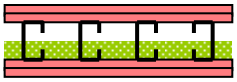	Rock fibre (Cavity insulation)
3		Rock fibre (External insulation)

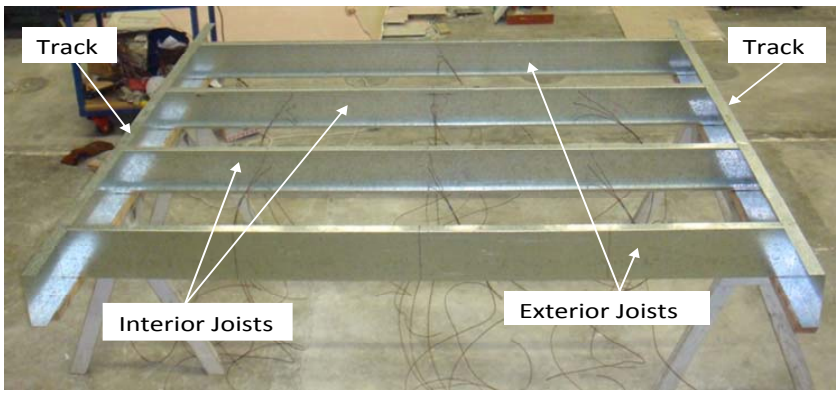

Figure 1: Floor frame

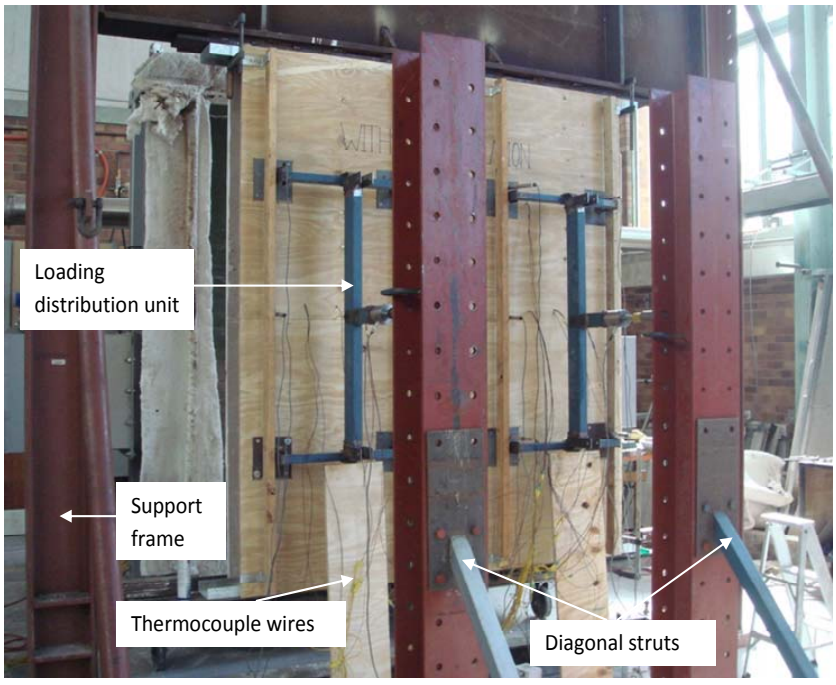

Figure 2: Test set-up

2.2 Test set-up

A heavy steel frame was specially constructed to support the test floor specimens. It consisted of two columns firmly bolted to the strong floor and a universal beam connecting the two columns to form an 'H' shaped portal frame (see Figure 2). The gas furnace only allowed test floor specimens to be set in a vertical position. Hence the transverse loads on the floor specimens were applied in a horizontal direction. In order to simulate a uniformly distributed loading present in LSF floor systems, a load distribution system was developed (see Figure 2) and the target load of 18 kN per jack (4.5 kN per loading point) was applied first and maintained throughout the fire test by the two hydraulic jacks. This target load was determined based on a load ratio of 0.4 where the load ratio is the target load in the fire test to the ultimate failure load of the floor specimen at ambient temperature predicted by FEA. The ultimate failure load at ambient temperature was predicted as 20 kN per joist using the AS/NZS 4600 design rules. A propane fired gas furnace was used in this research to undertake full scale fire tests of the three LSF floor specimens. Many Linear Variable Displacement Transducers were used to measure the lateral deflection of the test specimen. K type thermocouples were used to measure the temperature development across the joists. The average temperature rise as measured by these thermocouples served as the input to the computer controlling the furnace according to the standard cellulosic temperature-time fire curve in AS 1530.4.

2.3 Structural and fire behaviour of test specimens

In all the specimens, at the end of 4 minutes of starting the furnace, smoke was seen coming out from the top of the floor specimen due to the burning of the plasterboard paper on the exposed surface. After about 10 minutes thick smoke and steam were seen to escape from the outer edges from the top of the floor (see Figure 3 (a)). The presence of steam in the mixture of escaping gases was evident as heavy condensation of steam into water was clearly seen on the bottom flange, web of the top UB of the support frame and the top track of the specimens. There were periods of more smoke from the specimens for almost 30 to 40 minutes. This would probably indicate the burning of inside plasterboard paper.

From the beginning of the fire test, the floor specimens were observed to be bending towards the furnace. This continued until the failure and resulted in failing towards the furnace (see Figure 3 (b)). The lateral deflection was the largest in Test Specimen 2 with cavity insulation compared with Test Specimens 1 and 3 (external insulation and no insulation). This was due to higher temperature difference between hot and cold sides of the joists which caused noticeable higher thermal bowing in this test compared with other two tests.

Maintaining the load on the floor specimen was difficult at failure stage with the hand pump controlling the jacks being operated more frequently. The failure was sudden in all the specimens with the joists buckling in the inward direction. The ambient surface of floor specimen recorded temperature values well below the insulation failure temperature (140°C) during all three tests. The failure of the specimen was due to the structural failure of the joists.

(a) Smoke and steam escaping from the top side (b) Lateral deflection of the specimen

Figure 3: Structural and fire behaviour

2.4 Joist temperatures and failure

The failure of the specimens was always by the structural failure of the joists and not by insulation or integrity failure. In the case of cavity insulated specimen, the external plasterboards collapsed prior to joist failure thus hastening the collapse of the floor specimen by exposing the steel frame to direct furnace heat.

Table 2 gives a comparison of the thermal responses of the interior joists at the end of 30, 60, 90 and 120 minutes. Also temperature values are given at the respective failure time of each specimen. Joists of Specimens 1 and 2 reached higher temperatures compared to those in Specimen 3. This is because of the external insulation used in Specimen 3. The cold flange temperature values near the failed interior joists of Specimens 1 and 2 were 320°C and 105°C, respectively. The hot flange failure temperatures of these interior joists are very close to each other (i.e. 489°C). For these joists the temperature differences between hot and cold flanges were 143°C and 398°C, respectively. This may mean that joist failure is mostly governed by the (maximum) hot flange

temperature than the temperature difference between hot and cold flanges. Hence we can conclude that structurally similar LSF floor panels will fail once their joists reach a particular temperature and the fire resistance can be increased only by delaying the maximum temperature in the joists. This is confirmed by the increase in fire resistance time of Specimen 3, which was achieved by the delay in temperature rise in joists due to the use of external insulation.

As seen in Table 2, failure times (fire rating) of Test Specimens 1 to 3 were 107, 99 and 139 minutes. Hence these results demonstrate the improvements to fire resistance of LSF floors by the use of external insulation as proposed in this research. The results also showed that the use of cavity insulation was detrimental to fire resistance of LSF walls in comparison to not using it. In all three cases, failure was due to structural failure of joists by buckling inwards.

Table 2: Thermal responses of interior joists of all three specimens

	Test Specimen 1		Test Specimen 2		Test Specimen 3	
Time (min)	HF (^oC)	CF (^oC)	HF (^oC)	CF (^oC)	HF (^oC)	CF (^oC)
30	121	73	131	63	75	50
60	208	84	236	78	109	75
90	392	226	450	96	152	87
99	-	-	504	106	-	-
107	489	343	-	-	-	-
120	-	-	-	-	298	164
139	-	-	-	-	379	236

3.0 Numerical Study

3.1 General

A numerical study was performed to gain further insight into the buckling and ultimate strength behavioural effects of LSF floor joists under fire conditions, and to investigate the influence of key parameters on their fire resistance. Many finite element analysis programs are currently available. In this research, ABAQUS standard version 6.9 (HKS, 2009) was used for the analysis code. Considerable amount of time was spent in developing an appropriate finite element model for LSF floor joists under fire conditions. In the structural modelling of LSF floor systems, only the individual joists with appropriate loading and boundary conditions were used. The loading simulated the bending

action of joist under the applied transverse loads. In the experimental study, the end conditions were maintained as simply supported. Hence in the numerical study also the support conditions were modelled as simply supported.

3.2 Finite element type and mesh

Element type should be defined correctly to simulate true member behaviour. Based on convergence studies, shell element, S4R, was selected as the most suitable element which can explicitly model the behaviour of LSF joist sections subject to large deformations at higher temperatures. Appropriate selection of mesh size is critical in finite element analysis for improved accuracy of results. A fine mesh density is desirable for greater accuracy, but it may lead to excessive computation time and resources. Also, the aspect ratio of an element (length/width) may have an influence on the solution performance. It was found that a 5 mm x 5 mm (approximately) finite element mesh provides adequate accuracy in modeling the behaviour of joists.

3.3 Symmetry and boundary conditions

The symmetry is considered about a particular axis or a plane of a structure with respect to geometry, boundary conditions and loading patterns before and after the deformations. In the case of support conditions, only one support provides restraint against X-axis translation while keeping other degrees of freedom same. However, it can be considered as symmetrical about the mid-plane. Therefore it was possible to consider only half the span of the test beam, and apply the boundary conditions as shown in Figure 4 to all the nodes at its mid-span. The X-axis translation was prevented at the mid-span cross-section.

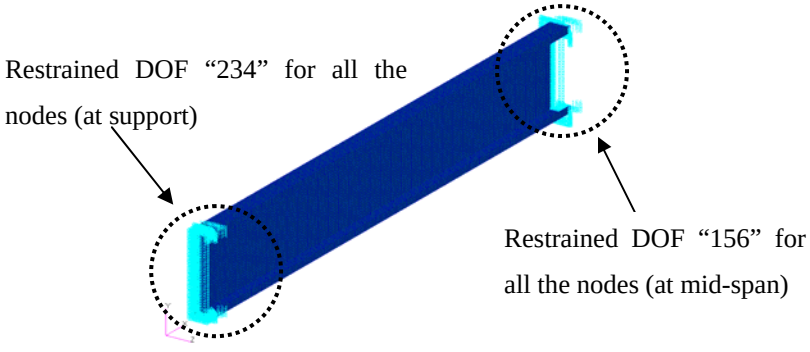

Figure 4: Boundary conditions at the support and mid-span of half-length experimental finite element model

The degrees of freedom notation “123” corresponds to translations in x, y and z axes whereas “456” relate to rotations about x, y and z axes, respectively.

Additional restraining effect provided by plasterboard lining on both sides of the joist was taken into account. For this purpose, the connection of steel joist with plasterboard was represented by a boundary condition restraining the lateral displacement of top and bottom flanges at 300 mm and 200 mm intervals, respectively, which represent the screw fastening locations. This boundary condition was applied to a single row of nodes across the section as shown in Figure 5.

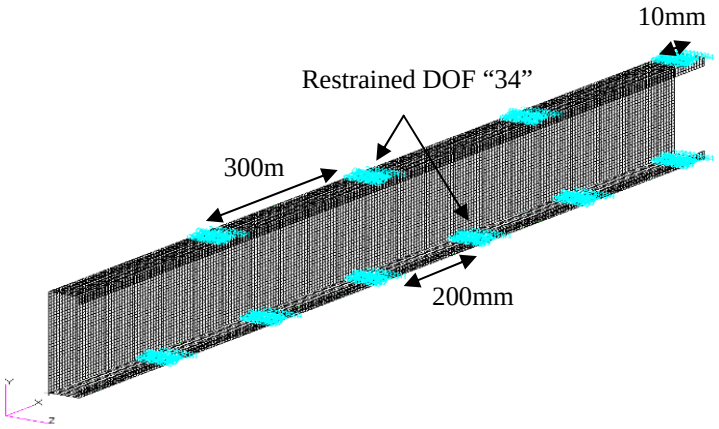

Figure 5: Lateral restraints provided by plasterboard

3.4 Loading conditions

Structural loading

The loading conditions used in the fire tests were simulated in the numerical model. A uniformly distributed loading was simulated as equal concentrated nodal loads over the upper flange of the joist.

Temperature loading

The temperature loading was created as amplitude curve with respect to step time. An amplitude curve allows arbitrary time variations of temperature to be given throughout a step (using step time) or throughout the analysis (using total time). ABAQUS offers different ways to define an amplitude curve: Tabular definition method was selected to define the measured temperature loading amplitude curve as a table of values at convenient points on the time scale. ABAQUAS interpolates linearly between these values, as needed. The temperature loads with time were created using *AMPLITUDE, NAME=name,

DEFINITION=TABULAR option. The temperatures of the steel joist profile at mid-length and quarter points were measured during the fire test. Measured average temperature values (see Figures 7(a)-(c)) were input to the model at three heights over the cross-section (cold flange, web and hot flange) and these temperatures were assumed to be constant over the beam length. The temperature inputs across the section are shown in Figure 6.

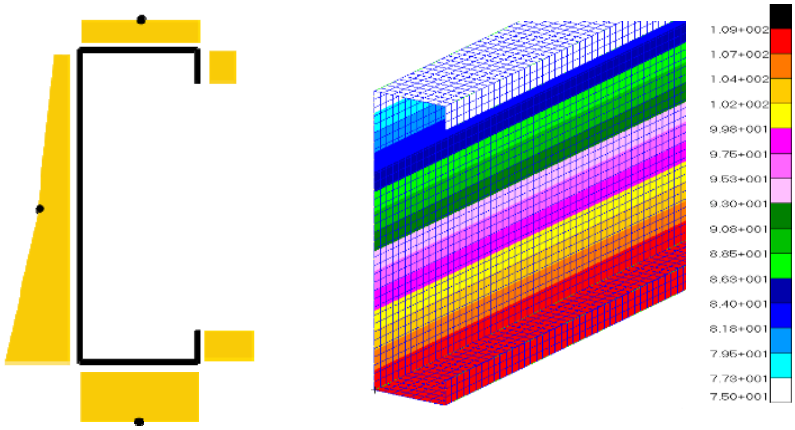

(a) Temperature measurement locations and input

(b) Temperature contours in FEA

Figure 6: Temperature loading across the section

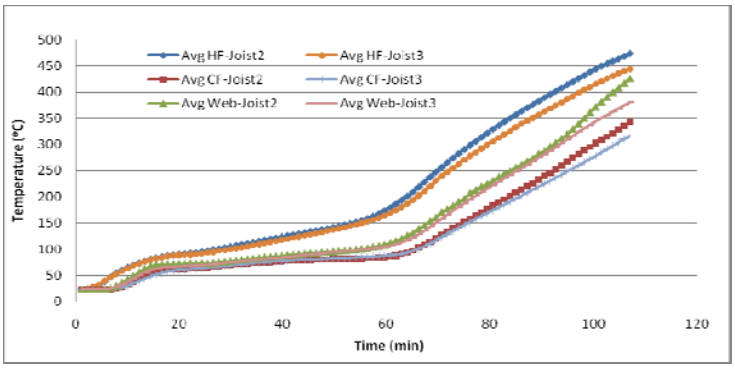

(a) Test Specimen 1

Figure 7: Measured Average Time - Temperature plots of flanges and web surfaces of joists

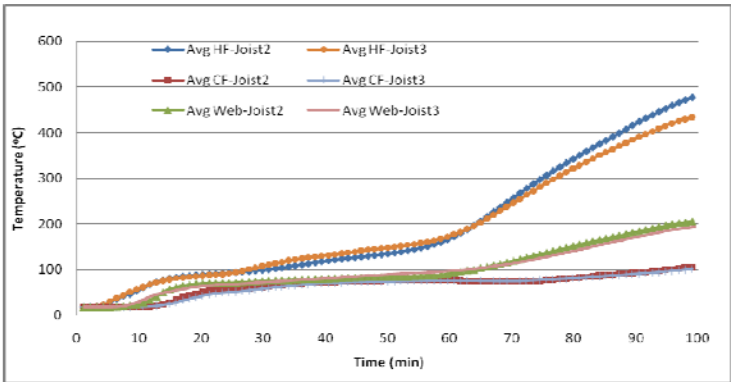

(b) Test Specimen 2

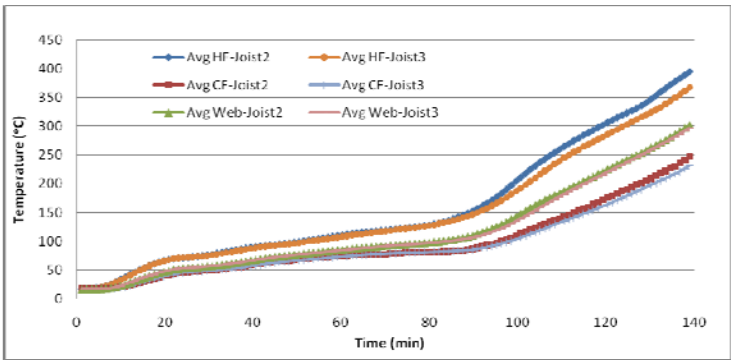

(c) Test Specimen 3

Figure 7: Measured Average Time - Temperature plots of flanges and web surfaces of joists

3.5 Material modeling

The mechanical properties are one of the most important factors in numerical simulations. The mechanical properties required for elastic and nonlinear analyses are Young's modulus of elasticity, yield strength and Poisson's ratio. They should be the same as those of tested specimens to verify the accuracy of developed finite element models. Therefore the yield strength values were

measured using tensile coupon tests at ambient temperature and these measured yield stresses were used in this model. The measured yield strength was 612 MPa while the modulus of elasticity was 210260 MPa, and they were used in the validation of ambient temperature test results. ABAQUS classical metal plasticity model was adopted in this research to include the material non-linearity effects. The reduction of mechanical properties at elevated temperature significantly influences the numerical analysis results. Therefore the mechanical properties should be explicitly considered in the finite element analyses for elevated temperatures. Dolamue Kankanamge (2009) undertook a study to investigate the mechanical properties (yield strength and elastic modulus) of cold-formed steels at elevated temperatures. Her predictive equations were used to determine the yield strength and elastic modulus of 1.15 mm G500 steel at elevated temperatures. The Poisson's ratio was taken as 0.3 and was assumed to remain unchanged with increasing temperature as stated in Ranby (1999). Also the coefficient of thermal expansion was taken as a constant value of 0.000014 $°C^{-1}$ even at higher temperatures.

The initial geometric imperfection values used in the previous studies varied among the past studies. Both local and global initial geometric imperfections were included in Schafer and Pekoz (1997). On the other hand an imperfection amplitude value of L/1000 was used in the studies of Kaitila (2002). However, due to the dominance of thermal bowing the effect of initial geometric imperfection does not have any significant effect on the behaviour of LSF joist at elevated temperature. The geometric imperfections in the joists were applied by modifying the nodal coordinates using a field created by scaling appropriate buckling eigenvectors obtained from an elastic bifurcation buckling analysis. The lowest buckling eigenmodes are usually the critical mode. Hence, a value of b/150 was used in this model after considering the modes from the bifurcation buckling analysis of LSF joists at ambient condition. Residual stresses diminish rapidly with increasing temperature. Therefore the effect of residual stresses was considered to be negligible at elevated temperatures in this model.

3.6 Validation of experimental finite element models at ambient conditions

In the ambient condition, joists were considered as fully laterally restrained by plasterboard and plywood at the top and bottom flanges. Therefore flexural capacity calculations from AS/NZS 4600 were used to validate the results of FEA at ambient condition. This is to ensure that the finite element model can be extended to simulate the desired buckling and ultimate strength behaviour of cold-formed steel joist at fire conditions. The design section moment capacities agree reasonably well with the FEA results as seen in Table 3.

The RIKS method uses the load magnitude as an additional unknown. It solves simultaneously for loads and displacements. Therefore another quantity must be used to measure the progress of the solution. ABAQUS uses the "arc length," along the static equilibrium path in load-displacement space (HKS, 2009). This approach provides solutions regardless of whether the response is stable or unstable. Large displacement theory was also considered in the analyses.

Table 3: Moment capacities of joists from FEA and design codes

Ultimate moment capacity (FEA-Non linear)	6.89 kNm
Section moment capacity (AS 4600)	5.98 kNm
Section moment capacity (Euro code)	6.68 kNm

3.7 Validation of experimental finite element models under fire conditions

Deflection curves

The finite element modelling was performed under dynamic condition where the joist was first subjected to the pre-determined applied load and then it was exposed to the measured temperature profiles. Finite element analyses were performed in three static analysis steps. The first step was an eigen buckling analysis at ambient condition, in which the buckling modes were obtained and the deformed profile of the lowest buckling mode was used to determine the joist initial imperfection. Nonlinear analyses were then performed for the remaining steps with Riks-off method. In the second step, the load was applied incrementally up to the target level. Temperature was then applied in the final step to follow the measured temperature profiles. The accuracy of the developed finite element models was validated using the time-lateral deflection curves obtained from the full scale fire tests. Figures 8 (a)-(c) show a close agreement between the deflection curves from fire tests and FEA. The agreement of these curves is very good compared to the previous numerical studies of LSF floors under fire conditions.

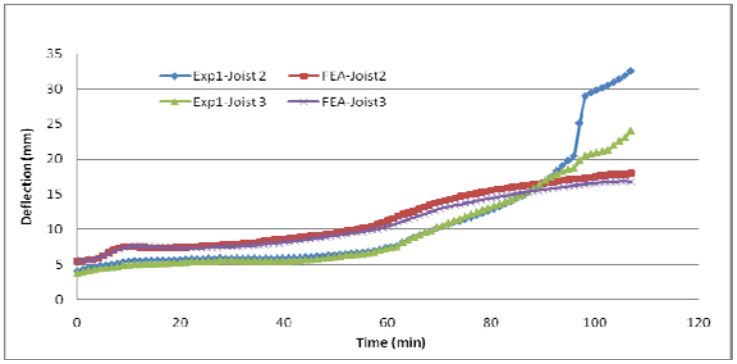

(a) Test Specimen 1

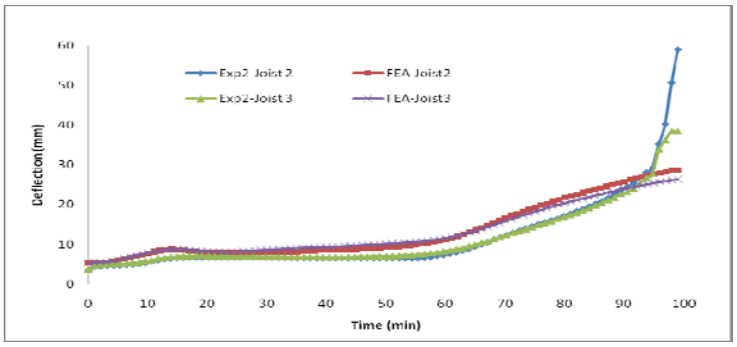

(b) Test Specimen 2

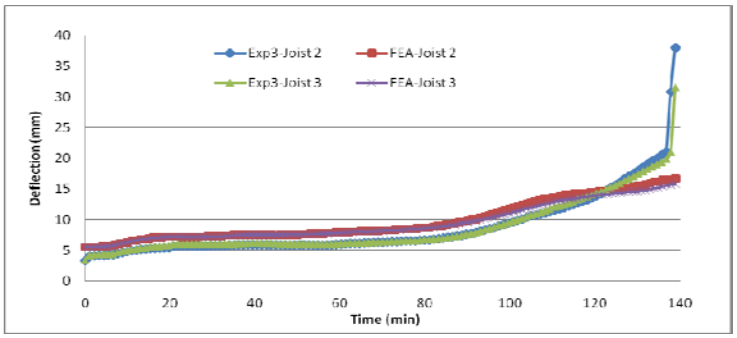

(c) Test Specimen 3

Figure 8: Lateral deflection plots obtained from fire tests and FEA

Failure modes

It was noted that flexural-torsional buckling and flexural buckling about the minor axis of joist were fully prevented by the lateral support offered by the dual layers of plasterboard throughout the test. The central joists in all the specimens experienced local failures at the support as shown in Figure 9 (c). Figure 9 (a) shows the failure mode of the joist where the local buckling waves were observed along the length. Figures 9 (a)-(c) show close agreement of the failure modes between experiment and FEA near the ultimate failure point.

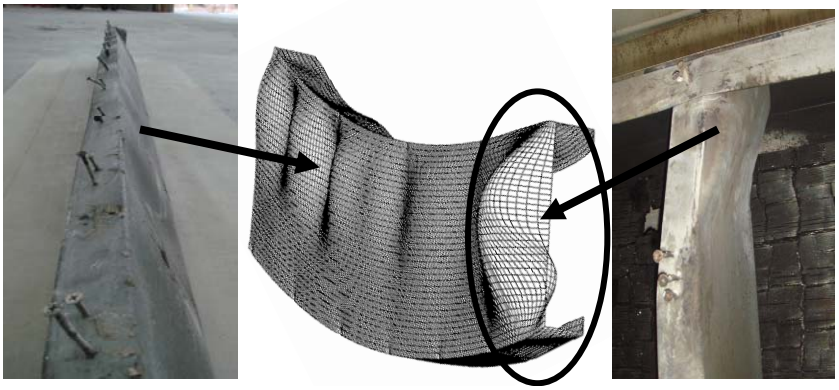

(a) Local web buckling along joists (b) Failure modes in FEA (c) Local failure at support

Figure 9: Failure modes of joists from Fire Tests and FEA

Predictions of failure times

For the convenience of comparison of FEA failure time with experimental failure time, the finite element analyses were performed under the steady-state condition in two steps. This means the temperature distributions in the steel cross-section are raised to the target levels and then kept unchanged in the first step. Following this, the load was applied in increments until failure with Riks-on in the next step. The joist temperatures are based on the measurements of joist temperatures at different times during the fire tests. Figure 10 shows the predicted failure times from FEA. From Figure 10, failure times can be predicted for the three fire tests based on the applied moment of 2.81 kNm and the results are given in Table 4. Table 4 results confirm that the failure times predicted by FEA agree reasonably well with the results from the fire tests.

Table 4: Failure times from experiments and finite element analyses

Test	Insulation	Failure Mode	Failure Time Expt. (min)	Failure Time FEA (min)
1	None	Structural	107	110
2	Rock fibre Cavity insulation	Structural	99	106
3	Rock fibre External insulation	Structural	139	156

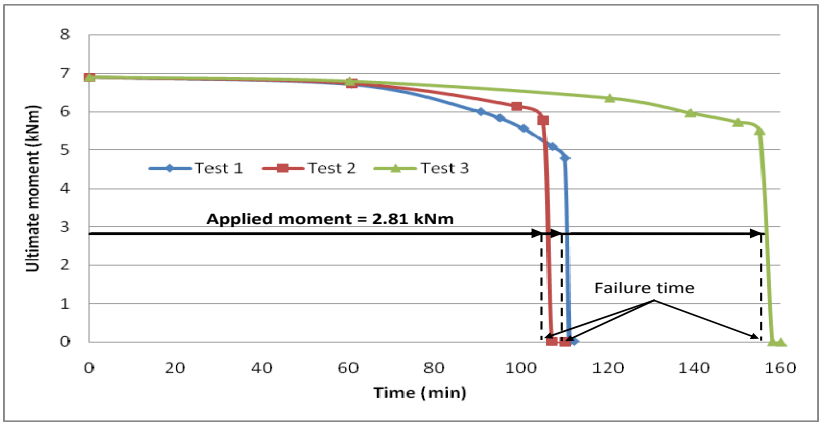

Figure 10: Failure time prediction

4.0 Conclusions

This paper has presented the details of three full scale fire tests of a new light gauge steel floor-ceiling system using external insulation and the results. This study has shown that the use of cavity insulation led to poor thermal and structural performance of LSF floors. In contrast, the thermal and structural performance of externally insulated LSF floor system was superior than the traditionally built floors with or without cavity insulation. Details of fire tests and the results are presented and discussed in this paper. The numerical models were developed and validated to fully understand the improvements offered by the new composite system and to confirm the fire test observations. The use of accurate numerical models allowed the inclusion of various complex thermal

and structural effects such as thermal bowing, local buckling and material deterioration at elevated temperatures.

Acknowledgment

The authors would like to thank Australian Research Council for the financial support to this project and the Queensland University of Technology for providing the necessary facilities and technical support.

References

Alfawakhiri, F. (2001), Behaviour of Cold-Formed-Steel-Framed Walls and Floors in Standard Fire Resistance Tests, PhD Thesis, Faculty of engineering, Carleton University, Ottawa, Ontario, Canada.

Baleshan, B. Mahendran, M. (2010), Full Scale Fire Tests of a New Light Gauge Steel Floor-Ceiling System, Proc. of the 4th International Conference on Steel and Composite Structures, Sydney, Australia. (Paper submitted)

Dolamue Kankanamge, N. (2009), Structural Behaviour and Design of Cold-formed Steel Beams at Elevated Temperatures, PhD Thesis, Queensland University of Technology, Brisbane, Australia.

European Committee for Standardization (CEN) Eurocode 3 (1996) ENV 1993-1-3, Design of Steel Structures, General Rules- Supplementary Rules for Cold-formed Thin Gauge Members and Sheeting, London, UK.

Hancock, G.J. (2005), Design of cold-formed steel structures, Australian Institute of Steel Construction, Sydney, Australia.

Hibbitt, Karlsson & Sorensen, Inc. (HKS) (2009). ABAQUS User's Manual, Hibbitt, Karlsson & Sorensen, Inc., Rhode Island, USA.

Kaitila, O. (2002), Finite Element Modelling of Cold-Formed Steel Members at High Temperatures, Licentiate of Science in Technology Thesis, Helsinki University of Technology, Finland.

Kolarkar, P. and Mahendran, M. (2008), Thermal Performance of Plasterboard Lined Stud Walls, Proc. of 19th International Specialty Conference on Cold-Formed Steel Structures, St. Louis, Missouri, U.S.A, pp.517-530.

MSC. Patran (2008). Patran Version 2008 r1, MSC.Software Corporation, California, USA.

Ranby, A. (1999), Structural Fire Design of Thin Walled Steel Sections, Licentiate Thesis, Division of Steel Structures, Department of Civil and Mining Engineering, Lulea University of Technology, Sweden.

Sakumoto, Y., Hirakawa, T., Masuda, H. and Nakamura, K. (2003), Fire Resistance of Walls and Floors Using Light-Gauge Steel Shapes, Journal of Structural Engineering, pp.1522-1530.

Schafer, B.W. (1997). Cold-formed Steel Behavior and Design: Analytical and Numerical Modeling of Elements and Members with Longitudinal Stiffeners, Ph.D. Thesis, Cornell University, Ithaca, New York, USA.

Standards Australia (SA) (2005), AS/NZS 4600, Cold-formed Steel Structures, Sydney, Australia.

Standards Australia (SA) (1997), AS 1530.4, Methods for fire tests on building materials, components and structures, Sydney, Australia.

Standards Australia (SA) (1998), AS/NZS 2588, Gypsum Plasterboard, NSW, Australia.

Sultan, M.A., Seguin, Y.P., Leroux, P., MacLaurin, J.W and Monette, R.C. (1998), Temperature Measurements in Full-Scale Fire Resistance Tests on Insulated and non-insulated Steel Joist Floor Assemblies, Internal Report, Institute for Research in Construction, National Research Council of Canada, Ottawa, Ontario, Canada.

VTT (2001), Fire resistance test on a load-bearing, separating floor construction, Test Report No.RTE3819/00, Technical Research Centre of Finland (VTT), Espoo, Finland.

Twentieth International Specialty Conference on Cold-Formed Steel Structures
St. Louis, Missouri, U.S.A., November 3 & 4, 2010

FEASIBILITY STUDY FOR A REPETITIVE MEMBER FACTOR FOR COLD-FORMED STEEL FRAMING SYSTEMS

By
S. Clayton[1] and S.F. Stephens[2]

Abstract

Cold-formed steel has become a preferred building material for structural framing in many different types of structures, commonly used as repetitive members such as floor joists, roof rafters, roof trusses and wall studs. For wood framed structures with repetitive members, a repetitive member factor increases the allowable bending stress from 1.00 to 1.50 times the reference design value, depending on both the type of material and the type of load. Currently, however, the bending strength of cold-formed steel repetitive members is not permitted to be increased, even though the method of framing is quite similar to that of wood except for the material properties. Typical light-frame wood construction consists of floor, roof, and wall systems, each with repetitive members connected by sheathing. A repetitive system is one of at least three members that are spaced not farther apart than 24-inches connected by a load distributing element. The behavior of the individual members, then, is affected by inclusion into this system. The effects of both composite action and load-sharing in a repetitive system increase the bending capacity of bending members. The same general principles of repetitive use should apply to cold-formed steel due to its similarity to wood construction. Based upon a preliminary analytical study of the effects of both composite action and load-sharing in cold-formed steel assemblies it has been concluded that a repetitive member factor for cold-formed steel members is feasible and should be further investigated.

[1] Graduate Student, Department of Architectural Engineering and Construction Science, Kansas State University, Manhattan, Kansas
[2] Associate Professor, Department of Architectural Engineering and Construction Science, Kansas State University, Manhattan, Kansas

1.0 Introduction

Cold-formed steel has become a preferred building material for structural framing in many different types of structures, commonly for structural systems such as floor joists, ceiling joists, roof rafters, and wall studs. For each of these systems, the cold-formed steel members are repetitive in nature; that is they are usually spaced at regular intervals of 12-inches (305 mm) to 24-inches (610mm) apart, which is very similar to conventional light frame wood construction. For wood framed structures with repetitive members, a repetitive member factor is permitted for individual members as long as they meet specific criteria. This adjustment factor has the effect of increasing the allowable bending stress for the member and ranges anywhere from 1.00 to 1.50. Currently, no repetitive member factor for cold-formed steel repetitive members exists, even though the method of framing is quite similar to that of wood.

The National Design Specification (AF&PA, 2005) allows the use of a repetitive member factor for members such as joists, truss chords, rafters, studs, planks, decking and other similar members. For sawn lumber construction, the repetitive member factor is 1.15. The required criteria are that there must be at least three members joined by a load distributing element such as sheathing, and they must be spaced no further apart than 24-inches (610 mm). Moreover, the repetitive member factor is only for bending and is applied as an adjustment factor to the reference design value for allowable bending stress.

The main goal of this study was to determine if a repetitive member factor is feasible for cold-formed steel members that meet the same criteria as sawn lumber repetitive members. The following sections discuss the factors that were used to develop repetitive member factor for wood systems, review relevant literature, and also review current repetitive member factors for different types of wood materials. The study also performs an analytical study of both composite action and load-sharing for a cold-formed steel assembly, and calculates a repetitive member factor.

2.0 Repetitive Assemblies and System Effects

The *Standard Guide for Evaluating System Effects in Repetitive-Member Wood Assemblies* (ASTM, 2003), which establishes the guidelines for evaluating repetitive wood assemblies, defines a repetitive-member wood assembly as a system in which three or more members are joined using a transverse load-distributing element. Also, the National Design Specification (AF&PA, 2005) defines a load-distributing element as “any adequate system that is designed or has been proven by experience to transmit load to adjacent members without

displaying structural weakness or unacceptable deflection." Sheathing, which includes plywood, oriented strand board (OSB), and gypsum wall board, is the most commonly used load-distributing element for most structures (Rosowsky, Yu, & Bulleit, 2005).

Bending strength of individual wood members is allowed to be increased when part of a repetitive assembly, due to assembly action. Assembly action is primarily composed of three effects: composite action, load-sharing, and residual capacity. The conservative reference design values for bending stress provided in the National Design Specification (NDS) also have an effect on the increased assembly strength.

2.1 Wood Design Values

It is important to understand the conservatism built into the NDS reference design values for bending stress. The strength of sawn wood products is highly variable because of inconsistencies in the material, such as knots, shakes, and slope of grain. To account for the effect that the material characteristics will have on the member's strength and stiffness, grading rules have been established. The most common method is to visually inspect each piece and sort them into grades based on their characteristics. The other method is to utilize machine grading, which uses non-destructive tests to sort the members into strength and stiffness classes. The coefficient of variation (COV) for stiffness or strength is relatively high for visually graded lumber, while the COV of machine graded lumber is somewhat less (WCLIB, 2009).

Current design methods specified in the NDS are based on individual member design. To assure adequately safe design strength for any single member requires a conservative member strength design value. The reference design values for bending stress is found by statistically analyzing test data and calculating the 5% exclusion value (ASTM, 2006).

This means that most members in a system will have a higher strength than the strength calculated using the NDS reference design values. The load-sharing effect, which is discussed later, is able to take advantage of these stronger members.

2.2 Composite Action

Composite action is the interaction of the sheathing and the bending member that creates T-Beam-like action, effectively increasing the moment of inertia of the bending member by moving the neutral axes of the components toward each

other (Wolfe, 1990). Typically in wood systems, the sheathing and the bending member are connected by nails, glue, or both. However, nails do not provide fully rigid connections between the member and the sheathing because of slippage due to shear, resulting in only partial composite action. Sheathing also comes in panels, and therefore many gaps occur between sheathing panels along the length of the "T-Beam." These gaps cause a discontinuity of the effective flange and therefore have an adverse effect on the amount of partial composite action that can occur (McCutcheon, 1977). Partial composite action is important because it can provide a significant amount of increased capacity. For example, for sawn lumber, it accounts for approximately 2/3 of the increased capacity (ASTM, 2007).

2.3 Load Sharing

Load-sharing between members is another main component of assembly action. As was discussed previously, the strength of a wood member can be highly variable, and the design strengths of the sawn lumber members are conservative. Load-sharing is able to take advantage of both of these concepts by transferring load from a weaker member to the surrounding stronger members. Transfer of load is possible mainly due to differential deflections between members, as stiffer members will deflect less than less rigid members (Wolfe, 1990). Figure shows an assembly made of three members connected by sheathing, which is acting as a load-distributing element.

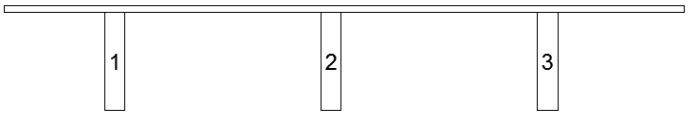

Figure 1 - Load Sharing Assembly

To illustrate load-sharing, assume that member 2 is a weak member surrounded by stronger members 1 and 3. If uniform load was applied to the assembly, the weaker member 2 would deflect more than members 1 and 3. However, due to its stiffness, the sheathing is assumed to transfer more load to 1 and 3 until their deflections reach that of member 2. In this way, the load-distributing element is able to transfer load away from weaker members to stronger ones. Because the stronger members are able to carry additional load, the strength of the assembly is greater than that of the weakest member. The amount of load that is able to be transferred to the surrounding members depends on many factors, including the effects of size and mutual restraint (Wolfe, 1990).

2.3.1 Effects of Size on Assembly Capacity

The size effect is dependent on the number of members in the assembly and the dimensions of the individual members (Wolfe, 1990). The failure of an assembly is defined as the point at which the first member in the assembly fails (ASTM, 2003). Load-sharing is dependent on having multiple members in the system, though the chances of including a weak member increase with increasing number or length of members (Rosowsky & Yu, 2004). Because the capacity of the assembly is dependent on first member failure, the higher chance of including a weak member will cause the assembly capacity to decrease. Thus, the calculation of the load-sharing factor, which will be discussed in Section 2.3.3, is highly dependent on the number of members in the assembly. For example, the load sharing factor for a 5-member assembly with a COV of 25% is 1.22, but decreases to 1.06 for a 50-member assembly.

2.3.2 Mutual Restraint

Mutual restraint is a measure of the stiffness of the load distributing element that will cause all of the members in the assembly to deflect together. It is the main component of load-sharing. Two theoretical systems can be used to illustrate the effects of mutual restraint.

The first theoretical system is known as a brittlest-link system. It has an infinitely rigid deck, and therefore the highest amount of mutual restraint (Zahn, 1970). Because the deck is infinitely rigid, all members in the assembly would be constrained to have the same deflection. In this system, the member with the least deflection capacity (brittlest-link) will fail first (Zahn, 1970). Members in a brittlest-link system will act as described previously, where load will be transferred from less stiff members to stiffer ones. This will lead to an increase in assembly capacity in wood products because a positive relationship between rigidity and strength exists. Alternatively, if the most rigid member is also the weakest, mutual restraint would have a detrimental effect on the assembly capacity because the weakest member would take the most load.

The other hypothetical system is one with an infinitely flexible deck, known as a weakest-link system (Zahn, 1970). This system would have no mutual restraint, as the members could deflect independently of each other. Here, the capacity of the assembly would be controlled by the weakest member in the system. A weakest-link system does not take advantage of the stronger members because no load is shared through the sheathing.

Realistically, repetitive assemblies fall somewhere between these two theoretical systems. Ultimately, the amount of mutual restraint that can occur is dependent

on the difference in deflections between adjacent members and stiffness of the sheathing. For this reason, the effects of mutual restraint increase with material variability.

2.3.3 Calculation of Load-Sharing Factor

The load-sharing factor is defined as the ratio of load at first member failure in an assembly to that of first member failure not in an assembly. A load-sharing factor can be found either analytically or empirically utilizing the guidelines given in ASTM D 6555 (ASTM, 2003).

The concept of a repetitive member factor was based primarily on the effects of load-sharing (ASTM, 1970), a concept originally introduced in 1962 in *Tentative Recommended Practice for Determining Design Stresses for Load-Sharing Lumber Member*s (ASTM, 1962). The standard was discontinued in 1968, but a 1.15 factor was adopted in 1970 in *Standard Methods for Establishing Structural Grades and Related Allowable Properties for Visually Graded Lumber* (ASTM, 1970). This load sharing factor was based on a simplified statistical analysis of three parallel bending members, known as an averaging model (ASTM, 1970). The allowable bending stress of a member in a load sharing system is found by using the following equation:

$$\bar{X} = \frac{F_b}{(1-k\Omega/\sqrt{n})} \qquad \text{(Equation 1)}$$

where F_b is the 5% exclusion limit of the allowable bending stress of an individual member**,** *k* is the distance from the mean to the lower percentile in terms of standard deviates, Ω is the coefficient of variation (COV), n is the number of members in the assembly, and $\bar{X}$ is the allowable bending stress of a member as a result of load-sharing (Wolfe, 1990). Based on a 95% inclusion value, k is found on a standard normal distribution chart to be 1.645. Typical visually graded sawn lumber has a COV of modulus of rupture (MOR) of 25% to 30% (Wolfe, 1990). If an assembly had three members and a COV of 25%, the calculation would be:

$$\bar{X} = \frac{F_b}{\left(1-\frac{(1.645)(0.25)}{\sqrt{3}}\right)} = 1.31F_b \qquad \text{(Equation 2)}$$

The same calculation with a COV of 30% yields a factor of 1.40. ASTM Committee D07, which has jurisdiction of most wood standards, proposed a conservative factor of 1.15, which coincides with a COV of approximately 16%. The committee also placed conservative guidelines for usage of the repetitive

member, including limits of spacing, number of members, and the size of lumber (ASTM, 2003).

2.4 Residual Capacity

Though one member in a system may fail, the whole assembly will not collapse in most cases. This is referred to as residual capacity and is based upon both composite action and load sharing. For sawn lumber, the residual capacity has been found to be as much as two to five times greater than the capacity of the weakest member in the system (ASTM, 2003). An assembly is an indeterminate system, and so many factors affect an assembly's residual capacity are not always obvious without detailed analysis. In deciding how to address residual capacity as it applies to member design, ASTM Committee D07 on Wood wrote the following:

> "The committee chose to discourage the use of residual capacity in system factor calculations based on the premise that traditional "safety factors" are calibrated to a member-based design system. The committee believes that is inappropriate to extend the same factors to entire systems. In other words, engineers should not design entire systems that have the same computed probability of failure as individual members in today's designs." (ASTM, 2003)

Even though an assembly can have a significant residual capacity, that capacity is not currently permitted in member design.

3.0 Literature Review

Since the establishment of the repetitive member factor, many studies and tests have been conducted to better understand the repetitive member behavior and how it should be calculated. The following sections review previous studies that are centered on the effects of both partial composite action and load-sharing.

3.1 Studies of Partial Composite Action

Sheathing attached to a joist or stud creates a T-Beam-like effect that increases the effective moment of inertia of the bending member (Wolfe, 1990). The relationship between loading, connection slippage, and gaps in the sheathing has been the focus of many studies.

For instance, McCutcheon (1977) presented a simplified method to calculate the deflection in partial composite sections. This calculation took into account the reduction of composite action because of connection slippage and sheathing gaps. To test the equations developed in this study, seven floors were

constructed with nine 2x8 (51mm x 204 mm) joists sheathed with tongue-in-groove plywood. Four of the floors were connected with 8d common nail fasteners, and the other three were nail-glued using rigid adhesive. The stiffness of each joist was found prior to construction using non-destructive bending tests. The floors were non-destructively tested with both concentrated and uniform loads, and the measured mid-span deflections were compared to the calculated values. Results showed 22 of 29 floors tested were within 5 percent of the calculated deflections, which suggests that the composite stiffness could be approximated by these simplified equations.

3.2 Load-Sharing Studies

Load sharing between members is a main component of the current repetitive member factor, but the amount of load that can be transferred to the surrounding members is dependent on many factors, including the effects of size, mutual restraint, and bridging (Wolfe, 1990): The size effect is dependent on the number of members in the assembly, the length, and the dimensions of the individual members; mutual restraint is a measure of the rigidity of the load distributing element; bridging is the ability of the components to transfer load around defects within an element (Wolfe, 1990).

Zahn (1970) conducted a statistical analysis of both brittlest-link and weakest-link systems to investigate the size effect and mutual restraint. He also utilized computer modeling to confirm that weakest-link and brittlest-link systems represent the lower and upper bounds of system capacity. For the statistical analysis of the weakest-link system, Zahn assumed load was equal on all members and concluded that increasing the number of members in a weakest-link system decreases the capacity of the system. Then, he modeled a brittlest-link system by constraining the mid-span deflections of all members to be equal. The statistical analysis of this system yielded a maximum load-sharing increase of 12.8 percent. Because a brittlest-link system is the upper bound of load-sharing, Zahn concluded the maximum load sharing increase should be 12% for sawn lumber systems. The study did not investigate bridging or partial composite action.

4.0 Investigation of a Repetitive Member Factor for Cold-Formed Steel Framing

Cold-formed steel is commonly used as repetitive members in similar applications to wood. The following sections discuss the application of the same principles used for establishing wood repetitive member factors to cold-formed steel.

4.1 Composite Action Effect

In wood assemblies, composite action accounts for approximately 2/3 of the repetitive member factor, while load-sharing accounts for the other 1/3. An analytical study of a cold-formed steel stud with attached sheathing was used to find the contribution of composite action in a cold-formed steel assembly. The section, shown in Figure 2, consists of an ASTM A1003 Structural Grade 33 Type H, 600S-162-33 cold-formed steel stud with 7/16-inch (11 mm) thick oriented strand board (OSB) with a 24/0 span rating.

The stud spacing was based on several assumptions. First, if the stud-spacing limitation used for wood is assumed for cold-formed steel, the maximum member spacing would be 24-inches (610 mm). 16-inch (407 mm) stud spacing is commonly used in walls; therefore a 16-inches (407 mm) spacing was used. The width of flange that can be used in composite calculations is limited in the design of both concrete T-Beams and steel composite construction, but no literature was found on the limitations of the effective flange width for wood sheathing. For simplicity, the full flange width was used for the calculations.

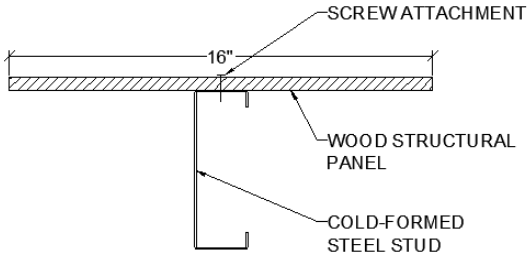

Figure 2 – Composite Section of CFS Stud and Wood Structural Panel

To simplify the calculations, the screw connection between the sheathing and stud was assumed to provide full composite action. Also, the cold-formed steel stud is assumed to be a solid section, with no holes punched in the web. The properties and the Allowable Stress Design (ASD) allowable strength of the cold-formed steel stud were found by utilizing a cold-formed steel analysis program, CFS (RSG Software, 2006). The results of the analysis are shown in Table 1.

Table 1: Cold-Formed Steel Stud Properties

Depth:	6	in	(152.4	mm)
Width:	1.625	in	(41.275	mm)
Thickness:	0.0346	in	(0.8788	mm)
Return Lip:	0.5	in	(12.7	mm)
F_y:	33	ksi	(228	MPa)
M_a:	11282	lb*in	(1274	Nm)
A:	0.343	in^2	(221.3	mm^2)
I_x:	1.784	in^4	(742557	mm^4)
S_x:	0.595	in^3	(9750	mm^3)
E:	29500	ksi	(203395	MPa)

Several assumptions were made in the selection of the rating of the sheathing and its properties. The OSB with the least modulus of elasticity was chosen because it would result in the least transformed area. Also, the study sought and found properties of sheathing in the weak direction with stress perpendicular to the strength axis to generate a conservative composite calculation.

The axial compressive strength of OSB with stress perpendicular to the strength axis is much stronger than the tensile strength. Due to the limited tensile strength, the composite effect was found to be negligible when composite action was calculated with tension assumed in the sheathing.

Some properties of both the sheathing and the cold-formed steel stud were not specifically given, and required calculations to find them. The modulus of elasticity (E) and the axial compressive strength (F_c) of the OSB sheathing, found in the *Panel Design Specification* (APA, 2004), were each given per unit area. Also, the maximum allowable stress of the cold-formed steel was not given by the analysis program, but the maximum moment was. The stress in the steel at maximum moment, found by dividing the moment by the section modulus (S_x), was set as the maximum allowable stress in the cold-formed steel member.

To find the effect of composite action, the transformed area method is used. First, the area of the OSB is transformed to an equivalent area of cold-formed steel so the section can be analyzed like one material. Next, the neutral axis and moment of inertia of the composite section are calculated. The maximum moment of the composite section is found by checking the maximum stresses at three critical locations in the composite section: the top of the sheathing, and the top and bottom of the cold-formed steel member. For this calculation, it is

assumed the maximum allowable stress of the composite cold-formed steel member cannot surpass the maximum allowable stress from the non-composite analysis. The composite factor is the ratio of the maximum moment of the composite section to that of the non-composite member.

Using these methods, the composite factor is calculated to be 1.24, which as previously stated, assumes that full composite action can be developed between the cold-formed steel member and the sheathing. For full composite action to be possible, the screws must be able to transfer the shear across the connection. Fastener capacity calculations determine whether the screws provide a connection that can transfer shear forces at the maximum moment. In order to calculate the shear force, an equivalent distributed load on an assumed 10-foot (3.05 m) span is found from the maximum moment. Using this shear force, the maximum shear force is checked against the fastener capacity.

The full shear force is found to be transferable across the connection at a screw spacing no more than 6-inches (152 mm) when the maximum moment is applied. It is important to note that because of the size of the load, the deflection would likely govern the design of the member. Additionally, composite action results in an increase of stiffness due to the increase of the moment of inertia of the section. Also, due to slippage in the connection, the actual deflection of the section will be higher than the deflection that could be calculated for the fully composite section. Finally, because there has been limited research into the slippage occurring between cold-formed steel studs and sheathing, this study does not allow for slippage.

These calculations were performed on a 6-inch (152 mm) deep member, but cold-formed steel sections are available in depths that commonly range from 3.625-inches (102 mm) to 16-inches (406 mm). To find the possible composite action for a deeper member as might be used in a roof or floor system, the same calculations on a 1200S162-68 member were performed. The composite factor for this 12-inch (305 mm) deep member was found to be 1.12.

4.2 Load Sharing Effect

The other effect to be considered is the load-sharing capabilities of the system. The effects of load-sharing are directly related to the differential deflection between system members. In general, steel has much more consistent material properties than wood products. Pekoz (1987) performed bending tests that can be applied to this study. The test used was of a beam with a stiffened compression flange. The result of that test is shown in Table 2:

Table 2 - Beam Test Results

Number Tested	Mean	C.O.V.
8	1.146	0.046

A load sharing factor can be calculated using this data as follows.

$$\text{Load Sharing Factor (LSF)} = \left(1 - k\Omega/\sqrt{n}\right)^{-1} \qquad \text{(Equation 3)}$$

k = 1.645 (5^{th} Percentile)

Ω = 0.046

n = 8

LSF = 1.027

Though steel has relatively little variation of stiffness when compared to wood, the variation is high enough that some load-sharing can occur. The COV for cold-formed steel is only 0.046, compared to 0.3 to 0.4 for sawn lumber.

4.3 Cold-Formed Steel Repetitive Member Factor

The calculations performed in the previous sections yield only preliminary results to support the feasibility of a repetitive member factor for cold-formed steel members. Though more rigorous testing is required, this study showed that a repetitive member factor can likely be applied to cold-formed steel in some applications. Because composite action is negligible when the sheathing is in tension, a repetitive member factor for applications where the sheathing is in tension is dependent only on load-sharing. For these assemblies, such as walls, a repetitive member factor of 1.02 was determined.

For assemblies where compression in the sheathing can be assured, both composite action and load-sharing can be considered. The preliminary calculations showed that strength increase due to composite action ranged from 1.12 to 1.24, depending on the depth of the cold-formed steel member. Combined with the load-sharing factor of 1.02, the repetitive member factor could be as high as 1.14 to 1.26. These numbers are based on full composite action and do not take into account gaps in the sheathing or slippage in the connections.

The calculations performed were based on several assumptions and limitations:

- Only 600S162-33 and 1200S162-68 sections without punchouts were investigated
- F_y = 33 ksi (228 MPa)
- Full composite action was assumed

- Flange width of sheathing 16-inches (40.64 cm) was assumed
- ½-in (12.7 mm) OSB sheathing

5.0 Conclusion

This study shows that the effects of partial composite action, load sharing, and residual capacity can all have positive effects on the flexural capacity of a repetitive system. Currently, the methods used in the NDS (AF&PA, 2005) permit only partial composite action and load sharing to be used in the calculation of a repetitive member factor for wood products.

Given the similarities between wood and cold-formed steel, this study investigated the feasibility of a repetitive member factor for cold-formed steel members using the same principles that apply to wood. When the sheathing is used in flexural compression, composite action resulted in an increase of member bending strength from 12 to 24 percent, depending on the depth of the member.

Next, though the variability of stiffness in cold-formed steel members is relatively small when compared to wood, it can still yield a positive effect on the capacity of an assembly. Based on test data used, a load-sharing factor for repetitive cold-formed steel members was calculated to be 1.02.

Therefore, when compression in the sheathing can be assured, the repetitive member factor for the limited scope of this study can range from 1.14 to 1.26, depending on the depth of the member. However, for applications where the sheathing is in tension, a repetitive member factor is limited to1.02.

This study has found that a repetitive member factor is feasible for cold-formed steel when the values are based only on load-sharing and full composite action. To determine a reliable factor for design however, research will need to be conducted to establish a number of items including but not limited to the effective flange width of sheathing, the type of sheathing, the effect of slippage in the connection, and the effect of gaps in the sheathing.

Appendix. – References

AF&PA. (2005). *National Design Specification for Wood Construction.* Washington, DC: American Forest & Paper Association.

ASTM. (2003). Standard Guide for Evaluating System Effects in Repetitive-Member Wood Assemblies. *ASTM D 6555* . Philadelphia, PA: American Society for Testing and Materials.

ASTM. (1970). Standard Methods for Establishing Structural Grades and Related Allowable Properties for Visually Graded Lumber. *ASTM D 245-70* . Philadelphia: American Society for Testing and Materials.

ASTM. (2006). Standard Practice for Establishing Structural Grades and Related Allowable Properties for Visually Graded Lumber. *ASTM D 245* . Philadelphia: American Society for Testing and Materials.

ASTM. (2007). Standard Specification for Establishing and Monitoring Structural Capacities of Prefrabricated Wood I-Joists. *D 5055* . Philadelphia: American Society for Testing and Materials.

ASTM. (1962). Tentative Recommended Practice for Determining Design Stresses for Load-Sharing Lumber Members. *ASTM D 2018-62T* . Philadelphia, PA: American Society for Testing and Materials.

McCutcheon, W. (1977). *Method for Predicting the Stiffness of Wood-Joist Floor Systems with Partial Composite Action.* Madison: USDA Forest Service.

Pekoz, T. (1987). Development of a Unified Approach to the Design of Cold-Formed Steel Members. Washington, DC: American Iron and Steel Institute.

Rosowsky, D., & Yu, G. (2004). Partial Factor Approach to Repetitive-Member System Factors. *Journal of Structural Engineering* , 1829-1841.

Rosowsky, D., Yu, G., & Bulleit, W. (2005). Reliability of Light-Frame Wall Systems Subject to Combined Axial and Transverse Loads. *Journal of Structural Engineering* , 1444-1455.

RSG Software. (2006). CFS Version 6.0.2. Lee's Summit, MO.

WCLIB. (2009, March). Assessing the Comparability of NDT Systems Using Standard Practices. West Coast Lumber Inspection Bureau.

Wolfe, R. (1990). Performance of Light-Frame Redundant Assemblies. *1990 International Timber Engineering Conference* (pp. 124-131). Tokyo, Japan: USDA Forest Service.

Zahn, J. (1970). *Strength of Multiple-Member Structures.* Madison: U.S. Forest Products Laboratory.

Appendix. – Notation

Ω : Coefficient of variation
A : Cross-sectional area
COV : Coefficient of variation
E : Modulus of elasticity
f : Stress
F_b : Allowable bending stress
F_c : Axial compressive strength
F_y : Yielding stress of steel
I_x : Moment of inertia about x-axis
k : Distance from the mean to the lower percentile in terms of standard deviates
M_a : Allowable moment
n : Number of members in the system
n : Transformed area conversion factor
P : Fastener capacity
Q : First moment of area about x-axis
S_x : Section modulus about x-axis
V : Shear force
w : Distributed load
$\bar{X}$: Allowable bending stress using averaging model

Twentieth International Specialty Conference on Cold-Formed Steel Structures
St. Louis, Missouri, U.S.A., November 3 & 4, 2010

Extending Direct Strength Design to Cold-Formed Steel Beams with Holes

Cristopher D. Moen[1], Benjamin W. Schafer[2]

Abstract

The extension of the American Iron and Steel Institute's Direct Strength Method (DSM) to cold-formed steel beams with holes is nearly in place. DSM was first introduced to the AISI specification in 2004 as an alternative to the effective width method, and is widely considered a major advancement in cold-formed steel component design. In DSM, the beam elastic buckling properties for a general cross-section are obtained with a computer analysis utilizing the finite strip method. A disadvantage of the finite strip method and DSM has been that discrete holes along the member length could not be easily accounted for, although the recent development of simplified elastic buckling approximations including holes has now alleviated the inherent shortcoming. This paper provides an introduction to the DSM approach for cold-formed steel beams with holes, where the critical elastic buckling moments for local, distortional, and global buckling are calculated including the presence of holes, and then input into strength prediction expressions modified to capture the strength reduction from yielding at the net section. A DSM design example of a joist with evenly spaced web holes is provided.

Introduction

Cold-formed joists are a popular structural component in the floor systems of low and midrise buildings. These thin-walled structural steel flexural members are manufactured by cold bending steel sheet into an open cross-section, most commonly a C-section. The joists are provided with evenly spaced web holes to accommodate the passage of electrical conduits, plumbing pipes, and HVAC ducts. Hole sizes and shapes vary by manufacturer, and the hole edges can be either unstiffened (Figure 1a) or stiffened (Figure 1b).

[1] Assistant Professor, Virginia Tech, Blacksburg, VA, 24061, USA. (cmoen@vt.edu)
[2] Professor, Johns Hopkins University, Baltimore, MD, 21218, USA. (schafer@jhu.edu)

(a)

(b)

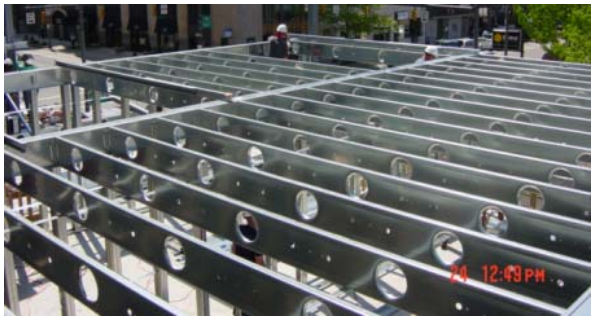

Figure 1 (a) Cold-formed steel joist with unstiffened punched web holes (b) C-section joists with stiffened circular holes (photos courtesy of Don Allen)

The broad range of hole shapes, sizes, and spacings in cold-formed steel construction today has exceeded the original scope of the American Iron and Steel Institute (AISI) design equations developed for beams with holes over the last four decades. The current AISI design equations were derived within the context of the effective width method (Yu 2000), and address the influence of unstiffened holes on local buckling dominated failures. The AISI provisions are written specifically for unstiffened holes in C-section webs, and are limited to a somewhat restricted range of hole sizes and spacings. For example, the effective width equations are only applicable when unstiffened web holes are provided with a centerline spacing of 457 mm (18 in.) or greater, and where the hole depth is less than 63 mm (2.5 in.) regardless of the cross-section dimensions (AISI-S100 2007, Section B2.4).

The AISI specification addresses the influence of unstiffened holes on local buckling through the effective width method, however holes are not currently considered for global buckling and distortional buckling limit states. When unstiffened holes are present in a cold-formed steel beam, the critical elastic

flexural-torsional buckling load decreases relative to the same beam without holes, which increases the global slenderness and decreases predicted strength (Moen and Schafer 2009a). For distortional buckling, a form of buckling related to intermediate and/or edge stiffeners commonly observed in open cross-sections, the presence of unstiffened web holes decreases the stabilizing influence of the web on the cross-section, reducing the critical elastic distortional buckling moment and increasing the tendency for distortional buckling to initiate at a hole (Kesti 2000; Moen and Schafer 2008; Moen and Schafer 2009a). A more general design method which considers the influence of holes across all cold-formed steel limit states is needed.

An AISI research program was recently completed that capitalizes on advances in cold-formed steel strength prediction, and specifically the AISI Direct Strength Method (DSM) (AISI-S100 2007, Appendix 1), to deliver a more general design approach for cold-formed steel beams with holes. DSM represents an important advancement in cold-formed steel design because it provides engineers and cold-formed steel manufacturers with the tools to predict member strength for a general cross-section. With the design approach summarized herein, DSM can now safely predict the strength of cold-formed steel flexural members with the ever expanding range of cross-section types, hole sizes, shapes and spacings common in industry. Note that this paper focuses on flexural strength prediction for beams with unstiffened holes. However, the DSM approach is also applicable to beams with stiffened holes, and work is underway to formalize the design equations and elastic buckling framework (Moen and Yu 2010).

The AISI Direct Strength Method

DSM for beams without holes

The AISI Direct Strength Method employs the elastic buckling properties of a general cold-formed steel cross-section to predict strength. For members without holes, the elastic buckling properties are obtained from an elastic buckling curve generated with freely available software, for example CUFSM (Schafer and Ádány 2006) and GBTUL (Bebiano et al. 2008), which perform a series of eigen-buckling analyses over a range of buckled half-wavelengths. An example of an elastic buckling curve is provided in Figure 2 for a cold-formed steel C-section beam, highlighting the three categories of elastic buckling considered in DSM – local, distortional, and global buckling – where $M_{cr\ell}$, M_{crd}, and M_{cre} are the respective elastic buckling moments.

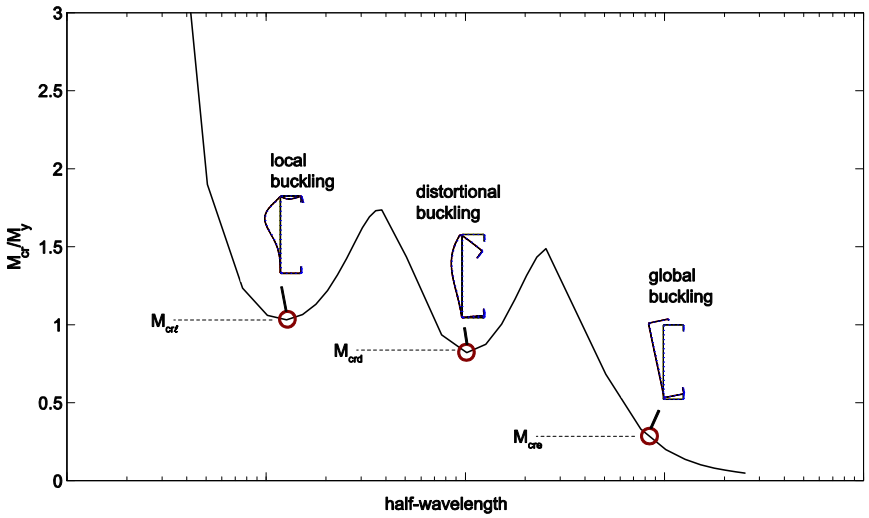

Figure 2 Elastic buckling curve for a cold-formed steel beam without holes

Flexural capacity is calculated with DSM considering three limit states – global buckling, local-global buckling interaction, and distortional buckling (AISI-S100 2007, Appendix 1). The global strength of an unbraced beam span, M_{ne}, is determined with the global slenderness, $\lambda_c=(M_y/M_{cre})^{0.5}$; $M_{n\ell}$ is calculated with the local slenderness, $\lambda_\ell=(M_{ne}/M_{cr\ell})^{0.5}$; and M_{nd} is obtained with the distortional slenderness, $\lambda_d=(M_y/M_{crd})^{0.5}$. When slenderness is high for global or distortional buckling limit states, i.e. when M_{cre} or M_{crd} is small relative to the yield moment of the beam, $M_y=S_fF_y$, flexural strength is limited by elastic buckling. (Note that S_f is the section modulus referenced to the outer fiber that yields first and F_y is the steel yield stress.) When λ_c or λ_d is low, the flexural strength is controlled by inelastic buckling and yielding. Considering the local-global buckling interaction limit state for unbraced beams, the flexural-torsional buckling capacity is reduced from M_{ne} to $M_{n\ell}$ to account for local buckling along the beam span. The minimum strength from the three limit states is taken as the beam's flexural capacity, i.e. $M_n=\min(M_{ne}, M_{n\ell}, M_{nd})$.

Strategy for extending DSM to beams with holes

A logical extension of the Direct Strength approach to cold-formed steel beams with holes is to maintain the assumption that elastic buckling properties can be used to predict strength. For a beam with holes, this means that the elastic buckling moments $M_{cr\ell}$, M_{crd}, and M_{cre}, are calculated including the influence of

holes. A suite of simplified methods for obtaining these elastic buckling moments was recently developed as an alternative to cumbersome thin-shell finite element eigen-buckling analysis. The elastic buckling moments, including the influence of holes, can be calculated with finite strip analysis or hand calculations derived from classical buckling solutions (Moen and Schafer 2009a; Moen and Schafer 2009b). The simplified elastic buckling prediction methods are demonstrated in an example at the end of this paper.

It was concluded in the AISI research program that the elastic buckling moments including the influence of unstiffened holes are viable parameters for predicting capacity in a Direct Strength approach (Moen 2008). However, when yielding controls strength, modifications to the existing DSM design expressions for beams without holes were needed to limit flexural capacity to that of the net section, i.e. $M_{ynet}=S_{fnet}F_y$, where S_{fnet} is the section modulus at the net section. Furthermore, the AISI research program concluded that inelastic buckling and collapse at a hole may control flexural strength with intermediate slenderness ranges (Figure 3), requiring a transition from the elastic buckling regime to the net section limit (Moen 2008). DSM distortional buckling design expressions presented in the following section have been modified to provide this transition. For local-global buckling interaction, $M_{n\ell}$ is capped at M_{ynet}, imposing the net section strength limit when flexural capacity is governed by inelastic buckling and yielding, i.e. when λ_ℓ and λ_c are both low.

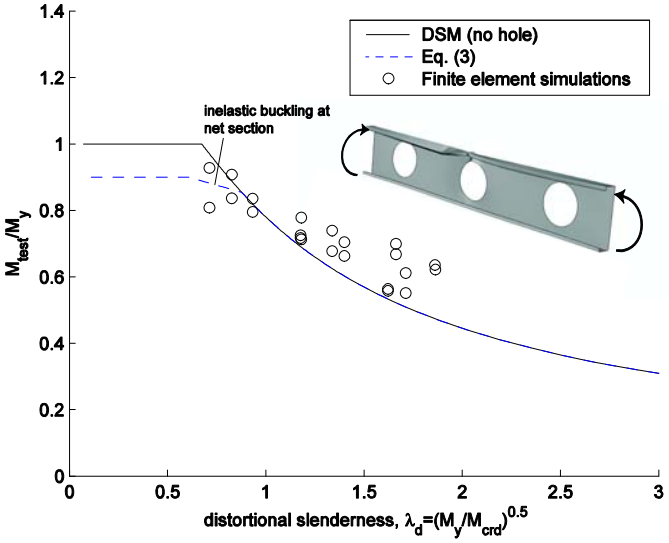

Figure 3 DSM distortional buckling curve for beams with holes

DSM design expressions for beams with holes

The nom inal strength of a col d-formed steel beam with holes shall be the minimum of M_{ne}, $M_{n\ell}$, and M_{nd} as given in the following sections.

Global Buckling

The nominal flexural strength, M_{ne}, for lateral-torsional buckling is:

$$\begin{aligned} M_{ne} &= M_{cre} \quad \text{for} \quad M_{cre} < 0.56M_y \\ &= \frac{10}{9}M_y\left(1-\frac{10M_y}{36M_{cre}}\right) \quad \text{for} \quad 2.78M_y \geq M_{cre} \geq 0.56M_y \\ &= M_y \quad \text{for} \quad M_{cre} > 2.78M_y \end{aligned} \tag{1}$$

where M_{cre} includes the influence of hole(s).

Local Buckling Interaction

The nominal flexural strength, $M_{n\ell}$, for local-global buckling interaction is:

$$\begin{aligned} M_{n\ell} &= M_{ne} \leq M_{ynet} \text{ for } \lambda_\ell \leq 0.776 \\ &= \left[1-0.15\left(\frac{M_{cr\ell}}{M_{ne}}\right)\right]^{0.4}\left(\frac{M_{cr\ell}}{M_{ne}}\right)^{0.4} M_{ne} \text{ for } \lambda_\ell > 0.776\,, \end{aligned} \tag{2}$$

where $\lambda_\ell=(M_{ne}/M_{cr\ell})^{0.5}$, and $M_{cr\ell}$ includes the influence of hole(s).

Distortional Buckling

The nominal flexural strength, M_{nd}, for distortional buckling is:

$$\begin{aligned} M_{nd} &= M_{ynet} \quad \text{for} \quad \lambda_d \leq \lambda_{d1} \\ &= M_{ynet} - \left(\frac{M_{ynet}-M_{d2}}{\lambda_{d2}-\lambda_{d1}}\right)\left(\lambda_d-\lambda_{d1}\right) \quad \text{for} \quad \lambda_{d1} < \lambda_d \leq \lambda_{d2} \\ &= \left(1-0.22\left(\frac{M_{crd}}{M_y}\right)^{0.6}\right)\left(\frac{M_{crd}}{M_y}\right)^{0.6} M_y \quad \text{for} \quad \lambda_d > \lambda_{d2}\,, \end{aligned} \tag{3}$$

where $\lambda_d=(M_y/M_{crd})^{0.5}$, $\lambda_{d1}=0.673(M_{ynet}/M_y)$, $\lambda_{d2}=0.673(1.7(M_y/M_{ynet})^{1.7}-0.7)$, M_{crd} includes the influence of hole(s), and

$$M_{d2}=\left(1-0.22\left(1/\lambda_{d2}\right)^{0.5}\right)\left(1/\lambda_{d2}\right)^{0.5}M_y\,. \qquad (4)$$

Design example

The DSM design approach outlined in Eq. (1) to Eq. (4) is employed to calculate the capacity of a perforated cold-formed steel joist (Figure 4) with an SSMA 550S162-33 lipped C-section (SSMA 2001), where F_y=55 ksi.

Joist geometry, boundary conditions, and loading

The joist carries a uniform vertical load and is assumed to be fully braced against lateral-torsional buckling (Figure 4). Distortional buckling and local buckling are viable strength limit states.

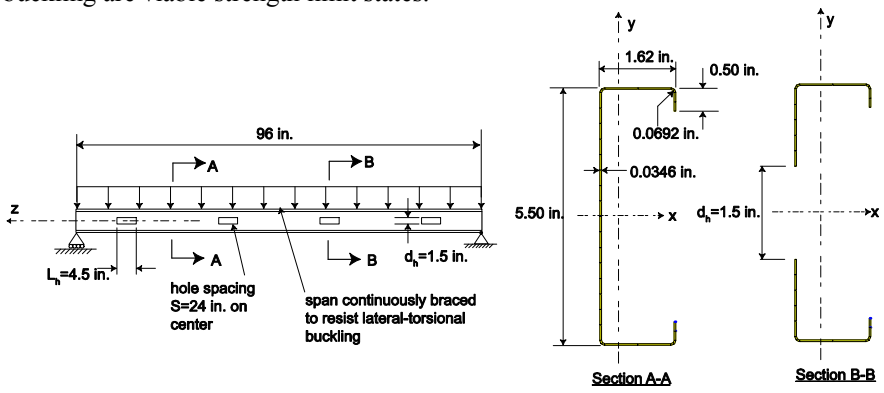

Figure 4 Column dimensions and boundary conditions

Gross and net section properties

The gross section and net section properties (Table 1) are calculated with the section property calculator in CUFSM. To determine the net section properties in CUFSM, assign a thickness of zero to the elements at the location of the perforations, but do not delete them. Assuming 55 ksi steel, M_y=29.15 kip·in. and M_{ynet}=28.95 kip·in.

Table 1 (a) gross section properties, (b) net section properties

(a)

A_g in.^{2}	I_x in.^{4}	I_y in.^{4}	r_x in.	r_y in.	J in.^{4}	C_w in.^{6}	x_o in.	y_o in.	I_{xo} in.^{4}	I_{yo} in.^{4}	r_{xo} in.	r_{yo} in.	r_o in.
0.327	1.46	0.11	2.11	0.59	0.000130	0.682	-1.11	0.00	1.86	0.11	2.39	0.59	2.46

(b)

A_{net} in.^{2}	I_{xnet} in.^{4}	I_{ynet} in.^{4}	r_{xnet} in.	r_{ynet} in.	J_{net} in.^{4}	C_{wnet} in.^{6}	x_{onet} in.	y_{onet} in.	I_{xonet} in.^{4}	I_{yonet} in.^{4}	r_{xonet} in.	r_{yonet} in.	r_{onet} in.
0.275	1.45	0.10	2.29	0.61	0.000110	0.677	-1.20	0.00	1.84	0.10	2.59	0.61	2.66

Elastic buckling analysis

Local buckling

Local buckling in a cold-formed steel beam with holes is assumed to occur as either buckling in the gross cross-section between holes ($M_{cr\ell nh}$) or buckling of the compressed strip adjacent to a hole ($M_{cr\ell h}$). The buckled mode shape with the lowest critical buckling load defines $M_{cr\ell}$, i.e. $M_{cr\ell}$=min($M_{cr\ell nh}$, $M_{cr\ell h}$). The elastic buckling curve for the gross cross-section (generated with CUFSM, see Figure 5) is used to obtain $M_{cr\ell nh}$. Taking the first minimum on the elastic buckling curve, $M_{cr\ell nh}$= 17.61 kip·in. at a half-wavelength $L_{cr\ell nh}$=3.0 in.

The net-section elastic buckling curve is generated in CUFSM by modifying the gross section node and element geometry such that one finite strip element with t=0 spans across the hole (Figure 6). A reference moment of 1 kip·in. is applied to the cross section and CUFSM (Properties screen) is used to calculate the corresponding stress distribution. The zero thickness element is then deleted, and the two corners of the cross-section in compression are restrained in the CUFSM z-direction. The resulting mode shape and elastic buckling curve is provided in Figure 6. The lowest buckling load of the unstiffened strip occurs at a half-wavelength less than the length of the perforation ($L_{cr\ell h}$ =4.25 in. versus L_{hole}=4.5 in.) meaning that the buckled half-wave can form within the length of the hole, and therefore $M_{cr\ell h}$=10.51 kip·in. (Note that $M_{cr\ell h}$ could be tabulated for standard punchout sizes and shapes as a convenience to the engineer!)

Local buckling is predicted to occur in the net cross section since $M_{cr\ell h}$<$M_{cr\ell nh}$ and therefore $M_{cr\ell}$= 10.51 kip·in. The local buckling moment is 40% lower at a hole, which means that buckling will tend to occur as unstiffened strip buckling rather than in the web of the gross cross-section between holes.

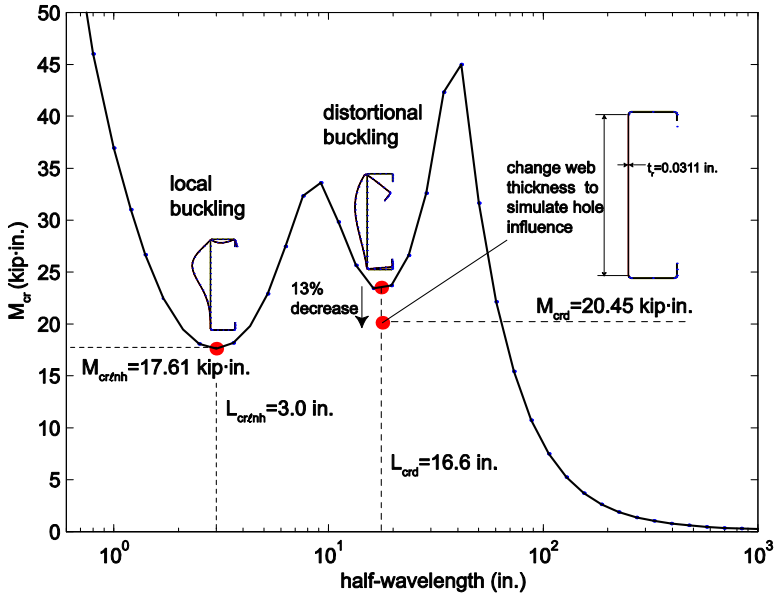

Figure 5 Elastic buckling curve for gross cross-section

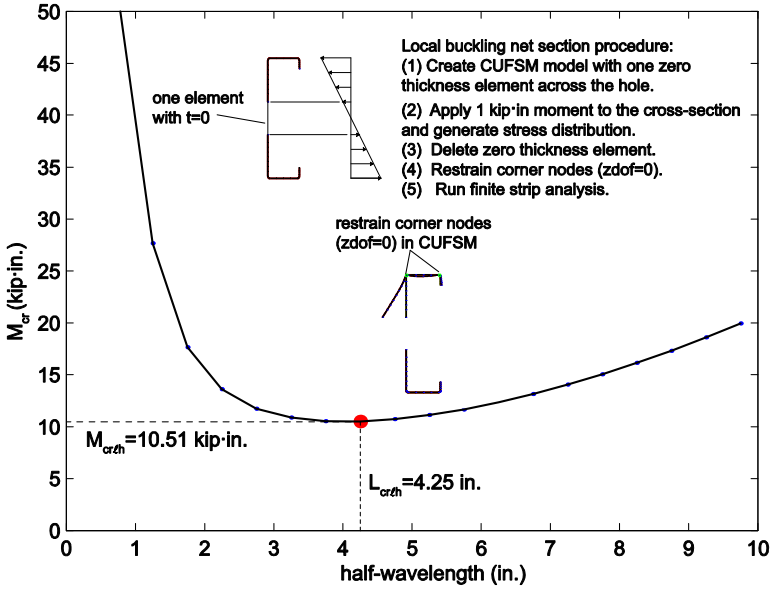

Figure 6 Local buckling curve for net cross-section

Distortional buckling

The critical elastic buckling moment for distortional buckling, including the influence of web holes, is calculated by first obtaining the distortional buckling half-wavelength from a finite strip analysis of the gross cross-section (L_{crd}=16.6 in., see Figure 5). The reduced web bending stiffness caused by a hole over one distortional half-wavelength is simulated by reducing the cross-section thickness of the web (Moen and Schafer 2009a):

$$t_r = \left(1 - \frac{L_h}{L_{crd}}\right)^{1/3} t \quad . \tag{5}$$

For L_h=4.5 in. and t=0.0346 in., t_r=0.0311 in. which is then implemented in a second finite strip analysis (Figure 5) performed just at L_{crd}=16.6 in., resulting in M_{crd}=20.45 kip·in. The presence of perforations reduces M_{crd} by 13% when compared to a distortional buckling moment of 23.43 kip·in for a beam without holes (Figure 5). Note that the beneficial influence of the moment gradient on M_{crd} (Yu 2005) is negligible and not considered because the beam's span length is much longer than L_{crd}.

Ultimate Strength Calculation

Inputs from the elastic buckling analysis include:

$M_y := 29.15 \cdot kip \cdot in$ $\quad M_{crL} := 10.51 \cdot kip \cdot in$

$M_{ynet} := 28.95 \cdot kip \cdot in$ $\quad M_{crd} := 20.45 \cdot kip \cdot in$

DSM global buckling strength Eq. (1)

$M_{ne} := M_y$ beam is fully braced against lateral-torsional buckling

$M_{ne} = 29.15 \cdot kip \cdot in$

DSM local buckling strength, Eq. (2)

$\lambda_L := \sqrt{\frac{M_{ne}}{M_{crL}}}$ $\quad \lambda_L = 1.6654$ (subscript "L" = "ℓ") local slenderness (including influence of holes)

$$M_{nL} := \begin{cases} \min\left(M_{ne}, M_{ynet}\right) & \text{if } \lambda_L \le 0.776 \\ \left[\left[1 - 0.15\cdot\left(\frac{M_{crL}}{M_{ne}}\right)^{0.4}\right]\left(\frac{M_{crL}}{M_{ne}}\right)^{0.4}\cdot M_{ne}\right] & \text{if } \lambda_L > 0.776 \end{cases}$$

$M_{nL} = 17.45\cdot kip\cdot in$

DSM distortional buckling strength, Eq. (3)

$\lambda_d := \sqrt{\frac{M_y}{M_{crd}}}$ $\quad \lambda_d = 1.1939$ distortional slenderness (including influence of holes)

$\lambda_{d1} := 0.673\cdot\left(\frac{M_{ynet}}{M_y}\right)$ $\quad \lambda_{d1} = 0.6684$

$\lambda_{d2} := 0.673\cdot\left[1.7\left(\frac{M_y}{M_{ynet}}\right)^{1.7} - 0.7\right]$ $\quad \lambda_{d2} = 0.6865$

$M_{d2} := \left[1 - 0.22\cdot\left(\frac{1}{\lambda_{d2}}\right)^{0.5}\right]\cdot\left(\frac{1}{\lambda_{d2}}\right)^{0.5}\cdot M_y$ $\quad M_{d2} = 25.8\cdot kip\cdot in$

$$M_{nd} := \begin{cases} M_{ynet} & \text{if } \lambda_d \le \lambda_{d1} \\ \left[M_{ynet} - \left(\frac{M_{ynet} - M_{d2}}{\lambda_{d2} - \lambda_{d1}}\right)\cdot\left(\lambda_d - \lambda_{d1}\right)\right] & \text{if } \lambda_{d1} < \lambda_d \le \lambda_{d2} \\ \left[\left[1 - 0.22\cdot\left(\frac{M_{crd}}{M_y}\right)^{0.6}\right]\left(\frac{M_{crd}}{M_y}\right)^{0.6}\cdot M_y\right] & \text{if } \lambda_d > \lambda_{d2} \end{cases}$$

$M_{nd} = 19.4\cdot kip\cdot in$

Predicted flexural capacity (including holes):

$M_n := \min\left(\left(M_{ne} \quad M_{nL} \quad M_{nd}\right)\right)$ LRFD (prequalified section)

$M_n = 17.45 \cdot kip \cdot in$ (M_{nL} controls)

$\phi_b := 0.90$

$\phi_b \cdot M_n = 15.7 \cdot kip \cdot in$

Local buckling at a hole is predicted as the governing failure mode, with a decrease in flexural strength of 15% when compared to the same beam without holes. This result is contrary to the AISI Main Specification Section B 2.4, which states that when $d_h/h<0.38$, holes do not influence local buckling capacity. It will be difficult to make definitely conclusions on the validity of the Main Specification versus DSM until more experimental data is generated for cold-formed steel joists with unstiffened holes. The elastic buckling prediction of the unstiffened strip employed in DSM is certainly more representative of the actual buckling behavior when compared to the Main Specification as the net section finite strip approach (see Figure 6) considers cross section interaction.

Conclusions

The AISI Direct Strength Method (DSM) for cold-formed steel beams with holes utilizes the critical elastic buckling loads of a beam, including the influence of holes, to predict strength. The elastic buckling predictions are obtained with a suite of recently developed simplified methods that employ finite strip analysis and hand calculations derived from classical buckling solutions. The existing DSM design expressions for beams without holes have been modified to limit flexural capacity to the strength of the net cross section, and in the case of distortional buckling, a transition from the net section capacity to the elastic buckling regime was added to predict flexural strength influenced by inelastic buckling at the net cross section. DSM provides an accessible design approach for cold-formed steel beams that can account for holes across global, local, and distortional buckling limit states with improved accuracy and generality when compared to existing strength prediction methods.

Ongoing research

The DSM approach presented in this paper has been developed and validated primarily with nonlinear finite simulations (Moen 2008) in part because of the lack of experimental data. An experimental program was recently completed by the first author considering cold-formed steel joists with unstiffened holes which will be used to supplement the ongoing validation effort.

References

AISI-S100. (2007). *North American Specification for the Design of Cold-Formed Steel Structural Members*, Am erican Iron and St eel Institute, Washington, D.C.

Bebiano, R ., Pina, P ., Silv estre, N ., an d C amotim, D. (2 008). "GB TUL - Buckling a nd Vibration Analysis of Thin-W alled Me mbers." DECivil/IST, Techn ical Un iversity o f Lisbon (http://www.civil.ist.utl.pt/gbt).

Kesti, J. (2000). "Local and Disto rtional Bu ckling of Perforated Steel Wall Studs," Dissertation/Thesis, Helsinki University of Technology, Espoo, Finland.

Moen, C. D. (2008). "Dir ect Stren gth D esign for C old-Formed Steel M embers with Perforations," Ph.D. Thesis, Johns Hopkins University, Baltimore.

Moen, C. D., and Yu, C. "Elastic buckling of thin-walled structural components with stiffe ned holes." *51th AIAA/ASME/ASCE/AHS/ASC Structures, Structural Dynamics and Materials Conference, April 12, 2005 - April 15, 2010*, Orlando, FL.

Moen, C. D. , and Schafer, B . W. (2008). "Experim ents on c old-formed steel columns with holes." *Thin-Walled Structures*, 46, 1164-1182.

Moen, C. D., and Schafer, B. W. (2009a). "Elastic buckling of cold-formed steel columns and beams with holes." *Engineering Structures*, 31(12), 2812-2824.

Moen, C. D., and Schafer, B. W. (2009b). "Elastic buckling of thi n plates with holes in c ompression o r b ending." *Thin-Walled Structures*, 47 (12), 1597-1607.

Schafer, B. W., and Ádány, S. "Buckling analysis of cold-formed steel members using C UFSM: con ventional an d c onstrained finite st rip m ethods." *Eighteenth International Specialty Conference on Cold-Formed Steel Structures*, Orlando, FL.

SSMA. (2 001). *Product Technical Information, ICBO ER-4943P*, Steel Stud Manufacturers Association, <www.ssma.com>.

Yu, C. (2005). "Disto rtional b uckling of co ld-formed steel members in bending," Ph.D. Thesis, Johns Hopkins University, Baltimore.

Yu, W. W. (2 000). *Cold-Formed Steel Design*, John W. W iley & Sons, New York, NY.

Twentieth International Specialty Conference on Cold-Formed Steel Structures
St. Louis, Missouri, U.S.A., November 3 & 4, 2010

On the Direct Strength Design of Continuous Cold-Formed Steel Beams

Cilmar Basaglia and Dinar Camotim[1]

Abstract

The work reported in this paper concerns an ongoing investigation aimed at developing an efficient methodology to design continuous cold-formed steel beams failing in modes that combine local, distortional and global features. At this stage, it is intended to assess how accurately can the load-carrying capacity of lipped channel continuous (two and three-span) beams subjected to non-uniform bending be predicted by means of the current Direct Strength Method (DSM) design curves. "Exact" ultimate strength values yielded by geometrically and materially non-linear shell finite element analyses are compared with estimates provided by the DSM equations and, on the basis of this comparison, it is possible to identify some features that must be included in a DSM approach applicable to continuous cold-formed steel beams.

Introduction

The vast majority of cold-formed steel members exhibit very slender cross-sections, a feature rendering them highly prone to geometrically non-linear effects, namely those related to local, distortional and global (flexural or flexural-torsional) buckling. Indeed, a fair amount of research work has been recently devoted to the development of efficient design rules for isolated (single-span) members, mostly subjected to uniform internal force and

[1] Department of Civil Engineering and Architecture, IST/ICIST, Technical University of Lisbon, Av. Rovisco Pais, 1049-001 Lisboa, Portugal.

moment diagrams. The most successful end product of this intense research activity is the "Direct Strength Method" (DSM), which (i) has its roots in the work of Hancock (1994), (ii) was originally proposed by Schafer & Peköz in 1998 and (iii) has been continuously improved since (*e.g.*, Schafer 2008). The DSM provides estimates of the load-carrying capacity of cold-formed steel members exhibiting local, distortional or global failure mechanisms, as well as those undergoing local/global interaction – design curves to account for interaction phenomena involving distortional buckling are currently under investigation (*e.g.*, Kwon *et al.* 2009, Silvestre *et al.* 2009). Since the member ultimate strength can be accurately predicted solely on the basis of its elastic (critical) buckling and yield stresses, the DSM is an efficient alternative to the more traditional "effective width method". Following the universal acceptance of the DSM approach to design cold-formed steel members, it has already been included in the latest editions of the corresponding North American (NAS 2007) and Australian/New Zealander (AS/NZS4600 2005) specifications.

Concerning the determination of the member elastic buckling stress, the current application of the DSM relies heavily on the use of finite strip analysis (FSA), easily accessible to a large number of designers, mostly due to the freely available software developed by Schafer & Ádány (2006). However, at the moment FSA can only handle accurately simply supported single-span members subjected to uniform internal forces and moments.

In practice, many cold-formed steel members exhibit multiple spans (*e.g.*, secondary elements such as purlins or side rails) and are often subjected to non-uniform bending moment diagrams combining positive (sagging) and negative (hogging) regions, a feature making their buckling behavior rather complex, as it may (i) combine local, distortional and global features and (ii) involve a fair amount of localization (*e.g.*, the occurrence of local and/or distortional buckling in the vicinity of intermediate supports, where there are relevant moment gradients and little restraint can be offered to the slender bottom/compressed flanges). Even so, it seems fair to say that it is still very scarce the amount of research devoted to the buckling and post-buckling behaviors of cold-formed steel beams subjected to non-uniform bending moment diagrams, namely continuous beams. In this context, it is worth noting the recent works of (i) Yu & Schafer (2007), who used shell finite element models to investigate the influence of linear bending moments on the distortional buckling and post-buckling behaviors of single-span steel beams,

and applied their findings to examine and extend the DSM design procedure to such members, (ii) Camotim *et al.* (2008), who employed Generalized Beam Theory (GBT) to analyze the buckling behavior of steel beams with several loadings and support conditions (including intermediate supports), and (iii) Pham & Hancock (2009), who proposed a DSM-based design criterion for purlin-sheeting systems using elastic lateral-torsional buckling moments evaluated through the so-called C_b-factor approach or finite element analyses.

The objective of this work is to report the available results concerning an ongoing investigation aimed at developing an efficient methodology to design continuous cold-formed steel beams failing in arbitrarily complex collapse modes. The first step consists of assessing how accurately can the ultimate strength of lipped channel continuous (two and three-span) beams subjected to non-uniform bending (due to uniformly transverse loads) be predicted by the current DSM design curves, developed primarily for single-span (isolated) members. In order to achieve this goal, one incorporates into the DSM expressions "exact" (i) critical load factors, evaluated by means of GBT analyses, and (ii) ultimate load (collapse load) factors, obtained from first-order elastic-plastic shell finite element (SFE) analyses carried out in the code ANSYS (SAS 2004). The DSM ultimate strength estimates are compared with "exact" values, yielded by geometrically and materially non-linear SFE analyses, also performed in ANSYS. The paper closes with the discussion of the results obtained – in particular, it is possible to draw some interesting (preliminary) conclusions concerning the features that must be incorporated in a DSM-based design approach applicable to continuous cold-formed steel beams similar to those considered in this work.

DSM Design Procedure

The current DSM approach adopts "Winter-type" design curves, calibrated against experimental and numerical results concerning the ultimate strength of single-span (isolated) members subjected to uniform compression and/or bending. In the case of beams, the nominal bending strengths against local (M_{nl}), distortional (M_{nd}) and global (M_{ne}) failures are given by the expressions

$$M_{nl} = M_y \qquad if \qquad \lambda_l = \sqrt{M_y / M_{crl}} \leq 0.776$$

$$M_{nl} = \left(1 - 0.15\left(\frac{M_{crl}}{M_y}\right)^{0.4}\right)\left(\frac{M_{crl}}{M_y}\right)^{0.4} M_y \qquad if \qquad \lambda_l > 0.776 \quad , \quad (1)$$

$$M_{nd} = M_y \qquad if \qquad \lambda_d = \sqrt{M_y / M_{crd}} \le 0.673$$

$$M_{nd} = \left(1 - 0.22\left(\frac{M_{crd}}{M_y}\right)^{0.5}\right)\left(\frac{M_{crd}}{M_y}\right)^{0.5} M_y \qquad if \qquad \lambda_d > 0.673 \quad , \quad (2)$$

$$M_{ne} = M_y \qquad if \qquad \lambda_e = \sqrt{M_y / M_{cre}} < 0.60$$

$$M_{ne} = \frac{10}{9}\left(1 - \frac{10M_y}{36M_{cre}}\right)M_y \qquad if \qquad 0.60 \le \lambda_e \le 1.336$$

$$M_{ne} = M_{cre} \qquad if \qquad \lambda_e > 1.336 \quad , \quad (3)$$

where (i) λ_l, λ_d, λ_e and M_{crl}, M_{crd} and M_{cre} are *local*, *distortional* and *global* slenderness and elastic critical buckling moment values, and (ii) $M_y = W_y f_y$ is the cross-section first yield moment – W_y is its elastic modulus.

Numerical Investigation: Scope and Modeling Issues

The continuous steel (*E=205GPa* and *v=0.3*) beams analyzed have (i) lipped channel cross-sections (dimensions in fig. 1(a)) and (ii) two or three identical spans (2s and 3s) with lengths *L=2.0m* (B2), *L=4.0m* (B4) and *L=5.0m* (B5). They are subject to a uniformly distributed load applied along the shear centre axis (causing only pre-buckling major-axis bending) and acting on either all spans (all) or just one of them (one) – see figure 1(b). The beam end sections are locally/globally pinned and may warp freely, and all the in-plane cross-section displacements are restrained at the intermediate supports.

Concerning the GBT analysis, the following modelling issues are worth noting:

(i) *Cross-Section Discretization*. Figure 2(a) shows the nodes considered in the lipped channel section. This discretization leads to *17* deformation modes, which are *global* (**1**-**4**), *distortional* (**5**-**6**) and *local* (**7**-**17**) – figure 2(b) shows the in-plane configurations of the most relevant ones.

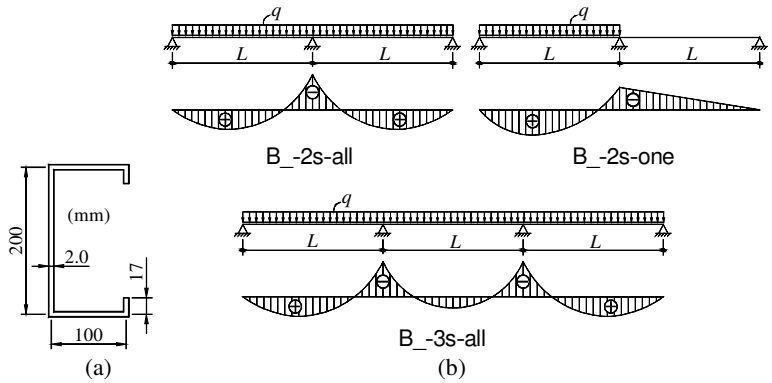

Fig. 1: Continuous beam (a) cross-section dimensions and (b) loading and first-order elastic bending moment diagrams

(ii) *Member Discretisation*. The equilibrium equations were solved using the beam finite element developed by Camotim *et al.* (2008): 2-node elements with 2*n* d.o.f. per node (*n* is the number of deformation modes included in the analysis), and mode amplitude functions approximated by Hermite cubic polynomials. Each beam span was discretized into *20* finite elements in all cases.

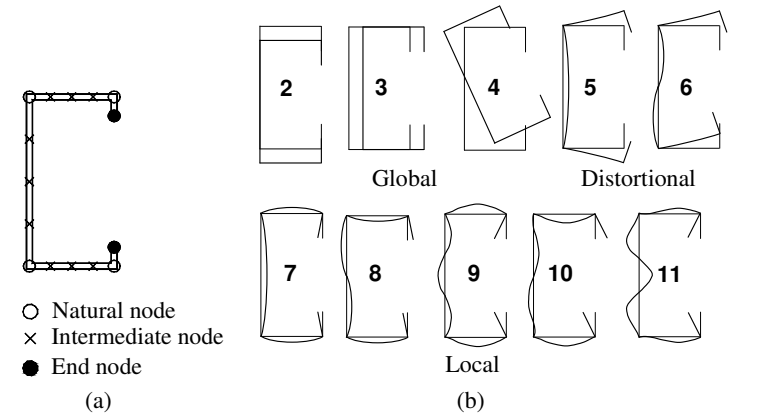

Fig. 2: (a) Lipped channel GBT discretization and (b) in plane shapes of the *10* most relevant deformation modes

Concerning the SFE analyses are concerned, the following issues are relevant:

(i) *Discretization*. The beam mid-surfaces were discretized into SHELL181 finite elements (ANSYS notation: isoparametric 4-node shell elements) – earlier investigations showed the adequacy of these elements. The beam discretization involved *20* elements along the cross-section mid-line and length-to-width ratios of about *1.3* (web and flanges) and *4* (lips).

(ii) *Support Conditions*. The support conditions were modeled in the "usual fashion": null transverse membrane and flexural displacement imposed at all cross-section nodes associated with the end and intermediate supports – in order to preclude the longitudinal rigid-body motion, the axial displacement was prevented at a beam mid cross-section node.

(iii) *Loading*. Transverse load distributions *q'* were applied along the cross-section mid-line covering the whole span length. These transverse loads are (iii_1) statically equivalent to a uniformly distributed load *q* applied along the beam shear centre axis (see fig. 3(a)) and also (iii_2) qualitatively similar to the first moment of the cross-section with respect to the its major axis (see fig. 3(b)).

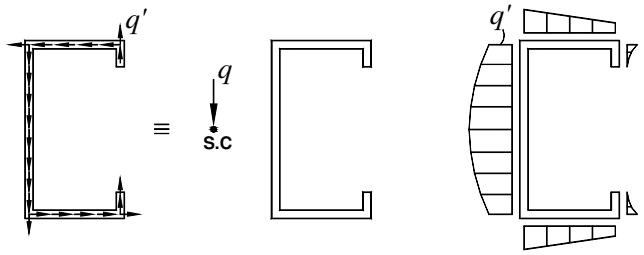

Fig. 3: (a) Applied transverse loads *q'* statically equivalent to a load *q* along the shear centre (S.C) axis and (b) cross-section distribution of the load *q'*

(iv) *Material Modeling*. The steel material behavior was deemed either linear elastic (bucking analyses) or a linear-elastic/perfectly-plastic with a von Mises yield criterion (post-buckling analyses).

(v) *Initial Imperfections*. All initial geometrical imperfections have the beam critical buckling mode shape and amplitude equal to either *10%* of the wall thickness (local/distortional buckling) or *L/1000* (global buckling).

Buckling Analysis

In all existing design procedures, a crucial step is the identification of the buckling mode nature, by no means clear in continuous beams. This can be confirmed by examining figure 4, which provides two representations of the B5-2s-all beam critical buckling mode shapes, namely (i) a 3D-view yielded by an ANSYS SFE analysis and (ii) the GBT modal amplitude functions. Note (i) the excellent agreement between the ANSYS and GBT results and (ii) how the critical buckling mode combines the three deformation mode types: contributions from local (**7**+**8**) and distortional (**5**+**6**) modes, mostly in the close vicinity of the intermediate support, and global (**3**+**4**) modes with higher participations at the mid-span regions.

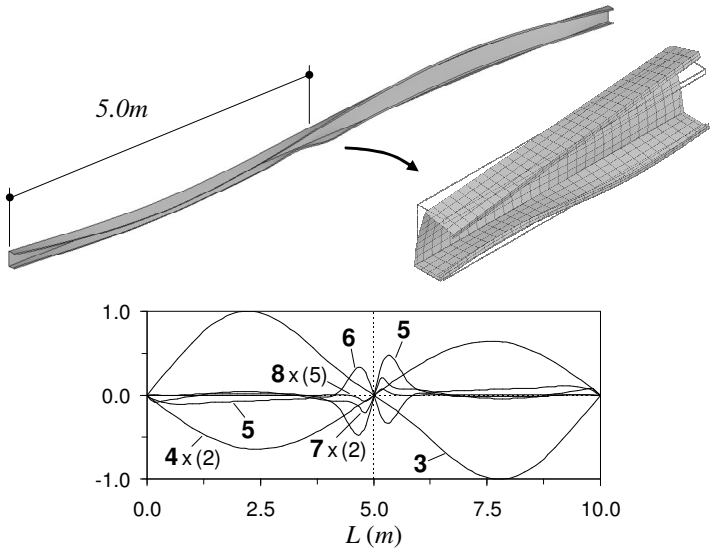

Fig. 4: ANSYS and GBT-based B5-2s-all beam critical buckling mode shapes

In order to attempt to establish the "dominant nature" of the beam critical buckling modes, GBT analyses were carried out including only global (**2**-**4**), distortional (**5**-**6**) and local (**7**-**17**) deformation modes. Table 1 shows the critical load values (q_{cr}), yielded by the ANSYS and GBT (including all deformation modes) analyses, and the relation between the "pure" global ($q_{b.e}$), distortional

($q_{b.d}$) and local ($q_{b.l}$) buckling loads and $q_{cr.GBT}$ – the "dominant buckling mode nature", given in the last column, reflects the "closeness" between the corresponding "pure" buckling load and $q_{cr.GBT}$ (lowest of the three ratios).

Table 1: Relation between the "pure" (q_b) and critical (q_{cr}) load values

Beam	Crit. Load (*kN/m*)		$\frac{q_{b.e}}{q_{cr.GBT}}$	$\frac{q_{b.d}}{q_{cr.GBT}}$	$\frac{q_{b.l}}{q_{cr.GBT}}$	Dominant buckling mode nature
	$q_{cr.GBT}$	$q_{cr.ANSYS}$				
B2-2s-all	46.66	46.78	5.193	1.399	1.032	Local
B4-2s-all	10.82	10.71	1.439	1.104	1.187	Distortional
B5-2s-all	6.06	5.92	1.074	1.172	1.391	Global
B2-2s-one	44.42	44.81	5.091	1.067	1.293	Distortional
B4-2s-one	10.21	10.00	1.416	1.044	1.505	Distortional
B5-2s-one	5.61	5.61	1.073	1.178	1.785	Global
B2-3s-all	53.19	52.42	4.585	1.074	1.021	Local
B4-3s-all	12.35	12.38	1.267	1.046	1.329	Distortional
B5-3s-all	6.13	6.09	1.063	1.303	1.805	Global

Post-Buckling Analysis

The ultimate load values q_u presented in the next sections were obtained through beam elastic-plastic SFE analyses carried out up to failure. To convey the meaning of these values, figure 5 (a) shows the post-buckling equilibrium paths (q *vs.* V_1) of the B2-2s-all beam with different yield stresses (f_y=*250*, *350*,*550*,*850 MPa*) – (i) the symbols □, △, ○ and ◇ indicate the ultimate loads and (ii) V_1 is the displacement selected to provide a better characterization of the beam post-buckling behavior, corresponding to the vertical displacement of the bottom flange-lip corner of the cross-section located in the beam left span, *23.4 cm* away from the intermediate support (see fig. 5(b)). As expected, the amount of post-critical strength reserve increases with the yield stress.

Figure 6 concerns the B2-2s-all beam with f_y=*250 MPa* and displays the deformed configurations and von Mises stress distributions associated with (i) the full yielding of the mid-cross-section (first plastic hinge formation), at q=*33.4 kN/m* (point **I** – fig. 5(a)), and (ii) the beam collapse, at q_u=*37.8 kN/m* (point **II**) and corresponding to the nearly simultaneous yielding of the two mid-span cross-sections. Note the very clear bending moment redistribution.

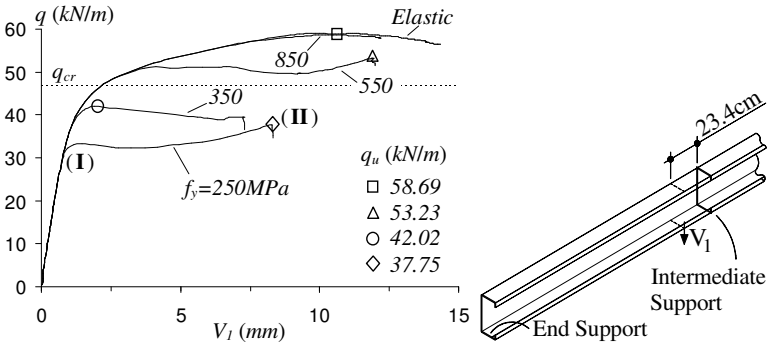

Fig. 5: B2-2s-all beam (a) equilibrium paths and (b) measured displacement

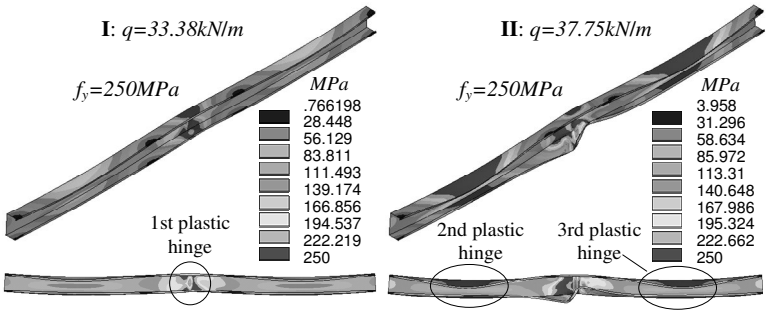

Fig. 6: B2-2s-all beam deformed configuration and von Mises stresses concerning the formation of the first plastic hinge and the beam collapse

Assessment of the DSM Strength Estimates

In beams subjected to non-uniform bending, it is convenient to replace the various "M_y and M_{cr} values" appearing in (1)-(3) by "first yield q_y and critical buckling q_{cr} load values" – in this case, the obvious choices are

$$q_y = M_y / 0.125L^2 \quad q_{cr} = M_{cr} / 0.125L^2 \quad \textit{for beams } \text{B\_-2s-all}$$

$$q_y = M_y / 0.0957L^2 \quad q_{cr} = M_{cr} / 0.0957L^2 \quad \textit{for beams } \text{B\_-2s-one}$$

$$q_y = M_y / 0.1L^2 \qquad q_{cr} = M_{cr} / 0.1L^2 \qquad \textit{for beams } \text{B\_-3s-all} \quad . \quad (4)$$

Note that using expressions (1)-(3) corresponds to neglecting (i) the cross-section elastic-plastic strength reserve, in both statically determinate and indeterminate beams, and (ii) the bending moment redistribution, in statically indeterminate beams – *i.e.*, overly conservative predictions are to be expected in statically indeterminate beams, particularly in the lower slenderness range.

Figures 7 to 9 show comparisons between the ultimate load predictions yielded by the current DSM design curves and the ultimate loads obtained through SFE analyses involving B_-2s-all, B_-2s-one and B_-3s-all beams with *15* different yield stresses, associated with yield-to-critical load ratios q_y/q_{cr} varying from *0.06* to *3.74* and covering a wide slenderness range – these results are summarized in table A1, presented in the Appendix of this paper). The numerical ("exact") ultimate loads, normalized w.r.t. q_y, are identified by the symbols ○, □ and △, for local, distortional and global buckling/failure modes. Since the beams exhibit buckling/failure modes that are not "pure", the DSM curve choice was based on their "dominant buckling mode nature", given in table 1 – however, λ_l, λ_d and λ_e are calculated with the "real" beam critical buckling load q_{cr}, which is neither "purely" local, distortional or global. The observation of these results/comparisons prompts the following remarks:

(i) The DSM predictions are (i_1) excessively safe in the low slenderness range, (i_2) slightly safe in the intermediate slenderness range and (i_3) too unsafe (local and distortional) or moderately safe (global) in the high slenderness range.

(ii) None of the DSM curves provides a set of efficient (safe and economic) predictions of the continuous beam ultimate loads, which is due to a combination of factors: (ii_1) neglecting both the cross-section elastic-plastic strength reserve and (mostly) the moment redistribution (low slenderness range) and (ii_2) the "mixed" nature of the failure mechanisms (high slenderness range).

(iii) Since the beam ultimate loads already incorporate the local, distortional and global buckling effects, it seems to make little sense to neglect the cross-section elastic-plastic strength reserve and moment redistribution. The recent work by Shifferaw & Schafer (2007) partially confirms this assertion, as it reports experimental and numerical evidence, involving simply supported isolated beams (no moment redistribution), of the

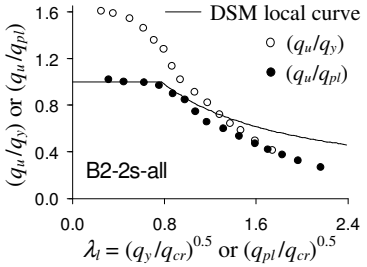

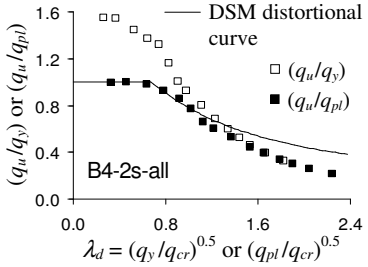

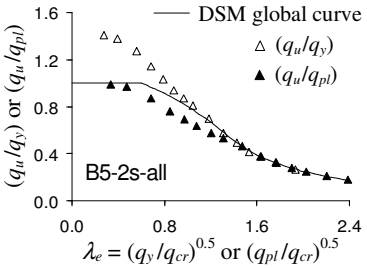

Fig. 7: B_-2s-all beams – comparison between the SFE ultimate loads and DSM design curve predictions

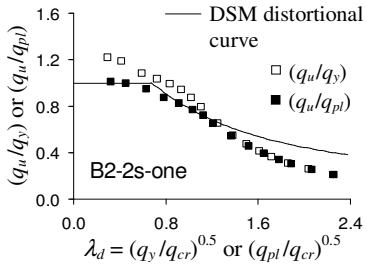

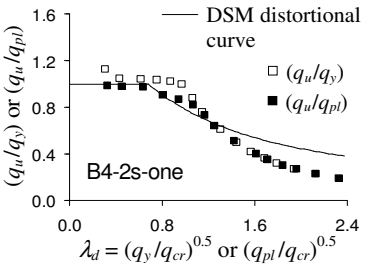

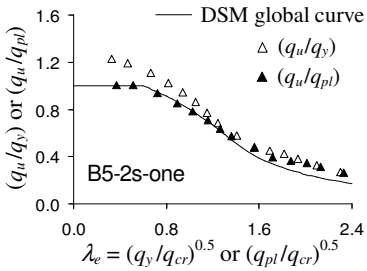

Fig. 8: B_-2s-one beams – comparison between the SFE ultimate loads and DSM design curve predictions

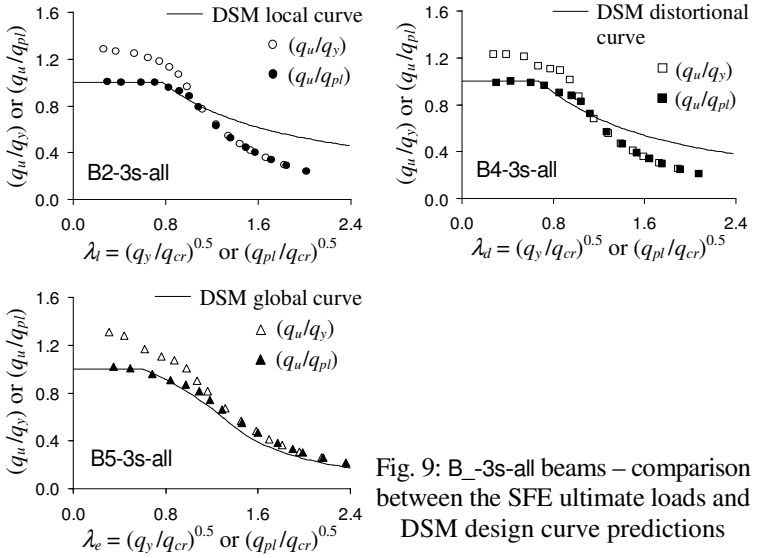

Fig. 9: B_-3s-all beams – comparison between the SFE ultimate loads and DSM design curve predictions

(logical) presence of a non-negligible inelastic strength in the low slenderness range – obviously due to the cross-section plastic strength.

(iv) The most rational approach to account for the beam inelastic strength reserve (including moment redistribution) is to replace the beam *first yield* loads q_y by (geometrically linear) *plastic collapse* loads q_{pl} in (1)-(3). Figures 7 to 9 also compare, for each beam, the ultimate load predictions yielded by the modified DSM design curves with the SFE values, now normalised w.r.t. q_{pl} and represented by the symbols ●, ■ and ▲. Moreover, figures 10 to 11 display all these results grouped according to the beam dominant buckling mode nature. The observation of this new set of results leads to the following comments:

(iv.1) In the low slenderness range, the modified DSM predictions are quite accurate (a few of them are slightly unsafe), which confirms the presence and relevance of the beam inelastic strength reserve.

(iv.2) In the intermediate slenderness range, most of the modified DSM predictions are fairly accurate, although there are a number of slightly unsafe (beams B2-2s-all and B2-2s-one) and safe (beams B4-2s-all, B4-2s-one, B5-2s-one, B2-3s-all, B4-3s-all and B5-3s-all)

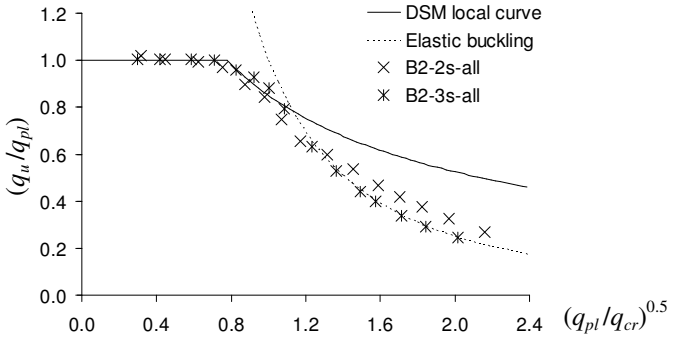

Fig. 10: SFE ultimate loads and modified DSM predictions (local failure)

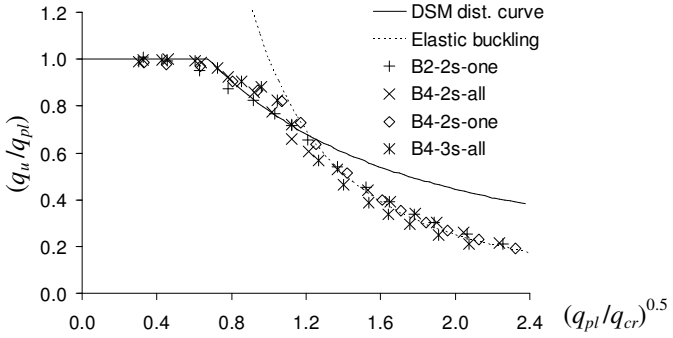

Fig. 11: SFE ultimate loads and modified DSM predictions (distort. failure)

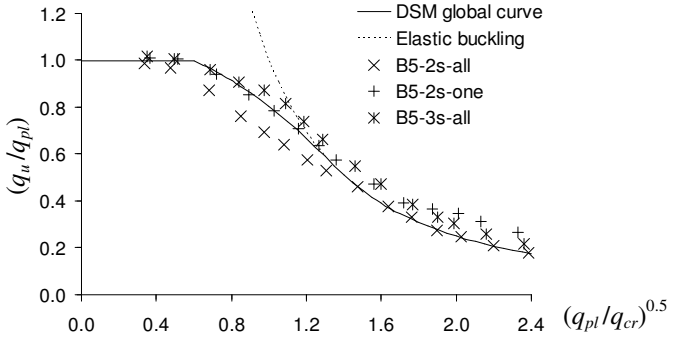

Fig. 12: SFE ultimate loads and modified DSM predictions (global failure)

estimates. The beam B5-2s-all predictions (predominantly global failures) are the exceptions, as they are clearly unsafe.

(iv.3) In the high slenderness range, there is practically no difference between the current and modified DSM predictions, due to the fact that failure stems mainly from stability effects (plasticity plays a lesser role). Indeed, in this slenderness range, the elastic critical buckling curves (dashed lines) provide almost always safe and accurate ultimate load estimates. The exception are now the beam B4-3s-all ultimate loads (predominantly distortional failures), which lie slightly below the corresponding elastic critical buckling curve.

Although considerable more research work is obviously needed before firm guidelines concerning the DSM design of continuous cold-formed steel beams can be established, it is possible to make some preliminary comments on the basis of the limited amount of results presented in this work:

(i) Since there are no "pure" buckling and failure modes, the DSM curve choice should be based on the concept of "dominant buckling/failure mode nature". Nevertheless, the local, distortional and global slenderness values are based on the "real" critical buckling load.

(ii) The first yield load (moment) should be replaced by the first-order plastic collapse load (moment), thus accounting for the cross-section elastic-plastic strength reserve and bending moment redistribution. Failing to do this will inevitably lead to overly conservative prediction in the low-to-intermediate slenderness range.

(iii) Apparently, the most rational approach is to develop and calibrate design curves based on (iii_1) the elastic-plastic collapse load, for stocky beams, and (iii_2) the elastic buckling load, for slender beams. Nothing can yet be said about intermediate beams (or about the slenderness limits separating the three ranges) – nevertheless, the current DSM design curves provide satisfactory ultimate load estimates in this range.

Conclusion

This work reported the available results of an ongoing investigation aimed at developing an efficient methodology to design continuous cold-formed steel beams failing in arbitrarily complex collapse modes. At this stage, it was assessed how accurately can the ultimate strength of continuous lipped channel beams (two and three spans) subjected to non-uniform bending

be predicted by the current DSM design curves. It was found that, in order to achieve a better accuracy, "exact" (i) critical load factors, evaluated by means of GBT analyses, and (ii) ultimate load factors, obtained from elastic-plastic first-order SFE ANSYS analyses, had to be incorporated into the DSM expressions. Then, the (modified) DSM ultimate strength estimates were compared with "exact" values, yielded by geometrically and materially non-linear SFE ANSYS analyses. The following aspects deserve to be mentioned:

(i) The beam buckling and failure modes combine at least two deformation mode types, which precludes a straightforward classification. Thus, one must resort to the "dominant buckling/failure mode nature" concept in order to choose of the appropriate DSM design curve.

(ii) The direct application of the current DSM design curves leads to either overly conservative (stocky beams) or clearly unsafe (slender beams) ultimate load predictions. After a few modifications, the "quality" of the DSM ultimate strength estimates improved significantly.

(iii) The numerical (SFE) ultimate loads obtained clearly indicated that (iii_1) the beams with low-to-intermediate slenderness exhibit a fair amount of inelastic strength reserve, stemming mostly from moment redistribution, and (iv_2) the ultimate loads of the slender beams are fairly well approximated by their critical buckling loads. Although further studies are required to confirm these preliminary findings, it seems that the incorporation of a few modifications in the current DSM design curves will make it possible to account efficiently for these two aspects.

Acknowledgements

The first author gratefully acknowledges the financial support provided by *"Fundação para a Ciência e Tecnologia"* (FCT – Portugal), through the post-doctoral scholarship nº SFRH/BPD/62904/2009.

References

AS/NZS4600 (2005). *Cold-formed Steel Structures.* Australian Standard/New Zealand Standard 4600, Standards Australia, Sydney.

Camotim D, Silvestre N, Basaglia C and Bebiano R (2008). GBT-based buckling analysis of thin-walled members with non-standard support conditions, *Thin-Walled Structures*, **46**(7-9), 800-815.

Hancock GJ, Kwon YB and Bernard ES (1994). Strength design curves for

thin-walled sections undergoing distortional buckling, *Journal of Constructional Steel Research*, **31**(2-3), 169-186.

Kwon YB, Kim BS and Hancock GJ (2009), "Compression tests of high strength cold-formed steel channels with buckling interaction", *Journal of Constructional Steel Research*, **65**(2), 278-289.

NAS (2007). *North American Specification for the Design of Cold-Formed Steel Structural Members* (AISI-S100-07), American Iron and Steel Institute (AISI), Washington (DC).

Pham C.H. and Hancock G. (2009). Direct strength design of cold-formed purlins, *Journal of Structural Engineering*, **135**(3), 229-238.

Schafer BW (2008). Review: the direct strength method of cold-formed steel member design, *Journal of Constructional Steel Research*, **64**(7-8), 766-778.

Schafer BW and Pekoz T (1998). Direct strength prediction of cold-formed steel members using numerical elastic buckling solutions, *Thin-Walled Structures - Research and Development* (ICTWS'98 – Singapore, 2-4/12) N. Shanmugam, J.Y.R. Liew, V. Thevendran (eds.), Elsevier, 137-144.

Schafer BW and Ádány S (2006). Buckling analysis of cold-formed steel members using CUFSM: conventional and constrained finite strip methods, *Proceedings of 18th International Specialty Conference on Cold-Formed Steel Structures* (Orlando, 26-27/10), R. LaBoube, W.W. Yu (eds.), 39-54.

Shifferaw Y and Schafer BW (2007). Inelastic bending capacity in cold-formed steel members, *Proceedings of SSRC Annual Stability Conference* (New Orleans, 18-21/4), 279-299.

Silvestre N., Camotim D. and Dinis P.B. (2009), "Direct strength prediction of lipped channel columns experiencing local-plate/distortional interaction", *Advanced Steel Construction – An International Journal*, **5**(1), 45-67.

Swanson Analysis Systems (SAS) (2004). *ANSYS Reference Manual* (vs. 8.1).

Yu C. and Schafer B.W. (2007). Simulation of cold-formed steel beams in local and distortional buckling with applications to the direct strength method, *Journal of Constructional Steel Research*, **63**(5), 581-590.

Appendix

Table A1 shows the ultimate load predictions yielded by current ($q_{u,y}$) and modified ($q_{u,pl}$) DSM design curves, as well as the "exact" ultimate loads obtained through SFE ANSYS analyses (q_u) of the beams dealt with in this work. Moreover, the beam dominant buckling mode nature (BM), which may be either local (L), distortional (D) or Global (G), is also provided.

Table A1: Comparison between the "exact" beam ultimate load values and the two DSM estimates

Beam	BM	SFE			DSM		$\frac{q_{u.y}}{q_u}$	$\frac{q_{u.pl}}{q_u}$
		q_y	q_{pl}	q_u (kN/m)	$q_{u.y}$	$q_{u.pl}$		
B2-2s-all	L	0.030	0.046	0.047	0.030	0.046	0.62	0.98
		0.059	0.093	0.094	0.059	0.093	0.63	1.00
		0.118	0.183	0.182	0.118	0.183	0.65	1.01
		0.177	0.266	0.258	0.177	0.266	0.69	1.03
		0.236	0.356	0.320	0.236	0.330	0.74	1.03
		0.295	0.447	0.377	0.291	0.385	0.77	1.02
		0.354	0.537	0.401	0.329	0.436	0.82	1.09
		0.413	0.642	0.420	0.366	0.490	0.87	1.17
		0.531	0.812	0.485	0.433	0.572	0.89	1.18
		0.649	0.992	0.532	0.494	0.652	0.93	1.23
		0.768	1.184	0.555	0.552	0.731	0.99	1.32
		0.886	1.359	0.570	0.606	0.799	1.06	1.40
		1.004	1.559	0.587	0.657	0.873	1.12	1.49
		1.181	1.809	0.590	0.730	0.960	1.24	1.63
		1.417	2.184	0.590	0.821	1.083	1.39	1.84
B4-2s-all	D	0.007	0.011	0.011	0.007	0.011	0.65	1.01
		0.015	0.023	0.023	0.015	0.023	0.65	1.00
		0.030	0.043	0.043	0.030	0.043	0.69	1.02
		0.044	0.066	0.061	0.044	0.061	0.73	1.00
		0.059	0.091	0.078	0.056	0.075	0.72	0.97
		0.074	0.111	0.086	0.066	0.086	0.76	1.00
		0.089	0.136	0.089	0.074	0.097	0.83	1.09
		0.103	0.158	0.096	0.082	0.107	0.85	1.12
		0.133	0.201	0.107	0.096	0.124	0.90	1.16
		0.162	0.251	0.111	0.109	0.141	0.98	1.27
		0.192	0.292	0.115	0.120	0.154	1.05	1.34
		0.221	0.342	0.116	0.131	0.169	1.13	1.45
		0.251	0.386	0.117	0.141	0.181	1.21	1.54
		0.295	0.447	0.116	0.155	0.196	1.33	1.69
		0.354	0.537	0.116	0.172	0.217	1.48	1.87
B5-2s-all	G	0.005	0.007	0.007	0.005	0.007	0.71	1.01
		0.009	0.013	0.013	0.009	0.013	0.73	1.03
		0.019	0.028	0.024	0.019	0.027	0.79	1.11
		0.028	0.043	0.032	0.027	0.038	0.84	1.18
		0.038	0.056	0.039	0.035	0.046	0.89	1.19
		0.047	0.069	0.044	0.041	0.052	0.94	1.19
		0.057	0.086	0.049	0.047	0.058	0.94	1.17
		0.066	0.101	0.053	0.051	0.060	0.96	1.13
		0.085	0.128	0.059	0.058	0.061	0.97	1.02

Table A1: Comparison between the "exact" beam ultimate load values and the two DSM estimates (cont.)

Beam	BM	SFE			DSM		$\frac{q_{u.y}}{q_u}$	$\frac{q_{u.pl}}{q_u}$
		q_y	q_{pl}	q_u (kN/m)	$q_{u.y}$	$q_{u.pl}$		
B5-2s-all	G	0.104	0.158	0.060	0.060	0.061	1.01	1.01
		0.123	0.183	0.061	0.061	0.061	1.00	1.00
		0.142	0.213	0.059	0.061	0.061	1.03	1.03
		0.161	0.243	0.061	0.061	0.061	1.00	1.00
		0.189	0.287	0.061	0.061	0.061	1.00	1.00
		0.227	0.337	0.061	0.061	0.061	1.00	1.00
B2-2s-one	D	0.039	0.047	0.047	0.039	0.047	0.82	0.99
		0.077	0.092	0.092	0.077	0.092	0.84	1.01
		0.154	0.176	0.167	0.154	0.176	0.92	1.05
		0.231	0.273	0.239	0.223	0.251	0.93	1.05
		0.308	0.372	0.306	0.272	0.309	0.89	1.01
		0.386	0.472	0.362	0.316	0.360	0.87	0.99
		0.463	0.562	0.403	0.356	0.402	0.88	1.00
		0.540	0.652	0.427	0.392	0.440	0.92	1.03
		0.694	0.832	0.451	0.458	0.510	1.01	1.13
		0.848	1.027	0.465	0.516	0.578	1.11	1.24
		1.003	1.207	0.473	0.570	0.634	1.20	1.34
		1.157	1.409	0.476	0.619	0.693	1.30	1.46
		1.311	1.580	0.478	0.665	0.740	1.39	1.55
		1.542	1.894	0.478	0.730	0.819	1.53	1.72
		1.851	2.259	0.478	0.809	0.904	1.69	1.89
B4-2s-one	D	0.010	0.011	0.011	0.010	0.011	0.89	1.02
		0.019	0.021	0.020	0.019	0.021	0.96	1.02
		0.039	0.041	0.040	0.039	0.041	0.96	1.03
		0.058	0.066	0.060	0.054	0.060	0.91	1.00
		0.077	0.091	0.079	0.066	0.074	0.84	0.94
		0.096	0.117	0.096	0.077	0.087	0.80	0.91
		0.116	0.140	0.102	0.086	0.097	0.85	0.95
		0.135	0.160	0.102	0.095	0.106	0.93	1.03
		0.174	0.206	0.105	0.111	0.123	1.05	1.16
		0.212	0.265	0.105	0.125	0.142	1.18	1.35
		0.251	0.298	0.105	0.137	0.152	1.30	1.44
		0.289	0.348	0.105	0.149	0.166	1.42	1.57
		0.328	0.392	0.105	0.160	0.178	1.52	1.68
		0.386	0.462	0.105	0.176	0.195	1.67	1.85
		0.463	0.552	0.105	0.195	0.215	1.85	2.04

Table A1: Comparison between the "exact" beam ultimate load values and the two DSM estimates (cont.)

Beam	BM	SFE			DSM		$\frac{q_{u.y}}{q_u}$	$\frac{q_{u.pl}}{q_u}$
		q_y	q_{pl}	q_u (kN/m)	$q_{u.y}$	$q_{u.pl}$		
B5-2s-one	G	0.006	0.008	0.008	0.006	0.008	0.82	0.99
		0.012	0.015	0.015	0.012	0.015	0.84	1.00
		0.025	0.029	0.027	0.024	0.028	0.88	1.01
		0.037	0.045	0.038	0.034	0.039	0.89	1.02
		0.049	0.059	0.047	0.041	0.046	0.89	1.00
		0.062	0.075	0.053	0.048	0.052	0.89	0.98
		0.074	0.090	0.057	0.052	0.055	0.91	0.97
		0.086	0.104	0.059	0.055	0.056	0.92	0.94
		0.111	0.137	0.065	0.056	0.056	0.87	0.87
		0.136	0.166	0.065	0.056	0.056	0.86	0.86
		0.160	0.197	0.072	0.056	0.056	0.78	0.78
		0.185	0.227	0.079	0.056	0.056	0.71	0.71
		0.210	0.255	0.080	0.056	0.056	0.70	0.70
		0.247	0.304	0.081	0.056	0.056	0.69	0.69
		0.296	0.355	0.081	0.056	0.056	0.69	0.69
B2-3s-all	L	0.037	0.047	0.047	0.037	0.047	0.78	0.99
		0.074	0.093	0.094	0.074	0.093	0.79	1.00
		0.148	0.183	0.184	0.148	0.183	0.80	1.00
		0.221	0.268	0.269	0.221	0.268	0.82	1.00
		0.295	0.363	0.349	0.295	0.349	0.85	1.00
		0.369	0.451	0.418	0.353	0.405	0.84	0.97
		0.443	0.536	0.473	0.400	0.454	0.84	0.96
		0.517	0.627	0.497	0.443	0.505	0.89	1.02
		0.664	0.812	0.514	0.524	0.599	1.02	1.17
		0.812	0.987	0.521	0.599	0.680	1.15	1.31
		0.959	1.185	0.524	0.668	0.767	1.27	1.46
		1.107	1.318	0.526	0.733	0.821	1.39	1.56
		1.255	1.559	0.526	0.795	0.915	1.51	1.74
		1.476	1.809	0.526	0.883	1.007	1.68	1.91
		1.771	2.159	0.526	0.993	1.127	1.89	2.14
B4-3s-all	D	0.009	0.011	0.011	0.009	0.011	0.81	1.01
		0.018	0.023	0.023	0.018	0.023	0.82	1.00
		0.037	0.045	0.045	0.037	0.045	0.82	1.01
		0.055	0.065	0.063	0.055	0.062	0.88	1.00
		0.074	0.090	0.082	0.068	0.078	0.84	0.96
		0.092	0.114	0.101	0.080	0.092	0.79	0.91

Table A1: Comparison between the "exact" beam ultimate load values and the two DSM estimates (cont.)

Beam	BM	SFE			DSM		$\frac{q_{u.y}}{q_u}$	$\frac{q_{u.pl}}{q_u}$
		q_y	q_{pl}	q_u (kN/m)	$q_{u.y}$	$q_{u.pl}$		
B4-3s-all	D	0.111	0.136	0.112	0.090	0.102	0.80	0.91
		0.129	0.156	0.113	0.099	0.112	0.88	0.99
		0.166	0.198	0.113	0.116	0.129	1.03	1.15
		0.203	0.243	0.113	0.131	0.146	1.17	1.30
		0.240	0.291	0.113	0.145	0.162	1.29	1.44
		0.277	0.333	0.113	0.158	0.176	1.40	1.56
		0.314	0.382	0.113	0.170	0.190	1.51	1.69
		0.369	0.452	0.113	0.186	0.209	1.66	1.86
		0.443	0.532	0.113	0.207	0.229	1.84	2.04
B5-3s-all	G	0.006	0.008	0.008	0.006	0.008	0.76	0.98
		0.012	0.015	0.015	0.012	0.015	0.78	1.00
		0.024	0.029	0.028	0.023	0.028	0.85	1.01
		0.035	0.043	0.039	0.033	0.039	0.84	0.98
		0.047	0.058	0.051	0.041	0.048	0.81	0.94
		0.059	0.073	0.059	0.048	0.054	0.81	0.91
		0.071	0.086	0.064	0.053	0.058	0.84	0.91
		0.083	0.102	0.067	0.057	0.061	0.85	0.90
		0.106	0.131	0.072	0.061	0.061	0.85	0.85
		0.130	0.156	0.074	0.061	0.061	0.83	0.83
		0.154	0.192	0.074	0.061	0.061	0.83	0.83
		0.177	0.222	0.074	0.061	0.061	0.83	0.83
		0.201	0.242	0.074	0.061	0.061	0.83	0.83
		0.236	0.286	0.074	0.061	0.061	0.83	0.83
		0.283	0.342	0.074	0.061	0.061	0.83	0.83

Twentieth International Specialty Conference on Cold-Formed Steel Structures
St. Louis, Missouri, U.S.A., November 3 & 4, 2010

Direct Strength Design of Cold-Formed C-Sections for Shear

Cao Hung Pham[1] and Gregory J. Hancock[2]

Abstract

The Direct Strength Method (DSM) recently included in the North American Specification and Australian/New Zealand Standard AS/NZS 4600:2005 gives design rules for compression and bending. No rules are presented at this stage for shear. Two series of tests on C-section can be used to develop and calibrate rules for design in shear. These are the University of Missouri Rolla tests of the 1970's and recent tests on high strength C-sections at the University of Sydney. Both series of tests use a similar test rig although different levels of tension field action have been observed. Two features researched are the effect of full section shear buckling (as opposed to web only shear buckling), and tension field action. Full section buckling is a feature of the DSM but requires software that can evaluate full sections for shear. The paper proposes DSM design rules for C-sections in shear both with and without tension field action. Both series of test results are compared with the proposed design rules.

1. INTRODUCTION

In both the Australian Standard and American Specification for the Design of Cold-Formed Steel Structures, which include the newly developed Direct Strength Method (DSM) of design, the method presented [Chapter 7 of AS/NZS 4600:2005 (Standards Australia, 2005)], Appendix 1 of the North American Specification (AISI, 2007)] is limited to pure compression and pure bending.

[1] Post-Doctoral Researcher, School of Civil Engineering, The University of Sydney, Sydney NSW 2006, Australia.
[2] Emeritus Professor, The University of Sydney, Sydney NSW 2006, Australia.

The Direct Strength Method (Schafer and Peköz, 1998) was formally adopted in the North American Design Specification in 2004 and in Australian/New Zealand Standard AS/NZS 4600:2005 as an alternative to the traditional Effective Width Method (EWM) in 2005. It uses elastic buckling solutions for the entire member cross section to give the direct strength rather than for elements in isolation. The first advantage of the DSM is that it allows direct computation of the capacity of cold-formed thin-walled members of complex section shape (eg. with intermediate stiffeners). Secondly, the interaction between local and overall modes, distortional and overall modes is easily taken into account. The DSM uses numerical solutions for elastic buckling and requires computer software such as THIN-WALL (CASE, 2006) or CUFSM (Schafer and Ádány, 2006) to evaluate elastic buckling stresses. There is no need to calculate cumbersome effective sections especially with intermediate stiffeners.

The development of the DSM for columns and beams including the reliability of the method is well researched. In the review of the DSM of cold-formed steel member design, Schafer (2006) noted that no formal provisions for shear currently exist for the DSM. However, as recommended in the AISI Direct Strength Design Guide (AISI, 2006), the existing provisions in the North American Design Specification and AS/NZS 4600:2005 could be suitably modified into the DSM format.

In order to extend DSM to purlin systems for shear, and combined bending and shear, vacuum rig tests on continuous lapped cold-formed purlins at the University of Sydney over a 10 year period, have been used to calibrate DSM design proposals for shear and combined bending and shear (Pham and Hancock, 2009a). The conclusions from this calibration are that the existing bending and shear equations in AS/NZS 4600:2005 in DSM format will provide reliable designs irrespective of whether the limiting design moment in the interaction equation is based on the lesser of the local buckling and distortional buckling moments (called Proposal 1) or the local buckling moment alone (called Proposal 2).

To further investigate these proposals, additional tests on C-sections including tests on both plain C- and SupaCee® purlin sections (Lysaght, 2003) in predominantly shear, combined bending and shear, and bending only (Pham and Hancock, 2009b, 2009c) have been performed at the University of Sydney. The high strength SupaCee® profile steel sections contain additional return lips and web stiffeners which enhance the bending and shear capacity of the sections. They are used widely in Australia as purlins in roof and wall systems. The basic design of the test rig was developed at the University of Missouri-Rolla. In the 1970's, LaBoube and Yu (1978) conducted a series of tests including a total of forty three beam specimens subjected primarily to shear stress. They found that, for shear, the

exact critical buckling load for beam webs is difficult to determine experimentally and the post-buckling strength of web elements due to tension field action increases as the h/t ratio of the web, the aspect ratio of the web, and the yielding point of the material increase. Further, the arrangement of connections has a significant effect on the ultimate shear capacity of the unreinforced webs. The current Effective Width Method for shear was calibrated against these tests.

The main objectives of this paper are:

- To summarise analyses of full sections in shear with a view to providing elastic shear buckling loads V_{cr} which can be used as input to the Direct Strength Method of design of complete sections in shear.
- To summarise both University of Sydney (UoS) and University of Missouri-Rolla (UMR) test results on cold-formed C- sections subjected primarily to shear.
- To summarise proposals for extension of the Direct Strength Method to shear. The proposals are made both with and without Tension Field Action (TFA) and are compared with both the UoS and UMR test results on the lipped C-sections.

2. SHEAR BUCKLING OF FULL SECTIONS

Analysis of the shear buckling stress of flat rectangular plates has been performed by many investigators (Timoshenko and Gere, 1961; Bulson, 1970; Bleich, 1952). The traditional approach has been to investigate shear plate buckling in the web alone and to ignore the behaviour of the whole section including the flanges. There does not appear to be any consistent theoretical or experimental investigation of the whole section buckling of thin-walled sections under shear. Recently, Pham and Hancock provided solutions to the shear buckling of complete channel sections (2009d) and plain C- lipped sections with an intermediate web stiffener (2009e) loaded in pure shear parallel with the web by using a Spline Finite Strip Method.

The Spline Finite Strip Method (SFSM) is a development of the semi-analytical finite strip method originally derived by Cheung (1976). It uses spline functions in the longitudinal direction in place of the single half sine wave over the length of the section, and has been proven to be an efficient tool for analyzing structures with constant geometric properties in a particular direction, generally the longitudinal one. The advantage of the spline finite strip analysis is that it allows more complex types of loading and boundary conditions other than simple

supports to be easily investigated and buckling in shear is also easily accounted for. Initially, the spline finite strip method was fully developed for the linear elastic structural analysis of folded plate structures by Fan and Cheung (1982).

The SFSM was then extended to buckling and nonlinear analyses of flat plates and folded-plate structures by Lau and Hancock (1986) and Kwon and Hancock (1991, 1993). The spline finite strip method involves subdividing a thin-walled member into longitudinal strips where each strip is assumed to be free to deform both in its plane (membrane displacements) and out of its plane (flexural displacements). The functions used in the longitudinal direction are normally B3 splines. The ends of the section under study are normally free to deform longitudinally but are prevented from deforming in a cross-sectional plane.

For the shear buckling analyses described by Pham and Hancock (2009d), three different methods, which represent different ways of incorporating the shear stresses in the thin-walled section, are used in this analysis as shown in Fig. 1.

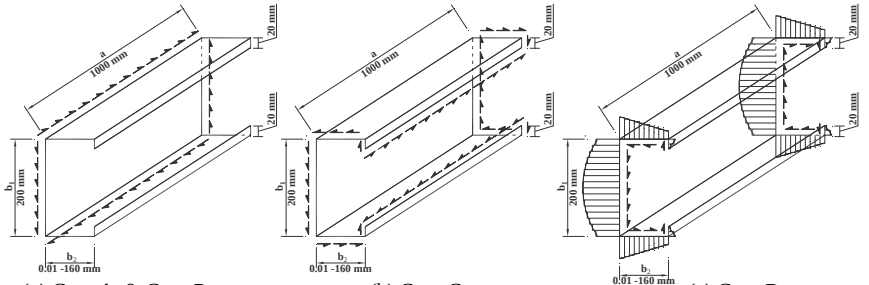

(a) Case A & Case B *(b) Case C* *(c) Case D*

Figure 1. Shear Flow Distributions in Lipped Channels

These include pure shear in the web only (Cases A and B), pure shear in the web and the flanges (Case C) , and a shear distribution similar to that which occurs in practice allowing for section shear flow (Case D). The stress states studied are not in equilibrium as shear can only be generated in a section by moment gradient. However, the studies allow the shear buckling to be isolated and investigated. Fig 2 from Pham and Hancock (2009d) shows the results of the buckling analyses of the lipped channel section of length a=1000 mm and the ratios of flange to web width (b_2/b_1) from 0.00005 to 0.8 (Case D). The corresponding buckling mode shapes are shown in Fig 3 (Case D). They demonstrate a range of buckling modes including section twisting for sections with narrow flanges, flange distortional buckling and web shear buckling depending upon the width of the flanges.

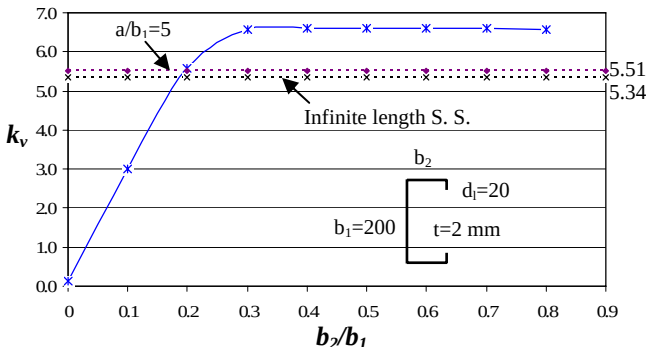

Figure 2. The Ratio of Flange and Web Widths (b_2/b_1) and The Shear Buckling Coefficients (k_v) for Case D

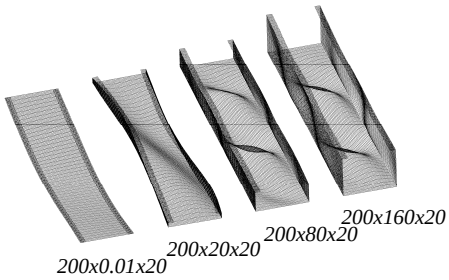

Figure 3. Buckling Mode Shape of Lipped Channel Section Length = 1000 mm, $a/b_1=5$ for Case D

3. EXPERIMENTS ON PLAIN C- LIPPED SECTIONS AND SUPACEE® SECTIONS IN SHEAR

3.1 Experimental Rig and Tests Specimens

The experimental program comprised a total of thirty six tests conducted in the J. W. Roderick Laboratory for Materials and Structures at the University of Sydney. All tests were performed in the 2000 kN capacity DARTEC testing machine, using a servo-controlled hydraulic ram. Two different commercially available plain C- lipped and SupaCee® sections of 150 and 200 mm depths as shown in Fig. 4 were chosen with three different thicknesses of 1.5, 1.9 and 2.4 mm (for plain C- lipped sections) and 1.2, 1.5 and 2.4 mm (for plain C- lipped sections).

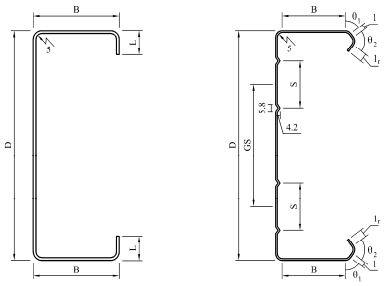

Figure 4. Dimensions of Plain and SupaCee® Channel Sections

The average measured dimensions and properties for the *V* series of both plain C-lipped and SupaCee® sections are given in Pham and Hancock (2009b, 2009c) respectively. A diagram of the test set-up is shown in Fig. 5 for shear *(V)* series. Although the tests described in LaBoube and Yu (1978) contained straps at the loading points as described later, tests both with and without straps are included in the test program described in this paper.

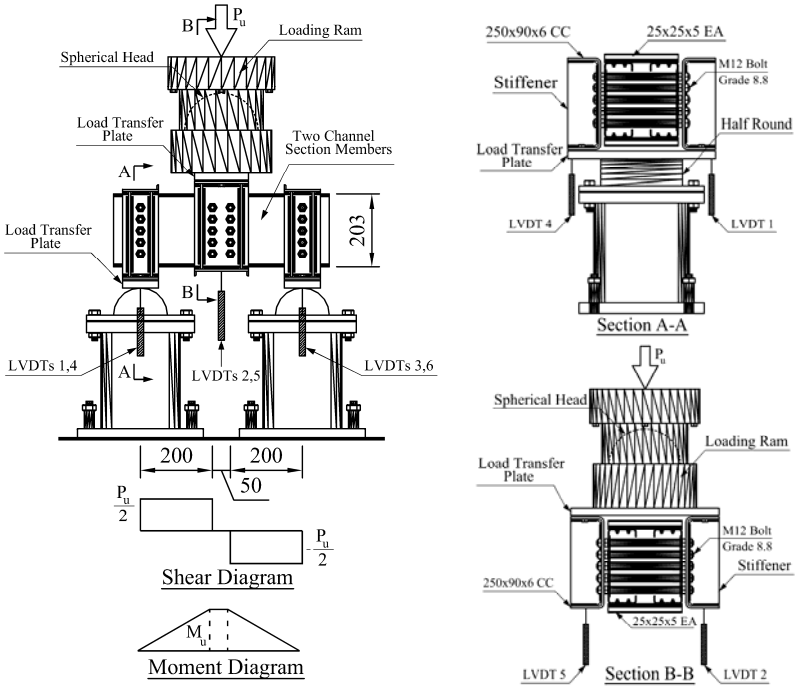

Figure 5. *V* Test Series Configuration (Dimensions for 200 mm Deep Section)

3.2 Test With and Without Straps Configurations

Twenty four tests (18 of plain lipped C- sections and 6 of SupaCee® sections) of the thirty six tests had four 25x25x5EA straps connected by self-tapping screws on each of the top and bottom flanges adjacent to the loading point and reactions as shown in Fig. 6(a). Twelve remaining tests (6 of plain lipped C- sections and 6 of SupaCee® sections) were tested without the two 25x25x5EA straps adjacent to the loading points on the top flange as shown in Fig. 6(b). The purpose of these two straps is to prevent distortion of the top flanges under compression caused by bending moment. The distortion may be a consequence of unbalanced shear flow or distortional buckling.

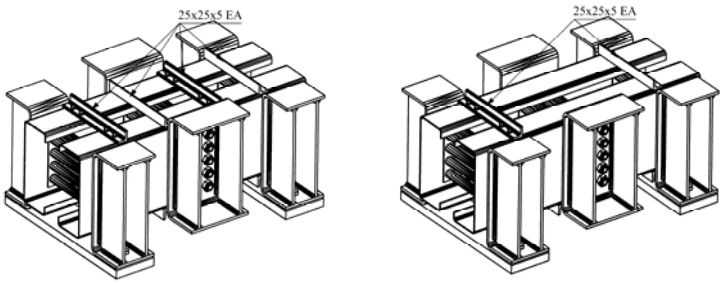

(a) With Straps (b) Without Straps

Figure 6. *V* Test Series Configuration With and Without Straps

3.3 University of Sydney (UoS) Plain Lipped C- and SupaCee® Section Shear Test Results

The full set of test results for the plain lipped C- and SupaCee® sections is given in the research reports by Pham and Hancock (2009b, 2009c). The tests results are compared with existing design methods in AS/NZS 4600:2005 and with the tension field action included using the rules of AS 4100:1998 (Standards Australia 1998). All slender section specimens in the *V* series were found to develop tension field action as the connection bolts at the loading and support points extended over the full depth of the section whether 150 mm (4 bolts) or 200 mm (5 bolts). The inclusion of straps attached to the flanges to prevent distortion at the loading and support points further enhanced the tension field action. They are compared with DSM design proposals in Section 3 following. All results of UoS tests for the predominantly shear *(V)* test series of both the plain C- sections and SupaCee® sections are summarized in Table 1.

Test	Section	V_T (kN)	V_y(AISI) (kN)	V_{cr} (kN)	$\sqrt{V_y / V_{cr}}$	V_T / V_y
V1	C15015	55.43	68.37	43.13	1.259	0.811
V2	C15015	56.08	68.26	43.21	1.257	0.822
V3	C15015	54.47	68.36	43.14	1.259	0.797
Vw	C15015	51.28	68.29	43.19	1.257	0.751
V1	C15019	76.78	84.99	88.23	0.982	0.903
V2	C15019	75.65	85.07	88.15	0.982	0.889
V3	C15019	77.85	84.95	88.27	0.981	0.916
Vw	C15019	70.87	84.85	88.37	0.980	0.835
V1	C15024	94.24	96.86	178.96	0.736	0.973
V2	C15024	96.04	96.73	179.19	0.735	0.993
V3	C15024	95.56	96.92	178.84	0.736	0.986
Vw	C15024	93.38	96.62	179.40	0.734	0.966
V1	C20015	56.14	88.58	31.84	1.668	0.634
V2	C20015	53.89	88.51	31.87	1.667	0.609
V3	C20015	57.76	88.56	31.85	1.667	0.652
Vw	C20015	50.82	88.61	31.83	1.669	0.573
V1	C20019	86.51	109.65	65.84	1.290	0.789
V2	C20019	86.06	109.66	65.83	1.291	0.785
V3	C20019	83.38	109.48	65.94	1.289	0.762
Vw	C20019	75.82	109.50	65.93	1.289	0.692
V1	C20024	115.45	131.69	132.19	0.998	0.877
V2	C20024	113.60	131.27	132.61	0.995	0.865
V3	C20024	112.61	130.92	132.96	0.992	0.860
Vw	C20024	103.31	131.81	132.07	0.999	0.784
V1	SC15012	42.13	59.93	27.00	1.490	0.703
Vw	SC15012	39.33	60.08	26.94	1.493	0.655
V1	SC15015	55.58	67.10	53.32	1.122	0.828
Vw	SC15015	51.87	67.58	52.94	1.130	0.768
V1	SC15024	97.99	102.71	219.62	0.684	0.954
Vw	SC15024	92.92	102.69	219.66	0.684	0.905
V1	SC20012	46.48	82.47	18.95	2.086	0.564
Vw	SC20012	45.55	82.57	18.92	2.089	0.552
V1	SC20015	62.07	91.35	37.44	1.562	0.679
Vw	SC20015	61.65	91.40	37.42	1.563	0.675
V1	SC20024	124.21	137.70	154.52	0.944	0.902
Vw	SC20024	117.31	137.04	155.26	0.939	0.856

Table 1. (UoS) *V* Series Test Results of Plain C- and SupaCee® Sections

3.4 University of Missouri-Rolla (UMR) Plain Lipped C- Section Shear Test Results

The full set of test results for the plain lipped C- sections is given in the research report by LaBoube and Yu (1978). A total of forty three shear tests have been conducted to determine the structural behavior of web elements subjected primarily to shear. All results of tests for the UMR shear *(V)* test series are summarized in Table 2.

In the report of LaBoube and Yu (1978), specimen Nos. S-10-1, S-10-2 and S-10-3 have been discarded due to combined bending and shear failure. Specimen No. S-9-3 has been discarded due to premature failure, and specimen Nos. S-19-1, S-19-2, S-20-1 and S-20-2 have been discarded due to web crippling, which resulted at the end supports because the connection rods were poorly arranged. They are therefore not included in Table 2. As can also be seen in Table 2, six additional tests (Nos. MS-2-1, MS-2-2, MS-3-1, MS-3-2, MS-8-1, MS-8-2) were performed with cover plates added to both the tension and compression flanges. In Table 2, the k_v values for the MS sections are simply those of the plain sections, as the restraint from the intermittently connected cover plates is difficult to quantify.

Beam Specimen	V_T **(kN)**	V_y**(AISI) (kN)**	k_v **Section**	V_{cr} **(kN)**	$\sqrt{V_y / V_{cr}}$	V_T / V_y
S-1-1	19.10	19.08	25.741	62.88	0.551	1.001
S-1-2	19.16	18.94	22.893	57.30	0.575	1.011
S-2-1	17.21	23.27	9.742	20.20	1.073	0.740
S-2-2	17.38	23.44	9.834	20.96	1.057	0.742
S-3-1	17.79	27.99	9.811	16.62	1.298	0.636
S-3-2	18.78	27.53	9.777	16.55	1.290	0.682
S-8-1	16.67	23.34	9.944	20.21	1.075	0.714
S-8-2	16.85	23.46	9.874	19.96	1.084	0.718
S-9-1	16.88	27.53	9.781	16.84	1.279	0.613
S-9-2	18.68	27.76	9.824	16.78	1.286	0.673
S-9-4	17.08	27.44	9.818	17.26	1.261	0.623
S-9-5	15.88	27.70	9.791	17.20	1.269	0.573
S-9-6	18.35	27.97	9.920	17.56	1.262	0.656
S-9-7	12.92	27.92	6.790	12.15	1.516	0.463
S-9-8	13.57	27.87	6.790	12.06	1.520	0.487
S-10-4	25.35	27.33	17.458	60.16	0.674	0.928
S-10-5	24.89	27.40	17.587	60.45	0.673	0.908
S-11-1	25.58	41.01	9.752	25.30	1.273	0.624
S-11-2	28.83	40.63	9.741	25.51	1.262	0.710
S-11-3	27.33	41.26	9.779	26.24	1.254	0.662
S-12-1	20.02	51.17	9.558	20.19	1.592	0.391
S-12-2	23.89	51.47	9.585	20.13	1.599	0.464
S-12-3	20.59	53.00	9.603	21.70	1.563	0.389
S-17-1	27.36	41.20	9.670	27.03	1.235	0.664
S-17-2	26.69	41.20	9.702	27.12	1.233	0.648
S-18-1	26.79	52.50	9.919	22.63	1.523	0.510
S-18-2	24.35	52.64	9.842	22.39	1.533	0.463
S-19-3	18.40	55.55	9.552	13.53	2.027	0.331
S-20-3	15.45	68.72	9.438	10.20	2.596	0.225
MS-2-1	17.50	23.35	9.758	19.81	1.086	0.750
MS-2-2	17.76	22.92	9.810	19.43	1.086	0.775
MS-3-1	17.51	27.92	9.815	16.67	1.294	0.627
MS-3-2	16.48	27.90	9.844	16.73	1.292	0.591
MS-8-1	18.03	23.18	9.943	20.34	1.068	0.778
MS-8-2	16.24	23.52	9.936	20.91	1.061	0.690

Table 2. (UMR) *V* Series Test Results of Plain C- Sections

4. PROPOSED DIRECT STRENGTH METHOD (DSM) OF DESIGN OF COLD- FORMED C- SECTIONS FOR SHEAR

4.1 Nominal Shear Capacity Based on AISI in DSM Format in Shear without Tension Field Action

The equations in Section C3.2.1 of the North American Specification (AISI, 2007) which are expressed in terms of a nominal shear stress F_v have been changed to DSM format by replacing stresses by loads as follows:

$$\text{For } \lambda_v \le 0.815 : V_v = V_y \tag{1}$$

$$\text{For } : 0.815 < \lambda_v \le 1.227 : V_v = 0.815\sqrt{V_{cr}V_y} \tag{2}$$

$$\text{For } : \lambda_v > 1.227 \; V_v = V_{cr} \tag{3}$$

where $\lambda_v = \sqrt{V_y / V_{cr}}$, V_y = yield load of web = $0.6A_w f_y$,

V_{cr} = elastic shear buckling force of web = $\dfrac{k_v \pi^2 E A_w}{12\left(1-\nu^2\right)\left(\dfrac{d_1}{t_w}\right)^2}$

d_1 = depth of the flat portion of the web measured along web plane,

t_w = thickness of web, A_w = area of web = $d_1 \times t_w$,

k_v = shear buckling coefficient for whole sections (as shown in Section 2)

To account for the shear buckling of the whole section rather than simply the web, the shear buckling coefficient *(k_v)* can be back-calculated from the shear buckling load V_{cr} (as summarized in Tables 1, 2 for both UoS and UMR test results) of the whole section as described in Pham and Hancock (2009d) (also in Section 2) by using the Spline Finite Strip Method. In this way, the DSM philosophy of section rather than element buckling can now be incorporated in the nominal shear capacity.

For the plain lipped C- sections, the computed values of the shear buckling coefficients *(k_v)* for the whole section increase from the theoretical value of a simply supported rectangular plate in shear of 9.34 for a Span:Panel Depth of 1:1 to 9.926 and 10.006 for the 150mm and 200 mm depth sections respectively. For the SupaCee® sections, the corresponding values are 12.204 and 11.709 as a result of the longitudinal intermediate stiffeners in the web.

4.2 Direct Strength Method based on AISI in DSM Format in Shear with Tension Field Action

The DSM nominal shear capacity *(V_v)* including Tension Field Action (TFA) is proposed based on the local buckling *(M_{sl})* equation where M_{sl}, M_{ol} and M_y are replaced by V_v, V_{cr} and V_y respectively as follows:

$$V_v = \left[1 - 0.15\left(\frac{V_{cr}}{V_y}\right)^{0.4}\right]\left(\frac{V_{cr}}{V_y}\right)^{0.4} V_y \qquad (4)$$

where V_y is yield load of web $V_y = 0.6A_w f_y$,

V_{cr} is elastic shear buckling force of web $V_{cr} = \dfrac{k_v \pi^2 E A_w}{12\left(1-\nu^2\right)\left(\dfrac{d_1}{t_w}\right)^2}$,

k_v = shear buckling coefficient for whole sections (as shown in Section 2)

The results of tests for the predominantly shear *(V)* test series of both UoS and UMR are plotted in Fig. 7. The TFA curve (Basler, 1961), the elastic buckling curve *(V_{cr})* and the DSM proposed curves for shear with and without TFA are also graphically reproduced in Fig. 7.

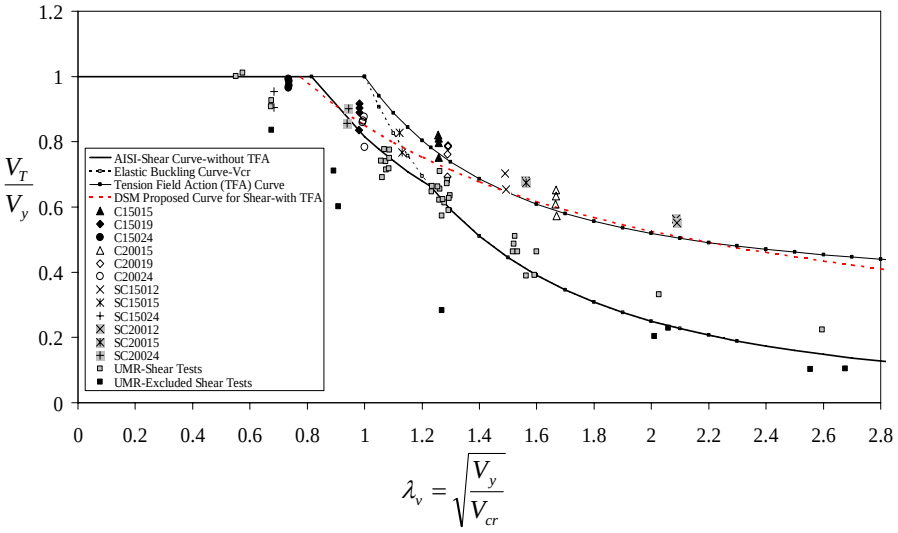

Figure 7. DSM Proposed Shear Curves and Shear Test Data (UoS and UMR)

Fig. 7 shows that all plain lipped C- and SupaCee® *V*-series tests of UoS lie close to the proposed DSM nominal shear capacity with TFA (see Eq. 4). The DSM proposed shear equation with TFA therefore gives a good mean fit to the *V*-series tests. They lie well above the AISI in DSM format equations (see Eqs. 1–3) presumably because significant tension field action was developed. Figs 8(a) and 8(b) show the corresponding buckling mode shapes of the SupaCee® section members with and without straps respectively for the *V*-series.

(a) With Straps

(b) Without Straps

Figure 8. Buckling Mode Shape of SupaCee® Section Members
V-Series – With and Without Straps

Fig. 7 also shows the UMR tests lie closer to the AISI in DSM format without TFA (see Eqs. 1-3). The reason for this is probably the inability of the deeper (and hence more slender) UMR sections to develop tension field action. This may be a result of keeping the same number of bolts for deeper sections although the test report does not fully specify the bolt configuration.

The mean (P_m) of the test results divided by the design model for each test series, and each design model (with and without TFA) is summarized in Table 3. The corresponding coefficient of variations (V_P) is also included in Table 3. The University of Sydney results are better predicted (P_m=1.022, V_P=0.068) by the DSM shear proposal with TFA, and the UMR results are better predicted (P_m=1.045, V_P=0.118) by the DSM shear proposal without TFA.

Test Program	**(Eqs. 1-3) DSM without TFA**		**(Eq. 4) DSM with TFA**	
	P_m	**V_P**	**P_m**	**V_P**
University of Sydney (Table 1)	1.293	0.295	1.022	0.068
University of Missouri-Rolla (Table 2)	1.045	0.118	0.835	0.128

Table 3. Comparison of P_m and V_P for UoS and UMR between DSM Shear Proposals with and without TFA

The development of TFA in the University of Sydney may be a result of the bolts connecting the webs of the channels spanning the full depth of the section for both 150 mm and 200 mm tests. The two vertical rows of bolts have increased the restraints to the web panel and act as web stiffeners. These increased restraints have improved the post-buckling strengths of the web for the *V*-series. It is interesting to note that the slender sections (e.g. C20015, SC15012, SC20012 and SC20015) are more conservative than stockier sections. This fact shows that the more slender sections have more tension field action contribution to the ultimate strength of the sections in shear.

3. CONCLUSION

The paper has presented proposals for the design of cold-formed steel sections in shear by the Direct Strength Method (DSM) as in the North American Specification and Australian/ New Zealand Standard. The proposals are compared with tests in predominantly shear of both the University of Missouri Rolla C-section tests of the 1970's and recent tests on high strength plain lipped C- and SupaCee® sections at the University of Sydney. One feature of the DSM is that the full section buckling including intermediate stiffeners under shear has been included rather than simple web buckling in shear. This proposal produces better correlation with the test data but requires special computer software such as the Spline Finite Strip Method (SFSM) to determine the shear buckling loads of full sections. The shear capacity, V_v, is based on the DSM proposals with and without

tension field action. The shear buckling load, V_{cr}, used in the DSM equations is based on the shear buckling coefficient of the full section and not just the web buckling in shear. The tests from the University of Sydney show that the DSM proposal curve for shear with tension field action gives a good mean fit to the shear tests and more accurate prediction on post-bucking strength of the C-sections in shear. The tests from the University of Missouri Rolla are better predicted by the DSM proposal curve for shear without tension field action. The increased restraints created by full bolt connections along the depth of the web panel at the supports and loading point may improve the post-buckling strengths of the web in shear. Research on this aspect is ongoing.

REFERENCES

AISI. 2006. "Direct Strength Method (DSM) Design Guide." *American Iron and Steel Institute*, Washington DC.

AISI. 2007. "North American Specification for the Design of Cold-Formed Steel Structural Members." *2007 Edition*, AISI S100-2007.

Basler, K. 1961. "Strength of Plate Girders in Shear." *Journal of the Structural Division, ASCE*, Vol. 87, No. ST7, 151-180.

Bleich, F. 1952. "Buckling Strength of Metal Structures." *McGraw-Hill, Book Co. Inc*, New York, N.Y.

Bulson, P. S. 1970. "Statbility of Flat Plates." *Chatto and Windus*, London.

CASE. 2006. "THIN-WALL – A Computer Program for Cross-Section Analysis and Finite Strip Buckling Analysis and Direct Strength Design of Thin-Walled Structures." Version 2.1, Centre for Advanced Structural Engineering, School of Civil Engineering, The University of Sydney.

Cheung, Y. K. 1976. "Finite Strip Method in Structural Analysis." *Pergamon Press, Inc.*, New York, N.Y., U.S.A.

Fan, S. C., and Cheung, Y. K. 1982. "Spline Finite Strip in Structural Analysis." *Proceedings, the International Conference on Finite Element Method*, Shanghai, China.

Kwon, Y. B. and Hancock, G. J. 1991. "Nonlinear Elastic Spline Finite Strip Analysis for Thin-Walled Sections." *Thin-Walled Structures*, Vol. 12, No. 4, pp 295-319.

Kwon, Y. B. and Hancock, G. J. 1993. "Post-Buckling Analysis of Thin-Walled Channel Sections Undergoing Local and Distortional Buckling." *Computers and Structures*, Vol. 49, No. 3, pp 507-516.

LaBoube, R. A., and Yu, W. W. 1978. "Structural Behavior of Beam Webs Subjected Primarily to Shear." *Final Report, Civil Engineering Study 78-2*, University of Missouri-Rolla, St Louis, Missouri, U.S.A.

Lau, S. C. W. and Hancock, G. J. 1986. "Buckling of Thin Flat-Walled Structures by a Spline Finite Strip Method." *Thin-Walled Structures*, Vol. 4, pp 269-294.

Lysaght. 2003. "NSW SupaCee® is trademark of Bluescope Steel Limited." *Bluescope Steel Limited trading as Bluescope Lysaght*.

Pham, C. H., and Hancock, G. J. 2009a. "Direct Strength Design of Cold-Formed Purlins." *Journal of Structural Engineering*, American Society of Civil Engineers, Vol. 135, Issue 3, pp. 229-238.

Pham, C. H., and Hancock, G. J. 2009b. "Experimental Investigation of High Strength Cold-Formed C-Section in Combined Bending and Shear.", *Research Report No R894*, School of Civil Engineering, The University of Sydney, NSW, Australia, April, 2009.

Pham, C. H., and Hancock, G. J. 2009c. "Experimental Investigation of High Strength Cold-Formed SupaCee® Sections in Combined Bending and Shear.", *Research Report No R907*, School of Civil Engineering, The University of Sydney, NSW, Australia, December, 2009.

Pham, C. H., and Hancock, G. J. 2009d. "Shear Buckling of Thin-Walled Channel Sections." *Journal of Constructional Steel Research*, Vol. 65, No. 3, pp. 578-585.

Pham, C. H., and Hancock, G. J. 2009e. "Shear Buckling of Thin-Walled Channel Sections with Intermediate Web Stiffener." *Proceedings, Sixth International Conference on Advances in Steel Structures*, Hong Kong, pp. 417-424.

Schafer, B. W. 2006. "Review: The Direct Strength Method of Cold-Formed Steel Member Design." *International Colloquium on Stability and Ductility of Steel Structures*, Lisbon, Portugal.

Schafer, B. W., and Ádány, S. 2006. "Buckling of Cold-Formed Steel Members using CUFSM, Conventional and Constrained finite strip methods." *Proceedings, Eighteen International Specialty Conference on Cold-Formed Steel Structures*, University of Missouri-Rolla, Orlando, Florida, U.S.A., pp. 39-54.

Schafer, B. W., and Peköz, T. 1998. "Direct Strength Prediction of Cold-Formed Steel Members using Numerical Elastic Buckling Solutions, Thin-Walled Structures, Research and Development." *Proceedings, Fourteenth International Specialty Conference on Cold-Formed Steel Structures*, St Louis, Missouri, U.S.A.

Standards Australia. 1998. "Steel Structures." *AS 4100:1998*, Standards Australia/ Standards New Zealand.

Standards Australia. 2005. "AS/NZS 4600:2005, Cold-Formed Steel Structures." Standards Australia/ Standards New Zealand.

Timoshenko, S. P. and Gere, J. M. 1961. "Theory of Elastic Stability." *McGraw-Hill Book Co. Inc*, New York, N.Y.

Twentieth International Specialty Conference on Cold-Formed Steel Structures
St. Louis, Missouri, U.S.A., November 3 & 4, 2010

Direct Strength Design of Cold-Formed C-Sections in Combined Bending and Shear

Cao Hung Pham[1] and Gregory J. Hancock[2]

Abstract

The paper describes a research program including tests on both plain C- and SupaCee® purlin sections in combined bending and shear, and bending only. The high strength SupaCee® profile steel sections contain additional return lips and web stiffeners which enhance the bending and shear capacity of the sections. They are used widely in Australia as purlins in roof and wall systems. The tests were performed at the University of Sydney with and without straps on the flange and thus allowed distortional buckling in the latter case. Design methods for these sections are normally specified in the Australian/New Zealand Standard for Cold-Formed Steel Structures or the North American Specification for Cold-Formed Steel Structural Members. Both the Effective Width Method (EWM) and the Direct Strength Method (DSM) can be used for the design of C-sections although rules for the DSM in combined bending and shear are not provided in either standard/specification. New DSM design rules for C-sections in shear both with and without tension field action are presented and discussed in a separate paper at this conference. This paper proposes DSM design rules for C-sections in combined bending and shear both with and without the effect of distortional buckling included. Both series of test results are compared with the proposed design rules.

[1] Post-Doctoral Researcher, School of Civil Engineering, The University of Sydney, Sydney NSW 2006, Australia.
[2] Emeritus Professor, The University of Sydney, Sydney NSW 2006, Australia.

1. INTRODUCTION

High strength cold-formed steel sections are commonly used in a wide range of applications which include lipped C and Z-purlin plain sections and SupaCee® sections in roof and wall systems. Sections are normally made from high strength steel up to 550 MPa yield stress. With the resulting reduction of thicknesses of high strength steel, the failure modes of such sections are mainly due to instabilities such as local, distortional and flexural-torsional buckling modes or the interaction between them. SupaCee® sections (Lysaght, 2003) are another type of purlin section which can increase buckling capacity and ultimate strength of thin-walled channel sections by introducing multiple longitudinal web stiffeners and return lips.

The development of the DSM for columns and beams, including the reliability of the method is well researched. In the review of the DSM of cold-formed steel member design, Schafer (2006) noted that no formal provisions for shear, and combined bending and shear currently exist for the DSM. However, as recommended in the AISI Direct Strength Design Guide (AISI 2006), the existing provisions in the North American Design Specification and AS/NZS 4600:2005 (Standards Australia 2005) could be suitably modified into the DSM format.

To investigate this proposition, vacuum rig tests on continuous lapped cold-formed purlins at the University of Sydney over a 10 year period, have been used to calibrate DSM design proposals for shear and combined bending and shear (Pham and Hancock, 2009a). The conclusions from this calibration are that the existing bending and shear equations in AS/NZS 4600:2005 in DSM format will provide reliable designs irrespective of whether the limiting design moment in the interaction equation is based on the lesser of the local buckling and distortional buckling moments (called Proposal 1) or the local buckling moment alone (called Proposal 2). To further investigate these proposals, additional tests on C-sections in combined bending and shear, and bending alone have been performed at the University of Sydney (Pham and Hancock, 2009b, 2009c).

The main purpose of this paper is to provide test data on simply supported channel sections, and to further refine the proposals based on tests which concentrated on combined bending and shear. The paper also summarises proposals for extension of the Direct Strength Method to combined bending and shear. The proposals are made both with and without Tension Field Action (TFA) and are compared with the test results on the lipped C-sections.

2. EXPERIMENTS ON PLAIN C- LIPPED AND SUPACEE® CHANNEL SECTIONS IN SHEAR, AND COMBINED BENDING AND SHEAR

2.1 Experimental Rig and Tests Specimens

Two testing programs on both high strength cold formed steel plain C- lipped sections and SupaCee® sections for the extension to the Direct Strength Method for shear, combined bending and shear, and bending only were performed. The first experimental program comprised a total of thirty six tests which included two test series conducted in the J. W. Roderick Laboratory for Materials and Structures at the University of Sydney. All tests were performed in the 2000 kN capacity DARTEC testing machine, using a servo-controlled hydraulic ram. Two different commercially available plain C- lipped channel sections of 150 mm and 200 mm depths as shown in Fig. 1 were chosen with three different thicknesses of 1.5 mm, 1.9 mm and 2.4 mm. The first series *(V)* is predominantly shear and is described in a separate paper at this conference. The second series *(MV)* is combined bending and shear. This series consisted of twenty four tests and used the test rig configuration as shown in Fig. 2. The third series is bending only *(M)* which used the common four point loading configuration as shown in Fig 3. A total of twelve tests of this series were conducted. Although the tests described in LaBoube and Yu (1978) contained straps at the loading points as described later, tests both with and without straps are included in the test program as shown in Fig. 4.

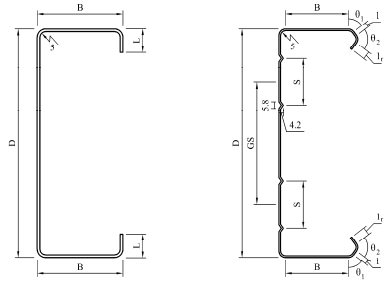

Figure 1. Dimensions of Plain and SupaCee® Channel Sections

The second testing program was also performed at the University of Sydney including a total of twenty four tests of commercially available SupaCee® sections as also shown in Fig. 1. Two different depths of 150 mm and 200 mm were chosen with three different thicknesses of 1.2 mm, 1.5 mm and 2.4 mm. Three test series, which were conducted identically to the first testing program,

also consisted of predominantly shear *(V)* (as also described in separate paper at this conference), combined bending and shear *(MV)*, and bending only *(M)* tests. These test series each included twelve tests each and used the same test rig configurations with the first test program.

The average measured dimensions and properties for the *MV* and *M* series of both plain C- lipped and SupaCee® sections are given in Pham and Hancock (2009b, 2009c) respectively. The basic design of the test rig was developed by LaBoube and Yu (1978). A diagram of the test set-up is shown in Fig. 2 for *MV* series. The detailed test configuration of the bending only series is shown in Fig. 3. The four point bending arrangement provided a central region of uniform bending moment and zero shear force. At the two supports, the rig assembly is exactly the same as that of the predominantly shear test set-up. The difference is at the loading points which have a similar configuration to the support points. The channel section members were loaded symmetrically at two points via a centrally loaded spreader I beam with stiffeners. The distance between the two half rounds bolted to the I beam at the loading points was 1000 mm. These two half rounds bore upon two 20 mm thick load transfer plates. The half round ensured that the applied loads were vertical. The distance between the support and the adjacent loading point was 800 mm.

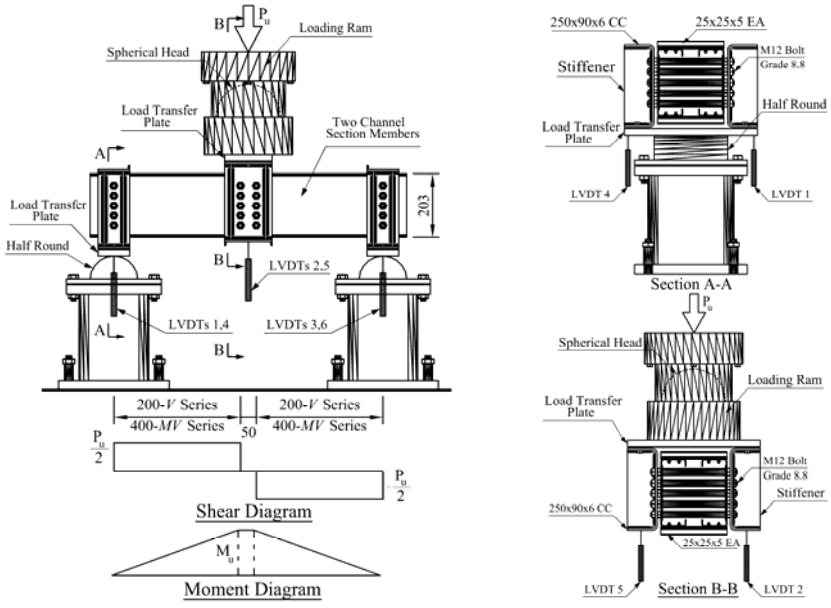

Figure 2. *MV* Test Series Configuration (Dimensions for 200 mm Deep Section)

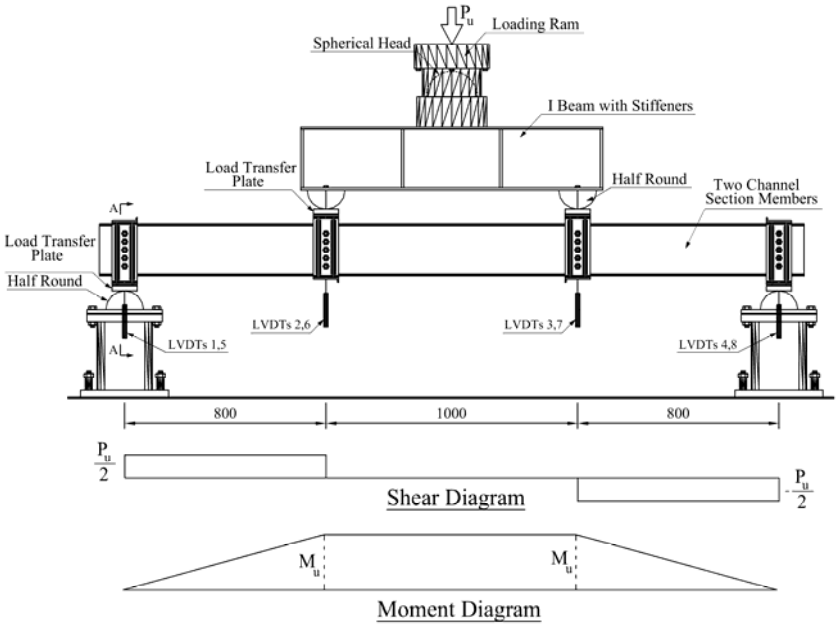

Figure 3. *M* Test Series Configuration (Dimensions for 200 mm Deep Section)

2.2 Test With and Without Straps Configurations

For the combined bending and shear *(MV)* test series, twenty four tests (18 of plain lipped C- sections and 6 of SupaCee® sections) of total thirty six tests had four 25x25x5EA straps connected by self-tapping screws on each of the top and bottom flanges adjacent to the loading point and reactions as shown in Fig. 4(a). Twelve remaining tests were tested without the two 25x25x5EA straps adjacent to the loading points on the top flange as shown in Fig. 4(b). The purpose of these two straps is to prevent distortion of the top flanges under compression caused by bending moment. The distortion may be a consequence of unbalanced shear flow or distortional buckling.

For the bending only *(M)* test series, twelve tests (6 of each plain lipped C- and SupaCee® sections) of total twenty four tests were tested with eight 25x25x5EA straps which were uniformly distributed in the pure bending moment region between the two loading points as shown in Fig. 5(a). The purpose of the straps is to force the channel members to buckle locally rather than by distortional

buckling. The twelve remaining tests in this series were tested without the six middle 25x25x5EA straps as shown in Fig. 5(b). Only two straps adjacent to the loading points were attached to the channel members to prevent distortion at the loading points.

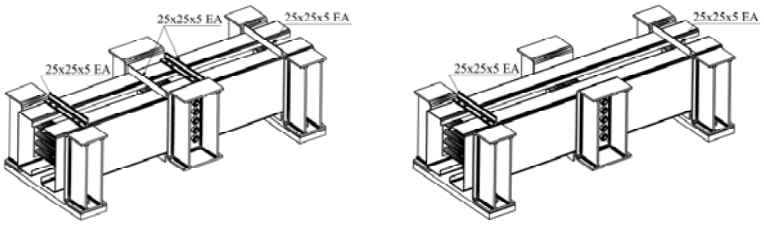

(a) With Straps (b) Without Straps

Figure 4. *MV* Test Series Configuration With and Without Straps

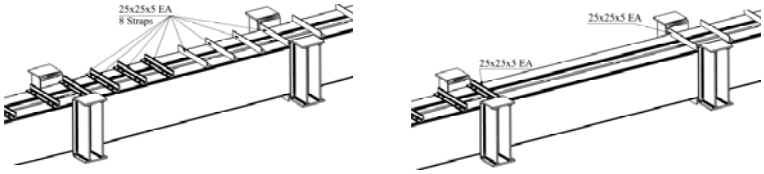

(a) With Straps (b) Without Straps

Figure 5. *MV* Test Series Configuration With and Without Straps

2.3 Plain Lipped C- Section Test Results

The full set of test results for the plain lipped C-Sections is given in the research report by Pham and Hancock (2009b). The tests results are compared with existing design methods in AS/NZS 4600:2005 and with the tension field action included using the rules of AS 4100:1998 (Standards Australia 1998). All slender section specimens in the *V* and *MV* Series were found to develop tension field action as the connection bolts at the loading and support points extended over the full depth of the section whether 150 mm (4 bolts) or 200 mm (5 bolts). The inclusion of straps attached to the flanges to prevent distortion at the loading and support points further enhanced the tension field action. They are compared with DSM design proposals in Section 3 following.

2.4 SupaCee® Section Test Results

The full set of test results for the SupaCee® sections is given in the research report by Pham and Hancock (2009c). The tests results are compared with existing design methods in AS/NZS 4600:2005 and with the tension field action included using the rules of AS 4100:1998 (Standards Australia 1998). As for the plain lipped C-Sections, all slender section specimens in the *V* and *MV* Series were found to develop tension field action. The inclusion of straps attached to the flanges to prevent distortion at the loading and support points further enhanced the tension field action.

3. DIRECT STRENGTH METHOD (DSM) OF DESIGN OF COLD-FORMED C- SECTIONS IN COMBINED BENDING AND SHEAR

3.1 DSM Design Rules for Flexure

The nominal section moment capacity at local buckling *(M_{sl})* is determined from Section 7.2.2.3 of AS/NZS 4600:2005 [Appendix 1, Section 1.2.2.2 of NAS (AISI 2007)] as follows:

$$\text{For } \lambda_l \le 0.776 \ : \ M_{sl} = M_y \tag{1}$$

$$\text{For } \lambda_l > 0.776 \ : \ M_{sl} = \left[1 - 0.15\left(\frac{M_{ol}}{M_y}\right)^{0.4}\right]\left(\frac{M_{ol}}{M_y}\right)^{0.4} M_y \tag{2}$$

where λ_l is non-dimensional slenderness used to determine M_{sl};

$\lambda_l = \sqrt{M_y / M_{ol}}$; $M_y = Z_f f_y$,

M_{ol} is elastic local buckling moment of the section; $M_{ol} = Z_f f_{ol}$,

Z_f is section modulus about a horizontal axis of the full section,

f_{ol} is elastic local buckling stress of the section in bending.

The nominal section moment capacity at distortional buckling *(M_{sd})* is determined from Section 7.2.2.4 of AS/NZS 4600:2005 [Appendix 1, Section 1.2.2.3 of AISI (2007)] as follows:

$$\text{For } \lambda_d \le 0.673 \text{ : } M_{sd} = M_y \tag{3}$$

$$\text{For } \lambda_d > 0.673 \text{ : } M_{sd} = \left[1 - 0.22\left(\frac{M_{od}}{M_y}\right)^{0.5}\right]\left(\frac{M_{od}}{M_y}\right)^{0.5} M_y \tag{4}$$

where λ_d is non-dimensional slenderness used to determine M_{sd} ;

$\lambda_l = \sqrt{M_y / M_{od}}$; $M_y = Z_f f_y$,

M_{od} is elastic distortional buckling moment of the section;

$M_{od} = Z_f f_{od}$,

Z_f is section modulus about a horizontal axis of the full section,

f_{od} is elastic distortional buckling stress of the section in bending.

3.2 Proposed DSM Design Rules for Shear

3.2.1 Nominal Shear Capacity Based on AISI in DSM Format in Shear Without Tension Field Action

The equations in Section 3.2.1 of the North American Specification (AISI 2007) which are expressed in terms of a nominal shear stress F_v have been changed to DSM format by replacing stresses by loads as follows:

$$\text{For } \lambda_v \le 0.815 \text{ : } V_v = V_y \tag{5}$$

$$\text{For } 0.815 < \lambda_v \le 1.231 \text{ : } V_v = 0.815\sqrt{V_{cr} V_y} \tag{6}$$

$$\text{For } \lambda_v > 1.231 \text{ : } V_v = V_{cr} \tag{7}$$

where $\lambda_v = \sqrt{V_y / V_{cr}}$, V_y = yield load of web = $0.6 A_w f_y$,

V_{cr} = elastic shear buckling force of web = $\dfrac{k_v \pi^2 E A_w}{12\left(1-\nu^2\right)\left(\dfrac{d_1}{t_w}\right)^2}$

d_1 = depth of the flat portion of the web measured along web plane,

t_w = thickness of web, A_w = area of web = $d_1 \times t_w$,

k_v = shear buckling coefficient for the whole channel sections.

To account for the shear buckling of the whole section rather than simply the web, the shear buckling coefficient k_v can be back-calculated from the shear buckling load V_{cr} of the whole section as described in Pham and Hancock (2009d) by using the Spline Finite Strip Method. In this way, the DSM philosophy of section rather than element buckling can now be incorporated in the nominal shear capacity.

The computed values of the shear buckling coefficients *(k_v)* for the plain channels increase from the theoretical value of a simply supported rectangular plate in shear of 9.34 for a Span:Panel Depth of 1:1 (*V* Series) to 9.926 and 10.006 for the 150mm and 200 mm depth sections respectively. For the SupaCee® sections, the corresponding values are 12.204 and 11.709 as a result of the longitudinal intermediate stiffeners in the web. For a Span:Panel Depth of 2:1 (*MV* Series), the shear buckling coefficients k_v for the plain channels increase from the theoretical value of a simply supported rectangular plate in shear of 6.34 to 7.122 and 7.237 for the 150mm and 200 mm depth sections respectively. For the SupaCee® sections, the corresponding values are 8.007 and 7.813.

3.2.2 Direct Strength Method based on AISI in DSM Format in Shear with Tension Field Action

All results of tests for the predominantly shear *(V)* test series of plain lipped C- and SupaCee® sections are summarized in a separate paper at this conference and in Pham and Hancock (2009b, 2009c). The DSM nominal shear capacity *(V_v)* is proposed based on the local buckling *(M_{sl})* equation where M_{sl}, M_{ol} and M_y are replaced by V_v, V_{cr} and V_y respectively as follows:

$$V_v = \left[1 - 0.15\left(\frac{V_{cr}}{V_y}\right)^{0.4}\right]\left(\frac{V_{cr}}{V_y}\right)^{0.4} V_y \qquad (8)$$

where V_y is yield load of web $V_y = 0.6A_w f_y$,

V_{cr} is elastic shear buckling force of web $V_{cr} = \dfrac{k_v \pi^2 E A_w}{12\left(1-\nu^2\right)\left(\dfrac{d_1}{t_w}\right)^2}$,

k_v is shear buckling coefficient for the whole channel sections (as shown in Section 3.2.1).

The development of tension field action may be a result of the bolts connecting the webs of the channels spanning the full depth of the section for both 150 mm and 200 mm tests. The two vertical rows of bolts have increased the restraints to the web panel and act as web stiffeners. These increased restraints have improved the post-buckling strengths of the web for the *V*-series.

3.3 Proposed DSM Design Rules for Combined Bending and Shear

In limit states design standards, the interaction is expressed in terms of bending moment and shear force so that the interaction formula for combined bending and shear of a section with an unstiffened web is given in Clause 3.3.5 of AS/NZS 4600:2005 [Section C 3.3.2 of AISI (2007)]:

$$\left(\frac{M^*}{M_s}\right)^2 + \left(\frac{V^*}{V_v}\right)^2 = 1 \qquad (9)$$

where M^* is bending action,
M_s is the bending section capacity in pure bending,
V^* is the shear action, and
V_v is the shear capacity in pure shear.

The equation for combined bending and shear with stiffened webs is also given in Clause 3.3.5 of AS/NZS 4600:2005 [Section C 3.3.2 of AISI (2007)]:

$$0.6\left(\frac{M^*}{M_s}\right) + \frac{V^*}{V_v} = 1.3 \qquad (10)$$

The interactions between (M_T/M_s) and (V_T/V_v) with and without the straps based on either AISI without TFA (Eqs. 5-7) or DSM proposed shear curve with TFA (Eq. 8) are graphically reproduced in Figs. 6-10 for both plain C- and SupaCee® section purlins. While the choice of the nominal section moment capacities, M_s, is based on the DSM, the nominal shear capacities, V_v, is based on AISI (without Tension Field Action) in DSM format (Figs. 6-7) and DSM proposed shear curve (with Tension Field Action) (Figs. 8-9) respectively.

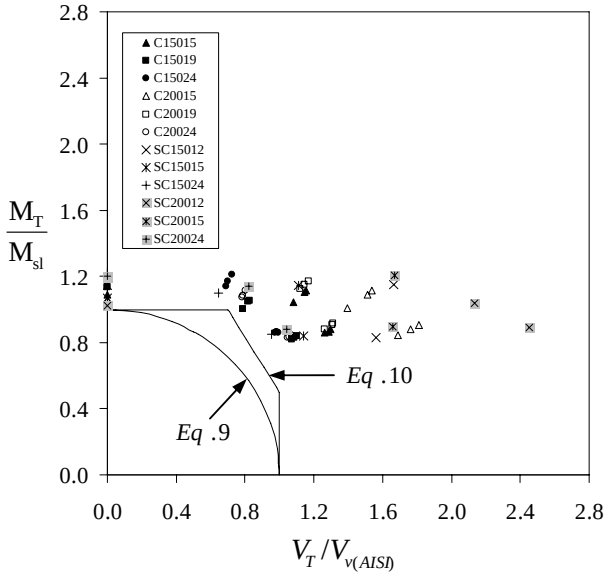

(a) With Straps

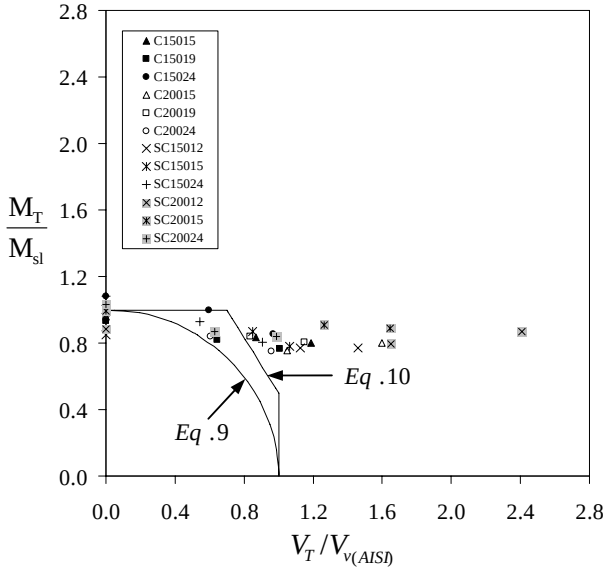

(b) Without Straps

Figure 6. Interaction between (M_T/M_s) and (V_T/V_v) with M_{sl} based on DSM, V_v based on AISI without TFA – Plain C- and SupaCee® Sections

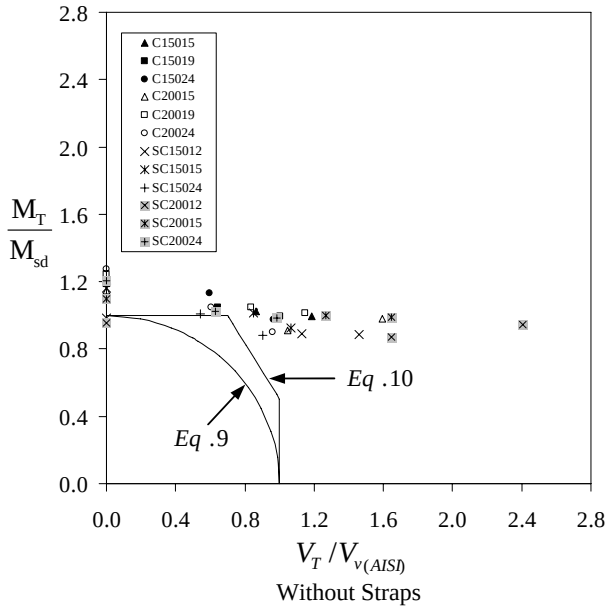

Figure 7. Interaction between (M_T/M_s) and (V_T/V_v) with M_{sd} based on DSM, V_v based on AISI without TFA – Plain C- and SupaCee® Sections

All results shown in Fig. 6(a) lie well above Eq. 10 trilinear so that the interaction between bending and shear is therefore not significant. The explanation for this fact is that the V_v, based on AISI, is calculated by using the elastic buckling stress of the whole sections which provides very conservative predictions, whereas the test results are based on the ultimate strength of the full section including tension field action. It is interesting to note that the slender sections (e.g. C20015 and SC20012) are more conservative than stockier sections. This fact shows that the more slender sections have more tension field action contribution to the ultimate strength of the sections in shear. Conversely, the stockier sections (e.g C15019, C15024, C20024, SC15024 and SC20024) of *(MV)* tests are more accurately predicted. In Fig. 6(b) for the tests without straps, the results are lower than those in Fig. 6(a) and mainly conservative except the stockier sections (e.g C15019, C15024, C20024, SC15024 and SC20024) of *(MV)* tests which lie just outside the circular domain limit (Eq. 9) and below Eq. 10 trilinear. In Fig. 7, the interaction between (M_T/M_s) and (V_T/V_v) without straps is similar to that in Fig. 6(b). The only difference is that the $M_s=M_{sd}$ is utilized instead of the $M_s=M_{sl}$ as it has a lower value. The results are shifted higher than those in Fig. 6(b) and lie above Eq. 10 trilinear. The interaction is therefore not as significant and very conservative.

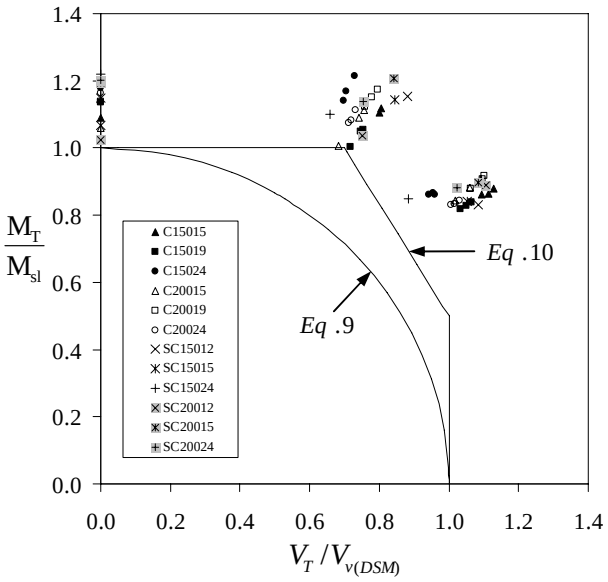

(a) With Straps

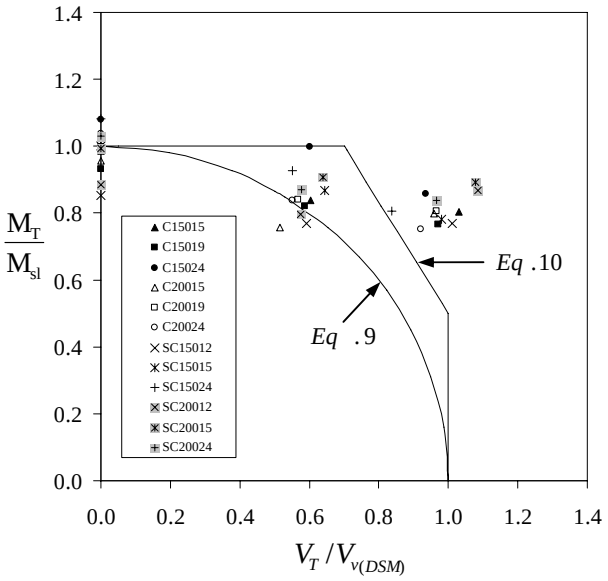

(b) Without Straps

Figure 8. Interaction between (M_T/M_s) and (V_T/V_v) with M_{sl} based on DSM, V_v based on DSM Proposal with TFA – Plain C- and SupaCee® Sections

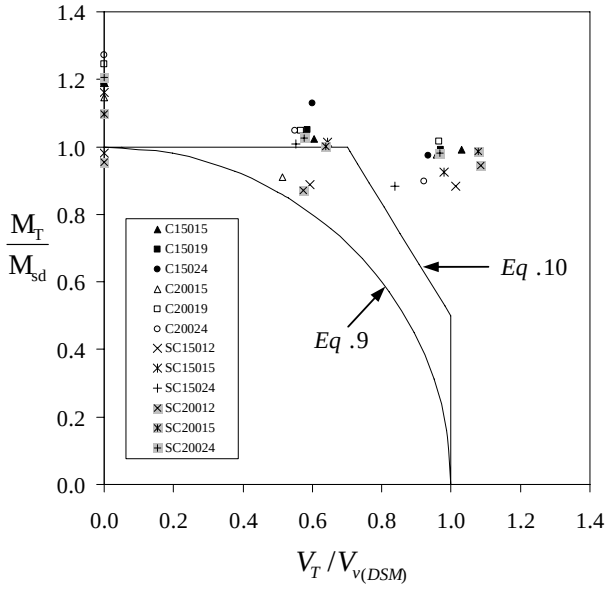

Figure 9. Interaction between (M_T/M_s) and (V_T/V_v) with M_{sd} based on DSM, V_v based on DSM Proposal with TFA – Plain C- and SupaCee® Sections

In Fig. 8(a), the mean of the ratios V_T/V_v for the *V* test series is almost equal to 1.0. This fact shows that the V_v based on DSM proposed shear curve with TFA gives the best prediction for the tested sections for nominal shear capacity of the whole section compared with that based on the AISI without TFA [see Fig. 6(a)]. The DSM proposed shear equation with tension field action gives a good mean fit to the *V* tests. The tests for the *(V)* and the *(MV)* also group very closely. This fact can be explained by the use of the shear buckling coefficient (k_v) for the whole channel sections instead of the web panel only. This method, therefore, gives more accurate prediction on the post-buckling strengths of the whole channel sections for bending and shear. Fig. 8(b) shows the interaction between (M_T/M_s) and (V_T/V_v) without straps where M_s is based on M_{sl} and V_v is based on the DSM proposed shear curve with TFA. It can be seen in this figure that the interaction between bending and shear is very significant. All tests for *(MV)* test series lie below Eq. 10 trilinear and are closer to Eq. 9 unit circle. The very slender sections (C20015, SC15012 and SC20012) even lie below the circular domain limit. This fact shows that it is unconservative to use Eq. 10 trilinear for design with M_{sl} and tension field action included. Therefore, Eq. 9 unit circle may be applicable in this case.

In Fig. 9, the $M_s=M_{sd}$ is utilized instead of M_{sl} as it is lower. The results are higher than those in Fig. 8(b) and generally lie above Eq. 10 trilinear. However, the tests with very slender sections (C20015, SC15012 and SC20012) of *MV* test series lie below Eq. 10 trilinear. The interaction is therefore less significant and conservative. The explanation is due to the fact that M_{sd} is normally lower than M_{sl} and it is conservative to use M_{sd} to predict M_s in the case of the tests without straps.

3. CONCLUSION

Two experimental programs were carried out at the University of Sydney to determine the ultimate strength of high strength cold-formed channel purlins subjected to combined bending and shear, and bending only. The high strength cold-formed channel purlins included plain C- sections and SupaCee® sections in each program respectively.

For combined bending and shear, all test results were plotted in this paper as interaction diagrams where V_v and M_s are determined by different methods. The nominal shear capacities, V_v, were based on AISI without tension field action in DSM format or DSM proposed shear curve with tension field action. The nominal section moment capacity, M_s, is based on either M_{sl} or M_{sd} of the DSM. The tests show that the DSM proposal with and without tension field action requires $M_s=M_{sl}$ to satisfy Eq. 10 trilinear interaction in cases of tests with straps. Also if tension field action is included in the DSM proposal, then Eq. 9 circular interaction must be used with both $M_s=M_{sl}$ and $M_s=M_{sd}$ in cases of tests without straps. Tension field action cannot be used with the DSM in case of tests without straps to satisfy Eq. 10 trilinear interaction.

REFERENCES

AISI. 2006. “Direct Strength Method (DSM) Design Guide.” *American Iron and Steel Institute*, Washington DC.

AISI. 2007. “North American Specification for the Design of Cold-Formed Steel Structural Members.” *2007 Edition*, AISI S100-2007.

LaBoube, R. A., and Yu, W. W. 1978b. “Cold-Formed Steel Web Elements under Combined Bending and Shear.” *Proc., 4th Int. Specialty Conf. on Cold-Formed Steel Structures*, University of Missouri-Rolla, St Louis, Missouri, U.S.A.

Lysaght. 2003. "NSW SupaCee® is trademark of Bluescope Steel Limited." *Bluescope Steel Limited trading as Bluescope Lysaght*.

Pham, C. H., and Hancock, G. J. 2009a. "Direct Strength Design of Cold-Formed Purlins." *Journal of Structural Engineering*, American Society of Civil Engineers, Vol. 135, Issue 3, pp. 229-238.

Pham, C. H., and Hancock, G. J. 2009b. "Experimental Investigation of High Strength Cold-Formed C-Section in Combined Bending and Shear.", *Research Report No R894*, School of Civil Engineering, The University of Sydney, NSW, Australia, April, 2009.

Pham, C. H., and Hancock, G. J. 2009c. "Experimental Investigation of High Strength Cold-Formed SupaCee® Sections in Combined Bending and Shear.", *Research Report No R907*, School of Civil Engineering, The University of Sydney, NSW, Australia, December, 2009.

Pham, C. H., and Hancock, G. J. 2009d. "Shear Buckling of Thin-Walled Channel Sections." *Journal of Constructional Steel Research*, Vol. 65, No. 3, pp. 578-585.

Schafer, B. W. 2006. "Review: The Direct Strength Method of Cold-Formed Steel Member Design." *International Colloquium on Stability and Ductility of Steel Structures*, Lisbon, Portugal.

Standards Australia. 1998. "Steel Structures." *AS 4100:1998*, Standards Australia/ Standards New Zealand.

Standards Australia. 2005. "AS/NZS 4600:2005, Cold-Formed Steel Structures." Standards Australia/ Standards New Zealand.

Twentieth International Specialty Conference on Cold-Formed Steel Structures
St. Louis, Missouri, U.S.A., November 3 & 4, 2010

FLEXURAL AND CYCLIC BEHAVIOUR OF HOLLOW AND CONCRETE- FILLED STEEL TUBES

Arivalagan .S[1], Kandasamy.S[2]

ABSTRACT

This paper presents a study on the flexural and cyclic behaviour of concrete filled steel hollow beam sections. The specimens in-filled with normal mix concrete, fly ash concrete, quarry waste concrete and low strength concrete (Brick-bat-lime concrete) and hollow steel sections were tested. Measurements of strains and deflections were made under two-point loading. A theoretical model was also developed to predict the moment carrying capacity. The capacities of the beams were compared with the ultimate capacity obtained using the international standards EC4-1994, ACI-2002 and AISC-LRFD-1999. The result of the experimental investigation showed that the moment carrying capacity increases based on the compressive strength of the filler materials. Energy absorption capacity also increase due to in filled materials. Analytical results show good agreements with experimental results.

Key words: 1) Steel hollow sections, 2) in-filled concretes, 3) static test
4) Cyclic test 5) FEM

[1]Dept.of Civil Engg., Dr M.G.R.Educational and Research Institute, Dept. of Civil Engg., Dr M.G.R.Educational and Research Institute,
Dr M.G.R.University, Chennai, TamilNadu, India.
e-mail:arivu357@yahoo.co.in.
[2]Dean, Anna University-Trichirappali,Ariyallur Campus, Ariyallur,TamilNadu, India.e-mail:kandasks@yahoo.com

1. INTRODUCTION

Concrete-Filled Hollow Steel sections (CFHS) are used in some special application. In the past,many research works were carried out on the behaviour of concrete-filled HSS columns and beam-columns. But relatively little research was reported on the structural behaviour of concrete-filled HSS beams. Assi.I.M., et al. tested thirty-four simply supported beams; 1000 mm long filled with lightweight concrete and foamed concrete (polyurethane) to obtain the ultimate moment capacity. Fully plastic stress block of the concrete at its maximum cylinder strength was used in the analysis. Analytical formulae for the ultimate moment capacity of concrete-filled RHS and SHS beams were suggested. They suggested that lightweight aggregate concrete and foamed concrete can be used in composite construction to increase the flexural capacity of steel tubular sections. Han L.M. conducted test on series of concrete filled square and rectangular beams, the depth to wall thickness ratio ranges from 20 to 50 and compressive strength of 28 days concrete cube of 30Mpa. to determine maximum moment capacity of the specimen and also to investigate the failure pattern. Elchakakani.M et al have tested 12 concrete filled steel CHS beams. The test specimens were selected to examine the effects of different d/t ratios ranging from 12 to 110 with the concrete cylinder strength 23.4 MPa. The test results showed that CFT were subjected to large deformations under pure bending, from which it was concluded that void filling prevented local buckling for very large rotations. Hussain K.M.A. conducted series of tests on thin walled composite beams with normal and lightweight volcanic pumice concrete as infill. It was observed the thin walled composite beam sections with volcanic pumice concrete exhibited satisfactory performance compared with normal concrete. Jane Helena.H. and Samuel Knight.G.M., carried out series of tests on hollow and concrete-filled cold-formed steel sections subjected to axial and bending forces. The effects of eccentricity ratio and strength of in-fill on the behaviour of these sections were studied. Even though the behaviour of concrete filled compression members are well understood the flexural behaviour of these sections needs to be investigated for better understanding. The objective of the present investigation is to study the flexural and cyclic load behaviour of rectangular hollow section beams in filled with different concrete materials and also to develop a empirical model for the analysis of the flexural behavior for concrete-filled HSS beams.

2. MATERIALS AND TESTING ARRANGEMENT

2.1 Material

All the experiments were carried out using commercially available RHS sections. They were produced by TATA STEEL INDUSTRIES, India. The ratio of tube depth to wall thickness (d/t) is 29.25. All the steel tubes used in this investigation were factory made products The length of the specimen was 1.2 m. The depth, breadth, and wall thickness of the rectangular section were 100×50×3.2 mm . The grade of steel was Yst310 as per IS 4923:1997 "INDIAN STANDARD HOLLOW STEEL SECTIONS FOR STRUCTURAL USE – SPECIFICATIONS". In order to determine the material properties of the steel tubes the coupon tests were conducted in accordance with the code of practices IS: 1608-1972 "METHOD FOR TENSILE TESTING OF STEEL PRODUCTS". Three coupons were cut from the three flat surfaces and the 0.2% proof stress was adopted as the yield stress for the steel tubes. The mean values of material properties of the steel specimens were shown in Table 1.For Concrete-Filled RHS beam specimens, ordinary portland cement (OPC-43 Grade) was used. The required quantity was procured in a single batch. The physical properties of the concrete were shown in Table 1. Locally available river sand conforming to zone II of IS: 383-1970 was used. The coarse aggregate of the granite stone 8 to 10 mm size was supplied by the local quarry. Ordinary potable water available in the laboratory was used for the experimental investigations and for curing purposes. Fly ash procured from Neyveli Thermal Power Plant had been used as replacement to cement. Quarry wastes procured from the quarry mines in and around Salem city and Fat limes were used.

2.2 Composite Beam Specimens

The details of the tested specimens filled with different types of concrete are shown in Tables 1 and 2 such as the specimen label, the sectional dimensions, the depth to wall thickness ratio (d/t), the type of mix, the yield strength of steel and characteristic compressive strength of concrete. Each mix proportions consist of three specimens. They are designated as Normal Mix Concrete (NMC), Fly Ash Concrete (FAC), Quarry Waste Concrete (QWC), Low Strength Concrete (LSC), and Rectangular Hollow Section (RHS).

Table 1 Group designation of the test specimen (Under Static Load)

Sl.No	Specimen Label	Sectional Dimensions D×B×t (mm)	d/t	Type of mix, f_y(MPa) and f_{ck}(MPa)
1	RHS-1	100×50×3.2	29.25	Rectangular Hollow Section f_y =338
2	RHS-2	100×50×3.2	29.25	
3	RHS-3	100×50×3.2	29.25	
5	NMC-R-1	100×50×3.2	29.25	Normal Mix Concrete f_{ck}=32.3
5	NMC-R-2	100×50×3.2	29.25	
6	NMC-R-3	100×50×3.2	29.25	
7	FAC–R-1	100×50×3.2	29.25	Fly Ash Concrete f_{ck}=27.5
8	FAC–R-2	100×50×3.2	29.25	
9	FAC–R-3	100×50×3.2	29.25	
10	QWC-R-1	100×50×3.2	29.25	Quarry Waste Concrete f_{ck}=21.63
11	QWC-R-2	100×50×3.2	29.25	
12	QWC-R-3	100×50×3.2	29.25	
13	LSC-R-1	100×50×3.2	29.25	Low Strength Concrete f_{ck}=0.88
14	LSC-R-2	100×50×3.2	29.25	
15	LSC-R-3	100×50×3.2	29.25	

Table 2 Group designation of the test specimen(Under Cyclic Reversal load)

Sl.No	Specimen Label	Sectional Dimensions D×B×t (mm)	d/t	Type of mix, f_y(MPa) and f_{ck}(MPa)
1	RHS-1	100×50×3.2	29.25	Rectangular Hollow Section f_y =338
2	RHS-2	100×50×3.2	29.25	
3	RHS-3	100×50×3.2	29.25	

4	NMC-R-1	100×50×3.2	29.25	Normal Mix Concrete f_{ck}=37
5	NMC-R-2	100×50×3.2	29.25	
6	NMC-R-3	100×50×3.2	29.25	
7	FAC–R-1	100×50×3.2	29.25	Fly Ash Concrete f_{ck}=35
8	FAC–R-2	100×50×3.2	29.25	
9	FAC–R-3	100×50×3.2	29.25	

The specimens were filled with concrete in many layers and carefully compacted by a steel rod to avoid voids inside the specimen. Three cubes of 150 mm size were prepared for each type of concrete to determine the average compressive strength. These cubes were cured in water and tested according to the guidelines specified in the code of practices (IS 456:2000).

Table 3 Average material properties of steel sections

Sectional Dimensions D×B×t (mm)	**Yield Stress f_y (MPa)**	**Ultimate Stress f_u (MPa)**	**Young's Modulus E_s (MPa)**	**f_u/f_y**
100×50×3.2	338	480	2.28×10^5	1.42
72×72×3.2	345	510	2.2×10^5	1.48

Table 4 Average Material Properties of in-filled Concrete

Filler material	**Density (kg/m^3)**	**Compression strength (MPa)**
Normal Mix Concrete (NMC)	2400	32.3& 37
Fly Ash Concrete (FAC)	2100	27.55& 35
Quarry Waste Concrete (QWC)	2150	21.63
Low Strength Concrete (LSC)	2000	0.88

2.3 Test On Static Load

Fifteen beam specimens consisting of three hollow steel specimens and twelve Concrete-Filled Steel Tubular beam specimens (CFSTs) were selected. The twelve Concrete-Filled Steel Tubular (CFST) beam specimen consists of three in-filled with normal mix concrete, fly ash concrete, quarry waste concrete and low strength concrete three members in each case. The sizes of RHS sections were selected as 100 × 50 × 3.2 mm. The length of the specimen was 1.2 m. The details of the test specimens are shown in Table 1. A simply supported beam set up was adopted. Beams were tested under two-point load in a 1000 kN capacity Universal Testing Machine. The beams were placed over simple supports with an effective span of 1.00m. Two point loading was applied at the centre of a very rigid plate, to ensure the distribution of the load as shown in Figure 1. The test specimens were instrumented to measure load, strains and deflections. Deflections of the beam specimens were measured by three dial gauges, one is placed at the mid span of the specimen, and the other two were placed under concentrated loads. Strain values were measured using the strain gauges at every incremental of load applications. The strain gauges were fixed at the centre, on the top and at the bottom flanges of the beam specimen to measure the tensile and compressive strain. A load interval of less than one-tenth of the estimated load capacity was used. Each load interval was maintained for about 2-3 minute at each load increment. Load and the corresponding deflections and strains were measured upto ultimate stage.

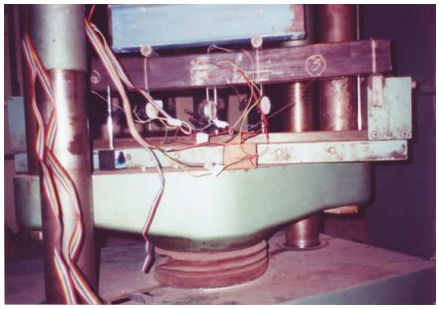

Figure 1 Test set up

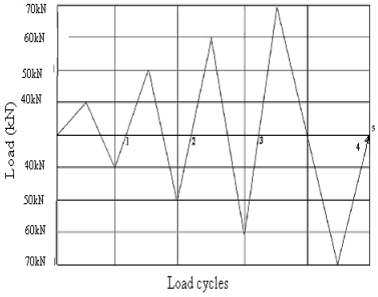

Figure 2 Cyclic loading diagram

2.4 Test On Cyclic Reversal Load

A total of nine specimens consisting of three hollow steel specimens and six Concrete-Filled Steel Tube beam specimens (CFSTs) consisting of three RHS in-filled with normal mix concrete and fly ash concrete specimens were casted and tested. The sizes of RHS sections were selected as 100 × 50 × 3.2 mm. The length of the specimen was 1.2 m. They are summarized in Table 2. The 400 kN capacity UTM (Universal Testing Machine) was used to perform the test. Each specimen was subjected to cyclic reversible bending. The test procedure of cyclic load is described below.

The test specimen was arranged in a simply supported condition. The load was applied by two-point method at one-third distance of the span of the specimen. The load was applied gradually through a jack at an increment of 5kN. In the first cycle, load was applied to a maximum of 40kN. Then the specimen was unloaded with a decrement load of 5kN. The load was brought to zero. Afterwards the specimen was turned over and arranged again in the position. Then cyclic test was performed as described above. Thus one complete cycle of loading and unloading was performed .In second, third, fourth and fifth cycles, the maximum load of each cycle was 50kN, 60kN, 70kN and 80kN respectively. Deflectometers were placed under the loading point and the centre (midspan) of the specimen to measure the deflections. Strain gauges were also used to measure the strain values. These are fixed at the centre (midspan) of the beam specimen and in the top and at the bottom faces of the beam specimen. The readings of the deflectometer and the strain gauge were recorded. From the deflection and strain values, Moment Vs Strain, Load Vs Deflection and Load Vs Strain behavior were studied. Figure 2 shows the cyclic loading arrangement.

3. ANALYTICAL STUDY

3.1 Ultimate moment of resistance based on strain compatibility at the interface (By Stress-Strain Block approach)

This analysis is based on the consideration of the hollow steel section for fully plastic at the time of failure. For the calculation of ultimate strength of concrete, the rectangular and semi parabolic stress block concept of

the reinforced concrete design is adopted (By Stress-Strain block approach) according to Indian code IS456-2000.

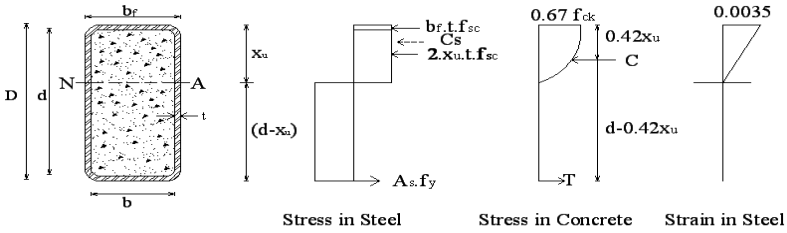

Figure3 Stress-Strain distribution in concrete-filled hollow steel section at Mu

where, b_f - External breadth of the section; b - Internal breadth of the section; D -External depth of the section; d - Internal depth of the section; t - Thickness of steel section; xu - Depth of neutral axis; f_{ck} - Characteristic strength of concrete; f_y - Yield strength of steel tube; f_{sc} -compressive stress on the extreme compression fiber of the tube; C_c-compressive force in concrete;C_s-Compressive force in steel, C-total compressive force;T-Total tensile force in tension flange of steel.

This is based on full plastic stress distribution in steel. A uniform compressive stress is assumed for concrete. Since the above consideration is approximate, an accurate model developed in the present investigation based on the stress block of IS: 456-2000. In addition to the usual assumptions of flexural theory, the following is assumed.

1. Initially plane sections remain plain after bending and normal to neutral plane.
2. At ultimate stage, steel in tension zone is subjected to yield stress of f_y.
3. The compressive stress on the extreme compression fiber of the tube is $f_{sc}=0.9f_y$.
4. At ultimate stage of bending the failure of the concrete deemes to have been reached, when the extreme fiber compressive stress ε_{cu} reaches 0.0035.
5. The maximum compressive strength of the concrete is assumed to be 0.67times of laboratory characteristic compressive strength $(\frac{2}{3} f_{ck})$.

6. The contribution of concrete in tension zone is ignored.

the ultimate moment of resistance can be obtained by taking moments about the tension flange of the composite section and the ultimate moment of resistance can be calculated using the equation 4.12,

$$M_u = 0.545\ f_{ck}\ b\ x_u(d - 0.42\ x_u) + f_{sc}\ A_{sc}\left(D - {x_u}/{2}\right)$$

------ (1)

3.2 Finite Element Analysis of the Flexural Behaviour of Hollow Steel and Concrete-Filled Beams

Material properties used for the steel and the concrete in the Finite Element Analysis are taken from the results of material testing. The average stress-strain curve for linear materials of the steel RHS and SHS tubes used in this model was determined by idealization from the tensile coupon tests. An elastic-perfectly plastic model was used. The stress-strain curve for concrete material provided by the ANSYS is linear. The boundary conditions were applied correctly, at support located at 100mm from end. At support nodal translations are restrained along all axes and rotations about x axis only permitted. A figure 3 shows the FEA Concrete-filled Beam model with boundary condition.

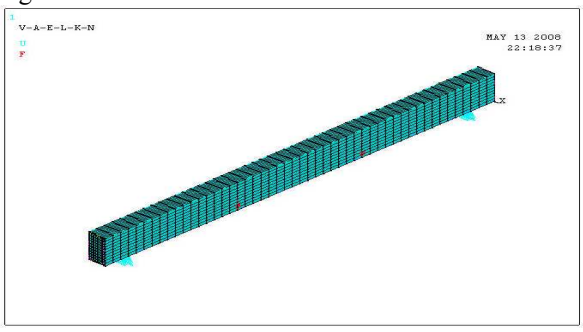

Figure 4 FEA Concrete-filled Beam model with boundary condition

The hollow steel is modeled by shell 43 elements. The shell 43 is well suited to model non-linear, flat or warped, thin to moderately thick shell structures. In concrete filled steel tubular sections the concrete core is meshed by three-dimensional solid concrete (solid 65) element. The model of the beam

is presented in the Figures 4 for concrete filled section. The model presented in the figure is global co-ordinate system represented in x, y and z-axes. The span of the beam is 1200 mm. A static linear analysis has been conducted .A reasonably fine mesh of 50 mm is adopted for mesh modeling of the steel shell and the concrete core. It is assumed that the strain compatibility exists at the steel-concrete interface.

4. RESULT AND DISCUSSION

4.1 Load Vs Deflection

Figure 5 presents the Load Vs Deflection behaviour of hollow steel section and hollow steel section filled with normal mix concrete, fly ash concrete, quarry waste concrete and low strength concrete. Both rectangular section and square section are taken into consideration. From the above figure it is observed that the initial stiffness increases due to the infill materials. The increase in stiffness in the case of normal mix concrete, fly ash concrete, quarry waste concrete is about 3 times more than that of the hollow steel sections. Even in low strength concrete, the initial stiffness increases by 2.25 times. From the Figure 5 it can be seen that in the case of normal mix concrete, fly ash concrete, quarry waste concrete increases the loads with slight increasing the deflection whereas in low strength concrete the increase in the deflection with reducing load is noticeable. This strength and deflection mainly depend on the strength of filler materials. The Figures 5 shows that concrete-filled beams yield load and the ultimate load is increased when compared to hollow steel specimens. It is also observed that in specimens filled with low strength concrete, only a marginal increase is observed.

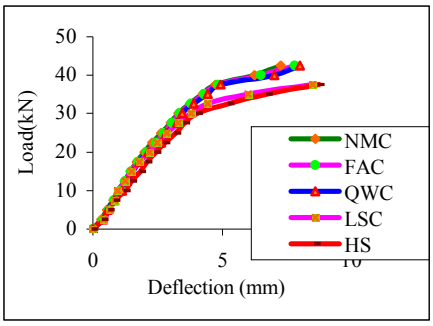

Figure 5 Load Vs Deflection

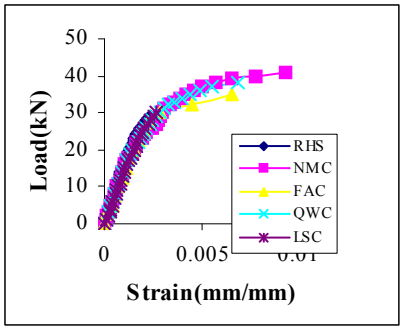

Figure 6 Tensile Strain

4.2 Load Vs Tensile Strain

In Figure 6 present tensile strains against load for different flexural members under each configuration of rectangular and square sections. Once again for concrete-filled specimens ultimate range and stiffness is noticeable although full curve is not available due to an early peeling of strain gauges. For all the specimens yield strain values are within the limits of 0.002 to 0.003. The Load Vs Strain plots in Figure 6 show the strain readings of hollow steel sections and their premature failure due to less stiffness. Its strain non-linearity gests start at 75% of its ultimate load value. From the above figures of Load Vs Deflection curves it can be observed that the stiffer curves of composite beams filled with different materials (NMC, FAC and QWC). In-case of in-filled sections filled with normal mix concrete, fly ash concrete and quarry waste concrete its strain non-linearity gets starts at 85% of its ultimate load value. For low strength concrete it strain non-linearity gets starts at 80% of its ultimate load value. Improved performance of the tensile concrete is due to the strength of filler materials.

4.3 Comparison of Moment Carrying Capacities

4.3.1 Moment Carrying Capacity of Hollow Steel Beams

The details of the RHS beam test specimen and its corresponding moments are presented in Table 5. A comparison of experimentally observed moment carrying capacity of the hollow steel section beams with plastic moment carrying capacity calculated with the Indian standard codal provisions is shown in Table 5. It is observed that the experimental values reasonably agree with the plastic moment capacity.

Table 5 Moment carrying capacities of Hollow steel Beams

Sl.No	Specimen Label	Sectional Dimensions DxBxt (mm)	f_y (MPa)	$M_{u(exp)}$ (kN m)	M_{Plas} (kN m)	$M_{u(exp)}/M_{Plas}$
1	RHS-1	100×50×3.2	338	10.56	10.00	1.056
2	RHS-2	100×50×3.2	338	10.40	10.00	1.04
3	RHS-3	100×50×3.2	338	10.40	10.00	1.04

4.3.2 Moment Carrying Capacity of Concrete-filled Beams

Twelve RHS beams filled with normal mix concrete, fly ash concrete, quarry waste concrete and low strength concrete members were tested under flexure. The detailed test results of its experimental and theoretical test values and its comparisons are presented in Table 6.Theoretical ultimate moment capacity of concrete-filled beams is calculated based on the analytical expression derived (Eqn.1)in the present work and it is presented in Table 6 along with the experimental moments. It can be seen that analytical expression closely predicts experimental ultimate moment carrying capacity.

Table 6 Moment carrying capacities for concrete-filled Beams

Sl.No	Specimen Label	Sectional Dimensions DxBxt (mm)	$M_{u(exp)}$ (kN m)	$M_{u(the)}$ (kN m)	$M_{u(exp)}/M_{u(the)}$
1	NMC-R-1	100×50×3.2	13.86	13.21	1.05
2	NMC-R-2	100×50×3.2	13.70	13.21	1.04
3	NMC-R-3	100×50×3.2	13.70	13.21	1.04
4	FAC–R-1	100×50×3.2	13.20	12.97	1.02
5	FAC–R-2	100×50×3.2	12.87	12.97	0.99
6	FAC–R-3	100×50×3.2	13.04	12.97	1.005
7	QWC-R-1	100×50×3.2	13.04	12.64	1.03
8	QWC-R-2	100×50×3.2	12.87	12.64	1.02
9	QWC-R-3	100×50×3.2	12.71	12.64	1.006

10	LSC-R-1	100×50×3.2	10.73	11.29	0.95
11	LSC-R-2	100×50×3.2	10.89	11.29	0.96
12	LSC-R-3	100×50×3.2	10.56	11.29	0.94

It is observed that when compared to hollow steel section, in the beams filled with normal mix concrete, fly ash concrete and quarry waste concrete there is an increase in moment carrying capacity. But in the case of specimen filled with low strength concrete only a marginal increase of moment carrying capacity is observed.

4.3.3 Moment Carrying Capacities of standards

A comparison of the moment carrying capacity between various standard codes and experimental results are shown in Table 7. The partial safety factor was not considered during comparison. It is observed that the codal equations of EC 4:1994, ACI-318:1989 and AISC-LRFD: 1999 considerably underestimate the experimentally obtained moment capacities of the specimens. The Eurocode(EC4) yield better predictions of the moment carrying capacity than ACI and AISC codes**.** It is observed that beam specimen filled with normal mix concrete, fly-ash concrete and Quarry waste concrete behaves in a similar manner. From the above results it is seen that the flexural capacity of tube is increased when it is filled with concrete materials and this increase depends on the strength of the filled materials.

Table 7Comparison of Moment Carrying Capacity between Experimental results and Standard Codes

Sl. No	Specimen Label	$M_{u(exp)}$ (kN m)	EC4		ACI		AISC	
			M_{EC4} (kN m)	M_{EC4} /$M_{u(exp)}$	M_{AIJ} (kN m)	M_{ACI} /$M_{u(exp)}$	M_{AISC} (kN m)	M_{AISC} / $M_{u(exp)}$
1	NMC-R-1	13.86	10.10	0.73	10.03	0.72	9.65	0.70
2	NMC-R-2	13.70	10.10	0.74	10.03	0.73	9.65	0.70
3	NMC-R-3	13.70	10.10	0.74	10.03	0.73	9.65	0.70
4	FAC-R-1	13.20	10.03	0.76	10.00	0.76	9.65	0.73
5	FAC-R-2	12.87	10.03	0.78	10.00	0.78	9.65	0.75
6	FAC-R-3	13.04	10.03	0.77	10.00	0.77	9.65	0.74
7	QWC-R-1	13.04	9.95	0.76	9.90	0.76	9.65	0.74

8	QWC-R-1	12.87	9.95	0.77	10.30	0.77	9.65	0.75
9	QWC-R-3	12.71	9.95	0.78	9.90	0.78	9.65	0.76
10	LSC-R-1	10.72	9.70	0.90	9.70	0.90	9.65	0.90
11	LSC-R-2	10.89	9.70	0.89	9.70	0.90	9.65	0.89
12	LSC-R-3	10.56	9.70	0.92	9.70	0.92	9.65	0.91

4.4 COMPARISON OF FINITE ELEMENT ANALYSIS REULTS WITH EXPERIMENTAL RESULTS

The loads Vs deflection response of the composite beams are plotted in the Figure 7. From the Figure7 of rectangular hollow steel section in filled with concrete, FEA yield load value is 5% and 10% is higher when compared to experimental yield load value. In general it has been observed that the difference between the predicted and observed values increases with increase in load. The higher values predicted by FEA may be attributed to the following limitations in the present analysis. In the present analysis, compatibility of steel and concrete at the interface during loading has been assumed. However, a more realistic approach is use interface elements with appropriate material model. Also elastic perfectly plastic behaviour has been used to model the behaviour of steel and ANSYS provide linear stress-strain behaviour for concrete. It is known that concrete develops cracks at higher load and crushes as well. Therefore the consideration of this aspect is required in modeling the behaviour of composite section. Analysis also carried out for a RHS without filling. The Load-deflection response of the comparison is presented in Figures 7. For the hollow steel section, a Finite Element result agrees well with the experimental results until the ultimate load is reached. After the ultimate load the experimental results showed sharp loss of stiffness and ductility which is due to the local buckling. While in comparison the analysis indicates the beam is stiffer than that observed in the experiments. Figure 8 shows the FEA diagram of filled beam.

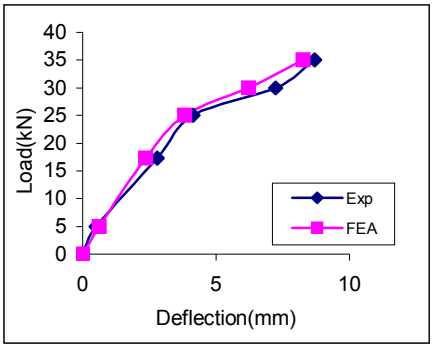

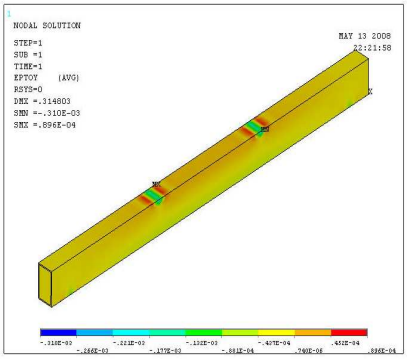

Figure 7 FEA and Experimental Load Vs Deflection Figure 8 FEA Strain Contour of Concrete-filled RHS Beam

4.5 Hysteretic Behaviour

4.5.1 Moment Vs Strain hysteretic Behaviour

The typical variation of moment carrying capacity with respect to strain for hollow steel and concrete-filled beams is shown in Figures 9. It is observed that Moment Vs Strain behaviour of tension flange of rectangular section filled with normal mix concrete, moment carrying capacity increases upto four cycles and thereafter it remains constant. The value of capacity beyond four cycles is slowly reduced. From the above observation it is observed that upto four to five cycles the moment carrying capacity increases after that once the local buckling takes place suddenly reduced the moment carrying capacity. The yield strain values are within 0.002 to 0.003.

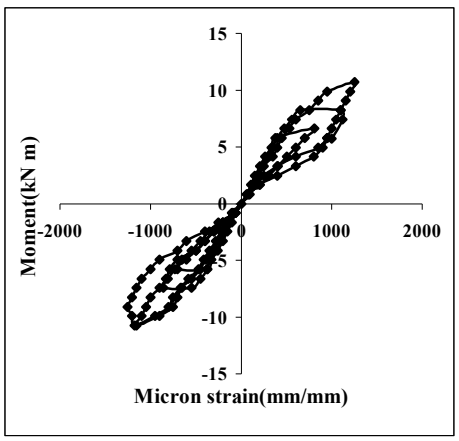

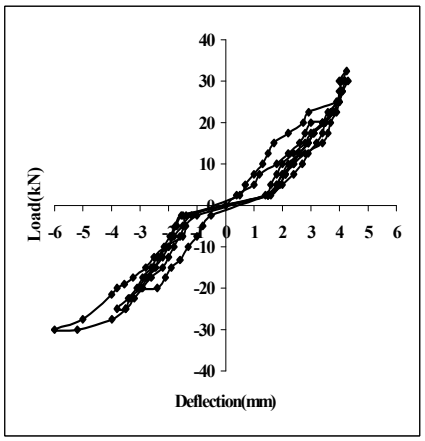

Figure 9 Cyclic Moment Vs Strain Figure10 Cyclic Load Vs.Load Vs Deflection

4.5.2 Load Vs deflection hysteretic Behaviour

The deflection variation for the rectangular section filled with normal mix concrete is presented in Figure 10. It can be seen that deflections are generally positive. The beam could not be deflected upward due to the resistance of the reversal load. The variation is uniform upto four cycles and after that due to reducing capacity the deflection become negative. It is observed that the increase of deformation is very difficult to control just after the peak, although the load is constant at certain loading level. Accordingly, the stiffness decreases rapidly in concrete-filled beams after it attains the ultimate load.

4.6 Energy Absorption Capacity

The concrete-filled specimens have showed significantly higher energy absorption capacity when compared to hollow steel beam specimens. The increased in energy absorption capacity of rectangular section filled with normal concrete and fly ash concrete is 1.53 times and 1.49 times when compared to hollow steel section.

5. CONCLUSION

1. Beam specimens filled with normal mix concrete, fly ash concrete, quarry waste concrete and low strength concrete behave flexurally and are capable of developing the full flexural strength of their sections.
2. The test results show that there is an increase of 28%, 27% and 25% in the moment carrying capacity of normal mix concrete, fly ash concrete and quarry waste concrete respectively when compared to hollow steel section.
3. The theoretical expression developed for the calculation of moment of resistance based on Indian code stress block (Equation 1) closely predicts the flexural behaviour.
4. The existing international codal formulae (without safety factor) under-estimates the moment carrying capacity of the concrete filled beams.
5. Concrete filling increases the residual load capacity of thin RHS and SHS beams to resist cyclic load especially when the transverse displacement increases.
6. Concrete filling increases the energy absorption especially for hollow steel sections.

6. Acknowledgement

The experiments were conducted as part of Ph.D. research programme at the strength of materials laboratory, Government College of Engineering, Salem, Tamil nadu, India. The author wishes to thanks the authorities of the facilities provided, the teaching and non teaching staff, P.G. students for their support and encouragement.

7.REFERENCE

1. Assi I.M., Qudeimat E.M. and Hunaiti Y.M., 'Ultimate Moment Capacity of Foamed and Fly ash Aggregate Concrete-Filled Steel Tubes', Steel and Composite Structures, Vol. 3, No. 3, 2003, pp-199-212.

2. Han,LH., "Flexural Behaviour of Concrete-Filled Steel Tubes", Journal of Constructional Steel Research, 60, 2004, pp.313-337.
3. Elchalakani,M.,Zhao, XL .and Grzebieta, R.H., "Concrete Filled Circular Steel Tubes Subjected to Pure Bending",Journal of Constructional Steel Research ,57(11), 2001, pp. 1141-1168
4. Hussain,K.M.A., "Experimental & Theoretical Behavior of Thin Walled Composite Filled Beams", Electronic Journal of Structural Engineering, 3, 2003,pp.117-139.
5. Jane Helena,H. and Samuel Knight,G.M., "Behaviour of Cold-Formed Steel Hollow and Conrete-Filled Members", Steel and Composite Structures, Vol.5,No.1,2005,pp.35-47.
6. I.S: 4923,"Indian Standard Hollow Steel Sections For Structural Use – Specification", Bureau of Indian Standards, NewDelhi, Second revision 1997.

NOTATIONS:

Asc : Area of steel tube under compression.

b_f : External breath of the section

b : Internal breath of the section

D : External depth of the section

d : Internal depth of the section

t : Thickness of steel section

xu : Depth of neutral axis

Z , Z_p , W_{pa} :Plastic section modulus of the hollow steel tube

W_{ps} : Plastic section modului of the reinforcement

W_{pa} , Z_{con} : Plastic section modului of the concrete part of section (for the calculation of W_{pc} the concrete is assumed to be uncracked)

f_c :Concrete cylinder strength

fc_d :Design strength for the concrete

f_{ck} : Characteristic strength of concrete

f_{cu} : Characteristic 28-day cube strength of concrete

f_{yr} : Yield strength of reinforcement steel

f_y : Yield strength of steel tube

f_{yd} :Design strength for the structural steel

f_{sd} :Design strength for the reinforcement

Twentieth International Specialty Conference on Cold-Formed Steel Structures
St. Louis, Missouri, U.S.A., November 3 & 4, 2010

Lateral torsional instability of single channels restrained by angle cleats

G.M. Bukasa[1] and M. Dundu[2] MASCE.

Abstract

A series of experiments on the lateral torsional instability of single channels is presented. The channels are restrained by a purlin – angle cleat connection and subjected to a two point loading system in order to simulate a distributed load. Failure of the channels occurred by local buckling of the compression zone of the flange and web and lateral torsional buckling of the channels between points of lateral support. Tests have shown the purlin–angle cleat connection to be capable of restraining the frames from failing due to lateral-torsional buckling. This eliminates the idea of having fly-bracings, which is normally done in practice to restrain torsional instability.

[1] Postgraduate Student, University of Johannesburg, Dept. of Civil Engineering Science, P. O. Box 524, Auckland Park, 2006, South Africa.
[2] Senior Lecturer, University of Johannesburg, Dept. of Civil Engineering Science, P. O. Box 524, Auckland Park, 2006, South Africa.

Introduction

Cold-formed channel beams and rafters in portal frames are usually restrained against lateral-torsional buckling behaviour from its top flange through an angle cleat-purlin connection. Additional restraint is usually provided by fly bracing. This restraining mode has disadvantages of either weakening the top flange of the main frames if it is in tension, due to tearing that occurs around the fastened points or fabrication costs of providing fly bracing. This study investigates a restraint that avoids the use of fly bracing and bolt holes in the top flange. Restraint of the beam or main frame is still provided by a purlin-angle cleat connection, however the angle is long enough so as to connect the main beam or frame in the web. This connection configuration is found to be better because it restrains both lateral and torsional movements of the member.

In these tests the beam, purlin and angle cleats are all cold-formed steel sections to make the structure light and connected together by bolting only. The sizes of the beam, purlin and angle cleat section are 300x75x20x3mm, 100x50x20x2mm and 100x75x20x3mm, respectively. In order to obtain different buckling modes, the length of the channels is varied from 1.8 to 6m. The support systems were designed to achieve simply supported end conditions in the vertical plane; however the channel beams were restrained against lateral deflections and twist rotations at the ends. Restraints were also provided at the loading points. The beans were subjected to a two-point loading system at the top flange in order to experience pure bending in the internal span. The objectives of the tests are to examine the ability of thin cold-formed angle cleat to restrict lateral-torsional buckling and compare the test results with unfactored resistances from design standards.

Material and section properties

The channel sections used are of commercial quality steel. A total of fifteen coupon test specimens were cut from the web and flange of channel beams. Corner coupons were not tested because of the lack of appropriate tools to prepare and test them. The coupon were prepared and tested in a 100kN capacity displacement controlled testing machine according to the guidelines provided by the British Standard, BS 18. The thickness and width of the reduced section of coupons were measured and recorded on the computer system so as to calculate the area and subsequently the stresses. The longitudinal strain gauges, attached to

the coupon at the centre of each face, were used to determine the strains. The tensile load was applied to the prepared coupon test at a constant rate of 3.0mm/min until failure. A 50mm gauge length was marked onto the tensile test specimens before testing. After fracturing the specimens the two parts are fitted together to measure the axial elongation of the coupons. The ductility of the steel is evaluated as a percentage of the elongation at failure, according to the following equation:

$$\varepsilon_f = \left(\frac{l_f - l_0}{l_0} \right) \times 100$$

where, l_0 is the initial length of gauge and l_f the final length measured after fracture.

The stress-strain relationship of the coupons, shown in Figure 1, is derived from the load-elongation relationship using its original cross-sectional area and the gauge length. The yield stress, ultimate stress and modulus of elasticity of the steel are determined from these stress-strain curves. The average yield stress and tensile stress of the web and flange coupons are summarized in Table 1. In this table, ε_y and ε_u are the yield and the ultimate strain respectively. In compliance with SANS-10162-1:2005, the material properties of the channels achieved the recommended ductility requirements, that is, the percentage elongation at failure exceeded 10% for a 50mm gauge length and the ratio of the specified ultimate tensile strength (f_u) to the specified yield strength (f_y) exceeded 1.08.

The measured dimensions for the channels under investigation were found to be very close to the nominal ones from the supplier. This allowed the use of section properties from the Southern Africa Steel Construction Handbook (2005).

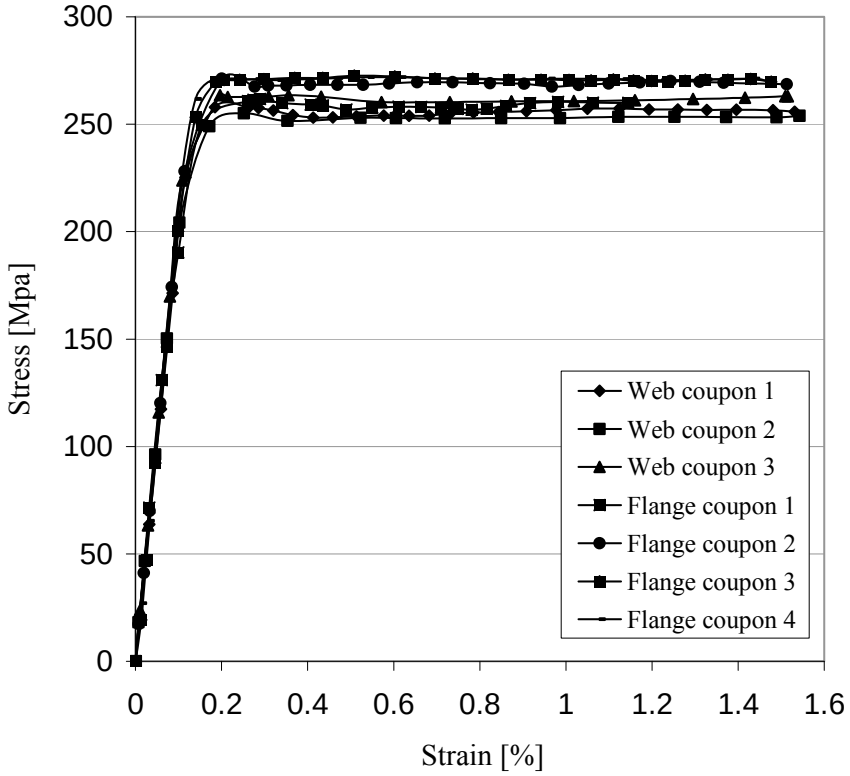

Figure 1 Stress-Strain Curve

Table 1 Average material properties of the channels

Specimen	f_y (MPa)	f_u (MPa)	f_u/f_y	ε_y	ε_u	$\varepsilon_u/\varepsilon_y$	ε_f (%)
Web	259.17	367.62	1.42	0.015	0.028	1.83	41.75
Flange	273.66	375.36	1.37	0.022	0.034	1.58	42.45

Test programme

Nine beams were tested under two point loading as illustrated by the schematic diagram in Figure 2. Two-point loading provides a constant moment region between the applied loads so that pure bending failure only is experienced. This loading arrangement simulates a distributed load over the entire span of the beam.

The span of the beams varied from 1.8m to 6 m. The support system was designed to ensure that the beam test is simply supported and, that both twisting and lateral deflections were prevented at the ends. Lateral and torsional bracing was also provided at the loading point as shown in the figure. Details of the span and points of bracing are shown in Table 2. The load was applied through the top flange of the channel sections, exactly at the restrained points to simulate the tests to the actual conditions to which a frame could be subjected under vertical load.

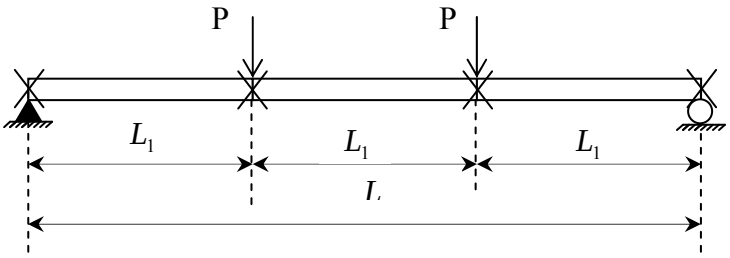

Figure 2 Sketch of test set-up

Table 2 Length of tested beams

Tests	Span, L (mm)	Length L_1 (mm)	Slenderness ratio of internal length
Test 1	1 800	600	23.9
Test 2	2 280	760	30.3
Test 3	2 790	930	37.1
Test 4	3 300	1 100	43.8
Test 5	3 780	1 260	50.2
Test 6	4 290	1 430	57.0
Test 7	4 800	1 600	63.7
Test 8	5 280	1 760	70.1
Test 9	6 000	2000	79.7

To allow for interaction to occur between members in an assembly, the beams were tested in pairs, as shown in Figure 3 (Baker and Eickhoff 1955, 1956; Baker et al. 1956; Dowling et al. 1982 and Dundu and Kemp 2006). The channels are oriented in the same direction as this offers greater stiffness than having the channels oriented in different directions (Dundu and Kemp 2006). The beam channels in each assembly are spaced at 1.84m, and as indicated before were

connected together by 100x50x20x2mm cold-formed purlin sections through 100x75x20x3mm cold-formed angle-cleats. Two, 12mm diameter bolts connects the angle-cleat to the web of the purlin whilst another two, 20mm diameter bolts connects the same angle cleat to the web of beam channel.

Figure 3 Typical test set-up

The beams were fully instrumented so that in-plane deflection, out-of-plane deflection, strains and torsion rotation of the beam could be measured. These measurements were recorded at the mid-span through a data logger. In-plane and out-of-plane deflections of the beam were measured using 3 linear variable differential transducers (LVDTs) as shown in Figure 3. Torsional rotation at mid-span of the beams was monitored by means of clinometers placed inside the web. Strains were measured in both the top flange and bottom flange of the channel in order to determine the moment-curvature behaviour of the frames. A 250kN hydraulic instron testing machine was used to apply the loads. Each test specimen was incrementally loaded at the rate of 2mm/min until failure. All measurements were taken at each load increment, until the beam tests buckled.

Experimental results

The results of the full scale beam tests are summarised in Table 3. P and M_u are the maximum point load and moment applied to the base, respectively, and M_r is the buckling moment resistance, determined using the South African structural steel code, SANS10162-2:2005. This code is based on the Canadian structural steel code, CAN-S16.1-M89. As expected, small in-plane deflections and higher ultimate load were observed in short beam tests by comparison with longer beams. The buckling moment of resistance of the middle unbraced length is determined, based on modified section properties (effective width of compression elements) to control local buckling. The effective width concept was first proposed by Von Karman (1932) and calibrated for use by Winter (1947). Since the load was applied at the top of the channels it had a distabilising effect on the channels. This implies that an effective length factor of 1 for bending about the minor axis (assuming a partially restrained member) and moment-gradient factor of 1 (uniform bending moment diagram) should be adopted. A comparison of the experimental moment and the buckling moment resistance shows the experimental moment to be significantly lower than the buckling resistance. This is because the some of the spans used are not long enough to encourage a larger moment to develop. Additional tests that favour a lateral torsional buckling mode of failure are being pursued.

Table 3 Test results

Tests	Unbraced-length (mm)	P (kN))	M_u (kNm)	M_r (kNm)
Test 1	600	21.92	13.2	33.69
Test 2	760	18.51*	12.8	33.69
Test 3	930	17.98	16.9	33.69
Test 4	1 100	15.48	17.0	33.69
Test 5	1 260	14.50	18.41	33.69
Test 6	1 430	13.9	20.0	33.68
Test 7	1 600	13.03	20.8	32.8
Test 8	1 760	11.29*	20	31.9
Test 9	2000	11.36	22.7	30.45

* Instron stopped during testing

Local buckling failure of the compression flange-web junction was observed in all tested channel beams. This mode of failure occurred at the point where the load was applied and was probably caused by stress concentrations emanating

from the load itself. Figure 4 shows the observed buckling mode. No evidence of lateral torsional buckling failure was witnessed, implying that the angle cleat-purling connection was able to control lateral torsional buckling.

Figure 4 Failure of the compression flange-web junction

Graphs of the relationship between load and displacement of frames are shown in Figure 5. The behaviour consists firstly of a linear response followed by a non-linear response. After this point large deformations take place and result in the collapse of the frame. As shown in this figure the buckling load decreases with increase in length of the channel. Note that the load and deflection in these graphs excludes the effect of the loading system.

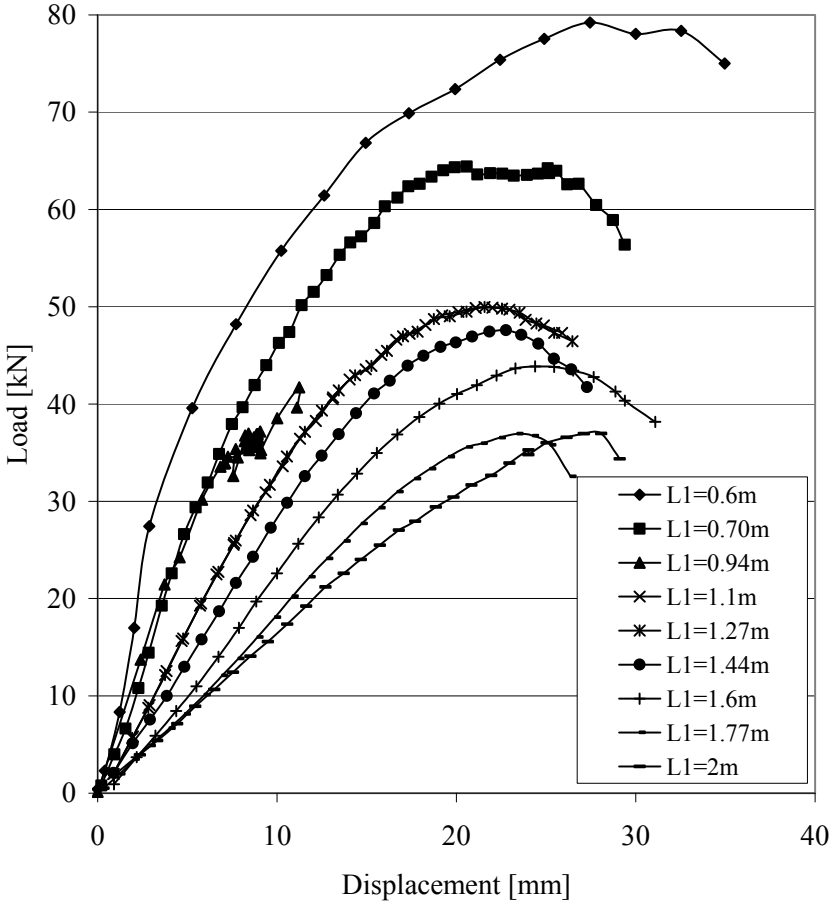

Figure 5 Load-Displacement curves

Conclusion

Tests on the lateral buckling of cold-formed channels beams under two- point loading have been described. The following conclusions are made:

- The lateral-buckling strength values obtained from the tests are in all cases less than the values predicted by the Canadian/South-Africa code of practice.

This is because some of the spans used are not long enough to encourage a larger moment to develop. Future tests are expected to correct this.

- In all cases failure occurred by local buckling of the compression flange-web junction. The capacity reached by the channels shows that a purlin-cleat restraining system is able to resist lateral buckling, and it can be used without adding fly bracing, as is normally done in practice to restrain torsion instability.

Acknowledgements

The authors wish to thank University of Johannesburg Research Committee (URC) for sponsoring this research.

REFERENCES

Baker, J.F. and Eickhoff, K.G., "The behaviour of saw-tooth portal frames", Proc., Conf. on the Correlation of Stresses and Displacements, Institute of Civil Engineering, U.K, 1955.

Baker, J.F. and Eickhoff, K.G., "A test on a pitched roof portal, preliminary publication", IABSE, 5th Congress, Lisbon, 1956.

Baker, J.F. and Eickhoff, K.G., "Tests on two north-light portals", Rep. FEI/49, British Welding Research Association, Cambridge, U.K, 1956.

BS 18, "British standard method for tensile testing of metals", British Standard Institution (BSI), 1987.

CAN – S16.1 – M89, "Steel Structures for Buildings – Limit States Design", Canadian Standards Association, Rexdale, Ontario, Canada, 1989.

Dundu, M. and Kemp, A.R., "Plastic and Lateral-Torsional Buckling Behaviour of Single Cold-Formed Channels Connected Back-to-Back", Journal of Structural Engineering, ASCE 2006, Vol. 132.

Dundu, M. and Kemp, A.R., "Strength requirements of single cold-formed channels connected back-to-back", Journal of Construction Steel Research 2006, 62, 250-261.

Karman, T.V., Sechler, E.E. and Donnell L.H., "The Strength of thin plates in Compression", Transactions, Applied Mechanics Division, ASME 1932, 54, APM 54-5, 53-57.

SANS 10162-2:2005, "South African Standard Code of Practice for the Structural use of Steel, Part 2 – Limit States Design of Cold-formed Steelwork", South African Bureau of Standards, Pretoria, 2005.

Southern African Institute of Steel Construction, "South African Steel Construction Handbook, Limit States Design", Southern African Institute of Steel Construction, Third Edition 2005

Winter, G., "Strength of thin Steel Compression Flanges", Transactions, ASCE 1947, 112, 527-554.

Twentieth International Specialty Conference on Cold-Formed Steel Structures
St. Louis, Missouri, U.S.A., November 3 & 4, 2010

EVALUATION OF THE FLEXURAL STRENGTH OF COLD-FORMED STEEL STUDS WITH EMBOSSED FLANGES

K. B. Reynolds[1], S. F. Stephens[2] and R. A. LaBoube[3]

Abstract

New advances and improvements in the manufacture of cold-formed steel shapes are continually being made. One such advancement in the manufacturing of steel studs is flange embossing, a technique used to facilitate the installation of drywall screws into the stud flange. Currently, embossed flanges are not specifically addressed in the *North American Specification for the Design of Cold-Formed Steel Structural Members* (AISI S100), thereby drawing into question the use of current design equations from being used to calculate member properties for an embossed stud.

A limited experimental investigation was undertaken to determine if light flange embossing affects the nominal flexural strength of cold-formed steel studs. Studs with embossed flanges were tested in bending and their actual flexural strength was determined. This data was then compared with the nominal flexural strength without embossing calculated using AISI S100-07 equations. The findings indicate that light flange embossing does not adversely affect the bending strength of the stud either negatively or positively and therefore, based on the scope of this study, the equations in AISI S100-07 for nominal flexural strength can be applied to lightly embossed studs.

---

[1]Former Graduate Student, Department of Architectural Engineering and Construction Science, Kansas State University

[2]Associate Professor, Department of Architectural Engineering and Construction Science, Kansas State University, Manhattan, Kansas

[3]Distinguished Teaching Professor, Department of Civil, Architectural and Environmental Engineering, Missouri University of Science and Technology, Rolla, Missouri

Introduction

One application of cold-formed steel is as wall studs in light frame and commercial construction. One common use for cold-formed steel studs is curtain walls. According to the AISI S200*, North American Standard for Cold-Formed Steel Framing—General Provisions* (AISI 2007b), a curtain wall is "[a] wall that transfers transverse (out of plane) loads and is limited to a superimposed vertical load, exclusive of sheathing materials, of not more than 100 pounds per foot or a superimposed vertical load of not more than 200 lbs." The studs tested in this investigation are designed for use in curtain walls. These studs are generally sheathed with gypsum or OSB attached with screws, and resist distributed out-of-plane loads applied to the surface of the sheathing. Under this loading, flexural strength is very important, while axial compressive strength is less so. One shape commonly used for steel studs is a C-section. This shape consists of relatively large web with top and bottom flanges, each with a stiffener. Traditionally, the only cold working done to the sheet steel is four bends to form the different elements of the shape, leaving the surface of each of the elements (web, flanges, and stiffeners) smooth along the entire length of the member.

Some manufacturers offer studs with embossed flanges. Embossing is a process where small indentations, often called knurls, are pressed into the flange of the stud as shown in Figure 1. Embossing is not done to enhance the strength of the member, but rather to improve the connection of screws into the flanges. However, as these embossed studs are not currently specifically addressed in AISI S100 for either determination of member properties or nominal strength. This brings into question the use of the AISI S100 design equations to determine the capacities of this stud configuration.

Purpose of Investigation

The purpose of this investigation was to determine whether flange embossing affects the member properties of cold-formed studs. Specifically, studs with embossed flanges were tested in bending in an effort to determine if embossed flanges adversely affect the nominal flexural strength of a curtain wall stud in a fully braced condition. The flexural strengths determined by testing were compared to the calculated nominal flexural strength assuming the embossments were not present to determine if the strength is altered by the presence of the embossments. Two common depths of cold-formed steel studs, 3.625 inches (92 mm) and 6 inches (152 mm), both 18 mil minimum thicknesses and with embossed flanges, were investigated. This material thickness was selected because the embossing was more pronounced than it would have been on a thicker section, so this should be the most severe situation.

Experimental Investigation

Material Properties and Cross-Sectional Geometry

The cold-formed steel studs used in this investigation were donated by Telling Industries of Cambridge, OH. Two sizes were tested; 362S125-18, and 600125-18. All studs had 1.5-in (38.1 mm) web punchouts spaced at 24" OC (610 mm), starting 12-in (305 mm) from the end of the stud.

To determine the actual mechanical properties of the steel, coupons were cut from the center of the webs to avoid a potential increase in F_y due to cold work of forming. Coupons were milled to width and subjected to an ASTM A370 standard tensile test. The results of the tensile test based on the measured uncoated cross sectional area are shown in Table 1.

Additionally, the full cross sections were carefully measured to determine the dimensions, including radii of bends and angles of the flange stiffeners. The dimensions of the embossments (Figure 2) were also measured, and are listed in Table 2.

The measured dimensions were then input into RSG Software's CFS program, Version 6.0.2, (RSG 2009), to compute the section properties and the nominal flexural strength of the sections using provisions from AISI S100 (AISI 2007a).

Test Specimens

Test specimens were constructed of two 8'-0" (2.44 m) long C-studs assembled in an open box configuration with their flanges toward the center of the specimen (Figure 3). A box section was used to provide a more laterally stable specimen than a single stud. The test was designed so that the failure mode would be flexure. The width of the specimen was 5.5 inches (139.7 mm).

All specimens were assembled with #8 x ¾-in (19 mm) self-drilling screws. ¾-in (19 mm) wide cold-rolled channel (CRC) were used to form the box-shaped test specimen. The channels were placed at 12-in (305 mm) on center along both top and bottom flanges (Figure 4). This spacing was chosen to represent the way gypsum board is often attached in the field, using screws at a maximum of 12-in (305 mm) on both sides of the stud.

To prevent web crippling, each specimen was reinforced with web stiffeners at the end supports and points of load application. Segments of cold-formed studs, with length equal to the depth of the specimen and oriented perpendicular to the specimen, were used as web stiffeners, which were attached to the specimens with five No. 8 screws. For the first three specimens tested of each size (specimens 3A, 3B, 3C, 6A, 6B, and 6D), the stiffeners were made from the

same size stud that was being tested. In the second set of tests, all web stiffeners were cut from 3.625-in (92 mm) studs, and stiffeners at the point of load application were also extended approximately ⅛" (3.2 mm) above the top flange, to provide load transfer directly to the web thus avoiding buckling of the flange from local stresses at the bearing plates. This change was made because in the first set of three tests it was discovered that loading directly on the flanges may have been causing a concentration of stresses leading to premature flange buckling. For this stiffener configuration, six No. 8 screws were used per stiffener to ensure full load transfer from the stiffener to the specimen web. All specimens were also braced against torsional buckling at the end reactions with dimensional 2x wood blocking (3"x5.5"x1.5" (76x140x38 mm) for the 3.625-in (92 mm) specimens and 5.5"x5.5"x1.5" (140x140x38 mm) for the 6-in (152 mm) specimens).

Test Setup

Specimens were tested in a simple span condition with two concentrated loads located at third points of the beam, 2'-8" (813 mm) (Figure 4,5,6) from beam ends creating a constant moment region with zero shear in the central span between the loads. Third points were selected for loading because they provided a constant moment region and provided balanced loading. Loads were applied to the specimens at the location of the web stiffeners through 4-in (102 mm) wide steel plates. Bearing plates at the end reactions were also 4-in (102 mm) wide, and one support was a sliding bearing plate to allow for longitudinal movement of the specimen.

To prevent lateral displacements of the test specimens, four large, hot rolled steel brackets were arranged with wooden shims to restrain the specimen laterally while still allowing it to deflect vertically. These braces were located at 8 inches from load points (Figure 6). One 3.625-in (92 mm) specimen (specimen 3E) 6'-6" (1.98 m) in length was also tested.

Test Procedure

Tests were conducted using an MTS Flextest GT unit, with a 22-kip actuator and load cell. Time, load, and stroke displacement were measured and recorded through a MultiPupose TestWare (MPT) program written to control the actuator. Additionally, a linear variable differential transformer (LVDT) was used at midspan to measure deflection. Deflection data was also continually recorded through the MPT software.

The actuator was run in a displacement-controlled manner at a rate of 0.1 inch (2.5 mm) per minute. Each specimen was loaded until it would take no more load.

Test Results and Evaluation of Data

A total of ten specimens were tested (five from 3.625-in (92 mm) studs and five from 6-in (152 mm) studs) and were loaded until local or distortional buckling reduced the resistance to the point that they would not take any more load. All of the specimens failed in a similar manner; by flange local buckling. In some cases, after the flange local buckling was observed, buckling of the web below the flange buckle was noted (Figure 7). After each specimen was tested, the tested flexural strength was computed for the specimen as a whole. The nominal flexural strength was also calculated using the CFS program based on AISI S100-07. These two values were then compared to determine the applicability of the AISI S100 flexural equations for embossed-flanged studs.

In 60% of the tests conducted, failure occurred at the punchouts (Figure 4). The punchouts were considered in the calculation of the nominal flexural strength. Failure by buckling at these locations is as expected since the section properties for bending are most critical at the punchouts.

Results for the 3.625-in (92 mm) Specimens

Table 3 summarizes the results obtained for the 3.625-in (92 mm) specimens. The first column shows the test yield stress, F_y found in the tensile tests. The next columns show the configuration of the test, referencing the dimensions shown in Figure 5. The total test load, P_t, is the total read from the load cell plus the weight of the bearing plates and spreader beam, and is the total of both point loads applied. The displacement shown was recorded by the load cell, and represents the displacement at the point of load application.

Figure 8 shows a graph of the force and displacement of a representative test of the 3.625-in (92 mm) test specimens. The graph starts at 100 pounds (445N) due to the weight of the plates and spreader beam on the specimen prior to the beginning of the test. The two peaks on this graph represent the two different studs that comprise the specimen buckling at slightly different loads. The predicted displacement is also displayed calculated using the section properties from CFS. As can be seen, once the predicted displacement line is shifted to exclude initial deflection, the measured displacements correlated with the predicted.

Table 4 shows the values of the maximum load resisted by each specimen based on the test results. From this, the tested moment capacity was calculated for a single stud. The computed nominal moment capacity, M_n, is also listed in table 4. Using the CFS software, checking both distortional and elastic local buckling, it was found that the governing limit state for this size stud was elastic local buckling based on the effective section modulus. Finally, the ratio of the

bending moment based on the test load to the calculated nominal flexural strength is shown.

Results for the 6-in (152 mm) Specimens

Table 5 summarizes the results of the bending tests on the 6-in (152 mm) specimens. The yield stress found in the coupon test is shown. The loading configuration data, again referencing Figure 5, is in the next three columns. The maximum load shown in the table is the total load applied by the load cell including the weight of the bearing plates and spreader beam to the overall specimen. The displacement recorded in the table represents the displacements at points of load application.

The graph shown in Figure 9 is a representative sample force-displacement graph for one of the 6-in (152mm) specimens. Again, the graph starts at 100 pounds (445 N) due to the spreader beams and load plates. This graph has a single peak, indicating that both members flange buckled simultaneously. This graph also shows the predicted displacement. For this specimen, once the initial deflection is accounted for the actual deflections again correlated with the predicted.

Table 6 shows the maximum load applied to each of the 6-in (152 mm) specimens. This was used to calculate the tested bending capacity of a single stud, shown in the next column. The nominal flexural strength as calculated per AISI S100 is also shown. For the 6-in (152 mm) studs, it was found that the distortional buckling calculated by the direct strength method was the governing limit state. The ratio of the bending moment based on the test load to calculated nominal flexural strength is presented in Table 6, as well.

Conclusions

For both stud sizes, the data was examined to determine if the presence of flange embossing resulted in a reduction in the flexural capacity for the stud below the nominal flexural strength computed by the provisions of the AISI S100-07.

For the 3.625-in (92 mm) studs, all tested moment capacities fall within 5% of the calculated value of M_n. The mean value for all 5 tests is 1.044 with a coefficient of variation of 0.0516. Comparing these results to the test data base used for the development of the design equations, these results would fall within the scatter of the previous testing programs.

For the 6-in (152mm) studs, once again, the tested moment capacities all surpass the computed values for M_n. The mean ratio of tested moment capacity to nominal flexural strength was 1.0361, with a coefficient of variation of 0.0274. Again, this data fits within the scatter of the previous test results. As an

example of this, on page 75 of the Direct Strength Method Design Guide (AISI 2006), Table 5 shows for 185 tested C-sections, the mean is 1.10, but the V_p is 0.11. This V_p is much larger than was obtained in this study, suggesting that this data would indeed fit into the scatter of the previous tests.

Based on the findings of this study, embossing of the flanges on the specimens tested did not adversely affect the flexural capacity of the studs. Therefore, it is concluded that the AISI S100 provisions may be appropriate for the determination of both section properties and nominal flexural strength.

The authors wish to thank Telling Industries, for their donation of the materials used in this testing program.

References

AISI (2006), *Direct Strength Method Design Guide,* American Iron and Steel Institute, Washington D.C.

AISI-S100 (2007a), *North American Specification for the Design of Cold-Formed Steel Structural Members,* American Iron and Steel Institute, Washington D.C.

AISI-S200 (2007b), *North American Standard for Cold-Formed Steel Framing—General Provisions* American Iron and Steel Institute, Washington D.C.

ASTM Subcommittee A01.13. (2008). *ASTM A370 - 09 Standard Test Methods and Definitions for Mechanical Testing of Steel Products.* ASTM International, West Conshohocken, PA

RSG Software. (2009) *CFS Version 6.0.2.* Lee's Summit, MO

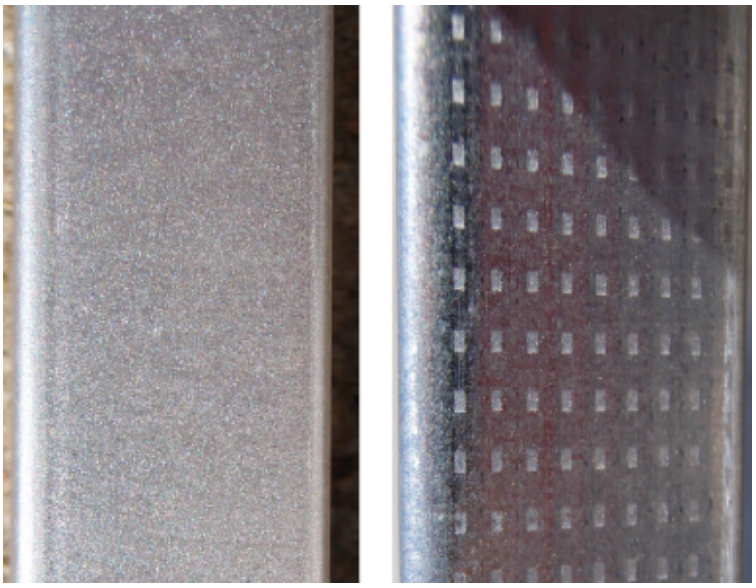

Figure 1: Flange of a smooth stud and an embossed flange.

Table 2: Tensile Test Results

Specimen	t (in.)	w(in.)	F_y (ksi)	F_u(ksi)	Percent Elongation
3A	0.0170	0.95	50.5	58.4	9.59
3B	0.0168	0.95	51.5	59.6	9.58
6A	0.0188	0.95	51.0	60.0	9.56
6B	0.0185	0.95	52.0	61.7	9.56
For SI: 1 in. = 25.4 mm, 1 ksi = 6.8 MPa					

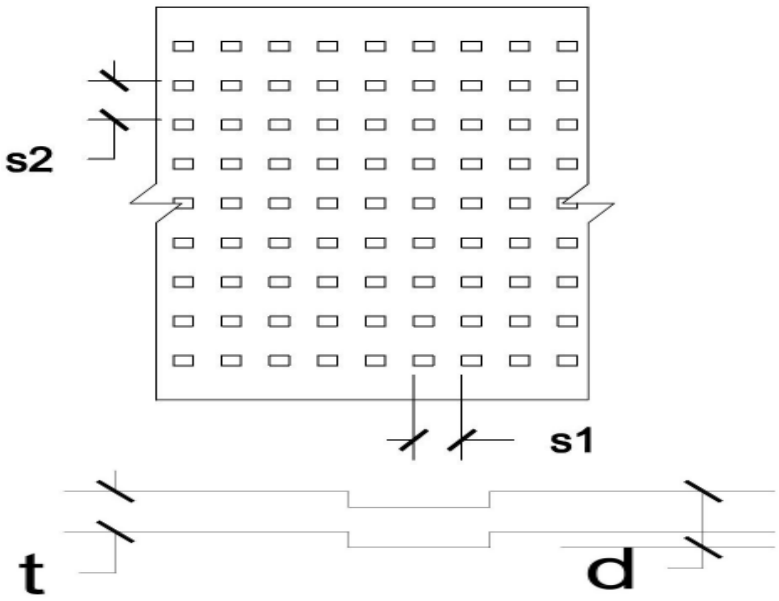

Figure 2: Dimensions for embossments.

Table 2: Embossment dimensions

Section	t	d	s1	s2
362S125-18	0.0171	0.019	0.116	0.116
600S125-18	0.0187	0.0211	0.116	0.116
Note:	All dimensions in inches (1 in = 25.4 mm).			

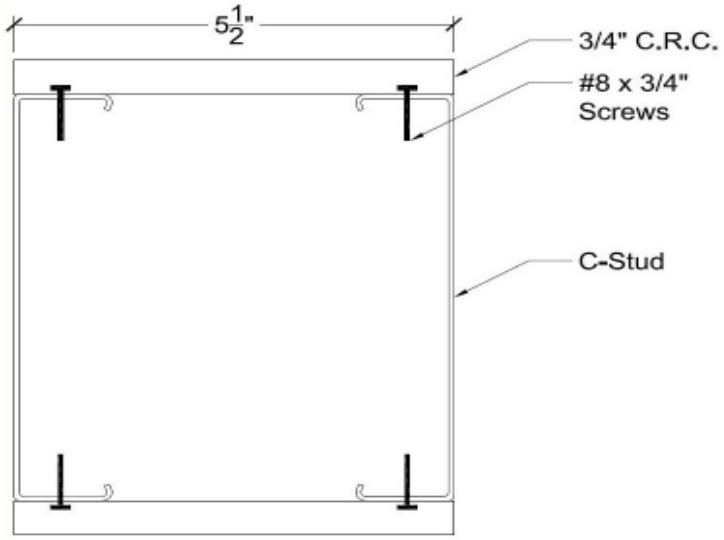

Figure 3: Typical test specimen cross section.

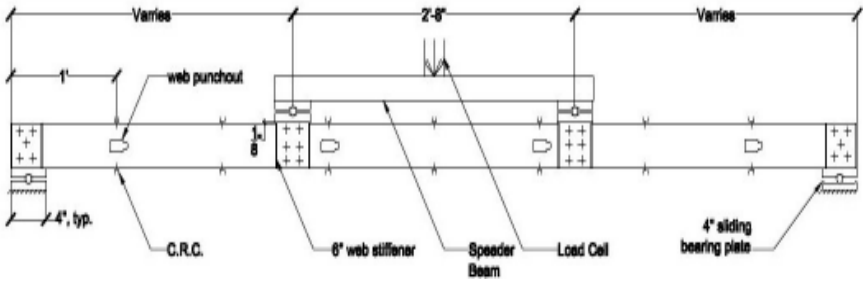

Figure 4: Test specimen (3.625-in (92 mm)) showing extended web stiffeners.

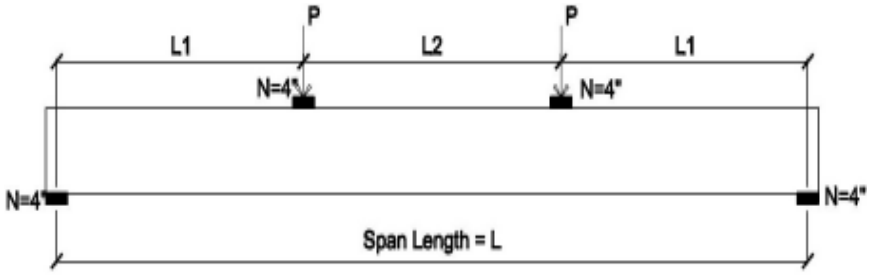

Figure 5: Typical loading configuration.

Figure 6: 6-inch (152 mm) test specimen set-up.

Figure 7: Typical flange buckling failure shown on a 6 in. (152 mm) specimen.

Table 3: Configuration and test loads for 3.625-in (92 mm) specimens.

Specimen	F_y (ksi)	Span L	Loading Dims L1	Loading Dims L2	P_t (lbs.)	Disp. (in.)
3 A	51	7'-8"	2'-8"	2'-8"	396.88	0.439
3 B	51	7'-8"	2'-8"	2'-8"	396.71	0.439
3 C	51	7'-8"	2'-8"	2'-8"	404.27	0.495
3 D	51	7'-8"	2'-8"	2'-8"	388.16	0.459
3 E*	51	6'-6"	1'-11"	2'-8"	494.61	0.411

Note:
P_t = Total test load
L1 and L2 (Refer to Figure 5)
*-This sample was shortened due to shipping damage at its ends.
For SI: 1 ksi = 6.8 MPa, 1 ft = 0.305 m, 1 lb = 4.45 N, 1 in = 25.4 mm

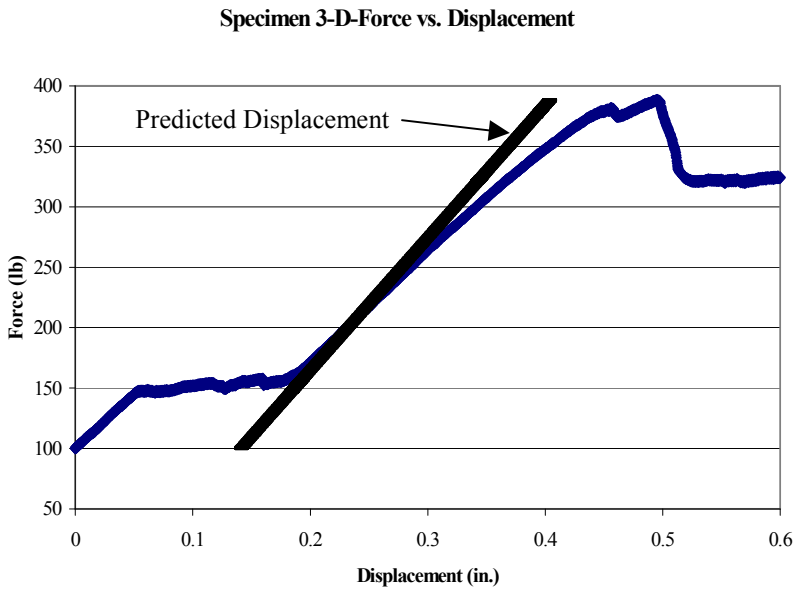

Figure 8: Force-Displacement graph for specimen 3D.

For SI: 1 lb. = 4.45 N, 1 in. = 25.4 mm

Table 4: Nominal flexural capacity comparison, 3.625-in. (92mm) specimen.

Specimen	P_t (lbs.)	M_t (k-in.)	M_n (k-in.)	M_t/M_n
3 A	396.88	6.350	5.951	1.067
3 B	396.71	6.347	5.951	1.067
3 C	404.27	6.468	5.951	1.087
3 D	388.16	6.210	5.951	1.044
3 E	494.61	5.688	5.951	0.956

Note: P_t = Total test load
M_t = Test moment
M_n = Computed nominal flexural strength
For SI: 1 lb.=4.45 N, 1 k-in.=113 Nm

Table 5: Configuration and test loading for 6-in (152 mm) specimens.

Specimen	F_y (ksi)	Span L	Loading Dims L1	Loading Dims L2	P_t (lbs.)	Disp. (in.)
6 A	51.5	7'-8"	2'-8"	2'-8"	706.39	0.444
6 B	51.5	7'-8"	2'-8"	2'-8"	716.09	0.442
6 C	51.5	7'-8"	2'-8"	2'-8"	702.12	0.415
6 D	51.5	7'-8"	2'-8"	2'-8"	745.71	0.396
6 E	51.5	7'-8"	2'-8"	2'-8"	736.83	0.363
Note:	P_t = Total test load L1 and L2 (Refer to Figure 5) For SI: 1 ksi=6.8 MPa, 1 ft = 0.305 m, 1 lb = 4.45 N, 1 in.=25.4 mm					

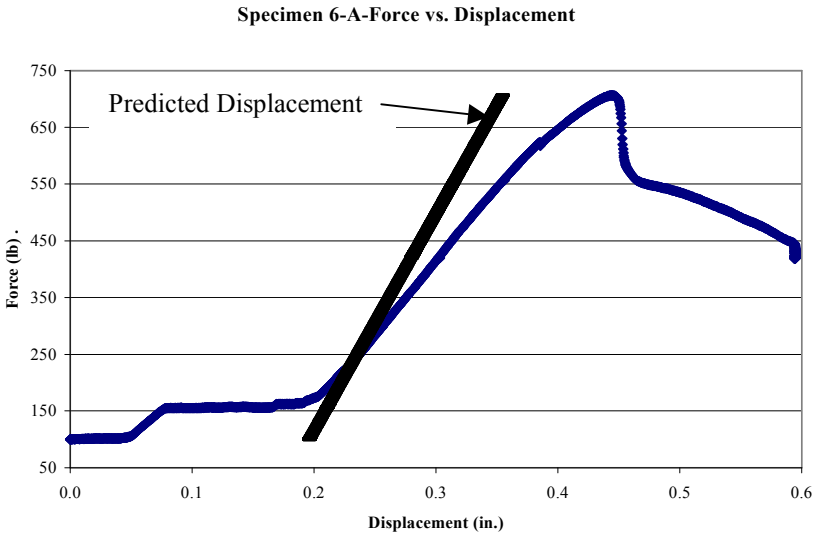

Figure 9: Force-Displacement graph for specimen 6A.

For SI: 1 in=25.4mm, 1 lb =4.45 N

Table 6: Nominal flexural capacity comparison, 6" (152 mm) specimens.

Specimen	P_t (lbs.)	M_t (k-in.)	M_n (k-in.)	M_t/M_n
6 A	706.39	11.302	11.141	1.015
6 B	716.09	11.457	11.141	1.028
6 C	702.12	11.234	11.141	1.008
6 D	745.71	11.931	11.141	1.071
6 E	736.83	11.789	11.141	1.058

Note: P_t = Total test load
M_t = Test moment
M_n = Computed nominal flexural strength
For SI: 1 ksi=6.8 MPa, 1 ft.=0.305 m, 1 lb.=4.45 N, 1 in.=25.4 mm

Twentieth International Specialty Conference on Cold-Formed Steel Structures
St. Louis, Missouri, U.S.A., November 3 & 4, 2010

Steel Roof Deck Diaphragms on Cold-Formed Steel Framing

Thomas Sputo[1]

Introduction

This paper addresses the design of steel roof deck diaphragms on cold-formed roof framing, either rafters or trusses, as shown in Figure 1. Criteria for design strength and stiffness of plywood diaphragms on cold-formed framing are available from several sources, but no equivalent resource exists for steel deck on cold-formed framing. Basic diaphragm theory is well established and is readily available in the Steel Deck Institute *Diaphragm Design Manual* (SDI, 2004) and the Metal Construction Association *Primer on Diaphragm Design* (MCA, 2004). This paper will not repeat this theory, and the reader is directed to these two publications for this basic information.

This paper will address the modifications that are needed to the basic SDI diaphragm theory to develop diaphragm design tables that account for the properties of the supporting framing. The tables contained in the *Diaphragm Design Manual* (SDI, 2004) assume support framing that is thick enough such that the behavior of the fastener in the support framing does not control. This paper will provide tables for screw-connected diaphragms of standard 1-1/2" steel roof deck on 33 mil and 43 mil support framing. Design tables assume lower bound material properties and industry standard thicknesses as shown in Table 1. No. 10 screws (d = 0.190 in) are assumed for sidelap fasteners and No. 12 (d = 0.216 in) or 14 (d = 0.250 in) screws are assumed for support fasteners. Screw fasteners shall conform to ASTM C1513. Proper detailing of the diaphragm to carry in-plane forces into and out of the diaphragm is assumed.

[1] Technical Director, Steel Deck Institute, 10 SW 1st Avenue, Gainesville, FL 32601 (email: sputoeng@mindspring.com)

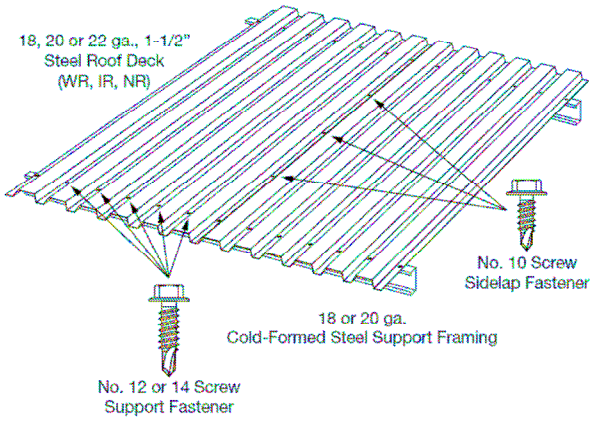

Figure 1. Steel Deck on Cold-Formed Framing

Table 1. Material Properties

		Design Thickness (in.)	Fy (ksi)	Fu (ksi)
Deck	22 gage	0.0295	33	45
Deck	20 gage	0.0358	33	45
Deck	18 gage	0.0474	33	45
Framing	20 gage	0.0346	33	45
Framing	18 gage	0.0451	33	45

Screw Strength

SDI (2004) equations for screw strength in support steel assume a minimum thickness of the support of 0.0385 inches. Because of this limitation, the screw strength equations contained in the AISI *North American Specification for the Design of Cold-Formed Steel Structural Members* (AISI, 2007) are used for this application.

$$Q_f = P_{ns} \text{ (per AISI (2007), E4.3.1)}$$

The SDI (2004) criterion for stitch screw strength is used

$$Q_s = 115\ d\ t$$

Screw Flexibility

The SDI (2004) equations for support screw flexibility do not consider the thickness of the support material. MCA (2004) provides a rational modification to the SDI equation that includes the thickness of the support framing when the support framing is less than 0.0478 inches in thickness. This equation applies for all load tables in this paper.

$$S_f = \{1.3 + (3.0\text{-}1.3)[(0.0478 - t_s)/(0.0478\text{-}t)]\} / (1000\ t^{0.5})$$

When the support thickness is greater than 0.0478 inches in thickness, the SDI (2004) equations may be used

$$S_f = 1.3 / (1000\ t^{0.5})$$

The SDI (2004) criterion for stitch screw flexibility is used

$$S_s = 3.0 / (1000\ t^{0.5})$$

Diaphragm Shear Stiffness

Using the SDI (2004) method, the diaphragm shear stiffness, assuming a deck span of 3 or more spans, is as follows

$$G' = K_2 / \{K_4 + (0.3D_{xx}/L_v) + (3K_1L_v)\}$$

The value of K_1 is found in the load tables (Tables 6-11), while the values of D_{xx}, K_2, and K_4 are found in Tables 2 and 3.

Table 2. K_2 and K_3

Deck Gage	K_2	K_4
22	870 kip/in	3.78
20	1056 kip/in	3.78
18	1398 kip/in	3.78

Table 3. Deck Warping Constant, Dxx (ft)

Deck Profile	Fastener Pattern *	22 Gage	20 Gage	18 Gage
WR	36/9	129	97	63
IR		226	169	111
NR		356	266	175
WR	36/7	129	97	63
IR		226	169	111
NR		356	266	175
WR	36/5	758	567	372
IR		886	663	435
NR		974	728	478
WR	36/4	1072	802	526
IR		1216	909	597
NR		1286	959	630
WR	36/3	2209	1652	1084
IR		2428	1816	1192
NR		2442	1827	1199
WR	30/6	129	97	63
IR		226	169	111
NR		356	266	175
WR	30/4	1377	1030	676
IR		1547	1157	760
NR		1608	1202	789
WR	30/3	1754	1312	861
IR		1943	1453	954
NR		1978	1480	971

* See SDI (2004) for fastener pattern types

Load Tables

Load tables are presented in the SDI (2004) format that is familiar to engineers designing steel deck diaphragms on hot rolled framing. Load tables were developed for 18, 20, and 22 gage, 1-1/2" steel roof deck on 18 gage and 20 gage support framing. No. 12 or 14 screws used as support fasteners are installed per fastener layouts shown in Figure 1. All calculations are conservatively based on No. 12 screws. The number of No. 10 sidelap screws per deck span are indicated in the tables. Load tables are as indicated in Table 4.

Table 4. Diaphragm Load Tables

Table No.	Deck Ga.	Framing Ga.	t_2/t_1	Q_f (lbs)	S_f (in/kip)	Q_s (lbs)	S_s (in/kip)
6	18	18	0.95	841	0.0145	1018	0.0138
7	20	18	1.26	858	0.0118	769	0.0159
8	22	18	1.53	774	0.0076	633	0.0175
9	18	20	0.73	565	0.0180	1018	0.0138
10	20	20	0.97	565	0.0164	769	0.0159
11	22	20	1.17	589	0.0142	633	0.0175

The tables provide nominal capacities as limited by shear strength and panel buckling. Applicable resistance factors (Φ) and safety factors (Ω), in accordance with AISI (2007) are as shown in Table 5.

Table 5. Resistance and Safety Factors

		Φ (LRFD)	Ω (ASD)
Panel Shear Strength	Seismic	0.65	2.50
	Wind	0.70	2.35
	Other	0.65	2.50
Panel Buckling	All	0.80	2.00

The design capacity of the diaphragm is the lesser of the shear strength and panel buckling capacities.

Design Example 1 - Seismic
Using allowable strength design (ASD), select a diaphragm for an in-plane seismic load of 330 plf, assuming 18 gage framing at 4 foot on center and 22 gage WR steel roof deck. Steel deck panels are 36 inches wide.

Referring to Table 8, select a 36/7 fastener pattern. Assuming 4 sidelap fasteners per span, check the panel shear strength:

S = 330 plf
S_n = 860 plf
Ω = 2.50 (seismic)
S_n / Ω = 860 / 2.50 = 344 plf > 330 plf OK

Next, check panel buckling

S_n = 3205 plf
Ω = 2.00
S_n / Ω = 3205 / 2.00 = 1602 plf > 400 plf OK
(Note: Panel buckling will rarely control design for most reasonable configurations)

The panel stiffness is calculated as follows

K_1 = 0.239 ft^{-1} (Table 8)
K_2 = 870 kip/in (Table 2)
K_4 = 3.78 (Table 2)
D_{xx} = 129 ft (Table 3)
L_v = 4 foot

G' = 870 / {3.78 +(0.3 x 129/4) +(3 x 0.239 x 4)} = 53.3 kip/in

Diaphragm deflections are calculated using rational design methods. Refer to SDI (2004) for additional information and design examples.

Other combinations of deck thickness and fastener spacing are possible.

Design Example 2 - Wind

Using allowable strength design (ASD), select a diaphragm for an in-plane wind load of 120 plf combined with 30 psf uplift, assuming 18 gage framing at 4 foot on center and 22 gage WR steel roof deck. Steel deck panels are 36 inches wide.

Referring to Table 8, select a 36/7 fastener pattern. Assuming 4 sidelap fasteners per span, check the panel shear strength:

S = 120 plf
S_n = 860 plf
Ω = 2.35 (wind)
S_n / Ω = 860 / 2.35 = 366 plf > 120 plf OK

Next, check panel buckling

S_n = 3205 plf

Ω = 2.00
S_n / Ω = 3205 / 2.00 = 1602 plf > 180 plf OK
(Note: Panel buckling will rarely control design for most reasonable configurations)

Next, check fastener uplift capacity, using No. 12 support screws (d = 0.216 in; d_h = 0.432 in)

T_n = 373 pounds (pullout) Controls
T_n = 860 pounds (pullover)
[Screw pullout and pullover calculated per AISI (2007)]
T_n / Ω = 373 / 3.0 = 124 pounds

k = 5(interior fasteners) + 2(edge fasteners)/2(shared)
= 6.0
β = k / panel cover = 6.0 / 3 feet
= 2.0
T = w_{up} (L_v/ β) = 30 (4/2.0)
= 60 pounds per screw
[Screw contributions k and β calculated per SDI (2004)]

Check interaction of uplift and shear per SDI (2004) criteria for combined shear and pullout on screw

$(\Omega T / T_n) + 0.85(\Omega S / S_n) < 1.0$ (ASD)
$(60/124) + 0.85\ (120/366) =$ 0.76 OK

Note 1: Interaction of screw pullout with shear for LRFD is: $(T_u / \Phi T_n) + 0.85(S_u / \Phi S_n) < 1.0$
Note 2: For interaction of screw pullover with shear, refer to AISI (2007) Section E4.5

The panel stiffness is calculated as for Design Example 1. Other combinations of deck thickness and fastener spacing are possible.

Nomenclature

d	=	Screw major diameter, inches
d_h	=	Screw head diameter, inches
D_{xx}	=	Panel warping constant, feet
G'	=	Diaphragm shear stiffness, kip/inch
k	=	Effective number of support fasteners per panel width

L_v	=	Panel span, feet
P_{ns}	=	Nominal shear strength (resistance) per screw
Q_f	=	Support fastener strength, kips
Q_s	=	Sidelap fastener strength, kips
S	=	Required allowable diaphragm shear strength, pounds (ASD)
S_f	=	Support fastener flexibility factor
S_n	=	Nominal shear strength of diaphragm, pounds
S_s	=	Sidelap fastener flexibility factor
S_u	=	Required design shear strength of diaphragm, pounds (LRFD)
T	=	Required allowable uplift capacity of screw, pounds (ASD)
T_n	=	Nominal uplift capacity of screw, pounds
T_u	=	Required design uplift capacity of screw, pounds (LRFD)
t	=	Deck thickness, inches
t_s	=	Support framing thickness, inches
t_1	=	Deck thickness in contact with screw head or washer, inches
t_2	=	Support framing thickness not in contact with screw head or washer, inches
w_{up}	=	Uplift on deck, psf
β	=	Fastener pattern factor
Φ	=	Resistance factor (LRFD)
Ω	=	Safety factor (ASD)

References

American Iron and Steel Institute (AISI) (2007). *North American Specification for the Design of Cold-Formed Steel Structural Members and Commentary*, Washington DC.

ASTM C1513 - 04(2009)e1 *Standard Specification for Steel Tapping Screws for Cold-Formed Steel Framing Connections.*

Metal Construction Association (MCA) (2004). *Primer on Diaphragm Design, 1st Edition*, Glenview, IL.

Steel Deck Institute (SDI) (2004). *Diaphragm Design Manual, 3rd Edition*, Fox River Grove, IL.

1.5(WR,IR,NR) t=design thickness= 0.0474 in. 18 Gage Φ(EQ): 0.65 Ω(EQ): 2.50
Support Framing t=design thickness= 0.0451 in. 18 Gage Φ(WIND): 0.70 Ω(WIND): 2.35
SUPPORT FASTENING: #12 or #14 screws Φ(Other): 0.65 Ω(Other): 2.50
SIDE-LAP FASTENING: #10 screws

FASTENER LAYOUT	SIDE-LAP CONN/SPAN	MAXIMUM NOMINAL SHEAR STRENGTH, PLF SPAN, FT 2.0	3.0	4.0	5.0	6.0	7.0	8.0	9.0	10.0	K1
36/9	0	1155	865	675	550	445	375	325	285	255	1.129
	1	1380	1080	870	720	615					0.739
	2	1530	1255	1040	875	755	660	580	510		0.549
	3	1635	1390	1180	1015	880	775	690	625	560	0.437
	4	1710	1495	1300	1135	995	885	795	715	655	0.363
	5	1760	1575	1395	1235	1100	985	885	805	735	0.310
	6	1800	1640	1475	1325	1190	1075	975	890	815	0.271
36/7	0	775	550	420	335	275	235	200	180	160	1.693
	1	1065	810	640	525	445					0.945
	2	1255	1010	825	690	590	515	455	405		0.656
	3	1375	1160	975	835	720	635	565	510	460	0.502
	4	1455	1270	1100	955	840	745	665	605	550	0.407
	5	1510	1355	1200	1060	945	845	760	690	635	0.342
	6	1545	1415	1275	1150	1035	935	850	775	710	0.295
36/5	0	655	485	360	310	255	215	185	165	145	2.031
	1	855	690	570	475	410					1.042
	2	955	825	710	610	535	475	425	380		0.701
	3	1010	910	810	720	640	575	520	470	430	0.528
	4	1045	965	880	800	725	660	600	550	505	0.424
	5	1065	1000	930	860	790	730	670	620	575	0.354
	6	1075	1030	970	905	845	785	730	680	635	0.304
36/4	0	500	375	290	235	190	160	140	120	110	2.540
	1	675	580	470	400	345					1.162
	2	750	665	585	515	460	410	370	335		0.753
	3	785	725	660	600	545	495	455	415	385	0.557
	4	800	760	710	660	610	565	520	485	450	0.442
	5	815	780	745	700	660	615	575	540	505	0.366
	6	820	795	765	730	695	655	620	585	555	0.313
30/6	0	710	530	375	300	245	210	180	160	140	2.258
	1	1025	765	605	495	415					1.202
	2	1230	980	795	665	565	490	435	385		0.819
	3	1360	1135	955	810	700	615	545	490	445	0.621
	4	1445	1255	1080	935	820	725	650	585	535	0.500
	5	1500	1340	1185	1045	925	830	745	675	620	0.419
	6	1540	1405	1265	1135	1020	920	835	760	700	0.360
30/4	0	610	455	355	290	245	200	175	155	135	2.540
	1	790	650	540	455	390					1.277
	2	880	770	670	580	510	455	405	370		0.853
	3	925	840	755	680	610	550	500	455	415	0.640
	4	950	890	820	750	685	625	575	530	490	0.513
	5	965	920	860	800	745	690	640	595	555	0.427
	6	975	940	890	840	790	740	695	650	610	0.366

* DESIGN SHEAR SHOWN ABOVE MAY BE LIMITED BY SHEAR BUCKLING. SEE TABLE BELOW.
THE SHADED VALUES DO NOT COMPLY WITH THE MINIMUM SPACING REQUIREMENTS FOR SIDE-LAP CONNECTIONS AND SHALL NOT BE USED EXCEPT WITH PROPERLY SPACED SIDE-LAP CONNECTIONS.

Φ(Buckling): 0.80 Ω(Buckling): 2.00

DECK PROFILE	I in^4/ft	NOMINAL DIAPHRAGM SHEAR DUE TO PANEL BUCKLING (S_n), PLF / SPAN, FT 2.0	3.0	4.0	5.0	6.0	7.0	8.0	9.0	10.0
NR	0.181	20850	9270	5215	3335	2320	1705	1305	1030	835
IR	0.196	22140	9840	5535	3545	2460	1805	1385	1095	885
WR	0.284	29240	12995	7310	4680	3250	2385	1830	1445	1170

NOTE:
ASD Required Strength (Service Applied Load) <= Minimum [Nominal Shear Strength / Ω(EQ or WIND), Nominal Buckling Strength S_n / Ω(Buckling)]
LRFD Required Strength (Factored Applied Load) <= Minimum [Φ(EQ or WIND) x Nominal Shear Strength, Φ(Buckling) x Nominal Buckling Strength S_n]

Table 6. 18 gage deck, 18 gage framing

1.5(WR,IR,NR) t=design thickness= 0.0358 in. 20 Gage Φ(EQ): 0.65 Ω(EQ): 2.50
Support Framing t=design thickness= 0.0451 in. 18 Gage Φ(WIND): 0.70 Ω(WIND): 2.35
SUPPORT FASTENING: #12 or #14 screws Φ(Other): 0.65 Ω(Other): 2.50
SIDE-LAP FASTENING: #10 screws

FASTENER LAYOUT	SIDE-LAP CONN/SPAN	MAXIMUM NOMINAL SHEAR STRENGTH, PLF SPAN, FT 2.0	3.0	4.0	5.0	6.0	7.0	8.0	9.0	10.0	K1
36/9	0	1180	875	685	545	450	390	330	295	260	0.695
	1	1355	1050	840	695	580					0.508
	2	1490	1195	975	815	695	600	520	460		0.398
	3	1590	1315	1095	925	800	700	615	545	490	0.328
	4	1665	1415	1200	1030	895	790	700	630	565	0.279
	5	1725	1495	1290	1120	985	870	780	705	640 *	0.242
	6	1770	1565	1370	1205	1065	950	850	770 *	705 *	0.214
36/7	0	790	560	425	335	280	235	205	180	160	1.042
	1	1025	760	585	490	405					0.668
	2	1195	930	745	620	525	455	395	350		0.491
	3	1315	1065	880	740	635	555	490	435	390	0.389
	4	1400	1175	990	845	730	645	570	515	465	0.322
	5	1465	1265	1085	940	825	730	650	585	535	0.274
	6	1510	1335	1170	1025	905	805	725	655	600 *	0.239
36/5	0	670	495	390	310	255	215	190	165	150	1.250
	1	830	660	535	445	380					0.748
	2	930	780	655	555	480	425	375	335		0.533
	3	990	865	750	650	570	505	455	410	375	0.415
	4	1030	925	820	730	650	580	525	475	435	0.339
	5	1055	970	880	790	715	645	590	540	495	0.287
	6	1075	1005	925	845	770	705	645	595	550	0.248
36/4	0	510	380	300	235	195	165	140	120	110	1.563
	1	655	535	440	370	315					0.849
	2	730	635	545	470	410	365	325	295		0.583
	3	775	695	620	550	490	440	395	360	330	0.444
	4	800	740	675	610	555	505	460	420	390	0.358
	5	815	765	710	655	605	555	515	475	440	0.301
	6	825	785	740	695	645	600	560	520	485	0.259
30/6	0	725	510	380	300	250	210	180	160	145	1.389
	1	975	720	560	455	375					0.856
	2	1160	895	715	590	500	430	375	330		0.619
	3	1290	1035	850	710	610	530	470	415	375	0.485
	4	1385	1155	965	820	710	625	555	495	450	0.398
	5	1450	1245	1065	920	800	710	635	570	520	0.338
	6	1500	1320	1150	1005	885	790	710	640	585	0.293
30/4	0	620	465	365	290	240	205	175	155	140	1.563
	1	770	820	505	425	365					0.919
	2	865	730	620	530	460	405	360	325		0.651
	3	910	805	705	620	545	485	435	395	360	0.504
	4	940	855	770	690	620	555	505	460	420	0.411
	5	960	895	820	745	680	615	565	520	480	0.347
	6	975	920	855	790	725	670	615	570	530	0.301

* DESIGN SHEAR SHOWN ABOVE MAY BE LIMITED BY SHEAR BUCKLING. SEE TABLE BELOW.
THE SHADED VALUES DO NOT COMPLY WITH THE MINIMUM SPACING REQUIREMENTS FOR SIDE-LAP CONNECTIONS AND SHALL NOT BE USED EXCEPT WITH PROPERLY SPACED SIDE-LAP CONNECTIONS.

Φ(Buckling): 0.80 Ω(Buckling): 2.00

DECK PROFILE	I in^4/ft	NOMINAL DIAPHRAGM SHEAR DUE TO PANEL BUCKLING (S_n), PLF / SPAN, FT 2.0	3.0	4.0	5.0	6.0	7.0	8.0	9.0	10.0
NR	0.128	13030	5790	3260	2085	1450	1065	815	645	520
IR	0.139	13865	6160	3465	2220	1540	1130	865	685	555
WR	0.198	18075	8035	4520	2890	2010	1475	1130	896	725

NOTE:
ASD Required Strength (Service Applied Load) <= Minimum [Nominal Shear Strength / Ω(EQ or WIND), Nominal Buckling Strength S_n / Ω(Buckling)]
LRFD Required Strength (Factored Applied Load) <= Minimum [Φ(EQ or WIND) x Nominal Shear Strength, Φ(Buckling) x Nominal Buckling Strength S_n]

Table 7. 20 gage deck, 18 gage framing

1.5(WR,IR,NR) t=design thickness= 0.0295 in. 22 Gage Φ(EQ): 0.65 Ω(EQ): 2.50
Support Framing t=design thickness= 0.0451 in. 18 Gage Φ(WIND): 0.70 Ω(WIND): 2.35
SUPPORT FASTENING: #12 or #14 screws Φ(Other): 0.65 Ω(Other): 2.50
SIDE-LAP FASTENING: #10 screws

FASTENER LAYOUT	SIDE-LAP CONN/SPAN	MAXIMUM NOMINAL SHEAR STRENGTH, PLF SPAN, FT 2.0	3.0	4.0	5.0	6.0	7.0	8.0	9.0	10.0	K1
36/3	0	1065	790	620	490	400	340	290	260	235	0.366
	1	1210	935	745	615	510					0.301
	2	1325	1055	860	715	610	520	450	400		0.255
	3	1415	1160	960	810	700	610	530	470	425 *	0.222
	4	1460	1245	1050	895	780	685	610	540 *	485 *	0.196
	5	1535	1320	1130	975	855	755	675 *	605 *	550 *	0.176
	6	1575	1390	1200	1050	920	820	735 *	665 *	605 *	0.159
36/7	0	715	505	385	300	250	210	180	160	145	0.549
	1	905	670	525	430	355					0.414
	2	1055	815	650	540	455	390	340	300		0.333
	3	1160	935	765	640	545	475	420	370	335	0.278
	4	1240	1030	860	730	630	550	490	440	400	0.239
	5	1300	1110	945	810	710	625	555	500	455 *	0.209
	6	1345	1175	1020	885	780	690	620	560 *	510 *	0.186
36/5	0	605	450	350	280	230	195	165	150	135	0.659
	1	740	585	470	395	335					0.474
	2	825	665	575	485	420	370	325	290		0.370
	3	880	760	655	565	495	440	390	355	320	0.304
	4	920	820	720	635	560	500	450	410	375	0.257
	5	945	860	770	690	620	560	505	465	425 *	0.223
	6	960	890	815	740	670	610	555	510	470 *	0.197
36/4	0	460	345	270	210	170	145	125	110	100	0.824
	1	585	470	385	325	275					0.554
	2	650	560	475	410	355	315	280	250		0.417
	3	690	615	545	480	425	380	340	310	285	0.334
	4	715	655	590	535	480	435	395	360	330	0.279
	5	730	680	630	575	525	480	440	410	375	0.240
	6	740	700	655	610	565	520	485	450	415	0.210
30/6	0	655	460	340	270	220	190	160	145	130	0.732
	1	865	630	495	395	330					0.538
	2	1020	780	620	510	435	370	320	285		0.425
	3	1135	905	735	615	525	455	400	355	320	0.351
	4	1220	1005	835	710	610	535	475	425	380	0.299
	5	1285	1090	925	790	690	605	540	485	440 *	0.261
	6	1335	1160	1000	870	760	675	605	545 *	495 *	0.231
30/4	0	560	420	330	260	215	180	155	140	125	0.623
	1	685	550	445	375	320					0.585
	2	760	645	540	465	400	355	315	280		0.454
	3	810	710	615	540	475	420	375	340	310	0.371
	4	840	760	675	600	535	480	435	395	360	0.314
	5	860	795	720	650	590	535	485	445	410	0.272
	6	875	820	755	695	635	580	535	490	455 *	0.240

* DESIGN SHEAR SHOWN ABOVE MAY BE LIMITED BY SHEAR BUCKLING. SEE TABLE BELOW.
THE SHADED VALUES DO NOT COMPLY WITH THE MINIMUM SPACING REQUIREMENTS FOR SIDE-LAP CONNECTIONS AND SHALL NOT BE USED EXCEPT WITH PROPERLY SPACED SIDE-LAP CONNECTIONS.

Φ(Buckling): 0.80 Ω(Buckling): 2.00

DECK PROFILE	I in⁴/ft	NOMINAL DIAPHRAGM SHEAR DUE TO PANEL BUCKLING (S_n), PLF / SPAN, FT 2.0	3.0	4.0	5.0	6.0	7.0	8.0	9.0	10.0
NR	0.099	9295	4130	2325	1485	1035	760	580	460	370
IR	0.108	9920	4410	2480	1590	1100	810	620	490	395
WR	0.152	12820	5700	3205	2050	1425	1045	800	635	515

NOTE:
ASD Required Strength (Service Applied Load) <= Minimum [Nominal Shear Strength / Ω(EQ or WIND), Nominal Buckling Strength S_n / Ω(Buckling)]
LRFD Required Strength (Factored Applied Load) <= Minimum [Φ(EQ or WIND) x Nominal Shear Strength, Φ(Buckling) x Nominal Buckling Strength S_n]

Table 8. 22 gage deck, 18 gage framing

1.5(WR,IR,NR)	t=design thickness= 0.0474 in.	18 Gage	Φ(EQ): 0.65	Ω(EQ): 2.50
Support Framing	t=design thickness= 0.0346 in.	20 Gage	Φ(WIND): 0.70	Ω(WIND): 2.35
SUPPORT FASTENING:	#12 or #14 screws		Φ(Other): 0.65	Ω(Other): 2.50
SIDE-LAP FASTENING:	#10 screws			

FASTENER LAYOUT	SIDE-LAP CONN/SPAN	MAXIMUM NOMINAL SHEAR STRENGTH, PLF SPAN, FT 2.0	3.0	4.0	5.0	6.0	7.0	8.0	9.0	10.0	K1
	0	775	575	450	365	300	255	220	190	170	1.395
	1	980	785	640	535	460					0.845
	2	1095	935	790	680	565	485	425	375		0.606
36/9	3	1165	1030	905	790	660	565	495	440	395	0.472
	4	1205	1100	990	885	755	645	565	500	450	0.387
	5	1235	1150	1055	960	850	725	635	565	510	0.328
	6	1250	1185	1100	1020	940	805	705	630	565	0.284
	0	520	370	280	225	185	155	135	120	105	2.093
	1	785	615	495	410	345					1.058
	2	925	775	655	525	440	375	330	295		0.708
36/7	3	995	880	770	640	535	455	400	355	320	0.532
	4	1040	950	855	755	630	540	470	420	375	0.426
	5	1065	995	915	840	720	620	540	480	435	0.355
	6	1080	1025	960	895	815	700	610	545	490	0.305
	0	440	325	255	205	170	145	125	110	100	2.511
	1	615	515	430	365	305					1.156
	2	680	610	540	475	400	340	300	265		0.751
36/5	3	710	660	610	555	490	420	370	330	295	0.556
	4	725	690	650	610	565	500	440	390	350	0.441
	5	730	705	675	645	610	575	510	455	410	0.366
	6	735	720	695	665	640	605	575	515	465	0.312
	0	335	250	195	155	130	110	95	80	75	3.140
	1	485	415	360	310	260					1.273
	2	525	485	445	405	355	305	265	235		0.798
36/4	3	545	520	490	455	425	385	335	300	270	0.581
	4	550	535	515	490	465	440	410	365	325	0.457
	5	555	545	530	510	490	470	450	425	385	0.377
	6	560	550	535	525	510	490	475	455	440	0.320
	0	480	335	255	200	165	140	120	105	95	2.791
	1	765	590	470	385	320					1.338
	2	910	760	620	495	415	355	310	275		0.880
30/6	3	990	870	760	610	510	435	380	340	305	0.655
	4	1035	945	850	725	605	515	450	400	360	0.522
	5	1060	990	910	830	695	595	525	465	420	0.434
	6	1080	1020	955	885	790	680	595	525	475	0.371
	0	410	305	240	195	160	135	115	105	90	3.139
	1	565	480	410	350	295					1.413
	2	620	565	505	455	390	335	290	260		0.912
30/4	3	645	605	565	520	480	415	365	320	290	0.673
	4	655	630	600	565	530	495	435	385	345	0.533
	5	660	645	620	595	565	535	505	450	405	0.442
	6	665	650	635	610	590	565	540	510	460	0.377

* DESIGN SHEAR SHOWN ABOVE MAY BE LIMITED BY SHEAR BUCKLING. SEE TABLE BELOW.
THE SHADED VALUES DO NOT COMPLY WITH THE MINIMUM SPACING REQUIREMENTS FOR SIDE-LAP CONNECTIONS AND SHALL NOT BE USED EXCEPT WITH PROPERLY SPACED SIDE-LAP CONNECTIONS.

Φ(Buckling): 0.80 Ω(Buckling): 2.00

DECK PROFILE	I in⁴/ft	NOMINAL DIAPHRAGM SHEAR DUE TO PANEL BUCKLING (S_n), PLF / SPAN, FT 2.0	3.0	4.0	5.0	6.0	7.0	8.0	9.0	10.0
NR	0.181	20860	9270	5215	3335	2320	1705	1305	1030	835
IR	0.196	22140	9840	5535	3545	2460	1805	1385	1095	885
WR	0.284	29240	12995	7310	4680	3250	2385	1830	1445	1170

NOTE:
ASD Required Strength (Service Applied Load) <= Minimum [Nominal Shear Strength / Ω(EQ or WIND), Nominal Buckling Strength S_n / Ω(Buckling)]
LRFD Required Strength (Factored Applied Load) <= Minimum [ΦΩ(EQ or WIND) x Nominal Shear Strength, Φ(Buckling) x Nominal Buckling Strength S_n]

Table 9. 18 gage deck, 20 gage framing

1.5(WR,IR,NR) t=design thickness= 0.0358 in. 20 Gage Φ(EQ): 0.65 Ω(EQ): 2.50
Support Framing t=design thickness= 0.0346 in. 20 Gage Φ(WIND): 0.70 Ω(WIND): 2.35
SUPPORT FASTENING: #12 or #14 screws Φ(Other): 0.65 Ω(Other): 2.50
SIDE-LAP FASTENING: #10 screws

FASTENER LAYOUT	SIDE-LAP CONN/SPAN	MAXIMUM NOMINAL SHEAR STRENGTH, PLF SPAN, FT 2.0	3.0	4.0	5.0	6.0	7.0	8.0	9.0	10.0	K1
36/9	0	775	575	450	360	295	250	215	190	170	0.961
	1	940	740	600	500	425					0.634
	2	1050	870	725	615	530	465	410	360		0.473
	3	1120	965	825	710	620	550	490	440	395	0.377
	4	1165	1035	905	795	705	630	565	500	450	0.313
	5	1200	1085	975	870	775	700	635	565	510	0.268
	6	1220	1130	1025	930	840	760	695	630	565	0.234
36/7	0	520	370	280	220	185	155	135	120	105	1.441
	1	735	560	445	365	310					0.812
	2	870	705	580	490	420	365	325	290		0.565
	3	950	810	690	590	515	455	400	355	320	0.434
	4	1000	885	775	680	600	535	470	420	375	0.352
	5	1030	935	840	750	670	605	540	480	435	0.296
	6	1055	975	890	810	735	665	610	545	490	0.255
36/5	0	440	325	255	205	170	145	125	110	95	1.729
	1	585	480	395	335	285					0.896
	2	655	570	495	430	380	335	300	265		0.605
	3	690	625	565	505	450	410	370	330	295	0.456
	4	710	660	610	560	510	465	430	390	350	0.367
	5	720	685	645	600	555	515	475	445	410	0.306
	6	730	700	665	630	590	555	520	485	455	0.263
36/4	0	335	250	195	155	125	105	90	80	70	2.162
	1	460	390	325	280	240					1.000
	2	510	460	410	365	325	290	265	235		0.650
	3	530	495	460	420	385	350	325	295	270	0.482
	4	545	520	490	460	425	395	370	345	320	0.383
	5	550	530	510	485	460	430	405	385	360	0.317
	6	555	540	520	500	480	455	435	415	390	0.271
30/6	0	480	335	250	200	165	140	120	105	95	1.921
	1	710	535	425	345	290					1.033
	2	850	685	560	470	405	350	310	275		0.706
	3	940	795	675	580	500	435	380	340	305	0.536
	4	990	875	760	665	590	515	450	400	360	0.433
	5	1025	930	830	740	660	595	525	465	420	0.362
	6	1050	970	885	800	725	660	595	525	475	0.312
30/4	0	410	305	240	190	160	135	115	100	90	2.162
	1	540	450	375	315	275					1.098
	2	600	530	465	410	360	320	290	260		0.736
	3	630	580	525	475	430	390	355	320	290	0.554
	4	645	605	565	520	480	445	410	380	345	0.444
	5	655	625	590	555	520	485	455	425	395	0.370
	6	660	640	610	580	550	520	490	460	435	0.317

* DESIGN SHEAR SHOWN ABOVE MAY BE LIMITED BY SHEAR BUCKLING. SEE TABLE BELOW.
THE SHADED VALUES DO NOT COMPLY WITH THE MINIMUM SPACING REQUIREMENTS FOR SIDE-LAP CONNECTIONS AND SHALL NOT BE USED EXCEPT WITH PROPERLY SPACED SIDE-LAP CONNECTIONS.

Φ(Buckling): 0.80 Ω(Buckling): 2.00

DECK PROFILE	I in^4/ft	NOMINAL DIAPHRAGM SHEAR DUE TO PANEL BUCKLING (S_n), PLF / SPAN, FT 2.0	3.0	4.0	5.0	6.0	7.0	8.0	9.0	10.0
NR	0.128	13030	5790	3260	2085	1450	1065	815	645	520
IR	0.139	13865	6160	3465	2220	1540	1130	865	685	555
WR	0.198	18075	8035	4520	2890	2010	1475	1130	895	725

NOTE:
ASD Required Strength (Service Applied Load) <= Minimum [Nominal Shear Strength / Ω(EQ or WIND), Nominal Buckling Strength S_n / Ω(Buckling)]
LRFD Required Strength (Factored Applied Load) <= Minimum [Φ(EQ or WIND) x Nominal Shear Strength, Φ(Buckling) x Nominal Buckling Strength S_n]

Table 10. 20 gage deck, 20 gage framing

1.5(WR,IR,NR) t=design thickness= 0.0295 in. 22 Gage Φ(EQ): 0.65 Ω(EQ): 2.50
Support Framing t=design thickness= 0.0346 in. 20 Gage Φ(WIND): 0.70 Ω(WIND): 2.35
SUPPORT FASTENING: #12 or #14 screws Φ(Other): 0.65 Ω(Other): 2.50
SIDE-LAP FASTENING: #10 screws

FASTENER LAYOUT	SIDE-LAP CONN/SPAN	MAXIMUM NOMINAL SHEAR STRENGTH, PLF SPAN, FT 2.0	3.0	4.0	5.0	6.0	7.0	8.0	9.0	10.0	K1
36/9	0	810	600	470	375	305	260	220	195	175	0.688
	1	950	740	595	495	410					0.489
	2	1050	855	705	590	505	440	390	340		0.379
	3	1125	945	795	680	590	515	460	410	365	0.310
	4	1175	1015	875	760	665	585	525	475	430 *	0.262
	5	1215	1075	940	825	730	650	585 *	530 *	485 *	0.227
	6	1240	1120	1000	885	790	710	640 *	585 *	535 *	0.200
36/7	0	540	385	290	230	190	150	140	125	110	1.032
	1	730	550	430	355	295					0.641
	2	855	680	550	460	390	340	295	265		0.464
	3	940	780	660	550	475	415	370	335	300	0.364
	4	1000	860	735	635	555	490	435	395	360	0.300
	5	1040	920	805	705	620	555	495	450	410	0.254
	6	1065	965	860	765	680	615	555	505	460 *	0.221
36/5	0	460	340	265	215	175	150	125	115	100	1.238
	1	585	470	385	320	275					0.714
	2	655	560	475	410	355	315	280	255		0.502
	3	695	620	545	480	425	380	340	310	285	0.387
	4	720	660	595	535	480	435	395	360	330	0.315
	5	740	690	635	580	530	485	445	410	375	0.265
	6	750	710	660	615	570	525	485	450	420	0.229
36/4	0	350	260	205	160	130	110	95	85	75	1.548
	1	465	380	315	270	230					0.808
	2	515	455	395	345	305	270	245	220		0.546
	3	540	495	450	405	365	330	300	275	250	0.413
	4	555	525	485	445	410	375	345	320	295	0.332
	5	565	540	510	475	445	410	385	355	335	0.277
	6	570	550	525	500	470	440	415	390	365	0.238
30/6	0	500	350	260	205	170	145	125	110	100	1.376
	1	700	520	405	330	275					0.820
	2	835	655	530	440	375	325	280	250		0.584
	3	925	760	635	535	460	405	355	320	290	0.453
	4	990	845	720	620	540	475	425	380	345	0.370
	5	1030	905	790	690	610	540	485	440	400	0.313
	6	1060	955	850	755	670	600	545	495	450 *	0.271
30/4	0	425	320	250	200	165	140	120	105	95	1.548
	1	545	440	365	305	265					0.878
	2	605	525	450	390	340	300	270	245		0.612
	3	640	575	510	455	405	365	330	300	275	0.470
	4	660	610	555	505	460	415	380	350	320	0.382
	5	670	630	590	545	500	460	425	390	365	0.321
	6	680	650	610	570	535	495	460	430	400	0.277

* DESIGN SHEAR SHOWN ABOVE MAY BE LIMITED BY SHEAR BUCKLING. SEE TABLE BELOW.
THE SHADED VALUES DO NOT COMPLY WITH THE MINIMUM SPACING REQUIREMENTS FOR SIDE-LAP CONNECTIONS AND SHALL NOT BE USED EXCEPT WITH PROPERLY SPACED SIDE-LAP CONNECTIONS.

Φ(Buckling): 0.90 Ω(Buckling): 2.00

DECK PROFILE	I in^4/ft	NOMINAL DIAPHRAGM SHEAR DUE TO PANEL BUCKLING (S_n), PLF / SPAN, FT 2.0	3.0	4.0	5.0	6.0	7.0	8.0	9.0	10.0
NR	0.099	9295	4130	2325	1485	1035	760	580	460	370
IR	0.108	9920	4410	2480	1590	1100	810	620	490	395
WR	0.152	12820	5700	3205	2050	1425	1045	800	635	515

NOTE:
ASD Required Strength (Service Applied Load) <= Minimum [Nominal Shear Strength / Ω(EQ or WIND), Nominal Buckling Strength S_n / Ω(Buckling)]
LRFD Required Strength (Factored Applied Load) <= Minimum [Φ(EQ or WIND) x Nominal Shear Strength, Φ(Buckling) x Nominal Buckling Strength S_n]

Table 11. 22 gage deck, 18 gage framing

Twentieth International Specialty Conference on Cold-Formed Steel Structures
St. Louis, Missouri, U.S.A., November 3 & 4, 2010

Overview of Recent Changes and Additions to AISI Standards

By Helen Chen[1], Roger Brockenbrough[2], Richard Haws[3]

Abstract

Since the publication of the 2007 editions of AISI standards, changes and additions have been made to some of the standards. This paper will provide an overview of the major revisions to those standards.

Introduction

During 2007, the American Iron and Steel Institute (AISI) Committee on Specifications and the Committee on Framing Standards have approved a series of design and testing standards, and established a new numbering system. A complete list of the published standards and the corresponding designated numbers is provided in Appendix A.

Among those standards, AISI S100-07, *North American Specification for the Design of Cold-Formed Steel Structural Members,* was developed and maintained by a joint effort of the AISI Committee on Specifications, the Canadian Standards Association Technical Committee on Cold Formed Steel Structural Members (S136), and Camara Nacional de la Industria del Hierro y del Acero (CANACERO). This Specification has been adopted in the United States by the American National Standards Institute (ANSI) as the American National Standards (ANS), in Canada by Canadian Standards Association (CSA) and endorsed by CANACERO in Mexico. AISI S100-07 has also been adopted by the International Building Code, 2009 edition, and NFPA 5000, Building Construction and Safety Code, 2009 edition.

[1] Manager, Construction Standards Development, American Iron and Steel Institute, Washington, DC.
[2] President, R. L. Brockenbrough & Associates, Pittsburgh, PA.
[3] Technical Services Manager, NUCONSTEEL, Denton, TX.

The North American Cold-Formed Steel Framing Standards series (See Appendix A) were developed and maintained by the AISI Committee on Framing Standards and its subcommittees. These standards have been developed with the intent for adoption by North American countries, and have been approved by ANSI as American National Standards. All the North American Cold-Formed Steel Framing Standards listed in Appendix A, except AISI S202, have also been adopted by the International Building Code, 2009 edition, and NFPA 5000, Building Construction and Safety Code, 2009 edition.

Fourteen Test Standards (AISI S901-08 to AISI S914-08) have been published in the 2008 edition of the AISI *Cold-Formed Steel Design Manual* (AISI, 2008). Among these test standards, AISI S901-08 to AISI S912-08 were updated and reformatted, and AISI S913-08 and AISI S914-08 were newly developed. All the test standards have been approved by ANSI as the ANS as well.

In 2008, AISI published a new seismic design standard S110-07, *Standard for Seismic Design of Cold-Formed Steel Structural Systems – Special Bolted Moment Frames*. This standard provides design provisions for a single story moment frame formed by cold-formed channel beams and tubular columns. The cold-formed special bolted moment frames are intended to be used for free standing mezzanines (light storage), elevated office support platforms, equipment support platforms and small buildings in all seismic areas. The system is limited to a single story of 35 feet (10.7 m) maximum in height, with the ability to extend over several spans and multiple bay widths. All lateral resistance frame lines use the same sections for the beams and columns and all connections will be of the same geometry. As is the case with other AISI standards, this standard has been approved by ANSI as the ANS in 2008.

During 2009 and 2010, the following supplements were published:

- S100-07/S1-10, *Supplement No. 1 to North American Specification for the Design of Cold-Formed Steel Structural Members*;
- S100-07/S2-10, *Supplement No. 2 to North American Specification for the Design of Cold-Formed Steel Structural Members*;
- S213-07/S1-09, *North American Cold-Formed Steel Framing-Lateral Design with Supplement No. 1;* and

- S110-07/S1-09; *Standard for Seismic Design of Cold-Formed Steel Structural Systems – Special Bolted Moment Frames with Supplement No. 1*

Note that S100-07/S2-10 also includes the changes and updates made in S100-07/S1-09.

In the following sections, an overview is provided for major technical changes and additions that are included in these supplements.

Technical Changes and Additions in Supplements

1. S100-07/S2-10, Supplement No. 2 to North American Specification for the Design of Cold-Formed Steel Structural Members.

Supplements No. 1 and No. 2 were published in 2009 and 2010, respectively. The major changes are summarized as follows:

(a) AISI S100 Section F1.1, Load and Resistance Factor Design and Limit States Design, is modified to recognize that the behavior and probability of failure for a composite interior partition wall stud differs from the direct load bearing system. A composite interior wall stud is a stud in an interior application with full-height gypsum sheathing that is screw attached to both flanges and supports, and no axial load other than self-weight. Instead of a safety factor (Ω) of 1.67 for lateral load resistance of load bearing wall studs, $\Omega = 1.5$ is used for lateral resistance of interior partition wall studs. This safety factor corresponds to a target reliability index $\beta_o = 1.6$. This low target reliability also reflects the fact that for composite interior partition wall studs, the consequences of failure are less severe than for other structural members. This change has been included in both Supplements No. 1 and No. 2.

(b) AISI S213-07/S1, *North American Standard for Cold-Formed Steel Framing – Lateral Design, 2007 Edition with Supplement No. 1*, was adopted by the Canadian Standards Association. This standard is, therefore, recognized in the US, Mexico and Canada, and was referenced in AISI S100 Section A9, Referenced Documents.

(c) For uniformly compressed elements with single or multiple identical and equally spaced stiffeners (AISI S100, Section B5.1.1), the buckling coefficient for local element buckling (k_{loc}) is revised to

$$k_{loc} = 4(b_o/b_p)^2 \qquad \text{(AISI S100 } Eq. \text{ B5.1.1-1)}$$

where b_o = total flat width of stiffened element; b_p = largest sub-element flat width. This change results in a better estimate of member strength.

(d) New provisions were added for cellular or composite decks (see Figure 1) with fastener spacing exceeding the requirements provided in AISI S100 Section D1.3, Spacing of Connections in Cover Plated Sections. The effective section properties of those composite decks can now be determined using newly added Section B2.5, Uniformly Compressed Elements Restrained by Intermittent Connections, and the strength of the section can then be determined according to the flexural member design provisions. The new provisions were developed based on the research work by Snow and Easterling (2008).

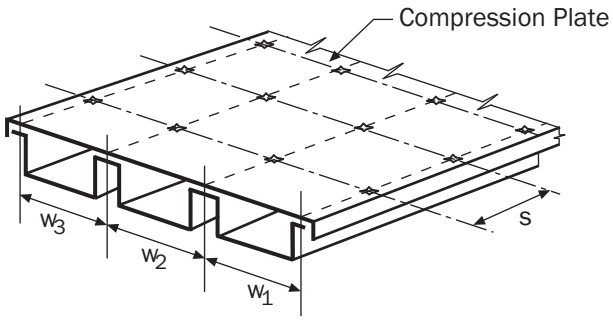

Figure 1 Built-Up Deck

(e) The simplified provisions for considering distortional buckling of flexural and compression members have been moved from the Specification to the Commentary. This change is due to the consideration that even though the simplified approach can be useful to quickly determine that distortional buckling does not control the design, the approach is often overly conservative and could lead to some confusion to designers.

(f) Tension Member Design Provisions for US and Mexico and Canada have been harmonized, and the provisions are now included in the main body of the Specification.

(g) The resistance factor for sections with stiffened or partially stiffened compression flanges as defined in AISI S100 Section C3.1.1, has been changed from 0.95 to 0.90 for LRFD. This change is based on the examination of more recent available test data (Shafer and Trestain, 2002; Yu and Schafer, 2003), and consideration of the fact that the higher resistance factor existed in part due to inelastic reserve strength, which is addressed in AISI S100 Section C3.1.1(b).

(h) In conjunction with the revisions of tension member design, significant changes and reorganizations were made to Chapter E, Connections and Joints. The complete chapter is included in Supplement No. 2. The major changes include:

(1) The design provisions for flare bevel groove welds were revised. Two new equations were added to accurately define the effective throat of the groove bevel welds. Filled flush throat depths were also modified to match those specified in AWS D1.1-2006.

(2) The provisions for checking combined shear and tension on arc spot welds were added.

For ASD

If $\left(\frac{\Omega_t T}{P_{nt}}\right)^{1.5} \le 0.15$, no interaction check shall be required.

If $\left(\frac{\Omega_t T}{P_{nt}}\right)^{1.5} > 0.15$,

$$\left(\frac{\Omega_s Q}{P_{ns}}\right)^{1.5} + \left(\frac{\Omega_t T}{P_{nt}}\right)^{1.5} \le 1$$

(AISI S100 *Eq*. E2.2.4.1-1)

For LRFD or LSD:

If $\left(\frac{\overline{T}}{\phi_t P_{nt}}\right)^{1.5} \le 0.15$, no interaction check shall be required.

If $\left(\frac{\overline{T}}{\phi_t P_{nt}}\right)^{1.5} > 0.15$,

$$\left(\frac{\overline{Q}}{\phi_s P_{ns}}\right)^{1.5} + \left(\frac{\overline{T}}{\phi_t P_{nt}}\right)^{1.5} \leq 1$$

(AISI S100 *Eq*. E2.2.4.2-1)

where

Ω_t = Corresponding safety factor for P_{nt} given by AISI S100 Section E2.2.3

T = Required allowable tensile strength of connection

P_{nt} = Nominal tension strength as given by AISI S100 Section E2.2.3

Ω_s = Corresponding safety factor for P_{ns} given by AISI S100 Section E2.2.2

Q = Required allowable shear strength of connection

P_{ns} = Nominal shear strength as given by AISI S100 Section E2.2.2

$\overline{T}$ = Required tensile strength [factored tension force] of the connection

= T_u for LRFD

= T_f for LSD

ϕ_t = Resistance factor corresponding to P_{nt} given in AISI S100 Section E2.2.3

P_{nt} = Nominal tension strength [resistance] as given by AISI S100 Section E2.2.3

P_{ns} = Nominal shear strength [resistance] as given by AISI S100 Section E2.2.2

$\overline{Q}$ = Required shear strength [factored shear force] of the connection

= Q_u for LRFD

= Q_f for LSD

ϕ_s = Resistance factor corresponding to P_{ns} given in AISI S00 Section E2.2.2

The new provisions were developed based on research work at the University of Missouri-Rolla (predecessor of Missouri University of Science and Technology) (Stinemann, LaBoube, 2007).

(3) For screws in tension, provisions for specific washer thickness are added. If the thickness of the sheet steel that is directly in contact with the screw head is less than 0.027 in. (0.69 mm), a washer a thickness of at least 0.024 in. (0.61 mm) must provided; otherwise, if the thickness of the sheet steel is greater than 0.027 in. (0.69 mm), a washer thickness of at least 0.050 in. (1.27 mm) must be provided.

(4) The tension and shear rupture design provisions for all the fasteners considered in the Specification are consolidated and included in Section 5.3, Rupture. The nominal tensile rupture strength, T_n, is defined as:

$T_n = F_u A_e$ (AISI S100 *Eq*. E5.2-1)

where

A_e = Effective net area subject to tension

$= U_{s\ell} U_{st} A_{nt}$ (AISI S100 *Eq*. E5.2-2)

where

$U_{s\ell}$ = Shear lag factor defined in Table AISI S100 Table E5.2-1

U_{st} = Staggered connectors factor

= 1.0 where staggered connectors are not present

= 0.9 where staggered connectors are present

A_{nt} = Net area subject to tension defined in AISI S100 Section E5.2.

AISI S100 Table E5.2-1
Shear Lag Factors for Connections to Tension Members

Description of Element	Shear Lag Factor, $U_{s\ell}$
(1) For flat sheet *connections* not having staggered hole patterns	
(a) For multiple connectors in the line parallel to the force	$U_{s\ell}$ = 1.0
(b) For a single connector, or a single row of connectors perpendicular to the force	
(i) For single shear and outside sheets of double shear connections with washers provided under the bolt head and the nut.	$U_{s\ell} = 3.33\ d/s \le 1.0$ (AISI S100*Eq.* E5.2-4)
(ii) For single shear and outside sheets of double shear connections when washers are not provided or only one washer is provided under either the bolt head or the nut.	$U_{s\ell} = 2.5\ d/s \le 1.0$ (AISI S100 *Eq.* E5.2-5)
(iii) For inside sheets of double shear connections with or without washers.	$U_{s\ell} = 4.15\ d/s \le 1.0$ (AISI S100 *Eq.* E5.2-6)
(2) For flat sheet *connections* having staggered hole patterns	$U_{s\ell}$ = 1.0
(3) For other than flat sheet connections:	
(a) When load is transmitted only by transverse welds	$U_{s\ell}$ = 1.0 and A_{nt} = Area of the directly connected elements
(b) When load is transmitted directly to all the cross sectional elements.	$U_{s\ell}$=1.0
(c) For connections of angle members not meeting (a) or (b) above.	$U_{s\ell} = 1.0 - 1.20\ \bar{x}/L \le 0.9$ (AISI S100 *Eq.* E5.2-7) but $U_{s\ell}$ shall not be less than 0.4
(d) For connections of channel members not meeting (a) or (b) above.	$U_{s\ell} = 1.0 - 0.36\ \bar{x}/L \le 0.9$ (AISI S100 *Eq.* E5.2-8) but $U_{s\ell}$ shall not be less than 0.5

(h) In the Direct Strength Design method, provisions are provided to permit applying the safety and resistance factors for pre-qualified members to non-qualified members. If a member falls outside the geometric and material limitations outlined in AISI S100 Table 1.1.1-1 for columns and Table 1.1.1-2 for beams, it is now possible to use the safety and resistance factors for pre-qualified members (i.e. those members with their geometric and material properties within the limitations). This is permitted if, through the use of AISI S100 Chapter F, the predicted resistance factor, ϕ, provides an equal or higher resistance factor compared to the resistance factor for pre-qualified members. In the use of AISI S100 Chapter F, P = Test-to-predicted ratio; P_m = Mean of test-to-predicted ratio; V_p = Coefficient of variation of P. If $V_p \leq 15\%$, C_p is permitted to be set to 1.0. At least three tests should be conducted.

2. S213-07/S1-09, North American Cold-Formed Steel Framing-Lateral Design with Supplement No. 1

This standard has been revised and updated in 2009 with the following major changes:

a. The definition of "amplified seismic load" was added. "Amplified seismic load" is defined as "Load determined in accordance with the *applicable building code* load combinations that include the system overstrength factor, Ω_o, for strength design (LRFD). [USA and Mexico]."

b. The ductility-related force modification factor, R_d, for diagonal strap braced walls has been adjusted to match the values approved by the Canadian National Committee on Earthquake Engineering (CANCEE) for inclusion in the National Building Code of Canada (NBCC) seismic provisions.

Design Coefficients and Factors for Seismic Force Resisting Systems in Canada
(Excerpt from AISI S213 Table A4-1)

Type of Seismic Force Resisting System	R_d	R_o	Building Height (m) Limitations [1]				
			Cases Where $I_E F_a S_a(0.2)$				Cases Where $I_E F_v S_a(1.0)$
			< 0.2	≥0.2 to <0.35	≥0.35 to ≤0.75	>0.75	>0.3
Diagonal Strap Braced (Concentric) Walls							
Limited ductility braced wall	1.9	1.3	20	20	20	20	20
Conventional construction	1.2	1.3	15	15	NP	NP	NP

c. Based on the research work at the University of North Texas (Cheng, 2009), new shear wall nominal shear strengths for wind and other in-plane loads were added for 0.027 in. (0.69 mm) one side steel sheet with height to width aspect ratio 2:1.

Nominal Shear Strength (R_n) for Wind and Other In-Plane Loads for Shear Walls for US and Mexico (Pounds Per Foot)
(Excerpted from AISI S213 Table C2.1-1

Assembly Description	Maximum Aspect Ratio (h/w)	Fastener Spacing at Panel Edges (inches)			
		6	4	3	2
0.027" steel sheet, one side	4:1	-	1,000	1085	1170
	2:1	647	710	778	845

d. The setback requirements have been revised. It is required that where setbacks of structural walls create an offset between them on an upper and lower story, the floor diaphragm and floor framing shall be designed to transfer overturning and shear forces through the offset in accordance with AISI S213 and the applicable building code.

e. The equations for design deflection of a blocked wood structural panel diaphragm for US Customary and SI units are consolidated into one expression.

3. S110-07/S1-09, Standard for Seismic Design of Cold-Formed Steel Structural Systems-Special Bolted Moment Frames with Supplement No. 1

To have the system adopted by ASCE 7, a series of analyses were performed following FEMA P-695 (FEMA, 2009). It was concluded from the analyses that the system would performance well with the following seismic performance factors.

Design Coefficients and Factors for Basic Seismic Force Resisting Systems							
Basic Seismic Force Resisting System	Response Modification Coefficient R	System Overstrength Factor Ω_o	Deflection Amplification Factor C_d	Height Limit (ft) Seismic Design Category			
				B & C	D	E	F
Building Frame Systems							
Cold-formed steel–special bolted moment frames[c]	3.5	3.0[a]	3.5[b]	35	35	35	35

[a] The seismic load effect with overstrength, E_{mh}, is permitted to be based on the expected strength determined in accordance with AISI S110, Section D1.2.3.

[b] Also see AISI S110 Section D1.3.

[c.] Cold-formed steel–special bolted moment frame is limited to one-story in height.

The values included in the table above are consistent with what has been adopted in ASCE 7-09 (ASCE, 2009).

References

American Iron and Steel Institute (2008), *Cold-Formed Steel Design Manual, 2008 Edition*, Washington, DC, 2008.

American Society of Civil Engineers (2009), ASCE/SEI 7-09, *Minimum Design Loads in Buildings and Other Structures*, Reston, VA, 2009.

Snow, G. L. and Easterling, W. S. (2008). "Section Properties for Cellular Decks Subjected to Negative Bending." Report No. CE/VPI – 08/06. Virginia Polytechnic Institute and State University, Blacksburg, VA, 88 pages.

Schafer, B.W., Trestain, T. (2002). "Interim Design Rules for Flexure in Cold-Formed Steel Webs." *Proceedings of the Sixteenth International Specialty Conference on Cold-Formed Steel Structures*, Orlando, FL. 145-160.

Yu, C., Schafer, B.W. (2003). "Local Buckling Tests on Cold-Formed Steel Beams." ASCE, *Journal of Structural Engineering*. 129 (12) 1596-1606.

FEMA, (2009), P695, "Qualification of Building Seismic Performance Factors," June, 2009.

Stirnemann, L.K., R. A. LaBoube (2007), "Behavior of Arc Spot Weld Connections Subjected to Combined Shear and Tension Forces," Research Report, University of Missouri-Rolla, Rolla, MO, 2007

Appendix A: AISI Standards and Designations

New Designation	Old Designation	Title
AISI S100	NASPEC	North American Specification for the Design of Cold-Formed Steel Structural Members
AISI S110	SEISIMIC	Standard for Seismic Design of Cold-Formed Steel Structural Systems-Special Bolted Moment Frames
AISI S200	GP	North American Cold-Formed Steel Framing – General Provisions
AISI S201	PRODUCT	North American Cold-Formed Steel Framing – Product Data
AISI S202	COSP	North American Cold-Formed Steel Framing – Code of Standard Practice
AISI S210	FRSD	North American Cold-Formed Steel Framing – Floor and Roof System Design
AISI S211	WSD	North American Cold-Formed Steel Framing – Wall Stud Design
AISI S212	HEADER	North American Cold-Formed Steel Framing – Header Design
AISI S213	LATERAL	North American Cold-Formed Steel Framing – Lateral Design
AISI S214	TRUSS	North American Cold-Formed Steel Framing – Truss Design
AISI S230	PM	North American Cold-Formed Steel Framing – Prescriptive Method
AISI S901	TS-1	Rotational-Lateral Stiffness Test Method for Beam-to-Panel Assemblies
AISI S902	TS-2	Stub-Column Test Method for Effective Area of Cold-Formed Steel Columns
AISI S903	TS-3	Standard Methods for Determination of Uniform and Local Ductility
AISI S904	TS-4	Standard Test Methods for Determining the Tensile and Shear Strength of Screws

(Continue)

AISI S905	TS-5	Test Methods for Mechanically Fastened Cold-Formed Steel Connections
AISI S906	TS-6	Standard Procedures for Panel and Anchor Structural Tests
AISI S907	TS-7	Test Standard for Cantilever Test Method for Cold-Formed Steel Diaphragm
AISI S908	TS-8	Base Test Method for Purlins Supporting a Standing Seam Roof System
AISI S909		Standard Test Method for Determining the Web Crippling Strength of Cold-Formed Steel Beams
AISI S910		Test Method for Distortional Buckling of Cold-Formed Steel Hat Shaped Compression Members
AISI S911		Method for Flexural Testing Cold-Formed Steel Had Shaped Beams
AISI S912		Test Procedure for Determining a Strength Value for a Roof Panel-to-Purlin-to-Anchorage Device Connection
AISI S913		Test Standard for Hold-Downs Attached to Cold-Formed Steel Structural Framing
AISI S914		Test Standard for Joist Connectors Attached to Cold-Formed Steel Structural Framing

Twentieth International Specialty Conference on Cold-Formed Steel Structures
St. Louis, Missouri, U.S.A., November 3 & 4, 2010

Review of AISI Design Guide for Cold-Formed Steel Purlin Roof Framing Systems – Component Stiffness Method

Michael W. Seek, PE[1]

Abstract

This paper reviews the Component Stiffness Method for determining anchorage forces in roof systems as presented in Chapter 5 of the new AISI *Design Guide for Cold-Formed Steel Purlin Roof Framing Systems*. The four steps in the general methodology of the component stiffness method are presented. First, the development of forces requiring anchorage in purlin roof systems is discussed. Next, calculation of the stiffness of each of the components of the roof system and the procedure for distributing these forces through the system is presented. The final step, evaluation of the effectiveness of the anchors in preventing deformation of the system, is discussed. The five numerical examples relating to the component stiffness method are outlined.

Introduction

In June 2009, the American Iron and Steel Institute published the *Design Guide for Cold-Formed Steel Purlin Roof Framing Systems* (2009). This publication originated primarily in support of the new roof bracing and anchorage provisions in the AISI *North American Specification for the Design of Cold-Formed Steel Structural Members* (2007). These provisions, now in Section D6.3.1, represent a new approach to quantifying anchorage forces using a systematic stiffness analysis of the roof system. The *Specification* outlines one method for performing the stiffness analysis. However, recognizing that there are a number of different ways to perform such an analysis, the *Specification* allows the use of other methods to determine the anchorage forces. The *AISI Design Guide* contains details for several methods to determine anchorage forces: Simplified Specification Solution, Matrix Solution, Frame Element Stiffness Model and Shell Element Stiffness Model and the Component Stiffness Method. As each method increases in computational requirements, each allows for more refined analyses on more complex systems. Table 1.1 in the *Design Guide* provides a matrix of applicability for each method.

---

[1]Assistant Professor, Department of Engineering Technology,
East Tennessee State University, Johnson City, TN, USA

The *AISI Design Guide* is arranged in five chapters. The first chapter provides an introduction to the components comprising typical cold-formed steel roof systems. The second chapter provides a discussion of purlin design using the R-factor method for through fastened systems subjected to uplift loading and the Base Test Method for standing seam systems. In Chapter 3, design assumptions for continuous span purlin design are discussed and two design examples are provided. Chapter 4 presents the new purlin anchorage provisions in the Specification with several design examples. In addition, a Simplified Specification Solution and a Matrix Solution are also introduced. Alternate analysis procedures are presented in Chapter 5. The bulk of this chapter is devoted to explaining the mechanics of purlin anchorage, the development of the Component Stiffness Method, and several examples. Chapter 5 also presents guidelines for determining anchorage forces using a frame element finite element model and a shell element finite element model.

The Component Stiffness Method can be applied to solve anchorage forces for single or multiple span systems with supports, third point, midpoint, supports plus third point lateral restraints and supports plus third point torsional restraints. The method is versatile and provides a thorough representation of the system of purlins. However, to provide this versatility and account for the variety of systems provided by the different manufacturers, the method requires the designer to apply more properties of the purlin, the sheathing and the connections between the purlin and sheathing and purlin and rafters. The increased complexity allows for a refined analysis.

The component stiffness method is fundamentally a stiffness analysis. To perform the analysis, there are 4 steps. The first is to determine the external forces acting at each node on the system. The second is to determine the stiffness of the system. Once the nodal forces and stiffness of the system is determined, forces can be distributed throughout the system according to stiffness. One important final step is to perform serviceability checks to evaluate the effectiveness of the anchors.

Forces in the System

In purlin supported roof systems, the load carrying capacity of a purlin is affected by its attachment to the sheathing. Purlins are designed based on the assumption of constrained bending. That is, despite the fact that Z-sections have rotated principal axes relative to their normal orthogonal axes and sloped roof systems are subjected to torsional downslope loading, the sheathing is assumed to restrict the lateral and rotational movements of the purlin, constraining

bending of the purlin to a plane perpendicular to the sheathing. Through-fastened systems are assumed to perfectly restrain the purlin when subjected to gravity loading. Standing seam systems have greater flexibility and are typically not as effective as a through fastened system at constraining the bending. Consequently, design of purlins attached to standing seam systems is based upon the Base Test Method. With the Base Test Method, a reduction is applied to the fully constrained bending strength in the form of an R-Factor. For the sheathing to constrain the bending of a purlin, forces are developed in the sheathing. Therefore, to insure validity of the assumption of constrained bending, the forces developed in the sheathing must be anchored externally. The Component Stiffness Method is a method of determining this anchorage force that closely mimics this interaction between the purlin and sheathing.

Each purlin, by virtue of the restraint provided by the sheathing, generates a force that must be resisted by the anchorage device. As gravity loads are applied, the sheathing attached to the top flange of the purlin partially restrains lateral and torsional movements of the purlin. Forces generated as a result of the interaction between the purlin and the sheathing must be transferred through the sheathing to the anchorage device. The first step in the Component Stiffness Method is to determine this force.

The interaction between a purlin and sheathing is complex. Resistance to lateral movement is a function of the diaphragm stiffness of the sheathing, G', which includes float in standing seam clips. Torsional resistance provided by the sheathing is affected by the type of fastener (standing seam clip or through fastened), by the location of the fasteners between sheathing and purlin, gage of purlin and sheathing material, and the presence of insulation. In the Component Stiffness Method, the connection between the purlin and sheathing is represented by a spring. The stiffness of the spring, k_{mclip}, is defined as the moment generated in the connection between the purlin and sheathing per unit torsional rotation of the purlin per unit length along the purlin.

To determine the force contributed by each purlin, displacement compatibility of the top flange of the purlin at midspan is considered. The greater the lateral and torsional restraint provided by the sheathing, the greater the anchorage force. As the restraint of the sheathing is reduced, the less anchorage force is generated as the purlin deviates from constrained bending. Consider the following example of a simple span purlin subjected to a uniformly applied gravity loading. In absence of the restraining effects of the sheathing, the Z-section, because of its rotated principal axes, when loaded uniformly in the plane of its web deflects laterally as shown in Figure 1 (a). In typical roof systems, the uniformly applied load is assumed to act at an eccentricity at the top flange (δb) causing an upslope

rotation of the purlin. The total lateral and torsional displacement of the purlin unrestrained by the sheathing is shown in Figure 1 (a).

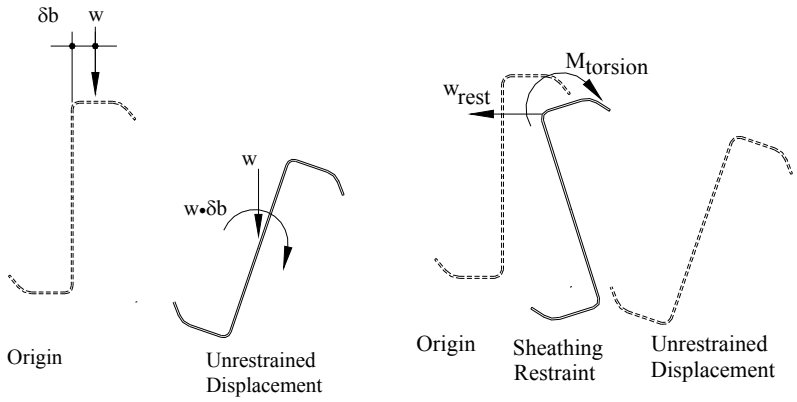

(a) Unrestrained Displacement (b) Sheathing Restraining Forces

Figure 1 Restraining Effect of Sheathing on Purlin Displacement

Figure 1 (b) shows the lateral and torsional restraining effects of the sheathing. As the purlin moves laterally, uniform resistance is provided by the diaphragm action in the sheathing. This effect is represented by a uniform horizontal load in the plane of the sheathing, w_{rest}. This horizontal load has the effect of pushing the purlin downslope towards its original undeflected position. Because this horizontal load is applied at the top flange of the purlin, it causes a downslope rotation of the purlin. The sheathing also resists torsional rotations of the purlin through the development of a moment, $M_{torsion}$, in the connection between the purlin and the sheathing.

By equating the deformation of the purlin in the absence of the sheathing with the restoring displacement provided by the sheathing, the uniform restraint force in the sheathing, w_{rest}, is determined. For a single span purlin with supports restraints,

$$w_{rest} = w \cdot \sigma \qquad (1)$$

Where

$$\sigma = \frac{\frac{5\left(\frac{I_{xy}}{I_x}\cos\theta\right)L^4}{384EI_{my}} + \frac{((\delta b + m)\cos\theta)d}{2}\tau + \frac{L^2\sin\theta}{8G'Bay}}{\frac{5L^4}{384EI_{my}} + \frac{d^2}{4}\tau + \frac{L^2}{8G'Bay}} \quad (2)$$

If the purlin is rigidly restrained by the sheathing, that is the sheathing prevents horizontal movement and torsional rotation, then $\sigma = I_{xy}/I_x$, and the purlin conforms to constrained bending. Typically, σ will range between I_{xy}/I_x (perfectly restrained) for a very rigid diaphragm and purlin-sheathing connection to zero, where no restraint is provided by sheathing. There are a few instances, such as high slope roofs or downslope facing purlins where $\sigma > I_{xy}/I_x$. Note that the uniform restraint force that is generated in the sheathing is resolved in the sheathing. The uniform restraint force along the length of the purlin is counteracted by a force at frame lines equal to $w_{rest} \cdot L/2$ as shown in Figure 2. The uniform restraint force in the sheathing is not directly transferred into the anchorage force.

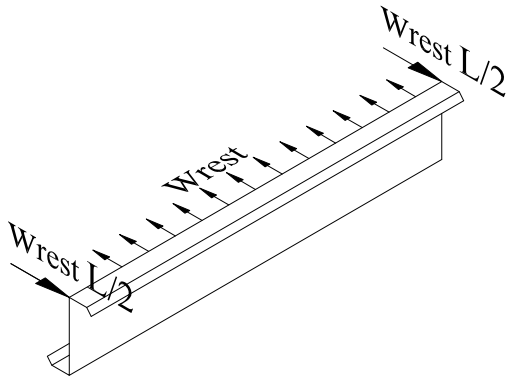

Figure 2 Uniform restraint force in sheathing

To determine the force each purlin adds to the system, moments are summed about the base of the purlin based on the free body diagram shown in Figure 3. For a sloped roof, the components of the gravity load are divided into a normal component, $w \cdot \cos\theta$, perpendicular to the plane of the sheathing and a downslope component, $w \cdot \sin\theta$, in the plane of the sheathing. The torsional moment,

$M_{torsion}$, is the moment that is generated in the connection between the purlin and the sheathing as the sheathing resists the tendency of the purlin to twist. For a supports restraint configuration, the torsional moment is calculated based on the torsional rotation of the purlin at midspan.

$$M_{torsion} = \tfrac{2}{3} k_{mclip} \cdot wL\left(\sigma \frac{d}{2} - (\delta b)\cos\theta\right)\tau$$

Where

$$\tau = \frac{\frac{a^2\beta}{GJ}}{1 + k_{mclip}\frac{\kappa}{GJ}}$$

Both laboratory testing and finite element models have shown bending of the top flange and subsequent deformation of the purlin cross section. For thinner purlins, as the purlin twists, less of the torsion is transferred to a moment in the connection between purlin and sheathing. To account for this local deformation and its effect on the anchorage force, a moment, M_{local}, is incorporated into the Component Stiffness Method.

$$M_{local} = -wL \cdot \delta b \cos\theta \frac{k_{mclip}}{k_{mclip} + \frac{Et^3}{3d}}$$

Summing moments about the base of the free body diagram shown in Figure 3, the net overturning effects are distilled into P_i, where

$$P_i = \frac{wL}{d}(\delta b \cos\theta - d\sin\theta) + M_{torsion} + M_{local}$$

The torsional moment varies for each restraint configuration and for single and multi-span configurations. In Section 5.1.6 of the *AISI Design Guide*, a summary of the equations required for the different restraint and span configurations is provided.

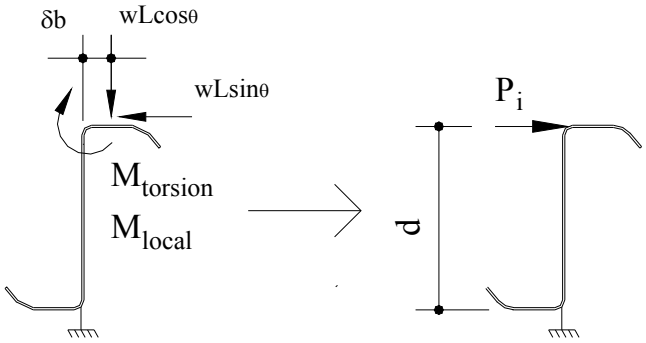

Figure 3 Free Body Diagram of Purlin Overturning Forces

Stiffness of Components

Resistance to the overturning forces generated by each purlin is provided mostly by the externally applied anchors and to a lesser extent by the connection between the purlin and sheathing and the connection between the purlin and rafter. The purlin overturning forces are distributed to each of these "components" of the system according to the relative stiffness of each. It is necessary, therefore, to quantify the stiffness of each of the components.

By determining the stiffness of each of the components in the system, the designer has greater flexibility and the result is a better approximation of the roof system. The component stiffness method allows the designer to account for the different stiffness of various purlin support conditions, effects of clip type and insulation.

Most of the total stiffness of a system of purlins comes from the anchorage devices. In the component stiffness method, anchorage devices are divided into two categories: support and interior. The stiffness of the anchorage is defined as the force developed in the anchor relative to the lateral displacement of the top flange at the anchorage device. Support anchors are subdivided into either an antiroll anchorage device or a discrete anchor. A discrete anchor is considered to only restrain the web of the purlin at a single point along the height of the web whereas and antiroll anchorage clamps the web at multiple locations along its height. Both types of anchorage are shown in Figure 4.

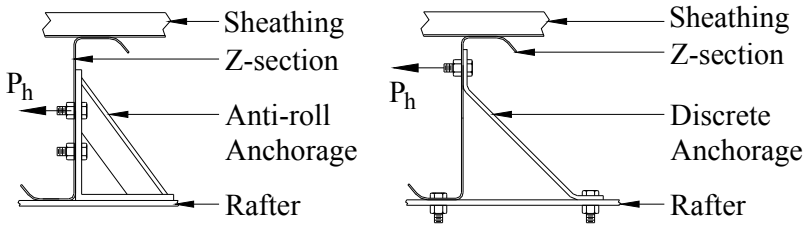

(a) Anti-roll Anchorage (b) Discrete Anchorage

Figure 4 Types of Support Anchorage Devices

Typically, there is flexibility in the web of the purlin between the top of the support anchor and the top flange of the purlin (see Figure 5). Therefore, for a supports anchorage configuration, the stiffness is the combined stiffness of the anchorage device and stiffness of the web of the purlin between the top of the anchorage device and top flange of the purlin. For interior restraints, flexibility of the purlin web is not considered and the stiffness of an interior restraint is simply the stiffness of the anchorage device itself. The *AISI Design Guide* provides derivations and equations for several anchor configurations.

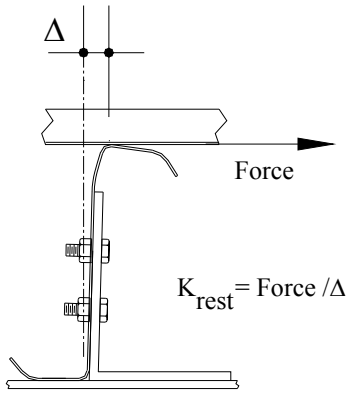

Figure 5 Stiffness of Anchorage Device

By virtue of its connection to the sheathing and connection to the rafter, a purlin has some inherent resistance to overturning. This inherent resistance is known

as the system effect. As a purlin is subjected to overturning, a moment is developed in the connection between the purlin and sheathing. The moment is proportional to the lateral deflection of the top flange. Therefore, the component of the sheathing stiffness, K_{shtg} is defined as the moment developed in the connection between the purlin and sheathing along the entire span of the purlin per unit lateral displacement of the top flange at the restraint location (see Figure 6) The sheathing stiffness is a function of type of connection between the purlin and sheathing, purlin span, thickness, and torsional properties. Procedures for determining sheathing stiffness are provided in the *AISI Design Guide.*

Similarly, for the connection of the purlin to the rafter, whether it is a flange bolted connection or a web plate, as overturning of the purlin occurs, a moment, M_{rafter}, is developed. The stiffness of the rafter connection is defined as the moment generated at the rafter per unit lateral displacement of the top flange of the purlin. The *AISI Design Guide* provides equations to approximate the stiffness for both flange bolted and web plate connections.

With the component stiffness method, anchorage forces are analyzed per line of restraint. The line of restraint includes all purlins in the bay. For example, a three-span continuous purlin system with anchors at the frame lines has 4 lines of restraint: one at each of the exterior frame lines and one for each interior frame line. For solution of the anchorage forces, the entire stiffness along the line of restraint is considered. This stiffness includes the stiffness of the anchors, stiffness of the purlin-sheathing connection tributary to the line of restraint, and the stiffness of the rafter connections. The stiffness included from the rafter connection includes all locations that do not have a support anchor. For interior restraint configurations (midpoints and third points) the rafter stiffness is conservatively ignored.

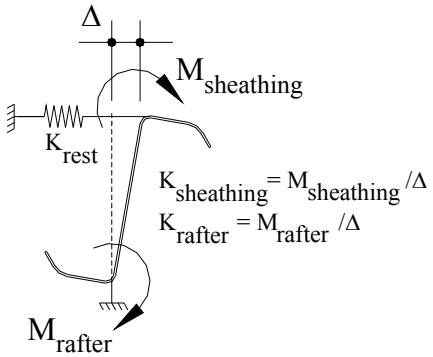

Figure 6 Stiffness of Rafter and Sheathing Components

Anchorage Force Determination

To solve for anchorage forces using the Component Stiffness Method, at each line of anchorage, the system of purlins is considered to have a single degree of freedom: the lateral displacement of the top flange at the restraint location. The sheathing or some other mechanism such as in strapping is assumed to rigidly link the purlins at the line of anchorage, so each purlin along the line of anchorage has the same lateral deflection. Because the stiffness of each component (anchors, purlin-sheathing connection and purlin-rafter connection) is related to this lateral deflection, forces are distributed throughout the system according to the relative stiffness. The total overturning force acting at the line of anchorage is the sum of the forces each purlin contributes to the system, P_i. The sum of these forces is then distributed to each anchor according to the stiffness of the anchor, K_{rest}, relative to the total stiffness at the line of anchorage, K_{total} (see Figure 7). In general, the anchorage force, P_L, is

$$P_L = \sum_{n_p} P_i \cdot \frac{K_{rest}}{K_{total}}$$

Anchorage force is a function of the height of the application of restraint. The stiffness of the anchor is affected by the height of restraint. Typically the lower the restraint from the top flange, the less the stiffness, which will typically reduce the anchorage force. However, since the anchorage force is determined by summing moments about the base of the purlin, as this moment arm is reduced, the anchorage force will increase by a factor of d/h. The anchorage force calculated at the height of the restraint, P_h, is

$$P_h = P_L \frac{d}{h}$$

In terms of anchorage force, the decrease in stiffness and decrease in moment arm will often negate each other. However, as the location of the anchorage is lowered from the top flange, there is an increase in the lateral movement of the top flange. Because the purpose of providing anchorage is to limit lateral deflection, it is recommended that anchorage be provided as close as possible to the top flange.

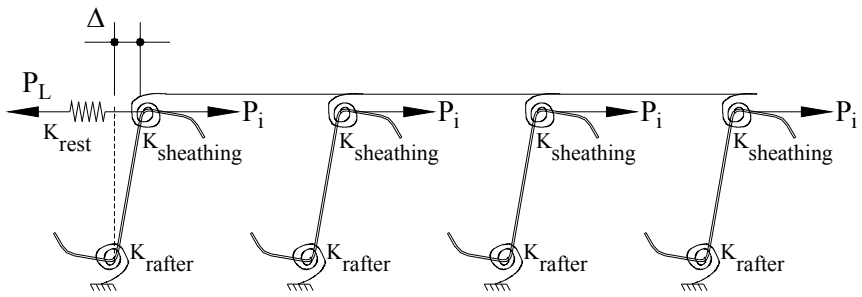

Figure 7 Anchor Force Along Line of Anchorage

Anchorage Effectiveness

Anchorage force is a function of the stiffness of an anchor relative to the stiffness of the system. As anchor stiffness is reduced relative to the system stiffness, the anchorage force is reduced. However, as anchor stiffness is reduced, lateral deflection of the purlin top flange increases. Therefore, to prevent excessive flexibility in a system of purlins, deflection limits were established in the 2007 *AISI Specification*. The *Specification* sets the following limits on the lateral movement of the top flange of a purlin at the line of anchorage.

$$\Delta_{tf} \le \frac{1}{\Omega}\frac{d}{20} \qquad \text{(ASD)}$$

$$\Delta_{tf} \le \phi\frac{d}{20} \qquad \text{(LRFD, LSD)}$$

The lateral deflection of the top flange of a purlin along the line of anchorage using the component stiffness method is

$$\Delta_{tf} = \frac{P_L}{K_{rest}}$$

Because the system of purlins depends upon the sheathing to partially restrain movements and transfer loads to the anchors, the sheathing must have sufficient diaphragm stiffness. For most bracing situations, the *Specification* limits the lateral deflection of the top flange of the purlin between lines of anchorage to

L/360. For bracing configurations where third point torsional braces are used in conjunction with lateral restraints along the frame lines, the lateral deflection limits are relaxed to L/180.

Away from the lines of anchorage, lateral deflection is a function of the uniform restraint force in the sheathing, $w \cdot \cos(\theta) \cdot \sigma$, and the downslope component of the applied load, $w \cdot \sin\theta$. For supports and supports plus third point torsional braces, maximum lateral deflection occurs at midspan of the purlin between frame lines. For low slope roofs, deflection will typically be upslope (considered a positive deflection) and as the slope of the roof increases, lateral deflection will shift downslope (negative deflection).

For interior restraint configurations (midpoints and third points), lateral deflection between lines of anchorage is checked at the frame lines. Lateral deflection will typically be negative (downslope) for low slope roofs with interior restraints. As the roof slope increases, the downslope lateral deflections will increase. Equations to calculate the lateral displacement between lines of anchorage are provided in Section 5.1.6 of the *AISI Design Guide*.

For supports plus third point lateral anchors, the lateral displacements between anchors will typically be very small, so lateral deflection is checked at the third point anchors using the above equation for top flange deflection at a restraint. The lateral deflection at the third point is compared to L/360.

The last aspect of anchor effectiveness that needs to be checked is the transfer of force from the sheathing to purlin, P_{sc}. At anchorage locations, the connection between the sheathing and the purlin must transfer significant loads. In many cases (particularly at anchors along the frame lines) this force will exceed the anchorage force. Although the *Specification* does directly address the connection, considering the magnitude of the forces transferred, the designer should acknowledge the need for a mechanism to transfer the force from the sheathing to purlin. The force P_{sc} varies for each restraint configuration, so equations for each configuration are provided in Section 5.1.6 in the *AISI Design Guide*.

Examples

The Component Stiffness Method is a complex solution to a complex problem that accounts for the many variables that affect anchorage forces. As such, the calculations are facilitated with the help of a computer. In the *AISI Design Guide*, five examples are provided. The first four examples (Examples 8 -11) are based upon a four-span continuous system of Z-sections with standing seam

sheathing. In each of the different examples, the system of purlins is subjected to different bracing configurations. Example 8 demonstrates the system of purlins with antiroll anchorage devices along the frame lines. In Example 9 anchorage is provided by third point anchors applied at the eave of the system of purlins. Example 10 demonstrates the calculation of anchorage forces for supports plus third point torsional braces. Example 11 takes the same third point anchors used in Example 9 but shows the effects of providing additional restraint along the frame lines. The last example has the same general roof configuration as Examples 8-11 but C-sections are used instead of Z-sections. The C-sections are lapped over the interior frame lines and anchorage is provided in the form of antiroll anchorage devices intermittently along the frame line.

Conclusion

The new *AISI Design Guide for Cold-Formed Steel Purlin Roof Framing Systems* is an indispensable source for the designer of purlin roof systems. The *Design Guide* provides insight into design methods and assumptions for purlins but the bulk of the guide is devoted to calculation of purlin anchorage forces, both the adopted by the *Specification* as well as several alternate methods allowed by the *Specification*. Among the alternate methods, the Component Stiffness Method is derived and described in detail. With a summary of equations and examples applying the Component Stiffness Method, the *Design Guide* provides valuable insight and analysis for purlin supported roof systems.

Appendix - References

AISI (2007) *North American Specification for the Design of Cold-Formed Steel Structural Members, 2007 Edition*, American Iron and Steel Institute, Washington, D.C.

AISI (2009) *Design Guide for Cold-Formed Steel Purlin Roof Framing Systems*, American Iron and Steel Institute, Washington, D.C.

Appendix – Notation

a	Torsional constant $\sqrt{\frac{EC_w}{GJ}}$
b	Width of C- or Z-section top flange (in.) (mm)
Bay	Total width of diaphragm perpendicular to span (ft) (m)
C_w	Torsional warping constant of cross-section ($in.^6$) (mm^6)
d	Depth of C- or Z-section (in.) (mm)
E	Modulus of elasticity (29,500,000 psi) (203,400 MPa)
G	Shear modulus (11,300,00 psi) (78,000 MPa)
G'	Diaphragm shear stiffness. Ratio of shear per foot to the deflection per unit width of diaphragm assembly. (lb/in.) (N/m)
h	Height of applied restraint measured from base of purlin parallel to web (in.) (mm)
I_{my}	Modified moment of inertia $\frac{I_x I_y - I_{xy}^2}{I_x}$
I_x	Moment of inertia of full unreduced section about axis perpendicular to the plane of the web ($in.^4$) (mm^4)
I_{xy}	Product of inertia of full unreduced section about major and minor centroidal axes ($in.^4$) (mm^4)
J	Saint-Venant torsion constant ($in.^4$) (mm^4)
k_{mclip}	Combined rotational stiffness of sheathing and connection between the purlin and sheathing per unit length along span of purlin (lb-in./ft) (N-m/m)
K_{rafter}	Moment developed in connection between purlin and rafter per unit lateral displacement of top flange of purlin at restraint (lb-in./in.) (N-m/m)
K_{rest}	Force restrained at top flange of purlin per unit lateral displacement of top flange at restraint location (lb/in.) (N/m)
K_{shtg}	Moment developed in connection between purlin and sheathing per

	unit lateral displacement of top flange of purlin at restraint (lb-in./in.) (N-m/m)
K_{total}	Total stiffness of system at anchor location.
L	Span of purlin (ft) (m)
m	Horizontal distance from shear center of C-section to mid-plane of web (m = 0 for Z-sections) (in.) (mm)
M_{local}	Moment developed in sheathing due to cross sectional deformation of purlin (lb-in.) (N-m)
M_{rafter}	Moment developed in connection between rafter and purlin due to lateral movement of top flange relative to base (lb-in.) (N-m)
M_{shtg}	Moment developed in sheathing along the span of the purlin due to lateral movement of top flange relative to base (lb-in.) (N-m)
$M_{torsion}$	Moment developed in sheathing due to twist of purlin relative to sheathing (lb-in.) (N-m)
P_h	Anchorage force per anchorage device at height of restraint (lb) (N)
P_i	Overturning force generated per purlin per half span (lb) (N)
P_L	Anchorage force per anchorage device at top of purlin (lb) (N)
P_{sc}	Shear force in connection between purlin and sheathing at anchorage location (lb) (N)
n_p	Number of purlins in a bay
w	Uniform loading on purlin (lb/ft) (N/m)
w_{rest}	Uniform diaphragm restraint force provided by sheathing (lb/ft) (N/m)
α	Coefficient for purlin direction
β	Torsional constant for beam subjected to uniform torsion (rad.)
δ	Coefficient for determining load eccentricity on purlin top flange (1/3)
Δ_{tf}	Horizontal deflection of the top flange of purlin at restraint (in.) (mm)
η	Number of up slope facing purlins minus the number of down slope facing purlins
κ	Torsional constant for beam subjected to parabolically varying torsion (rad·in.^{2}) (rad·mm^2)
σ	Proportion of uniformly applied load transferred to a uniform restraint force in the sheathing
θ	Angle between the vertical and the plane of the purlin web (degrees)
τ	Torsional constant for beam subjected to uniform torsion with uniformly distributed rotational springs resistance (rad/lb) (rad/N)

Twentieth International Specialty Conference on Cold-Formed Steel Structures
St. Louis, Missouri, U.S.A., November 3 & 4, 2010

The 2008 AISI Cold-Formed Steel Design Manual

Richard C. Kaehler, P.E.[1] and Helen Chen, Ph.D., P.E.[2]

Abstract

The 2008 edition of the AISI Cold-Formed Steel Design Manual has been published. The new edition includes updated examples and design aids as well as newly developed example problems and design aids covering new material in the 2007 edition of the *North American Specification for the Design of Cold-Formed Steel Structural Members.* Also included are all current AISI structural Test Standards.

Introduction

The American Iron and Steel Institute (AISI) has published the 2008 edition of its Cold-Formed Steel Design Manual (manual). The manual was produced for AISI by Computerized Structural Design, S.C. under the direction of Subcommittee 26 – Design Manual of the AISI Committee on Specifications.

The manual is a companion to the 2007 edition of the *North American Specification for the Design of Cold-Formed Steel Structural Members* (*NA Specification*). As in earlier editions, the 2008 manual provides worked example problems, tabulated and graphed design aids, AISI test standards and other supplemental information for use by designers, students, educators and code officials.

[1] Vice President, Computerized Structural Design, S.C., Milwaukee, WI
[2] Manager, Construction Standards Development, American Iron and Steel Institute, Washington, D.C.

The 2008 edition of the manual is based on the 2007 *North American Specification for the Design of Cold-Formed Steel Structural Members*, a joint publication of AISI, the Canadian Standards Association and CANACERO. The 2007 *NA Specification* covers Load and Resistance Factor Design and Allowable Strength Design for use in the US and Mexico, and Limit State Design for use in Canada with equal emphasis. Country specific provisions applicable to Canada, Mexico and the U.S. are included for cases where joint provisions were not possible. New to the 2007 *NA Specification* are Appendices covering the Direct Strength Method and Second-Order Analysis. Provisions are provided in dimensionless terms where possible or in US customary units and two separate metric systems where that is not possible.

To keep the manual to a reasonable size and appeal to the majority of potential users, all example problems and other calculated values are presented in US customary units using the US country specific provisions. Manuals with Canadian or Mexican country specific provisions or metric units are not available at this time.

All of the previous tables and charts have been updated according to the provisions of the 2007 *NA Specification*. New tables were added to incorporate new design provisions wherever appropriate. A total of 50 illustrative examples are included in this manual. All example problems from the 2002 manual were reviewed and updated to improve presentation of the material and illustrate new and revised *NA Specification* provisions. Eleven new example problems were added to illustrate new and revised *NA Specification* provisions. To provide users with a better understanding of the design information included in each part of the manual, discussions on cold-formed member behavior and failure modes considered in design have been added to the relevant parts of the manual.

As in the 2002 edition, the *Specification* and *Commentary* are not included as chapters in the manual, due to space limitations. Both are available as part of the Cold-Formed Steel Design Manual Set. The 2007 *Specification* and the *Commentary* should be used in conjunction

with the manual. Highlights of the features and changes in the other sections of the manual follow.

Part I – Dimensions and Properties

The table of referenced ASTM steels has been updated to reflect recent changes in steels approved for cold-forming.

Many of the design aids and example problems are based on the "representative cross sections" that are tabulated in Part I. The cross section from the previous edition of the manual have been carried over, including industry standard Steel Stud Manufacturers Association (SSMA) and Light-Gage Steel Institute (LGSI) cross sections for such shapes as studs, C- and Z-sections.

The discussion of the calculation of effective section properties has been expanded to help clarify the procedure. Formulas for calculating distortional buckling properties have been added. The effective section property examples have been updated to reflect changes in Chapter B of the 2007 *NA Specification*.

Part II – Beam Design

To provide an overall understanding to cold-formed steel beam design, new discussions of cold-formed flexural member behavior and limit states, including distortional buckling, have been added to the introductory section.

Three new design tables have been added to aid in evaluation of the distortional buckling limit state. These tables provide design coefficients and nominal distortional buckling strengths for the C-shapes, SSMA studs and Z-shapes tabulated in Part I. A sample of one of these tables is shown in Figure 1. In addition, the smallest possible nominal distortional buckling strength is noted (with diamonded shape) on the each beam's nominal flexural strength curve in Charts II-1 to II-3. The lower bound of the available distortional buckling strength for a

given beam can be calculated via the value on the chart and be used to estimate whether the distortional buckling controls the beam design.

Five new example problems have been added.

1. Distortional Buckling of C-Section illustrates the calculation in detail of the distortional buckling strength of a C-Section braced by OSB per *NA Specification* Section C3.1.4.

2. Tubular Section – Rectangular illustrates the calculation of the flexural strength of a square HSS using *NA Specification* Section C3.1.2.2, including a comparison between the AISI and AISC methods.

3. C-Section with Combined Bending and Torsional Loading illustrates the calculation of the combined flexural and torsional strength of a C-section subject to an eccentric transverse loading per *NA Specification* Section C3.6.

4. Web Crippling illustrates the calculation of the available bearing strength of a stud with a reinforcing bearing stiffener attached according to *NA Specification* Section C3.7.

5. Web-Stiffened C-Section by the Direct Strength Method – Flexure illustrates the computation of the strength of a flexural member having a complex cross section using the Direct Strength procedure from *NA Specification* Appendix 1.

Part III – Column Design

New discussions of cold-formed compression member behavior and limit states have been added to the introductory section.

Three new design tables have been added to aid in evaluation of the distortional buckling limit state. These tables provide design coefficients and nominal distortional buckling strengths for the C-

shapes, SSMA studs and Z-shapes tabulated in Part I. A sample of one of these tables is shown in Figure 2.

Five new example problems have been added.

1. C-Section Subject to Distortional Buckling – Compression illustrates the new distortional buckling provisions for columns included in *NA Specification* Section C4.2.

2. Stiffened Z-Section with One Flange Fastened to a Standing Seam Roof – Compression illustrates the calculation of the axial strength of a Z-purlin in a standing seam roof system per the provisions of *NA Specification* Section D6.1.4.

3. Square HSS Section – Bending and Compression illustrates the calculation of compression strengths and combined compressive and flexural strengths of a square HSS according to *NA Specification* Sections C4 and C5, including a comparison between the AISI and AISC methods.

4. Frame Design by Second-Order Analysis illustrates the new second-order analysis and design provisions given in *NA Specification* Appendix 2.

5. Web-Stiffened C-Section by the Direct Strength Method – Compression illustrates the computation of the strength of a compression member having a complex cross section using the Direct Strength procedure from *NA Specification* Appendix 1.

Part IV – Connection Design

New discussions of connection design limit states were added to the introductory sections for welded, bolted and screwed connections.

A new design table, Arc Spot Welds – Shear of Sheet Welded to an Identical Sheet has been added, in which the nominal strength is based

on the sheet strength. Each of the six screw strength tables from the last edition has been duplicated using the typical SSMA design thicknesses, to allow convenient use with SSMA shapes without the need for interpolation.

The design examples have been revised to reflect technical and editorial changes in the 2007 *NA Specification*.

Part V – Supplemental Information

There is once again a cross reference table showing where each illustrated provision of the *NA Specification* can be found in the example problems.

The material previously published as Section 2 – Laterally Unbraced Compression Flanges has been removed. The long published "9 step" or "10 step" method provided a means of calculating the combined flange and web buckling strength of sections such as hats. This mode of buckling is now recognized as "distortional buckling" and can now be evaluated using the provisions of the Direct Strength method in Appendix 1 of the 2007 *NA Specification*.

The previously published Section 4 – Suggested Cold-Formed Steel Structural Framing, Engineering, Fabrication, and Erection Procedures for Quality Construction has been removed. The information in this document has been superseded by the 2006 Edition of the *AISI Code of Standard Practice for Cold-Formed Steel Structural Framing*.

Part VI – Test Methods

All existing and new test standards have been given new identifying numbers consistent with the new AISI document numbering standard. For example, the test method Rotational-Lateral Stiffness Test Method for Beam-To-Panel Assemblies which was referenced as AISI TS-1-02, is now AISI S901-08, where the 'S901' is the unique designation for this standard and '08' indicates the year of the edition. A cross

reference table is included in the beginning of Part VI, which lists the old and new numbering for each standard.

Several previously included standards have been updated and six new test standards have been added to this edition:

1. *AISI S909-08: Standard Test Method for Determining the Web Crippling Strength of Cold-Formed Steel Beams*. This test standard establishes procedures for conducting tests to determine the web crippling strength of single-web, multiple-web and built-up web flexural members.

2. *AISI S910-08: Test Method for Distortional Buckling of Cold-Formed Steel Hat Shaped Compression Members*. This test standard establishes procedures for determining the distortional buckling strength of cold-formed steel compression members with a hat shaped cross section.

3. *AISI S911-08: Method for Flexural Testing Cold-Formed Steel Hat Shaped Beams*. This test standard establishes procedures for determining the nominal flexural strength of cold-formed steel compression members with a hat shaped cross section subject to negative bending moment.

4. *AISI S912-08: Test Procedure for Determining a Strength Value for a Roof Panel-to-Purlin-to Anchorage Device Connection*. This test standard establishes procedures for determining lower bound strength values for roof panel-to-purlin-to-anchorage device connections in through-fastened and standing seam, multi-span, multi-purlin line roof systems, with or without intermediate braces.

5. *AISI S913-08: Test Standard for Hold-Downs Attached to Cold-Formed Steel Structural Framing*. This test standard establishes procedures for determining the strength and deformation behavior of hold-downs used in cold-formed steel light-frame construction.

6. *AISI S914-08: Test Standard for Joist Connectors Attached to Cold-Formed Steel Structural Framing*. This test standard establishes procedures for determining the strength and deformation behavior of joist connections used in cold-formed steel light-frame construction.

Availability

The 2008 Edition of the Cold-Formed Steel Design Manual Set, which includes the 2008 Cold-Formed Steel Design Manual, the 2007 *NA Specification* and the *Commentary*, can be obtained from the AISI e-store at: http://www.steel.org.

Conclusion

The 2008 AISI Cold-Formed Steel Design Manual represents a refinement and updating of the previous edition. The changes will make the manual both more convenient and useful to the range of users it serves.

Appendix - References

American Iron and Steel Institute, *Cold-Formed Steel Design Manual*, Washington, D.C., 2008.

American Iron and Steel Institute, AISI S100-07, *North American Specification for the Design of Cold-Formed Steel Structural Members*, Washington, D.C., 2007.

American Iron and Steel Institute, *Code of Standard Practice*, Washington, D.C., 2007.

Figure 1 – Example Flexural Distortional Buckling Table

Table II - 8

Distortional Buckling Properties
SSMA Studs – Flexural Strength
C-Sections With Lips

Ω_b = 1.67 (ASD)
ϕ_b = 0.90 (LRFD)

	L_{cr} in.	$k_{\phi fe}$ kips	$\tilde{k}_{\phi fg}$ in.^{2}	$k_{\phi we}$ kips	$\tilde{k}_{\phi wg}$ in.^{2}	F_d/β ksi	$M_n^1{}_{(\beta=1)}$ F_y=33 ksi kip-in.	$M_n^1{}_{(\beta=1)}$ F_y=50 ksi kip-in.
1200S250-97	17.9	1.05	0.0256	1.06	0.0142	53.2	171	226
1200S250-68	21.7	0.328	0.0128	0.326	0.00698	33.1	105	136
1200S250-54*	24.5	0.156	0.00811	0.154	0.00441	24.7	75.9	97.5
1200S200-97	15.7	1.07	0.0189	1.18	0.0180	60.9	159	212
1200S200-68	19.0	0.334	0.00953	0.352	0.00889	37.2	98.2	128
1200S200-54*	21.5	0.158	0.00606	0.164	0.00562	27.5	70.9	91.4
1200S162-97	12.1	1.15	0.0162	1.54	0.0292	59.1	140	186
1200S162-68	14.5	0.359	0.00845	0.435	0.0146	34.5	85.1	110
1200S162-54*	16.4	0.169	0.00543	0.196	0.00925	24.9	60.7	78.1

Figure 2 – Example Axial Compression Distortional Buckling Table

Table III – 4

Distortional Buckling Properties
Axial Strength
C-Sections With Lips

Ω_c = 1.80 (ASD)
ϕ_c = 0.85 (LRFD)

Section	Per Section 4.2(b)							
	L_{cr} in.	$k_{\phi fe}$ kips	$\tilde{k}_{\phi fg}$ in.^{2}	$k_{\phi we}$ kips	$\tilde{k}_{\phi wg}$ in.^{2}	F_d ksi	$P_n^1{}_{(Lm\geq Lcr)}$ F_y=33 ksi kips	$P_n^1{}_{(Lm\geq Lcr)}$ F_y=55 ksi kips
12CS4x105	32.7	0.712	0.0322	0.521	0.0280	20.5	44.3	57.6
12CS4x085	35.2	0.363	0.0223	0.277	0.0195	15.3	31.2	40.2
12CS4x070	37.8	0.196	0.0158	0.154	0.0139	11.8	22.6	28.9
12CS3.5x105	30.2	0.721	0.0267	0.521	0.0328	20.9	42.5	55.4
12CS3.5x085	32.5	0.367	0.0184	0.277	0.0229	15.6	30.0	38.6
12CS3.5x070	35.0	0.198	0.0130	0.154	0.0162	12.0	21.7	27.8
12CS2.5x105	24.6	0.750	0.0175	0.521	0.0492	19.1	36.7	47.6

Twentieth International Specialty Conference on Cold-Formed Steel Structures
St. Louis, Missouri, U.S.A., November 3 & 4, 2010

COLD-FORMED STEEL FOR STUDENTS: A WEBSITE

R.A. LaBoube[1] and C.M. Stratman[1]

INTRODUCTION

Cold-formed steel members for decades have been used in numerous applications, for example curtain wall framing, partition wall framing, and as floor and roof deck for both steel framed and concrete framed structures. Also cold-formed members have been used as purlins in metal buildings. In recent years cold-formed steel members have also been assigned the task of providing the axial load bearing system for low- and mid-rise structures. With the increased use of cold-formed steel members and connections there is a more pressing need to have engineers educated on the design aspects of cold-formed steel.

Unfortunately, for most engineering students, at no time during their formal education are they exposed to cold-formed steel design or cold-formed steel framing applications. To better inform undergraduate college engineering students, a student website has been developed (http://ccfssonline.org/Student/Student.html). This development effort, the work of the Wei-Wen Yu Center for Cold-Formed Steel Structures (CCFSS), was initially motivated and encouraged by the Cold-Formed Steel Engineers Institute (CFSEI).

[1]Wei-Wen Yu Center for Cold-Formed Steel Structures, Missouri University of Science and Technology, Rolla, MO

The initial objective of the website was to provide a college student resource for information pertaining to applications of and the design, fabrication and erection of cold-formed steel structures. Because cold-formed steel design is typically not taught in undergraduate education programs a primary audience for the website is the senior level students enrolled in a capstone design course.

At Missouri University of Science and Technology (formerly University of Missouri-Rolla), the website is also used as a resource in a sophomore level Architectural Engineering course titled Architectural Materials and Methods of Construction.

A student is a learner or one who studies. Therefore, an equally important secondary objective of the website is to provide a resource for the practicing engineer. This may be an engineer who is seeking an initial introduction into the use of cold-formed steel applications and design or who desires to expand his or her knowledge of cold-formed steel design.

WEBSITE CONTENT

The website provides such fundamentals of cold-formed steel design as:

- Terminology (e.g. curtain wall, load bearing wall, purlin, girt, deck and panel, etc.)
- Applications for cold-formed steel (e.g. framing, deck, racks, metal buildings, etc.)
- Student design aids
- Software resource (e.g. CFS and AISIWIN, are free downloads for the student).

The website is designed to provide an introduction for such topics as the possible applications, cross-section shapes and design criteria. Figure 1 presents the Home page for the website.

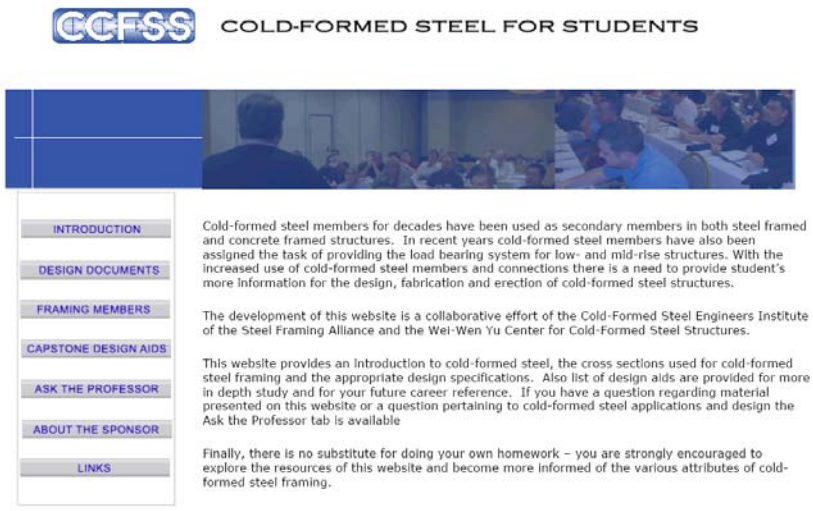

Figure 1 Website Homepage

Introduction:

The introduction page (Figure 2) is intended, through the use of PowerPoint slides, to provide information regarding the application of cold-formed steel framing members, the relevant AISI design documents to include the *North American Specification for the Design of Cold-Formed Steel Structural Members* and the AISI framing standards.

Design Documents

As illustrated by Figure 3, information is provided to introduce the student to cold-formed steel design.

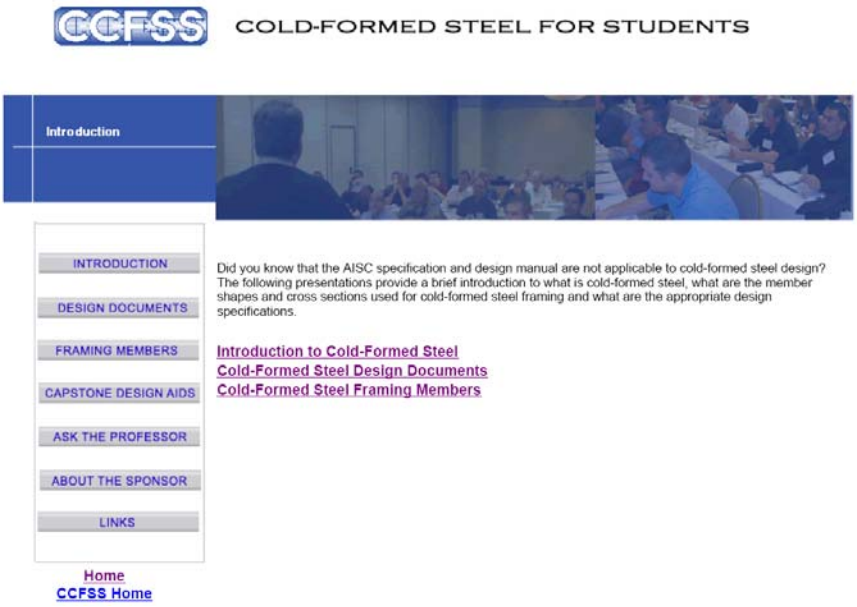

Figure 2 Introduction Web Page

AISI Design Tool. This is a document developed by Dr. Helen Chen of AISI Staff that presents (Figure 4):

- Overview of the *North American Specification for the Design of Cold-Formed Steel Structural Members*, S100-2007
- Overview of the *AISI Cold-Formed Steel Design Manual*, D100-2008
- Overall considerations for cold-formed steel design
- Flow charts for compression member strength, flexural member strength and built-up members

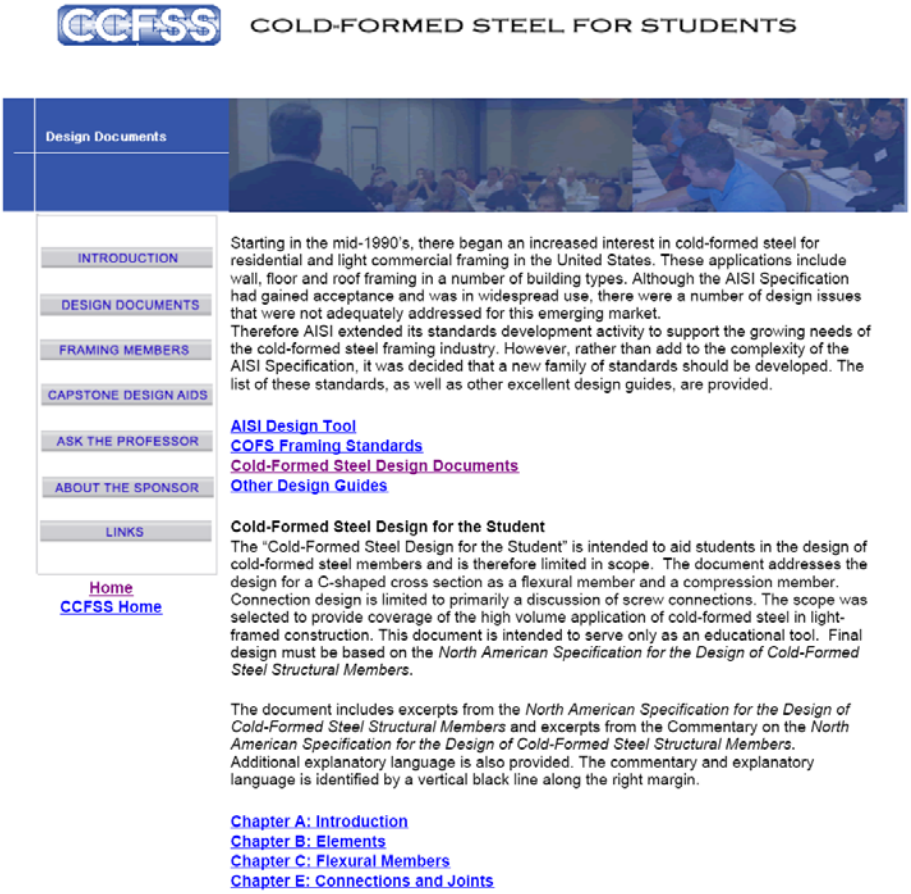

Figure 3 Design Documents Webpage

Figure 4 AISI Design Tool

Cold-Formed Steel Framing Standards. Clicking this tab will provide the user with a compilation of the following AISI framing standards.

- AISI S200-07, *North American Standard for Cold-Formed Steel Framing – General Provision* (2007), American Iron and Steel Institute
- AISI S201-07, *North American Standard for Cold-Formed Steel Framing – Product Data* (2007), American Iron and Steel Institute
- AISI S210-07, *North American Standard for Cold-Formed Steel Framing – Floor and Roof System Designs* (2007), American Iron and Steel Institute

- AISI S211-07, *North American Standard for Cold-Formed Steel Framing – Wall Stud Design* (2007), American Iron and Steel Institute
- AISI S212-07, *North American Standard for Cold-Formed Steel Framing – Header Design* (2007), American Iron and Steel Institute
- AISI S213-07, *North American Standard for Cold-Formed Steel Framing – Lateral Design* (2007), American Iron and Steel Institute
- AISI S214-07, *North American Standard for Cold-Formed Steel Framing – Truss Design* (2007), American Iron and Steel Institute
- *Standard for Cold-Formed Steel Framing – Code of Standard Practice* (2005), American Iron and Steel Institute

Cold-Formed Steel Design Documents. Listed on the website is the AISI design specification, AISI S100, as well as other design related documents.

Other Design Guides. For additional design guidance the student may refer to the following listed documents:

- *Cold-Formed Steel Framing Design Guide*, D110-07, (2007), American Iron and Steel Institute
- *Bracing Cold-Formed Steel Structures: A Design Guide* (2005), ASCE
- *Cold-Formed Steel Design* (2000), W. W. Yu, Wiley-Interscience

Cold-Formed Steel Design for the Student. The document "Cold-Formed Steel Design for the Student" is an abridged version of AISI S100 intended to aid the student in the design of cold-formed steel members and connections. The document is limited in scope

and addresses the fundamental design requirements for a C-shaped cross section used as a flexural member or a compression member. Connection design is limited to primarily a discussion of screw connections. The scope of this document was selected to provide coverage of the high volume application of cold-formed steel in light-framed construction. This document is intended to serve only as an educational tool. Final design must be based on the *North American Specification for the Design of Cold-Formed Steel Structural Members*.

The document includes excerpts from the *North American Specification for the Design of Cold-Formed Steel Structural Members* and excerpts from the *Commentary on the North American Specification for the Design of Cold-Formed Steel Structural Members*. Additional explanatory language is also provided. To distinguish the specification from the commentary, the commentary and explanatory language are identified by a vertical black line along the right margin.

Framing Members

The Framing Members tab provides a copy of AISI S201-07, *North American Standard for Cold-Formed Steel Framing – Product Data*. This document defines standardized light-steel framing profiles such as stud or joist, track furring channel, u-channel and angle.

Capstone Design Aids

Typically Civil and Architectural Engineering undergraduate programs do not teach courses on cold-formed steel design. But the students enrolled in a capstone design course often encounter the challenge of developing a design using cold-formed steel members. Senior capstone design courses attempt to introduce the student to the challenge of designing a complete project to include

main structural framing as well as curtain walls. The student thus will likely encounter cold-formed steel design when developing a design for a curtain wall.

To assist students with their design project, general information or rule of thumb information is provided such as:

- Rule number one when designing cold formed steel bearing walls:
  LINE UP THE WALLS.
  It is critical that cold formed steel bearing walls align vertically. If you are not able to vertically align the bearing walls then you should consider other framing schemes.
- Avoid welds in the field.
- PAF and screw connections are typically preferred by cold formed steel contractors. Be aware that these connectors have low allowable load capacities.
- 0.14" diameter is the preferred powder actuated fastener (PAF) size by most cold formed steel contractors.
- Identify shear wall locations and indicate main frame lateral forces to be accommodated in the shear wall design.
- Design the foundations at the shear wall anchorage. Provide enough dead load to resist uplifting force at each end of the shear wall

Also a comprehensive list of design office references is provided along with standard construction details, and available software as illustrated by Figure 5.

Figure 5 Capstone Design Aids

Also included in the list of design office references are websites for associations that represent cold-formed steel applications:

- American Iron and Steel Institute (AISI)
- Cold-Formed Steel Engineers Institute (CFSEI)
- Metal Building Manufactures Association (MBMA)
- Steel Deck Institute (SDI)
- Steel Stud Manufacturers Association (SSMA)
- Steel Framing Alliance (SFA)

Ask the Professor – Message Board

It is impossible for cold-formed steel organizations to provide comprehensive nationwide coverage of cold-formed steel design in seminars, short courses, conferences etc., however, the interaction

such seminars create can be partially re-created on the web through message boards and the like. Therefore the student website has a message board monitored by the CCFSS to provide interaction with the students. Thus, given the manner in which students of all ages consume information today, a web optimized resource has significant merit.

CONCLUSION

To better enlighten both undergraduate engineering college students and practicing engineers regarding the fundamentals and application of cold-formed steel, a student website has been developed. This development effort, the work of the Wei-Wen Yu Center for Cold-Formed Steel Structures (CCFSS), was motivated and encouraged by the Cold-Formed Steel Engineers Institute (CFSEI).

ACKNOWLEDGEMENTS

The authors value the guidance and encouragement provided by the AISI staff (Jay Larson) and CFSEI staff (Don Allen and Brian Berger). Thanks are also extended to Dr. Ben Schafer and his students at Johns Hopkins University for their review and comment during the development of the website. Review and comment provided by Missouri S&T students were helpful during the development and gratefully acknowledged.

Twentieth International Specialty Conference on Cold-Formed Steel Structures
St. Louis, Missouri, U.S.A., November 3 & 4, 2010

FRAME ANALYSIS AND DESIGN OF INDUSTRIAL COLD-FORMED STEEL RACKS

Teoman Peköz, PhD[1], Ali Karakaplan, Eng.Sc.D[2], Ali Koç[3],

Abstract

Industrial cold-formed steel racks have semi-rigid joints between the columns and beams. Frame analysis of such structures call for special considerations that are studied in this paper. The current design approach uses a linear idealization of the moment-rotation relation relationship based on an empirically decided secant to the nonlinear moment rotation curve.

This study presents a refined analytical approach to the analysis such frames using the state-of-art finite element based nonlinear analysis program LARSA 4D. Parametric studies are carried out to obtain an accurate design approach for using computer programs that treat linear moment-rotation relationships.

INTRODUCTION

Beams and columns of cold-formed steel industrial racks shown in Fig. 1 have mechanical connections. When loaded, the moment-rotation relationship at these joints is nonlinear. In this paper rotation is defined as the change in angle between a beam and a column. The Rack Manufacturers Institute Specification for The Design, Testing And Utilization Of Industrial Steel Storage Racks (to be referred to herein as the RMI Specification) [Rack Manufacturers Institute, 2010] idealizes the moment-rotation relationship as linear. The linearization obtained by taking a secant to the moment-rotation curve for all levels of loading can be quite inaccurate as will be shown in this paper. This study is aimed at exploring the accuracy of such approaches and reaching a more accurate basis for analysis.

[1] Professor Emeritus, Cornell University, Ithaca, NY USA
[2] President, LARSA, Inc, Melville, NY USA
[3] Director, Research, Development and Support, LARSA, Inc, Melville, NY USA

Fig. 1 Examples of Pallet Racks

MOMENT-ROTATION RELATIONSHIP

Moment-rotation relationship at the joint between the columns and the beams are determined by three different types of tests according to the RMI Specification. Each type is preferable depending on the information required. The three types of tests are:

- Portal test illustrated in Fig. 2 is stated in the RMI Specification to be appropriate for getting the moment-rotation behavior to evaluate the sidesway behavior and stability. This is a rather difficult test to run.

- Cantilever test illustrated in Fig. 3 is specified for determining the moment capacity and according to the RMI Specification Commentary rigidity of the connection. The rigidity obtained from this test is lower than that obtained by portal tests.

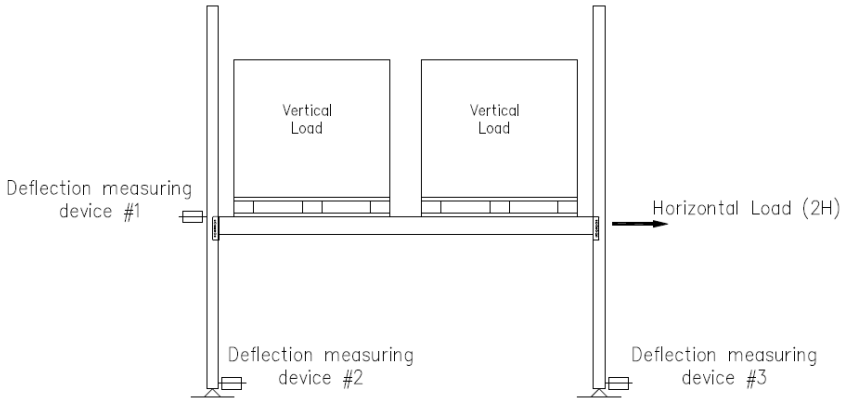

Fig. 2 Portal test Setup

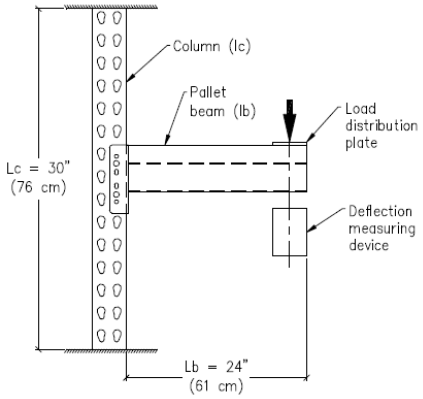

Fig. 3 Cantilever Test Setup

- Cyclic test illustrated in Fig. 4 is specified to determine the moment-rotation characteristics of the beam-to-column connections. This type of test is new in the RMI Specification and could be the most accurate type of testing to obtain moment-rotation relationship.

Since the objective of the study was to obtain a general approach, several moment-rotation relationships were used. The study covered a wide range of parameters, but this paper will demonstrate only one case. However, the conclusions were applicable to other cases studied as well.

The relationship between the moment and the angular change at a joint is not linear. The RMI Specification Commentary states that in evaluating cantilever tests it appears reasonable to use constant value, F for relating moment, M , to angular change, θ , between the members at a joint.

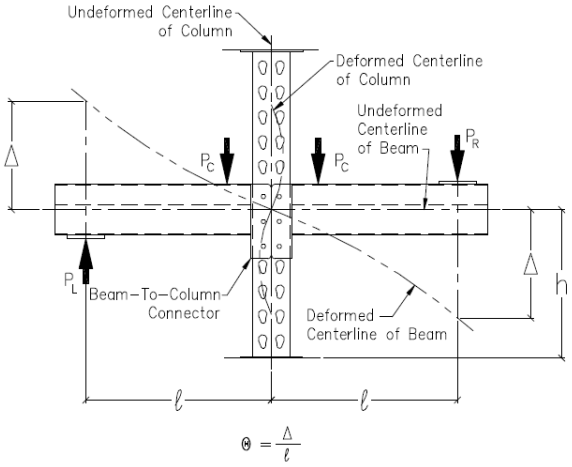

Fig.4 Cyclic test Setup

The value of M used for the determination of F is 85% of the ultimate moment, $M_{.85}$, and the value of θ is the rotation at $M_{.85}$. A reduction factor of 2/3 is applied to determine $F_{.85}$ the value of F to use in design of beams. No reduction factor is used for design of columns.

The RMI Specification states that “the portal test is to be performed when the value of F is be used to obtain a joint spring constant needed for a semi-rigid frame analysis”. In the portal test the tightening of the joint due to vertical loads in the actual rack is better represented. A reduction factor of 2/3 is applied to the value of F determined for design of beams as well as columns.

According to the RMI Specification “a horizontal force equal to the horizontal design load corresponding to the vertical load on the assembly shall be applied to the assembly, equally distributed between the two columns, at the level of the top of the beams, and in the direction of the beams. Deflection due to the horizontal loading shall be measured at the level of the top of the beams. The procedure shall be repeated at a load

twice the design load." To determine the design load one needs the spring constant F . To determine the load to apply in the portal frame test one needs the design load. The process is thus an iterative one.

The portal test is difficult to run and get consistent reproducible results. The cyclic load tests that is included in the 2010 edition of the RMI Specification appears to be the most reasonable test to obtain the spring constant F . There are many cycles of loading involved in this test procedure. Thus one has to select the most relevant stress cycle for the purpose of determining the spring constant F .

The possibility of using one value of F, for example, $F_{.85}$, for all load levels was studied and the results are discussed below.

TYPES OF RACKS AND LOADINGS STUDIED

Several numerical examples were studied to see the implications of using various ways of determining frame load carrying capacity. Two types of racks were studied as numerical examples. One was a rack having cold-formed steel members (designated CF Rack), the other was a rack having hot-rolled steel members. Only the results on CF rack will be discussed here.

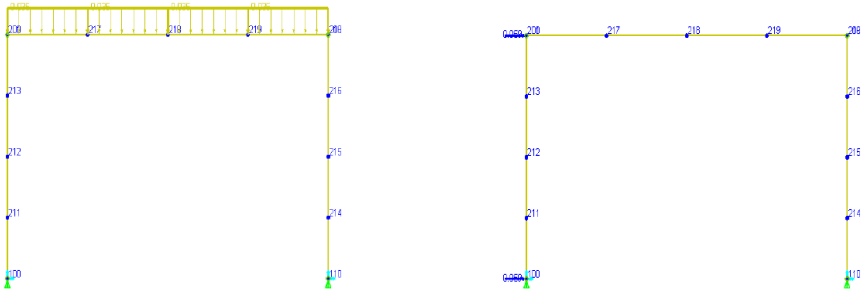

Fig. 5 Portal Frame Studied

Two rack frame configurations were studied. These were the portal frame shown in Fig. 5 and the multistory frame shown in Fig. 6. These figures are from the LARSA 4D Models which will be described below. Load cases and the node numbers are also shown on these figures.

The CF Rack members had the following properties:
Column $A_g = 0.936in^2$, $I_x = 1.27in^4$, $S_x = 0.8647in^3$, Beam
$A_g = 0.78in^2$, $I_x = 1.701in^4$.

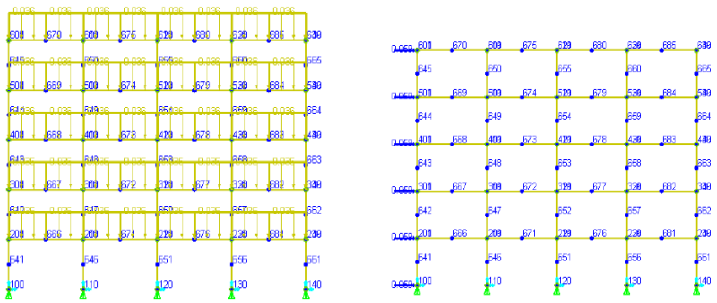

Fig. 6 Multi Story Frame Studied

Bending axis is the x axis of the members.

The beam center line to beam centerline dimension as well as the distance from the first level beam centerline to floor distance was 60 inches. Centerline to centerline dimension of columns was 99 inches.

Loading is applied as follows:

- Stage 1: Vertical load are applied in increments of 0.1 times the typical total factored load of 3.53 k per beam applied uniformly in 10 increments.

- Stage 2: While the total vertical load is on the rack, horizontal load is applied in increments of 0.1 times the vertical load divided by 240. The horizontal loads are applied up to 30 increments. The combination of the vertical load and horizontal load is intended to simulate earth quake loading. In the Tables the parameters are in general reported for the increment 10 of the horizontal loads since this corresponds to the intended design load.

The modulus of elasticity is reduced by 80 percent as required by the AISI Specification [American Iron and Steel Institute, 2007] to a value of 23,600 ksi for second order analysis.

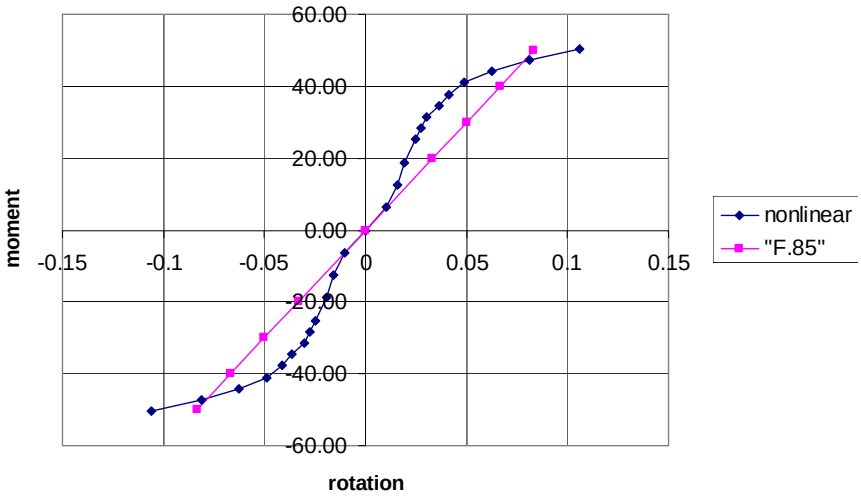

Fig. 7 Moment-Rotation curve for the CF steel rack studied

TYPES OF JOINT PROPERTIES STUDIED

Moment-rotation curve of the cold-formed steel rack joint was assumed to be as shown in Figs. 7 and 8. This curve was a modified version of a cantilever test result. A typical cantilever test result was made stiffer to

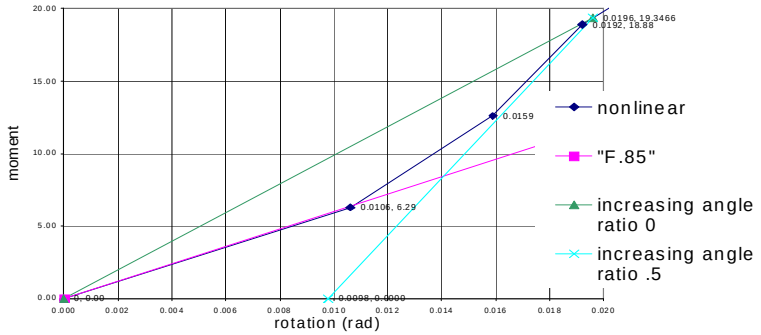

Fig. 8 Joint idealization

represent the tightening due to vertical loads. The line designated F.85 is a secant drawn from the origin to the nonlinear curve where the moment reaches 0.85 times the maximum value of the moment obtained in the test.

Cyclic testing data is shown for a series of tests in Fig. 9. The process of extraction of the moment-rotation curves to be used for semi-rigid frame analysis requires careful study.

Column base fixity was considered for two reduced values of 2,400 and 600 in-k/rad. In this paper the results for the former value are discussed.

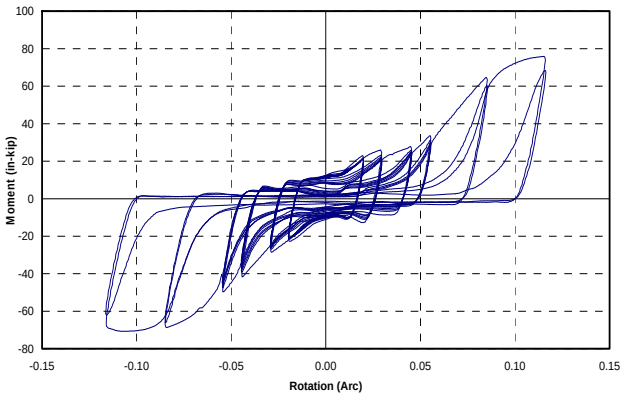

Fig. 9 Cyclic Test Results for a Rack Joint

ANALYSIS METHODS

Computer programs MASTAN and LARSA 4D were used for the analyses. MASTAN analyzes frames only with linear semi-rigid joints. As will be shown later this is a serious limitation for racks and the procedure developed here need to be used to apply to nonlinear semi-rigid joints. However, this procedure may lead to results that are quite conservative.

LARSA 4D is a state of the art finite element based nonlinear analysis program described at the site http://www.larsausa.com/ . This program was used for the parametric studies described in this report. This program enables the modeling of semi-rigid joints by true nonlinear springs characterized by moment-rotation values obtained by tests. This program also has a “staged construction” capability which makes it possible to change the spring properties between stages. As described in the next section this was used when the spring characteristics needed to be changed after vertical loads are applied and the application of horizontal loads starts. The loading in any stage can be applied incrementally. Increments are also referred to as Steps.

PORTAL FRAME ANALYSIS

First the portal frame shown in Fig. 5 was analyzed for the loads mentioned above. Deflected shapes of the frame are shown in Fig. 10. During the application of the vertical loads (gravity loads) the angle between the columns and the beam decreases. When the horizontal load is subsequently applied, the angle on the left side begins to increase and the angle on the right side continues to decrease. This is shown in Fig. 10 as well as the plot in Fig. 11.

For increasing rotations, the spring moment-rotation curve is nonlinear as seen in Fig. 7. Though the moment rotation curve for the increasing rotations is determined in the tests, the tests do not show exactly what the decreasing curve should be for an arbitrary point on the increasing rotation curve. For this study, it was assumed that the decreasing moment rotation relationship is linear. When the moment becomes zero, there could be a residual rotation as seen in Fig. 8. This residual rotation can be defined as a percentage of the rotation at which the rotation began to decrease. The percentage is designated “ratio”. If the “ratio” is zero then there is no residual rotation. If the “ratio” is 1.00 then the residual rotation is equal to the rotation at which rotation began to increase. This is illustrated in Fig. 8 for ratios equal to 0 and 0.5. Analyses were carried out for various values of “ratio”. Highest deflection and moment is obtained for “ratio”=0. Very significant decrease in deflections and moments were observed when nonlinear moment rotation relationships are used. Results are discussed more in detail for multistory frames, but the conclusions are valid for this portal frame as well.

MULTISTORY FRAME ANALYIS

The overall frame configuration and the deflected shapes of the multistory rack studied are shown in Fig. 11 for various stages of loading.
The spring rotations obtained by LARSA 4D are plotted in Fig. 12. It is seen that the rotations at these lateral loads are much smaller than the rotations corresponding to $F_{.85}$; namely when the moment is 85% of the

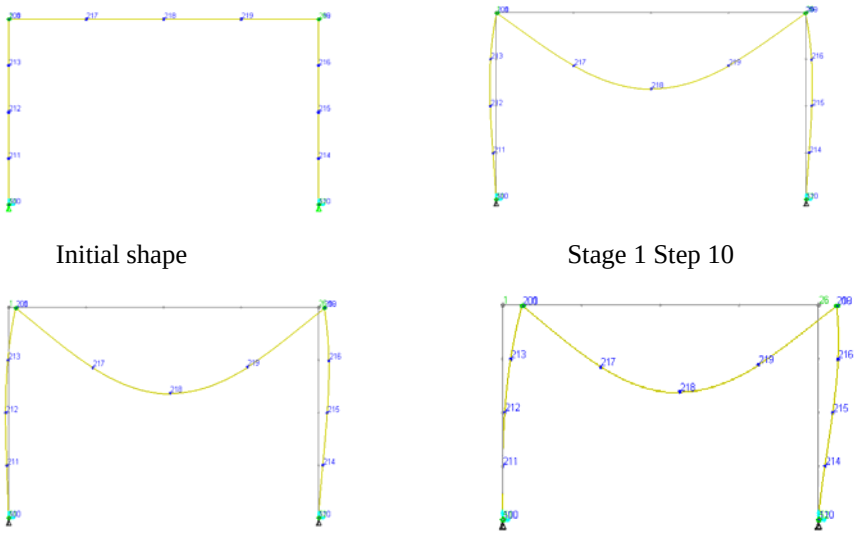

Initial shape | Stage 1 Step 10

Stage 2 Step 10 | Stage 2 Step 30

Fig. 10 Portal Frame deflected shapes

maximum moment obtained in a joint test. The rotation at each joint is different when the horizontal load is applied. Determining the rotations at all joints when the horizontal loads start to be applied is tedious but essential for the decreasing rotation behavior of each spring where the angle between the columns and beams starts to increase. The solution for this difficult task was made possible by a special macro prepared for LARSA 4D which determined the rotation at each joint on the left end of each beam when the horizontal load was applied. The macro also inserted a different linear spring value F for the moment-rotation for the left end of each beam.

For second order analysis the values of F as well as the column base fixity was reduced by a factor of 0.85 in as required by the AISI Specification [American Iron and Steel Institute, 2007].

The deflections and moments are obtained by LARSA 4D analysis are given in Table 1. Linear joint results by MASTAN analysis are given in Table 2.

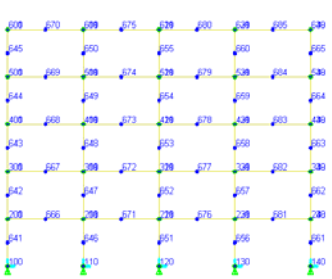

Initial shape

Stage 1 Step 10

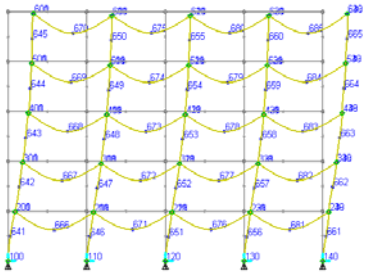

Stage 2 Step 10

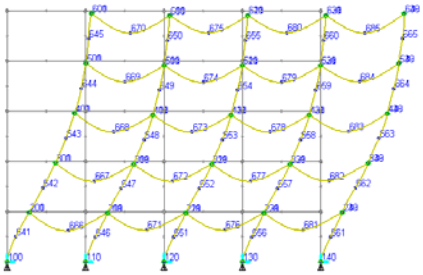

Stage 2 Step 30

Fig. 11 Multistory Rack Deflected Shapes

The following are some additional observations and conclusions based on the results:

- Assuming “ratio” = 0 gives more conservative results than assuming “ratio” greater than zero. Definition of “ratio” is given in previous section. Determining ratio or the exact shape of the reducing branch of the moment curve for all values of maximum moment experimentally is not practical or possible. It is certain that “ratio” should be greater than 0. For the sake of comparison, the numbers given below are based on “ratio”=0. Similar comparisons were made for other values of “ratio” and column base fixity.

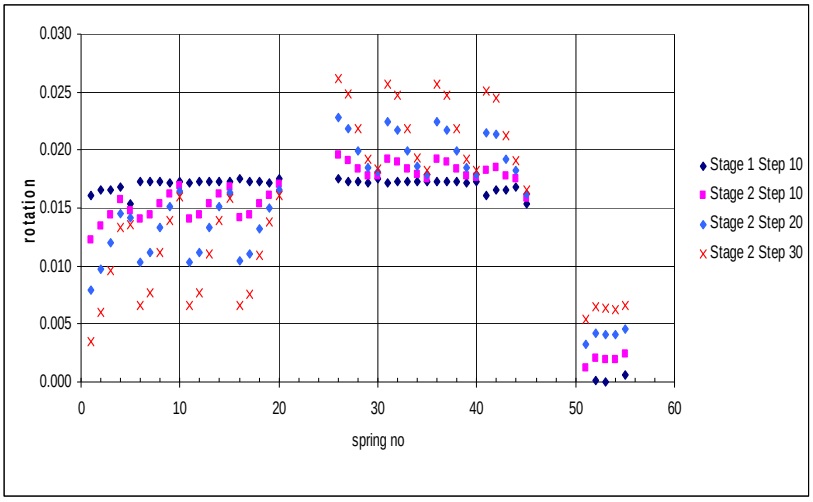

Fig. 12 Multistory Rack Spring Rotations

(Note: Springs 1 through 20 are on the right end of the beams where the rotation is increased with horizontal load. Springs 26 through 45 are on the left end of the beams where rotation is decreased with horizontal load. Springs 51 through 55 are column base springs)

- From Table 1, it is seen that assuming rigid joints in the analysis is grossly unconservative. A maximum horizontal deflection of 0.3768 in is determined for rigid frame compared to 1.005 in for the semi-rigid frame determined as explained in the Note 3 this Table.

- There are significant benefits of using the nonlinear joint characteristics of joints. For the maximum moment is 8.879 in-k for linear semi-rigid joints using $F_{.85}$ versus 4.912 in-k for non-linear semi-rigid joints with "ratio"= 0 and 3.801 in-k for "ratio"=0.8.

ratio	Deflection top beam	M_{max} 2nd column base	P_{max} 2nd column base	Note
Na	0.3768	3.100	18.13	6
Na	2.4239	8.879	17.79	1
Na	0.7811	4.291	17.75	2
0	1.0050	4.912	17.76	3
0	2.4697	9.004	17.70	4
0	1.2531	5.600	17.74	5
0.4	0.8240	4.386	17.76	3
0.8	0.6306	3.801	17.76	3

Note:

1 For linear left and right joints using F=750 ($F_{reduced}$=600k-in/rad)

2 For nonlinear both ends beams for vertical and horizontal loads

3 For nonlinear for vertical loads for both ends of beams
For horizontal loads applied subsequently, springs nonlinear for right end linear for left end

4 All Linear springs with right and left stiffer spring const 6.293/0.0106 (=593.68) . For these values see Fig. 8.

5 All linear springs with right and left stiffer spring const 18.88/0.0193 (978.24). For these values see Fig. 8.

6 Rigid joints by MASTAN Analysis

Na not applicable

Table 1 Multistory frame LARSA 4D analysis results

- The use of $F_{0.85}$ also gives very conservative results. For example a deflection of 2.424 in is obtained using $F_{0.85}$ versus 1.005 in using the nonlinear moment rotation curve.

$F_{.85}$	.8 $F_{.85}$	Horizontal Deflection at top beam level, in.	Maximum Column Moment, in-k.	Maximum Column axial Load, k.	Deflection at bottom beam level, in	Maximum Beam end Moment, in-k
rigid		0.377	3.074	18.13	0.124	
1200	960	1.278	5.688	17.74	0.327	19.67
1125	900	1.370	5.954	17.73	0.346	19.27
1000	800	1.574	6.536	17.72	0.387	18.59
875	700	1.883	7.406	17.71	0.448	17.92
750	600	2.408	8.861	17.71	0.551	17.36

Table 2 Multistory frame MASTAN analysis results

- The significant difference between using linear semi-rigid joints with $F_{0.85}$ and using the non-linear moment rotation relationship can be explained as follows: using $F_{0.85}$ assumes that the moments and rotations are much larger than the analysis would show. It can be seen in Fig. 7 that $F_{0.85}$ line crosses the nonlinear moment-rotation curve between a moment between 47.20-50.35 in-k and between a rotation between 0.0809-0.1062 rad. However the non-linear analysis with the non-linear moment rotation curves shows rotations plotted in Fig. 12 around 0.017 rad.

- The range of rotations and moments obtained by the nonlinear analysis with the nonlinear moment-rotation curves are shown in Fig. 7. In this range, it is interesting to see in Table 1 that the analyses carried out with linear joint rotation spring constant 18.88/0.0192 (Note 5 in the Table) give better results than $F_{0.85}$ or a spring constant 6.293/0.0106 (Note 4 in the Table). The slope of the moment-rotation curve to the left of 6.293/0.0106 is almost identical with the $F_{0.85}$ where as the slope to the left of 18.88/0.0192 is significantly different.

- These conclusions apply to other the moment-rotation curves used in this study. The results were sensitive to the shape of moment rotation curves. It is necessary to look at data for other joints before general conclusions are drawn.

- If the moments at the beam ends due to vertical loads are closer to the ultimate moments of the joints the benefits obtained by using an analysis that includes the nonlinearity of the joints may not be as large as demonstrated in this study.

A POSSIBLE DESIGN APPROACH

Analytically it is most accurate and proper to use a program such as LARSA 4D that accounts for nonlinear moment-rotation behavior of joints. The following is a conservative procedure to use a computer program as MASTAN which applies to frames with joints linear moment-rotation relationship:

- Based on the moment-rotation relationship draw a moment versus secant plot as shown in Fig. 13.

- Based on MASTAN analysis results given in Table 2, plot a maximum beam end moment versus 0.8 $F_{.85}$ as shown in Fig. 14.

- Based on MASTAN analysis results given in Table 2, plot a maximum column moment versus 0.8 $F_{.85}$ as shown in Fig. 15.

- Start the analysis of the frame by MASTAN using 0.8 $F_{.85}$. In the case of the frame being analyzed here for beam end fixity coefficient of 0.8 $F_{.85}$ = 600 in k/rad and determine maximum beam end moment anywhere in the frame. In the case of the frame being analyzed the maximum beam end moment is 17.36 in-k.

- The value of the secant to the moment-rotation curve at a moment of 17.36 is approximately 960 as seen in Fig. 13.

- Analyze the frame by MASTAN using a beam end fixity coefficient of 960.

- The maximum end moment obtained is about 19.67 in-k as seen in Table 2.

- Fig. 13 indicates that the secant value or the beam end fixity coefficient should be 900 thus the process has converged and the end moment is 19.27 in k.

- Determine maximum column moment anywhere in the frame for beam end fixity coefficient of 900 in-k/rad. This can be determined from Table 2 or plot of Fig. 15. The value of the maximum column moment is 5.964 in-k.

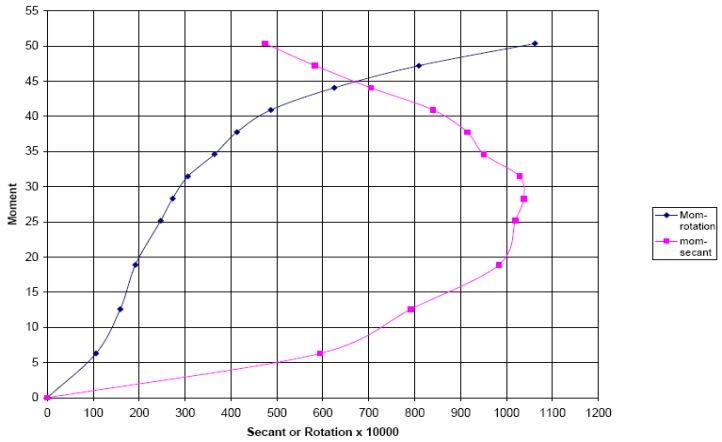

Fig. 13 Moment-rotation and moment-secant curves
Note: Moment-secant curve is based on the moment-rotation curve

- The value of the secant to the moment rotation curve at a moment of 8.861 is approximately 600 as seen in Fig. 14.

- Analyze the frame by MASTAN using a beam end fixity coefficient of 960. The maximum beam end moment obtained is about 19.27 in k

- Fig. 14 shows that the secant value or the beam end fixity coefficient should be 900 in-k/rad, thus the process has converged and the beam end moment is determined to be 19.27 in k and the maximum column moment is 5.964 in-k. These values are conservative compared to the maximum beam end moment of 17.76 in-k and maximum column moment 4.912 in-k by LARSA 4D analysis given in Table 1 with Note 2. The degree of conservatism for this example is 21.4% for the column moment and 8.5% for the column moment.

- It may be possible to reduce the degree of conservatism of the procedure above by taking other values of the moments rather than the maximums in the above procedure. This will be studied in future.

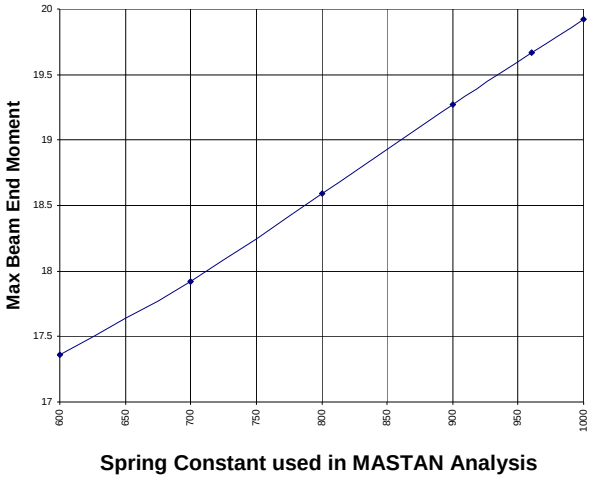

Fig. 14 Maximum beam end moment in the frame versus spring constant used in MASTAN analysis based on Table 2.

- Other moment rotation curves were tried and similar results were obtained.

CONCLUSIONS

A study of industrial rack frames with nonlinearly semi-rigid joints was carried out. The results show that care must be used to treat the moment-rotation relationship as linear. The LARSA 4D program was found to be particularly suitable to treat the nonlinear nature of the moment-rotation relationship of the joints. A procedure for using idealizing the joint moment-rotation relationship as linear was developed. This approach may be too conservative for certain range of parameters.

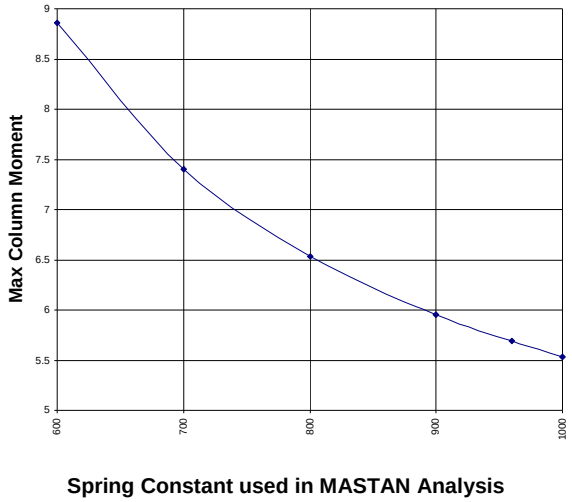

Fig. 15 Maximum column moment in the frame versus spring constant used in MASTAN analysis based on Table 2.

ACKNOWLEDGEMENTS

Support of the Rack Manufacturers Institute (RMI) and the help of John Nofsinger, Dan Clapp, James Crews and the entire RMI Specification Advisory Committee are gratefully acknowledged.

REFERENCES

American Iron and Steel Institute, 2007, AISI S100-2007 North American Specification for the Design of Cold-Formed Steel Structural Members, 2007

Rack Manufacturers Institute, 2010, MH16.1:2010. Specification for the Design, Testing and Utilization of Industrial Steel Storage Racks, 2010.

Twentieth International Specialty Conference on Cold-Formed Steel Structures
St. Louis, Missouri, U.S.A., November 3 & 4, 2010

Cross-aisle Shear Stiffness Tests on Rack Upright Frames

S.R. Sajja[1], R.G. Beale[2] and M.H.R. Godley[3]

Abstract

The US Rack Manufacturers Institution (RMI) code uses a theoretical formula derived by Timoshenko and the new Eurocode EN15512 requires testing. There is a considerable difference in the stiffness values determined by two approaches. This paper describes the experiments conducted on 80 full sized upright frames at Oxford Brookes University varying upright size, number of panels in the frame, aspect ratio of the panel (panel length/depth), restraints at the intermediate nodes of the frame, loading pattern, lacing pattern (channels back to back or front to front) and bolt tightness. The experimental data reported can be used in proposing revised design procedures.

1. Introduction

The cross-aisle shear stiffness of upright pallet rack frames is determined in Europe by testing using BS EN15512 (2009) whereas the US Rack Manufacturer's code (RMI, 2005) uses a theoretical method proposed by Timoshenko (Timoshenko and Gere, 1961). A pilot test program conducted at Oxford Brookes University by Chwan (2001) revealed that there was

[1] Senior Engineer, Amey, Lewes, East Sussex, UK
[2] Principal Lecturer, School of Technology, Oxford Brookes University, Oxford, UK
[3] Senior research Fellow, School of the Built Environment, Oxford Brookes University, Oxford, UK

considerable difference in the shear stiffness values obtained by the two methods, showing that the international codes for the evaluation of shear stiffness are not consistent and at least one not accurate. Chwan's tests were based on provisions of the code derived by the Federation Europeene de la Manutention (FEM 2000) which was used as the basis for BS EN 15512 (2009). A review of the literature (Rao et al 2004) indicated that the number of test results available was not enough to find the reasons for the difference in shear stiffness values determined by the two methods. Hence, a detailed experimental study was undertaken to identify the factors affecting the shear stiffness, which could be used for developing accurate and more rational design method. The test data were also used as a basis for generating numerical models using LUSAS that helped to quantify the affect of various parameters.

In the test program, experiments were conducted on full sized upright frames. In a preliminary study, three tests were carried out to check the repeatability of experiments and to confirm earlier findings from Chwan. Later a detailed test program was designed by varying the following parameters: upright size, number of panels in the frame, aspect ratio of the panel (panel length/depth), restraints at intermediate nodes of the frame, loading pattern and the lacing pattern (channels back-to-back or lip-to-lip). The affect of bolt tightness was also studied. In total, 80 tests were conducted at the detailed stage.

2. Shear Stiffness Tests

The test program was aimed at the following objectives and scope:

- To confirm the findings from previous research.
- To find the effect of the number of panels in the frame or length of upright, the aspect ratio of the panels, the boundary conditions and the influence of half-panels, on the shear stiffness of upright frames.
- To study the connection behaviour.
- To study the behaviour of different types of lacing patterns.
- To generate more experimental data that can be used in proposing a rational design method for industry practice.

3. Test specimens

Tests were conducted on full sized upright frames made of cold formed steel sections conforming to BS EN 10147 (2000). The uprights were open perforated lipped channels with additional bends and the bracing members were lipped channels. Typical upright and bracing members used in testing are shown in Fig.1.

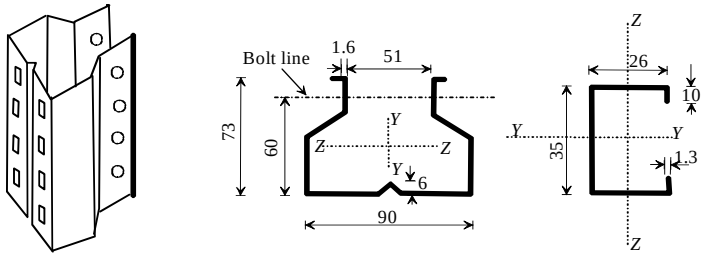

Fig.1: Upright and bracing layout

In the experimental programme, two different sizes of uprights and bracing members were used; one in the preliminary study (Series 1) and the other in the extended series (Series 2) of tests. Cross-sectional properties of upright and bracing members that were used for testing are presented in Table 1. 1.8 mm thick bracing members were used in series 1 tests, whereas 1.5 mm thick bracing members were used in series 2 tests. In Table 1, G_Y is the distance of the centroid of the upright from its back face centre line. The upright frames used in testing varied in size as the number of panels and aspect ratio of the panels (panel length/depth) were changed. The panel length (i.e. centre-to-centre distance between joints, where diagonals intersect) was kept as 1200mm and the depth of the frame varied from 605mm to 1050mm leading to panel aspect ratios ranging from 1.14 to 1.98. The test frames were 1200mm to 3600mm long with 1, 1.5, 2, 2.5 and 3 panels.

Table 1: Sectional properties of upright and bracing members

Member	**Series**	**Net Area (mm^2)**	**Second Moment of Area (mm^4)**		**Centroid (mm)**	**Torsion constant (mm^4)**
			I_Y	I_Z	G_Y	J
Upright	1	324.0	372205	163060	22.91	294
	2	788.9	522444	1.02×10^9	33.96	2062
Bracing member	1	167.1	30879	14307	9.73	180
	2	139.5	27187	10923	8.87	105

The lacing patterns of the frames used in the testing were single layer diagonal, X and N. As the lacing members in the frames were channels, they can either be connected lip-to-lip or back-to-back to the uprights. Frames with both these connection patterns were studied even though a lip-to-lip lacing pattern is not now used commonly in the industry. This pattern was chosen to enhance eccentricity effects.

The test layout and arrangement of displacement transducers (LVDTs) are shown schematically in Fig. 2 and a typical arrangement of a frame under test at Oxford Brookes University laboratory can be seen in Fig. 3.

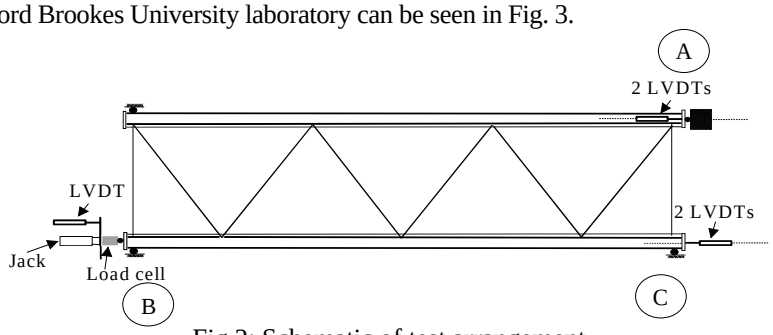

Fig.2: Schematic of test arrangement

Fig. 3: Frame under test

The positions of the rollers were adjusted so that the frame just fitted snugly between them with no looseness. The roller condition at the nodes was achieved by putting two PVC sheets in between the uprights and packing the test rig. This arrangement led to an upright frame with restraints at all nodes (RAN) and satisfied the FEM code provisions (FEM, 2000). But in practice, cross-aisle frames have limited restraint from beams. Hence frames were also tested with only corner restraints (OCR) to reflect actual conditions of the frames during their usage.

The pinned support achieved at point A in the frame (Fig. 2), by using ball type arrangement, restrained all three translational displacements but allowed upright sections to rotate freely in all three directions. The FEM code procedure assumed that the out-of-plane rotation of the frame would be negligible and hence would not affect the shear stiffness in the cross-aisle direction. However, there might have been some movement at the support under the application of load. Therefore, two displacement transducers were placed at A in the direction of the upright to determine any movement of the support. The load was applied

along the centroid of the other leg, at point B in Fig. 2. A load cell of 6 kN capacity was connected to a 230 kN jack and an LVDT was placed there to control the loading. Load was applied gradually using the jack at the rate of 0.1 kN/sec. The maximum load applied in the test was kept low (approximately 5 kN) so that there was no visible damage to the specimens. After reaching the maximum load, the frames were unloaded to approximately 0.5 kN. The frames were reloaded and unloaded between loads 0.5 kN and 5 kN for 5 to 6 cycles in each test. This was carried out to avoid any error in evaluating shear stiffness due to bolt slip at the joints connecting diagonal bracing members and upright sections. Two LVDTs were placed at point C as shown in Fig. 2 to measure the displacement of the loaded upright along its own axis. LVDTs were placed at bottom and top of the upright base plate to measure any difference in displacements. In some of the tests LVDTs were also placed at the four corners of the frame to measure any horizontal movement of the frame and also to capture out-of-plane deformations of uprights, if any. The data obtained was used to plot a load-deformation curve and then to calculate the shear stiffness of the frame.

The load – displacement curves of upright frames in shear stiffness testing have two slopes (k_{ti}); one during initial loading (0 – 5 kN, *OP* portion in the graph) and the other during remaining cycles. The slope for the second portion was obtained by fitting a linear trend line to the cyclic loading applied in the test omitting the first cycle.

For example, in the case of the graph shown in Fig. 4, the slope of line *OP* is 1.49 and the slope of trend line is 6.14. The difference in the slopes is about four in the chosen test and can be attributed to initial settlement, bedding of the joints and bolt slip during the first cycle of loading. The slope of *OP* yields conservative results and was recommended by the FEM code for shear stiffness calculation. But, the slope of *OP* depends on the looseness of joint, which was considered in the paper by Godley and Beale (2008). Hence, the data from initial loading was omitted hereafter. The slope was calculated from trend line. In this case, the slope of trend line is 6.14 and hence k_{ti} is 6.14. Note that the shear stiffness is often influenced by joint looseness.

After getting k_{ti} values from graphs, shear stiffness values can be easily determined using equation 1

$$S_{ti} = k_{ti} D^2 / H \tag{1}$$

For the case considered, the length of the frame (*H*) was 3600 mm and the distance between the centroidal axes of the upright sections (*D*) was 1050 mm. Hence, the experimental shear stiffness value for this case is 1880 kN. Once the procedure for testing and derivation of results was established, tests were carried out to confirm findings of earlier research and to fill gaps in the research, by varying the different parameters mentioned earlier. Results of these tests are given in Table 2 and discussed below.

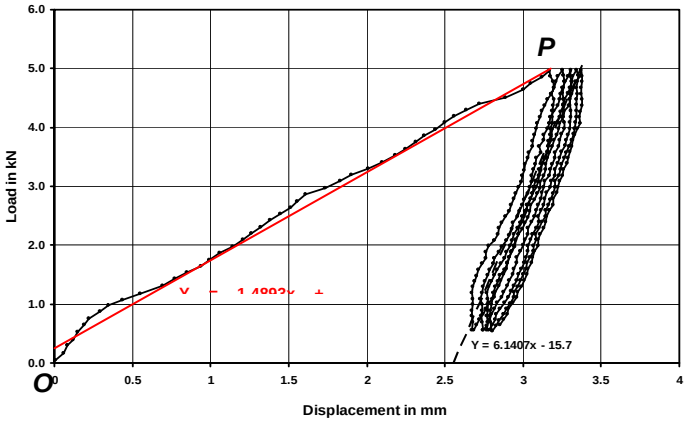

Fig. 4: A typical load-deformation curve

The mean value of the three frames tested in the preliminary study was 1808 kN. The results suggest that the repeated tests will yield results within 10% range from the mean value. Results from testing are compared against the RMI values (calculated based on Timoshenko's theory) and it can be noticed that the RMI values are approximately eight times higher than the test values.

4. Test results

4.1 Effect of lacing pattern or eccentricity

In Europe, cross-aisle frames are constructed by bolting bracing sections to uprights. Generally, channel sections are used as bracing members no consideration is given to the way they connect i.e. lip-to-lip or back-to-back. However tests show that frames with a back-to-back bracing pattern have almost double the stiffness values compared to similar size lip-to-lip panel frames due to the larger eccentricity in load transfer between upright members and bracing sections.

Hence, this factor was considered and both lacing patterns were tested. Fig. 5 shows the two configurations. In the results in Table 2, for frames restrained at corners only for size 1 frames (centre-centre distance of 1032 mm) the mean stiffness for the back-to-back configuration was 1718 kN and for the front-to-front case was 644 kN.

Table 2: Geometric properties and test results of the upright frames tested

Reference to Experiments	Panel Depth (mm) c/c	Length of frame (mm)	No. of Panels	Bracing Pattern	Support conditions	Test Stiffness (kN)	RMI stiffness (kN)	Comments
Prelim-inary Study	1050	3600	3	B/B	RAN	1881	14070	Hi - Lo Frames Repea-tability
	1050	3600	3	B/B	RAN	1606	14070	
	1050	3600	3	B/B	RAN	1937	14070	
Single Layer Diagonal Bracing	1032	3600	3	F/F	OCR	963	11005	Horizontal displa-cement
	1032	3600	3	F/F	RAN	1210	11005	
	1032	3600	3	B/B	OCR	1566	11005	
	1032	3600	3	B/B	RAN	1683	11005	
Tests for Bolt Loose-ness (Single Layer Diagonal Bracing)	1032	3600	3	F/F	RAN	643	11005	Torque = 20Nm
	1032	3600	3	F/F	OCR	554	11005	
	1032	3600	3	F/F	OCR	263	11005	Torque = 10Nm
	1032	3600	3	F/F	RAN	387	11005	
	1032	3600	3	F/F	OCR	589	11005	Torque = 15Nm
	1032	3600	3	F/F	RAN	702	11005	
	1032	3600	3	F/F	RAN	363	11005	Torque = 5Nm
	1032	3600	3	F/F	OCR	294	11005	
	1032	3600	3	F/F	RAN	589	11005	Torque = 12.5Nm
	1032	3600	3	F/F	OCR	409	11005	
	1032	3600	3	F/F	RAN	1043	11005	Torque =17.5Nm
	1032	3600	3	F/F	OCR	674	11005	
Size 2 (Single Layer Diagonal Bracing)	902	3600	3	B/B	OCR	1974	11248	
	902	3600	3	B/B	RAN	2790	11248	
	902	3600	3	F/F	OCR	896	11248	
	902	3600	3	F/F	RAN	1204	11248	
	902	3000	2.5	F/F	OCR	624	11248	
	902	3000	2.5	F/F	RAN	949	11248	
	902	3000	2.5	B/B	RAN	1143	11248	
	902	3000	2.5	B/B	OCR	1003	11248	
Size 1 (Single Layer Diagonal Bracing)	1032	3000	2.5	B/B	RAN	1255	11005	
	1032	3000	2.5	B/B	OCR	1179	11005	
	1032	3000	2.5	F/F	RAN	887	11005	
	1032	3000	2.5	F/F	OCR	667	11005	
	1032	2400	2	B/B	RAN	1585	11005	
	1032	2400	2	B/B	OCR	1192	11005	

Reference to Experiments	Panel Depth (mm) c/c	Length of frame (mm)	No. of Panels	Bracing Pattern	Support conditions	Test Stiffness (kN)	RMI stiffness (kN)	Comments
	1032	2400	2	F/F	OCR	623	11005	
Size 2	902	2400	2	B/B	OCR	1653	11248	
	902	2400	2	B/B	RAN	1011	11248	
	1032	2400	2	F/F	RAN	754	11005	
Size 2	902	2400	2	F/F	OCR	761	11248	
	902	2400	2		RAN	874	11248	
Size 1, 1.5 Panel Frame	1032	1800	1.5	B/B	OCR	1339	11005	
	1032	1800	1.5	B/B	RAN	2600	11005	
	1032	1800	1.5	F/F	OCR	425	11005	
	1032	1800	1.5	F/F	RAN	580	11005	
Size 2 (Single Layer Diagonal Bracing)	902	1800	1.5	F/F	OCR	741	11248	
	902	1800	1.5	F/F	RAN	847	11248	
	902	1800	1.5	B/B	OCR	1007	11248	
	902	1800	1.5	B/B	RAN	1175	11248	
	902	1200	1	B/B	OCR	1264	11248	
	902	1200	1	B/B	RAN	1286	11248	
Size 1, 1 Panel Frame	1032	1200	1	B/B	OCR	1223	11005	
	1032	1200	1	B/B	RAN	1272	11005	
Size 2	902	1200	1	F/F	OCR	601	11248	
	902	1200	1	F/F	RAN	545	11248	
Size 1, 1 Panel Frame	1032	1200	1	F/F	OCR	762	11005	
	1032	1200	1	F/F	RAN	578	11005	
Loading Pattern tests	1032	1200	1	F/F	OCR	461	11005	Load Pattern 1
	1032	1200	1	B/B	OCR	1207	11005	
	1032	1200	1	B/B	OCR	1279	11005	Load Pattern 2
	1032	1200	1	F/F	OCR	799	11005	
Tests for Joint rotation	1032	1200	1	F/F	OCR	Not measured	11005	distortion of joint studied
	1032	1200	1	B/B	OCR		11005	
	1032	1200	1	B/B	OCR		11005	
	1032	1200	1	F/F	OCR		11005	
X bracing Frames	1032	1200	1	B/B	OCR	1207	11005	
	1032	1200	1	F/F	OCR	976	11005	
N bracing Frames	1032	1200	1	F/F	OCR	683	11000	Loading Pattern 2
	1032	1200	1	B/B	OCR	976	11000	

Reference to Experiments	Panel Depth (mm) c/c	Length of frame (mm)	No. of Panels	Bracing Pattern	Support conditions	Test Stiffness (kN)	RMI stiffness (kN)	Comments
	1032	1200	1	B/B	OCR	1029	11000	Loading Pattern 1
	1032	1200	1	F/F	OCR	692	11000	
Single Layer Diagonal Bracing	1032	3600	3	F/F	OCR	434	11005	Loading Pattern 2
	1032	3600	3	F/F	OCR	443	11005	
	1032	3600	3	F/F	OCR	508	11005	Repeatab-ility of
	1032	3600	3	B/B	OCR	730	11005	Loading
	1032	3600	3	B/B	OCR	757	11005	Pattern 2
	1032	3600	3	B/B	OCR	723	11005	Repeatab-ility
Size 3 (Single Layer Diagonal Bracing)	1032	3600	3	F/F	OCR	582	11005	Loading Pattern 1
	1032	3600	3	B/B	OCR	897	11005	
	605	3600	3	F/F	OCR	390	10400	
	605	3600	3	B/B	OCR	373	10400	

Notes: B/B = Back-to-Back bracing pattern; F/F = Front-to-Front or Lip-to-Lip bracing pattern; OCR = Only Corner Restraints; and RAN = Restraints at All Nodes

For the size 2 frames (centre-centre distance of 902 mm) the corresponding mean values were 1380 kN for the back-to-back case and 725 kN for the lip-to-lip case. Hence the authors' recommendation is that all rack frames should be constructed with faces in the back-to-back configuration.

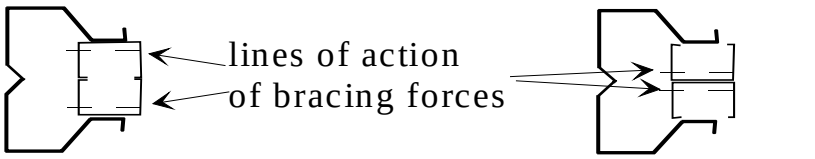

(a) 2 lipped channels face-to-face

(b) 2 lipped channels back-to-back

Fig. 5: Bracing configurations

4.2 Effect of external restraints at joint (RAN vs OCR)

The experimental study was started with conducting tests on frames with both external support conditions i.e. restraints at all the nodes (intersection of bracing members and upright sections and with supports at corner nodes only.

The restraints at the nodes were achieved by placing PVC sheets between upright section and either the testing frame or packing. Two PVC sheets were used at each location to simulate roller behavior at the joints. As can be seen from Table 2, shear stiffness values for frames with restraints at all nodes were higher than the shear stiffness values for frames with restraints at corner nodes only. The variability in the two values ranges from 10 to 50%.

The external supports were achieved with the help of packing where the amount of fixity was not quantified. This resulted in uncontrolled and additional frictional resistance on the test frames and thus in larger stiffness values for frames with restraints at all nodes compared to the frames with only corner restraints. Therefore, in 2004 (Ra et al, 2004) the authors recommended that shear stiffness tests be carried out with only corner restraints (OCR). This recommendation has been included in the Eurocode (BS EN 15512, 2009). The assumption may be conservative as there will be some amount of restraint from the down-aisle beams. However the results will be consistent and indeterminate stiffness will not be introduced.

4.3 Effect of bolt torque

In the experimental program, tests were carried out to find the significance of bolt tightness (connection between bracing members and uprights) on shear stiffness of upright frames.

It was concluded from the experimental results (Tests 12-23) that a bolt torque above 12.5 Nm would produce consistent results for the specimens tested. Hence, a bolt torque of 15 Nm was used in all further experiments. Further details of these tests are given in Rao et al (2004). The authors also recommend that when testing frames preliminary bolt tightness tests be undertaken to ensure consistency of results.

4.4 Effect of horizontal movements

The test frames were supported at nodes. However there is a possibility of frames undergoing rigid body motion due to looseness in the test set up. This could influence shear deformations and hence the effect has been studied to measure the difference in shear stiffness values. The horizontal displacements were measured by placing LVDTs parallel to the frame at the four corners as shown in Fig. 6. The change in displacements measured at the free end of the

loaded upright can be either additive or subtractive depending upon the rotation of the frame. If the frame rotates anti-clockwise as shown in Fig. 6 the difference to be subtracted from actual measurements at the free end or vice versa.

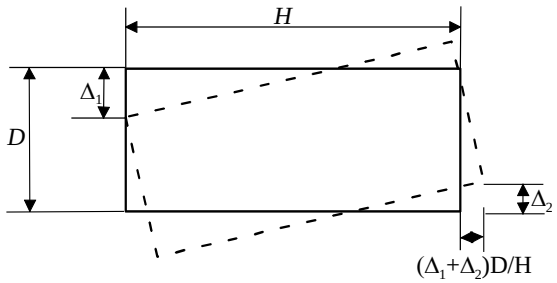

Fig. 6: Schematic showing rigid body motion of the frame

The results were sensitive to rigid body rotation. For example, a 3-panel back-to-back braced frame with centre-to-centre distance of uprights of 902 mm (3PBS2OCR) had a slope without considering horizontal displacements of 8.33 resulting in a shear stiffness value of 1882 kN. But the slope of the curve when the contribution to the total longitudinal displacement due to rigid body rotation was subtracted was 8.73, which resulted in shear stiffness value of 1974 kN. The error in estimate of shear stiffness due to neglecting rigid body rotation in this case was approximately 5%. Variations from other experiments where horizontal displacements were measured were approximately 5 – 15 %. However the horizontal displacements were not measured in some of the experiments as the number of LVDTs was limited in the laboratory. In these cases a correction of 10% was applied to the test results.

4.5 Effect of aspect ratio of frame

In Timoshenko's theory shear stiffness is influenced by the aspect ratio (defined as the ratio of the total length of the panels to the centre-to-centre distance of uprights) of the panel and remains constant irrespective of the length of the frame. Tests were carried out to check if there was any variation in the results.

The aspect ratio of the frame increases as the number of panels increases for a given depth and hence this effect was studied in terms of number of panels. As it had been previously concluded that frames with restraints at all nodes resulted in inconsistent high values (see section 4.2), test results with only corner restraints were used for comparison. The general trend noted was that shear stiffness values increased with increased length of the frame. This could be due to reduced impact of local effects. However the test results for the half panel cases appear anomalous.

At the time of testing the effect of the asymmetry of the half panel configuration was unknown and hence further tests were carried out to study this effect by loading the frame in two alternative patterns, which is discussed in the next section.

4.6 Effect of loading pattern

Diagonal bracing in the frames results in unsymmetrical frames. For example, a one panel frame can be loaded in two different patterns. In one case, the diagonal and upright meet at the loading point (loading pattern 1) and in other case the diagonal member will not be there (loading pattern 2), which will influence load transfer in the frames leading to a variation in shear deformations. The internal force distribution and reactions are shown in Fig. 7. Note that the restraints used at the load point and at the two corner nodes not loaded with horizontal restraint can only take compressive loadings into the restraint. Tensile reactions were not supported by the restraint applied. This effect has been studied on one panel and three panel frames with only corner restraints.

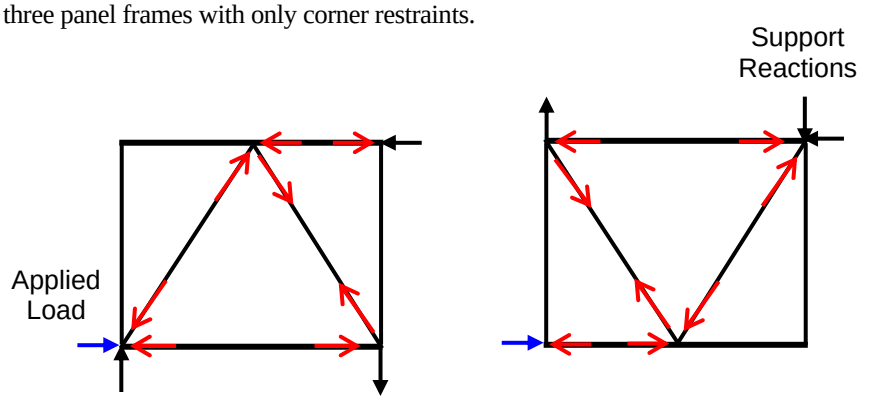

Fig. 7: Force distribution

The shear stiffness values determined by tests with load pattern 2 were consistently larger than the load pattern 1 test results. The difference becomes less important when number of panels in frames is high. But normally frames consisting of 2.5 to 3 panels only will be tested due to costs and difficulties involved with large frames. There are considerable differences in the load distributions between frames with panels with a whole number of panels and those with frames with half panels at one end. Hence care should be taken while testing frames for shear stiffness and both load patterns must be tested or full cyclic loading used. It is recommended that if the difference between the two values is not more than 10%

then the average of the two values can be taken as shear stiffness. Otherwise the lowest value should be taken as the shear stiffness of the frame.

4.7 Effect of bracing shape

Three different bracing shapes i.e. X – bracing, diagonal bracing and N – bracing, were tested. These tests were carried out to compare test results with different formulae proposed by Timoshenko. These are shown in Fig. 7.

(a) Diagonal bracing

(b) X bracing

(c) N bracing

Figure 7: Bracing configurations

Different brace shapes were treated by the ratios of their areas of the cross-sections of the bracing sections and to that of the upright in one panel. Note that in these ratios the area of the bracing at the end of each frame was not considered. These ratios give an indication of the material used per panel and the corresponding shear stiffness values. Hence, bracing values for the frames were 0.35 (diagonal bracing) and 0.70 (for both X – bracing and N - bracing). The results of tests carried out on X-braced frames and on N – braced frames of depth 1032mm test

68-73) are given in Table 2. Note that these tests were carried out on single panel frames. The results presented in Table 2 clearly demonstrate that N – braced frames are not efficient in resisting shear for given material. Theoretically X – braced frames should have double the shear stiffness values to diagonal braced frames but this was not observed in practice.

5 Conclusions

Based on the test results, the following can be concluded:

- Test results do not compare with theoretical values of Timoshenko (1961) and they differ by between 5 to 25 times.
- Frames with a back-to-back bracing pattern have almost double the stiffness values compared to similar size lip-to-lip panel frames. It is due to the larger eccentricity in load transfer between upright members and bracing sections.
- Frames with external supports at all the nodes produced larger stiffness values compared to the frames with only corner restraints. However these are not consistent and do not represent true behavior.
- Frames with an N-bracing configuration are inefficient and do not have any better performance than a diagonally braced frame of the same dimensions.
- Shear stiffness values of the same frames were also affected by loading arrangement during testing and hence full cyclic loading through zero should be undertaken to get representative values.

References

BS EN10147, (2000), *Continuously hot-dip zinc coated structural steels strip and sheet. Technical delivery conditions*, British Standards Institute, London.

BS EN 15512 (2009), *Steel Static Storage Systems – Adjustable pallet racking systems – Principles for Structural Design*, British Standards Institute, London.

Chwan K, (2001), *Investigations into the Shear Stiffness of Pallet Rack Uprights*, BEng. Thesis, School of Architecture, Oxford Brookes University.

FEM 10.2.02 (2000), T*he Design of Steel Pallet Racking*, Section X of the Equipement et Proceeds de Stockage, Federation Europeénne de la Manutention.

Godley, M H R, Beale, R G, (2008), Investigation of the effects of looseness of bracing components in the cross-aisle direction on the ultimate load-carrying capacity of pallet rack frames, *Thin-walled Structures*, 46 (7-9), 848-854.

Rao S S, Beale R G, Godley M H R, (2004), Shear stiffness of pallet rack upright frames. *Proceedings of 17th International Specialty Conference on Cold-formed Steel Structures*, Orlando, USA, 295–311.

RMI (2005), The Rack Manufacturers' Institute: *Specification for the design, testing and utilisation of industrial steel storage racks*.

Sajja S R, Beale R G, Godley M H R, (2008), Shear stiffness of pallet rack upright frames, *Journal of Constructional Steel Research*, 64, 867–874.

Timoshenko, S P, Gere J M, (1961), *Theory of Elastic Stability*, 2nd Edition, McGraw-Hill Book Company Inc., New York.

Appendix: notation

D	Distance between centroidal axes of the uprights
G_y	Distance of centroid of upright from back face centre line
H	Length of frame
I_y	Moment of inertia of upright about minor axis
I_z	Moment of inertia of upright about major axis
J	Torsion constant
OCR	Restraints applied at corner nodes only
RAN	Restraints applied at all nodes
S_{ti}	Shear stiffness of frame
YY	Principal major bending axes of sections
ZZ	Principal minor bending axes of sections
k_{ti}	Slope of regression line (Load against displacement)
Δ_1	Horizontal displacement of frame in the cross-aisle direction at one end of frame
Δ_2	Horizontal displacement of frame in the cross-aisle direction at the other end of frame

Twentieth International Specialty Conference on Cold-Formed Steel Structures
St. Louis, Missouri, U.S.A., November 3 & 4, 2010

Experimental Evaluation of a Vehicular Access Door Subjected to Hurricane Force Wind Pressures

Tian Gao[1] , Cristopher D. Moen [2]

Abstract

This paper describes an experimental study of a rolling sheet door under uniform positive and negative pressure, i.e. wind pushing the door into the building and wind suction pulling the door out of the building. Rolling sheet vehicular access doors are a commonly provided feature in metal building systems. The edges of the door slide freely during regular usage in tracks connected to cold-formed steel jambs. During an extreme wind event, the door engages the jambs with wind locks distributed along both vertical edges of the door to prevent excessive out-of-plane deformation. The goal of the study was to measure the forces in the wind locks and evaluate the performance of the door curtain and cold-formed steel door jambs. Axial and bending stresses in the wind locks, door curtain out-of-plane deflections, and jamb deflections were simultaneously measured using strain gauges and position transducers. The relationship between curtain deflection and wind lock forces was observed to be nonlinear and dependent upon the stiffness of the cold-formed steel jambs. The experimental observations are being used to develop and validate engineering expressions for predicting wind lock and door jamb design forces in rolling sheet vehicular access door systems.

Introduction

Vehicular access doors are a commonly provided feature in metal building system applications. The most popular type of door is a rolling sheet door (Figure 1a), where a cold-formed steel curtain spans between a door frame constructed of structural steel and\or cold-formed steel components. Steel

[1] Graduate Research Asst, Virginia Tech, Blacksburg, VA, 24061, USA. (gaot@vt.edu)
[2] Assistant Professor, Virginia Tech, Blacksburg, VA, 24061, USA. (cmoen@vt.edu)

restraints, called wind locks because of their ability to engage with the door frame in the case of a wind event, are riveted to the vertical edges of the curtain. The wind locks are free to move up and down under typical service conditions within a cold-formed steel guide attached to the door frame (Figure 1b). During an extreme wind event the wind locks engage with a wind bar, also attached to the door jambs, preventing excessive out-of-plane deformation through a combination of metal-on-metal friction and the support provided by the door jamb.

(a)  (b) 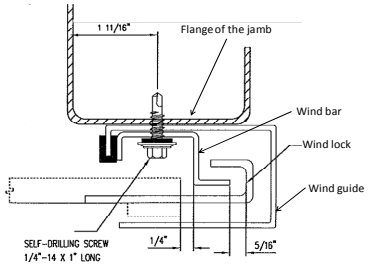

Figure 1 (a) Steel curtain rolling sheet door (view from the inside of a building) and (b) typical details for a rolling sheet door provided with wind locks

The demand forces that develop in the wind lock, typically referred to as catenary forces in industry, are difficult to predict because of the complicated support conditions at the door-frame interface and the changing geometry of the steel curtain as the wind pressure is applied. For a stiffer door frame with masonry walls serving as jambs, the out-of-plane sheeting deformation will be small and the catenary design forces will be high, resulting in the potential for a connection failure at the wind lock or wind bar location. With a more flexible cold-formed steel door jamb, the catenary design forces will be lower but the out-of-plane deformation of the door will be larger, resulting in a potential failure mode where the wind locks slip off the wind bar.

The experimental study described herein was jointly sponsored by the Metal Building Manufacturers Association (MBMA) to study the behavior of a typical rolling sheet vehicular access door under a hurricane force wind pressure. The objectives were to quantify the structural behavior of a rolling sheet vehicular access door and the attached frame under both positive pressure (pushing the door into the building) and negative pressure (suction pulling the door away from the building), including the direct measurement of the catenary forces in the wind locks with strain gauges. The results will be used to improve existing design methods for a rolling sheet vehicular access door and supporting frame.

Rolling Sheet Doors Dimensions and Structural Details

Two identical 10 ft. by 10 ft. steel curtain rolling sheet doors fitted with wind locks were tested in a custom pressure chamber at a rolling sheet door manufacturing plant (Figure 1a). The door frame component sizes and dimensions are provided in Figure 2, and Figure 3 provides pictures of the frame connections. Purlin bearing leg panels (i.e. PBR panels) with the dimensions described in Figure 4 were attached to the outside of the building frame with self-tapping machine screws.

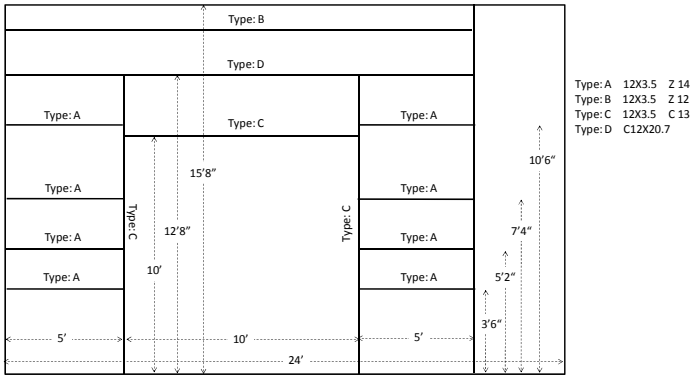

Figure 2 Frame dimensions

Figure 3 Door frame details (picture taken from the inside of the building)

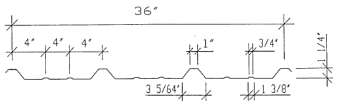

Figure 4 PBR panel cross-section (dimensions shown are for a 22 or 24 gauge panel)

Test Procedure

Two rolling sheet doors were experimentally evaluated. Door #1 was loaded with a negative pressure (Door #1N, -80 psf max) followed by three separate positive pressure loading sequences (Door #1P-1,60 psf max; Door #1P-2, 80 psf max; Door #1P-3, 140 psf max). Door #2 was loaded with a negative pressure (Door #2N, -80 psf max). The wall system supporting the door, including the cold-formed steel jambs and girts, was replaced before testing Door #2N. The pressure on the door was digitally recorded with a pressure transducer, and simultaneously monitored with a well-type manometer. For each test, the door was preloaded with a pressure of 10 psf and then released. The pressure was then reapplied in 10 psf increments until the maximum pressure output was reached from the blower or failure of the door occurred. Several unanticipated loading and unloading steps occurred during each of the five tests when the seal was lost in the vacuum chamber. The pressure time history for each test is provided in Figure 5 and Figure 6.

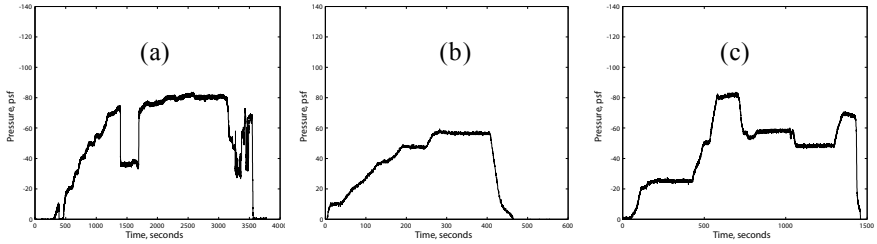

Figure 5 Pressure time history for (a) Door #1N (b) Door #1P-1, (c) Door #2N

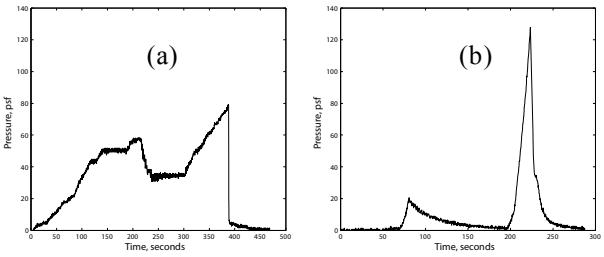

Figure 6 Pressure time history for (a) Door #1P-2 (b) Door #1P-3

Data Acquisition

A Vishay Micro-Measurements Model 5100B data acquisition system was used to digitally record 42 data channels at 5 points per second, including strain in the

wind locks, deflection of the steel sheeting with wire potentiometers, deformation of the cold-formed steel door jambs with Linear Variable Differential Transformer (LVDTs), and chamber pressure with a pressure transducer. All channels were zeroed immediately prior to testing. Figure 7 summarizes the gauge type and location, and the following sections provide details on their use and installation.

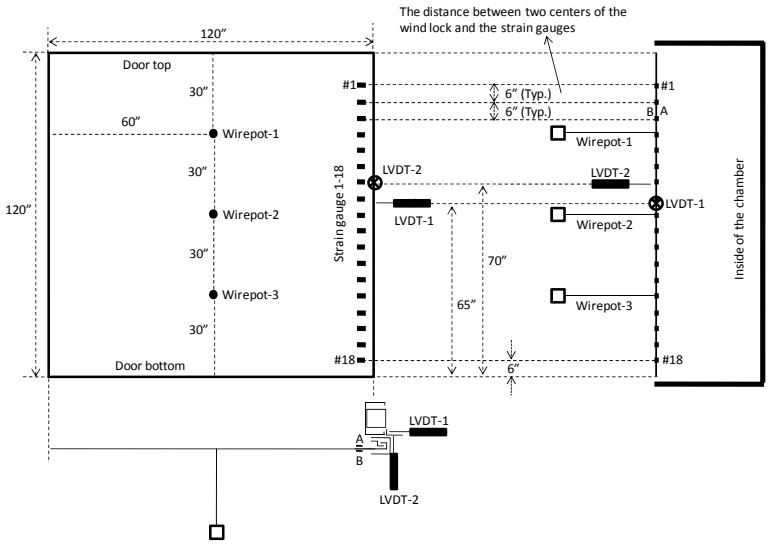

Figure 7. Wire pot, LVDT, and strain gauge locations

Strain Gauges

To accommodate the placement of strain gauges on the wind locks, the typical wind lock detail for a rolling sheet door was lengthened as shown in Figure 8. The modifications shifted the position of the riveted connection away from the wind guide, allowing the placement of the strain gauges (and associated wires) such that they did not interfere with the installation and operation of the door. The distance of the strain gauges from the riveted connection was set at approximately 2 times the width of the wind lock to ensure a uniform strain distribution in accordance with St. Venant's principle (Ugural and Fenster 2003).

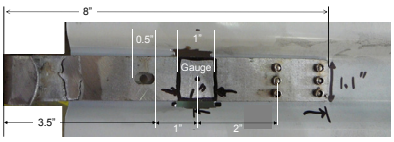

Figure 8. Lengthened wind lock and strain gauge location

A strain gauge was applied on each face of a wind lock. Strain gauge A faces towards the outside of the building, and Strain gauge B faces towards the inside of the building. Axial force, P (lbs), and moment, M (lb·in), in the wind lock at the gauge location were calculated with the formulas:

$$P = \left(\frac{\varepsilon_A + \varepsilon_B}{2} \right) EA, \quad (1)$$

and

$$M = \left(\frac{\varepsilon_A - \varepsilon_B}{2} \right) ES, \quad (2)$$

where ε_A and ε_B are the strains measured by gauge A and B respectively (note positive strain is tension), and A and S are the cross-sectional area and section modulus of the wind lock respectively. The modulus of elasticity for steel, E, was assumed as 30,000,000 psi. Eq. (1) and Eq. (2) are derived based on the assumption that the steel in the wind locks remained elastic at the strain gauge locations, which is consistent with the measured strain magnitudes (Gao and Moen 2009). Note that $+P$ represents tension in the wind lock, and $+M$ represents a bending moment that creates tension on the face of the wind lock oriented toward the outside of the building.

Out-of plane Steel sheeting Deflections

The steel sheeting deflection was recorded using wire potentiometers (wire pots) at 3 locations oriented along the vertical centerline of the door (see Figure 7). The wire pots were clamped to a steel column anchored to the concrete floor outside the pressure chamber as shown in Figure 9. The wire from each potentiometer was extended and attached to the door with sheet metal screws.

Figure 9 Wire pots were measure out-of-plane displacement

Cold-formed Steel Jamb Deflections

LVDT-1 and LVDT-2 measured the in-plane displacement, *a*, and rotation of the jamb, *b*, respectively as pressure was applied to the door (Figure 10). LVDT-1 was attached to a horizontal girt (the location is described in Figure 7, also see Figure 11), and LVDT-2 was clamped on a steel frame isolated from the door system.

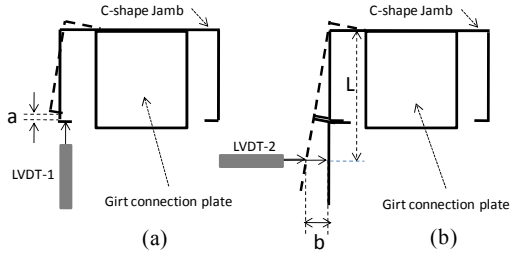

Figure 10 LVDTs measured (a) in-plane jamb displacement and (b) rotation of the jamb

Figure 11 LVDT-1 and LVDT-2 measured jamb displacements

Test Results

Curtain Deflection vs. Pressure

In both negative pressure tests (suction on the door pulling it out of the building) and positive pressure tests (pushing the door into the building), a bi-linear pressure-displacement curve was observed as shown in Figure 12 and Figure 13. In the linear region (<10 psf or >-10 psf), the wind locks were unrestrained by the wind bar (see Figure 12 and Figure 13). As the pressure increased past ±10 psf, the out-of-plane curtain deformation increased until the wind locks fully engage the wind bar at approximately ±30 psf. The restraint of the door jamb limited further in-plane curtain deformation, which led to an increase in stiffness denoted by the sharp change in slope in Figure 12 and Figure 13. The curtain demonstrates a higher unloading stiffness than loading stiffness (note the steeper descent in Figure 12 and Figure 13) which is hypothesized to occur from arching action until the wind locks disengage from the wind bars.

For the negative pressure tests (Figure 12), the top and middle wire pots measured similar displacements at -60 psf (-11 in. for Door #1N top, -11 in. for Door #1N middle), while for the positive pressure test (Figure 13), there is a difference of 2 in. between the top and middle wire pots at 60 psf (10 in. for Door #1P-1 top, 12 in. for Door #1P-1 middle). It is hypothesized that this difference in displacements stems from the contribution of the barrel to the curtain deformation pattern as shown in Figure 14. The barrel limited the door deflection in a negative test, but had a minimal impact on curtain deflection for a positive pressure test. It is also noted that in all tests the slope of the pressure-displacement curve for the bottom wire pot is higher than the middle and the top, demonstrating the increased stiffness provided by the angle fastened to the bottom of the curtain. (For Door #1P-3 which was loaded to 140 psf, the bottom angle was plastically deformed as shown in Figure 15.)

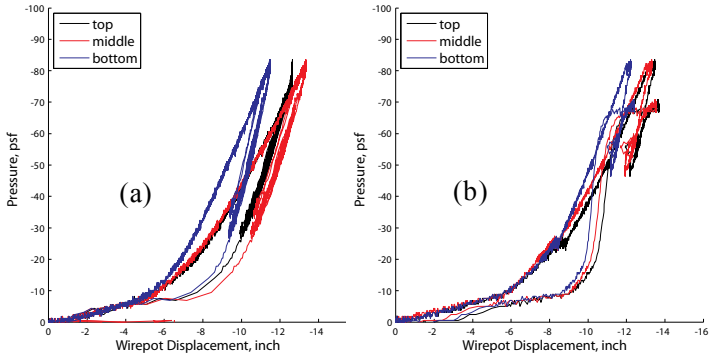

Figure 12 Curtain deflection in negative pressure for (a) Door#1N and (b) Door#2N

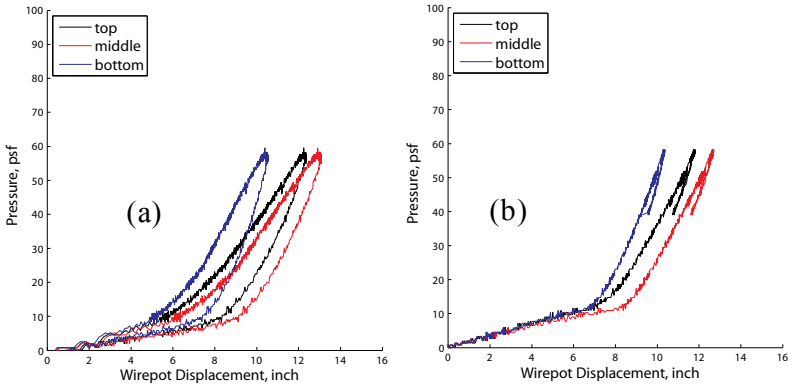

Figure 13 Curtain deflection in positive pressure for (a) Door#1P-1 and (b) Door#1P-2

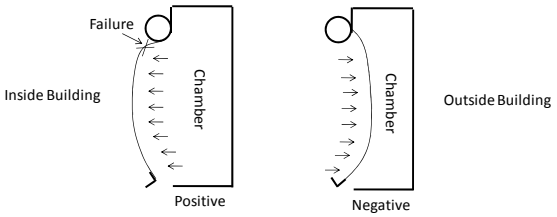

Figure 14 Curtain deflected shape varies with a positive or negative pressure

Figure 15 Bottom door angle was severely deformed after Door #1P-3 (+140 psf max)

The influence of multiple positive pressure loading sequences on a door is demonstrated in Figure 16b. In the first positive pressure test on Door #1, Door #1P-1, the wind locks engaged the wind bar at approximately +6 in. of middle wire pot deflection. In the second positive pressure test on Door #1, Door #1P-2, the wind locks did not engage the wind bar until the middle wire plot deflected approximately +8 inch. Note that Door #1P-2 was tested shortly after Door #1P-1 without replacing the door frame or jambs. The 2 in. difference is hypothesized to occur because of a permanent in-plane displacement of the jamb after the Door #1P-1 testing. This could have occurred due to permanent deformation in the jamb or slippage in the bolted connected of the girt to the jamb, permanent deformation in the wind lock, or binding of the sheet door in the guide. (Note that oversized holes were used in the bolted connections.) Furthermore, the Door #1P-2 test has a higher loading stiffness (steeper slope in) than Door #1P-1 test, supporting the hypothesis that the jamb stiffness increased in the second test from full bearing in the bolted connections.

The difference in pressure-deformation response of the door between a positive pressure test and negative pressure test can be observed in Figure 16c . Door #1N has a higher loading stiffness than Door #1P-1. It is hypothesized that the higher stiffness in the negative pressure tests occurs, at least in part, because of the direction of the catenary forces on the jamb. As shown in Figure 17, the jamb is inherently stiffer in the direction of the catenary forces applied by the negative pressure test when compared to those applied by a positive pressure test because the moment arm between the catenary force and the pivot point on the jamb is smaller in the negative pressure test.

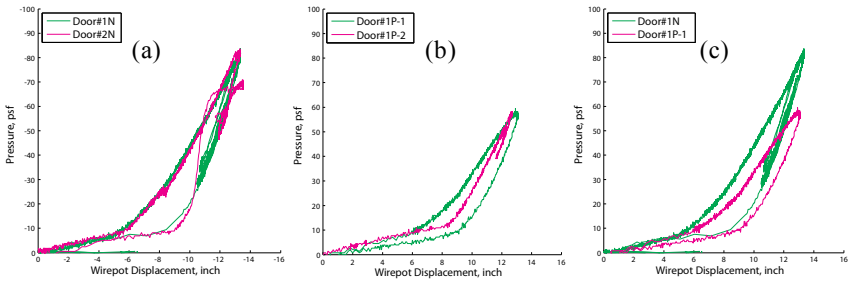

Figure 16 Out-of-plane curtain deflection at midheight: (a) Door#1N vs. Door#2N demonstrates consistency between tests, (b) Door#1P-1 vs. Door#1P-2 shows influence of multiple tests on the same door, and (c) Door#1N vs. Door#1P-1 highlights the different door behavior (stiffness) for positive and negative pressure loading

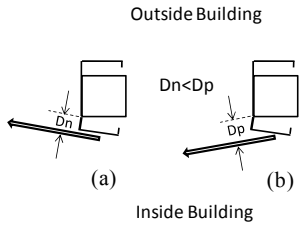

Figure 17 Direction of catenary forces on the jamb in (a) the negative pressure test and (b) the positive pressure test

Axial Force in Wind Lock vs. Pressure

The axial force, *P*, per wind lock, as calculated from the strains in the negative and positive pressure testing in Eq. (1), are summarized in Figure 18. For the negative pressure tests, the axial force does not develop until the wind lock engages the wind bar between -10 psf and -30 psf. (This trend is consistent with the pressure-displacement curves in Figure 12.) After wind lock engagement, the axial force increases as pressure is applied, confirming that catenary forces are influenced by the interaction between the curtain and the jamb. The axial force at -80 psf (Door #1N) ranges between -200 lbs compression to +650 lbs tension as summarized in Figure 18a and Table 1.

The wind lock axial forces for the positive pressure tests demonstrate a similar trend to the negative pressure tests. The axial force increases after 10 psf and the wind locks engage. At +80 psf (Door #1P-1), the axial force at each wind lock ranged from -75 lbs to +450 lbs as summarized in Figure 18b and Table 1. There is no observable correlation between girt location and wind lock forces.

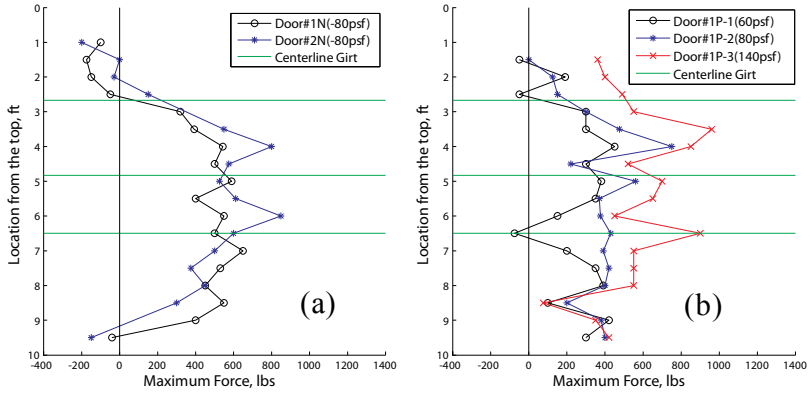

Figure 18 Maximum axial forces per wind lock for (a) negative pressure and (b) positive pressure tests.

Table 1 Summary of maximum wind lock axial forces

Location from top of door	Door #1N (-80 psf)	Door #2N (-80 psf)	Door #1P1 (+60 psf)	Door #1P2 (+80 psf)	Door #1P3 (+140 psf)
ft.	lbs	lbs	lbs	lbs	lbs
1	-100	-200			
1.5	-175	0	-50	0	360
2	-150	-30	190	125	400
2.5	-50	150	-50	150	490
3	320		300	300	550
3.5	390	550	300	475	960
4	540	800	450	750	850
4.5	500	575	300	220	520
5	590	525	380	560	700
5.5	400	610	350	370	650
6	550	850	150	375	450
6.5	500	600	-75	430	900
7	650	500	200	390	550
7.5	530	375	350	420	550
8	450	450	390	400	550
8.5	550	300	100	200	75
9	400		420	380	350
9.5	-40	-150	300	400	420
Max	650	850	450	750	960
Min	-175	-200	-75	0	75

Bending Moment vs. Pressure

The moment in the wind locks at the gauge locations for both negative and positive pressure tests are shown in Figure 19 and Figure 20. In the negative pressure test (Figure 19), below -10 psf the wind locks are not engaged and the moments in the wind locks are negligible. After the wind locks engage, a positive moment increases as a function of pressure until reaching a constant magnitude at approximately -40 psf. The peak moments in each wind lock are summarized in Figure 21a.

The sign of the moment (i.e. a positive moment) is consistent with the observed deformation pattern for a negative pressure test as shown in Figure 22a. Figure 21a does not show any discernable effect of the girt location on the maximum moment.

For the positive pressure tests in Figure 20, the moment is initially negative, but then transitions to a positive moment at approximately +30 psf. This transition from negative to positive moment occurs as the wind lock contacts the wind guide as shown in Figure 22b, resulting in double curvature in the wind lock and a reversal of moment, and ultimately severe plastic deformation of the wind guide and wind bar (Figure 23). The moment plateaus and slightly decreases for all positive pressure tests (Figure 20) due to yielding of the wind lock and the wind guide.

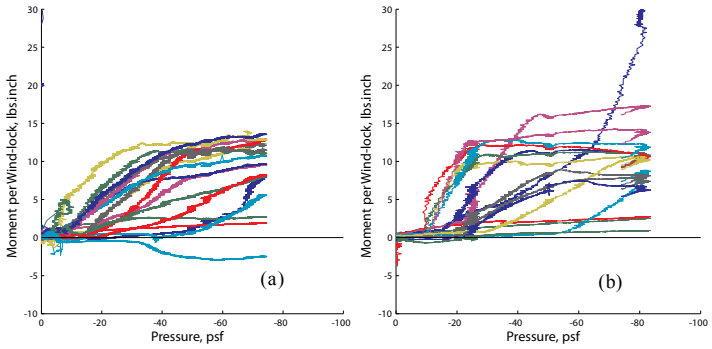

Figure 19 Moment at gauge location per wind lock in negative pressure. (a) Door #1N and (b) Door #2N

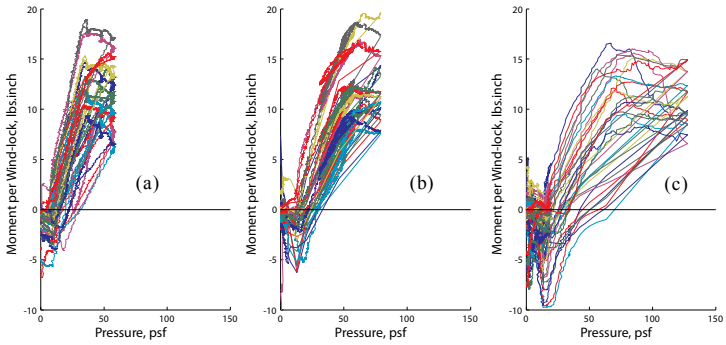

Figure 20 Moment at gauge location per wind lock in positive pressure. (a) Door #1P-1, (b) Door #1P-2 and (c) Door #1P-3

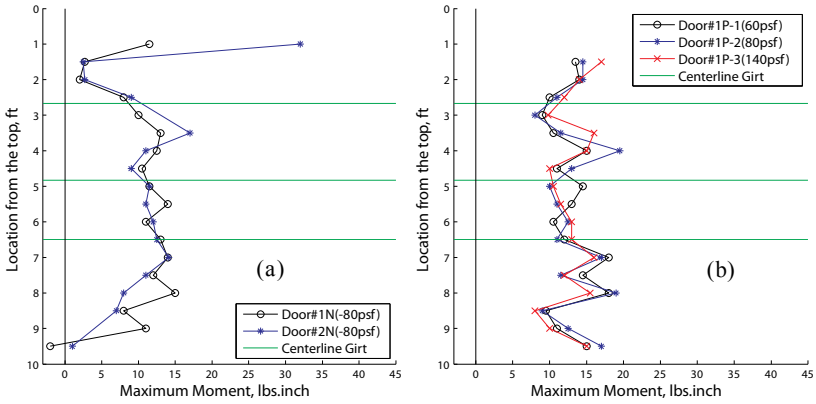

Figure 21 Maximum bending moment at gauge location per wind lock for (a) negative and (b) positive pressures

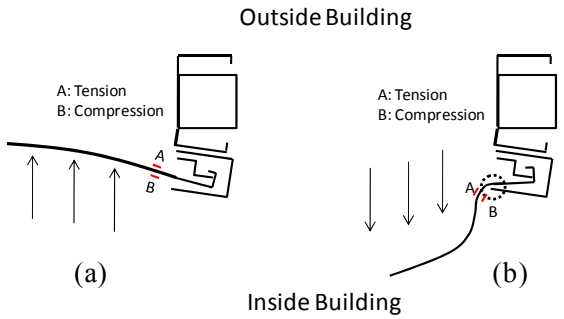

Figure 22 Wind lock system in (a) negative and (b) positive pressure

Figure 23 Plastically deformed wind lock and wind-guide after positive pressure testing

Jamb Displacement vs. Pressure

The in-plane displacement of the jamb, *a*, was measured with LVDT-1 (see Figure 10). By observing the slope of the pressure-displacement curves in Figure 24, the jamb behavior in the negative pressure testing is concluded to be stiffer than in positive pressure testing, supporting the hypothesis described in Figure 17. Note that the in-plane displacement measurement with LVDT-1 is a combination of jamb flange-web rotation (Figure 10a) and global deformation of the door frame which could not be separated with the measurements taken during the experiments. Also note that the out-of-plane jamb measurements from LVDT-2 (see Figure 10b) were deemed unreliable and are not presented here.

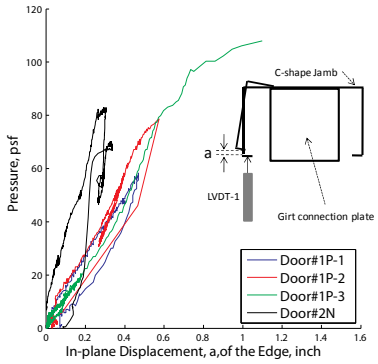

Figure 24 In-plane displacement of the jamb due to the rotation of the flange

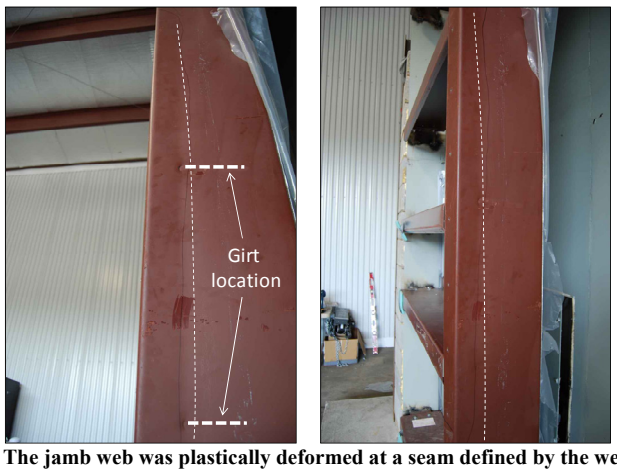

Figure 25 The jamb web was plastically deformed at a seam defined by the welded girt connection plate

Conclusions

Wind pressure experiments were conducted on two steel curtain rolling sheet doors to quantify the catenary forces present in the wind locks and to evaluate overall structural behavior under both negative and positive pressure loadings. The out-of-plane door deformation increased rapidly until the wind locks engaged with the wind bar at ± 10 psf for both negative and positive pressure tests. Once the wind locks were engaged, the system stiffness increased, resulting in catenary forces applied to the door jambs. The direction of the wind lock forces on the jamb was observed to influence the in-plane system stiffness, and there was no observed connection between girt location and wind lock force. For positive pressure on the building, the wind locks contacted the wind guide, causing plastic bending of the wind lock and the wind guide at pressures above +40 psf. The jamb flexibility was observed to be an important parameter when predicting the wind lock forces and the out-of-plane deflections of the rolling sheet door.

Acknowledgements

DBCI provided the use of their test facility in Douglasville, GA and supplied the rolling sheet doors used in the tests. Special thanks are extended to DBCI personnel, especially Mr. Bray Allen, who worked tirelessly to carry out the test plan. NCI Building Systems supplied the cold-formed framing members to assemble the typical metal building wall used in the test assembly. Mr. Jerry Hatch of NCI provided valuable guidance throughout the test program. Dr. Thomas Murray provided expertise as a testing consultant with respect to the project. Coordination with the sponsor was provided by Dr. Lee Shoemaker and Mr. Dan Walker of MBMA. Mr. Joe Hetzel of DASMA also made important contributions to the project.

References

Gao, T., and Moen, C. D. (2009). "Experimental Evaluation of a Vehicular Access Door Under Hurricane Force Wind Pressures." Virginia Tech Dept. of Civil and Environmental Engineering, Report No. CE/VPI-ST-09/03.

Ugural, A. C., and Fenster, S. K. (2003). *Advanced Strength and Applied Elasticity, Fourth Edition*, Prentice Hall, Upper Saddle River, NJ.

Twentieth International Specialty Conference on Cold-Formed Steel Structures
St. Louis, Missouri, U.S.A., November 3 & 4, 2010

Shear Behaviors of Light-gauge Composite Walls under Monotonic and Cyclic Loading

Yuanqi LI[1], Fei LIU[2], Zuyan SHEN[1], Xingyou YAO[2]

Abstract

Shear properties of cold-formed thin-walled steel composite walls are affected by many factors, including the section of light-gauge studs, the space of self-drilling screws, the panel on both sides of wall, the distribution of hold down device, etc, which makes it is difficult to estimate the shear strength. In this paper, twelve Q345 light-gauge composite wall specimens with a dimension of 2400mm wide and 3000mm high were designed for shear capacity test. Two kinds of panel combination in the specimens were considered, one is gypsum board on one side and OSB board on another side, the other is gypsum board on one side and corrugated steel sheet on another side. In order to understand the effect of opening holes in the wall on the shear behavior, three kinds of opening patterns, i.e., window openings of 600X1200 mm and 1200X1200 mm, and door openings of 1200 X2100 mm were simulated in the tests. It was shown that, the main failure modes of the test specimens were local fragmentation of gypsum boards, shear buckling of corrugated steel sheets, and yielding of end stud near the bottom. Based on the test data, lateral stiffness, shear strength, displacement ductility and energy dissipation coefficient of the composite walls under different loading conditions were studied. Finally, based on domestic and foreign research achievements, analysis method of shear strength of the light-gauge composite walls considering opening under monotonic and cyclic loading was investigated, and design methods for horizontal shear resistance and aseismic design were proposed.

Introduction

Cold-formed thin-walled steel structures are widely used in foreign countries, such as the United States, Japan, Australia, etc. The low-rise cold-

[1] Professor, Tongji University, Shanghai, China
[2] Doctoral candidates, Tongji University, Shanghai, China

formed thin-walled steel structures also come into use in China recently, and the market application prospect is broad, it is necessary to carry out systematic researches on design theory and method of this new structure system. Currently, building structures in China mainly use Q235 and Q345 or identical steel material, the Technical code of cold-formed thin-walled steel structures (GB50018-2002) is primarily concerned with these two kinds of steel material, and it prescribes that the thickness of main load-bearing members is between 2~6mm. Composite walls composing of open c section studs and coated panels (gypsum board, oriented strand board, rib corrugated sheet, etc.), are the main load-bearing structure components of this new structure system. The shear properties of light-gauge steel composite walls are affected by many factors, including the cross-section of keel studs, spacing of self-tapping screws, the panels on both sides of wall, the distribution of hold down devices, which makes it is difficult to estimate the shear strength.

Cold-formed thin-walled steel structures are widely used in foreign countries, such as the United States, Japan, Australia, etc. The low-rise cold-formed thin-walled steel structures also come into use in China recently, and the market application prospect is broad, it is necessary to carry out systematic researches on design theory and method of this new structure system. Currently, building structures in China mainly use Q235 and Q345 or identical steel material, the Technical code of cold-formed thin-walled steel structures (GB50018-2002) is primarily concerned with these two kinds of steel material, and it prescribes that the thickness of main load-bearing members is between 2~6mm. Composite walls composing of open c section studs and coated panels (gypsum board, oriented strand board, rib corrugated sheet, etc.), are the main load-bearing structure components of this new structure system. The shear properties of light-gauge steel composite walls are affected by many factors, including the cross-section of keel studs, spacing of self-tapping screws, the panels on both sides of wall, the distribution of hold down devices, which makes it is difficult to estimate the shear strength.

Reliable aseismic behaviour of whole structure should be ensured in promotion process of this new cold-formed thin-walled steel residential building system in China, as the key members of lateral resistant structure system, light-gauge composite wall is the emphasis object for investigation, some relevant researches were carried out on the shear properties of composite walls abroad, such as L.A.Fülöp and D.Dubina (2004), Tae-Wan Kim (2006), Hassan Moghimi (2008), Lei Xu (2006) , Reynaud Serrette (2009), Jörg Langea(2006), Raffaele Landolfo (2006). The model test and theoretical analysis also began in our nation, such as Zhou Tian-hua (2006), Zhou Xuhong (2006), Guo Lifeng (2004), Nie Shaofen (2006), Guo Peng (2008). However , the test specimens were mainly standard walls without opening, the influence of opening on composite shear walls was studied by Xiong Zhigang (2008) and Li Bin (2008), the test applied monotonic loading scheme, cyclic loading on hysteretic characteristics of composite shear walls

with openings were seldom seen in domestic study. Tongji University cooperated with Shanghai Best Steel Group, carried out experimental investigation on shear behaviour of Q345 cold-formed thin-walled steel composite walls with different conformation and opening sizes. Based on testing results, aseismic performance of composite walls were studied, and design method for shear walls considering openings was proposed.

Experimental investigation

The purposes of this experiment were: (1) studying the hysteretic performance of composite walls under monotonic and cyclic loading, and finding out the degradation regulation of strength and stiffness. (2) gaining the quantitative indexes for aseismic behaviour of composite walls; (3) investigating the design method for shear strength of composite wall with opening.

Test specimens

Twelve composite wall specimens were designed and supplied by Shanghai Best Steel Group, which had the same dimension and conformation as practical engineering. The wall specimens were divided into two groups according to conformation of coated panels, i.e., specimens of first group with OSB board plus gypsum board, specimens of second group with ribbed corrugated steel sheet plus gypsum board. The group and opening sizes of specimens, and loading scheme was shown in table 1.

The material of steel keel was Chinese standard Q345 and wall stud section was C9008, the standard space of wall studs was 600mm.The dimension of gypsum board was 2.4m height, 1.2m width and 12mm thickness; the dimension of OSB board was 2.44m height, 1.22m width and 12mm thickness; the dimension of rib corrugated sheet was 2.4m height, 1.2m width and 0.5mm thickness. Due to limitation of panel size, the coated panels should be cut to fit the inner steel keel, and they were connected to steel frame by self-tapping screws, the spaces of connected screws were 150mm in borderline and 300mm inside. The hold-down devices were set at both side wall studs with M16 bolts and connected to web of studs.

The opening sizes were considered in design of composite wall specimens, specimens 4 to 9 were walls with openings of different width, height and position; specimens 10 to 12 were walls with another typical panel construction form. The vertical load was basing on completed two floor full scale shaking table test model, the load level of 2.4m width wall was 20kN. The typical composite wall specimens with openings were shown in Fig 1(a), (b), the cross section of wall stud was shown in Fig 1 (c).

Table 1 Composite wall specimens

Specimen number	Wall construction	Opening Sizes (mm)	Test scheme	
			Loading scheme	Vertical load
SW1	Q345 steel	—	monotonic	20kN

SW2	2400 width X3000 mm height column section: U9008 panel :12mm gypsum board 12mm OSB board	—	monotonic	20kN
SW3		—	cyclic	20kN
SW4		600X1200	monotonic	20kN
SW5		600X1200	monotonic	20kN
SW6		600X1200	cyclic	20kN
SW7		1200X1200	cyclic	20kN
SW8		1200X2100 (middle)	cyclic	20kN
SW9		1200X2100 (side)	cyclic	20kN
SW10	Q345 steel 2400 width X3000 mm height column section: U9008 Panel :12mm gypsum board 0.5 mm OSB board	—	monotonic	20kN
SW11		—	cyclic	20kN
SW12		600X1200	cyclic	20kN

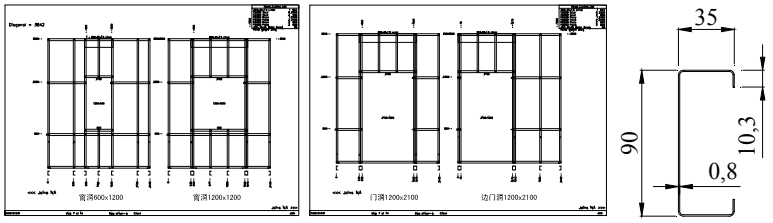

(a) Window opening (b) Door opening (c) Stud section

Fig.1 Structure specimens

Material property

The steel keel of wall specimens was Chinese standard Q345, the thickness of wall stud section was 0.8mm, mechanic tests were carried out on the four sheet samples, the elastic modulus, yield strength, ultimate strength and elongation was gained through material tension test, the results were shown in table 2.

Table 2 Mechanic property of Q345 sheet

Specimen number	f_y (MPa)	f_u (MPa)	Elongation (%)	E (x10^5MPa)
MS08-1	439.49	530.40	28.60	1.945
MS08-2	452.65	521.60	30.86	1.852
MS08-3	445.89	525.800	30.66	2.201
MS08-4	454.59	520.46	31.00	2.107
Average value	448.15	524.57	30.28	2.026
Standard variation	5.95	3.91	0.98	0.136
Variability coefficient	0.013	0.008	0.032	0.067

The above test showed that: (1) For the sheet with thickness less than 2mm, the actual yield strength was higher than nominal yield strength, and it reached 430Mpa; (2) The stress-strain curve of thin steel sheet had obvious

yield plateau, and long stress strengthening phase, the material exhibited good ductility and plastic development ability.

Setup of test

The test was completed in structure laboratory of Department of Building Engineering, Tongji University, the equipments were jack and counter-frame. The loading of vertical force used oil jacks of 50t measurement range, the horizontal load also used pushing and pulling jacks of 50t measurement range, the maximal stroke of jacks was ± 250mm, the height of horizontal counter-frame was 6m. The entire loading process applied manual control, the test devices were shown in fig.2. The vertical load applied on the midpoint of distribution beam with oil jack, the horizontal loading beam on top of the wall specimen acted as a rigid beam, it transferred the concentrated load from up distribution beam to uniform load. On the top of vertical loading jack, there was a rolling instrument, it can rolled along the counter-force beam, so the relative position of vertical load to shear wall specimens did not change during test process At the end of top loading beam, there was an end plate with screw holes to connect with horizontal oil jack and achieve cyclic loading scheme. The test data was collected by data acquisition instrument. Assistant devices were designed to restrict the bottom of specimen edge and reduce relative slip between wall specimen and the pedestal beam. The test devices and data acquisition instrument were shown in Fig. 2.

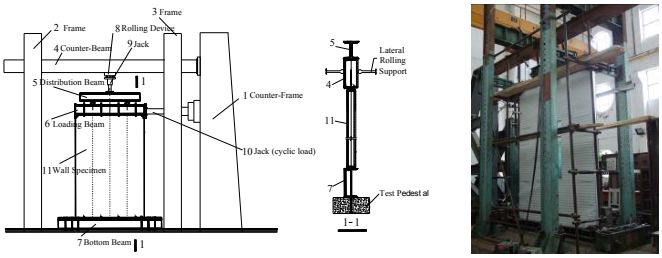

(a) Sketch map (b) whole device

Fig.2 Setup of test

Measuring points

In the test, displacement meters and strain gauges were arranged on wall specimen, the deformation in different positions of specimen was expected, and the data can be converted to the net shear deformation of structure. The layout scheme of sensors was shown in Figure 3 (a), Strain gauges were arranged on mid span of both side wall studs to test the axial strain of studs in loading process, Figure 3(b) and 3(c) were photos of sensors.

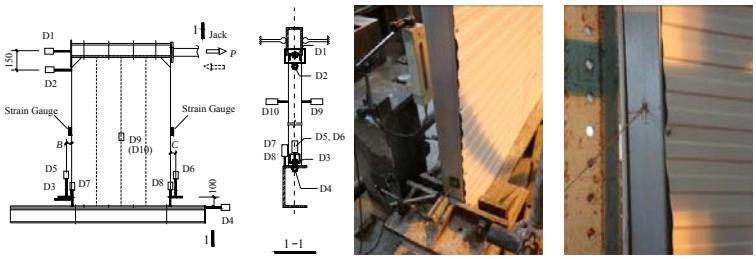

(a) layout of sensors (b) displacement meter (c) strain gauge

Fig.3 Sensors

Loading cases

(1) Monotonic loading process: Firstly, the vertical load was applied and keep constant, then horizontal load was applied in the incremental grade of 2kN, the load-displacement P-Δ curve was observed and recorded through data acquisition instrument. When the slope curve changed significantly, displacement control loading was applied instead of force control loading, until the destruction of test sample and test finished.

(2) Cycle loading process: Firstly, the vertical load was applied and keeping constant, according to test results of monotonic loading, horizontal yield displacement Δy of specimen was determined approximately. The yield load was divided into 4 levels and applied on specimen with single cycle, after yield load level, displacement control loading was applied instead of force control loading, each level was increased with 1/2Δy displacement and three cycles, until the failure of sample and test finished.

Test phenomena

The steel keel of wall specimens was assembled in situation of laboratory, the experimental phenomena was described respectively according to groups of test specimens.

Wall specimens SW1 to SW9

It could be seen from the observed phenomena, gypsum board was the typical brittle material with poor ductility, therefore, the failure of the specimens emerged from gypsum board firstly. When the loading level was not large, two gypsum boards at junction began to have relative rotation, and the rotation displacement increased with load's increasing. Gypsum boards at junction region extruded seriously, and the gypsum slag fell off much.

Screws embedded into gypsum board due to insufficient strength of gypsum material, subsequently, down rails and edges of side studs experienced distortion failure. The self-tapping screws had apparent dislocation,

especially in the seams at the bottom. In the end, most of screws connected gypsum boards failed.

The phenomena of low cyclic loading tests was basically the same as monotonic loading, the extrusion of gypsum boards occurred in the joint position, and regional failure of gypsum boards were found, stress concentration of board corner was clear, the failure phenomena of wall specimen SW3 was shown in Fig.4. Self-tapping screws were drilled into or pulled out of coated panels, while OSB board itself did not damage. In the structural system, resisting of overturning moment mainly relied on side stud and hold down devices, the moment finally converted to axial tension and compression force of side studs. When horizontal load level and lateral displacement was large, the edge studs yielded finally due to great overturning moment generated by horizontal and vertical load, and the self-tapping screws connecting hold-down devices and bottom edge of wall studs were pulled out, the specimen failed due to loss of anti-overturning ability. However, the hold-down device itself did not damage, which indicated that the strength and stiffness of hold-down device met seismic resistant requirements.

(a) extruding failure (b) failure at joint region (c) yield of side stud

Fig.4 Test phenomena of wall SW3

In the test process, it can be found that opening holes of the specimens became stress concentration region , they were weak parts of composite wall structures. The failure modes of wall specimens were similar to standard specimens without openings, i.e., dislocation of panels at junction and extrusion failure. The 45^0 principal stress penetrating crack appeared in the opening corner clearly, in sequence, the crack of upper side extended, which indicated the intensification stress was transferred along the oblique direction of opening corners. Figure 6 showed the phenomena of specimen SW4, with the increasing of horizontal load, opening holes region had serious deformation, from original rectangular shape to parallelogram. Self-tapping screws on both sides of wall head almost went into the gypsum board.

The test showed that the phenomena of composite walls with openings were basically similar to that of walls without openings. Since the existence of the hole, its level of shear strength and stiffness decreased significantly relative to standard composite walls. Due to the up lintel of door and window openings, the shear force could be effectively transferred.

The location of opening holes had no apparent influence on mechanical property of composite walls from test phenomena of SW8 and SW9. Specimen SW9 set side door opening, due to the effective arrange of double studs at door side, hold down devices and lintel, no regional weakened part appeared in the structure, and the position of door opening had little effect on shear strength of composite walls. Only the different phenomenon from previous test was that, for the opening rate increased, the ultimate bearing capacity of composite wall declined, so axial force transferred to side wall stud also decreased , the side studs did not yield in test process.

(a) baroclinic stress concentration (b) relative rotation (c) deformation of opening

Fig.5 Test phenomena of wall SW4

Wall specimens SW10 to SW12

As for another common construction form of the composite walls, i.e., interior gypsum board plus outer ribbed corrugated sheet, specimens SW10 to SW12 were designed. Due to variation of coated panels, the failure modes also changed. Fig.6 showed the test phenomena of specimen SW10 to SW12, the failure modes of two specimens were similar. The original self-drilling screws at the gypsum board junction had dislocation with each other, the gypsum boards extruded with each other seriously, screws embedded into gypsum board. At the same time, the bottom of left side stud experienced distortion, the ribbed corrugated steel sheets had been resulting in oblique shear ripple due to the existence of horizontal loads, the screw holes had rapid expansion in the connection region bearing large shear force, and steel sheet was torn, which resulted in connection failure, all the central self-drilling screws fell off, and the flange of side steel stud yielded associated with crippling of sheet. As the out plane stiffness of gypsum board and ribbed corrugated steel sheet was significantly different, when the horizontal load increased, gypsum board experienced local rupture, and the stiffness decreased greatly, the panels can not provide adequate support for wall studs, finally, the studs destructed with overall instability, the total gypsum boards failed with fragmentation.

(a) out of plane deformation and rupture

(b) detachment of corrugated sheet

(c) shear buckling (d) instability of wall studs (e) pulling out of hold down screws

Fig.6 Test phenomena of wall SW10 to SW12

Specimen SW12 with cyclic loading scheme had the similar failure modes with specimen SW11. Due to the presence of holes, failure modes of ribbed corrugated sheet had some change, because the overlap length of sheet was shorter, the seam was relatively weaker, the detachment of corrugated sheets in the junction was very clear, the screw holes of side stud enlarged, and the sheet was torn finally. As the existence of openings, the mechanism of load distribution had some change, and the limit load was relatively small, the axial force of side wall studs was relatively small, the overall instability of wall studs did not appear.

The phenomena of all the composite wall tests was summarized, four kinds of failure modes can be concluded: (1) connections between panel and steel frame; (2) crushing of gypsum board and shear buckling of corrugated steel sheet; (3) buckling of side wall stud; (4) detachment of hold-down device from wall stud, and invalidation of lateral resistant system.

Test analysis

Basing on the data of displacement meters and force transducer, the load (P)-displacement (Δ) hysteretic curve, skeleton curve, ductility coefficient, energy dissipation coefficient and load bearing capacity results were studied.

Load-displacement curve

The main data in this test was the horizontal shear force and displacement of wall specimen top. According to the original test data and conversion rules,

the net shear deformation of composite walls can be gained, and load-displacement curves of test specimens can be drawn. Fig.7 (a) showed the typical load-displacement curves of wall specimens in monotone loading test, it can be seen, due to the presence of vertical loads, the load-displacement curve had a significant descending stage.

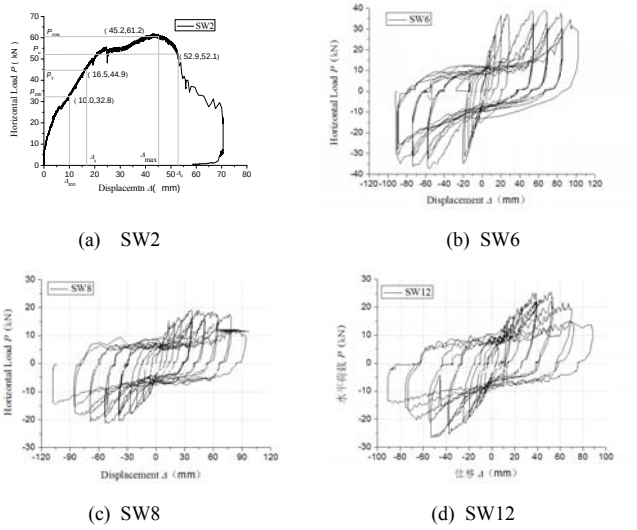

(a) SW2 (b) SW6

(c) SW8 (d) SW12

Fig.7 Load-displacement curves of typical wall specimens

Fig.7 (b), (c) and (d) showed the typical load-displacement hysteretic curves of wall specimens in cyclic loading test. The major shapes of hysteretic curves for structure member included four forms：shuttle, arc , anti-S, and Z shaped, different failure mechanisms of structure members can be seen from the shape of hysteretic cycle; shear failure often emerged as S and Z shapes, this was called “pinch effect” in earthquake engineering. The load-displacement hysteretic curve of cold-formed thin-walled steel composite walls also had similar property. To compare test results of monotonic loading and cyclic loading, the envelope of load-displacement curve, i.e., skeleton curve was drawn.

From the above figure, it can be observed that all the hysteretic curves of composite walls had similar direction. The shape of hysteretic loop changed with the number of repeated load cycles, in elastic stage, the hysteretic curve was basically a straight line, the stiffness remained unchanged; when the load increased, the specimen gradually came into elastic-plastic stage, the hysteretic curve gradually became spindle shape, area of hysteretic loop also increased significantly, residual deformation existed when unloading to zero. When load continued to increase, the hysteretic curve became bow-shaped, the area of hysteretic loop became larger, load-displacement curves took on "pinch effect" phenomenon; when the load

achieved yield value, the area of hysteretic loop was more full, the hysteretic curve developed from bow-shape to anti-S shape, "pinch effect" was more obvious, this was because the self-tapping screw holes became tight and loose in test process due to extrusion of coated panels, when the holes became tight, the stiffness of specimen went up at once, which was similar to "crack surface effect" in reinforced concrete structures. When shear deformation was large, this phenomenon was obvious. In the damage phase of test, when the load achieved maximal value, the specimen had significant degradation of stiffness and strength, the slip distance of composite wall was large, the horizontal segment of hysteretic loop was long, the performance of hysteretic loop became Z-shaped and energy dissipation capacity of the wall was very low at this time. The shape and area of hysteretic loop can be used to measure energy dissipation capacity and failure mechanism of specimen, the reduction of hysteretic loop area indicated the degradation of energy dissipation capacity. From load-displacement skeleton curve of wall specimens, it can be seen that the structure under cyclic loading experienced the three stages of elasticity, yield and limit.

Strain gauges were set on side keel studs of the composite wall specimens in the test, to ensure the reasonable loading scheme and verify the displacement meter data. In particular, for the wall specimens with door or window opening, strain gauges were also arranged on the side studs of opening. The rule of load-strain hysteretic curve accorded with load-displacement curves well, which reflected the variational axial force of side wall studs in cyclic loading tests.

Load-carrying capacity

As for the experimental data obtained by load-displacement (P-Δ) curves, there was no obvious yield point, according to “Specification of test methods for earthquake resistant building” (JGJ101-1996) , it prescribed the maximum load $p_{\max}$ of peak point in P-Δ curve and corresponding deformation $\Delta_{\max}$; the ultimate load p_u was defined as 85% of maximum load in descending segment of the curve. The confirmation of yield load point in skeleton curve was according to the principle of reciprocal area, limited to the layout, the method was not explained in detail. Displacement ductility factor reflected the ductility of entire structure member, the ductility factor was defined as following formula: $\mu = \Delta_u / \Delta_y$, which was the reflection of structural plastic deformation capacity, and also an important index to measure its seismic performance.

The whole test results of the wall specimens were shown in Table 3. For wall specimen 1, due to improper connection mode between steel keel and coated panels, the failure mode and bearing capacity result was unreasonable; for wall specimen 4, as the bottoms of coated panels contacted the pedestal firmly, the OSB board directly bare the toppling moment and transferred it to the pedestal, the decline segment of load-displacement curve was

not gained during test process, the result didn't reflect the actual load bearing capacity of wall structure, only the valid data was used in data processing.

Table3 Test Results of wall specimens

Specimen number	H/300 load		Yield load		Maximal load		Ultimate load		Ductile coefficient	Energy dissipation coefficient
	P_{300} (kN)	$\triangle_{300}$ (mm)	P_y (kN)	$\triangle$ y (mm)	P_{max} (kN)	$\triangle_{max}$ (mm)	P_u (kN)	$\triangle$ u (mm)	μ	*Ec*
SW1	—	—	—	—	—	—	—	—	—	—
SW2	32.8	10.0	44.9	16.5	61.2	45.2	52.1	52.9	3.21	—
SW3	22.6	10.0	31.7	21.7	50.3	44.3	37.7	65.4	3.01	1.508
SW4	—	—	—	—	55.6	65.3	—	—	—	—
SW5	24.0	10.0	40.4	30.6	53.6	78.0	49.7	101.9	3.33	—
SW6	12.6	10.0	36.8	33.2	54.9	40.7	34.6	96.0	2.89	1.598
SW7	17.0	10.0	21.6	20.6	30.6	53.9	26.0	57.1	2.77	1.796
SW8	10.2	10.0	14.7	22.7	19.6	60.0	16.7	87.0	3.83	1.841
SW9	12.8	10.0	17.2	18.0	23.6	39.8	20.1	52.8	2.93	1.667
SW10	12.9	10.0	33.0	13.3	39.1	32.1	33.2	48.0	3.61	—
SW11	15.7	10.0	33.1	26.9	42.5	59.9	36.2	71.9	2.67	1.765
SW12	13.5	10.0	19.0	22.2	26.8	58.9	22.8	65.2	2.94	1.755

The full-scale models of composite shear wall tests completed by Zhou Tian-hua (2006), Guo Peng (2008) and Xiong Zhigang (2008) contained different kinds of coated panels, i.e., gypsum board, OSB board, and ribbed corrugated sheets. The results showed that, the shear strength of specimens was between 12 to 14kN/m, and the shear strength of wall specimen in cyclic loading test was 10% lower than that of monotonic loading tests. The ductile coefficients of shear wall were between 3.08 to 3.84, and the energy coefficients *E* were about 1.0. In seismic fortification zone of China, ductility requirements must be met to achieve the principle of "no collapse under rare earthquake", ductility coefficient is the important parameter used to indicate the plastic deformation of structure component.

From the above table, it can be seen that, for specimens with opening, the shear strength and stiffness was lower than whole wall specimens, but ductile coefficient was higher, shear strength of wall specimens in cyclic loading test decreased about 10% ~ 25% grade compared with those in monotonic loading. The test data showed that, when the hole size was larger, the limit displacement was also relatively large. It was due to the change of limb slenderness ratio for the composite wall. When the opening area was large, it means that slenderness ratio of single wall limb was greater, so the limit deformation was larger.

Conclusion

Full-scale model test was the effective method to study shear capacity of cold-formed thin-walled steel composite walls, the test in this paper contained wall specimens with different opening sizes. The following conclusions can be gained through test phenomena and data analysis:

(1) The destruction of wall specimens occurred in the connections of coated panels and wall studs, extrusion destruction of the coated panels, slippage, tilting and pulling out of self-drilling screws. For cold-formed steel composite walls, the panels provided effective lateral support for wall studs, so when connections failed, shear strength and stiffness of wall specimen reduced. The horizontal joint of rib corrugated sheets, vertical joints of OSB boards and gypsum boards were weak parts for shear behaviour of composite walls, it was recommended that panel joints were as less as possible. Double open c-shape studs were proposed to set on both sides of wall edges and opening hole.

(2) The ribbed corrugated steel sheet experienced shear wave and large out-plane deformation due to shear buckling in test process. In practical engineering, it was proposed that the rib height of steel sheet was increased to improve the out of plane stiffness and reduce bulge deformation.

(3) The failure phenomena of wall specimens under cyclic loading were serious than those under monotonic loading test, and the shear strength reduced. From the test results, displacement ductility factors of composite walls with double sides panels were between 2 to 4, which accorded with completed experimental research. The energy dissipation coefficients of composite wall specimens were between1.5 to 2, the energy consumption of composite walls mainly relied on the relative deformation between steel keel studs and coated panels.

(4) The change in hole sizes will change the slenderness ratio of single wall limb, with increase of wall limb slenderness ratio, deformation shape took on bending type, so the displacement limits of composite walls became greater. The strength and stiffness of composite walls was basically proportional to the effective length, opening holes caused decrease of strength and stiffness, however, the ductility factors were greater than the whole composite walls.

(5) Test results of monotonic loading and cyclic loading were compared, the loading scheme had little effect on initial stiffness, the difference of initial stiffness value was no more than 20%. The situation of ductility factor was similar, it had 10% ~ 25% decrease in cyclic loading test. As for maximal shear strength, the maximal load-carrying capacity in cyclic loading test had the decline of 20%-30% comparing with monotonic loading test.

Limited to the layout, some other theoretical analysis fruit was not described in this paper. Based on current research, further study of cold-formed steel composite wall structures can be carried out, to investigate the seismic analysis method under rare earthquake:

(1) The shear properties of cold-formed steel composite walls included many factors, other factors such as the height-to-width ratio of wall, spacing

of wall studs, sections of wall studs, etc., remains to be investigated by model test and theoretical analysis.

(2) To further study various parameters affecting seismic performance of composite walls and establish the macro restoring model of shear walls with openings, and to verify the rationality by full-scale model test and numerical validation, endeavor to integrate the model into whole structure and perform non-linear static and dynamic time-history analysis.

Notation

f_y = yield strength (MPa) ;
f_u = ultimate tensile strength (MPa);
E = Young's modulus (MPa);
P = horizontal load (kN);
Δ = net shear deformation of wall specimen (mm);
μ =displacement ductile coefficient;
E_c = energy dissipation coefficient;
P_{300} = load corresponding to 1/300 story height deformation (kN);
$\triangle_{300}$ = shear deformation corresponding to 1/300 story height(mm) ;
P_y = defined yield load of wall specimen (kN);
$\triangle_y$ = defined yield displacement of wall specimen (mm);
P_{max} = maximal load of wall specimen (kN);
$\triangle_{max}$ = displacement corresponding to maximal load point (mm);
P_u = ultimate load of wall specimen (kN);
$\triangle_u$ = displacement corresponding to ultimate load point (mm);

Reference

GB50018-2002, Technical code of cold-formed thin-wall steel structures [S].
GB50011-2001, Code for seismic design of buildings [S].
Guo Lifeng. Shear Behavior of light-guage steel stud walls in residential buildings [D]. *Xi'an: Xi'an University of Architecture & Technology*, 2004. (in Chinese)
Guo Peng. Experimental and theoretical study on shear performance of cold-formed steel framing walls [D]. *Xi'an: Xi'an University of Architecture & Technology*, 2008. (in Chinese)
Hassan Moghimi, Hamid R. Ronagh. Performance of light-gauge cold-formed steel strap-braced stud walls subjected to cyclic loading [J]. *Engineering Structures*, 2008, 07:1-15.
JGJ101-1996, Specification of test methods for earthquake resistant building [S].

Jörg Langea, Bernd Naujoks, Behaviour of cold-formed steel shear walls under horizontal and vertical loads [J]. *Thin-Walled Structures*, 2006, 44: 1214-1222.

L.A.Fülöp, D.Dubina. Performance of wall-stud cold-formed shear panels under monotonic and cyclic loading. Part I: Experimental research [J]. *Thin-Walled Structures*, 2004, 42: 321–338.

L.A.Fülöp, D.Dubina. Performance of wall-stud cold-formed shear panels under monotonic and cyclic loading. Part II: Numerical modelling and performance analysis [J]. *Thin-Walled Structures*, 2004, 42: 339-349.

Lei Xu, Joel Martinez. Strength and stiffness determination of shear wall panels in cold-formed steel framing [J]. *Thin-Walled Structures*, 2006, 44 :1084-1095.

Li Bin. Shear resistance of cold-Formed steel compound wall with openings [D]. *Suzhou: Suzhou University of Science and Technology*, 2008. (in Chinese)

Nie Shaofeng. Research on simplified method of calculation for shear resistance of cold-formed steel stud composed wall [D]. *Xi'an: Chang'an University*, 2006. (in Chinese)

Raffaele Landolfo, Luigi Fiorino, Gaetano Della Corte, Seismic Behavior of sheathed cold-formed structures: physical tests [J]. *Journal of Structural Engineering*, 2006,132(4):570-581.

Raffaele Landolfo, Luigi Fiorino, Gaetano Della Corte, Seismic behavior of sheathed cold-formed structures: numerical study [J]. *Journal of Structural Engineering*, 2006, 132(4):558-569.

Reynaud Serrette, David P. Nolan, Reversed Cyclic Performance of shear walls with wood panels attached to cold-formed steel with pins [J]. *Journal of Structural Engineering*, 2009, 8, 959-967.

Tae-Wan Kim, James Wilcoski. Shake table tests of a cold-formed steel shear panel [J]. *Engineering Structures*, 2006, 28:1462-1470.

Xiong Zhigang. Study on the behavior of cold-formed steel framing shear walls with openings in residential structures [D]. *Xi'an: Chang'an University*, 2008. (in Chinese)

Zhou Tian-hua, Shi Yu, He Bao-kang, etc. Experimental research on the shear resistance of cold-formed steel stud composed wall [J]. *Journal of Xi'an University of Architecture & Technology*. 2006, 38(1):83-88. (in Chinese)

Zhou Xuhong, Shi Yu, Zhou Tianhua, etc. Study on shear resistance of cold-formed steel stud walls in residential structures [J]. *Journal of Building Structures*, 2006, 6: 42-47. (in Chinese)

Twentieth International Specialty Conference on Cold-Formed Steel Structures
St. Louis, Missouri, U.S.A., November 3 & 4, 2010

Experimental Investigation on 6 Feet Wide Cold-Formed Steel Framed Shear Walls with Steel Sheet Sheathing

Cheng Yu[1], Yujie Chen[2]

ABSTRACT

An AISI sponsored research project on the performance of 6 feet wide cold-formed steel (CFS) framed shear walls with single sided steel sheet sheathing is recently completed at the University of North Texas. This research project is aimed at determining the required seismic detailing for 6 feet wide 8 feet high CFS shear walls using two steel sheets, one is 4 feet wide, and the other is 2 feet wide. Both monotonic and cyclic tests are conducted and various parameters in the framing and sheathing details are considered in the test program. Those parameters include framing member thickness (33 mil, 43 mil, 54 mil), framing member size (3.5 inches, 6 inches), steel sheet thickness (30 mil, 33 mil), fastener size (No. 8 and No. 10), sheet joint configuration, and the option in bracing and blocking. This paper presents the testing details, test results, and analyses on the performance of 6 feet wide CFS framed shear walls. Recommendations for framing and sheathing are provided in order to achieve satisfactory seismic performance. The nominal shear strength for the tested shear wall configurations are also presented in this paper.

.

1. Assistant Professor, Department of Engineering Technology, University of North Texas, Denton, TX, US. cheng.yu@unt.edu

2. Graduate Student, Department of Engineering Technology, University of North Texas, Denton, TX, US. chenyujie711@hotmail.com

INTRUDUCTION

The cold-formed steel stud framed shear wall using steel sheet sheathing (CFS sheet steel shear wall) is a code approved lateral force-resisting system for residential and low-rise commercial buildings. The previous experimental studies of CFS sheet steel shear walls (Serrette 1996, 1997, 2002; Yu 2007) have focused on wall aspect ratios (height vs. width) 2:1 and 4:1, in which 4 ft. and/or 2 ft. wide steel sheet were used. The published nominal shear strengths of CFS steel sheet shear walls in the Steel Framing Standard - Lateral Design by American Iron and Steel Institute (AISI S213, 2007) are based on the experimental results 4 ft. wide 8 ft. high and 2 ft. wide 8 ft high walls. However the 6 ft. wide CFS shear walls are also practically used in the field and such structures have not been fully studied yet. The objective of the research presented in this paper is to identify the appropriate framing and sheathing details for 6 ft. wide CFS shear walls using 2 ft. and 4 ft. wide steel sheets to achieve satisfactory performance in cyclic loading. The test program includes both monotonic and cyclic tests, the test results are used to establish nominal shear strength for studied CFS sheet steel shear walls.

TEST PROGRAM

Test Setup

The monotonic tests and the cyclic tests were performed on a 16 ft. span, 12 ft. high adaptable structural steel testing frame. Figure 1 illustrates the testing frame with an 8 ft. × 6 ft. steel shear wall installed. All the shear wall specimens were assembled in a horizontal position and then installed vertically in the testing frame. The shear walls were bolted to the base beam and loaded horizontally at the top. For shear walls using 3.5 in. framing members, a 5 in. × 5 in. × 1/2 in. structural steel tubing was used for the base beam. For shear walls using 6 in. framing members, 10 in. × 5 in. × 1/2 in. structural steel tubing was used for the base beam. The base beam was attached to a W16×67 structural steel I beam that was attached to the concrete floor slab.

The lateral force was applied to the shear wall top via a load beam made of a structural steel T shape. The T shape was attached to the top track of the shear wall by self-drilling tapping screws placed every 3 in. on center. The out-of-plane displacement of the wall was prevented by a series of steel rollers on each side of the T shape. Five position transducers were employed to measure the horizontal displacement of the top of wall, and the vertical and horizontal displacements of the bottoms of the two boundary studs. The applied force and

the five displacements were measured and recorded instantaneously during the test.

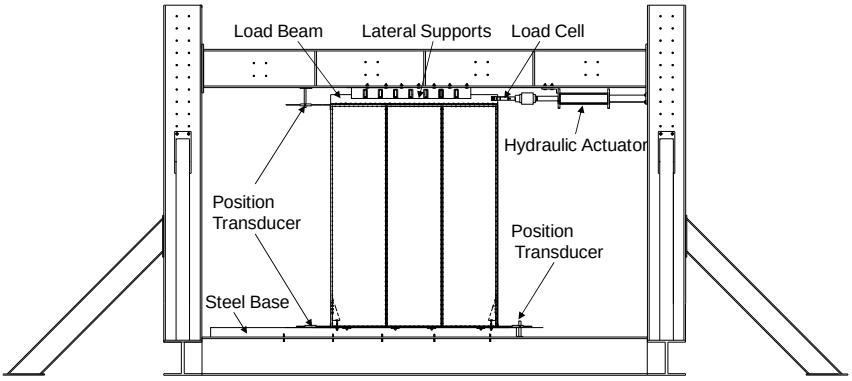

Figure 1 Shear wall test setup

Testing Procedure

Both the monotonic and the cyclic tests were conducted in a displacement control mode. The procedure of the monotonic tests was compliant with ASTM E564 (2006) "Standard Practice for Static Load Test for Shear Resistance of Framed Walls for Buildings." The CUREE protocol with 0.2 Hz loading frequency was chosen for the cyclic tests. The CUREE protocol is in accordance with the method C in ASTM E2126 (2007) "Standard Test Methods for Cyclic (Reversed) Load Test for Shear Resistance of Vertical Elements of the Lateral Force Resisting Systems for Buildings." The specific displacement amplitudes in CUREE are determined by the shear wall's displacement capacity obtained from the monotonic tests. If the shear wall has not failed at the end of the 40 cycles, additional cycles which increased of 50% over the previous primary cycle shall be added. The added magnitude is 75% of the primary for the two followed trailing cycles.

Test Specimens

This research was focused on the performance of shear walls subject to seismic loads, therefore two identical cyclic tests with CUREE protocol for each specimen configuration were performed. In general, one monotonic test was conducted prior to the cyclic tests. The purpose of the monotonic test was to

determine the ultimate displacement capacity which was used to define the reference displacement for the CUREE protocol.

In order to determine the appropriate detailing in framing and the joint of sheathing, a total of 4 wall configurations were investigated in the test program. Figure 2 shows the wall configuration A. The sheathing consisted of one 8 ft. × 4 ft. and one 8 ft. × 2 ft. steel sheet. The two sheets were butted and attached to the frame by single line of screws at the panel edges as well as in the field of sheathing. The studs were 24 in. apart, and double studs were used at the boundary and the sheet joint. One 5/8 in. shear bolt was installed on the bottom track in each section of the frame. The wall configuration B is similar to the configuration A except that one single stud was installed at the sheet joint.

The wall configuration C, illustrated in Figure 3, was developed from the configuration B with additional special detailing to improve the seismic performance. The details include the following.

- No. 10-16 × 3/4-in. modified truss head self-drilling tapping screws were used for connect sheathing and framing. The screws were placed in the stagger pattern at boundary and sheathing joint studs and in single line on tracks.
- 1-1/2-in. × 33 mil flat strap was installed at the mid height on both sides of the frame. No. 8 × 1/2-in. screws were used to attach the strap to the stud and blocking.
- Stud/track blocking with the same material as the framing members was installed at the mid height in the two end sections of the frame. The strapping and blocking details were in accordance with AISI S230 Standard for Cold-Formed Steel Framing – Prescriptive Method for One and Two Family Dwellings (AISI S230, 2007) Section E.

The wall configuration D adopted the same framing detail as configuration B except that three 8 ft. × 2 ft. steel sheets were used. The sheets were attached to the frame at the panel edge by single line of screws.

Figure 4 illustrates the labeling method. Table 1 provides the details for the tested shear walls. Since the research was focused on the seismic detailing for 8 ft. × 6 ft. CFS shear walls, the majority of the tests were cyclic. In general, one monotonic test was conducted prior to the cyclic tests. The purpose of the monotonic tests was to determine the shear wall's ultimate displacement capacity which was used to define the reference displacement in the CUREE protocol for cyclic tests. Two identical cyclic shear wall tests were conducted for each wall configuration, if the difference was greater than 10% of the first test, a third test would be performed.

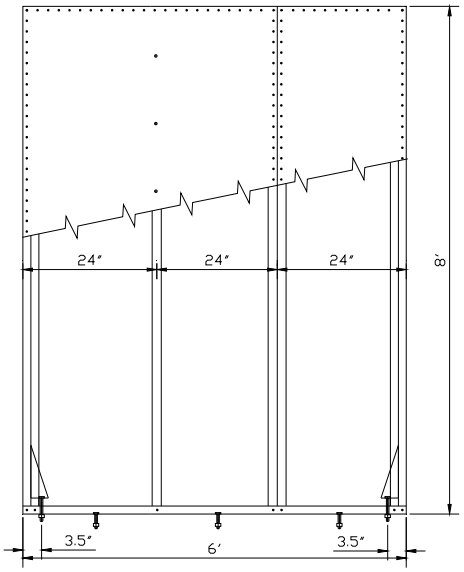

Figure 2 Dimensions of 8 ft. × 6 ft. wall assembly – Configuration A

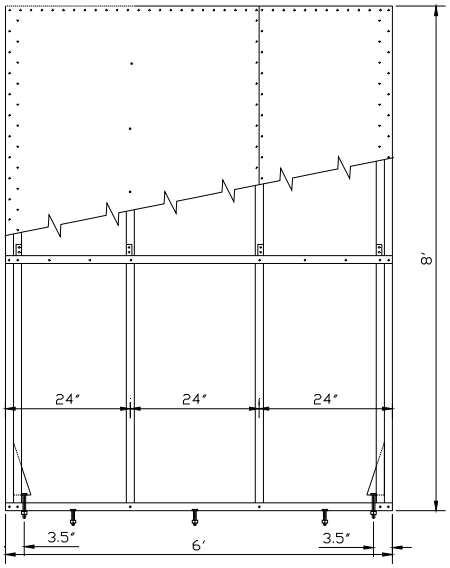

Figure 3 Dimensions of 8 ft. × 6 ft. wall assembly – Configuration C

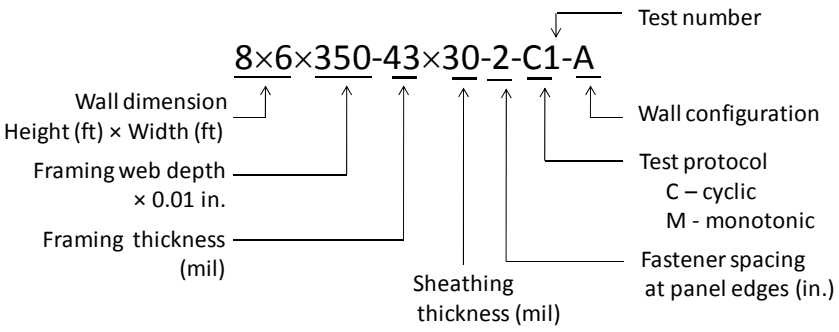

Figure 4 Specimen labeling method

Table 1 Details of 8 ft × 6 ft shear walls

Specimen label	Fastener
8×6×350-43×30-2-C1-A	#8×1/2”
8×6×350-43×30-2-C1-B	#8×1/2”
8×6×350-43×33-2-M1-C	#10×3/4”
8×6×350-43×33-2-C1-C	#10×3/4”
8×6×350-43×33-2-C2-C	#10×3/4”
8×6×350-43×30-2-M1-C	#10×3/4”
8×6×350-43×30-2-C1-C	#10×3/4”
8×6×350-43×30-2-C2-C	#10×3/4”
8×6×600-43×33-2-M1-C	#10×3/4”
8×6×600-43×33-2-C1-C	#10×3/4”
8×6×600-43×33-2-C2-C	#10×3/4”
8×6×350-54×33-2-M1-B	#8×1/2”
8×6×350-54×33-2-C1-B	#8×1/2”
8×6×350-54×33-2-C2-B	#8×1/2”
8×6×350-43×27-2-M1-D	#10×3/4”
8×6×350-43×27-2-C1-D	#10×3/4”
8×6×350-54×33-2-M1-C	#10×3/4”
8×6×350-54×33-2-C1-C	#10×3/4”
8×6×350-54×33-2-C2-C	#10×3/4”

Material Properties

Coupon tests were conducted in accordance with the ASTM A370 (2006) "Standard Test Methods and Definitions for Mechanical Testing of Steel Products" to obtain the actual properties of the test materials in this project. The coupon test results are summarized in Table 2. The coating on the steel was removed by hydrochloric acid prior to the coupon tests. A total of four coupons were tested for each member, and the average results are provided in Table 2.

Table 2 Coupon test results

Member	Uncoated Thickness (in.)	Yield Stress Fy, (ksi)	Tensile Strength Fu (ksi)	Fu/Fy	Elongation for 2 in. Gage Length (%)
33 ksi 18 mil steel sheet	0.0189	51.0	55.0	1.08	21%
33 ksi 27mil steel sheet	0.0294	46.8	54.9	1.18	27%
33 ksi 30 mil steel sheet	0.0286	48.9	55.6	1.08	24%
33 ksi 33 mil steel sheet	0.0358	47.2	53.6	1.14	33%
33 ksi 33 mil stud	0.0341	49.8	58.1	1.17	35%
33 ksi 43 mil stud	0.0430	47.6	55.1	1.15	29%
50 ksi 54 mil stud	0.0535	55.4	73.8	1.33	20%
33 ksi 33 mil track	0.0339	67.5	87.5	1.30	16%
33 ksi 43 mil track	0.0420	43.1	55.6	1.29	25%
50 ksi 54 mil track	0.0534	62.3	82.3	1.32	20%

The test results indicate that the measured uncoated thickness of 30 mil sheet, 43 mil track, and 54 mil stud and track is less than the required minimum base metal (i.e., uncoated) thickness per the AISI S201 Product Data (2007) Table B2-1. All the coupons meet the minimum ductility requirement by North American Specification for Design of Cold-Formed Steel Structural Members 2007 Edition (NASPEC 2007), which requires the tensile strength to yield strength ratio greater than 1.08, and the elongation on a 2 in. gage length higher than 10%.

TEST RESULTS AND DISCUSSION

A total of 19 8 ft. × 6 ft. CFS sheet steel shear walls were tested. The test results are summarized in Table 3. In Table 3, the ductility factor, μ, was calculate using the equivalent energy elastic plastic model (EEEP) (Park 1989). Figure 5 illustrates the EEEP model in which a bilinear curve (EEEP curve), represents

an ideal elastic-plastic shear wall system that is capable of dissipating an equivalent amount of energy as compared with the real shear wall. The slope of the elastic region of the EEEP curve is calculated by $K_e = \frac{F_{400}}{\Delta_{400}}$, where Δ_{400} is the shear wall height divided by 400, F_{400} is the load on the actual test curve corresponding to the lateral displacement of Δ_{400}. The ductility factor is determined as $\mu = \frac{\Delta_{max}}{\Delta_e}$, where the maximum displacement, Δ_{max}, and the maximum elastic displacement, Δ_e, can be obtained from Figure 5. The ductility factor has been commonly used in evaluating the ductility of CFS shear walls (Kawai et al. 1997, Fulop and Dubina 2004, Branston et al. 2006).

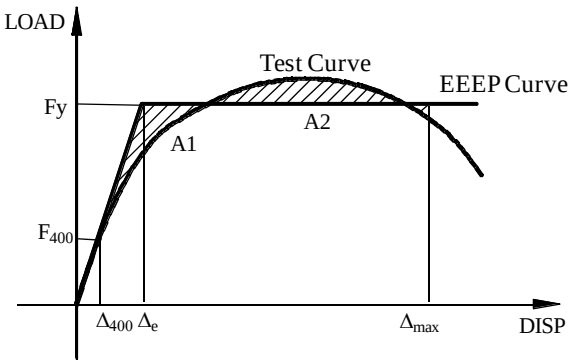

Figure 5 EEEP model

Table 3 Shear wall test results

Test label	Average peak load (plf)	Average disp. (in.)	Ductility factor
8×6×350-43×30-2-C1-A	1045	1.35	6.24
8×6×350-43×30-2-C1-B	1243	1.61	5.91
8×6×350-43×33-2-M1-C	1215	1.74	6.38
8×6×350-43×33-2-C1-C	1529	1.10	3.39
8×6×350-43×33-2-C2-C	1485	1.27	4.16
8×6×350-43×30-2-M1-C	1255	1.41	4.31
8×6×350-43×30-2-C1-C	1341	1.52	4.29
8×6×350-43×30-2-C2-C	1372	1.42	5.07
8×6×600-43×33-2-M1-C	1354	1.72	2.95
8×6×600-43×33-2-C1-C	1497	1.59	2.56
8×6×600-43×33-2-C2-C	1477	1.01	3.90
8×6×350-54×33-2-M1-B	1699	1.87	3.40
8×6×350-54×33-2-C1-B	1845	1.64	3.96
8×6×350-54×33-2-C2-B	1898	1.34	3.14
8×6×350-43×27-2-M1-D	1380	1.36	4.88
8×6×350-43×27-2-C1-D	1466	1.42	4.20
8×6×350-54×33-2-M1-C	1989	2.49	3.40
8×6×350-54×33-2-C1-C	1994	1.65	4.11
8×6×350-54×33-2-C2-C	2174	1.56	3.66

This research started with two pilot cyclic tests on 30 mil sheet shear walls with two wall configurations, A and B. Configuration A used double studs at the sheet joint, while Configuration B used a single stud at the sheet joint. Figure 6 shows the test hysteresis and failure mode for a shear wall with configuration A (8×6×350-43×30-2-C1-A). The test 8×6×350-43×30-2-C1-A failed by flexural buckling of the single interior stud and screw pull-out at the joint, which caused the separation of the double studs. Sheathing screw pull-out was also observed at the panel corners and on the single interior stud. Figure 7 shows the test hysteresis and failure mode of a shear wall with configuration B (8×6×350-43×30-2-C1-B). The test 8×6×350-43×30-2-C1-B failed by flexural buckling of the interior studs and sheathing screws pulled out at the corner and in the field of the panel. The shear wall with configuration B yielded a 19% higher peak load than that of the configuration A wall. Both shear walls demonstrated similar ductility. The boundary studs in both tests were able to provide sufficient overturning resistance. However the failure of the interior stud occurred in both tests, which could cause collapse of the structures in earthquakes or strong winds.

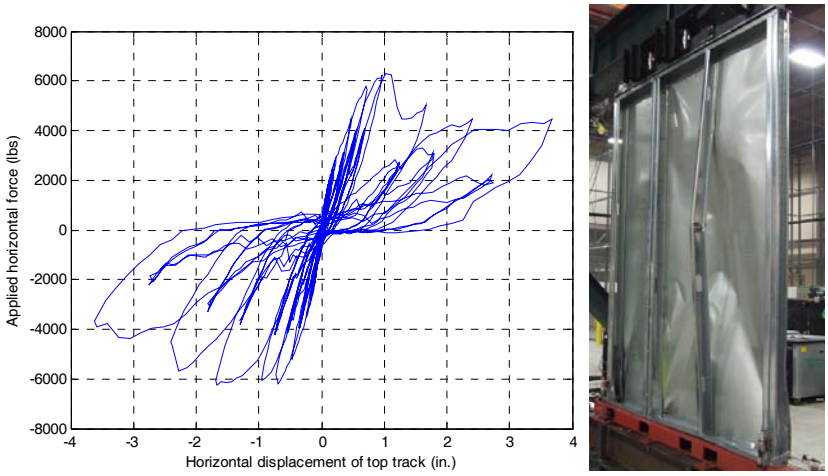

Figure 6 Test hysteresis and Failure mode for 8×6×350-43×30-2-C1-A

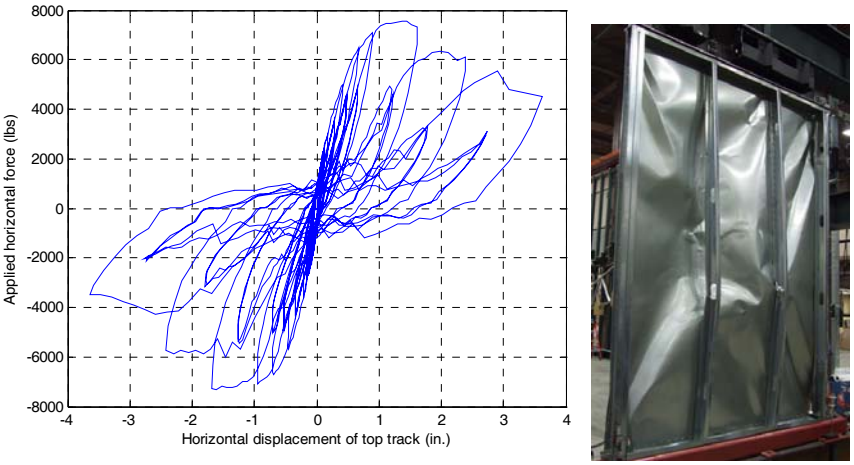

Figure 7 Test hysteresis and failure mode for 8×6×350-43×30-2-C1-B

In order to avoid failure in the studs, a wall configuration C was developed by adding special detailing to the configuration B. As stated in the previous section, the special details included No. 10×3/4" screws to replace No. 8×1/2" screws, the use of blocking and strapping, and the use of a staggered screw pattern at the end and joint studs. Figure 8 shows the 30 mil sheet steel shear walls with configuration C after testing. The flexural buckling of the interior studs was successfully restricted by the added blocking and strapping. The flange of the interior stud in the panel field was damaged due to the pull-out of the sheathing

screws. The special details also improved the shear strength of the shear wall. For the 30 mil sheet steel shear wall, a 9% increase in the peak load was found on configuration C walls compared with configuration B walls.

The special detailing (wall configuration C) was also applied to 43 mil 6 in. framed shear walls with 33 mil sheathing. Figure 9 shows failure mode of the test 8×6×600-43×30-2-C1-C. Moderate distortion of the interior stud at the field of the 4 ft. sheet occurred, and screw pull-out was observed at the deformed interior stud and at the bottom of the joint stud. The 6 in. framed shear walls did not give higher shear strength than the 3.5 in. framed shear walls using the same sheathing and fastener configurations. The two cyclic tests on 6 in. framed wall with 33 mil sheathing yielded 1487 plf in average. The two cyclic tests on 3.5 in. framed wall with 33 mil sheathing yielded 1507 plf in average. It suggests that the nominal strength for 3.5 in. framed shear walls can be used for 6 in. framed shear walls with the same details in framing, sheathing, and the fastener configurations.

Figure 8 Failure mode of test 8×6×350-43×30-2-C1-C

Figure 9 Failure mode of test 8×6×600-43×30-2-C1-C

Monotonic and cyclic tests were also performed on 54 mil framed shear walls sheathed with 33 mil sheets with and without the special detailing. 54 mil framed wall without the special detailing. Figure 10 shows the failure mode of a 54 mil shear wall without using the special details. The wall failed by the screw pull-out from the center of the interior stud and from the bottom of the boundary studs. The screw pull-out also caused distortion of the stud flange. However the studs were able to maintain their original shape after the tests. The special

detailing increased the shear strength of the 54 mil framed shear wall by an average of 11.4% for the cyclic loading. The ductility of the shear wall was also improved as the cyclic tests showed an average of 21.7% increase in the ductility factor for the 54 mil framed shear walls with the special detailing compared with the walls without special detailing.

The wall configuration D uses three 2 ft. wide steel sheets, which is a feasible method to assemble a 6 ft. wide shear wall. The tests on configuration D included one monotonic test and one cyclic test on 8 ft. × 6 ft. 33 mil framed shear wall sheathed with three 27 mil 8 ft. × 2 ft. sheets. The special detailing was not installed for these two tests. Figure 11 shows the failure mode of the cyclic test. The shear wall failed by the interior stud distortion and the flange distortion at panel corners. Compared with 8 ft. × 4 ft. shear walls with 27 mil sheathing in Yu (2007) the 8 ft. × 6 ft. walls yielded higher unit shear strength due to the stronger framing members being used (43 mil vs. 33 mil). However the special detailing is recommended for the 6 ft. wide shear walls using multiple steel sheets to avoid potential damage on the studs.

Figure 10 Failure mode of test 8×6×350-54×33-2-C1-B

Figure 11 Failure mode of test 8×6×350-43×27-2-C1-D

Following the guidance in ICC-ES AC322 Acceptance Criteria for Prefabricated, Cold-Formed, Steel Lateral-Force-Resisting Vertical Assemblies (AC322 2009), the nominal shear strength for seismic loads for those studied shear walls can be obtained by taking the average of identical tests for each configuration. The computed nominal shear strength is provided in Table 4. The nominal strengths

listed in Table 4 are adjusted only by the variation in the material thickness between the design values and the actual values in steel sheets. Footnotes to the table address the variation in the material yield strength.

Table 4 Tested nominal shear strength for seismic loads for shear walls[1]

Assembly description[2]	Aspect ratio (h:w)	Nominal thickness of framing	Required screw size	Blocking and strapping requirement[4]	Nominal shear strength (plf)
0.033" steel sheet	3:2	43 mil[2]	10	Yes	1507
0.030" steel sheet	3:2	43 mil[2]	10	Yes	1357
0.033" steel sheet	3:2	54 mil[3]	8	No	1872
0.033" steel sheet	3:2	54 mil[3]	10	Yes	2084
0.033" steel sheet	3:2	43 mil[2]	10	Yes	1575

Note:

1. Screws shall be installed 12 in. o.c. in the field of panel, and 2 in. o.c. at the panel edges.
2. Steel sheet installed on one side. Sheet steel sheathing, wall studs, tracks, and blocking shall be of ASTM A1003 Grade 33 Type H steel with minimum yield strength, Fy, of 46 ksi and a minimum tensile strength, Fu, of 55 ksi.
3. Wall studs, tracks, and blocking shall be of ASTM A1003 Grade 50 Type H steel with minimum yield strength, Fy, of 55 ksi and a minimum tensile strength, Fu, of 74 ksi.
4. Blocking and strapping shall be the same thickness as the framing. Strapping shall be of 33 mil minimum, installed on both sides of the wall.

CONCLUSIONS

CFS sheet shear walls with various configurations in framing and sheathing were experimentally studied to investigate the behavior and necessary detailing for 6-ft. wide CFS shear walls. A special seismic detailing was developed by a series of cyclic tests on 8 ft. × 6 ft. shear walls with 2 in. fasteners at panel edges to prevent potential damage on the studs. The special detailing includes blocking and strapping at middle height and No. 10×3/4-in. self-drilling screws staggered at boundary and joint studs. It is recommended to use a single stud at the sheet joint. The test results indicate that the special detailing will increase the nominal strength as well as improve the ductility of the shear wall. Apart from the special detailing, it was found that 8 ft. × 6 ft. shear walls with 33-mil sheathing using 54-mil frame without the special detailing could also give satisfactory performance under cyclic loading. It can be concluded that the special seismic detailing shall be installed for 33-mil or 43-mil framed shear walls with steel sheathing thickness equal to or less than 33-mil. The nominal strength for representative shear walls with the special seismic detailing is established.

ACKNOWLEDGEMENT

The funding by American Iron and Steel Institute and the donation of materials by Steel Stud Manufacturers Association, Nuconsteel Commercial Corp., and Simpson Strong-Tie Company, Inc. are gratefully acknowledged. The authors would like to thank UNT undergraduate students, Kyle Durham, Devin Hyde, Travis Stivors, and Taylor Cheney for their assistance in preparing the specimens and conducting tests.

REFERENCES

AISI S201 (2007). "North American Standard for Cold-Formed Steel Framing – Product Data, 2007 Edition," American Iron and Steel Institute, Washington, DC.

AISI S213 (2007). "North American Standard for Cold-Formed Steel Framing – Lateral Design 2007 Edition," American Iron and Steel Institute, Washington, DC.

AISI S230 (2007). "North American Standard for Cold-Formed Steel Framing – Prescriptive Method for One and Two Family Dwellings 2007 Edition," American Iron and Steel Institute, Washington, DC.

ASTM A1003/A1003M. "Standard Specification for Steel Sheet, Carbon, Metallic-and Nonmetallic-Coated for Cold-Formed Framing Members" American Society for Testing and Materials, West Conshohocken, PA.

ASTM A370 (2006). "A370-06 Standard Test Methods and Definitions for Mechanical Testing of Steel Products," American Society for Testing and Materials, West Conshohocken, PA.

ASTM E2126 (2007). "Standard Test Methods for Cyclic (Reversed) Load Test for Shear Resistance of Vertical Elements of the Lateral Force Resisting Systems for Buildings," American Society for Testing and Materials, West Conshohocken, PA.

ASTM E564 (2006). "E564-06 Standard Practice for Static Load Test for Shear Resistance of Framed Walls for Buildings," American Society for Testing and Materials, West Conshohocken, PA.

Branston, Boudreault, Chen, and Rogers (2006). "Light-gauge steel-frame – wood structural panel shear wall design method", Canadian Journal of Civil Engineering, 33:872-889.

Fülöp and Dubina (2004). "Performance of wall-stud cold-formed shear panels under monotonic and cyclic loading Part I: Experimental research", Thin-Walled Structures, 42 (2004) 321-338

ICC-ES AC322 (2009) “Acceptance Criteria for Prefabricated, Cold-Formed, Steel Lateral-Force-Resisting Vertical Assemblies”, ICC Evaluation Service, Inc., Washington, DC

Kawai, Kanno, and Hanya (1997). “Cyclic shear resistance of light-gauge steel framed walls”, ASCE Structural Congress, Poland.

NASPEC (2007). “North American Specification for Design of Cold-Formed Steel Structural Members 2007 Edition,” American Iron and Steel Institute, Washington, DC.

Park, R. 1989. Evaluation of ductility of structures and structural assemblages from laboratory testing. Bulletin of the New Zealand National Society for Earthquake Engineering, Wellington, New Zealand.

Serrette, R.L., Nguyen, H., Hall, G. (1996). “Shear wall values for light weight steel framing,” Report No. LGSRG-3-96, Santa Clara University, Santa Clara, CA.

Serrette, R.L. (1997). “Additional Shear Wall Values for Light Weight Steel Framing,” Report No. LGSRG-1-97, Santa Clara University, Santa Clara, CA.

Serrette, R.L. (2002). “Performance of Cold-Formed Steel-Framed Shear Walls: Alternative Configurations,” Final Report:LGSRG-06-02, Santa Clara University, Santa Clara, CA.

Yu, C. (2007). “Steel Sheet Sheathing Options for Cold-Formed Steel Framed Shear Wall Assemblies Providing Shear Resistance”, Report No. UNT-G76234 submitted to American Iron and Steel Institute, Washington, DC.

Twentieth International Specialty Conference on Cold-Formed Steel Structures
St. Louis, Missouri, U.S.A., November 3 & 4, 2010

Performance of Knee-Braced Cold-Formed Steel Shear Walls Subjected to Lateral Cyclic Loading

Mehran Zeynalian Dastjerdi[1] and Hamid Reza Ronagh[2]

Abstract

Light weight Steel Framed structures currently in use in Australia, are normally braced using face mounted thin straps, cross braces that are of the same shape as studs, or compressed cement boards screwed to the face of the walls. While these are found adequate in low seismic regions of Australia, an investigation into the earthquake resistance properties of LSF have led authors to investigate alternative bracing types that may present a more favourable ductility. Knee braces that are specially designed for this purpose are introduced in the paper and studied in a specially designed testing rig. The tests are on four full scale walls of 2.4 m × 2.4 m and are of a cyclic nature. Of particular interest are the specimens maximum lateral load capacity and the load-deformation behaviour. The study also looks at the failure modes of the system and investigates the main factors contributing to the ductile response of the LSF walls in order to suggest improvements so that the shear steel walls respond plastically with a significant drift and without any risk of brittle failure such as connection failure or stud buckling. The walls tested have different length of Knee-elements with or without brackets which have same length of Knee-elements. The study shows that although the performance of this kind of LSF lateral resistant system under cyclic loads is satisfactory, its shear strength is significantly lower than those LSF lateral resistant systems which are currently in use in Australia. In regions with medium to high seismic activity, the use of these braces would not be sufficient purely as to the lateral resistance.

[1] PhD Student, School of Civil Engineering, The University of Queensland, Australia
[2] Senior Lecturer, School of Civil Engineering, The University of Queensland, Australia

Introduction

Light Weight Steel Frames are widely used in housing industry especially in low rise residential buildings. They are cost-effective, light and easy to work with. Compared to common hot rolled steel structures, the structural behaviour of LSF structures is more complicated as they are very thin-walled members and suffer from intersection plate instability. Steel Framed structures currently in use in Australia, are normally braced using face mounted thin straps, cross braces that are of the same shape as studs, or compressed cement boards screwed to the face of the walls. While these are found adequate in low seismic regions of Australia, an investigation into the earthquake resistance properties of LSF have led authors to investigate alternative bracing types that may present a more favourable ductile response. Knee braces that are specially designed for this purpose are introduced in the paper and studied in a specially designed testing rig.

Of particular interest in this study are the effects of Knee-element length and the use of brackets on the lateral performance. Knee elements maintain a considerable reserve of post-local buckling strength prior to yielding. So, it is expected that their presence would facilitate a more ductile response. The brackets also add to the redundancy of the system and as such increase the ductility of the system in a similar manner.

The walls which are studied here are unlined and the positive effect of gypsum board on the lateral performance of the frame under cyclic loading is ignored; that is because post-earthquake observations of the timber frame structures in the Northridge earthquake have also shown that many gypsum board shear walls failed under imposed dynamic load (Serrette and Ogunfunmi, 1996). Also, some design codes (US Army Corps of Engineers, 1998) have recommended neglecting the gypsum board contribution and relying only on the bare steel frames. Scrutinizing the obtained results and comparing the results to other experiments which performed by the authors and other researchers, show that although this failure is ductile, the strength is not high enough, and as such the use of this kind of LSF structure is not preferable particularly in medium to high seismic regions.

Test Setup

The general configuration of the testing rig is shown in Figure 1. Each specimen was installed on the rig in between the fixed support beam at the bottom and a rigid loading beam at the top using four M16 high strength bolts in the vicinity

of chords and middle of the tracks either side. The bolts were tightened by a torque wrench to a torque of about 190 Nm that was corresponding to about 53 KN tension in the bolt. A strong combination of washers and nuts were used to ensure that there was no slip possibility between the tracks and the beams. Also, as shown in the figure, four hold-down angles were used at the four corners of the wall in order to lower the possibility of overturning and providing a proper load path from the braces to the wall chords and studs. An accurate Horizontal Drift (DH) transducer was used to evaluate the horizontal displacement of the top track. In order to evaluate the amount of uplift, four transducers were placed at the four corners of the walls in between the frame and the tracks. Also, one load-cell was used to measure the racking resistance. All data from the transducers and load-cell were analysed and transferred to the computer using Lab View Signal Express software (LabVIEW, 2007); and then the lateral performance of each frame was plotted.

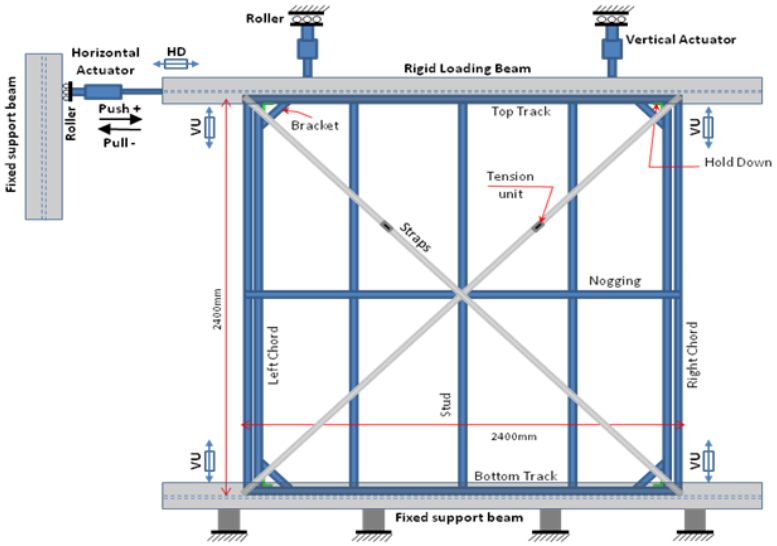

Figure 1- Testing Rig Diagram and notation convention

The cyclic loading regime that has been used in this research study is based on Method B of ASTM Standard (E2126-07, 2007), which was originally developed for ISO (International Organization for Standardization) standard 16670. This loading methodology consists of one full cycle at 0.5, 1, 2, 3, 4 mm and three full cycles at 8, 16, 24, 32, 40, 48, 56, 64, and 72 mm, unless failure or

a significant decrease in the load resistance occurs earlier. The mentioned lateral amplitudes are corresponding to 1.25%, 2.5%, 5%, 7.5%, 10%, 20%, 40%, 60%, 80%, 100%, 120%, 140%, 160%, and 180% of the ultimate lateral displacement of the walls. It is worth noting that Method B of ASTM E2126-07 stipulates that the amplitude of cyclic displacements has to be selected based on fractions of monotonic ultimate displacement. If it was to be used here, since each specimen has its own ultimate displacement, the loading regime would vary for different specimen types. However, as set out earlier, one of the current research objectives is the comparison of different types of Knee-braced configurations of the shear walls. This would necessitate using identical cyclic amplitudes for different walls, as represented earlier. Hence, Method B is therefore used in this study with lateral amplitude independent of monotonic testing. Moreover, although 75 mm, or 3.125%, inter-story drift ratio was the maximum amplitude of our actuator, it was considered adequate as the maximum allowable story drift ratio specified by Standard FEMA450 is 2.5% (BSSC, 2003). The average loading velocity was about 2mm/s which is compatible with the ASTM E2126-07 which recommends the loading velocity must be in the range of 1–63mm/s.

Experimental Program

The program consisted of four 2.4 to 2.4 m full scale frames to investigate the hysteretic lateral performance of different configuration of Knee-braced walls as shown in Figures 2 to 5. Specimens N1 and N3 included concurrent Knee-braced system and brackets in the four interior corners of the wall. This was to investigate the effects of brackets on the frames performances. In order to reduce the number of geometric variants, the length of knee elements and brackets were considered equal. The Knee-elements length was $300\sqrt{2}$mm which is equal to thirteen times the half wave-length (HWL) of local buckling of the stud section in specimen N1, and $200\sqrt{2}$mm (eight times the local buckling HWL) in specimen N3. The diagonal elements were connected to the middle of elements exactly as shown in Figures 2 and 4.

These walls were tested in the Structural Laboratory of the School of Civil Engineering, the University of Queensland using a specially made testing rig illustrated previously. All of the frame elements, such as: top and bottom tracks, noggins, studs and Knee-elements were made by an identical C section of dimensions 90x36x0.55. The section structural properties are shown in Table 1; and its detailed section geometry is shown in Figure 6.

All components were connected together at each flange using just one rivet with the shear strength capacity and tensile strength capacity of 3.3 KN and 3.8KN respectively.
The effects of different components such as: the use of bracket, length of bracket, length of Knee element, are monitored and investigated in this research by changing them from one specimen to another specimen.

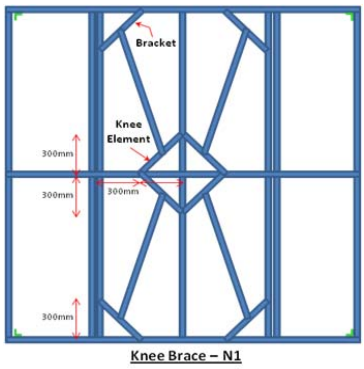

Figure 2 - Specimen N1

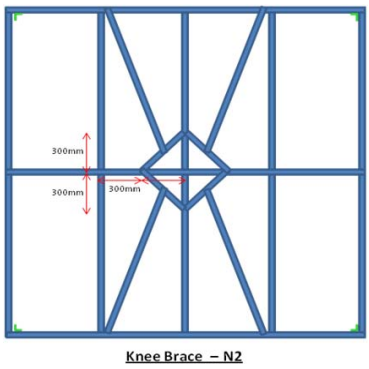

Figure 3 - Specimen N2

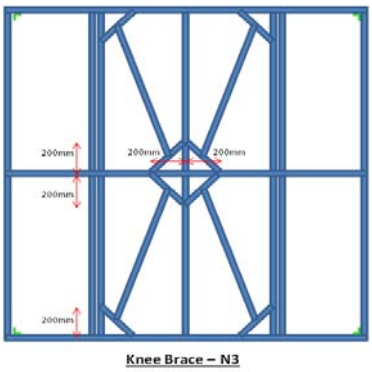

Figure 4 - Specimen N3

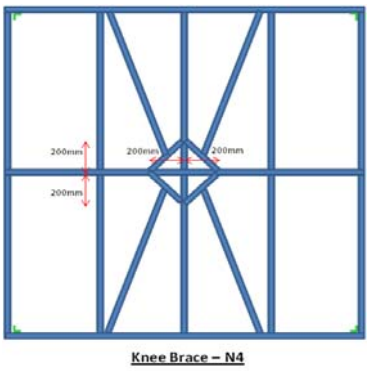

Figure 5 - Specimen N4

Nominal Grade	550 MPa	Yield Strain	0.45 %
Nominal Thickness	0.55 mm	Ultimate Stress, Fu	617.25 MPa
Elastic Modulus	168.93 GPa	Ultimate Strain	2.86 %
Yield Stress, Fy	592.26 MPa	Fu/Fy	1.04

Table 1 - Mechanical properties of the C Section Stud

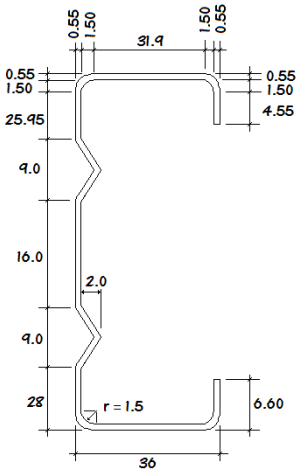

Figure 6 - C90x36x0.55

Experimental Results

The first specimen, N1, as depicted in Figure 2 was consisted of a wall panel with four brackets in the interior corners. To prevent buckling in the side chords, double studs sections were used. Interestingly, the panel performance was perfect and no failure mode was observed up to the end of the test that was corresponding to maximum drift cycle of 74 mm, though some plastic local buckling were occurred in the Knee-elements connections at the central part of the frame which was followed by plastic bending in the middle of the brackets. The hysteretic envelope curves and Load-Deflection Hysteretic Cycles for all

Specimens are shown in Figure 7 to 11. The envelope curves are derived from the load-deflection hysteretic cycles which are obtained from racking tests using accurate transducers and Lab View software (LabVIEW, 2007). The outputs of the software are in the EXCEL format, and can be used for the required post-experimental analyses such as the described envelope curves.
For specimen N2 (presented in Figure 3), after the application of the lateral loads, early plastic local buckling occurred in the Knee-elements connections; however the frame lost its capacity only after the rivet pull-out at the end of diagonal braces. This was considered as the main failure mode of the frame and was corresponding to the third cycle of 56 mm drift in the upward cyclic loading. Next specimen was N3 (shown in Figure 4). It was similar to specimen N1 with a smaller length for Knee-elements and brackets.

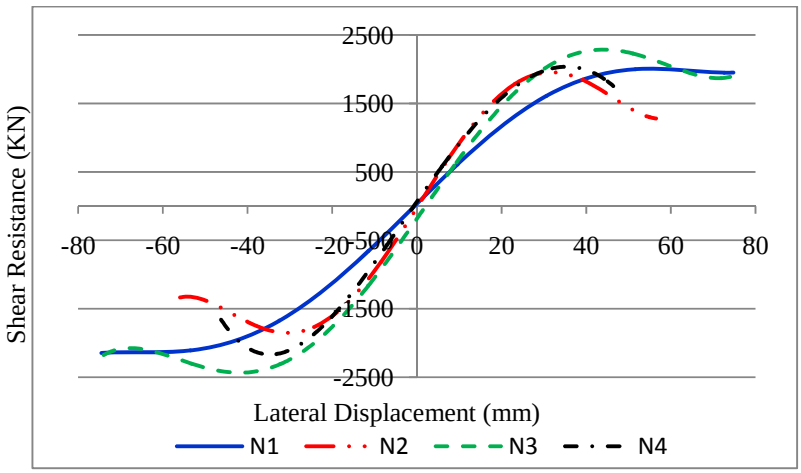

Figure 7 - Hysteretic Envelope Curve for all Specimens

Again for specimen N3 no specific failure mode was observed up to the end of the test. The only phenomenon was plastic local buckling in the Knee-elements connections followed by plastic bending in the brackets. Figure 5 shows the final shear wall, N4, which was tested. The major failure mode for this wall was a plastic global buckling in the longer Knee elements followed by the rivet pull-out corresponding to the second cycle of 48 mm drift.

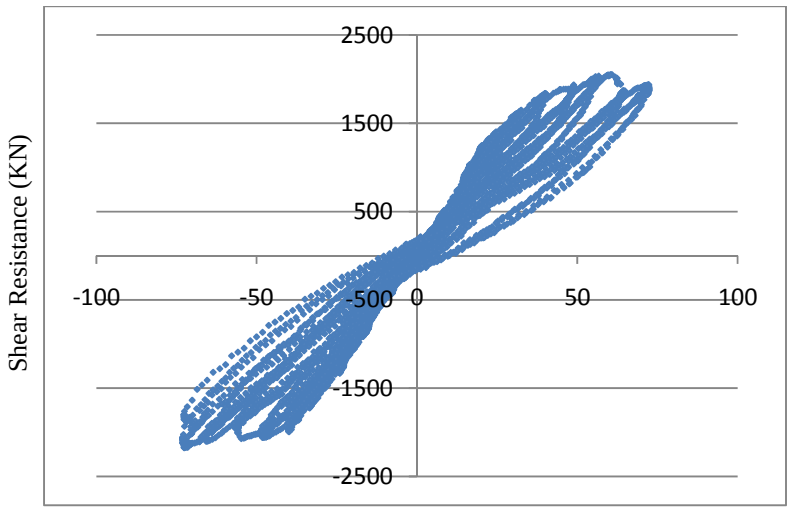

Figure 8 - Load-deflection hysteretic cycles for Specimen N1

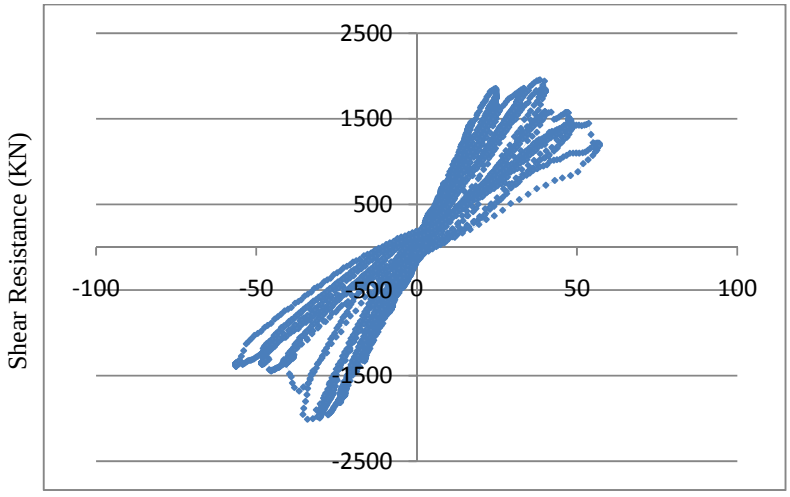

Figure 9 - Load-deflection hysteretic cycles for Specimen N2

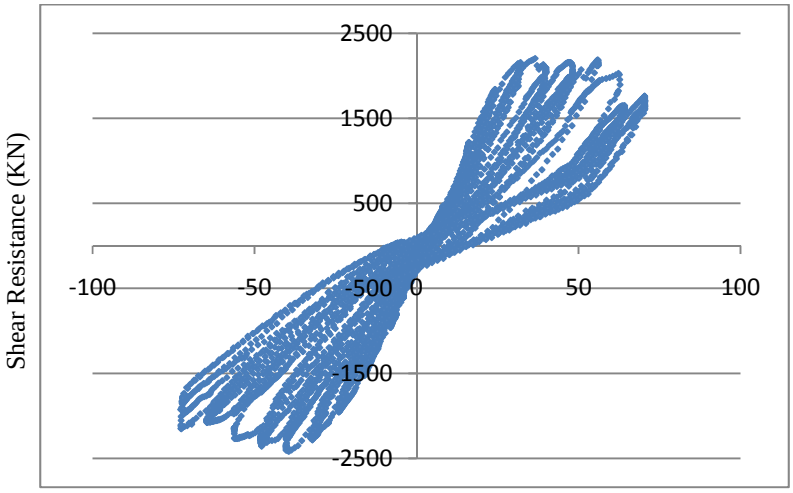

Figure 10 - Load-deflection hysteretic cycles for Specimen N3

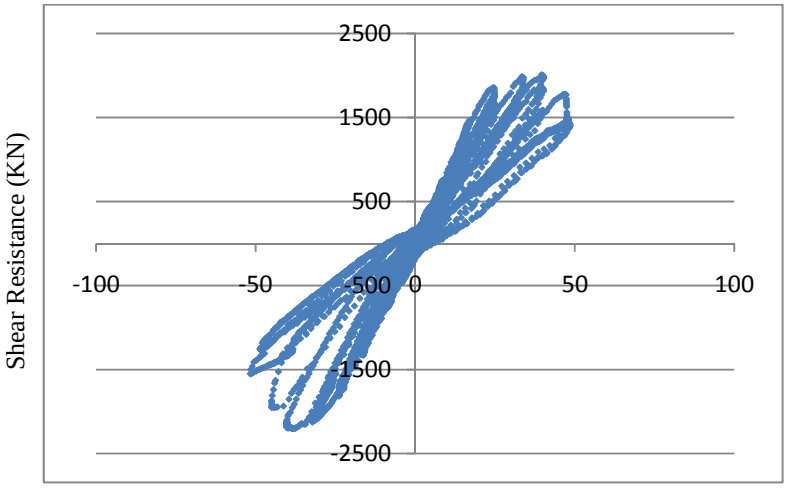

Figure 11 - Load-deflection hysteretic cycles for Specimen N4

Conclusions and Recommendations

According to the current research results, comparing the associated envelope curves and load-deflection hysteretic cycles in Figures 7 to 11, following conclusions can be made:

1- Using brackets at four interior corners of a Knee braced wall panel improves the lateral performance of the panel considerably, including both shear wall strength and the panel ductility. Besides supporting the chords and the tracks against buckling by reducing the buckling length of the members, one great advantage of using brackets is to use the plastic bending capacity of the brackets as an additional plastic energy dissipating mechanism in the frame. It is necessary to mention that using double stud sections for the chord members is essential to improve the lateral performance of the walls when brackets are incorporated as it increases the chord buckling capacity.

2- The performance of the Knee Brace lateral resistant system would be improved by decreasing the length of Knee-elements from $300\sqrt{2}$mm (thirteen times the half wave-length of local buckling of the stud section) to $200\sqrt{2}$mm (eight times the local buckling half wave-length). In another word, although the lateral performances of both specimens N1 and N3 which include the brackets were acceptable and no specific failure modes were observed during the tests and the ultimate drifts were approximately similar, the maximum absolute shear load for specimen N3 which had shorter Knee-elements was higher than that of N1. As is evident in Figure 7, the area which is enclosed by the Equivalent Energy Elastic Plastic (EEEP) curve and the capacity of energy dissipation for specimen N3 is higher than other specimens.

3- Comparing the envelop curves of specimens N2 and N4, it is seen that a shorter Knee-element leads to a greater shear strength for the wall but at the expense of a lower ductility. That is because larger Knee-elements provide more post local buckling reserve which allows the walls to deform further under the lateral loads.

4- Investigating the test results and the final failure modes for different specimens, a suggestion would arise with regard to preventing the brittle failure of the walls (with no bracket) associated with rivet pull-out; and this is to use appropriate washers under the rivets or use a rivet with wider head. This suggestion has been implemented in the current study and as seen confirmed by the results.

5- It is noted that the frame performance depend on the accuracy of the manufacturing of LSF elements. Existing gap (The lack of continuity of the web element) in the Knee-elements to stud elements connections causes the early

plastic local buckling in the connections that finally leads to undesirable failure modes such as tearing in the connections; and as such the real capacity of frame cannot be utilized. Also, as the bending capacity of studs is low, it is essential to connect different Knee-elements at the same point or as close to each other as it possibly can be to prevent any lever arm and bending moment development in the studs.

6- Considering the aforementioned results and comparing those to the results of strap bracing performed by (Moghimi and Ronagh, 2009), it is concluded that although the performance of Knee-braced cold-formed steel lateral resistant system under cyclic loads with respect to ductility is satisfactory, the shear strength of this kind of lateral resistant system is much lower than what a typical LSF house needs especially in medium to high seismic regions. Hence; it seems that Knee-brace system is not a preferable choice as an efficient lateral resistant system.

REFERENCES

BSSC, B. S. S. C. (2003) FEMA 450 - NEHRP Recommended Provisions for Seismic Regulations for New Buildings and other Structures - Part 1: Provisions. USA, Building Seismic Safety Council (BSSC).

E2126-07, A.-. (2007) Standard Test Methods for Cyclic (Reversed) Load Test for Shear Resistance of Walls for Buildings. USA.

LABVIEW (2007) LabVIEW SignalExpress. 2.0 ed. Austin, Texas, National Instruments Corporation.

MOGHIMI, H. & RONAGH, H. R. (2009) Performance of light-gauge cold-formed steel strap-braced stud walls subjected to cyclic loading. *Engineering Structures,* 31**,** 69-83.

SERRETTE, R. & OGUNFUNMI, K. (1996) Shear resistance of gypsum-sheathed light-gauge steel stud walls. *Journal of structural engineering New York, N.Y.,* 122**,** 383-389.

US ARMY CORPS OF ENGINEERS (1998) TI 809-07, Technical Instructions, Design of Cold-Formed Loadbearing Steel Systems and Masonry Veneer / Steel Stud Walls. Washington, DC 20314-1000.

Twentieth International Specialty Conference on Cold-Formed Steel Structures
St. Louis, Missouri, U.S.A., November 3 & 4, 2010

INNOVATIVE DAMAGE CONTROL SYSTEMS USING REPLACEABLE ENERGY DISSIPATING STEEL FUSES FOR COLD-FORMED STEEL STRUCTURES

Fuminobu OZAKI [1], Yoshimichi KAWAI [2] Hiroshi TANAKA [2],
Tadayoshi OKADA [3], Ryoichi KANNO [4]

Abstract

This paper describes the development of innovative seismic technologies for cold-formed steel structures; a rocking steel shear wall system with replaceable energy dissipating steel fuses for low rise housing units. In this system, the fuses are placed at the base of a folded-steel sheet wall connecting an anchor bolt and the steel sheet wall. It is designed so that most of the earthquake energy can be dissipated by plastic deformation of the fuse elements, while the shear wall remains intact and resists vertical and horizontal forces caused by large earthquakes.

As expected in seismic events, the fuses at the base move cyclically into plastic regions when the wall behaves in a rocking manner. As a result, the wall system is expected to show a stable energy absorption behavior. To maximize its energy absorption capability in this research, the shape of the fuse is optimized, such that a butterfly shape is employed to have a greater yielding region.

To verify the seismic performance of the proposed system, static shear wall tests and earthquake response analyses were respectively conducted. It was confirmed, with both results, that the developed fuses have high energy absorbing capacity and the rocking shear wall systems using them also have high seismic performance in comparison with conventional shear wall systems. The proposed system contributes to increased sustainability of the building systems through which damaged fuses are replaced after strong earthquakes.

1) Researcher, Steel Structure Development Center, Nippon Steel Corporation., Japan
2) Senior Researcher, Steel Structure Development Center, Nippon Steel Corporation., Japan
3) Chief Researcher, Steel Structure Development Center, Nippon Steel Corporation., Japan
4) General Manager, Steel Structure Development Center, Nippon Steel Corporation., Japan

1. Introduction

To minimize damages of both structural and nonstructural members in a building structure during strong earthquakes, a damage control system using replaceable energy dissipating elements is widely applied as one of the effectively advanced seismic technologies. The energy dissipating elements, namely fuses, have been developed by using various materials, for instance, steels, leads, superplastic alloys and viscoelastic polymers. Steel is renowned for its advantages over other materials, for instance, low costs by mass productions, compatibility of strength with ductility and insensitivity for both velocity and temperature under repeated stress. It is also advantageous for the fuse. In fact, buckling restrained braces and shear panels using the steel fuses have been respectively put to practical use.

While both damage control systems and fuses are applied to various types of structures, they are not necessarily optimized for individual structural characteristics. This is explained by an example in the case of shear wall structures. The shear wall structure generally possesses a high stiffness in a horizontal direction by the high in-plan shear stiffness of the shear wall. Drift angles of this structure remain small when it behaves elastically. On the other hand, the fuses are generally required to be placed at positions where work loads of external forces, that is, both external forces and deformations become large. Placed in parallel to the shear wall, they cannot effectively absorb the energy while the shear walls behave elastically. They are finally effective after the shear walls have been widely damaged with increasing plastic deformations. It is strongly suggested that the conventional damage control system is unsuitable for the shear wall structure and a specialized system must be developed.

This paper proposes an innovative damage control system for cold formed steel structures including the shear walls. This paper focuses on a controlled rocking system for low-rise housing units. Recently, it is recognized that the controlled rocking system using the fuses is one of the effective seismic technologies to realize a damage control system. Several systems have been proposed in previous studies (Midorikawa et al., 2006, 2010; Luth et al., 2008; Hajjar et al., 2010; Deierlein et al., 2010; Kishiki et al., 2010). They mainly focus on rigid or braced steel frames, concrete shear walls and detached wooden houses. In contrast, we have individually developed a controlled rocking system for low-rise housing units, in particular, cold formed steel structures. In this paper, both rocking systems and high performance steel fuses are respectively proposed. Seismic performances of the proposed systems are minutely investigated by experimental and numerical approaches.

2. Concepts of Rocking Shear Wall Systems including the Steel Fuses

Figure 1 shows a schematic diagram of the rocking shear wall system equipped with the steel fuses. This is a multi-storied shear wall system for a low-rise cold formed steel structure. In the system, high strength fasteners are respectively placed at both the upper and bottom of the shear wall at each floor. Two shear walls placed adjacent to the up and down floors are rigidly connected by the fasteners and anchor bolts cutting through steel channels of the floor joists. By rigid connections between the stories, an entire wall from the bottom to upper stories behaves as one body.

A web panel of the shear wall is made by a folded steel sheet (corrugated steel shear walls) with both high yield strength and high elastic stiffness (Tipping et al., 2008; Tanaka et al., 2009). All sides of the web panel are connected to the steel channel members by drilling screws. Hold down fasteners are respectively placed at the left and right bottoms of the shear walls at the basement floor and connected to anchor bolts standing from footing concrete slabs. The conventional hold down fasteners are elastically resistant to overturning moments of the shear wall during a strong earthquake. In this case, most of the earthquake energy is generally dissipated by plastic deformations of the shear walls, that is, the damages to

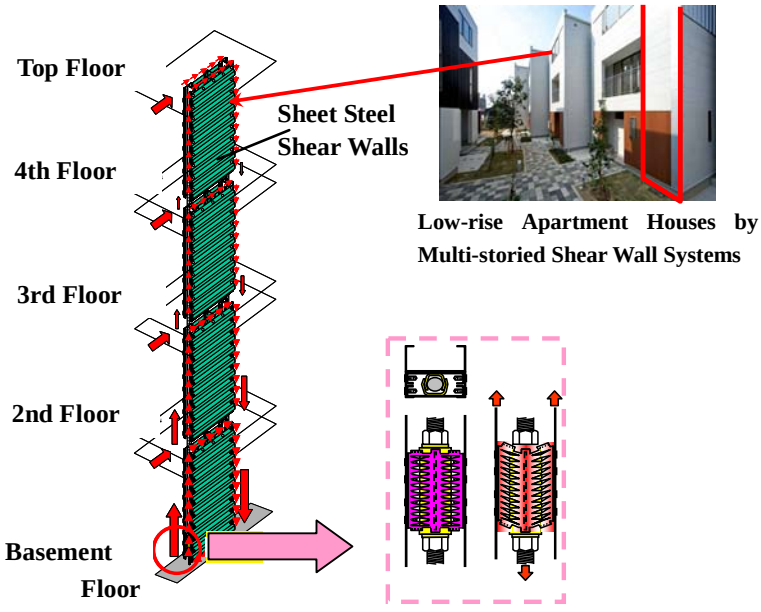

Fig-1 Rocking Shear Wall Systems using Fuses

themselves. On the other hand, a new concept proposed in this paper is that the hold down fasteners function as the fuse. While they dissipate the energy, the multi-storied shear wall wholly behaves in a rocking manner with up and down movements in a gravity direction.

Figure 2 shows the schematic diagrams of the hold down fastener equipped with the fuse function (hereafter, HDFF). A fuse panel of the HDFF is made by a steel plate pre-cutting using a laser beam machine. It bisymmetrically possesses plural rhomboid slits to create multiple energy dissipating elements. They are sandwiched between up and down rhomboid slits and have a butterfly shape; its cross section at the center is minimized and linearly increased toward both right and left ends. Both strength and stiffness of the HDFF can be controlled by numbers of butterfly elements. The steel fuse panels including the slits have been, for instance, proposed by past studies (Hitaka et al., 2003; Luth et al., 2008; Hajjar et al., 2010; Deierlein et al., 2010).

The fuse panel is connected to a fitting steel channel by a slot weld. A pair of fuse panels faces each other and is inserted into an inner hollow space of the steel channel attached to the shear wall. Finally, the HDFF is respectively connected to the steel channel and the anchor bolt by the drilling screws and nuts.

In a medium-grade earthquake, the HDFF behaves elastically and does not absorb the earthquake energy. In a strong earthquake, it moves cyclically into the plastic regions and most of the energy is dissipated by the plastic deformations of the butterfly elements. The severely damaged HDFFs after the earthquakes are detached from the shear walls and replaced by the intact HDFFs.

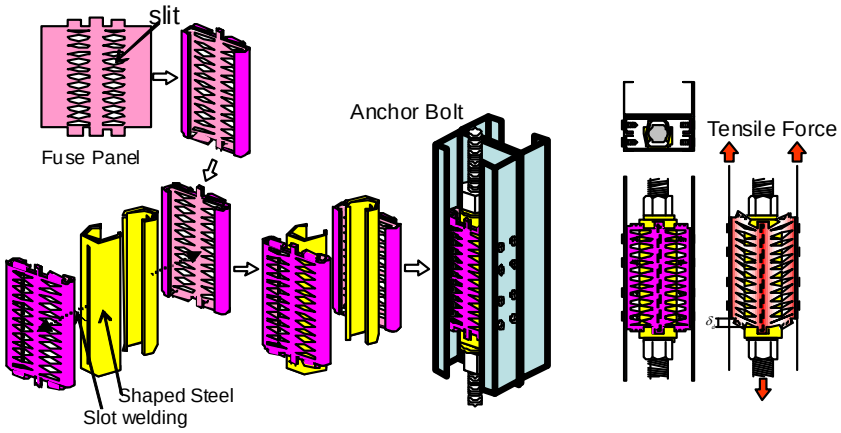

Fig-2 Hold Down Fastener Equipped with Fuse Functions

To maximize energy dissipating performance, both working forces and deformations must be concentrated in the HDFFs. The multi-storied shear wall can satisfy the above condition by large pull out forces induced by the overturning moments. On the other hand, it is necessary that the multi-storied shear wall remains intact while the HDFFs absorb the energy. Minimizing the damage of the shear wall is one of the most significant factors to guarantee the performance of the rocking shear wall system. As a matter of course, the HDFFs must have large plastic deformability maintaining a high resistant force. If these conditions cannot be satisfied, the energy absorbing capacities might decrease.

3. Static Experiments of the Rocking Shear Wall using the HDFF

3. 1 Summaries of the Experiments

To verify the seismic performance of the HDFFs, statically loaded experiments were conducted. Figure 3 shows the experimental system. The shear wall is set in the center of the system. Its section and steel material are respectively I-500x200x16x10 and JIS (Japan Industrial Standard)-SS400 (design yield strength 235N/mm^2 and design tensile strength 400N/mm^2). Both strength and stiffness of the shear wall are extremely larger than those of the HDFF. It is, consequently, considered that the shear wall behaves as a rigid body. Two steel channels are rigidly connected to both the right and left vertical sides of the shear wall by the drilling screws. Two HDFFs are symmetrically placed into both the right and left bottoms of the shear wall and respectively connected to both the steel channel and anchor bolt by the same process described in Fig. 2. Figure 4 shows the HDFF placed into the steel channel.

In the experiment, two types of energy dissipating elements are respectively used: the steel fuse panel with the butterfly shapes and rhomboid slits (Specimen A) and that with the rectangular shapes and rectangular slits (Specimen B). Figure 5 shows the fuse panels of the specimens. To verify the influence on plastic strain zones in the fuse elements, the butterfly and rectangular shapes are respectively conducted. To expand the plastic zones in the butterfly element (Specimen A), its sectional areas are optimized by the following equations.

$$\frac{M}{Z_e} = \sigma_y \tag{1}$$

$$\frac{1.5N}{A_c} = \frac{\sigma_y}{\sqrt{3}} \tag{2}$$

Where,

M : bending moment at the ends of the energy dissipating element,

N : shear force at the center of the energy dissipating element,
Z_e : section module at the ends of the energy dissipating element,
A_c : sectional area at the center of the energy dissipating element,
σ_y : yield stress of the fuse plate.

The equations (1) and (2) indicate that most parts in the butterfly elements start to simultaneously yield by both shear and bending stresses.

The steel material of the fuse panel is SS400. Its material property is shown in Table 1. The thickness of the fuse plates is given by 2.0 mm. Yield forces N_y of the HDFFs are given by the same value (33.3kN) for two specimens.

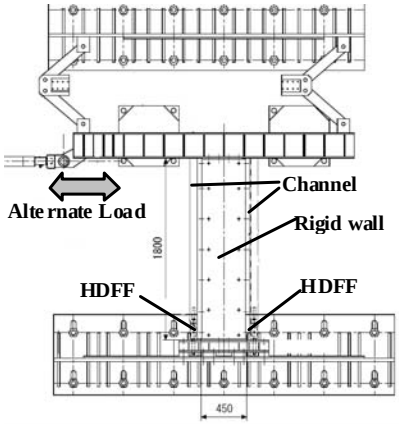

Fig-3 Overview of Experimental Systems

Fig-4 HDFF

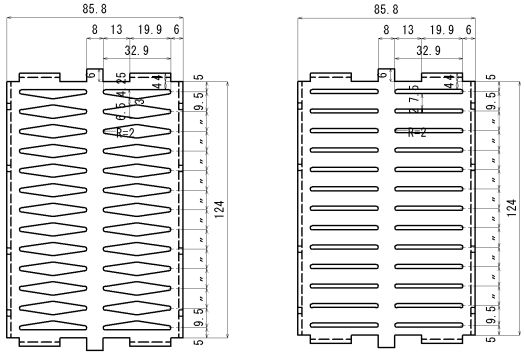

Specimen A **Specimen B**

Fig-5 Fuse Panels of the Specimens

A peak to peak alternative horizontal load at the top left of the shear wall is systematically applied by controlling the drift angle of the shear wall. The uplift deformation of the shear wall rapidly increases after the fuse panel of the HDFF moves into the plastic regions. The experiments were conducted until the fuse panels were fractured.

Table-1 Material Properties of JIS-SS400

	YS(MPa)	TS(MPa)	EL(%)	YR(%)
SS400	362.3	506.5	34.1	71.5

3.2 Experimental Results

Figure 6 shows the experimental results of both Specimen A and B. In the left figures, the horizontal and vertical axes respectively show the drift angle of the shear wall θ_A and the horizontal shear force Q. In the right figures, they respectively show the vertical deformation δ_d and the vertical force N for the HDFFs. Areas enclosed by the hysteresis of the force N - displacement δ_d relationships indicate the energy absorbing capacity of the HDFF. Its total energy value E is shown in Table 2. Both specimens exhibited ductile fractures of the energy dissipating elements.

From observations of the experimental results, Specimen B has a smaller energy absorbing capacity than Specimen A. This is because the rectangular elements have narrow plastic zones and plastic strains are concentrated at both the left and right ends. Consequently, they fractured at the early stages of the deformations as shown in Fig. 6. In contrast, the maximum deformations of the HDFFs of Specimen A (the butterfly elements) exceed over 10 mm. Its total energy absorbing value is, also, twice as large as Specimen B. It is considered that the large plastic zone of the butterfly elements contributes to maximization of both energy absorbing capacity and plastic deformability.

Table-2 Experimental Results of the HDFFs

	Specimen A	Specimen B
	Butterfly	Rectangular
Elastic Stiffness (kN/mm)	34.5	44.4
Yield strength (kN)	33.4	33.4
Tensile strength (kN)	45.8	53.5
Maximum deformation (mm)	12.5	7.5
Total Energy absorbing value (kNmm)	5 700	2 500

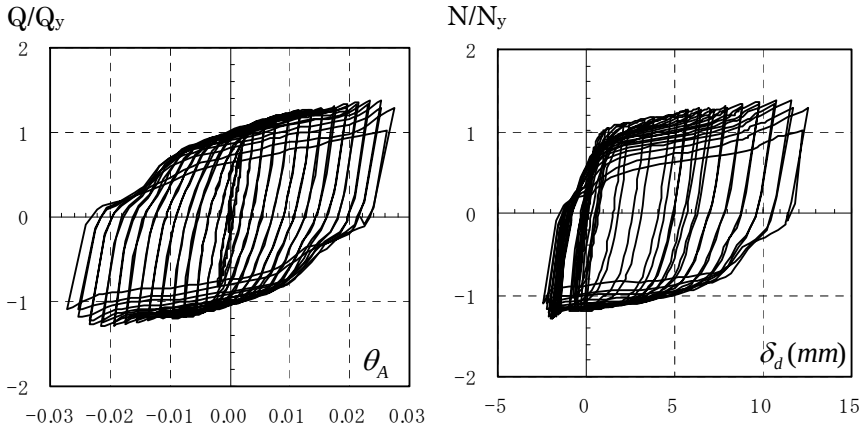

(a) Specimen A (Left : Shear Wall, Right : HDFF)

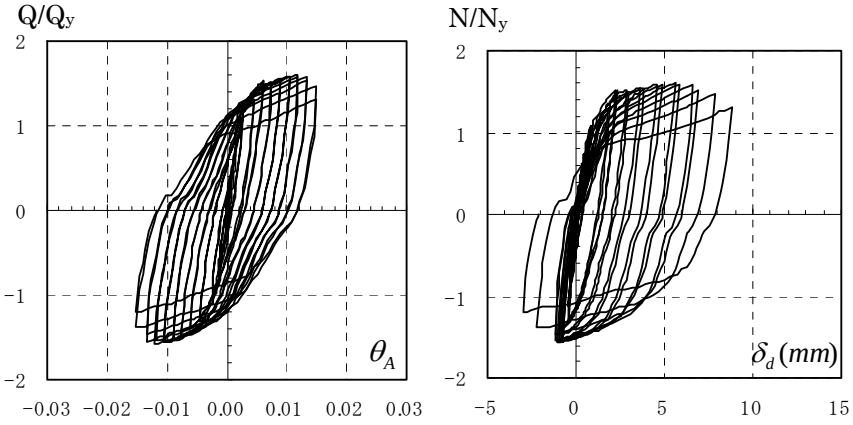

(b) Specimen B (Left : Shear Wall, Right : HDFF)

Fig-6 Experimental Results of Static Shear Walls with HDFFs

4. Earthquake Response Analyses of the Rocking Shear Wall System with the HDFF

4.1 Analytical model

In this chapter, behaviors of the rocking shear wall system with the HDFFs are minutely investigated using an earthquake response analysis

which takes into account both material and geometrical nonlinear effects (Tada et al., 2006).

Figure 7 shows a plane analytical model of four-storied and one span multi-storied shear wall structures. Uniformly concentrated masses are respectively placed on the nodes. The total weight of the masses is given by 50 kN. Two elasto-plastic springs which play the role of the HDFFs are respectively inserted at the bases of the frame. The hysteresis rule of the spring element in the plastic region is based on a kinematic hardening law. The values of the elastic stiffness, yield strength and secondary hardening are respectively illustrated in Fig. 7. Rectangular and line elements are respectively used for the shear walls and channel members. Both elements always behave in the elastic region. The primary natural frequency of the model is 0.72 seconds. It is assumed that the damping factor of the model is given by 0.01.

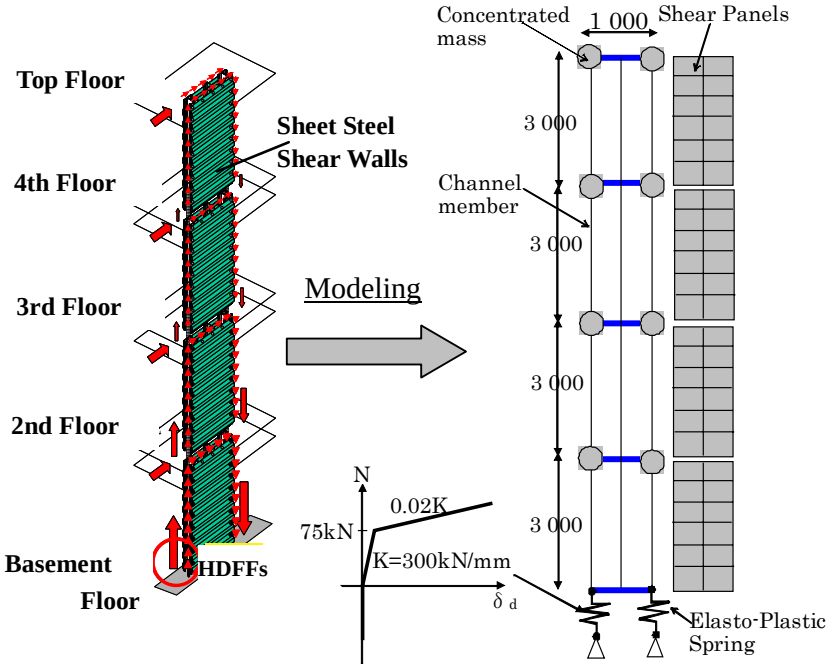

Fig-7 Analytical Models of Multi-Storied Shear Wall Structure using HDDFs

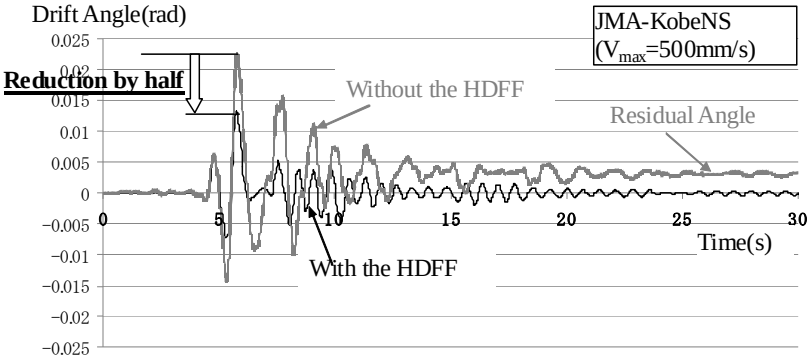

(a)Analytical results of JMA KobeNS

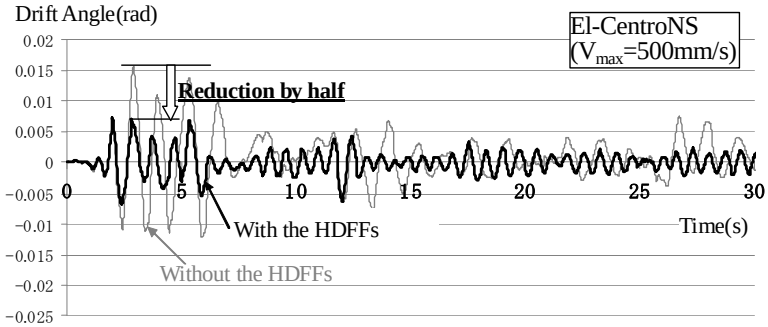

(b) Analytical results of El Centro-NS

Fig-8 Analytical Results of Drift Angles of Shear Wall

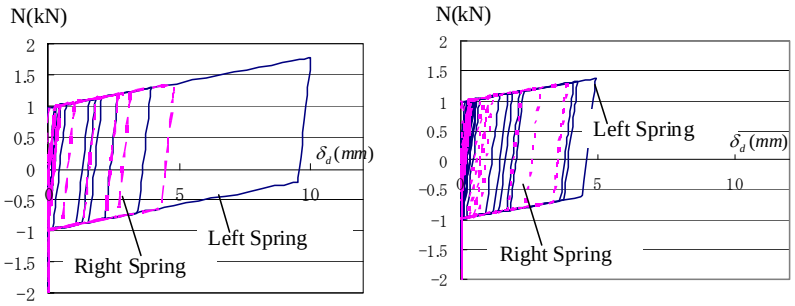

(a)Analytical results of JMA KobeNS **(b) Analytical results of El Centro-NS**

Fig-9 Analytical Results of HDFFs

4.2 Analytical Results

Figures 8 and 9 show the analytical results in the cases when normalized earthquake motions of JMA Kobe-NS (1995) and El Centro-NS (1940) are respectively used. Both maximum velocities are normalized to 500 mm/s. The above value corresponds to a generally required design value (Level 2 earthquake) recommended by the national Building Standard Law of Japan. Maximum accelerations of the two earthquake motions are respectively given by 4 540 mm/s^2 (JMA Kobe-NS) and 5 110 mm/s^2 (El Centro-NS). In Fig. 8, two types of analytical cases under the same conditions (the same base shear coefficient at push-over analyses) are illustrated. They are the analytical results with/without the HDFFs. In the analytical case without the HDFFs, the spring elements are changed from the elasto-plastic element to the elastic type. Conversely, the shear panel elements are changed from the elastic rectangular element to the elasto-plastic type to absorb the energy instead of the HDFFs (Tada et al., 2006). The energy absorbing capacity of the shear panel is smaller than that of the HDFF so that its behavior is ruled by a slip hysteresis law in the plastic region.

As in Figs. 8 and 9, it is recognized that the drift angle of the first floor is reduced by the energy absorbing capacities of the HDFFs. The maximum drift angle is approximately reduced by 50%. From the observations of response behaviors around 30 seconds, the residual drift angle of the shear wall with the HDFFs is almost non-observable (black lines). Or, the overall frame is returned to the original positions without self-centering or post-tensioning force. Conversely, the analytical results without the HDFFs exhibit large residual deformations (gray lines), particularly, in the case of JMA Kobe-NS motion. This indicates that the shear walls remain significantly damaged and major repair works are needed for continuous use.

5. Summaries of Seismic Designs based on Energy Balance

We discuss general schemes of seismic designs based on an energy balance for the proposed systems. A total energy balance equation during the earthquake is given by the following equation (Akiyama, 1985).

$$W_k + W_g + (W_e + W_p) + W_h = W \qquad (3)$$

Where,

W_k : kinetic energy at earthquake end,

W_g : potential energy by the uplift movements at earthquake end,

W_e : elastic strain energy at earthquake end,

W_p : total plastic strain energy during the earthquake,

W_h : total damping energy during the earthquake,

W : total input energy during the earthquake.

Figure 10 shows an example of the analytical result of each energy value. The analytical model is the same as that in Fig. 8. As shown in Fig. 10, most of the total input energy W is absorbed by both damping of the structure and plastic strains of the HDFFs.

In accordance with a notification of the national Building Standard Law of Japan, the energy on the damages of the structures, that is, restoring force energy in a strong earthquake can be estimated by the following equation (Hasegawa et al., 2004; MLIT (Ministry of Land, Infrastructure, Transport and Tourism of Japan), 2005).

$$W_e + W_p = W - W_h - W_k - W_g = 0.5mV^2 \quad (4)$$

Where,

m : total masses on the structures,

V : necessarily reduced velocities in a strong earthquake.

The necessarily reduced velocities V are dependant upon the primary natural frequency T_d and ground classes (soil types) as in Fig. 11. The above equation (4) has been verified by several parametrical analyses of various structural types (Hasegawa et al., 2004; MLIT, 2005). Assuming that HDFFs only move into the plastic region in a strong earthquake and W_e is much smaller than W_p (Fig. 10), the energy absorbing capacities of all HDFFs in the structure must satisfy the following equation.

$$W_p = 0.5mV^2 < \sum_{i=1}^{n} E_i \quad (5)$$

Where,

E : energy absorbing capacity that each HDFF possesses,

n : total numbers of the HDFFs in the structure.

The value of E is dependent upon the yield strength of the HDFFs, that is, the numbers of butterfly elements. To give an example, Table 3 shows relationships between the yield strength and the energy absorbing capacity, which are estimated using the experimental result of Specimen A.

When the above equation (5) is valid, the overall structures can absorb the earthquake energy by the work of the HDFFs during the earthquake.

Conversely, if it is not valid, specifications of the HDFFs must be changed to increase the energy absorbing capacity. In this case, numbers of the HDFFs or yield strength per unit HDFF must be increased. Additionally, both shear walls and footing members must be strengthened according to need.

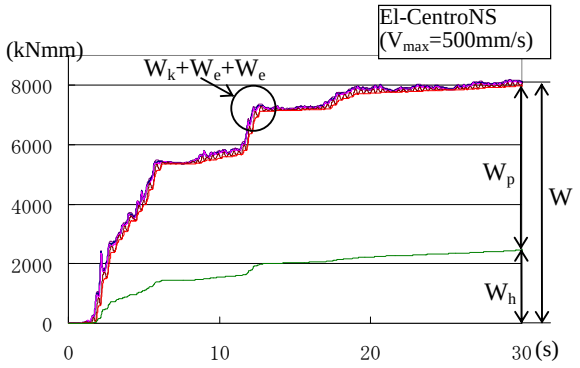

Fig-10 Analytical Results on Energy balance

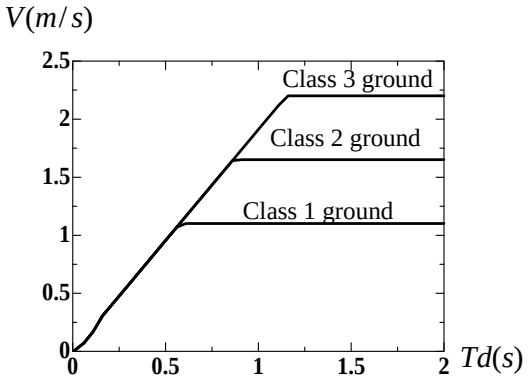

Fig-11 Relationships between Necessarily Reduced Velocities and Primary Natural Frequency

Table-3 Relationships between Ny and E of the HDFF

Yield Strength Ny (kN)	Energy Absorbing Capacity E (kNmm)
30	5 000
60	10 000
90	15 000
120	20 000

5. Conclusions

This paper draws the following conclusions:

1) We proposed an innovative seismic technology for a cold formed steel structure, which is a rocking multi-storied shear wall system using hold down fasteners with the fuse function (HDFF). The HDFFs are placed at the bases of the multi-storied shear walls and absorb the earthquake energy while the multi-storied shear walls exhibit the rocking behaviors with the uplift movements.

2) To verify the seismic performance of the HDFFs, statically loaded experiments of the shear wall with the HDFFs were conducted. From the observations of the results, it was clarified that the HDFFs possessed both high plastic deformability and large energy absorbing capacity.

3) Both seismic behaviors and performance of the rocking multi-storied shear wall system with the HDFFs were minutely investigated using the earthquake response analyses. Earthquake shaking was remarkably reduced by the large energy absorbing capacities of the HDFFs. It is considered that the proposed rocking shear wall system can offer among high seismic performance, low cost construction and increased sustainability for advanced seismic performance designs.

REFFERENCES

Midorikawa, M., Azuhata, T., Ishihara, T. and Wada, A. (2006): "Shaking table tests on seismic response of steel braced frames with column uplift", *Earthquake Engineering and Structural Dynamics, 35(14)*

Midorikawa, M., Ishihara, T., Azuhata, T., Asari, T., Hori, H. and Kusakari, T. (2010): "Seismic Behavior of Steel Rocking Frames by Three-Dimensional Shaking Table Test", *Joint Conference Proceedings 7th International Conference on Urban Earthquake Engineering, 5th International Conference on Earthquake Engineering, March 3-5, 2010, Tokyo Institute of Technology, Tokyo, Japan*

Luth, G., Krawinkler, H. and McDonald, B. (2008): "USC School of Cinema An Example of Reparable Performance Based Design", *Proceedings of SEAOC 2008 Convention*

Hajjar, J. F., Eartherton, M., Ma, X., Deierlein, G, G. and Krawinkler, H. (2010): "Seismic Resilience of Self-Centering Steel Braced Frames with Replaceable Energy-Dissipating Fuses – Part I", *Joint Conference Proceedings 7th International Conference on Urban Earthquake Engineering, 5th International Conference on Earthquake Engineering, March 3-5, 2010, Tokyo Institute of Technology, Tokyo, Japan*

Deierlein, G, G., Ma, X., Hajjar, J. F., Eartherton, M., Krawinkler, H., Takeuchi, T., Midorikawa, M., Hikino, T. and Kasai, K. (2010): "Seismic Resilience of Self-Centering Steel Braced Frames with Replaceable Energy-Dissipating Fuses – Part II; E-Defence Shake Table Test", *Joint Conference Proceedings 7th*

nternational Conference on Urban Earthquake Engineering, 5th International Conference on Earthquake Engineering, March 3-5, 2010, Tokyo Institute of Technology, Tokyo, Japan

Kishiki, S. and Wada, A.(2010): "Shaking Table Test on Controlled Rocking Frame of Wooden Structures", *Joint Conference Proceedings 7th International Conference on Urban Earthquake Engineering, 5th International Conference on Earthquake Engineering, March 3-5, 2010, Tokyo Institute of Technology, Tokyo, Japan*

Tipping, S. and Stojadinovic, B.(2008): "Innovative Corrugated Steel Shear Walls for Multi-Story Residential Buildings", *Proceedings of the 14th World Conference on Earthquake Engineering October 12-17, Beijing, China*

Tanaka, H. and Kawai, Y.(2009): "In-plain Shear Tests of Corrugated Sheet Walls for Steel Houses", *Summaries of Technical Paper of Annual Meeting 2009., AIJ, August 26-29,Tohoku, Japan* (In Japanese).

Hitaka, T. and Matsui C. (2003): "Experimental Study on Steel Shear Wall with Slits", *J. of Structural Engineering, ASCE 209(5)*.

Tada M., Hanya K., Yamashita N. and Ishikawa K.(2008): "The Elasto-plastic Model of Drilling Screw Demonstrating Slip Behavior in Steel Framed Houses", *J. of Steel Construction Engineering., JSSC 46B* (In Japanese).

Akiyama H. (1985): "Earthquake-Resistant Limit-State Design for Buildings", *University of Tokyo Press.*

Hasegawa T., Nishiyama K., Mukai A., Ishikawa T. and Kamura H. (2004): "Seismic Response Prediction of Steel Frames with Hysteretic Dampers based on Energy Ba*lance", J. of Struct. Const. Eng., AIJ, 582, 147-154* (In Japanese).

Ministry of Land, Infrastructure, Transport and Tourism of Japan (2005); "NotificationNo.631 Earthquake-resistant structural calculation based on energy balance" *June 28, 2005* (In Japanese).

Twentieth International Specialty Conference on Cold-Formed Steel Structures
St. Louis, Missouri, U.S.A., November 3 & 4, 2010

A Life-Cycle Assessment of Cold-Formed Steel Enclosures verses Alternative Enclosures in Commercial Buildings

K. J. Van Ooteghem[1] and L. Xu[2]

ABSTRACT

In North America, the operation of buildings accounts for approximately one third of the total energy use and greenhouse gas emissions each year.

Over the life of a building, the total energy use is a combination of the embodied energy in the building materials and the operating energy of the building. Building enclosures (walls and roofs) have a huge impact on both the embodied energy and the operating energy of buildings. Historically, steel has been blacklisted as a material with a high embodied energy. This has led to a misconception that steel enclosures use significantly more energy than other enclosure types. A study was conducted at the University of Waterloo to investigate cold-formed steel enclosures compared to other enclosure types in commercial buildings. After 50 years for a building located in Toronto, Canada, it was found that cold-formed steel enclosures are very competitive compared to other enclosure types in terms of total energy use and greenhouse gas emissions.

1.0 Introduction

The building industry in North America is changing. Over the past few decades, there has been an industry movement towards the design and construction of more energy efficient buildings. In recent years, numerous green building protocols such as: LEED® (North America), BREEAM (United Kingdom), Green Star (Australia), and many others have emerged in response to the demand for more environmentally conscious buildings. However, the building

[1] Research Assistant, The Canadian Cold-Formed Steel Research Group, Dept. of Civil and Environmental Engineering, University of Waterloo, Canada
[2] Professor, The Canadian Cold-Formed Steel Research Group, Dept. of Civil and Environmental Engineering, University of Waterloo, Canada

industry continues to have an overwhelming impact on the environment. In the U.S., buildings account for around 39% of primary energy use, 38% of all carbon dioxide emissions, and nearly 40% of all raw material use annually (USGBC, 2010). The trends in Canada are much the same. Each year in Canada the operation of buildings is responsible for approximately the same total secondary energy use as the entire transportation sector (NRCan, OEE, 2010).

Over the past two decades, cold-formed steel has become an increasingly popular building material for residential and commercial construction. This increased use can be attributed to the numerous advantages that cold-formed steel has over traditional building materials. Meanwhile, there has been a growing body of research investigating the life-cycle assessment (LCA) of buildings. These studies vary drastically in terms of their approach, the building components that are studied, and their degree of complexity. There is a need for a comprehensive comparison of cold-formed steel enclosures (walls and roofs) to alternative enclosures in commercial buildings, using the latest LCA techniques. Summarized in this paper are some of the results from a comprehensive LCA study of building enclosures that was conducted at the University of Waterloo.

2.0 Background Terminology

Embodied Energy of Buildings: There are two kinds of embodied energy: initial and recurring. Initial embodied energy is the energy consumed to manufacture the building materials, transport them to site, and then construct the building. Recurring embodied energy is the energy consumed to maintain, repair, or replace any parts of a building over its lifespan. In a typical office building in Toronto, Canada, the total embodied energy (initial + recurring) is about 15% of the total energy use after 50 years (Cole & Kernan, 1996).

Operating Energy of Buildings: The operating energy is the amount of energy consumed by a building to meet the demand for heating, cooling, lighting, ventilation, equipment, etc. In a typical office building in Toronto, Canada, the operating energy is about 85% of the total energy use after 50 years (Cole & Kernan, 1996).

Global Warming Potential (GWP): The term, GWP was developed to compare one GHG to another in terms of their ability to trap heat in the Earth's atmosphere. GWP is measured in mass of CO_2 equivalent. Carbon dioxide equivalency (CO_2eq.) is a measure of the equivalent amount of CO_2 that would have the same GWP as a mixture of CO_2 and other GHGs in the Earth's atmosphere.

Life-Cycle Assessment (LCA) of Buildings: A LCA is a process of evaluating the environmental burdens of a building throughout its lifespan. This involves calculating the environmental burdens associated with all aspects of a building from manufacturing the building materials, to constructing the building, to operating the building, to renovating or disposing of it at the end of its life.

3.0 Methodology

3.1. Description of Exterior Infill Wall Enclosures

A total of 11 different exterior infill walls were examined in this study. A detailed description of each wall assembly that was investigated can be found in the Appendix. The wall assemblies that were chosen for this study represent a broad sample of exterior infill walls that are typical of commercial buildings in Canada (many are also applicable to residential construction).

The 11 wall assemblies are classified based on their predominant structural system: concrete masonry unit walls (CMU), metal structural insulated panel walls (MSIP), cold-formed steel stud walls (SS), wood stud walls (WS), pre-engineered steel building walls (PENG), and aluminum curtainwalls (CWALL). Where appropriate, Ontario (standard) clay brick cladding was specified for the wall enclosures. The interior finish was assumed to be regular gypsum board with latex paint, or latex paint alone, depending on typical practice. With the exception of the MSIP wall, the insulation varied from 2 in. (50 mm) of exterior installed extruded polystyrene to cavity filled fiberglass batt insulation.

3.2. Description of Roof Enclosures

A total of eight roof enclosures were examined in this study. A detailed description of each roof assembly can be found in the Appendix. The roofs that were chosen for this study represent a broad sample of typical assemblies for a commercial building in Canada. The eight roofs are classified based on their predominant structural system: concrete hollow core roofs (CHC), open web steel joist roofs (OWSJ), cold-formed steel roofs (CFS), glulam roofs (GLU), and metal structural insulated panel roofs (MSIP). With the exception of the MSIP roof, a 4-ply built-up asphalt roof assembly with 3 in. (75 mm) polyisocyanurate insulation was specified. A suspended acoustic tile ceiling was also specified.

Not all roof joists can span the same distance. Some reach their optimum design state when spanning longer distances and some at shorter spans. To account for this variability, each roof joist was designed for a typical span that it would likely be used for, rather than for one standard span for all. This ensured that

undue advantage/disadvantage was not placed on one system over another, by designing it for a span for which it was not intended. Each roof was designed for structural loads according to Part 4 of the NBCC 2005 (Canadian Commission on Building and Fire Codes, 2006) using the typical design span.

3.3. Evaluating Embodied Energy (and Embodied GWP)

The ATHENA® Environmental Impact Estimator (EIE) for Buildings v4.0.64 (The Athena Institute, 2010) was used to calculate the embodied primary energy and embodied GWP for each building enclosure over a 50 year lifespan in Toronto. In addition to primary energy consumption and GWP, the ATHENA® EIE for Buildings is also capable of calculating acidification potential, human health respiratory effects potential, ozone depletion potential, photochemical smog potential, eutrophication potential, and weighted raw resource use. However, these additional measures are beyond the scope of this paper.

The ATHENA® EIE for Buildings is the only North American specific software tool that can evaluate both entire buildings and individual building components and is based on internationally accepted LCA methodology. The software is based on one of the most comprehensive Life-Cycle Inventory databases in the world and the most comprehensive for the North American building industry. The software considers the full life-cycle impacts of: resource extraction, material manufacturing, construction, transportation, occupancy/maintenance effects, demolition, disposal, and recycling at the end of the building's life.

3.4. Evaluating Operating Energy (and Operating GWP)

To estimate the impact that each alternative building enclosure had on the operating energy use of a building, a baseline building was defined. Using this baseline and holding all other variables constant, the exterior infill walls and roof were systematically replaced with the enclosures identified in this study and the change in the building's operating energy use was recorded.

The ATHENA® EIE for Buildings is unable to calculate the operating energy consumption of a building directly. In this study, operating energy was calculated using eQUEST v3.63 (Hirsch, 2009). eQUEST is based on the DOE-2 building simulation engine. DOE-2 is the most widely respected building energy simulation program available and has been around since the 1970's. It is important to mention that eQUEST calculates secondary energy use. Secondary energy use only includes the energy used by the final consumer unlike primary energy which includes the total requirements for all uses of energy including: secondary energy, energy required to transform one form of energy to another (e.g. coal to electricity), energy used to bring energy to the consumer, and more.

Fortunately, the ATHENA® EIE for Buildings has the ability to convert estimates of secondary energy use to primary energy use. Therefore, the secondary energy use from eQUEST was converted to primary energy use using the ATHENA® EIE converter. This allowed for a direct comparison of the operating energy results with the embodied energy results.

3.5. Baseline Building Description

The baseline building was established based on a combination of ASHRAE Standard 90.1-2007 (ASHRAE, 2007) requirements for climate zone 6 (Toronto, Canada) and the RSMeans Assemblies Cost Data (RSMeans, 2003). A summary of the baseline building is provided:

- Located in Toronto, Canada
- 50 year lifespan
- Single-storey, stand alone retail building
- Gross floor area of 6,300 ft^2 (586 m^2)
- Hours of operation: Monday-Saturday 8am-9pm and Sunday 9am-6pm
- Roof (see BASE ROOF in Appendix)
- Exterior infill walls (see BASE WALL in Appendix)
- 17% window-to-wall ratio
- Cooling equipment: direct expansion (DX) coils (electric)
- Heating equipment: combustion furnace (natural gas)
- Zoning: 100% perimeter zone

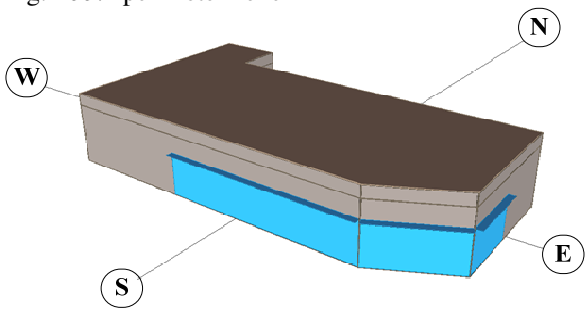

Figure 1: eQUEST Model of Baseline Building

4.0 Results and Discussion

4.1. Life-Cycle Assessment Results for Baseline Building

A LCA was performed on the baseline building in order to establish a datum from which a sensitivity analysis of the walls and roof could be performed.

4.1.1. Total Embodied Energy (and Total Embodied GWP) of Baseline Building

A LCA of embodied energy (and embodied GWP) was performed for the exterior infill walls and roof of the baseline building. The baseline building wall assembly (BASE WALL) consisted of EFIS with 2.5 in. (64 mm) extruded polystyrene insulation and 6 in. (150 mm) steel studs at 24 in. (600 mm) on center. Over a 50 year lifespan, this wall system resulted in approximately 927 MJ/m^2 of embodied primary energy and emission of about 49 kg of $CO_2eq./m^2$.

The baseline building roof assembly (BASE ROOF) consisted of a 4-ply built-up asphalt roof assembly with 3 in. (75 mm) polyisocyanurate insulation and OWSJ at 4 ft (1.2 m) on center. Over a 50 year lifespan, this roof system resulted in approximately 4,684 MJ/m^2 of embodied primary energy and emission of about 213 kg of $CO_2eq./m^2$.

4.1.2. Total Energy (and Total GWP) of Baseline Building

Simulations were performed on the baseline building to determine the total operating energy use (and total operating GWP). It was found that over a 50 year lifespan in Toronto, operation of the baseline building resulted in $48.90x10^6$ MJ of primary energy use (1,669 $MJ/m^2/yr$) and emission of $2.25x10^6$ kg of $CO_2eq.$ (77 kg of $CO_2eq./m^2/yr$).

4.1.3. Comparison of Baseline Building to Average Retail Building in Canada

The average retail building in Canada uses about 1,707 $MJ/m^2/yr$ of energy and emits about 94 kg of $CO_2eq./m^2/yr$ (NRCan, OEE, 2010). The baseline building in this study consumes about 2% less energy per year and emits approximately 18% less $CO_2eq.$ per year than the average retail building in Canada.

4.2. Life-Cycle Assessment Results for Exterior Infill Wall Enclosures

4.2.1. Total Embodied Energy (and Total Embodied GWP) of Walls

The total embodied energy (and total embodied GWP) for the walls identified in this study were calculated. The results of this analysis are illustrated in Figure 2. The total embodied energy (and GWP) for the walls ranged from 580 MJ/m^2 (and 29 kg of $CO_2eq./m^2$) respectively for W9 (PENG) to 1,607 MJ/m^2 (and 105 kg of $CO_2eq./m^2$) respectively for W1 (CMU). W10 (CWALL) actually had a slightly higher GWP (122 kg of $CO_2eq./m^2$), but had less embodied energy (1,590 MJ/m^2). For the steel stud walls, the corresponding energy and GWP ranged from 921 MJ/m^2 and 63 kg of $CO_2eq./m^2$ respectively for W6 (SS) to 1,065 MJ/m^2 and 68 kg of $CO_2eq./m^2$ respectively for W3 (SS).

The total embodied energy (and GWP) of the steel stud walls were higher than that of the comparable wood stud walls by a maximum of about 12% (and 18%) respectively. When altering the steel stud spacing from 16 in. (400 mm) on center to 24 in. (600 mm) on center, it resulted in a decrease in total embodied energy and in total embodied GWP of about 2%. Compared to W10 (CWALL) and W1 (CMU), the steel stud walls performed much better. In fact, the worst performing steel stud wall, W3 (SS), still consumed about 34% less energy and had about 35% less GWP than W1 (CMU).

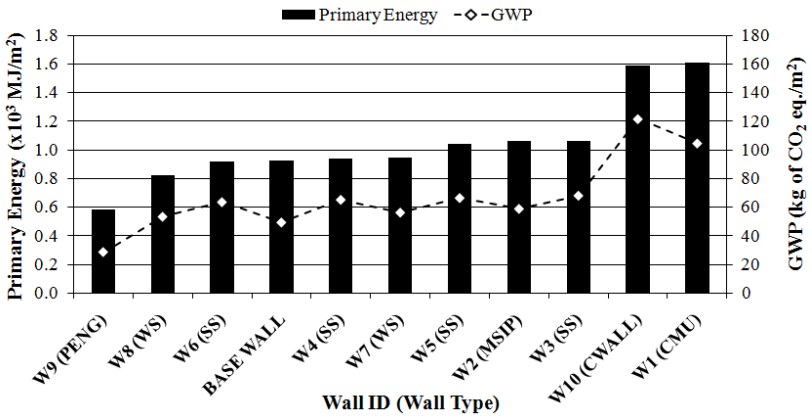

Figure 2: Total Embodied Energy (and GWP) of Exterior Infill Walls after 50 Year Lifespan in Toronto

4.2.2. Total Life-Cycle Energy (and Total Life-Cycle GWP) of Walls

The total life-cycle energy and total life-cycle GWP for each enclosure was calculated for a 50 year lifespan in Toronto. The total life-cycle energy of each enclosure equals the total embodied energy of the enclosure, plus the difference in the total operating energy from the baseline building, after changing the baseline building enclosure to the alternative enclosure (the total life-cycle GWP is calculated in a similar way, but using GWP numbers instead of energy).

The total life-cycle energy (and GWP) for each of the walls are displayed in Figure 3. As it can be seen from the figure, the walls with the lowest total energy (and total GWP) after 50 years were not necessarily the ones with the lowest embodied energy (and embodied GWP). In fact, an increase in total life-cycle energy (and total life-cycle GWP) was found to correspond to a general decrease

---

Note: 1 MJ/m^2 = 88.055 Btu/ft^2 and 1 kg of CO_2 eq./m^2 = 0.205 lb of CO_2 eq./ft^2

in overall assembly R-value. This suggests that operating energy (and therefore enclosure R-value) plays a more significant role over the life of a building than the embodied energy of the building materials, in terms of energy use and GWP.

The best performing wall enclosure was W2 (MSIP), which resulted in a decrease of about 2,027 MJ/m^2 from the baseline wall after 50 years. The worst performing wall enclosure was W10 (CWALL), which resulted in an increase of about 9,300 MJ/m^2 from the baseline wall after 50 years. The best performing steel stud wall enclosure was W5, which over a 50 year lifespan resulted in a decrease of about 49 MJ/m^2 of primary energy compared to the baseline wall. The worst performing steel stud wall enclosure was W4, which over a 50 year lifespan resulted in an increase of about 2,507 MJ/m^2 of primary energy compared to the baseline wall.

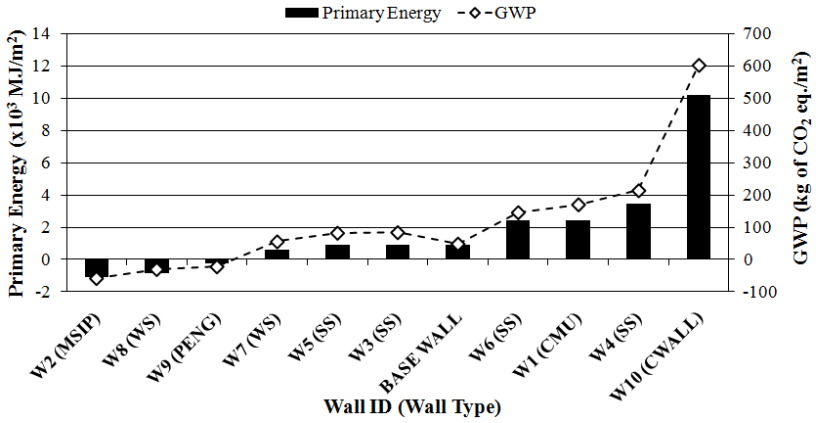

Figure 3: Total Life-Cycle Energy (and GWP) of Exterior Infill Walls after 50 Year Lifespan in Toronto

Changing the stud spacing from 16 in. (400 mm) to 24 in. (600 mm) on center for the steel stud walls with continuous exterior installed insulation, only decreased the total life-cycle energy use by 2% and the total life-cycle GWP by 2%. However, a similar change to the stud spacing for the steel stud walls with cavity installed batt insulation, decreased the total life-cycle energy use by 30% and the total life-cycle GWP by 32%. The wood stud walls consumed less energy after 50 years than the comparable steel stud walls.

Note: 1 MJ/m^2 = 88.055 Btu/ft^2 and 1 kg of CO_2 eq./m^2 = 0.205 lb of CO_2 eq./ft^2

4.3. Life-Cycle Assessment Results for Roof Enclosures

4.3.1. Total Embodied Energy (and Total Embodied GWP) of Roofs

The total embodied energy (and total embodied GWP) for each of the roof enclosures identified in this study was evaluated and the results are displayed in Figure 4. The total embodied energy (and GWP) for the roof enclosures ranged from as little as 1,210 MJ/m^2 (and 73 kg of CO_2eq./m^2) respectively for R8 (MSIP) to as high as 5,002 MJ/m^2 (and 244 kg of CO_2eq./m^2) respectively for R1 (CHC). For the cold-formed steel roof enclosures, the corresponding energy and GWP ranged from 4,419 MJ/m^2 and 196 kg of CO_2eq./m^2 respectively for R3 (CFS) to 4,615 MJ/m^2 and 213 kg of CO_2eq./m^2 respectively for R6 (CFS).

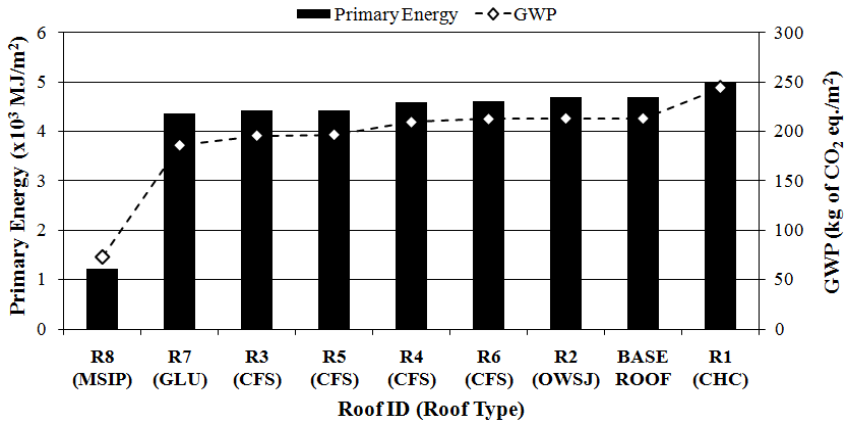

Figure 4: Total Embodied Energy (and GWP) of Roof Assemblies after 50 Year Lifespan in Toronto

Excluding the MSIP and CHC roofs, the remaining roofs only differed by about 7% in terms of total embodied energy and 13% in terms of total embodied GWP after 50 years. All of the roof enclosures (except the MSIP roof) had a 4-ply built-up asphalt roof and 3 in. (75 mm) of continuous polyisocyanurate insulation. The results suggest that the total embodied energy (and GWP) of the roof enclosures were more influenced by insulation levels and roof coverings than by the differences in the supporting structure.

Note: 1 MJ/m^2 = 88.055 Btu/ft^2 and 1 kg of CO_2 eq./m^2 = 0.205 lb of CO_2 eq./ft^2

4.3.2. Total Life-Cycle Energy (and Total Life-Cycle GWP) of Roofs

The total life-cycle energy (and total life-cycle GWP) for each of the roof enclosures identified in this study are displayed in Figure 5. The best performing roof enclosure was R8 (MSIP), which resulted in a decrease of about 5,180 MJ/m^2 from the baseline roof after 50 years. The worst performing roof enclosure was R1 (CHC).

All of the CFS, GLU, and OWSJ roofs consumed about equal amounts of primary energy and had nearly the same GWP after 50 years. This was due to the fact that all of these roofs had the same insulation and 4-ply built-up asphalt roof covering. An increase in total life-cycle energy (and GWP) corresponded in general to an increase in total life-cycle embodied energy (and GWP), but only because the R-values of these roofs (except R8) were very similar. Therefore, there was very little difference in life-cycle operating energy (and GWP). The CFS roofs did perform better than R2 (OWSJ), but marginally so. Looking at the roof systems with a span of 25 ft (7.6 m) or longer, the cold-formed steel roof truss systems performed slightly better than the conventional OWSJ enclosure.

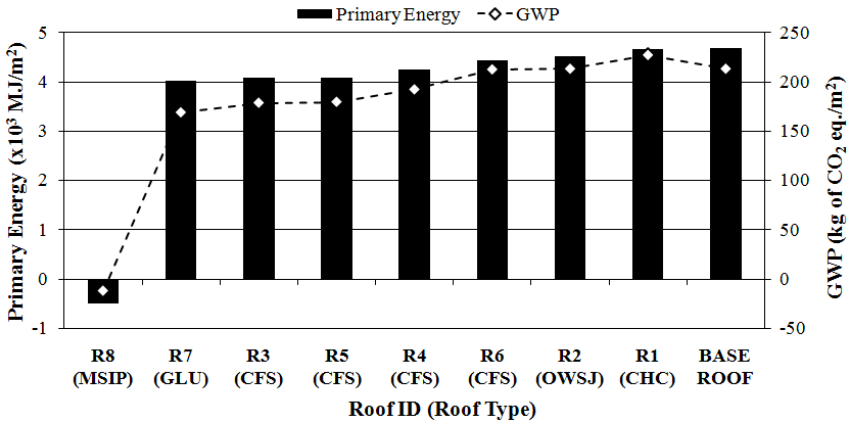

Figure 5: Total Life-Cycle Energy (and GWP) of Roof Assemblies after 50 Year Lifespan in Toronto

Note: 1 MJ/m^2 = 88.055 Btu/ft^2 and 1 kg of CO_2 eq./m^2 = 0.205 lb of CO_2 eq./ft^2

5.0 Conclusions

Exterior Infill Wall Enclosures

1. At most, the wood stud walls had 12% less total embodied energy and 18% less total embodied GWP than the steel stud walls after 50 years. However, the steel stud walls performed between 30% to 50% better than the concrete masonry unit wall and aluminum curtainwall
2. It was found that an increase in total life-cycle energy (and total life-cycle GWP) corresponded in general to a decrease in overall assembly R-value. Therefore, assembly R-value played a far more significant role in terms of energy use and GWP over the life of the building, than any differences in embodied effects between the building materials
3. Changing the stud spacing from 16 in. (400 mm) to 24 in. (600 mm) on center for the steel stud walls with continuous exterior insulation, only decreased the total life-cycle energy use and the total life-cycle GWP by 2%. A similar change in stud spacing for the case of the steel stud walls with cavity installed batt insulation, resulted in a decrease in total life-cycle energy use of 30% and total life-cycle GWP of 32%

Roof Enclosures

1. After 50 years, the differences in total embodied energy (and total embodied GWP) for the various roof enclosures were minimal, if the same level of insulation and roof covering were provided
2. It was found that an increase in total life-cycle energy (and GWP) corresponded to an increase in total life-cycle embodied energy (and GWP) in this case, but only because the R-values of all of these roofs (except R8) were extremely similar
3. The cold-formed steel roof truss enclosures used slightly less total energy (and total GWP) after 50 years than the typical OWSJ system

References

ASHRAE. (2007). *ASHRAE Standard 90.1-2007: Energy Standard for Buildings Except Low-Rise Residential Buildings I-P Edition.* Atlanta, GA: American Society of Heating, Refrigerating and Air-Conditioning Engineers, Inc.

Canadian Commission on Building and Fire Codes. (2006). *User's Guide-National Building Code 2005: Structural Commentaries (Part 4 of Division B).* Ottawa, ON: National Research Council Canada.

Cole, R. J., & Kernan, P. C. (1996). Life-Cycle Energy Use in Office Buildings. *Building and Environment , 31*, 307-317.

Hirsch, J. J. (2009). *eQUEST*. Retrieved March 29, 2010, from DOE2 Website: http://www.doe2.com/eQuest/

NRCan, OEE. (2010). *Energy Use Data Handbook Tables (Canada).* Retrieved March 18, 2010, from Natural Resources Canada, Office of Energy Efficiency Website: http://oee.nrcan.gc.ca/corporate/statistics/neud/dpa/handbook_tables.cfm?attr=0

RSMeans. (2003). *Assemblies Cost Data 2004*. Kingston, MA: Construction Publishers & Consultants.

The Athena Institute. (2010, February 18). *The Impact Estimator for Buildings*. Retrieved March 29, 2010, from Athena Institute Website: http://www.athenasmi.org/tools/impactEstimator/index.html

USGBC. (2010). *Green Building Research*. Retrieved March 18, 2010, from U.S. Green Building Council Website: http://www.usgbc.org/DisplayPage.aspx?CMSPageID=1718

Appendix - Descriptions of Enclosures

Wall Assemblies

BASE WALL — **COLD-FORMED STEEL STUD WALL (SS)**

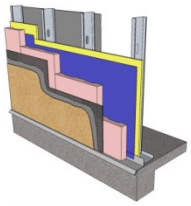

Assembly Layers: ***Outside,*** EFIS coating over metal mesh, 64mm extruded polystyrene rigid insulation, Vertical drainage channels in insulation, Self-adhesive membrane with primer (AB, VB, WB), 16mm non paper-faced gypsum sheathing, 39mm x 152mm x 1.52mm steel studs @ 600mm o/c *(includes 0.2kg of screws and fasteners per stud plus top and bottom steel tracks),* Regular 16mm gypsum board, Latex paint, ***Inside***
R-Value = 15.6 (RSI-Value = 2.75)

W1 (CMU) — **CONCRETE MASONRY UNIT WALL (CMU)**

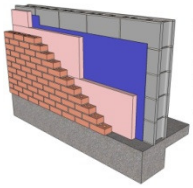

Assembly Layers: ***Outside,*** Ontario (standard) clay brick cladding, 25mm air gap, 50mm extruded polystyrene rigid insulation, Self-adhesive membrane with primer (AB, VB, WB), 200mm standard weight concrete block *(includes #15M bars @ 400mm o/c with grout),* Latex paint, ***Inside***
R-Value = 13.3 (RSI-Value = 2.34)

W2 (MSIP) — **METAL STRUCTURAL INSULATED PANEL WALL (MSIP)**

Assembly Layers: ***Outside,*** Latex based paint, 0.46mm galvanized commercial steel cladding (WB), 100mm polyurethane foam insulation, 0.46mm galvanized commercial steel cladding (AB, VB), Latex based paint, 1.90mm galvanized 200mm Z-girts @ 1200mm o/c *(self-weight: 6.3 kg/m = 4.2 lb/ft),* ***Inside***
R-Value = 24.5 (RSI-Value = 4.31)

W3 (SS) — **COLD-FORMED STEEL STUD WALL (SS)**

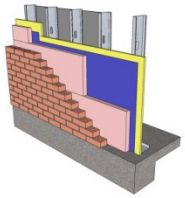

Assembly Layers: ***Outside,*** Ontario (standard) clay brick cladding, 25mm air gap, 50mm extruded polystyrene rigid insulation, Self-adhesive membrane with primer (AB, VB, WB), 16mm non paper-faced gypsum sheathing, 39mm x 152mm x 1.21mm steel studs @ 400mm o/c *(includes 0.2kg of screws and fasteners per stud plus top and bottom steel tracks),* Regular 16mm gypsum board, Latex paint, ***Inside***
R-Value = 14.2 (RSI-Value = 2.49)

W4 (SS) — **COLD-FORMED STEEL STUD WALL (SS)**

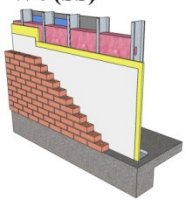

Assembly Layers: ***Outside,*** Ontario (standard) clay brick cladding, 25mm air gap, Building wrap (WB), 16mm non paper-faced gypsum sheathing, 39mm x 152mm x 1.21mm steel studs @ 400mm o/c *(includes 0.2kg of screws and fasteners per stud plus top and bottom steel tracks),* 140mm fiberglass batt insulation, 6mil poly (AB, VB), Regular 16mm gypsum board, Latex paint, ***Inside***
R-Value = 10.6 (RSI-Value = 1.86)

Wall Assemblies (Cont.)

W5 (SS) — **COLD-FORMED STEEL STUD WALL (SS)**

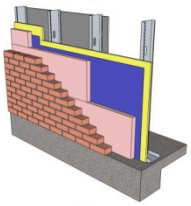

Assembly Layers: Outside, Ontario (standard) clay brick cladding, 25mm air gap, 50mm extruded polystyrene rigid insulation, Self-adhesive membrane with primer (AB, VB, WB), 16mm non paper-faced gypsum sheathing, 39mm x 152mm x 1.52mm steel studs @ 600mm o/c *(includes 0.2kg of screws and fasteners per stud plus top and bottom steel tracks)*, Regular 16mm gypsum board, Latex paint, **Inside**

R-Value = 14.1 (RSI-Value = 2.49)

W6 (SS) — **COLD-FORMED STEEL STUD WALL (SS)**

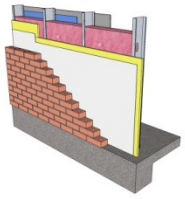

Assembly Layers: *Outside,* Ontario (standard) clay brick cladding, 25mm air gap, Building wrap (WB), 16mm non paper-faced gypsum sheathing, 39mm x 152mm x 1.52mm steel studs @ 600mm o/c *(includes 0.2kg of screws and fasteners per stud plus top and bottom steel tracks),* 140mm fiberglass batt insulation, 6mil poly (AB, VB), Regular 16mm gypsum board, Latex paint, ***Inside***

R-Value = 12.2 (RSI-Value = 2.16)

W7 (WS) — **WOOD STUD WALL (WS)**

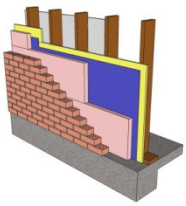

Assembly Layers: *Outside,* Ontario (standard) clay brick cladding, 25mm air gap, 50mm extruded polystyrene rigid insulation, Self-adhesive membrane with primer (AB, VB, WB), 16mm non paper-faced gypsum sheathing, 38mm x 140mm wood studs @ 400mm o/c *(wood studs are kiln-dried to a MC of at least 19%; include 110 g/m^2 steel nails @ 400mm o/c; and includes double top plate and one sill plate),* Regular 16mm gypsum board, Latex paint, ***Inside***

R-Value = 14.4 (RSI-Value = 2.53)

W8 (WS) — **WOOD STUD WALL (WS)**

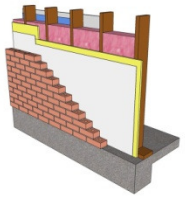

Assembly Layers: *Outside,* Ontario (standard) clay brick cladding, 25mm air gap, Building wrap (WB), 16mm non paper-faced gypsum sheathing, 38mm x 140mm wood studs @ 400mm o/c *(wood studs are kiln-dried to a MC of at least 19%; include 110 g/m^2 steel nails @ 400mm o/c; and includes double top plate and one sill plate),* 140mm fiberglass batt insulation, 6mil poly (AB, VB), Regular 16mm gypsum board, Latex paint, ***Inside***

R-Value = 19.0 (RSI-Value = 3.34)

W9 (PENG) — **PRE-ENGINEERED STEEL BUILDING WALL (PENG)**

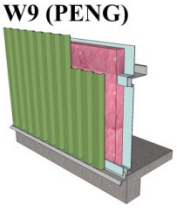

Assembly Layers: *Outside,* Latex based paint, 0.46mm galvanized commercial steel cladding (WB), 140mm fiberglass batt insulation, 6mil poly (AB, VB), 1.90mm galvanized 200mm Z-girts @ 1200mm o/c *(self-weight: 6.3 kg/m = 4.2 lb/ft),* ***Inside***

R-Value = 17.9 (RSI-Value = 3.15)

Wall Assemblies (Cont.) & Roof Assemblies

W10 (CWALL) **CURTAINWALL (CWALL)**

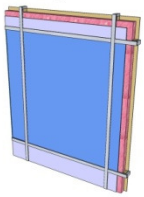

Assembly Layers: ***Outside,*** Opaque glazing spandrel panel (WB) *(one pane of 6mm glazing),* Self-supporting aluminum curtainwall grid system with thermal break *(100mm deep mullions spaced 2m o/c vertically and 1.5m o/c horizontally),* 90mm high density fiberglass insulation, Metal backpan (AB, VB), ***Inside***

R-Value = 6.3 (RSI-Value = 1.10)

R1 (CHC) **CONCRETE HOLLOW CORE ROOF (CHC)**

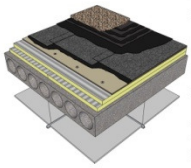

Assembly Layers: ***Outside,*** Ballast (aggregate stone), 4-ply built-up asphalt roof assembly (WB) *(type III glass felt & roofing asphalt),* Basesheet *(modeled as #15 organic felt),* Roofing asphalt, 12mm coverboard *(modeled as moisture resistant gypsum),* Continuous 75mm polyisocyanurate insulation, 200mm concrete hollow core roof slab (AB, VR) *(9% flyash, 45+ MPa, typical reinforcement),* 16mm suspended acoustical ceiling, Misc. fasteners, nails, and galvanized sheet, ***Inside***

R-Value = 22.8 (RSI-Value = 4.02); Design Span = 7.6 m

BASE ROOF / R2 (OWSJ) **OPEN WEB STEEL JOIST ROOF (OWSJ)**

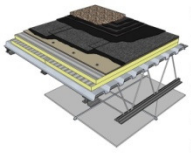

Assembly Layers: ***Outside,*** Ballast (aggregate stone), 4-ply built-up asphalt roof assembly (WB) *(type III glass felt & roofing asphalt),* Basesheet *(modeled as #15 organic felt),* Roofing asphalt, 12mm coverboard *(modeled as moisture resistant gypsum),* Continuous 75mm polyisocyanurate insulation, 39mm x 0.76mm galvanized corrugated metal deck (AB, VB), 550mm open web steel joists @ 1200mm o/c *(self-weight: 10.3 kg/m = 6.9 lb/ft),* 16mm suspended acoustical ceiling, Misc. fasteners, nails, and galvanized sheet, ***Inside***

R2 (OWSJ) → R-Value = 21.5 (RSI-Value = 3.79); Design Span = 9.1 m

BASE ROOF → R-Value = 20.8 (RSI-Value = 3.67)

(R-Value for R2 (OWSJ) is based on THERM simulation. R-Value for BASE ROOF is based on ASHRAE 90.1-2007 minimum building envelope requirements for climate zone 6)

R3 (CFS) **COLD-FORMED STEEL ROOF (CFS)**

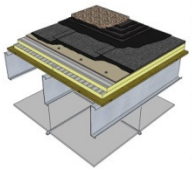

Assembly Layers: ***Outside,*** Ballast (aggregate stone), 4-ply built-up asphalt roof assembly (WB) *(type III glass felt & roofing asphalt),* Basesheet *(modeled as #15 organic felt),* Roofing asphalt, 12mm coverboard *(modeled as moisture resistant gypsum),* Continuous 75mm polyisocyanurate insulation, 19mm plywood deck (AB, VR), 39mm x 245mm x 1.52mm galvanized cold-formed steel C-joists @ 600mm o/c *(self-weight: 4.2 kg/m = 2.8 lb/ft),* 16mm suspended acoustical ceiling, Misc. fasteners, nails, and galvanized sheet, ***Inside***

R-Value = 22.4 (RSI-Value = 3.95); Design Span = 5.0 m

R4 (CFS) **COLD-FORMED STEEL ROOF (CFS)**

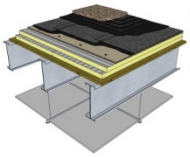

Assembly Layers: ***Outside,*** Ballast (aggregate stone), 4-ply built-up asphalt roof assembly (WB) *(type III glass felt & roofing asphalt),* Basesheet *(modeled as #15 organic felt),* Roofing asphalt, 12mm coverboard *(modeled as moisture resistant gypsum),* Continuous 75mm polyisocyanurate insulation, 19mm plywood deck (AB, VR), (2) - 39mm x 245mm x 1.52mm galvanized cold-formed steel C-joists back-to-back @ 600mm o/c *(self-weight: 8.4 kg/m = 5.6 lb/ft),* 16mm suspended acoustical ceiling, Misc. fasteners, nails, and galvanized sheet, ***Inside***

R-Value = 22.4 (RSI-Value = 3.95); Design Span = 7.6 m

R5 (CFS) **COLD-FORMED STEEL ROOF (CFS)**

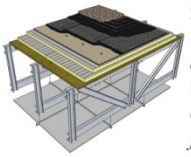

Assembly Layers: ***Outside,*** Ballast (aggregate stone), 4-ply built-up asphalt roof assembly (WB) *(type III glass felt & roofing asphalt),* Basesheet *(modeled as #15 organic felt),* Roofing asphalt, 12mm coverboard *(modeled as moisture resistant gypsum),* Continuous 75mm polyisocyanurate insulation, 19mm plywood deck (AB, VR), 9100mm long x 600mm deep cold-formed steel trusses spaced 600mm o/c *(self-weight: 4.5 kg/m = 3.0 lb/ft),* 16mm suspended acoustical ceiling, Misc. fasteners, nails, and galvanized sheet, ***Inside***

R-Value = 22.4 (RSI-Value = 3.95); Design Span = 9.1 m

R6 (CFS) **COLD-FORMED STEEL ROOF (CFS)**

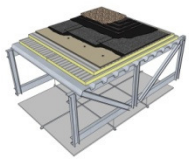

Assembly Layers: ***Outside,*** Ballast (aggregate stone), 4-ply built-up asphalt roof assembly (WB) *(type III glass felt & roofing asphalt),* Basesheet *(modeled as #15 organic felt),* Roofing asphalt, 12mm coverboard *(modeled as moisture resistant gypsum),* Continuous 75mm polyisocyanurate insulation, 39mm x 0.76mm galvanized corrugated metal deck (AB, VB), 9100mm long x 762mm deep cold-formed steel trusses spaced 1200mm o/c *(self-weight: 8.9 kg/m = 6.0 lb/ft),* 16mm suspended acoustical ceiling, Misc. fasteners, nails, and galvanized sheet, ***Inside***

R-Value = 21.5 (RSI-Value = 3.79); Design Span = 9.1 m

R7 (GLU) **GLULAM ROOF (GLU)**

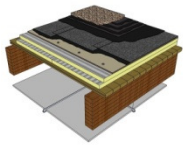

Assembly Layers: ***Outside,*** Ballast (aggregate stone), 4-ply built-up asphalt roof assembly (WB) *(type III glass felt & roofing asphalt),* Basesheet *(modeled as #15 organic felt),* Roofing asphalt, 12mm coverboard *(modeled as moisture resistant gypsum),* Continuous 75mm polyisocyanurate insulation, 38mm SPF tongue & groove solid wood plank decking (AB, VR), 80mm x 494mm 24f-E glulam joists @ 1800m o/c, 16mm suspended acoustical ceiling, Misc. fasteners, nails, and galvanized sheet, ***Inside***

R-Value = 23.1 (RSI-Value = 4.07); Design Span = 9.1 m

R8 (MSIP) **METAL STRUCTURAL INSULATED PANEL WALL (MSIP)**

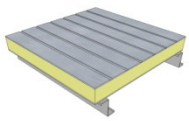

Assembly Layers: ***Outside,*** Latex based paint, 0.46mm galvanized commercial steel cladding (WB), 150mm polyurethane foam insulation, 0.46mm galvanized commercial steel cladding (AB, VB), Latex based paint, 1.90mm galvanized 229mm Z-shape purlin @ 1200mm o/c *(self-weight: 6.6 kg/m = 4.4 lb/ft),* Misc. fasteners, nails, and galvanized sheet, ***Inside***

R-Value = 36.2 (RSI-Value = 6.37); Design Span = 5.0 m

Twentieth International Specialty Conference on Cold-Formed Steel Structures
St. Louis, Missouri, U.S.A., November 3 & 4, 2010

Behavior and Design of Axially Compressed Sheathed Wall Studs

L.C.M. Vieira Jr.[1] and B.W. Schafer[2]

Abstract

The objective of this paper is to summarize efforts in a multi year project dedicated to developing a reliable design method for cold-formed steel wall studs that rely on sheathing for bracing. Testing on single columns with sheathing, and full-scale walls with sheathing, are summarized. Particular emphasis is placed on the observed limit states given the different sheathing conditions. The sheathing supplies beneficial restraint to the wall studs and the stiffness of this sheathing-based restraint is characterized experimentally and analytically. A unique application of the Direct Strength Method of design is explored where the sheathing-based restraint is used explicitly in determination of the elastic buckling loads of the wall studs, and then these elastic buckling loads are utilized to determine the strength. The test results are compared with the newly proposed design method as well as with previous design methods adopted by the AISI Specification. Good agreement is demonstrated for the new approach both in terms of strength and limit states prediction.

1 Introduction

Cold-formed steel walls have long relied on bracing to prohibit detrimental global buckling modes and to develop the full capacity of the wall. In the simplest case bracing is supplied by an explicit member, such as the bridging channel shown in Figure 1a. However, since at least the 1940s, the additional resistance supplied to a cold-formed steel stud due to its connection to sheathing, Figure 1b, has intrigued researchers and designers. Sheathing bracing offers the potential for significant economy since the sheathing is already supplied for the walls basic functioning. An isolated, but sheathed, column (wall stud) is shown in Figure 1c, and in this work tests were conducted on both

[1] Graduate Research Assistant, Johns Hopkins University, Baltimore, MD, USA
[2] Professor, Johns Hopkins University, Baltimore, MD, USA

isolated and full walls. It has been common in the past to simplify the role of the bracing of the column to an in-plane spring column model, as shown in Figure 1d. In this work, the stiffness provided by the sheathing is pursued for both in-plane and out-of plane restraint, as shown in Figure 1e, as it was found that each of these restraints play an important role in bracing the wall stud.

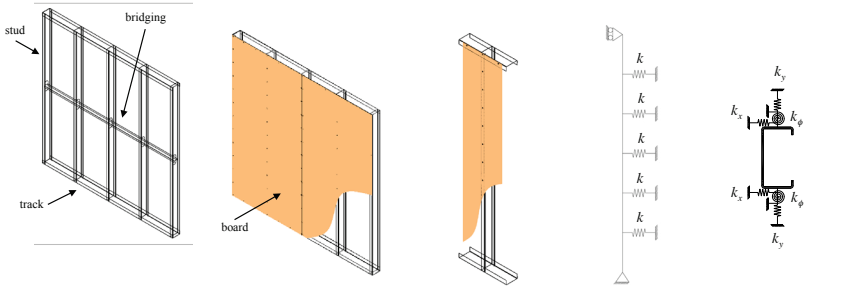

a) Bare wall with bridging | b) Sheathed wall, no bridging | c) Single column | d) Spring-column model | e) Springs on the cross-section

Figure 1 – Stud bracing

This paper summarizes the results of a larger project that aims to understand the behavior of sheathed wall studs and translate that knowledge into a reliable design method. The design method is corroborated by experimental tests. Single column tests, full wall tests, and rotational and translational stiffness tests were all conducted in support of the larger effort to develop a design method.

2 Experiments on sheathed studs and walls

The single column and full-scale sheathed wall tests summarized in this paper are covered in detail in progress reports: Shifferaw et al. (2009) and Vieira and Schafer (2009). The reports cover a series of thirteen full-scale walls and twenty-seven single columns all tested under axial compression. The studies concentrated on the impact of attaching different types of sheathing to the side of the wall, specifically bare (no sheathing), oriented strand board (OSB) or Gypsum (Gyp), under a variety of different combinations.

The cold-formed steel studs used in the test are 362S162-68's (50 ksi) (SSMA/ASTM nomenclature) throughout. Two types of sheathing are employed: OSB (7/16 in., rated 24/16, exposure 1) and Gypsum (½ in. Sheetrock). Number 6 screws (Simpson #6 x 1 5/8'') were used to connect to the Gypsum boards and number 8 screws (Simpson #8 x 1 15/16'') to connect to the OSB boards. The single column tests covered short (two feet), intermediate

(four and six feet) and long columns (eight feet). The walls have five studs of 8 feet equally spaced between two tracks of the same length. The boards are connected to the studs every 6 inches at the edge studs of the walls and every 12 inches in the field studs of the walls and the single column tests.

2.1 Observed Strength

Strength and observed failure mode for the single column tests as a function of column length and sheathing type are summarized in Table 1. Not provided are a series of studies on the end boundary conditions (Shifferaw et al. 2009) that examine the impact of the track and the sheathing on the strength and failure mode. It was found that the sheathing should not be allowed to bear against the end platens of the test fixture or artifically high strength is observed.

For the full-scale wall tests, strength and observed failure mode are summarized in Table 2. Multiple tests are conducted on each nominally identical sheathing arrangement and the mean value is also reported. To compare the full-scale walls with the single column tests, the per stud strength (mean value divided by 5 studs) is reported. The results reveal that the attachment of boards to the side of the wall can increase the axial strength of the wall by as much as 91%, for example, when comparing the case of Bare-Bare to that of OSB-OSB. However, detrimental results were also observed; specifically, the OSB-Bare walls had no post-buckling reserve as they failed in a dramatic flexural-torsional mode. In walls with symmetric sheathing (OSB-OSB and Gyp-Gyp), the observed failure mode of the stud was local buckling, and exhibited deformations essentially identical for the two sheathing types. However, for the case with asymmetric sheathing (OSB-Gyp) local buckling failure modes as well as other failure modes (primarily distortional buckling) were also observed in the studs.

As expected the peak load follows in an ascending order of Bare-Bare, OSB-Bare, Gyp-Gyp, OSB-Gyp and OSB-OSB, with little exception. Comparing Table 1 to Table 2 the limit states are the same for 8 ft single column tests and the full 8 ft x 8 ft wall, nonetheless, the peak load is usually slightly lower in the wall tests, except for the OSB-Bare tests. This is somewhat surprising as it demonstrates that full sheathing resistance is developed even with only one line of vertical fasteners, as in the single column tests. Postulated reasons for the slight decrease in the full-scale wall tests, when compared with the single columns tests: (a) local buckling in the outermost studs of the wall do not always fully bear on the track since they are at the ends of the track (b) the tributary area of the board designated to each stud in the wall as engaged for sheathing resistance is modestly less than in the single column tests, (c) bracing forces in the sheathing accumulate and may have a modestly detrimental influence, (d)

when the weakest of the 5 studs in the wall fail the forces must be carried by the other studs, thus observed strengths may be more of a weakest link strength as opposed to the idealized redistribution of a fully parallel system.

For the OSB-Bare case the failure is in flexural-torsional buckling and the full wall has a higher observed per stud mean strength than the single column, but the variability is significant and the failure mode in the full walls is dramatic and without any post-peak reserve.

Table 1 – Column tests, peak load and limit state

Length (feet)	Sheathing Configuration	Peak Load (kips)	Limit State
2	Bare-Bare	19.77	Distortional
	OSB-Bare	21.45	Local
	Gyp-Gyp	21.74	Local
	OSB-Gyp	21.99	Local
	OSB-OSB	23.10	Local
	OSB-OSB	22.84	Local
4	Bare-Bare	19.03	FT
	OSB-Bare	21.99	Local
	Gyp-Gyp	22.39	Local
	OSB-Gyp	21.62	Local
	OSB-OSB	22.26	Local
6	Bare-Bare	13.59	FT
	OSB-Bare	18.01	FT
	Gyp-Gyp	19.94	Local
	OSB-Gyp	20.40	Local
	OSB-OSB	22.38	Local
8	Bare-Bare	12.84	Flexural
	OSB-Bare	15.64	FT
	Gyp-Gyp	21.37	Local
	OSB-Gyp	22.45	Local
	OSB-OSB	23.09	Local

Table 2 – Wall tests, peak load and limit state

Sheathing Configuration	Peak Load (kips)	Limit State	Mean
Bare-Bare	56.33	FT and F	56.33 (56.33/5=11.27)
OSB-Bare	81.57	FT	87.67 (87.67/5=17.53)
	89.21	FT	
	92.23	FT	
Gyp-Gyp	94.07	Local	96.39 (96.39/5=19.28)
	96.66	Local	
	98.44	Local	
OSB-Gyp	103.05	Local	104.92 (104.92/5=20.98)
	105.71	Local	
	105.99	Local	
OSB-OSB	106.04	Local	107.80 (107.8/5=21.56)
	109.55	Local	

2.2 Observed Behavior

The observed limit states for the 8 ft x 8ft walls and the 8 ft long single columns are nearly identical. Only in the Bare-Bare case was some difference observed, as a few of the studs in the full wall test failed in flexural-torsional buckling instead of pure weak-axis flexural buckling. For the shorter length single column tests as the length of the columns gets shorter the global modes are less pronounced and the local mode dominates. In nearly all tests the local buckling failure occurs at the ends of the stud. It is postulated that as the stud is squeezed to fit into the track a large initial imperfection is applied at the end, ultimately triggering failure at this location.

The visually observed global buckling modes are consistent with fixed end conditions. This is likely due to (a) the studs were fully seated in the tracks during assembly and (b) the bearing surface for the track are stiff and level, as they are steel end fixtures. The impact of this condition may be readily observed

in Figure 2 where the bare column tests are compared to the values predicted by AISI-S100-07. As can be seen, the assumption of pinned ends (K=1.0) is overly conservative and the ideal fixed end conditions (K=0.5, i.e., $K_x=K_y=K_t=0.5$) leads to a fine approximation. Note, supplemental analysis by the authors, but not provided here, has shown the importance of applied axial load in closing gaps and restraining warping deformations at the ends, and allowing the full fixity to develop. Also, see LaBoube and Findlay (2007) for more on the impact of stud-to-track gaps on performance. Finally, Figure 2 also provides a comparison between the effective width method of column design utilized in the main Specification of AISI-S100-07 and the Direct Strength Method (DSM) of column design utilized in Appendix 1 of AISI-S100-07. The two methods provide nearly the same result for the studied column without sheathing.

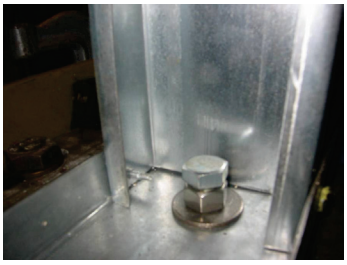

a) Contact stud and track

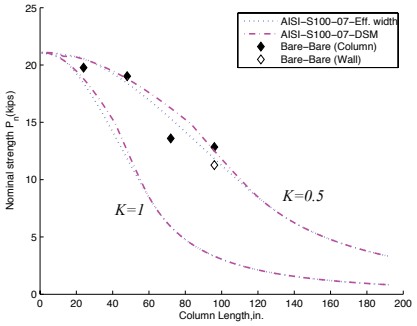

b) Tests and code prediction

Figure 2 – Bare tests and code predictions

3 Estimating restraint supplied by sheathing

With the strength and failure modes established the focus of the work switches to understanding how the sheathing restrains the wall studs. In specific, how the springs of Figure 1e are developed in actual walls is the focus of this section (Section 3), while the impact of the developed springs on the stability of the studs is the focus of Section 4. Finally, the impact on strength is explored in Section 5.

3.1 In-plane lateral (k_x) resistance

Several design models have been developed based on the in-plane stiffness provided by the sheathing to the stud. For instance, Winter's (1960) model assumes that the critical bracing stiffness and strength that sheathing supplies to

the stud is derived at the fastener location in direct shear. In essence, arguing that only local deformations must be understood. Simaan and Peköz's (1976) model ignored (simplified) the fact that the shear diaphragm must be resolved through the fasteners and only included flexibility from the diaphragm (the sheathing) itself. Diaphragm stiffness develops as the sheathing itself undergoes shear, which also translates into a lateral resistance at the fastener locations.

Here, it is found that both local and diaphragm resistance exist, and should be included. The importance of including both local and diaphragm stiffness is illustrated with a test on a full-scale wall. Where, instead of sheathing the wall with full boards, OSB strips (2 in. wide) were connected to the studs (Figure 3a). The use of strips negates the shear diaphragm resistance (k_d). The wall failed in flexural buckling at 69.5 kips, Figure 3b, slightly above the bare wall strength, and well below the fully sheathed strength (which fails in local buckling). Sheathing bracing derives from both the local and diaphragm resistance.

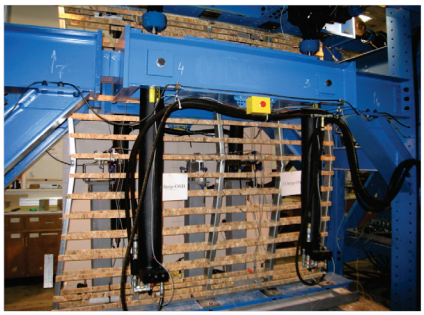

a) Full wall test, strips instead of full boards

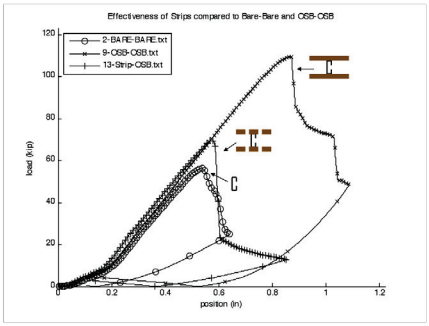

b) Comparison between loading curves

Figure 3 – Effectiveness of strips compared to Bare-Bare and OSB-OSB

To date, existing design methods have provided somewhat contradictory explanations for the manner in which sheathing braces studs, with some methods indicating a strong dependence on stud spacing, others ignoring it altogether. However, if one realizes that the local fastener stiffness is in series with the sheathing diaphragm stiffness then the explanation becomes clear. If local stiffness is low enough (and just as importantly diaphragm stiffness high enough) one will only see the local stiffness in the response and stud and fastener spacing will be largely irrelevant. Conversely, if local stiffness is high enough, say for example from a welded specimen with a steel sheet (and diaphragm stiffness low enough) then only the diaphragm stiffness will be important and stud spacing will be enormously important. Mathematically this may be handled by realizing k_x may be approximated as

$$k_x = 1/(1/k_\ell + 1/k_d) \quad (1)$$

where k_ℓ is determined experimentally, and k_d, as will be shown, can be found using Eq. 2. For bracing strength the local model (and its associated testing) includes the most critical strength limiting failure modes: bearing, tilting, edge pull-out, and screw shear. Failure of the sheathing itself, in shear, and not at the connector location is possible (e.g. in a shear wall), but is generally not an expected failure mode for sheathing only acting as bracing.

In the tests conducted in this work to determine k_ℓ the following variables were taken into account: sheathing type, stud spacing, fastener spacing, edge distance, environmental conditions, and construction flaws. The results provide characterization of the local stiffness and strength that is supplied as the fasteners bear and tilt in a stud-sheathing assembly, Figure 4.

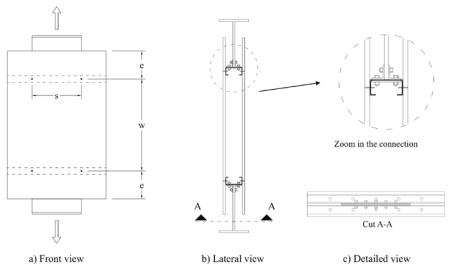

Figure 4 – Test setup design

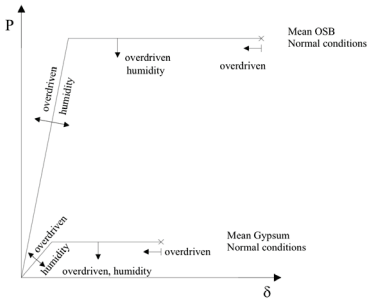

Figure 5 – P-δ of OSB vs. Gypsum

A stylized load-displacement curve, Figure 5, provides a graphical depiction of the average results and dramatically shows the difference between the two sheathing types. As indicated in the figure the impact of humidity and over-driving the fasteners is the same for both sheathing types. Humidity decreases stiffness and strength. Over-driving the fasteners increases stiffness, but decreases strength and deformation capacity.

A condensed summary of the test results is provided in Table 3, where normal conditions refer to w = 24 in.; s = 4, 12, or 20 in.; e = 6 in. (Figure 4); kept for seven days at a temperature of 20C and 65% humidity. The overdriven condition has the same w, s, and e but the screw is overdriven by 1/8''. The humid (saturated) condition has dimensions w = 8 in.; e = 2 in.; and s = 4, 6, 9, 12, and 20 in.; and are kept immersed in water for 7 days.

Table 3 – Condensed summary of test results

		k initial		Pmax		δ @ Pmax	
		mean (kip/in)	coef. variation	mean (kip)	coef. variation	mean (in)	coef. variation
OSB	Normal Conditions	7.08	0.07	0.58	0.03	0.62	0.02
	Overdriven	9.36	0.10	0.41	0.05	0.34	0.27
	Humid (saturated)	6.32	0.10	0.26	0.04	0.51	0.21
Gypsum	Normal Conditions	2.43	0.02	0.09	0.03	0.34	0.13
	Overdriven	3.49	0.14	0.07	0.02	0.15	0.57
	Humid (saturated)	0.24	-	0.02	-	0.42	-

For nominally identical studs, fasteners, and spacing: the lateral stiffness of an OSB sheathed specimen is 3 times greater than gypsum board; the shear capacity in OSB is nearly 7 times greater than gypsum board as the failure mode switches from screw shear to tear out; and the displacement at peak load is 2 times greater in OSB than in gypsum. An additional fifteen tests were conducted comparing plywood samples from Canada and the United States, the results can be found in the report by Vieira and Schafer (2009).

To determine the diaphragm stiffness, k_d, an analytical model was developed based on a plate deformed laterally following a sine-wave curve, Figure 6. In the model the stiffness at a fastener location is the force at the fastener, developed from an integration of the shear stress over the tributary area of the fastener, divided by the deformation, at the fastener location. For sheathing with a low shear modulus or where the panel is wide and short, both typical for the sheathing considered in wall studs, then the stresses are controlled by shear deflections consistent with diaphragm action.

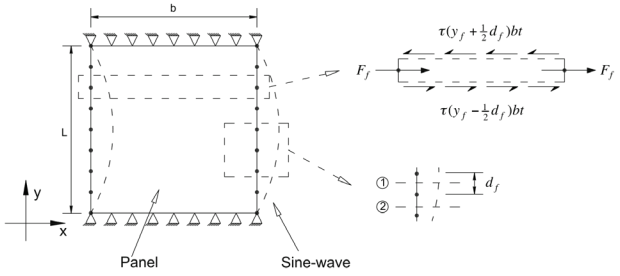

Figure 6 – Plate Model

Vieira and Schafer (2009) provide the full derivation for k_d, that leads to:

$$k_d = \frac{2\pi G t w_{tf}}{L} \cdot \sin\left(\frac{\pi d_f}{2L}\right) \cong \frac{\pi^2 G t w_{tf} d_f}{L^2} \qquad (2)$$

The variables in Eq. 2 are defined in Figure 6 except for shear modulus of the material, G, thickness of the board, t, and tributary width of board, w_{tf}. The primary limitation of Eq. 2 is that the tributary area of fasteners in the field should not be greater than 6 x the tributary area of the fasteners on the edge (perimeter). As the distance between fasteners in the field is increased over this limit the edge fasteners behave as if there were no fasteners in the field and the stiffness goes back to the case of only being connected at the edges. The limitation is not a practical problem since the relation between tributary areas is typically no greater than 4 x (e.g., 6 in. on the edge, 12 in. in the field).

3.2 Rotational (k_ϕ) resistance

As the flange attempts to rotate (due to buckling or other deformations) local tilting of the fastener combined with bending of the sheathing and contact between the flange and sheathing restricts this movement in a manner that may be idealized by a rotational resistance, k_Φ. Rotational tests were performed on the configurations tested herein (same studs, boards, fasteners, and fastener spacing) to check the methodology developed by Schafer et al. (2007), Table 4. Schafer et al. (2010) fully discuss the procedure to find k_Φ, which is represented in Figure 1e and in the paper assumes the nomenclature $k_{\Phi 2}$.

Table 4 – Rotational stiffness tests on 362S162-68 studs
(Stiffness reported in units lbf-in./in./rad)

Test	k_ϕ	$k_{\phi w}$	$k_{\phi c}$	k_ϕ - 10%Mmax
BBB-GYP-12-6-6-01	68	283	90	77
BBB-GYP-12-6-6-03	78	-	-	67
BBB-GYP-12-6-6-04	79	255	115	79
BBB-GYP-12-6-6-05	58	193	82	52
average	70.8	243.7	95.7	68.9
COV	0.14	0.19	0.18	0.18

Test	k_ϕ	$k_{\phi w}$	$k_{\phi c}$	k_ϕ - 10%Mmax
BBB-OSB-12-8-6-02	81	288	113	103
BBB-OSB-12-8-6-06	64	201	95	85
BBB-OSB-12-8-6-07	67	212	98	86
BBB-OSB-12-8-6-08	69	243	97	91
average	70.3	236.0	100.8	91.4
COV	0.11	0.17	0.08	0.09

The semi-empirical method developed in Schafer et al. (2007) may be summarized in three equations shown below. Eq. 3 provides the stiffness due to the connection itself, as a function of the stud thickness t (in in.) and steel modulus, E (in ksi). Eq. 4 gives the rigidity provided by the sheathing $(EI)_w$ for different materials and grain orientations (as commonly tabled by APA (2002) and others), and different tributary width, L. Finally Eq. 5 combines both stiffnesses as two rotational springs in series.

$$k_{\phi c} = 0.00035Et^2 + 75 \quad (3)$$

$$k_{\phi w}=(EI)_w/L \quad (4)$$

$$k_\phi=1/(1/k_{\phi c} + 1/k_{\phi w}) \quad (5)$$

The test values may be compared to the values predicted by the Eq.'s 3-5. For the connection stiffness, Eq. 3 predicts a $k_{\phi c}$ of 123 lbf-in./in./rad, while the mean measured values are 96 lbf-in./in./rad in the gypsum and 101 lbf-in./in./rad in the OSB, as reported in Table 4. Noting that the standard deviation on the original data used to calibrate Eq. 3 was 24 lbf-in./in./rad the measured connection stiffness is 1 standard deviation below the average values, reasonable if not perfect agreement.

For the sheathing stiffness $k_{\phi w}$ is determined by Eq. 4 and the appropriate industry standard $(EI)_w$ values. For gypsum, $k_{\phi w}$ is expected to be between 125 and 333 lbf-in./in./rad (from min and max values reported by GA 2001) compared with an average measured $k_{\phi w}$ of 243 lbf-in./in./rad. The limited rotational capacity of gypsum sheathed specimens is again noted. For OSB Eq. 4 predicts $k_{\phi w}$ of 111 lbf-in./in./rad for stress perpendicular to strength axis (as-tested here) and 541 lbf-in./in./rad for stress parallel to the strength axis, which may be compared with an average measured $k_{\phi w}$ of 236 lbf-in./in./rad. The APA (2004) values are again shown to provide a conservative estimate.

3.3 Out-of-plane lateral (k_y) resistance

Traditionally, when considering sheathing as bracing, the out-of-plane resistance of the sheathing is ignored. In-plane the sheathing restrains weak-axis bending and torsion of the stud, while out-of-plane the sheathing increases major-axis bending stiffness. As flexural-torsional buckling is a common mode in wall studs, this out-of-plane restraint may be influential. The out of plane stiffness that develops from the sheathing under major-axis bending, Figure 7, is the ratio of the force in each fastener to the respective deflection at the fastener. The force at each fastener can be found by the difference in the shear force over the tributary length, thus Eq. 6 gives the out-of-plane stiffness.

$$k_y = \frac{2E_w I\pi^3}{L^3} \cdot \sin\left(\frac{\pi d_f}{2L}\right) \tag{6}$$

If the sheathing is fully composite with the stud, then the inertia of the board *I*, takes its upperbound value : $I=bt_s^3/12+bt_s(y_{GC}+t_s/2)^2$). Or, if no composite action develops then I is simply $bt_s^3/12$ resulting in a lower bound value. Industry tabled values for EI as utilized for $k_{\phi w}$ determination may provide this lower bound approximation.

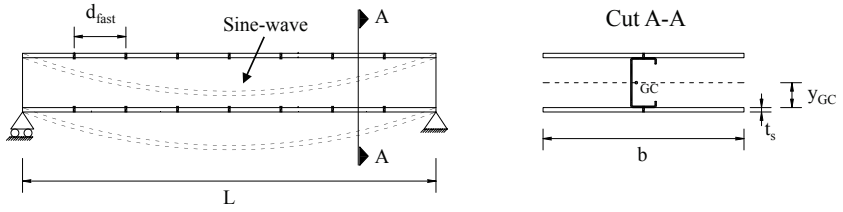

a) Stud under a sine-wave curve on the major axis b) Cross-section

Figure 7 – Analytical model for k_y

4 Stability of sheathing restrained studs

4.1 Unrestrained wall studs

The buckling modes of a pin-pin, unrestrained 362S162-68 SSMA cross-section, the same cross-section used in the columns and walls tests, are provided in the finite strip analysis "signature curve" results of Figure 8. Each buckling mode has an associated buckling half-wavelength (the length of the buckled wave). Understanding how sheathing, or equivalently the springs of Figure 1e, can or cannot change these buckling modes is critical to developing a sheathing braced design method.

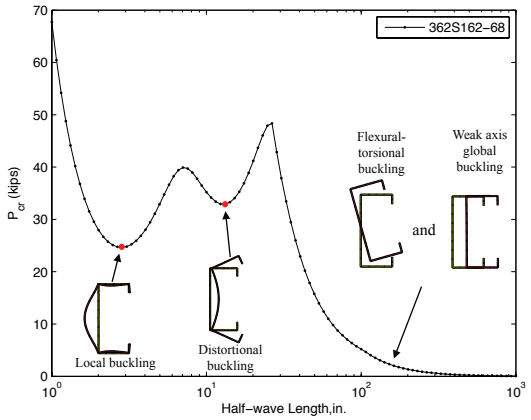

Figure 8 – Buckling curve and modes for pin-pin, unrestrained 362S162-68 SSMA cross-section

4.2 Sheathing restrained wall studs

The following results show how the elastic buckling modes of a cold-formed steel stud are influenced by the sheathing restraint, including different levels of restraint and for dissimilar restraint (different types of sheathing connected to the two flanges). For sheathing on one-side only, i.e. the OSB-Bare tests, Figure 9a compares the results to the unrestrained case. Introduction of the restraint changes the global buckling mode from weak-axis flexure to flexural-torsional buckling, and the resulting flexural-torsional mode is dependent on the level of out-of-plane resistance developed (i.e. lower bound vs. upper bound).

For sheathing on both sides, here the OSB-OSB values are used. Figure 9b compares the buckling results to the unrestrained case. Local buckling is not affected by the restraint, distortional buckling is modestly increased, while global buckling is altered significantly. If only the in-plane resistance is included, at practical lengths, weak-axis flexural buckling is replaced by flexural-torsional buckling. Introduction of the out-of-plane (k_y) resistance increases the flexural-torsional buckling load, and a strong sensitivity to the magnitude of k_y is found. The difference between using the lower bound and upper bound value for k_y is dramatic and should be carefully handled.

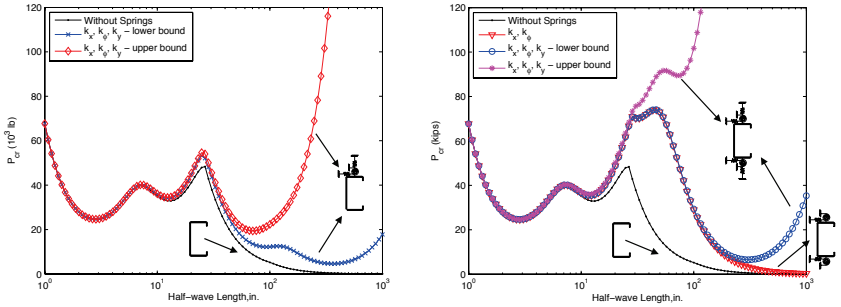

a) Springs on one flange

b) Springs on both flanges

Figure 9 – Buckling curves for springs on one flange and both

4.3 Local

Sheathing does not affect local buckling. The sheathing restrains the flange, but local buckling is largely driven by the web anyway. Even theoretically k_x and k_ϕ have no influence on local buckling, only k_y. The out-of-plane stiffness, k_y, is derived consistent with global bending resistance and not localized resistance. For local buckling predictions it is recommended to ignore the sheathing.

4.4 Distortional

Distortional buckling is mainly influenced by k_ϕ. The AISI-S210-10 (2010) standard provides general methods for finding k_ϕ. The rotational stiffness is the recognized means of primary resistance against distortional buckling and is derived and determined in a manner consistent with distortional buckling deformations. The in-plane stiffness, k_x, has little to no influence on distortional buckling in most cases, for very deep webs the additional restraint supplied by k_x could be influential so it may be included if desired. However, the out-of-plane stiffness, k_y, should not be added to k_ϕ, in part because k_ϕ itself derives from a moment couple that includes k_y at the connector and bearing between the flange and sheathing. Further k_y's deformations are consistent with beam bending, not rotation of the flange. For distortional buckling predictions it is appropriate to use k_x and k_ϕ, but ignore k_y.

4.5 Global

Global buckling modes are (a) weak-axis flexure and (b) flexural-torsional buckling. In most cases weak-axis flexure is the lowest mode and thus k_x is critical to this resistance and should be included. For flexural-torsional buckling the torsional component is restrained primarily by the couples created from the k_x springs (but also marginally from the k_ϕ springs), while the k_y spring restricts the major axis flexural component. For global buckling predictions at a minimum k_x should be included, but it is appropriate to include k_ϕ and k_y as well. In the absence of testing the lowerbound k_y value is the most rational choice.

5 Design Method

5.1 Proposed Methodology

The proposed design methodology is a unique application of the Direct Strength Method (DSM) of AISI-S100-07 Appendix 1. To design via the DSM approach the critical elastic buckling loads for local ($P_{cr\ell}$), distortional (P_{crd}), and global (P_{cre}), are required. Typically these P_{cr} values are for the isolated member cross-section; though work on distortional buckling has shown that if restraint is supplied to a member the P_{cr} (i.e. P_{crd}) can be analyzed with the restraint in place and the increased P_{cr} that results utilized in the DSM strength expressions for prediction of capacity (P_n).

Following the guidance of Sections 4.3-4.5 appropriate restraint (springs) are added to the model of the cross-section to predict $P_{cr\ell}$ and the sheathing-restrained P_{crd} and P_{cre}. The spring stiffness values are selected based on the results of Section 3 and applied to the cross-section by means of foundation stiffness (instead of a discrete spring at the fastener locations). Table 5 presents the spring stiffnesses and sheathing material properties considered.

In addition, and reflecting the findings of Section 2.2, Figure 2b, both pin-pin and fixed-fixed end boundary conditions are considered (for all three buckling modes). The traditional pin-pin models are developed using CUFSM 3.12 (Schafer and Adany (2006)) while the fixed-fixed models are performed in an in-house research version of CUFSM developed by Li and Schafer (2010).

Table 5 – Spring stiffnesses values and material properties considered

Board	k_x (kip/in/in)	k_y-upper bound (kip/in/in)	k_y-lower bound (kip/in/in)	k_ϕ (kip.in/in/rad)	E (ksi)	G (ksi)
OSB	0.2706	0.0355	0.0001710	0.0703	900	45
Gypsum	0.0485	0.0045	0.0000285	0.0708	100	5

5.2 Comparison with tests

As discussed previously, and demonstrated in Figure 2, the bare column (no sheathing) behaves essentially as a member with fixed-fixed end conditions, rather than pin-pin. As a result, both the traditional pin-pin, and upper bound fixed-fixed boundary conditions are explored in the following.

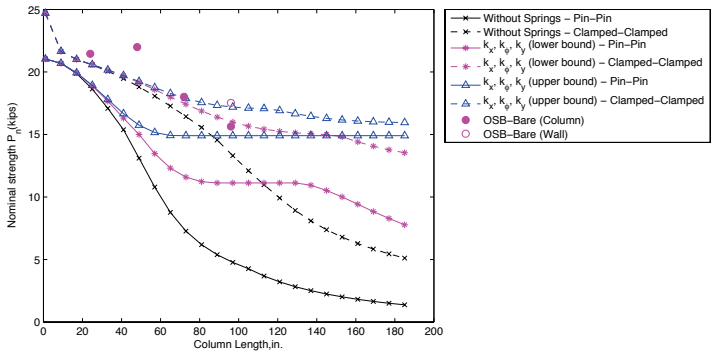

Figure 10 – Bare stud and stud restrained on one side compared to the possible design curves

Figure 10 provides a comparison of design assumptions for the OSB-Bare columns and walls. The tests all failed in a highly restrained version of flexural-torsional buckling. The test data most closely follows the assumption of fixed-fixed end conditions. In fact, up to 72 in. (6 ft), the end conditions are more influential than the sheathing restraint. For longer columns the importance of the sheathing restraint grows significantly. For the fixed-fixed end conditions, the lower bound (noncomposite) approximation for the sheathing contribution to the major–axis bending of the stud (k_y) is sufficiently accurate.

For the columns and walls with sheathing restraint on both sides: Gyp-Gyp, OSB-Gyp and OSB-OSB Figure 11 provides a comparison with potential design assumptions (to provide some clarity the spring values employed in the design curves are those for OSB-OSB). All of the tested columns fail in local buckling, at approximately the same per stud strength. In stark contrast to the case with one-sided sheathing (OSB-Bare) having springs on both flanges dramatically decreases the impact of the end boundary conditions. Even when only considering the in-plane resistance (k_x and k_ϕ) this restraint is enough to strongly restrict weak-axis bending and torsion, and up through 72 in. (6 ft) length the end conditions have only a small influence on the result. However, for longer than 72 in. (6 ft) the major-axis bending becomes increasingly important to restrain – either fixed-fixed end conditions or fully composite bending action with the sheathing (k_y upper bound) is required. The assumption of fixed-fixed end conditions and the noncomposite lower bound for k_y is again found to be a good predictor of the behavior. Pin-pin end conditions and only in-plane resistance (in essence the traditional model) is observed to be (a) a conservative predictor, and (b) one that reasonably follows the observed experimental trends.

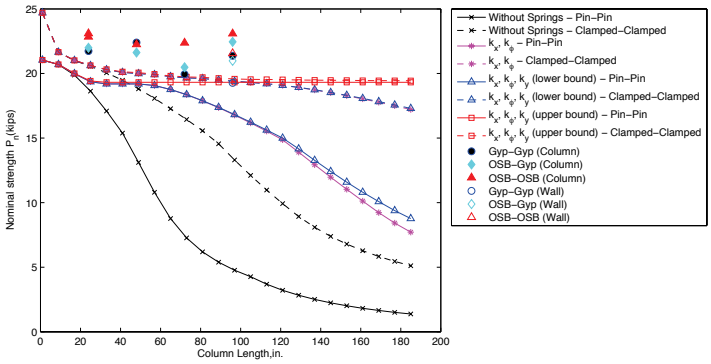

Figure 11 – Studs restrained on both sides compared to possible design curves

Finally, the proposed design method (using DSM and employing fixed-fixed end conditions, k_x and k_ϕ in-plane restraint and the non composite k_y lower bound resistance) is compared to the tests and other currently available design methods. In addition, the actual spring values for OSB and Gypsum board are utilized (per Table 5). The test data compares well with the proposed method and the small differences between OSB-OSB, OSB-Gyp, and Gyp-Gyp are even reflected in the predicted strength, along with the relatively pronounced decrease as a function of length for the one-sided sheathing case: OSB-Bare. The strength prediction is a significant improvement over AISI-S100-01 (essentially the Simann and Peköz 1976 method), Figure 12. The method is also an improvement over AISI-S210-07 both conceptually (AISI-S210-07 simply assumes one fastener is defective and calculates the strength of a column with a length equal to twice the fastener spacing) and in terms of strength prediction.

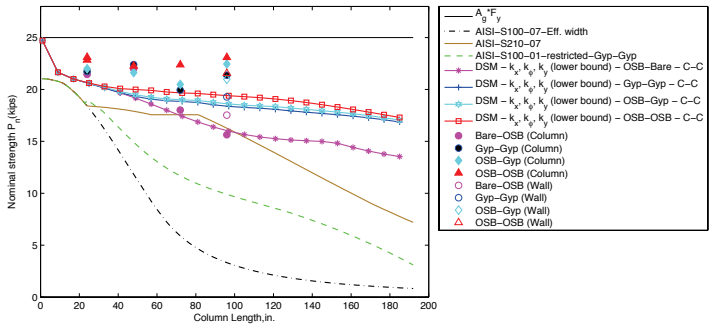

Figure 12 – Test results compared to former, current and proposed design methods

5.3 Fastener demands and future research

A significant and final feature of the proposed design method is still under development: the prediction of fastener demands. As the sheathing braces the studs forces develop at the fastener locations, failure of a fastener means loss of the bracing stiffness, thus the stud strength may be limited by the fastener strength. This may be particularly important for Gypsum sheathing. Preliminary work has been completed to predict the fastener demands as a function of the initial imperfections of the column, for both flexural and flexural-torsional buckling. Verification with nonlinear finite element modeling and development of a design procedure are underway.

6 Conclusions

The Direct Strength Method is shown to be an effective procedure for designing sheathing-braced wall studs. However, the problem must be handled carefully, as the sheathing-based restraint: in-plane, out-of-plane, and rotational must be determined with some care. A combination of experimental and analytical methods is presented herein for determining the restraint (bracing stiffness) associated with sheathing. The end boundary conditions for the studs are found to be fixed-fixed under test conditions, this is particularly important for un-sheathed studs, or studs sheathed on one-side only. For studs sheathed on both sides the end boundary conditions have a much smaller influence on the behavior, this is because the restraint provided by the sheathing largely dominates the response. For wall studs with sheathing on both sides, in the proposed design method, and in the testing, local buckling is the failure mode. Work is now underway to develop predictions of the fastener demands and complete a new procedure for the design of sheathing-braced wall studs covering similar, dissimilar, and one-sided sheathing configurations.

Acknowledgments

The authors gratefully acknowledge the Steel Stud Manufacturers Assoiation and the American Iron and Steel Institute for funding this research, Simpson Strong-Tie for donating the fasteners, and Nickolay Logvinovsky, Lauren Thompson and Hannah Blum for all their aid during the testing. In addition, the work benefitted from the input of the AISI Committee on Framing Standards Project Monitoring Task Group chaired by Nabil Rahman with significant input from Don Allen, Roger Laboube, Sutton Stephens, and Tom Trestain.

References

AISI (1962). Light Gage Cold-Formed Steel Design Manual. American Iron and Steel Institute, New York, NY (now Washington, D.C.)

AISI (2004) North American Specification for the Design of Cold-Formed Steel Structural Members. American Iron and Steel Inst., Wash., D.C.

AISI (2007). North American Standard for Cold-Formed Steel Framing–Wall Stud Design. AISI-S211-07, Am. Iron and Steel Inst., Washington, D.C..

AISI-S210 (2010). “North American Standard for Cold-Formed Steel Framing – Floor and Roof System Design.” American Iron and Steel Institute, Washington, D.C., ANSI/AISI-S210-10, 28 pp.

APA (2004) “Panel Design Specification”, APA – The Engineered Wood Association.

LaBoube, R.A.; Findlay, P.F. (2007). “Wall Stud-to-Track Gap: Experimental Investigation” Journal of Architectural Engineering, Vol. 13, No.2, June 1, 2007.

Li, Z. and Schafer, B.W. (2010) The constrained finite strip method for general end boundary conditions. Structural Stability Research Council - Proceedings of the 2010 Annual Stability Conference, Orlando, FL, USA, 2010; p 573-591

Miller, T., Peköz, T. (1994). "Behavior of Gypsum-Sheathed Cold-Formed Steel Wall Studs." ASCE, Journal of Structural Eng. 120 (5) 1644-1650.

Schafer, B. W., and Adany, S. (2006), "Buckling analysis of cold-formed steel members using CUFSM: Conventional and constrained finite strip methods." Proc. of the 18th Int'l. Spec. Conf. on Cold-Formed Steel Structures, 39-54.

Shifferaw, Y., Vieira Jr, L. C. M., Schafer, B.W. (2009). "Compression Testing of Single Column Studs with Sheathing Configurations" AISI Progress Report. www.ce.jhu.edu/bschafer/sheathedwalls

Simaan, A. Peköz, T. (1976). "Diaphragm Braced Members and Design of Wall Studs." ASCE, Journal of the Structural Division, 102 (ST1) 77-92.

Vieira Jr, L. C. M., Schafer, B.W. (2009). "Full-scale testing of sheathed cold-formed steel wall stud systems in axial compression" AISI Progress Report. www.ce.jhu.edu/bschafer/sheathedwalls

Winter, G. (1960). "Lateral Bracing of Beams and Columns." ASCE Transactions, Paper No. 3044, per footnote "published in 1958 in the Journal of the Structural Division"

Twentieth International Specialty Conference on Cold-Formed Steel Structures
St. Louis, Missouri, U.S.A., November 3 & 4, 2010

Shear Behavior of Screw Connections for Cold-Formed Thin-Walled Steel Structures

Yuanqi LI[1], Rongkui MA[2] and Xingyou YAO[2]

Abstract

Self-drilling screws are the primary means to fasten cold-formed thin-walled steel members in construction. There are several failure modes for shear connections with self-drilling screws, including screw tilting, hole bearing, edge tearing, tensile fracture in net section of connected elements and shear fracture of screws. Meanwhile, the "group effect" will exist when a large number of screws are used in a shear connection. A series of tests (75 specimens) on single lap shear connections with self-drilling screws has been carried out and the results reported in this paper. The end distance, screw spacing, pattern of screws arrangement and number of screws was varied to determine their influence on shear connection strength. The study focused on the analysis of factors affecting the shear connection strength, the shear strength estimation of self-drilling screw connections based on different failure modes and the influence of group effect. Finally, a proposed design method and recommendations for Chinese specification GB50018 are presented.

Introduction

Self-drilling screws are the primary means to fasten cold-formed thin-walled steel members in construction. Because of the high efficiency of screw connections, only a few days are required to build up a cold-formed steel structural building. Because of the excellent performance, screw connections have received more and more attention in recent years. Generally speaking, there are several failure modes for shear connections with screws, including screw tilting, hole bearing, edge tearing, tensile fracture in net section of connected elements and shear fracture of screws.

Pekoz (1990) first recommended a series of design equations for estimating the strength of steel-to-steel screw connections, and these equations were derived from a study of more than 3500 connection test

[1] Professor, Tongji University, Shanghai, China.
[2] Doctoral candidate, Tongji University, Shanghai, China.

results. Based on Pekoz's study, the 1996 AISI Specification for the Design of Cold-Formed Steel Structural Members introduced provisions for estimating the connection strength which was based on the failure in the connected elements.

LaBoube and Sokol (2002) found that, with screw and sheet sizes held constant, increasing the number of screws decreased the strength per screw in a connection. The decrease in strength was defined as the "group effect", and the group effect factor R is given by Eq. (1). The shear strength of a connection with more than one screw is estimated by Eq. (2).

$$R = \left(0.535 + \frac{0.467}{\sqrt{n}} \right) \leq 1.0 \tag{1}$$

$$P = nP_1R \tag{2}$$

where R = group effect factor; n = number of screws in a connection; P = shear connection strength; and P_1 = shear strength for a single screw connection.

The R factor was derived from test data of connections which had 3d (d being the nominal screw diameter) screw spacing. The method is applied to estimate the bearing or titling and bearing shear strength.

The current Chinese specification GB50018 (2002) is used to estimate the shear connection strength that is controlled by tilting and bearing. The specification does not have provisions for determining the shear strength based on other typical failure modes. Therefore, a project that included 75 single lap connections was conducted in Tongji University. The end distance, screw spacing, pattern of screws arrangement and number of screws was varied to determine their influence on shear connection strength. The study focused on the analysis of factors affecting the shear connection strength, the shear strength estimation of self-drilling screw connections based on different failure modes and the influence of group effect. Finally, an improved design method and recommendations for Chinese specification GB50018 were presented.

Test

Specimen and Testing Machine

The experiments involved a total of 75 single lap screw connection specimens, all of which were made up of normal ductility steel sheets with the thickness of 1 mm. Three different widths (45mm, 60mm and 80mm) of steel sheets were provided according to the variation of screw arrangement. The material properties of the steel sheets derived from tensile tests are presented in Table 1. Self-drilling screws (type P/W8×13) with nominal diameter of 4.2mm and length of 13mm were used. Three different screw

arrangements, including screws arranged in a line parallel to the force (L), in a row perpendicular to the force (T) and interlacingly or in several lines by several rows (I), were employed and the number of screws was varied from 1 to 9. Seven different screw spacings were used, including 3*d*, 4*d*, 5*d*, 7*d*, 10*d*, 15*d* and 20*d*. Three end distances were used, including 2*d*, 3*d* and 4*d*. The minimum edge distance of the specimens was 2*d*.

All of the tests were conducted on the CSS-44100 universal tension testing machine (Fig. 1). The specimens were denoted in the form of "SC5-4D-L-1", where "SC" means self-drilling screws, "5" means there are 5 screws in a connection, "4D" means the screw spacing is 4 times the nominal diameter of a screw. When there is only one screw in a connection, "4D" is the end distance. "L" means the screw pattern. "1" is the serial number of specimens with the same details.

Table 1. Material properties of steel sheets

Parameter	Specimen				Mean value
	MS-1	MS-2	MS-3	MS-4	
F_y (MPa)	297.42	302.76	304.13	306.11	303
F_u (MPa)	365.02	365.12	370.22	363.85	366
Elongation (%)	39.18	42.25	38.83	36.88	39.3

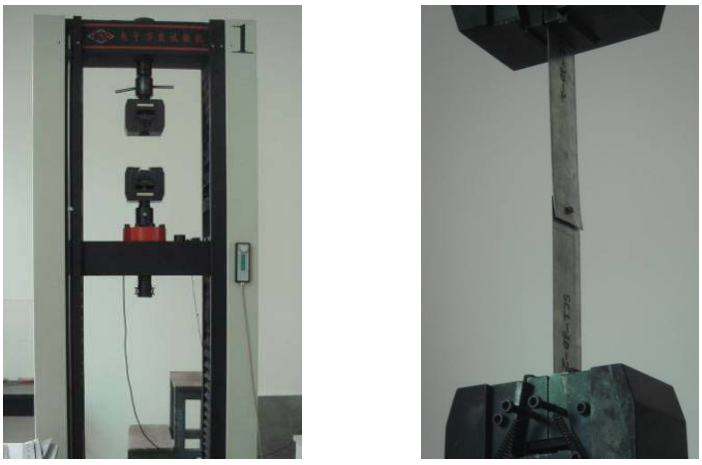

(a) tension testing machine (b) Testing jaw

Fig. 1. Testing setup

General Results

The shear strength of screw connections and their performance are affected by many factors, such as number of screws, screw pattern, screw spacing

and end distance, etc. Connections with a small number of screws usually failed in titling and bearing or the combination of several modes; and for the connections with a large number of screws, the steel sheets would fracture. Only the screws in specimen “SC3-5D-I-1” fractured in shear. Fig. 2 has presented the failure modes of screw connections. For certain specimens that had the same details, different failure modes were sometimes observed, but their strengths were similar.

It was found from the tests that for connections with several rows of screws the failure almost always occurred in the row closest to the jaws of testing machine. And when steel sheet fractured, it always occurred in the sheet that had the screw threads exposed (Fig. 2(c)).

(a) Titling

(b) Bearing

(c) Steel sheets fracture

(d) Screws fracture

Fig. 2 Failure modes of screw connections

Factors Affecting the Shear Strength of Screw Connections

End Distance

Three different types of single screw connections (SC1-2D, SC1-3D and SC1-4D), totaling 9 specimens, were tested to study the influence of end distance on shear strength. All nine connections exhibited the same failure mode (titling and bearing). The mean test strengths of SC1-2D, SC1-3D and SC1-4D were 2.834kN, 3.044kN and 3.083kN, respectively. SC1-3D and SC1-4D have 7.4% and 8.8%, respectively, more strength than SC1-2D, which indicates that there is a visible decrease in shear strength when the end distance is 2*d*. When the end distance is more than or equal to 3*d*, it has little influence on shear strength.

Screw Spacing

For connections with 5 screws, six different screw spacings were used, including 3*d*, 4*d*, 5*d*, 10*d*, 15*d* and 20*d*. A comparison of shear strength with different screw spacing is presented in Fig. 3.

Fig. 3 presents the relationship of shear strength of five-screw connections with different screw spacing. Connections have more strength as the screw spacing increases within a certain range (5*d* screw spacing); and as the range is exceeded, it seems to have no influence on shear strength.

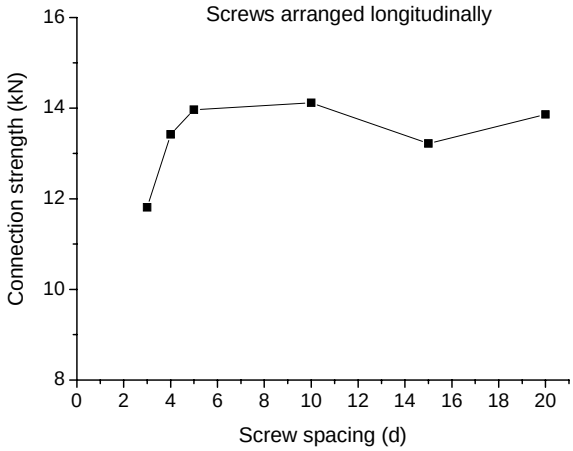

Fig. 3. Effect of screw spacing on shear strength

Pattern of Screws Arrangement

Twelve different geometric screw patterns, totaling 36 specimens, were conducted to research the influence of screw patterns on shear strength. When there were a less number of screws and less screw spacing in a connection, the connections with screws arranged longitudinally had more strength than those with screws arranged transversely. The data in Table 2 shows that SC2-3D-L and SC3-3D-L have 2.3% and 7.4% more strength than SC2-3D-T, SC3-3D-T, respectively. Yet, the situation was opposite as the number of screws or screw spacing increased in a connection. Table 2 shows that SC3-5D-L, SC3-7D-L, SC4-3D-L and SC5-3D-L have 6.3%, 7.8%, 3.6% and 16.4% less strength than SC3-5D-T, SC3-7D-T, SC4-3D-T and SC5-3D-T, respectively.

Table 2. Effect of screw pattern on shear strength

Specimen	Mean shear strength (kN)		$(P_L\text{-}P_T)/P_T$
	P_L (L-Pattern)	P_T (T-Pattern)	
SC2-3D	5.468	5.344	2.3%
SC3-3D	7.731	7.201	7.4%
SC3-5D	8.494	9.061	-6.3%
SC3-7D	8.811	9.557	-7.8%
SC4-3D	10.286	10.672	-3.6%
SC5-3D	11.810	14.130	-16.4%

Number of Screws

A typical relationship between shear strength and the number of screws is presented in Table 3. All the connections listed in Table 3 failed in the mode of titling and bearing.

Table 3. Effect of number of screws on shear strength

Specimen	P (kN)	P/P_1	Specimen	P (kN)	P/P_1
SC2-3D-L	5.468	1.77	SC2-3D-T	5.344	1.73
SC3-3D-L	7.731	2.51	SC3-3D-T	7.201	2.34
SC3-5D-L	8.494	2.76	SC3-5D-T	9.061	2.94
SC3-7D-L	8.811	2.86	SC3-7D-T	9.557	3.10
SC4-3D-L	10.286	3.34	SC4-3D-T	10.672	3.46
SC5-3D-L	11.810	3.83	SC5-3D-T	14.130	4.58
SC5-4D-L	13.420	4.35			
SC5-15D-L	13.221	4.29			

Based on the ratio of mean shear strength P to the single screw connection shear strength P1 (the mean strength of SC1-4D), conclusions can easily be obtained. No matter how the screws were arranged, the strength per screw in

a connection diminished as the number of screws increased, with the exception of SC3-7D-T. That is, for example, the strength of a connection with three screws is less than three times the strength of a similar connection with one screw. The phenomenon was defined as the “group effect” by Laboube and Sokol (2002).

Proposed Method for Shear Strength Estimation

Tilting and Bearing

Titling and bearing was the main failure mode, and a total of 64 connections failed in this mode. Table 4 presents a series of comparisons, such as the comparison of P_0 (the nominal shear strength calculated by GB50018 (2002)) to P (the test strength), and P_R (the estimated shear strength including the group effect factor R) to P. As listed in Table 4, the estimated shear strength P_0 of single screw connections agree well with P, and connections with a large number of screws have unconservative estimated strengths compared with P, with ratios in a range of 0.858 to 1.242. When the group effect factor R was employed in GB50018 (2002), the situation improved. As shown in Table 4, all the ratios of P_R to P are less than or equal to 1.0, within a range of 0.69 to 1.0; most of the ratios for connections which had 3d screw spacing are in the range of 0.8 to 0.9, and for connections which had more than 3d screw spacing, the ratios are mainly in the range of 0.7 to 0.8.

Table 4. Comparison of estimated strength to test strength

Specimen	Test strength P (kN)	P_0/P	R	P_R/P
SC1-2D-1	2.579	1.076	1.000	1.076
SC1-2D-2	3.045	0.911	1.000	0.911
SC1-2D-3	2.878	0.964	1.000	0.964
SC1-3D-1	2.948	0.941	1.000	0.941
SC1-3D-2	3.034	0.915	1.000	0.915
SC1-3D-3	3.150	0.881	1.000	0.881
SC1-4D-1	3.023	0.918	1.000	0.918
SC1-4D-2	2.992	0.927	1.000	0.927
SC1-4D-3	3.233	0.858	1.000	0.858
SC2-3D-T-1	5.430	1.022	0.865	0.884
SC2-3D-T-2	5.309	1.046	0.865	0.904
SC2-3D-T-3	5.293	1.049	0.865	0.907
SC2-3D-L-1	5.557	0.999	0.865	0.864
SC2-3D-L-2	5.625	0.987	0.865	0.854
SC2-3D-L-3	5.222	1.063	0.865	0.919
SC3-3D-T-1	6.705	1.242	0.805	1.000
SC3-3D-T-2	7.486	1.112	0.805	0.895
SC3-3D-T-3	7.412	1.123	0.805	0.904

SC3-3D-L-1	8.111	1.027	0.805	0.826
SC3-3D-L-2	7.658	1.087	0.805	0.875
SC3-3D-L-3	7.424	1.121	0.805	0.903
SC3-5D-T-1	8.442	0.986	0.805	0.794
SC3-5D-T-2	9.430	0.883	0.805	0.711
SC3-5D-T-3	9.312	0.894	0.805	0.720
SC3-5D-L-1	8.427	0.988	0.805	0.795
SC3-5D-L-2	8.653	0.962	0.805	0.775
SC3-5D-L-3	8.402	0.991	0.805	0.798
SC3-5D-I-2	8.174	1.019	0.805	0.820
SC3-5D-I-3	8.122	1.025	0.805	0.825
SC3-7D-T-1	9.692	0.859	0.805	0.692
SC3-7D-T-2	9.708	0.858	0.805	0.690
SC3-7D-T-3	9.270	0.898	0.805	0.723
SC3-7D-L-1	9.305	0.895	0.805	0.720
SC3-7D-L-2	8.718	0.955	0.805	0.769
SC3-7D-L-3	8.411	0.990	0.805	0.797
SC4-3D-T-1	10.382	1.069	0.769	0.822
SC4-3D-T-2	10.300	1.078	0.769	0.829
SC4-3D-T-3	11.334	0.979	0.769	0.753
SC4-3D-L-1	10.217	1.087	0.769	0.836
SC4-3D-L-2	10.534	1.054	0.769	0.810
SC4-3D-L-3	10.106	1.098	0.769	0.845
SC4-5D-I-1	10.954	1.013	0.769	0.779
SC4-5D-I-2	10.762	1.031	0.769	0.793
SC4-5D-I-3	10.799	1.028	0.769	0.791
SC5-3D-T-1	14.002	0.991	0.744	0.737
SC5-3D-T-2	13.597	1.021	0.744	0.759
SC5-3D-T-3	14.791	0.938	0.744	0.698
SC5-3D-L-1	11.819	1.174	0.744	0.873
SC5-3D-L-2	11.674	1.189	0.744	0.884
SC5-3D-L-3	11.938	1.162	0.744	0.865
SC5-4D-L-1	13.417	1.034	0.744	0.769
SC5-4D-L-2	13.311	1.042	0.744	0.776
SC5-4D-L-3	13.531	1.025	0.744	0.763
SC5-5D-L-2	13.884	0.999	0.744	0.744
SC5-5D-L-3	14.122	0.983	0.744	0.731
SC5-5D-I-1	12.920	1.074	0.744	0.799
SC5-5D-I-2	12.320	1.126	0.744	0.838
SC5-5D-I-3	12.139	1.143	0.744	0.850
SC5-10D-L-3	13.812	1.005	0.744	0.747
SC5-15D-L-1	13.197	1.051	0.744	0.782
SC5-15D-L-2	13.206	1.051	0.744	0.782
SC5-15D-L-3	13.261	1.046	0.744	0.779
SC5-20D-L-1	13.536	1.025	0.744	0.763
SC5-20D-L-2	13.748	1.009	0.744	0.751

Tensile Fracture in Connected Elements

Tensile fracture of the steel sheets occurred in 10 specimens. All the specimens had multiple screws in the line parallel to the force. Table 5 presents a comparison of the mean stress σ_{net} of steel sheet net section to the ultimate stress F_u, where σ_{net} was derived from the test strength P divided by the net section area A_n. All the ratios of σ_{net} to F_u are close to 1.0, within a range of 0.93 to 1.18. There is not an obvious stress concentration in net section. And the ratio of σ_{net} to F_u is higher as the number of screws in a row perpendicular to the force increased. For connections with three screws in a row, the ratios are near to 1.2.

Table 5. Comparison of σ_{net} of steel sheet net section to F_u

Specimen	Net section area A_n (mm^2)	Test strength P (kN)	σ_{net} (MPa)	$\frac{\sigma_{net}}{F_u}$
SC5-5D-L-1	40.8	13.892	340.5	0.93
SC5-10D-L-1	40.8	14.381	352.5	0.96
SC5-10D-L-2	40.8	14.157	347.0	0.95
SC5-20D-L-3	40.8	14.300	350.5	0.96
SC9-5D-L-1	40.8	14.071	344.9	0.94
SC9-5D-L-2	40.8	14.346	351.6	0.96
SC9-5D-L-3	40.8	14.353	351.8	0.96
SC9-5D-I-1	47.4	20.287	428.0	1.17
SC9-5D-I-2	47.4	20.441	431.2	1.18
SC9-5D-I-3	47.4	20.444	431.3	1.18

Note: For the first seven specimens, width of sheets is 45mm and number of screws in net section is 1; for the last three, width of sheets is 60mm and number of screws in net section is 3.

AS 4600 (2005) has specified the design method for the tensile fracture in the connected elements. For connections with screws in the line parallel to the force, the nominal tensile strength of net section of the connected elements is specified by Eq. (3); and for connections with a single screw or a single row of screws perpendicular to the force, it is specified by Eq. (4)

$$N_t = A_n F_u \tag{3}$$

$$N_t = \left(2.5d / s\right) A_n F_u \le A_n F_u \tag{4}$$

where N_t = nominal tensile strength of net section of the connected elements; F_u = ultimate stress; A_n = net area of connected elements; d = nominal screw diameter; and s = spacing of screws perpendicular to the line of the force; or width of sheet, in the case of a single screw.

The ratios of σ_{net} to F_u in Table 5 are consistent with Eq. (3) specified in AS 4600 (2005). For connections with a single screw or a single row of screws perpendicular to the force, no steel sheet fractured in the tests.

Shear Fracture of Screws

Only screws in specimen SC3-5D-I-1 fractured in shear during the tests. To avoid shear fracture of screws, AS 4600 (2005) requires that the nominal shear strength of screws be not less than 1.25 times the nominal shear strength, which is limited by titling and bearing. The equation is denoted as the formed of Eq. (5)

$$N_s \geq 1.25 N_v \tag{5}$$

where N_s = nominal strength limited by shear fracture of screws; N_v^s = nominal shear strength limited by titling and bearing.

Yet, the requirement may not be met as the thickness or strength grade of connected elements increases. AISI-NAS (2007) has required that the shear connection strength is dependent on the strength of screws, in addition to the strength of the connected elements. And the strength limited by shear fracture of screws should be obtained by standard testing.

Conclusions and Recommendations

Based on the test data of 75 steel-to-steel single lap screw connections, a better understanding of the behavior of screw connections was obtained. Factors affecting the shear strength of screw connections were analyzed in this paper. The findings of the study indicated that screw spacing influenced the screw connection strength significantly. Connections have more strength as screw spacing increases within a certain range (5*d* screw spacing), and as the range is exceeded, it seems to have no influence on shear strength.

The group effect will exist when a large number of screws are used in a shear connection. According to comparisons in Table 4, the estimated shear strength including the group effect factor *R* is more conservative for connections with screws arranged by more than 3*d* spacing. The *R* factor is also involved with screw spacing in addition to the number of screws.

Specimens, which had steel sheets fractured, always had multiple screws in the line parallel to the force. There is not an obvious stress concentration in net section of steel sheets, and the ratios of the mean stress of steel sheet net section to the ultimate stress are close to 1.0.

Notation

The following symbols are used in this paper:

A_n = net area of connected elements;
d = nominal screw diameter;

F_y = yield stress of steel sheet;
F_u = ultimate stress of steel sheet;
N = number of screws in a connection;
N_s = nominal strength limited by shear fracture of screws;
N_t = nominal tensile strength of net section of connected elements;
N_v = nominal shear strength limited by titling and bearing;
P = test shear strength;
P_0 = nominal shear strength calculated by GB50018 (2002);
P_1 = test shear strength for a single screw connection;
P_R = estimated strength employed the group effect factor R;
R = group effect factor;
s = spacing of screws perpendicular to the line of the force; or width of sheet, in the case of a single screw; and
σ_{net} = mean stress of steel sheet net section.

Acknowledgements

The first author gratefully acknowledgements the financial support provided by *key projects in the National Science and Technology Pillar Program during the eleventh five-year plan period* (No: 2008BAJ08B13) and *National Natural Science Foundation Projects of China* (No: 50878168).

References

AISI-NAS. (2007). “North American specification for the design of cold-formed steel structural members.” AISI, Washington, D.C.

AS 4600. (2005). “Cold-formed steel structures.” Standards Australia, Sydney, Australia.

GB50018. (2002). “Technical code of cold-formed thin-wall steel structures.” Beijing, China.

LaBoube, R. A. and Sokol, M. A. (2002). “Behavior of screw connections in residential construction.” J. Struct. Eng., 128(1): 115-118.

Pekoz, T. (1990). “Design of cold-formed steel screw connections.” Proc., 10th Int. Specialty Conf. on Cold-Formed Steel Structures, Univ. of Missouri-Rolla, Rolla, St. Louis, 576-587.

Twentieth International Specialty Conference on Cold-Formed Steel Structures
St. Louis, Missouri, U.S.A., November 3 & 4, 2010

Single Shear Bolted Connection tests of G500 1.20mm Thin Sheet Steel at Elevated Temperatures

Shu Yan [1] and Ben Young [2]

ABSTRACT

The current design rules on bolted connections of thin sheet steels for cold-formed steel structures are applicable for ambient temperature condition only. Research on such kind of connections at high temperatures is limited. In this study, 47 single shear bolted connection specimens fabricated from G500 1.20mm thin sheet steel and 9 coupon specimens were conducted by using steady state test method in the temperature range from 22ºC to 900ºC. Two failure modes were observed in the single shear bolted connection tests, namely the net section tension, and bearing. The test results were compared with the predicted values calculated from the American, Australian/New Zealand and European specifications for cold-formed steel structures. In calculating the nominal strengths of the connections, the reduced material properties were used due to the deterioration of material at elevated temperatures. It is shown that the strengths of the single shear bolted connections predicted by the specifications are generally conservative at elevated temperatures. Furthermore, the comparison between the deterioration of the strengths of connections and that of the material properties due to high temperatures showed a similar tendency of reduction.

[1] Research Student, Department of Civil Engineering, The University of Hong Kong, Hong Kong.
[2] Professor, Department of Civil Engineering, The University of Hong Kong, Hong Kong.

INTRODUCTION

Cold-formed structural members which are fabricated from sheet steels are widely used in light-weight steel structures, like low-rise residence houses, office buildings and garages. Small buildings can be made entirely of cold-formed sections, and relatively large buildings are often made of welded steel plate rigid frames with cold-formed sections used for girts, purlins, roofs and walls (Yu 2000). In cold-formed steel structures construction, bolted connections are one of the most popular connection types. The North American Specification AISI S100 (2007) and Australian/New Zealand Standard AS/NZS 4600 (2005) for cold-formed steel structures provide design equations of bolted connections for different types of failure modes. Rogers and Hancock (1998a, 1998b, 1999 and 2000) conducted hundreds of bolted connection tests at ambient temperature that focused on the bearing strength of the connections, based on which the North American Specification AISI S100 (2007) and Australian/New Zealand Standard AS/NZS 4600 (2005) have improved the design rules of bolted connections subjected to bearing failure. However, investigation on the structural behavior of bolted connections of thin sheet steels at elevated temperatures is limited. Outinen (1999), Outinen et al. (2001) and Chen and Young (2006 and 2007) conducted a series of tests on hot-rolled steel and cold-formed steel material at elevated temperatures. Numerical investigation of bolted moment-connections of cold-formed steel members at ambient temperature (Lim and Nethercot 2003) and elevated temperatures (Lim and Young 2007) have been conducted. It should be noted that the bolted connection design rules in the North American Specification AISI S100 (2007), Australian/New Zealand Standard AS/NZS 4600 (2005) and Eurocode 3 (2006) are only applicable at ambient temperature condition.

In this paper, the mechanical properties of G500 1.20mm thin sheet steel which were used to fabricate the single shear bolted connection specimens were firstly determined by tensile coupon tests using the steady state test method for the temperature ranged from 22ºC to 900ºC. The coupon test results obtained from this study showed a similar trend of deterioration of the material properties at elevated temperatures with

those obtained by Chen and Young (2007). Based on the reduction of yield stress and ultimate stress of the G500 1.20mm thin sheet steel at elevated temperatures, 7 critical temperature levels were selected for the bolted connection tests in this study. The structural behavior of bolted connections were investigated by varied the bolt size, the number and arrangement of the bolts in 5 series of tests. Two failure modes, namely the net section tension failure and bearing failure were observed from the tests. The test results of the single shear bolted connections were also compared with the deterioration of the material properties at elevated temperatures.

COUPON TESTS

Testing Device

An MTS 810 Universal testing machine was used to conduct the tensile coupon tests. The testing device and test set-up of the coupon tests are shown in Fig. 1. The heating device of MTS model 653.04 high temperature furnace that contains three independent-controlled heating chambers with a maximum temperature up to 1400ºC was used. There is an internal thermal couple located inside each heating chamber for the measurement of air temperature. Due to the distance between the internal thermal couples and the coupon specimen, therefore, the temperature obtained from the internal thermal couples is slightly different to the temperature of the coupon specimen. Hence, an external thermal couple was used to measure the actual temperature of the coupon specimen. The external thermal couple was inserted inside the furnace and contacted on the surface of the coupon specimen at mid-length. The specimen temperature reported in this paper was obtained from the external thermal couple. The heating rate of the furnace for the coupon tests was approximately 50ºC /min.

The strain of the middle section of the coupon specimen was measured by an MTS model 632.54F-11 high temperature axial extensometer. The gauge length of the extensometer was 25mm with a range limitation of ±2.5mm. In order to obtain the complete stress-strain curve of the coupon specimen, the extensometer was reset once it

approaches the range limit during testing.

Test Specimen

The coupon test specimens were designed according to the Australian Standard AS 2291 (1979) using 6mm wide coupons and a gauge length of 25mm. The coupon specimens were taken from the thin sheet steel along the longitudinal rolling direction of the steels. A total of 9 specimens were conducted to obtain the material properties of the thin sheet steel at elevated temperatures using steady state test method. The base metal thickness of the specimens was obtained by removing the galvanized zinc coating of the specimens using 1:1 hydrochloric acid. It is more accurate to determine the cross sectional area of the coupon specimens using the uncoated sheet (base metal) thickness.

Testing Procedure

Steady state test method was used for both the coupon and bolted connection tests in this study. The specimen was firstly heated up to a certain temperature. The axial load was slowly applied until the specimen fail at a constant temperature throughout the test. After reaching the pre-selected temperature level, the constant temperature was maintained for a period of 7 to 15 minutes, which depended on the pre-selected temperature level. This process allows the heat to transfer into the specimen. The thermal expansion of the coupon and bolted connection test specimens were allowed in this study by unrestrained the bottom end of the specimens. Therefore, the specimens were free to expand during heating with no axial force applied on the specimens before the stabilization of the specimen temperature was achieved. A constant loading rate of 0.15mm/min was used which is in accordance with the Australian Standard AS 2291 (1979).

Testing Results

The mechanical properties of G500 1.20mm thin sheet steel obtained at ambient temperature are presented in Table 1. The initial elastic modulus (E_{normal}), 0.2% proof stress ($f_{0.2,\ normal}$), tensile strength ($f_{u,}$

$_{normal}$), ultimate strain ($\varepsilon_{u,\ normal}$) and maximum strain after fracture ($\varepsilon_{f,\ normal}$) based on a gauge length of 25mm at normal room temperature (ambient temperature) are shown in Table 1. The ultimate strain ($\varepsilon_{u,\ normal}$) was determined by taking the strain corresponding to the tensile strength. The deterioration of the material properties is expressed by a series of reduction factors, as listed in Table 2. The test results of the G500 1.20mm thin sheet steel are plotted in Figure 2. The vertical axis of these graphs is the normalized reduction factors $f_{0.2,\ T} / f_{0.2,\ normal}$ and $f_{u,\ T} / f_{u,\ normal}$, while the horizontal axis plotted against the actual specimen temperature. The values of 0.2% proof stress ($f_{0.2,\ T}$) and ultimate strength ($f_{u,\ T}$) at elevated temperatures were determined from stress-strain curves of the coupon tests. The deterioration of the materials as the temperature increases are clearly shown in Figure 2. Furthermore, the reduction factors $f_{0.2,\ T} / f_{0.2,\ normal}$ and $f_{u,\ T} / f_{u,\ normal}$ calculated using the equations proposed by Chen and Young (2007) are also plotted in Figure 2. It is shown that the 0.2% proof stress ($f_{0.2}$) and tensile strength (f_u) dropped rapidly in the temperature range 300 – 600ºC.

SINGLE SHEAR BOLTED CONNECTION TESTS

Specimen Design

The test program consisted of 5 types of single shear bolted connection specimens varied in the size of bolt, the number of bolts and the arrangement of bolts. The details of the specimen dimension are illustrated in Fig. 3. Table 3 lists the dimension values of the notations in each bolted connection specimen in Fig. 3. The length of the specimen between two grips maintained 560mm after assembly despite the different length of the steel plates for each type of specimen, which ensure the bolted connection part always located at the center position of the furnace.

Two different sizes of bolts were used in this study: M6 Grade 12.9 bolts, M8 Grade 12.9 bolts. The corresponding size of steel washers and nuts were used. Table 4 lists the nominal and actual dimensions of

these bolts and the corresponding washers. Standard size of bolt holes (d_o) were adopted according to the AS/NZ 4600 (2005), namely the size of bolt hole is 1mm larger than the nominal bolt diameter (d) when d is smaller than 12mm, otherwise the size of bolt hole is 2mm larger than d. In this study, d_o in all specimens is 1mm larger than d. Grade 8.8 bolts were used during the trail tests, and it was found that most of the bolted connection specimens having one bolt failed by bolt shear. Therefore, Grade 12.9 bolts were used to avoid bolt shear failure in this study.

The distance between the center of the bolt hole and the end of the plate were chosen as three times of the nominal diameter of the bolt, which is the minimum requirement for the bearing failure in the AS/NZ 4600 (2005). It should be noted that the 3d rule has not been experimentally investigated at elevated temperatures. In this study, the minimum dimension of 3d at elevated temperatures due to the material deterioration is investigated. Moreover, tear out failure which usually accompanies brittle tear cracks in the sheet steels may appear when the edge distance is relatively short.

The test specimens were assembled so that initial bearing of the bolt did not occur, rather a random amount of clearance on the sides of the holes existed, as found in typical construction (Rogers and Hancock 1998a). All bolts were hand-tightened to a torque of approximately 10Nm to allow the slipping of the connection after small tension was applied.

Bolted Connection Specimen Labeling

In Table 3, each specimen was labeled by three or four segments in order to identify the nominal thickness of the sheet steel, the number of bolt, the bolt arrangement and the bolt size and bolt type of the test specimen. For example, the labels 120-B1-M6 and 120-B2-V-M6 define the following specimens:

- The first three numbers indicate the thickness of the thin sheet steel used in the specimens (120 = 1.20mm);

- The following symbols are the number of bolt in the specimen

(B1 means one-bolt connection, and B2 means two-bolt connection);

- The third segment of the label, which is omitted in one-bolt connection, represents the arrangement of the bolts in the specimen. For instance, the notation 'V' means the two bolts were perpendicular arranged with the loading direction, while the notation 'P' represents the two bolts in the specimen were arranged parallel with the loading direction;

- The last part of the label represents the nominal bolt size and bolt type (M6 has the nominal bolt diameter of 6mm Grade 12.9, and M8 has the nominal bolt diameter of 8mm Grade 12.9).

Test Set-up

A total of 47 single shear bolted connection specimens including some repeated test specimens were experimentally investigated in this study under 7 different elevated temperature levels. In general, it is found that both $f_{0.2,\,T}$ and $f_{u,\,T}$ reduce rapidly between around 300ºC to 600ºC. Hence, the nominal temperatures were broken down into 7 levels, namely 22ºC, 150ºC, 300ºC, 450ºC, 600ºC, 750ºC, and 900ºC, so that the critical temperature will not be missed, and the number of specimens can be reasonably optimized.

The bolted connection tests were conducted by the same MTS testing machine which was used for the coupon tests. The test set-up of single shear bolted connections of G500 1.20mm thin sheet steel at the normal room temperature and elevated temperatures are shown in Figs. 4(a) and 4(b), respectively. A pair of grip apparatus was specially fabricated in order to provide pin assembly at both ends of the test specimen and offer purely vertical in-line loading. Clips linked with iron wire were used to prevent the extent of out-of-plane curling at the end of the steel plate. A couple of transducers were set especially for the ambient temperature test to measure the deflection occurred in the overlapped section, while they were not used for elevated temperature tests.

Test Procedure

Steady state testing method was adopted. The specimen was firstly set up with clamping the top end while keeping the bottom free. An external thermocouple was set to contact on the surface of the sheet steel in the overlap section. The furnace was finally closed and raised the temperature to a pre-selected level. The thermal expansion was allowed by the unrestrained bottom end of the specimen during the heating process. The temperature was held usually around 10 minutes after the temperature rose to the expected level, and then the bottom end of the specimen was gripped after the stabilization of the temperature was achieved. The tensile loading was applied with a loading rate of 1mm/min until the loading dropped at least 25% of the ultimate load or the stroke of the hydraulic actuator reached 20mm movement.

Test Results

The test strengths ($P_{u,\ normal}$ and $P_{u,\ T}$) of the single shear bolted connection specimens at normal room and elevated temperatures are given in Table 5. The repeated test specimens were tested mainly at around 450ºC due to the consideration of the rapid drop of $P_{u,\ T}$ occurred in vicinity of this temperature level. Fig. 5 exemplifies the test curves of specimen 120-B1-M8 at 7 different temperature levels. All the curves have been shifted to remove the displacement due to the bolt-slipping during the initial loading stage.

COMPARISON OF TEST STRENGTHS WITH PREDICTED STRENGTHS

The predicted strengths (P_n) of single shear bolted connections were calculated using the design equations given by the AISI S100 (2007), AS/NZS 4600 (2005) and EC3 (2006) with consideration of the deterioration of the material properties at elevated temperatures. Table

5 shows the comparison of the test results with the predicted values calculated from the three specifications. Generally, the design rules for single shear bolted connections in the AISI S100 are identical to those in the AS/NZS 4600. Therefore, the predicted values obtained from these two specifications are identical. It is found that the predicted strengths ($P_{n\text{-}AISI}$) of the bolted connections predicted by the AISI S100 and AS/NZS 4600 are generally less conservative or unconservative at temperature less than or equal to 300ºC, while the predications ($P_{n\text{-}EC3}$) based on the EC3 are generally more conservative than the AISI S100 and AS/NZS 4600. However, the current design formulas in the three specifications by substituting the reduced material properties at elevated temperatures drastically underestimate the bearing strength of the single shear bolted connections, especially when the temperature is higher than 450ºC.

It is shown that the strengths of the bolted connections predicted by the AISI S100 and AS/NZS 4600 specifications are generally conservative, whereas the EC3 predications are even more conservative at elevated temperatures. For instance, in Table 5(b), the mean values of $P_{u,\,T}$ / $P_{n\text{-}AISI}$ and $P_{u,\,T}$ / $P_{n\text{-}EC3}$ are 1.07 and 1.29 with the coefficients of variation (COV) of 0.197 and 0.238, respectively, for specimen 120-B1-M8 at different temperature levels. It is also found that the AISI S100 and AS/NZS 4600 generally provide unconservative predictions for net section tension failure as shown in Tables 5(e). The mean values of $P_{u,\,T}$ / $P_{n\text{-}AISI}$ are 0.88 with the corresponding COV of 0.076 for specimen 120-B2-V-M6 in Table 5(e). However, this is not the case for EC3 predictions. The EC3 generally provides conservative predictions for net section tension failure. The mean values of $P_{u,\,T}$ / $P_{n\text{-}EC3}$ are 1.07 with the corresponding COV of 0.092 for specimen 120-B2-V-M6 in Table 5(e).

The comparison ($f_{u,\,T}$ / $f_{u,\,normal}$) of the tensile strength of material at elevated temperatures with that at ambient temperature can be directly viewed as the comparison ($P_{n,\,T}$ / $P_{n,\,normal}$) of the predicted strength of single shear bolted connection at elevated temperatures ($P_{n,\,T}$) with that at ambient temperatures ($P_{n,\,normal}$), because all of the coefficients in the design formulas for the calculation of single shear bolted connections

(P_n) are identical for ambient and elevated temperatures. Fig. 2 shows the deterioration of the test strengths of the single shear bolted connections of G500 1.20mm thin sheet steel as the temperature increases. The horizontal axis plotted the temperature. The vertical axis represents the normalized $f_{u,\,T}$ / $f_{u,\,normal}$ and $P_{n,\,T}$ / $P_{n,\,normal}$. The test strengths of the bolted connections demonstrated a rapid decrease from 300ºC to 600ºC with approximately 80% strength lost, which is similar to the deterioration of the tensile strength of the material properties.

VARIATION OF THE FAILURE MODES AT ELEVATED TEMPERATURES

The observed failure modes of each specimen are listed in Table 5. 'B' represents the bearing failure; 'N' means the net section tension failure; 'T' is short for tear out failure; 'BS' stands for the bolt shear failure. Some specimens failed by combined failure modes, such as 'B+N' that represents the specimen failed by combination of bearing and net section tension failure modes. Generally, most of the specimens were failed by bearing failure. Based on the experimental observation, it is found that the characteristics of the bearing failure mode, such as the bolt hole elongated, the tilting of the bolts, the steel material piling up in front of the bolts developed in high temperature. Fig. 6 shows the bearing failure for specimen 120-B1-M8 at relatively higher temperature range from 300 ºC to 900 ºC.

The bolt shear failure mode was observed for most of the specimens at the temperature of 900ºC except for 120-B2-P-M8. This specimen did not fail at the connection, but failed in the sheet steel beyond the overlapped connection part at 900ºC, which was defined as material failure and the symbol (MF) is used. The net section tension failure mode was found in specimens 120-B2-P-M8 and 120-B2-V-M6. The bearing effect became more and more exaggerated as the temperature increases for these two specimens. Based on the tested specimens, the minimum distance requirement for bearing according to most of the standards, namely 3d from the center of bolt hole to the end of the plate or between centers of bolt holes, could generally maintain the bearing

failure for fire conditions. Although the bolt shear failure was deliberately avoided in the design of the test specimens at ambient temperature, this failure mode was observed for most of the specimens at 900ºC, except for specimen 120-B2-P-M8 failed by the material failure mode.

CONCLUSIONS

An experimental investigation on the strengths and failure modes of single shear bolted connections of G500 1.20mm thin sheet steel at elevated temperatures has been presented. The coupon tests were conducted in order to investigate the deterioration of the material properties at elevated temperatures and to determine the critical temperatures for the bolted connections. A total of 47 connection specimens varied in bolt size and bolt arrangement were tested in 7 different temperature levels. The coupon tests and the connection tests were conducted using the steady state test method. The 0.2% proof stresses ($f_{0.2}$) and tensile strengths (f_u) of G500 1.20mm thin sheet steel obtained from the coupon tests were compared with the values predicted by Chen and Young's proposed equations (Chen and Young 2007). The comparison shows a rapid drop in both $f_{0.2}$ and f_u in the temperature range 300 – 600ºC.

The test strengths of the single shear bolted connections obtained from the tests were compared with the predicted values calculated using the American, Australian/New Zealand and European specifications for cold-formed steel structures by substituting the reduced material properties at elevated temperatures. It is shown that the American and Australian/New Zealand predications are generally conservative, whereas the European predications are even more conservative at elevated temperatures. The comparison of the test strengths of single shear bolted connections with the tensile strengths of the material properties of the G500 1.20mm sheet steel obtained from the coupon tests has a similar tendency of deterioration at elevated temperatures.

ACKNOWLEDGMENT

The writers are grateful to BlueScope Lysaght (Singapore) Pte Ltd for supplying the test specimens.

APPENDIX - REFERENCES

AISI S100 (2007). *North American Specification for the Design of Cold-Formed Steel Structural Members*, AISI S100-2007, AISI Standard, American Iron and Steel Institute.

AS. (1979). *Methods for the tensile testing of metals at elevated temperatures*, AS 2291:1979, Standards Australia, Sydney, Australia.

AS/NZS 4600 (2005). *Cold-formed Steel Structures*, Australian/New Zealand Standard, Standards Australia, Sydney, Australia.

EC3. (2006). *Eurocode 3 – Design of Steel Structures – Part 1-3: General Rules Supplementary Rules for Cold-formed Members and Sheeting*. EN 1993-1-3:2006, European Committee for Standardization, Brussels.

Chen, J. and B. Young. (2006). "Corner properties of cold-formed steel sections at elevated temperatures." *Thin-Walled Structures*, 44(2), 216-223.

Chen, J. and B. Young. (2007). "Experimental investigation of cold-formed steel material at elevated temperatures." *Thin-Walled Structures*, 45(1), 96-110.

Lim, J.B.P. and D.A. Nethercot. (2003). "Ultimate strength of bolted moment-connections between cold-formed steel members." *Thin-Walled Structures*, 41, 1019-1039.

Lim, J.B.P. and B. Young. (2007). "Effects of elevated temperatures on bolted moment-connections between cold-formed steel members." *Engineering Structures*, 29(10), 2419-2427.

Outinen, J. (1999). *Mechanical properties of structural steels at elevated temperatures*. Licentiate thesis, Helsinki University of Technology, Helsinki, Finland.

Outinen, J., Kaitila, O., and Mäkeläinen, P. (2001). "High-temperature testing of structural steel and modelling of structures at fire temperatures." *Research report TKK-TER-23*, Helsinki University of Technology Laboratory of Steel Structures, Helsinki, Finland.

Rogers, C.A. and G.J. Hancock. (1998a). "New bolted connection design formulae for G550 and G300 sheet steels less than 1.0mm thick." *Research Report No. R769*. Department of Civil Engineering, the University of Sydney, Centre for Advanced Structural Engineering, the University of Sydney, Sydney.

Rogers, C.A. and G.J. Hancock. (1998b). "Bolted connection tests of thin G550 and G300 sheet steels." *Journal of Structural Engineering*, 124(7), 798-808.

Rogers, C.A. and G.J. Hancock. (1999). "Bolted connection design for sheet steels less than 1.0 mm thick." *Journal of Constructional Steel Research*, 51, 123-146.

Rogers, C.A. and G.J. Hancock. (2000). "Failure modes of bolted-sheet-steel connections loaded in shear." *Journal of Structural Engineering*, 126(3), 288-296.

Yu, W.W. (2000). *Cold-formed Steel Design*. 3rd. Wiley, New York.

APPENDIX - NOTATION

The following symbols are used in this paper:

d = nominal bolt diameter
d_o = nominal diameter of the hole (Standard hole)
E_{normal} = elastic modulus at normal room temperature
E_T = elastic modulus at temperature TºC
$f_{0.2}$ = 0.2% proof stress
$f_{0.2,\,normal}$ = 0.2% proof stress at normal room temperature
$f_{0.2,\,T}$ = 0.2% proof stress at temperature TºC

f_u = tensile strength of sheet steel
$f_{u,\ normal}$ = tensile strength of sheet steel at normal room temperature
$f_{u,\ T}$ = tensile strength of sheet steel at temperature T°C
P_n = predicted strength of single shear bolted connection
$P_{n\text{-}AISI}$ = predicted strength of single shear bolted connection based on AISI S100 and AS/NZS 4600
$P_{n\text{-}EC3}$ = predicted strength of single shear bolted connection based on EC3
$P_{u,\ normal}$ = test strength of single shear bolted connection at normal room temperature
$P_{u,\ T}$ = test strength of single shear bolted connection at temperature T°C
t = uncoated sheet (base metal) thickness
$\varepsilon_{f,\ normal}$ = strain at fracture at normal room temperature
$\varepsilon_{u,\ normal}$ = ultimate strain at normal room temperature
ε_u = ultimate strain
$\varepsilon_{u,\ T}$ = ultimate strain at temperature T°C

E_{normal} (GPa)	$f_{0.2,\ normal}$ (MPa)	$f_{u,\ normal}$ (MPa)	$\varepsilon_{u,\ normal}$ (%)	$\varepsilon_{f,\ normal}$ (%)
215	613.7	627.3	4.5	9.0

Table 1. Coupon test results of G500 1.20mm sheet steel at normal room (ambient) temperature

519

Nominal Temperature (ºC)	22	150	300	380	450	520	600	750	900
Specimen Temperature (ºC)	22	146	299	378	445	514	592	745	892
$f_{0.2,\ T} / f_{0.2,\ normal}$	1.000	0.966	0.892	0.712	0.546	0.259	0.088	0.053	0.044
$f_{u,\ T} / f_{u,\ normal}$	1.000	1.002	0.960	0.766	0.612	0.311	0.127	0.059	0.056
E_T / E_{normal}	1.000	0.930	0.930	0.870	0.767	0.535	0.465	0.302	0.195
$\varepsilon_{u,\ T} / \varepsilon_{u,\ normal}$	1.000	0.587	0.475	0.386	0.565	1.105	2.982	1.374	1.276

Table 2. Reduction factors of material properties obtained from coupon tests

Specimen	L (mm)	d_o (mm)	w (mm)	e_1 (mm)	e_2 (mm)	s_1 (mm)	s_2 (mm)
120-B1-M6	363	7.0	50.0	18.0	-	-	-
120-B1-M8	369	9.0	50.0	24.0	-	-	-
120-B2-P-M6	372	7.0	50.0	18.0	18.0	-	-
120-B2-P-M8	381	9.0	50.0	24.0	24.0	-	-
120-B2-V-M6	363	7.0	50.0	18.0	-	18.0	16.0

Table 3. Bolted connection specimen dimensions

Bolt Type	Grade	Nominal Diameter (mm)	Actual Diameter (mm)
M6	12.9	6	5.9
M8	12.9	8	7.8

(a) Details of bolts

Washer Type	Outer Diameter (mm)	Inner Diameter (mm)	Thickness (mm)
M6	12.2	6.4	1.1
M8	15.9	8.5	1.4

(b) Details of washers

Table 4. Details of bolts and washers

Nominal T (°C)	Coupon T (°C)	Specimen T (°C)	$P_{u,\,normal}$ or $P_{u,\,T}$ (kN)	$\frac{P_{u,T}}{P_{u,normal}}$	$\frac{P_{u,normal}}{P_{n-AISI}}$ or $\frac{P_{u,T}}{P_{n-AISI}}$	$\frac{P_{u,normal}}{P_{n-EC3}}$ or $\frac{P_{u,T}}{P_{n-EC3}}$	Failure Mode		
							AISI and AS/NZS	EC3	Tests
22	22	22	12.69	1.00	0.94	1.14	B+T	B	B
150	146	158	11.63	0.92	0.86	1.04	-	-	B
		159	12.04	0.95	0.89	1.08	-	-	B
300	299	301	11.08	0.87	0.85	1.04	-	-	B
		298	11.42	0.90	0.88	1.07	-	-	B
450	445	445	8.79	0.69	1.06	1.29	-	-	B
		446	8.65	0.68	1.04	1.27	-	-	B
600	592	597	2.29	0.18	1.33	1.62	-	-	B
750	745	740	1.14	0.09	1.44	1.75	-	-	B
900	892	885	0.89	0.07	1.16	1.41	-	-	BS
				Mean	1.04	1.27			
				COV	0.207	0.253			

Note: B = Bearing failure; T = Tear out failure; BS = Bolt shear failure

(a) Comparison of Specimen 120-B1-M6

Nominal T (°C)	Coupon T (°C)	Specimen T (°C)	$P_{u,\,normal}$ or $P_{u,\,T}$ (kN)	$\frac{P_{u,T}}{P_{u,normal}}$	$\frac{P_{u,normal}}{P_{n-AISI}}$ or $\frac{P_{u,T}}{P_{n-AISI}}$	$\frac{P_{u,normal}}{P_{n-EC3}}$ or $\frac{P_{u,T}}{P_{n-EC3}}$	Failure Mode		
							AISI and AS/NZS	EC3	Tests
22	22	22	15.39	1.00	0.86	1.04	N	B	B
150	146	166	15.21	0.99	0.85	1.02	-	-	B
300	299	302	15.60	1.01	0.91	1.10	-	-	B
		307	14.35	0.93	0.84	1.01	-	-	B
450	445	448	11.16	0.73	1.02	1.23	-	-	B
		446	10.68	0.69	0.98	1.18	-	-	B
600	592	597	2.75	0.18	1.21	1.46	-	-	B
		595	2.80	0.18	1.23	1.49	-	-	B
750	745	741	1.37	0.09	1.30	1.57	-	-	B
		738	1.29	0.08	1.22	1.48	-	-	B
900	892	892	1.36	0.09	1.35	1.63	-	-	BS
				Mean	1.07	1.29			
				COV	0.197	0.238			

Note: N = Net Section tension failure.

(b) Comparison of Specimen 120-B1-M8

Nominal T (°C)	Coupon T (°C)	Specimen T (°C)	$P_{u,\,normal}$ or $P_{u,\,T}$ (kN)	$\frac{P_{u,T}}{P_{u,normal}}$	$\frac{P_{u,normal}}{P_{n-AISI}}$ or $\frac{P_{u,T}}{P_{n-AISI}}$	$\frac{P_{u,normal}}{P_{n-EC3}}$ or $\frac{P_{u,T}}{P_{n-EC3}}$	Failure Mode		
							AISI and AS/NZS	EC3	Tests
22	22	22	22.18	1.00	0.98	1.00	T	B	B
150	146	146	22.35	1.01	0.99	1.00	-	-	B
300	299	298	20.52	0.93	0.95	0.96	-	-	B
450	445	444	16.62	0.75	1.20	1.22	-	-	B
		445	17.22	0.78	1.25	1.27	-	-	B
600	592	590	3.58	0.16	1.25	1.27	-	-	B
		593	3.45	0.16	1.20	1.22	-	-	B
750	745	743	1.62	0.07	1.22	1.24	-	-	B
900	892	890	1.55	0.07	1.22	1.24	-	-	BS
				Mean	1.14	1.16			
				COV	0.127	0.129			

(c) Comparison of Specimen 120-B2-P-M6

Nominal T (°C)	Coupon T (°C)	Specimen T (°C)	$P_{u,\,normal}$ or $P_{u,\,T}$ (kN)	$\frac{P_{u,T}}{P_{u,normal}}$	$\frac{P_{u,normal}}{P_{n-AISI}}$ or $\frac{P_{u,T}}{P_{n-AISI}}$	$\frac{P_{u,normal}}{P_{n-EC3}}$ or $\frac{P_{u,T}}{P_{n-EC3}}$	Failure Mode		
							AISI and AS/NZS	EC3	Tests
22	22	22	28.51	1.00	0.95	1.14	T	N	B+N
150	146	153	29.11	1.02	0.96	1.17	-	-	B+N
300	299	300	26.53	0.93	0.92	1.11	-	-	B+N
450	445	440	19.49	0.68	1.06	1.28	-	-	B+N
		444	19.81	0.69	1.08	1.30	-	-	B+N
600	592	592	4.67	0.16	1.22	1.48	-	-	B+N
		591	4.60	0.16	1.20	1.45	-	-	B+N
750	745	740	1.78	0.06	1.01	1.22	-	-	B+N
900	892	890	1.59	0.06	0.93	1.13	-	-	MF
		892	1.57	0.06	0.92	1.12	-	-	MF
				Mean	1.03	1.24			
				COV	0.113	0.136			

Note: MF = Material failure.

(d) Comparison of Specimen 120-B2-P-M8

Nominal T (°C)	Coupon T (°C)	Specimen T (°C)	$P_{u,\,normal}$ or $P_{u,\,T}$ (kN)	$\frac{P_{u,T}}{P_{u,normal}}$	$\frac{P_{u,normal}}{P_{n-AISI}}$ or $\frac{P_{u,T}}{P_{n-AISI}}$	$\frac{P_{u,normal}}{P_{n-EC3}}$ or $\frac{P_{u,T}}{P_{n-EC3}}$	Failure Mode		
							AISI and AS/NZS	EC3	Tests
22	22	22	21.31	1.00	0.79	0.96	N	B	N
150	146	148	21.22	1.00	0.78	0.95	-	-	N
300	299	303	21.89	1.03	0.84	1.03	-	-	N
450	445	440	14.73	0.69	0.89	1.08	-	-	N
600	592	591	3.23	0.15	0.94	1.15	-	-	N+B
750	745	742	1.48	0.07	0.93	1.14	-	-	N+B
900	892	890	1.48	0.07	0.97	1.18	-	-	BS
				Mean	0.88	1.07			
				COV	0.076	0.092			

(e) Comparison of Specimen 120-B2-V-M6

Table 5. Comparison of test results with predicted values for single shear bolted connections

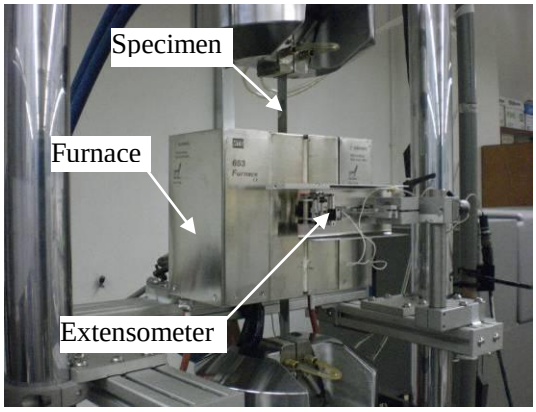

Fig. 1. Testing device of coupon tests

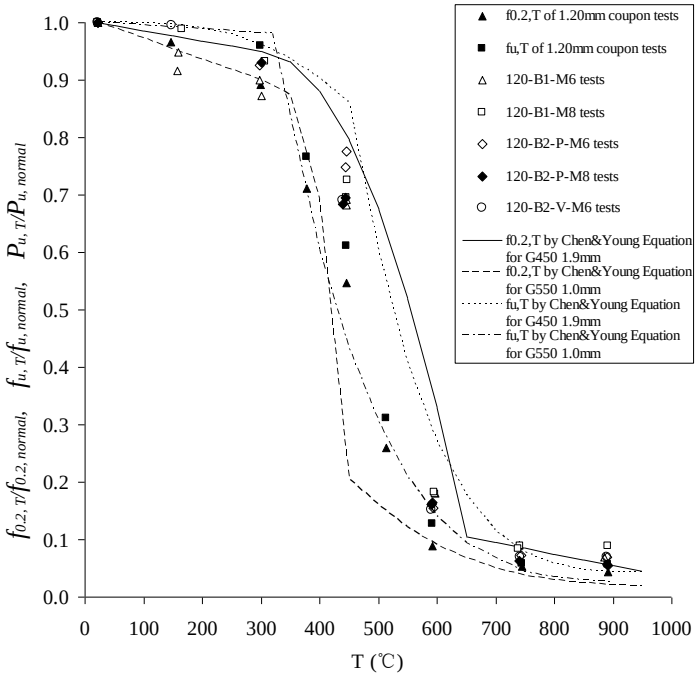

Fig. 2. Comparison of test results with material tests of G500 1.20mm steel and Chen & Young (2007) proposed equations

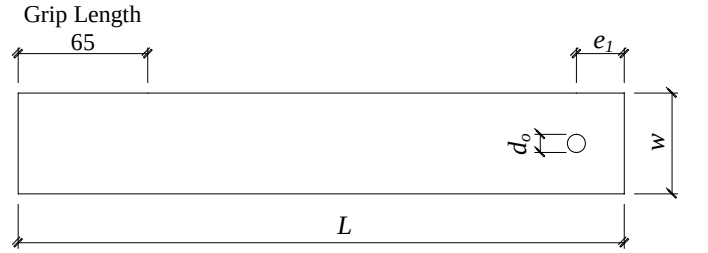

(a) B1 test specimen

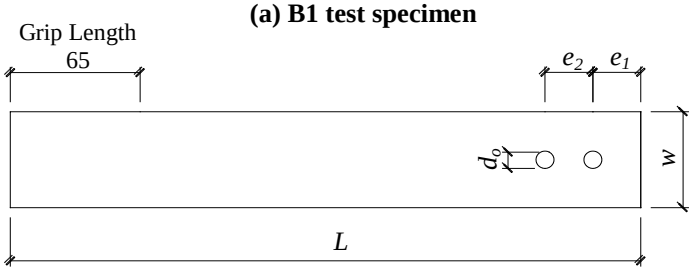

(b) B2-P test specimen

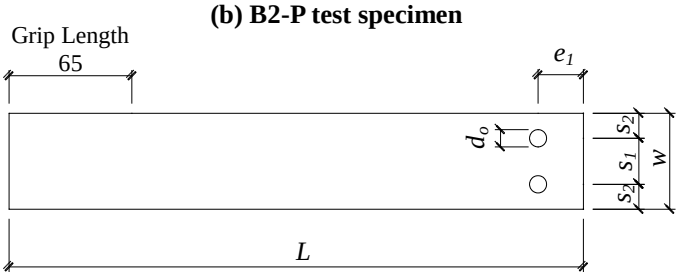

(c) B2-V test specimen

Fig. 3. Design details of single shear bolted connection specimens

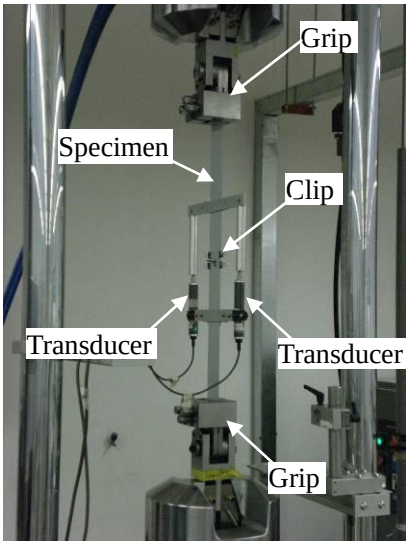

(a) Normal room (ambient) temperature

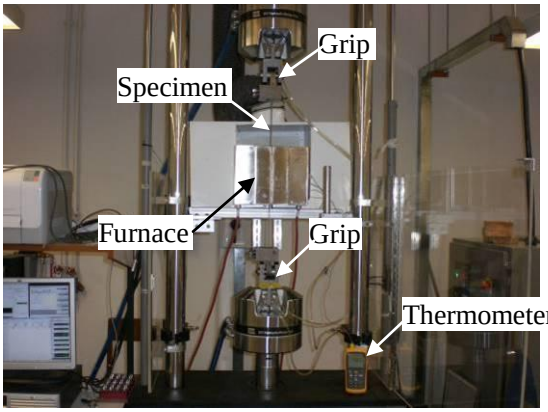

(b) Elevated temperature

Fig. 4. Test set-up of the single shear bolted connection specimens

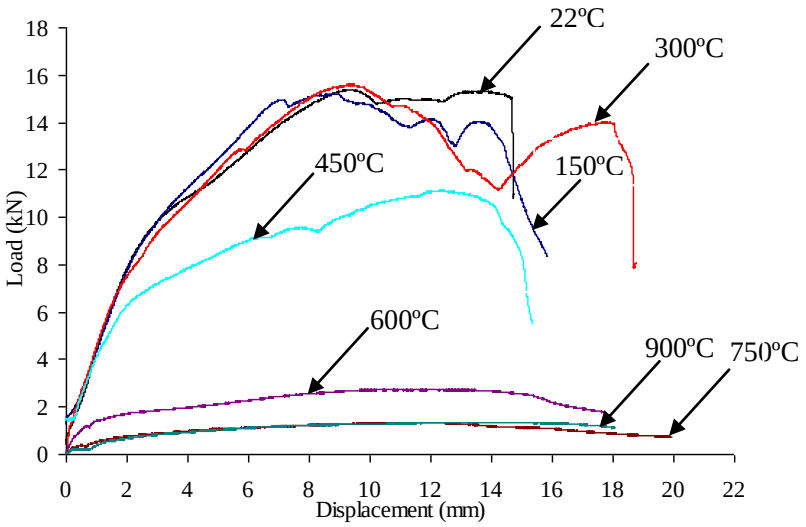

Fig. 5. Test curves of 120-B1-M8

(a) 302 ºC

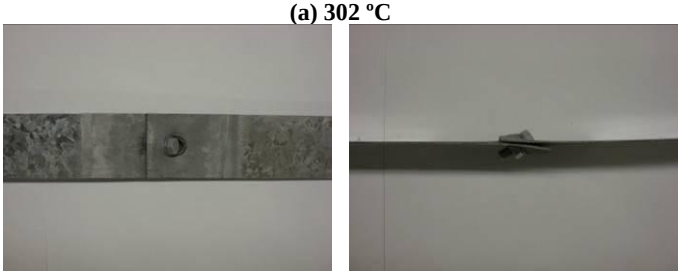

(b) 448 ºC

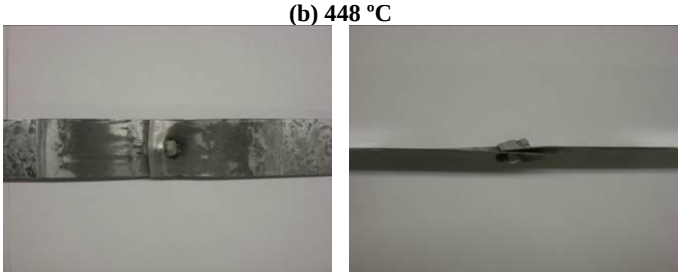

(c) 595 ºC

(d) 741 ºC

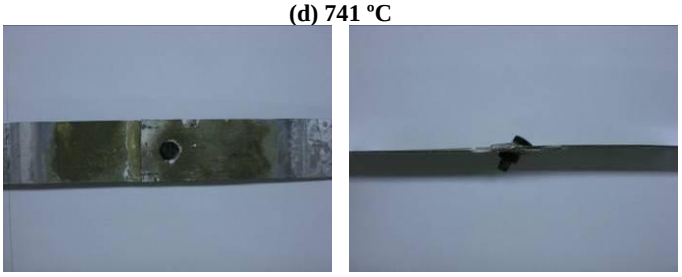

(e) 892 ºC

Fig. 6. Failure modes of 120-B1-M8 specimens at elevated temperatures

Twentieth International Specialty Conference on Cold-Formed Steel Structures
St. Louis, Missouri, U.S.A., November 3 & 4, 2010

Arc-Spot Welds for Multi-Overlap Roof Deck Panels

N. Guenfoud[1] , R. Tremblay[2], and C.A. Rogers[3]

Abstract

Roof deck construction often incorporates cold-formed steel panels that are connected to the underlying framing with the use of arc-spot welds. The welds are commonly located in areas where multiple layers of roof deck exist, such as at sidelaps or endlaps. CSA S136 restricts the use of multi-layer connections to being less than 2.5 mm thick; as well, the thickness of the supporting steel must exceed 2.5 times the aggregate thickness of the deck. In effect, the standard does not allow for the use of arc-spot welds for 18 ga (1.21 mm) and 16 ga (1.52 mm) roof deck panels. Nonetheless, it is not unusual for these deck panels to be used in construction; a solution to the arc-spot weld restrictions and a new welding protocol was needed. This situation led to the initiation of a research program on the shear resistance and tension resistance of multi-layer arc spot welds. The paper describes the welding protocol that was developed to obtain adequate quality and size arc-spot welds in up to four layers of 16 ga. deck. Weld test specimens were fabricated through one, two or four layers of steel sheets with thicknesses ranging from 22 ga. (0.76 mm) to 16 ga. (1.52 mm). Various sheet steel / weld configurations found in roof deck construction were included. A total of 72 tension tests and 107 shear tests were completed. Adequate weld quality could be achieved in all cases except that welds were undersized when the total sheet thickness becomes twice as large as the thickness of the underlying material. The results were compared with the current provisions of CSA S136 and modifications to the existing design equations are recommended.

[1] Graduate Student, Department of Civil, Geological and Mining Engineering, École Polytechnique, Montreal QC, Canada.
[2] Professor, Canada Research Chair in Earthquake Engineering, Department of Civil, Geological and Mining Engineering, École Polytechnique, Montreal QC, Canada.
[3] Associate Professor, Department of Civil Engineering & Applied Mechanics, McGill University, Montreal QC, Canada.

Introduction

In North America roof deck diaphragms are commonly used as part of the lateral load resisting system. These diaphragms are composed of corrugated steel panels that may be connected to the underlying structure by arc-spot welds. Due to uplift actions caused by wind loads the welded connections must also resist tension forces. At the perimeter of each panel, the sidelap and endlap fasteners connect adjacent panels to the structure; this can result in connections comprising two and four layers of deck (Fig. 1).

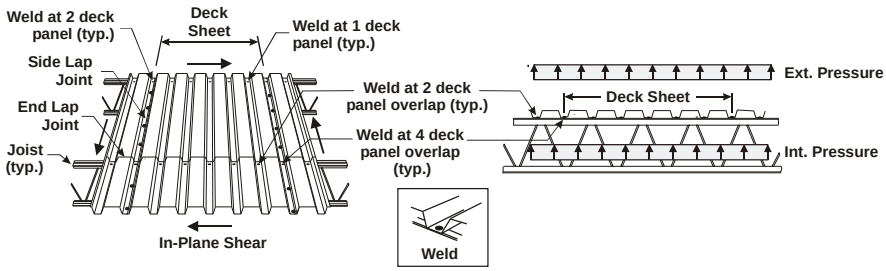

Figure 1: Steel deck panel connections and loading

CSA S136 (2007) contains provisions to determine the shear resistance and tensile resistance of arc-spot welds. These provisions, mainly based on tests that were carried out using thin deck (22 & 20 ga. (0.76 mm & 0.91 mm)), can be traced to the work of Peköz & McGuire (1979) and LaBoube & Yu (1991). CSA S136 limits the total thickness of sheet steel (deck thickness times the number of deck layers) for an arc spot weld connection to 3.81 mm. Section E2.2a of Appendix B (Canada) states that the maximum single sheet thickness shall be 2.0 mm and that the maximum aggregate sheet thickness of double sheets shall be 2.5 mm. The thickness of the supporting member must be at least 2.5 times the aggregate steel sheet thickness. Furthermore, the 2005 NBCC (NRCC, 2005) and CSA S16 (2001) necessitate the use of a capacity based seismic design approach which requires the roof deck diaphragm to have a shear resistance greater than the probable resistance of the vertical bracing system (Rogers & Tremblay, 2010). Consequently, the use of 18 (1.21 mm) and 16 ga. (1.52 mm) deck has become more common as stronger diaphragms are required.

Snow & Easterling (2008) performed shear tests on single, double and four-layer arc-spot weld connections for deck ranging from 0.76 mm to 1.52 mm. These deck-to-frame connections were fabricated using a shielded metal arc welding (SMAW) procedure that involved an E4310 (E6010) electrode. It was concluded that arc-spot welds can be adequately fabricated in single and double layers of sheet steel if the total thickness does not exceed 3.81 mm. It was also reported

that welds with sufficient penetration could not be fabricated in four layers of sheet steel. The 3.81 mm limit is exceeded when 16 and 18 ga. deck panels in the four layer sidelap/endlap configuration are required.

This research was initiated due to the lack of Canadian design information for arc-spot weld connections for the thicker deck panels. The scope of research was set to address the performance of multi-layer connections. The objective was to first identify a procedure that could be used to weld the connections, and to then verify if the current design provisions in CSA S136 for arc-spot welds are applicable to these thick deck sheet assemblies. The scope of research involved the testing of arc-spot weld connections fabricated through one, two or four layers of steel sheets with thicknesses ranging from 22 ga. (0.76 mm) to 16 ga. (1.52 mm). The findings of this research project are summarized herein; details on the test program can be found in Guenfoud *et al.* (2010).

Experimental Program

Welding Protocol and Procedure

In collaboration with a welding engineer and experienced certified welders a SMAW procedure for multi-overlap deck connections was first established; the key parameters affecting weld quality were identified as being the electrode type, the current setting and the welding technique. E4311 (E6011) electrodes were selected because they provided better penetration than other commonly used electrodes as observed by Peuler *et al.* (2002). Preliminary welding sessions were organized to verify the quality of welds fabricated and to refine the welding procedure. The final parameters used for the fabrication of the test specimens were: a) Circular welds having a visible diameter from 16 mm to 19 mm, b) 3.2 mm (1/8 in.) diameter E4311 (E6011) electrodes, and c) AC current set at 195 A when welding 16 and 18 ga. steel sheets, and 160 A when welding 20 and 22 ga. steel sheets. The welding procedure, similar to that elaborated by Peuler (2002), was selected because it facilitated piercing through thicker sheets while minimizing porosity. The weld was performed in the flat position. Once the arc was sparked, the electrode was pushed down vertically through the material to drill through the sheets until proper fusion of the underlying hot rolled steel was obtained. The electrode was then gradually withdrawn with a circular motion to allow the hole to be filled with molten metal. The arc was then broken vertically. The proposed settings represent laboratory conditions; field conditions might use this as a starting point but the final choice for optimum methods can vary depending on ambient conditions, welding equipment and the preferences of the welder.

Test Specimens and Set-up

The test program (Fig. 2) involved the two loading conditions encountered in roof deck construction, *i.e.* in-plane shear due to lateral loads and tension due to uplift wind pressure. Shear and tension connection test specimens were fabricated using four nominal sheet steel thicknesses: 0.76, 0.91, 1.21 and 1.52 mm. All specimens were made from galvanized ASTM A653 SS230 sheet steel with zinc thickness corresponding to Z275 (275 g/m^2, total of two faces).

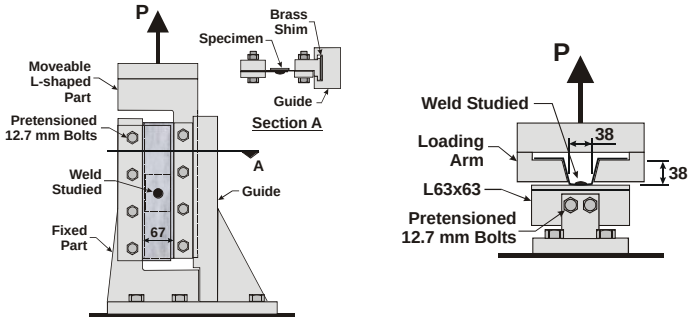

Figure 2: Steel deck panel shear and tension test set-up

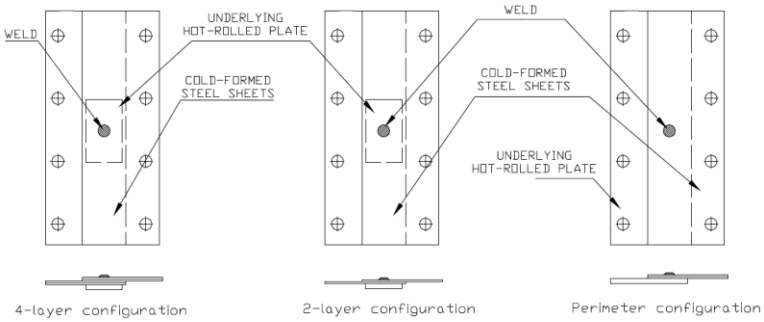

Figure 3: Steel deck panel shear test specimens

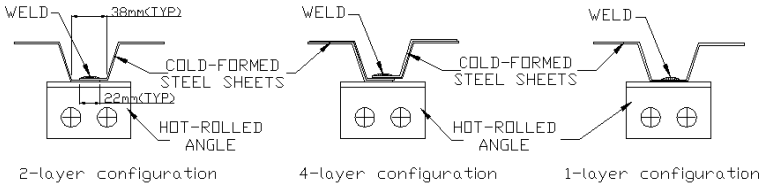

Figure 4: Steel deck panel tension test specimens

The shear specimens were made of two 102 x 280 mm overlapped steel sheets connected by a single weld (Fig. 3). To represent the underlying joist top chord or beam top flange, a 51 mm x 76 mm plate with thicknesses of 6.4 mm and 3.2 mm was used. These plates were made of CSA G40.21-350W steel with a one-coat primer. The set-up used to test the tension strength of the arc-spot welds was similar to that developed by LaBoube & Yu (1991). Steel sheets (100 mm long) were cut and cold bent to model one flute from the common 38 mm deep x 914 mm wide trapezoidal deck profile with flutes spaced 152 mm o/c (Fig. 4). At the bottom flange of the simulated flute, the sheets were welded to hot rolled CSA G40.21-350W steel L63x63 angles (one-coat primer) with thicknesses of 6.4 mm (1/4") and 3.2 mm (1/8") representing typical steel joist top chords.

Loading and Displacement Protocols

A monotonic loading protocol was used for all tension tests and 76 shear tests. The remaining 31 shear tests were carried out using a reversed cyclic loading protocol. Prior to running the cyclic tests, the data from the monotonic shear tests were compiled to provide an estimate of the average ultimate shear strength ($P_{u,avg.}$) for each connection configuration from which a loading protocol specific to each configuration was then determined.

Test Matrix

A listing of the connection test configurations is provided in Table 1. The first letter of the specimen number relates to the loading (M = monotonic, C = cyclic, and T = tension), "xx" is the gauge, followed by the number of plies, and "z" is the specimen number in a series. The letter "P" or "T" is added to identify the shear specimens at the perimeter of the diaphragm and when the thinner (3.2 mm) underlying material is used, respectively. The number of specimens is associated with a letter that gives the observed failure mode, as discussed below.

Test Results

Failure Modes

Three different failure modes were observed during the shear tests: weld shear failure (W), sheet tearing failure (T) and sheet bearing failure (B). Weld shear failure is characterized by fracture of the specimen through the weld nugget. Small displacements, a sudden loss in resistance and overall brittle behaviour are associated with this failure mode. Weld shear occurs mainly for the configurations that have a low weld diameter to total thickness ratio. When the effective diameter is relatively small compared to the thickness of the sheet steel

the critical load causing failure through the weld plane is reached before the sheet steel can exhibit significant deformations. When sheet tearing occurs (high *d*/*t* ratios), the failure initiates on the tension side of the weld and then spreads on a line perpendicular to the applied load. Out-of-plane deformations occur in the sheet steel on the compression side of the weld. Sheet bearing failure is characterized by piling of the steel in front of the weld nugget and by shearing of the sheet around the contour of the weld on lines parallel to the applied load.

During tension strength tests, two failure modes were encountered: weld failure (W) and sheet tearing failure (T). Weld failure, associated with small displacements, occurred for configurations with low *d*/*t* ratios. Sheet tearing is characterized by tearing of the sheet steel along the contour of the weld. A peeling effect caused by the geometry of the overlap connection was also observed.

Table 1 Test matrix and observed failure modes[1]

Specimen No.	Sheet thickness (mm) / Gauge			
	0.76 / 22	0.91 / 20	1.21 / 18	1.52 / 16
Mxx2z Mxx4z	4T 2W+1T+1B	4T 2W+1T+1B	4T 4W	4B 4W
Mxx2zP	2W+2T	1W+3T	4W	4W
Mxx2zT Mxx4zT	4T 2W+1T+1B	3T 1W+1T+2B	4T 3W	3W 3W
Cxx2z Cxx4z	4T 1W+1T+2B	4T 1W+1T+2B	4T 3W	4B 4W
Txx1z Txx2z Txx4z	3T 4T 3T	4T 4T 1W+3T	4T 4T 1W+3T	4T 3W+1T 3W
Txx2zT Txx4zT	5T 4T	3T 1W+2T	3W 3W	3T 3W

[1]Note: W = Weld failure, T = Sheet tearing failure, B = Bearing failure.

Effective Weld Diameter

In CSA 136 the resistance of welds subject to shear or tension is related to the effective weld diameter, d_{eff}. The cross-section of the weld nugget typically has a conical shape and, therefore, the diameter of the weld decreases over its depth. The visual weld diameter, d_{vis}, is measured at the surface of the weld whereas d_{eff} is located at the failure plane of the weld. The effective weld diameter is measured along the mid-thickness of the steel sheets for the four- and two-ply

shear specimens. Conversely, d_{eff} is at the interface between the cold-formed steel sheets and the hot rolled steel for the two-ply shear specimens representing an end lap connection to the perimeter beams and for the four-, two- and single-ply tension specimens. The difference between the visual diameter and the effective diameter increases as the total thickness of sheet steel above the expected failure plane, t, is increased:

$$d_{eff} = 0.7d_{vis} - 1.5t \leq 0.55d_{vis} \qquad \text{[E2.2.1.2-5]} \qquad (1)$$

The effective weld diameter was determined for all shear and tension specimens where weld failure occurred. A measure of pitting and porosity was deducted from the effective gross weld area to calculate the effective net weld area, A_{ne}, which was then used to obtain d_{eff}:

$$d_{eff} = \sqrt{4A_{ne}/\pi} \qquad (2)$$

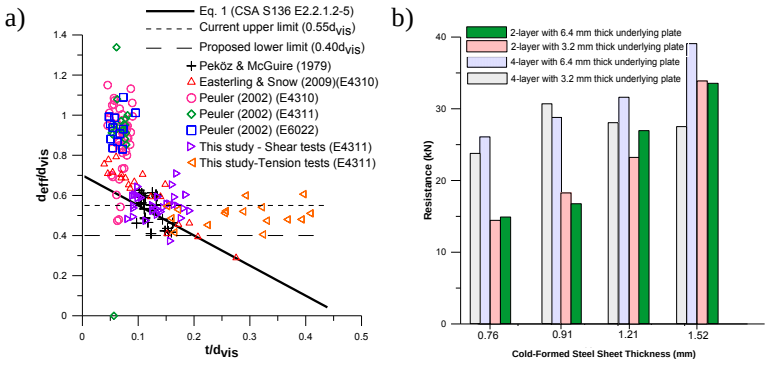

Figure 5 a) Effective weld diameter results; b) Influence of the thickness of the underlying plate on the shear strength of two-ply and four-ply specimens

Equation 1 has previously been found to be conservative because the measured effective weld diameters by Peuler (2002) were on average 50% higher than predicted. More recently, Snow & Easterling measured effective weld diameters that were on average 30% higher than those calculated using Eq. 1. It must be noted that the values published by Peuler as well as Snow & Easterling did not include a reduction to account for the porosity of the welds. A plot of the data recorded from the shear and tension specimens of this test program and the data reported from previous studies by Peköz & McGuire, Peuler and Snow & Easterling is provided in Fig. 5a. Specimens with "full-time welds" were plotted for the study by Snow & Easterling, the time spent making "full-time welds" being the minimum time

required to produce visual, average and effective diameters consistent with the dimensions required by the 2001 AISI Specification (AISI 2001). The measured values of d_{vis} were used to plot the data from this study.

The results show that Eq. E2.2.1.2-5 of CSA S136 accurately predicts d_{eff} for the t/d_{vis} range where tests had previously been carried out. This study also provided data in a t/d_{vis} range where few tests had previously been done. Figure 5a shows that Eq. E2.2.1.2-5 becomes overly conservative as t/d increases; a lower limit should be added if welds are fabricated with a welding procedure using an E4311 (E6011) penetrating electrode:

$$d_{eff} = 0.7d_{vis} - 1.5t\,, \text{ with } 0.4d_{vis} \le d_{eff} \le 0.55d_{vis} \quad (3)$$

Influence of the Thickness of the Underlying Framing Material

The failure modes and ultimate resistance of the shear and tension specimens fabricated with 3.2 mm and 6.4 mm framing material were compared. For the shear specimens, the failure mode was not influenced by the plate thickness. For two-layer specimens, the strength was found not to be affected by the thickness of the supporting material, regardless of the sheet thickness (Fig. 5b). The same holds true for the four-layer connections made with 22 to 18 ga. steel sheets. However, for the 4-layer specimens fabricated with 16 ga. (1.52 mm) material and 3.2 mm thick plates, the average measured shear resistance was 32% lower than the average measured shear resistance of the 4-layer specimens with 6.4 mm thick plates (Fig. 5b). The measured d_{vis} and d_{eff} were respectively 13% and 28% lower for specimens fabricated with 3.2 mm thick plates. These results show that when the plate material to total sheet steel thickness ratio is less than 0.5 the welder may experience more difficulty in producing welds with consistent effective weld diameters, which can result in reduced and more variable connection strength. No shear strength reduction was observed when the plate material to total sheet steel thickness ratio was equal to or greater than 0.7 (four 1.21 mm thick sheets on 3.2 mm plate), which is significantly less than the current minimum value of 2.5 specified in Appendix B of CSA S136.

The thickness of the angle had no influence on the behaviour and strength of the tension specimens fabricated with 22 and 20 ga. steel sheets. For specimens with 18 and 16 ga. steel sheets, a decrease in resistance was observed when 3.2 mm thick angles were used. It was observed that the angles deformed upon loading, causing stress concentrations along the perimeter of the weld thereby reducing the tension resistance of the weld. Such deformations did not occur with the 6.4 mm thick angles. In OWSJs the local flexibility of top chord angles will depend on several factors such as the angle size, the spacing and the stiffness of the joist

web members, etc., and it is therefore not possible to prevent angle deformations on the sole basis of a minimum angle to total sheet thickness ratio. Further research is needed to properly address this issue. In the test specimens, however, the average measured visible weld diameter of the 18 and 16 ga. steel sheet specimens with 3.2 mm thick angles was 17% smaller than for specimens fabricated with thicker underlying angles, leading to a smaller effective weld size and reduced capacity, similar to the shear tests. For the 4-layer specimens with 3.2 mm thick angles, the average measured A_{ne} of 16 ga. specimens was 20% less than that of the specimens composed of 18 ga. steel sheets. As such, welders may experience difficulty producing quality welds through 4 layers of 16 ga. (1.52 mm) steel sheet if the angle does not provide an adequate heat sink.

Analysis of CSA S136 Shear Resistance Equations

The results of the 76 monotonic shear tests were used to validate the CSA S136 equations. In tests with weld fracture, the resistance of the specimen is governed by the effective diameter of the weld. For sheet failure, the thickness of the steel sheets above the plane of maximum shear, and the visible weld diameter influence the shear strength. When considering the 33 shear tests with weld failure, the comparison of the measured effective weld diameter with the values predicted by Eq. E2.2.1.2-5 from CSA S136 provided an average test-to-predicted ratio of 1.13 with a coefficient of variation of 0.15. Equation E2.2.1.2-5 accurately predicts the d_{eff} for the range of t/d_{vis} corresponding to the shear specimens ($0.06 < t/d_{vis} < 0.2$). Equation 4 is used to evaluate the resistance of the connection specimens with regard to the weld shear failure mode:

$$P_u = \frac{\pi d_{eff}^2}{4} 0.75 F_{xx} \qquad \text{[E2.2.1.2-1]} \qquad (4)$$

Using the nominal tensile strength of the weld metal (F_{xx} = 430 MPa) and the measured d_{eff}, the average test-to-predicted resistance ratio for the shear specimens that failed due to weld fracture is 1.42 with a coefficient of variation of 0.15. This trend is consistent with that obtained by Peköz & McGuire who reported an average test-to-predicted ratio of 1.22 with a coefficient of variation of 0.30 for similar tests. The relationship between P_u and Eq. E2.2.1.2-1 is plotted in Fig. 6. The comparison shows that Eq. 4 consistently under-predicts the shear resistance of welded connections for the range of d_{eff} examined. This is likely caused by the difference between the actual and nominal values of the tensile strength of the weld metal. It is difficult to measure F_{xx} of the weld metal as it can vary significantly over the weld failure plane. The results show that Eq. E2.2.1.2-1 can safely be used to determine the shear resistance for arc spot weld failures in multi-overlap configurations.

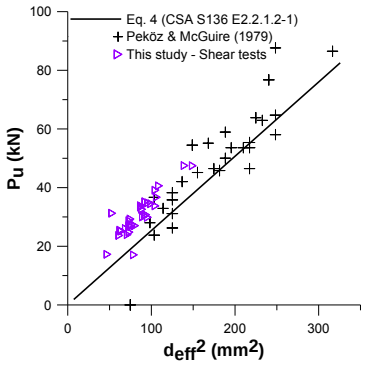

Figure 6 Relationship between P_u and d_{eff}^2 of CSA S136 Eq. E2.2.1.2-1

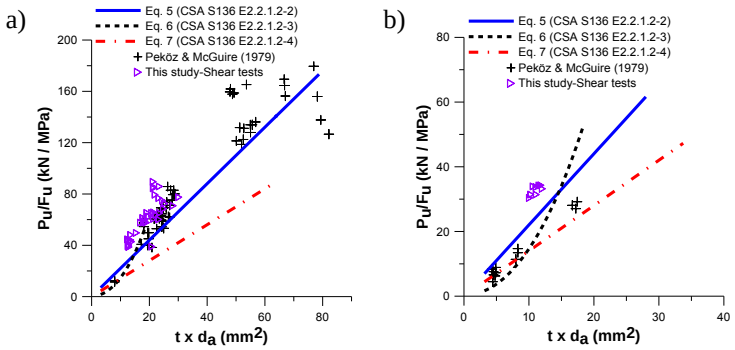

Figure 7 Relationship between measured arc spot weld shear strength and $t \times d_a$ for: a) Bearing failure; b) Tearing failure

Equations E2.2.1.2-2 to E2.2.1.2-4 in CSA 136 are used to predict the shear strength when shear failure occurs in the sheet material:

$$for\ (d_a/t) \le 0.815\sqrt{E/F_u}:$$

$$P_u = 2.20 t d_a F_u \qquad \text{[E2.2.1.2-2]} \qquad (5)$$

$$for\ 0.815\sqrt{E/F_u} < (d_a/t) < 1.397\sqrt{E/F_u}:$$

$$P_u = 0.280\left[1 + 5.59\frac{\sqrt{E/F_u}}{d_a/t}\right] t d_a F_u \qquad \text{[E2.2.1.2-3]} \qquad (6)$$

$$for\ (d_a/t) \ge 1.397\sqrt{E/F_u}:$$

$$P_u = 1.40 t d_a F_u \qquad \text{[E2.2.1.2-4]} \qquad (7)$$

In these equations, $d_a = d_{vis} - t$, where t is the thickness of steel above the plane of maximum shear in the weld, *i.e.* the plane where d_{eff} was measured for the specimen with weld failure, and F_u is the tensile strength of the steel sheet. The test data was compared to the predicted values using the measured values of d_{vis} and F_u. Of all monotonic shear specimens, 35 were governed by Eq. 5. This equation is associated with a bearing failure mode. In Fig. 7a, Eqs. 5 to 7 are plotted with the test results and the data by Peköz & McGuire.

A trend can be observed where the measured resistance is generally higher than the predicted resistance. The average test-to-predicted resistance ratio was 1.44 with a coefficient of variation of 0.14 for the group of specimens tested in this experimental program. Likewise, Peköz & McGuire reported an average test-to-predicted resistance ratio of 1.15 with a coefficient of variation of 0.17 while Snow & Easterling reported a ratio of 1.28 with a coefficient of variation of 0.09 for similar specimens. The difference between the three ratios may be attributed to differences in weld quality. Although this data was not recorded, some specimens may not have had efficient connectivity along the entire perimeter of the weld, which would inevitably lower the resistance of the specimen. When analysing the data collected during this experimental program the best fit formula to replace equation E2.2.1.2-2 was found to be:

$$P_u = 2.40 t d_a F_u \ , \ for \ (d_a / t) \le 0.815\sqrt{E/F_u} : \tag{8}$$

This proposed equation was analyzed in accordance with Section F.1 of CSA S136 which specifies the statistical treatment to determine the structural performance for limit states design. The average test-to-predicted ratio was 1.32 with a coefficient of variation of 0.14. A reliability index of 4.0 can be attained with a resistance factor $\phi = 0.6$.

A total of 8 specimens were governed by Eq. 6 because of the d_a/t range. The average test-to-predicted resistance ratio for specimens governed by this equation is 1.58 with a coefficient of variation of 0.04. The data measured in this study and the data by Peköz & McGuire are compared to the predicted values in Fig. 7b. Equation 6 generally underestimates the resistance of the tested specimens. However, too few specimens were governed by this equation during this test program to warrant the modification of the current CSA S136 equation. Based on the available test data, it seems that Eq. 6 can safely be used to predict the shear resistance of specimens with multi-overlap configurations when $0.815\sqrt{E/F_u} < (d_a / t) < 1.397\sqrt{E/F_u}$. Further research targeting this specific range of specimens should however be carried out to validate the accuracy of Eq. E2.2.1.2-3. Of all the specimens tested during this experimental

program, none presented a d_a/t ratio indicating that Eq. E2.2.1.2-4 would govern, hence no conclusions have been drawn regarding its accuracy.

Analysis of CSA S136 Tension Resistance Equations

The results showed that when the specimen behaviour was governed by weld fracture d_{eff} influenced the tension resistance. When the tension specimens were governed by sheet failure, the total thickness of sheet steel above the underlying material and the average weld diameter influenced the tension resistance. As discussed, the thickness of the underlying joist angle also influenced the resistance of the specimens as thinner supporting material can distort upon loading and create stress concentrations that can adversely affect the resistance of the specimen. The deformation of the support can be avoided by using hot rolled angles with a minimum thickness of 6.4 mm. Section E2.2.2 of CSA S136 is used by designers to determine the tensile resistance of arc-spot welds:

$$P_u = \frac{\pi d_{eff}^2}{4} F_{xx} \qquad \text{[E2.2.2-1]} \qquad (9)$$

$$P_u = 0.8\left(F_u/F_y\right)^2 t d_a F_u \qquad \text{[E2.2.2-2]} \qquad (10)$$

Equation 9 is related to weld failure in tension whereas Eq. 10 addresses the sheet tearing failure mode. CSA S136 specifies a 30% reduction for welds fabricated in sidelap joints. This reduction applies to sheet tearing when part of the weld connects to the overlapped sheet; this was not the case as the unstiffened flange width was larger than the visible weld diameter in all tests.

A total of 16 tension specimens failed due to weld fracture. The majority of these specimens (14) were fabricated with 1.21 and 1.52 mm thick steel sheets, the remaining two being made with 0.91 mm sheets. The resistance of such specimens is related to the effective weld diameter of each specimen. Figure 8a contains a plot of Eq. 9 without the 30% reduction in resistance. The data set is divided into two groups: 9 specimens where bending of the underlying angle was observed (3.2 mm thick angle with 18 ga. and thicker sheets) and 7 specimens where bending of the angles was not observed (6.4 mm thick angle or 20 ga. and thinner sheet steels). Test data for weld failure in tension reported by LaBoube & Yu (1991) for 4 non sidelap connections are also shown. Good match is found between Eq. E2.2.2-1 and the test data by LaBoube & Yu. The data produced in this test program is generally lower, with average test-to-predicted ratios of 0.50 and 0.56 for the entire data set and the subset where angle bending was not observed, respectively. Test specimens by LaBoube &

Yu had smaller effective diameters and washers were used in the welds, which favoured uniform stress distribution over the weld area. In this test program, the larger effective weld diameters and the absence of washer likely led to tensile stress concentrations along the perimeter of the welds, resulting in lower capacities; this phenomenon was probably accentuated when bending of the angle legs occurred. Considering that steel joists with thin angles are not uncommon in practice, it is proposed that Eq. 9 [E2.2.2-1] be modified based on the entire test data set by introducing a reduction factor of 0.5:

$$P_u = \frac{\pi d_{eff}^2}{4} 0.5 F_{xx} \tag{11}$$

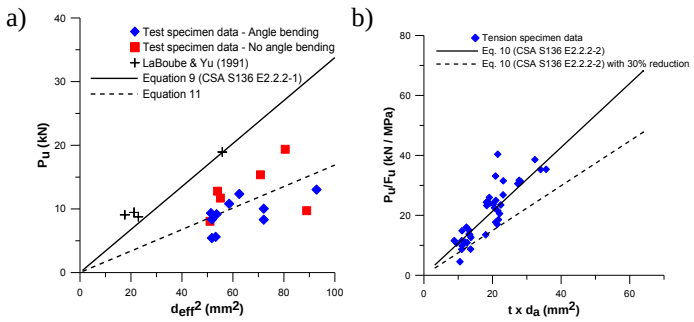

Figure 8 Relationship between measured arc spot weld tension strength and: a) d_{eff}^2 for weld failure; b) $t \times d_a$ for sheet tearing failure.

Using Eq. 11 (Fig. 8a), the average test-to-predicted ratio is equal to 1.0 with a coefficient of variation of 0.27; the resistance factor must be lowered to 0.32 to attain a reliability index of 4.0. If only the subset of 7 specimens for which angle bending was not observed is considered, a reduction factor of 0.56 is needed to achieve a test-to-predicted ratio of 1.0. The coefficient of variation is then equal to 0.26 and a resistance factor of 0.29 is required to obtain a reliability index of 4.0. In practice, Eq. [E2.2.2-1] will be used with effective diameter values obtained from Eq. (3). In this equation, the total thickness of sheet steel was used as the failure plane was located between the steel sheets and the steel angle. On average over the 16 test specimens, the so-computed effective weld diameter from Eq. 3 was equal to 1.22 times the measured effective diameters.

A total of 40 tension specimens with 2-layer and 4-layer configurations failed due to sheet failure. Equation 10 predicts the tensile resistance of specimens when sheet failure is involved and Section E2.2.2 specifies that this resistance be

reduced by 30% for arc-spot welds fabricated in sidelap configurations. Figure 8b illustrates Eq. E2.2.2-2 with and without the 30% reduction in capacity. The results obtained during the testing program are also plotted in Fig. 8b as a function of the measured visible weld diameter determined with the sheet steel thickness equal to half of the total thickness as failure always occurred at the mid-thickness of the steel sheets. The test data indicates that the 30% reduction does not apply to the specimens examined in this study. LaBoube & Yu (1991) proposed the 30% reduction to account for the fact that the unstiffened flange width of their specimens was small compared to d_{vis}. Using the measured specimen properties and the non reduced resistance from Eq. E2.2.2-2, the average test-to-predicted resistance ratio is equal to 1.17 with a coefficient of variation of 0.28. On this basis, a resistance factor of 0.38 must be applied to attain the reliability index of 4.0.

Conclusions

The type of electrode (E4311 (E6011)), high current setting and proper welding technique affect the quality of arc-spot welds in multi-layer connections. A lower limit for the net effective weld diameter was proposed. The shear resistance of arc-spot welds that are governed by weld failure are influenced by the net effective diameter of the weld. For specimens that are governed by sheet failure the total thickness of the steel sheets and the average weld diameter influence the shear resistance of the specimen. The tests also revealed that the shear strength of arc spot welds was not reduced when the thickness of the underlying material to the total sheet thickness was greater than 0.7. The data obtained during the shear resistance tests showed that Eq. E2.2.1.2-2 (bearing failure) was generally conservative; as such a modification to the coefficient was proposed.

Tension test specimens governed by weld fracture are influenced by the net effective weld diameter of the weld. The thickness of the underlying joist angle can also influence the resistance of the specimens if the loading causes deformations in the support. The resistance of tension specimens governed by sheet failure is influenced by the total thickness of sheet steel and the average weld diameter.

When tension weld failure governs, the results indicate that a 50% reduction in capacity should be applied to the resistance obtained from Eq. E2.2.2-1. A resistance factor $\phi = 0.32$ is proposed. These recommendations should apply to all connections, including those made of single sheets, because there is no evidence to suggest that the multi-overlap configuration influences the resistance of specimens governed by this failure mode. Test data for tension

failure by sheet tearing suggests that a reduced resistance factor $\phi = 0.38$ should be used in Eq. E2.2.2-2.

Acknowledgements

The authors thank NSERC, the CSSBI and the SSEF for their support in sponsoring this project. Additionally, appreciation is extended to G. Trigo from Consultarc for his valuable contribution on welding procedures.

References

AISI (2002) Cold-formed steel design manual, American Iron and Steel Institute, Washington, USA.

AISI (2001) North American specification for the design of cold-formed steel structural members, 2001 Edition, With 2004 supplement, American Iron and Steel Institute, Washington, USA.

CSA (2001) S16, Limit states design of steel structures, Canadian Standards Association, Toronto, Canada.

CSA (2007) S136, North American specification for the design of cold-formed steel structural members, Canadian Standards Association, Toronto, Canada.

Guenfoud, N., Tremblay, R., Rogers, C. (2010) Experimental program on the shear capacity and tension capacity of arc spot weld connections for multi-overlap roof deck panels, Rept. No. SR-10-01, Dept. of Civil, Geological, and Mining Eng., Ecole Polytechnique, Montreal, Canada.

LaBoube, R.A., Yu, W.W. (1991) Tensile strength of welded connections, Final Rpt., Civil Eng. Studies 91-3, University of Missouri-Rolla, Rolla, USA.

NRCC (2005) National building code of Canada 2005,12th ed., National Research Council of Canada, Ottawa, Canada.

Peköz, T., McGuire, W. (1979) Welding of sheet steel, Report SG-79-2, American Iron and Steel Institute, Washington, USA.

Peuler, M. (2002) Inelastic response of arc-spot welded deck-to-frame connections for steel roof deck diaphragms, Project Report, Dept. of Civil Engineering and Applied Mechanics, McGill University, Montreal, Canada.

Peuler, M., Rogers, C.A., Tremblay, R., (2002) Inelastic response of arc-spot welded deck-to-frame connections for steel roof deck diaphragms, Proc. 16th Int. Spec. Conf. on Cold-Formed Steel Struct., Orlando, USA, 763-778.

Rogers, C.A., Tremblay, R. (2010) Impact of diaphragm behaviour on the seismic design of low-rise steel buildings, Eng. J., AISC. (in press)

Snow, G.L., Easterling, W.S. (2008) Strength of arc-spot welds made in single and multiple steel sheets, Proc. 19th Int. Spec. Conf. on Cold-Formed Steel Struct., St. Louis, USA, 607-622.

Twentieth International Specialty Conference on Cold-Formed Steel Structures
St. Louis, Missouri, U.S.A., November 3 & 4, 2010

Strength Prediction Model for Power Actuated Fasteners Connecting Steel Members in Tension and Shear– North American Applications

J.R. Ubejd Mujagic,[1] Perry S. Green[2] and William G. Gould[3]

ABSTRACT

Power-actuated fasteners (PAFs), also referred to as pins, are small nail-like or threaded stud type connectors. They can be used in conjunction with several materials and in a number of different applications. Typical applications in steel include attachments of deck sheeting or diaphragms, architectural or mechanical components, or miscellaneous support brackets or connections to supporting steel members. Traditionally, the design strength of the connections featuring power-actuated fasteners has been determined through standardized testing protocols. In the United States, this protocol is embodied in the American Society for Testing and Materials (ASTM) Standard E 1190. The purpose of this study was to create a generic strength prediction model for pins embedded in steel substrate and subjected to either shear or tension, and to present the equations in a limit states format applicable to the North American practice and applications.

1 INTRODUCTION

The purpose of this study was to create a generic and comprehensive strength prediction model for power-actuated fasteners (PAFs) embedded in steel substrate and subjected to either shear or tension. Although strength

[1]Structural Engineering Consultant, Atlanta, GA
[2]Consultant, Former Technical Director, SJI, Myrtle Beach, SC
[3]Director of Engineering, HILTI, Tulsa, OK

provisions for PAFs exist in European practice, as embodied by EN 1993-1-3 (ECS 2006), they were not able to be directly incorporated into North American practice given differences in definitions of nominal strength, safety and reliability related adjustments, and somewhat different scope compared to the data available as a part of this study. However, EN 1993-1-3 Table 8.3 provided valuable guidance to this study with respect to the definition of limit states, scope, etc. Therefore, a separate effort, as described in the following sections was required to provide an acceptable and generic strength prediction model for PAFs.

Typical applications in steel include attachments of deck sheathing or diaphragms, architectural or mechanical components, or miscellaneous support brackets or connections to the supporting steel members. Typical fasteners used in conjunction with steel embedment are shown in Figure 1 (HILTI 2009).

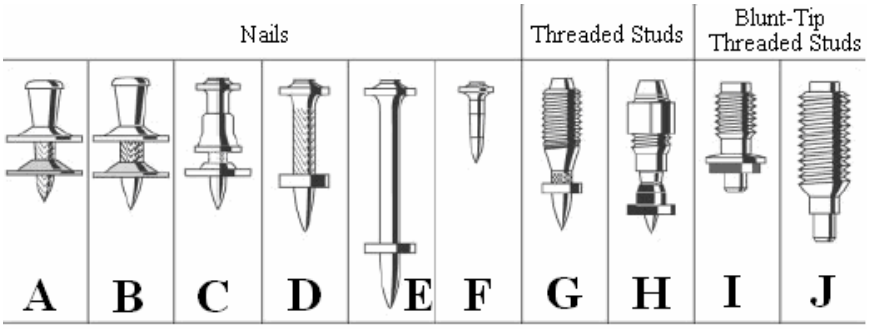

Figure 1 Typical Pin Types (HILTI 2009)

PAFs plastically deform and displace the embedment material when installed into it. Connection strength in tension is derived from the propensity of the displaced material to partially return to its original position. Specifically, this tendency on the part of the displaced material creates hoop stresses around the perimeter of the embedded fastener which results in friction forces resisting pullout. In addition to this tension strength mechanism, high temperatures developed during fastener driving into an embedment substrate cause the surface of the fastener to be partially fused with the surrounding substrate (Beck et al. 2003), providing additional resistance against pull-out. Alternatively, a PAF connection loaded in tension could also fail by fastener fracture and sheet pull-over over the fastener head. One of the most instrumental properties for the

PAF penetration into embedment steel is its hardness. To successfully penetrate the substrate material, fasteners must have a hardness of 4 to 5 times the embedment material (Beck & Reuter 2005), and are usually manufactured with Rockwell C scale (HRC) hardness between 49 and 58, depending on intended application and fastener geometry. Hardness increases with increasing content of carbon in steel. Typical pre-hardened steels used in manufacturing of PAFs are AISI 1060, 1070 and 1080, as defined in ASTM A 29 (ASTM 2008a), although different proprietary steel types may exist. In shear, the PAF connection could fail by shear fracture of the fastener, bearing failure of the connected substrate, tilting of the fastener followed by its pullout in shear, or by fracture of the connected net section including block shear.

Traditionally, the design strength of connections featuring PAFs has been determined through standardized testing protocols. In the United States, this protocol is embodied in the American Society for Testing and Materials (ASTM) Standard E 1190. Acceptability of the strengths established by following this standardized testing protocol, must then be established for construction through an evaluation process under the auspices of International Code Council Evaluation Services (ICC-ES). The acceptance criteria (AC) for PAFs are established in ICC-ES document AC70 (2010). Among other aspects, AC70 stipulates acceptable testing procedures (i.e., ASTM E 1190), establishment of proper material limitations, application limitations, establishment of combined loading limit states, and determination of factors of safety. A separate evaluation is required for each PAF type, each application, each connection configuration, as well as the geometry of each fastener. Strength values determined for any given PAF satisfying the corresponding AC and reduced by an appropriate factor of safety are then provided in published manufacturer's catalogs, and are then available to be used in design.

2 OBJECTIVE, APPROACH AND SCOPE

As noted above, the objective of the study was to generate a strength prediction model, whereby the design strength of connections featuring PAFs embedded in steel substrates, loaded in shear and tension, can be numerically determined for any applicable limit state.

Test reports containing test data for PAFs embedded in a steel substrate and loaded in shear and tension were provided by four of the major product

manufacturers of fasteners in North America: HILTI (2009, 2010), ITW Ramset (2009), Power Fasteners (2009) and Simpson Fasteners (2009). All the test reports submitted by the manufacturers document the tests performed in accordance with ASTM E 1190, thus eliminating variation in test data among different reports caused by any slight differences in their respective test setups.

The approach taken was to isolate tests featuring a specific loading condition (shear or tension) mode of failures in separate groups of data, and then generate a strength prediction model for each of the applicable failure modes. The design strength was then established based on the governing mode of failure for any given connection configuration, similar to the strength determination model for screws presently contained in the North American Specification for the Design of Cold-Formed Steel Structural Members, S100 (AISI 2007). The test data with incomplete, conflicting, or obviously flawed information was excluded.

3 TENSION LIMIT STATES

The modes of failure observed in tensile PAF tension test reports are PAF pull-out, tensile fracture, and sheet pull-over. The subsequent sections discuss each of the applicable limit states, and the analysis pertaining thereto. Various geometric variables used in this and other sections of this text are illustrated in Figure 2.

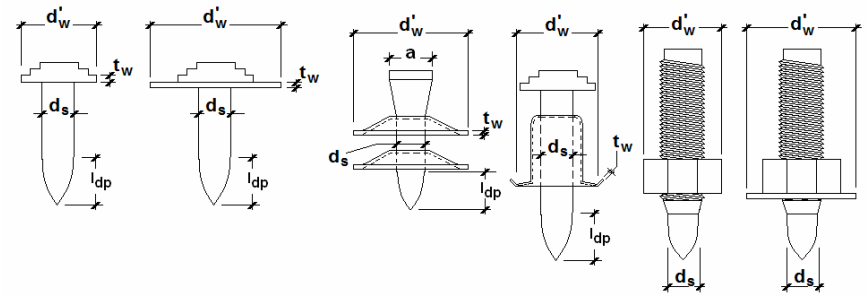

Figure 2 PAF Geometric Variables Used in the Strength Prediction Model

3.1 PAF FRACTURE IN TENSION

Tension fracture failures in PAFs embedded in steel are relatively rare. In fact, out of 1623 tension tests available to this study, only 10 specimens, with diameters of 0.146 and 0.150 in., experienced this mode of failure. This failure mode, however, is viable, and must be considered in practical design. Computing tensile strength, P_{tp}, is a trivial matter from a theoretical standpoint, and can be readily accomplished with Eq. 1.

$$P_{tp} = (d_s / 2)^2 \pi F_{uh} \quad \text{(Eq. 1)}$$

Where:

d_s = diameter of PAF shank, in.
F_{uh} = ultimate tensile strength of hardened PAF steel, psi

The nominal values of F_{uh} can be found only in some manufacturer's catalogs (ITW Ramset 2007) and are commonly not indicated in the test reports. However, HRC values are generally reported in most manufacturers' catalogs and all test reports, including those available to this study. There are several published works and standards relating various hardness scales to ultimate tensile strength, including ASTM A 370 (ASTM 2009). A formula relating the two generally takes the shape of Eq. 2, where ρ and ζ are constants derived through regression of available data. It was found that for the data available to this study, the best fit is provided by $\rho = 66000$ and $\zeta = 1/40$, which closely relates to the data published in BS 860:1967 (BSI 1967). Given the limited data sample of tension fracture tests, this validation was performed on shear fracture tests (Sec. 4.1), by relating shear and tension fracture strength by a factor of 0.6.

$$F_{uh} = \rho e^{(HRC/\zeta)} \quad \text{(Eq. 2)}$$

It should be noted that a range of tensile strengths derived by this expression based on typical range of HRC values found in PAFs is very small. Therefore, and also considering inherent statistical scatter, very little can be gained in view of accuracy by using Eq. 2 over simply using a uniform average value of F_{uh} of 260 ksi over the range of HRC values from 52 to 56, which is the array of values seen in this study. Considering the limited database of 10 tests performed on two different fasteners, Equation 1 yields an average ratio of tested-to-predicted strength (RTPS) of 0.95 with a coefficient of variation (COV) of 0.11 if the F_{uh} is computed using Eq. 2, and a RTPS of 0.97 and a COV of 0.10 if F_{uh} is taken as 260 ksi.

3.2 PAF PULL-OUT

The basis for establishment of pull-out strengths in the United States represent the code referenced test procedure standard, and an evaluation criteria, typically ASTM E 1190 (ASTM 2008b), and AC70 (ICC-ES 2010), respectively. In European practice, both the testing provisions and evaluation criteria are contained in CUAP (DIBt 2004), which is more specific than its U.S. equivalents in that it is also defines the application scope. The basis for establishment of the PAF pull-out represents the most dominant and most tested mode of failure among all types of PAFs and in nearly all connection configurations. The nature and specific mechanics of pull-out in PAFs is very unique given their specific design features and resistance mechanics. Pull-out strength is derived from the partial fusion stresses, f_f, and hoop confinement stresses, f_c, that result in resistive friction stresses, μf_c. A mechanical model that could be used to determine the pull-out strength of pins is represented graphically in Fig.3. In this particular case, the Fig. 3 considers the embedment case II from Fig. 4.

As can be seen, the pull-out resistance, T_p, can be defined as a mathematical function (Eq. 3) by integrating resisting stresses along the embedded surface of the PAF. Unfortunately, the solution of the integral given in Eq. 3 is a complicated polynomial requiring significant computing effort. Also, Eq. 3 would require modification when embedment condition changes to one of four other possible cases (I, III, IV and V in Fig. 4).

A further complication and found to be impossible to codify is the minute, but varying differences present in the geometric features that seem to have a profound impact on the PAF capacity in pullout. For instance, PAF points and shank knurling are one of the most dominant features impacting pullout resistance sometimes resulting in a pullout strength twice that of a non-knurled fastener of a similar diameter (ITW Ramset 2009). However, virtually every knurled PAF examined in this study featured a unique knurling pattern, each of which was based on a proprietary manufacturer's design. Further, specific metallurgical properties of PAFs and the embedment material, including weldability, hardness, carbon content, etc. cannot be codified in a comprehensive and general form, although each may have a minor to significant impact on the PAFs ability to partially fuse to the embedment hole surface, as well as on the ability of the displaced embedment material to confine the fastener.

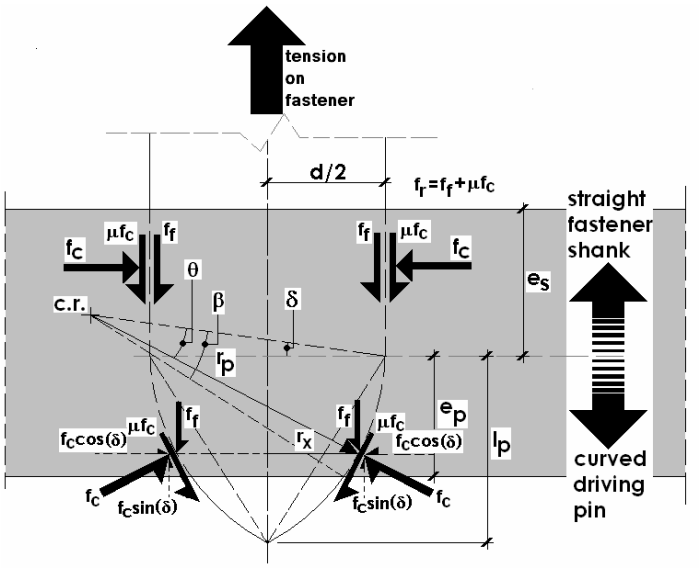

Figure 3 Pullout Strength Mechanical Model for PAFs

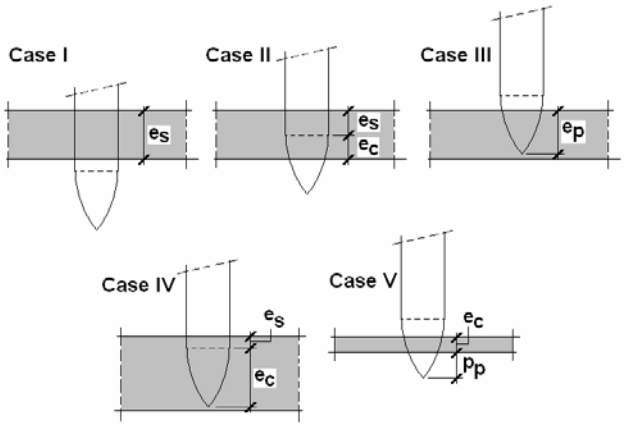

Figure 4 PAF Embedment Cases

$$T_p = f_r \pi e_s \left(\frac{d_s}{2}\right)^2 + \int_0^{\beta} f\left(d_s, l_p, f_r, e_s, e_p\right) d\theta \qquad \text{(Eq. 3)}$$

In short, while unique values of μf_c and f_f might be successfully determined for one fastener, an entirely different set of values may apply to another pin. As a final point, many PAFs have very complex geometric features affecting pullout strength, such as multiple point diameters, sloping shanks, multiple shank diameters, etc. Capturing all such features in a code-based equation would be an impossible task.

All the above facts render the concept embodied in Fig. 3 and Eq. 3 practically obsolete. Behavior and parametric impact on PAF strength was extensively studied by Beck & Reuter (2005) who found that the PAF pull-out strength depends heavily on depth of penetration. Fig. 5 shows the plot of strength vs. penetration distance for 127 tests of a particular PAF examined in this study. As can be seen, the data appears dispersed in three distinct clouds, with data confined by boundary A distinctly supporting findings by Beck & Reuter (2005). The data outside the boundary A appears also related to penetration distance, but nonetheless also affected by a system effect, including excessive driving energy which was found to have a significant deteriorating effect on pullout strength (Beck & Reuter 2005).

Where PAF points fully penetrate the embedment material (i.e., Case I in Fig. 4), correlation can be found between the embedment length and pull-out strength. This is illustrated in Fig. 6, which depicts such a correlation for 60 tests of a fastener installed in three different thicknesses. The intercept of the trend line in Fig. 6 is zero; therefore there is a direct correlation with the embedment length. However, Beck & Reuter found that although this correlation exists, the strength is not directly proportional to the embedment area of contact.

Based on the limitations presented above, it is clear that a comprehensive generic strength prediction model for PAF pullout is not possible, and that PAF strength in pullout should be determined through testing. As a matter of practical convenience, however, it seemed useful to generate a lower bound solution whereby strength of a smooth shank PAF can be presented in a tabular form for several typical applications. For the purpose of this study, this lower bound is defined as the largest capacity that can be justified for all smooth shank fasteners of the same diameter and the same embedment for which a factor of safety of 3.0 can be justified.

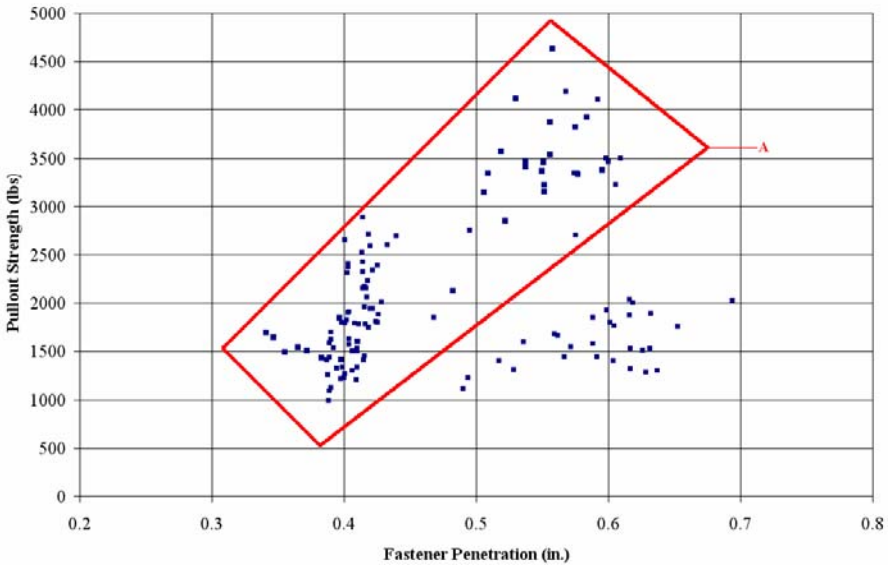

Figure 5 Depth of Penetration vs. Pull-out Strength

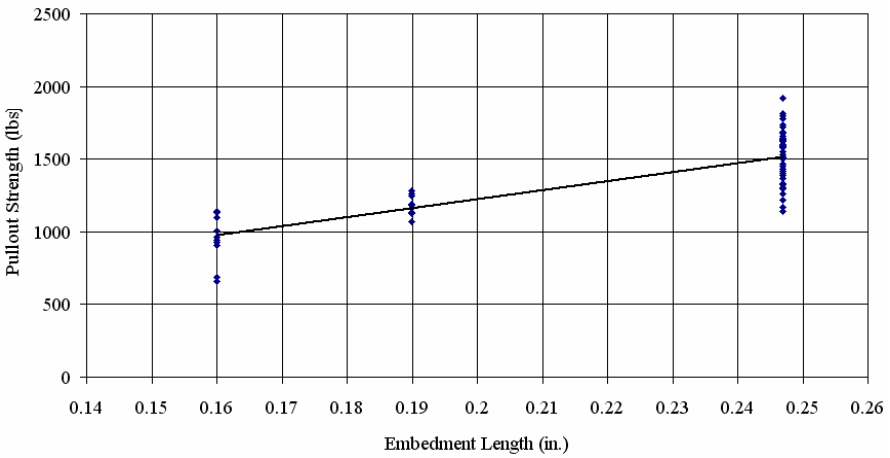

Figure 6 Embedment vs. Pull-out Strength

Table 1 summarizes such strengths based on analysis of 854 tests featuring 13 smooth shank fasteners from all four manufacturers, and then

reduced based on applicability limits and typical system effect considerations. Table 1 can safely be applied to knurled shank fastener connections, although only smooth shank fastener tests are in its development. Knurled PAF tests were omitted to avoid erroneous application of the safe table loads to knurled fasteners not covered by this study. Furthermore, Table 2 stipulates shank embedment (i.e., Case I in Fig. 4). Many fasteners do not achieve shank embedment in plates exceeding 5/16 in. in thickness, but rather some portion of, or the entire, PAF point becomes an embedded part of the fastener, often causing failure at lower loads than PAFs with shank embedment in 1/4-in. thick plates. Embedment is the function of a fastener's ability to penetrate a steel member, which in turn depends on the relative hardness difference between the PAF and the embedment material, power-actuated tool settings and driving energy, manufacturer or project specifications, etc. As the objective of this approach is the ability to conveniently and rapidly determine a safe load, rather than supercede actual tested strength reported by the manufacturer, the lower tested strengths corresponding to embedment I, III-V (Fig. 4) have been used to develop the Table 2; however, full embedment (Case I in Fig. 4) is stipulated to avoid unconservative outcomes pertaining to partial embedment and geometries not captured in the data available to this study. It is emphasized that the values provided do not assure the same degree of safety across the board, but rather only assure that the application of factor of safety of 3.0 will ensure the minimum degree of reliability for connections per Chapter F of AISI S100-2007. This solution is intended as a convenient tool for either preliminary or rapid safe design, rather than an alternative to tested pull-out date where available. The manufacturer's applicability limits and installation requirements must be adhered to, and they may preclude the usage various diameter-plate thickness combinations for a particular fastener.

Table 1 PAF Lower Bound Nominal Design Values

	Embedment Plate Thickness, in.		
d_s, in.	1/8	3/16	1/4
0.11-0.15	450	915	1230
0.18-0.21	-	-	1970

3.3 SHEET PULL-OVER

Fundamental behavioral aspects with respect to the pull-over limit state in PAF connections are basically identical to those of pull-over in screw

connections. The geometric and other properties affecting the strength are, with exception of fastener head geometry, solely a function of top connected member subject to pull-over. This study found three distinct behavioral types with respect to predicting pull-over strength. Specifically, the pullover strength featuring PAFs with distinct shank and head with or without a washer that does not appreciably differ from screws in their appearance (D, E, and F from Fig. 1) is predicted very well with the model presently contained in Sec. E4.4.2 of AISI S100-2007. A second type represents the connections with PAFs that derive their pullover strength from friction and interlocking of a loose washer with tapered fastener head. This type of fastener is shown as Types A and B in Fig. 1. Essentially, depending on the proportions of the fastener head, the pull-over load will cause the loose washer to ride up the tapered head and lock in place when the washer opening equals head diameter. The fasteners of Type A (Fig. 1) investigated in this study for which $\boldsymbol{a/d_s \geq 1.6}$, and $\boldsymbol{a - d_s \geq 0.12}$ **in.**, consistently achieved the full strength predicted by AISI S100-2007 Sec. E4.4.2, while those with $\boldsymbol{a/d_s \geq 1.4}$, and $\boldsymbol{a - d_s \geq 0.08}$ in. achieved only about 80% of that strength. There is no basis for establishing the strengths for other head proportions for this type of fasteners from the standpoint of the data available to this study, and such strengths should be addressed through testing. Finally, the third type of behavior observed relates to fasteners with compressible spring washers (Type C in Fig. 1). The top of the mushroom shaped washer (although other shapes are available as well) partially collapses when the PAF is installed into the steel member, thus creating an elastic-spring like mechanism that restrains the member subject to pullover in the vicinity of the fastener confined over an area corresponding to the diameter of the washer bottom, as illustrated in Fig. 7. Specifically, the image on the left represents a typical screw-like fastener, whereby a washer deforms along with the top member until distortions in the washer and top member around the hole and/or fastener head are large enough for the tearing and pull-over to occur. The image to the right depicts a fastener with collapsible spring washer.

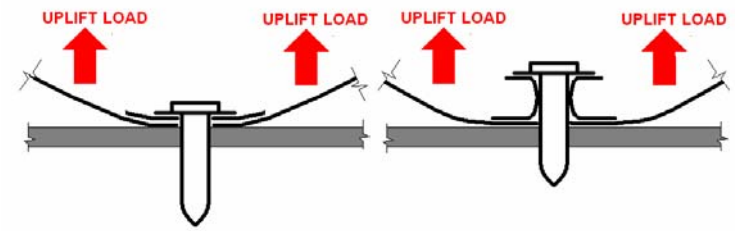

Figure 7 Mechanics of Pull-Over in Power Actuated Fasteners

As can be seen, the washer effectively extends the perimeter of the pull-over failure plane, and thus increases pull-over capacity, by clamping the member in contact with a washer to the base material. This type of fastener consistently yielded connection pullover strengths about 30% higher connection pull-over strengths than that predicted by the AISI S100-2007 model. The model predicting pull-over strength, P_{nov}, can therefore be summarized as shown in Eq. 4.

$$P_{nov} = \alpha_w t_1 d'_w F_{ut1} \quad \text{(Eq. 4)}$$

where:

α_w = 1.5 for screw-, bolt-, and nail-like flat heads, with or without head washers (Fig. 1, Types D-F)
= 1.5 for threaded stud pins and for pins with tapered standoff heads that achieve pull-over by friction and locking of the loose washer with the pin head (Fig. 1 Types A and B, with a/d_s ratio of no less than 1.6 and $(a - d_s)$ of no less than 0.12 in. (3 mm).
= 1.25 for threaded stud pins and for pins with tapered standoff heads that achieve pull-over by friction and locking of the loose washer with the pin head (Fig. 1 Types A and B, with a/d_s ratio of no less than 1.4 and $(a - d_s)$ of no less than 0.08 in. (2 mm).

t_1 = thickness of member in contact with the fastener head, in.
= 2.0 for pins with collapsible spring washer (Fig. 1, Type C).

d'_w = actual diameter of the washer or the fastener head in contact with the retained substrate. It shall not exceed 0.60 in. (15 mm) in computations, although the actual diameter may be larger.

F_{ut1} = ultimate tensile strength of the member in contact with fastener head (psi)

Figure 8 shows a very good agreement of tested and predicted data. The strength computation model presented as Eq. 4, based on 198 tests on 4 different fasteners, yields an average RTPS of 1.08 and a COV of 17%.

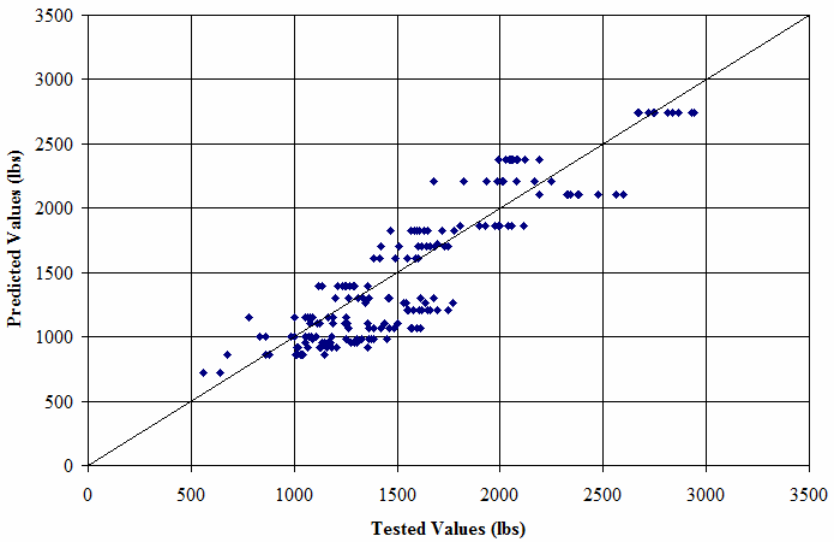

Figure 8 Distribution of Predicted vs. Tested Pullover Strengths

The pullover tests available to this study did not feature any of the blunt-head or sharp-head threaded studs (G through J in Fig. 1). However, in the opinion of the authors, and considering the experimental evidence of other types of fasteners, such fasteners can be considered using Eq. 4 if the variable d'_w is defined as shown in Fig. 2.

4 SHEAR LIMIT STATES

The modes of failure observed in tension PAF test reports are PAF pull-out in shear, shear fracture, bearing, net section strength, and connection strength limited by edge distance. The subsequent sections discuss each of the applicable limit states, and the analysis pertaining thereto.

4.1 SHEAR FRACTURE

The shear fracture strength of a PAF can be computed using Eq. 5. The determination of F_{uh} is discussed in Section 3.1.

$$P_{nsp} = 0.6(d_s / 2)^2 \pi F_{uh} \qquad \text{(Eq. 5)}$$

Equation 5, assessed on the basis of 304 tests featuring 14 different fasteners with diameters ranging from 0.106 – 0.197 in., yields a mean RTPS of 1.14 and a COV of 19% if F_{uh} is computed using Eq. 2, and a RTPS of 1.16 and a COV of 19% if F_{uh} is taken as 260 ksi. Distribution of predicted to tested strengths are depicted in Fig. 9. As can be seen, Eq. 5 tends to be more conservative for PAFs with higher nominal strengths. This can be explained by the fact that at higher loads PAF rotation becomes significant, thereby the fastener becomes loaded in a combination of shear and tension. Since the tensile strength of a fastener is larger, these fasteners yield a higher overall capacity. This, however, is also dependent on the size of the embedment member, which facilitates rotation when it is relatively flexible. From a practical standpoint, and attempting to maintain model simplicity, this phenomenon need not be considered, as typical connections with very high shear fracture strength will typically yield a lower strength due to another governing limit state.

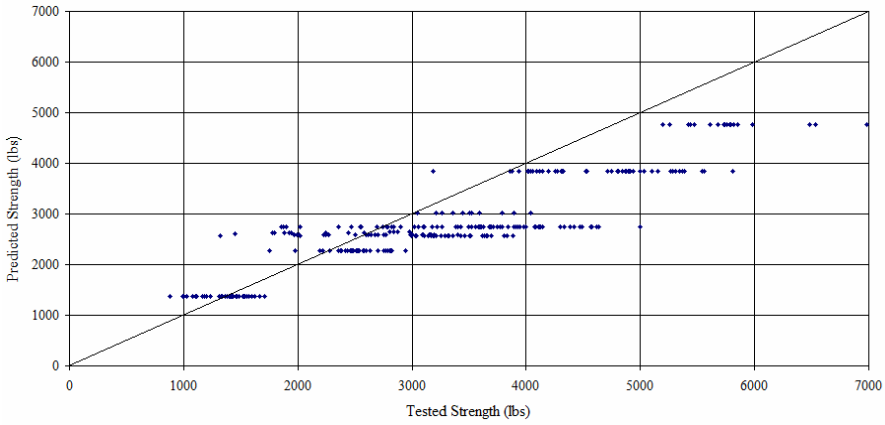

Figure 9 Distribution of Predicted vs. Tested Pullover Strengths

4.2 SHEAR PULL-OUT

Shear pull-out is a limit state widely reported in shear tests. It is an ultimate consequence of fastener tilting associated with significant deformations in the embedment base steel member. Given the configuration of the test setup,

nearly all shear pullout test data available to this study reported only the thickness of one member thickness (i.e., PAF is installed into only one member). Therefore it was not possible to assess the ratio t_2/t_1 at which bearing transitions into tilting for any given fastener. Also, several test groups contained both test samples failing in bearing and shear pull-out, thus indicating that pullout in shear is possible even at higher t_2/t_1 ratios. The approach taken in this study was to develop an equation for bearing that would be applicable to connections with t_2/t_1 of 2 or greater, which was the range of available data with reported bearing failure (Section 4.3).

Another equation predicting the PAF pull-out in shear was developed over the entire range of available data over which such a failure was reported. Specifically, 237 tests, featuring 7 fasteners ranging from 0.106 – 0.206 in. in diameter embedded in members of thicknesses ranging from 0.113 – 0.75 in., for which pull-out in shear was a reported mode of failure, and for which the strength properties of the embedment material and the fastener embedment condition was reported, were isolated and used in the equation development. The AISI S100-2007 equation for prediction of tilting strength in screws was found inapplicable, as it provided a very poor fit with the available data over nearly the entire range. However, the model developed by Mujagic et al. (2007) for predicting the shear pull-out strength in standoff screws was found to provide an excellent match with the data. This model is presented as Eq. 7. Some of its constants were slightly modified to provide the best statistical fit with the data. Fig. 10 shows the distribution of tested to predicted strengths for shear pull-out. The model presented as Eq. 7 yields an average RTPS of 1.03 and a COV of 17%.

$$P_{nos} = \frac{d_{ae}^{1.8} t_2^{0.2} \left(F_{y2} E^2\right)^{1/3}}{95} \qquad \text{(Eq. 7)}$$

where:

F_{y2} = yield strength stress of the member not in contact with fastener head, psi
E = elastic modulus of steel = 29000 psi
d_{ae} = average embedded PAF diameter, in.
= d_s when e_s in Fig. 4 equals t_2

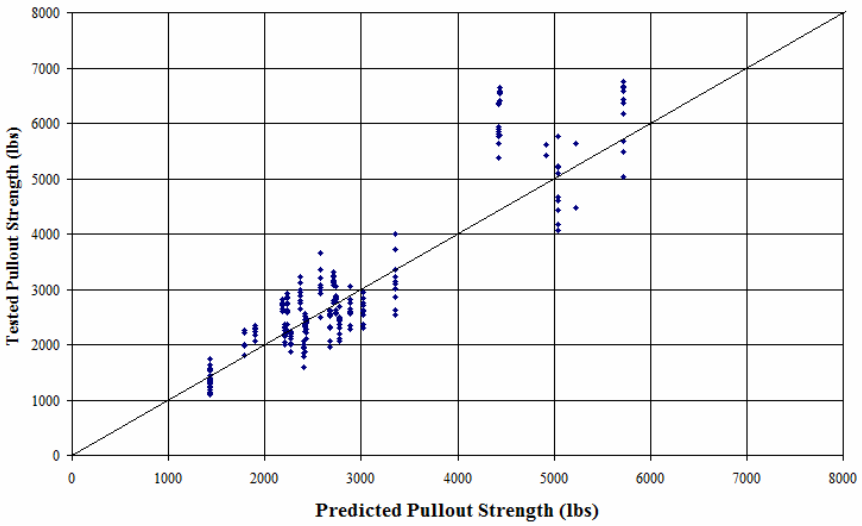

Figure 10 Distribution of Predicted vs. Tested Pull-out Strengths

4.3 BEARING, EDGE DISTANCE, SPACING AND NET SECTION CHECKS

The spacing and edge distances reported for many of the test specimens considered were in the order of 8 to 10 times the PAF shank diameter. Such large distances are considered excessive, and in many practical situations difficult to achieve. The ASTM standard governing testing procedures for power-actuated fasteners, E 1190-1995/2007 (ASTM 2008) provides a set of edge and spacing distances deemed to eliminate the effects of fastener grouping and edge distance. These limits are summarized in Table 2, and are recommended with the application of this strength prediction model.

Table 2 Minimum Required Edge and Spacing Distances

Pin Shank Diameter (in.)	Minimum Pin Spacing (in.)	Minimum Edge Distance (in.)
0.100-0.199	1.0	0.5
0.200-0.250	1.6	1.0

It should be noted that the model presented in this paper does not account for the effects of fastener grouping and edge distance on the computed strength, as such effects could not be evaluated from the available data. Therefore, the model cannot be applied to connections not satisfying the limitations of Table 3, whose strength should be established through testing.

Tests reported by Beck and Englehardt (2002) show that the net section strength of a steel member with installed PAFs consistently exceeds the strength of net sections with drilled holes of equivalent diameter. Therefore, the net section checks currently prescribed by AISI S100-2007 for other types of connections can safely be applied to the connections featuring power actuated fasteners. As a result of the same study, the authors recommended that the hole diameter be taken as 1.10 times the pin diameter in net section check calculations. This recommendation has been adopted for use with this model.

Bearing strength is generally defined as the product of fastener diameter, thickness of the bearing material, bearing material ultimate tensile strength, F_{ut1}, and a constant. This constant has values of 2.7 for screws (AISI 2007), 3.2 for power actuated fasteners in EN 1993-1-3 model (ECS 2006), and between 2 and 3 for structural bolts (AISC 2005) depending on edge and hole deformation considerations. Furthermore, in the AISI model, the tilting must be considered when the ratio of thickness of member not in contact with the fastener head, t_2, to the thickness of the member in contact with fastener head, t_1, does not exceed 1. The tilting check does not apply when this ratio equals 2.5 or more, and linear interpolation between the governing strengths at t_2/t_1 of 1 and 2.5 is used to determine the strengths in the intermediate range. Tilting reflects the fact that when two connected members are of similar thickness, connections tend to rotate with respect to the axis of applied force thus tilting the connection fastener which eventually pulls out.

The bearing strength of PAF connections was assessed in this study on the basis of 127 tests featuring 3 fastener models of Type A and C from Fig. 1 . Based on the analysis of the available data, it was shown that a constant multiplier of as high as 4.2 could be justified, which is much higher than in the case of either screws or bolts. The source of this higher strength most likely rests in washer clamping, sheet hardening and folding effects around the perimeter of the hole. However, 3.7 was chosen as the constant multiplier, as shown in Eq. 7.

$$P_b = 3.7 d_s t_1 F_{ut1} \qquad \text{(Eq. 7)}$$

Specifically, Fig. 11 depicts the plot or RTPS based on Eq. 8 versus t_2/t_1 ratio. As can be seen, and as expected, as this ratio decreases so does the strength defined solely by the bearing check of Eq. 7, thus indicating presence of tilting at lower ratios of t_2/t_1. Given the relatively limited data space, the actual transition point where tilting applies cannot be determined with certainty. However, if the model is limited to a minimum t_2/t_1 ratio of 2 (minimum for the data available in this study), which covers vast majority of shot fired pin applications, combined with setting the intercept of the average RTPS to about 1.0 for the group of tests with the lowest considered t_2/t_1 ratio (in this case 2), the model can safely predict the bearing and tilting strength without the need for a separate tilting formula. A constant of 3.7 accomplishes this goal. It should be noted that the model represented by Eq. 8 does not require any checks on the member not in contact with the fastener head; since the model is limited to configurations where $t_2/t_1 \geq 2$, bearing on the member not in contact with the PAF head will not govern the connection capacity when this model is used.

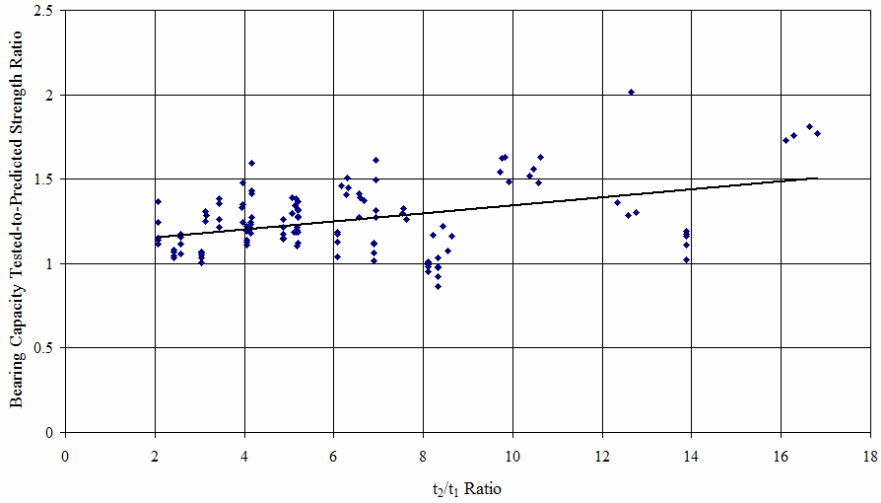

Figure 11 Influence of t_2/t_1 Ratio on Bearing RTPS

In terms of statistical performance over the entire sample group, a mean RTPS of 1.26 and a COV of 0.16 are calculated. For the group of data with $t_2/t_1 = 2$, the mean RTPS is 1.20 and COV is 0.08. To eliminate bias of any deterministic considerations pertaining to the test sample, the resistance and

safety factors for bearing and tilting presented in Section 5 are based on both the overall statistics and those pertaining to the group with $t_2/t_1=2$.

The test database featured fastener diameters ranging from 0.146 – 0.177 in. and top member thickness ranging from 0.018 to 0.06 in. Furthermore, based on the range of the test sample, Eq. 8 should be used only when $t_2 \geq 1/8$ in.

5 RELIABILITY ASSESSMENT AND SAFETY PROVISIONS

The resistance and safety factors for the limit states investigated in this study were established using the first-order second-moment reliability method presented in Chapter F of AISI S100-2007. The professional factor, P_m, was varied based on the actual RTPS. The materials factor, M_m, was taken as 1.10, and its coefficient of variation, V_M, was taken as 0.10 for all limit states except for bearing and pull-out in shear, where $V_M = 0.08$. The fabrication factor, F_m, and its associated coefficient of variation V_F, were taken as 1.00 and 0.05, respectively, for all limit states except for bearing and tilting, and pull-out shear, where V_F was taken as 0.05. The reliability index, β, of 3.5 was considered for U.S. applications and β of 4.0 was considered for Limit States Design (LSD).

The above values match those provided for screws in AISI S100-2007 Chapter F. They can be justified by relative comparisons of statistical indices of screws and PAFs. Specifically with respect to M_m and V_M, materials used in manufacturing screws are very similar. While PAFs are typically made of hardened AISI 1060 - 1080 steels, screws are typically made using similar AISI 1018 – 1040 steels using identical case hardening technology. Lower V_M for bearing and tilting is justified, as the value of 0.08 corresponds to the strength properties of mild steels typically found in supporting members associated with PAFs (Galambos & Ravindra 1978), and bearing and tilting and shear pull-out checks are depended on the strength properties of the supporting material, rather than those of the fasteners.

With respect to fabrication parameters F_m and V_F, PAFs again appear at no disadvantage to screws. A review of typical shop drawings for screws (Sealtite 2006) with those of PAFs (HILTI 2009, ITW Buildex 2009) indicate similar, or in some more conservative, fabrication tolerances for PAFs when

compared to the screws. Furthermore, minute geometric features of PAFs, such as knurling and point geometry, are critical to their performance, particularly in tension pullout, and are manufactured to tighter tolerances than any specific features associated with screws. Manufacturers generally monitor the COV of individual test groups throughout testing protocols. Those with COV in access of 15% are closely studied, and design features are often adjusted to achieve greater consistency and reliability.

Fig. 12 depicts a distribution of COV for 114 pullout groups of tests, with each group comprising between 5 and 30 tests. With a P_m of 1.0 and a COV of approximately 0.21 will result in a factor of safety of 3.0. As can be seen, 81% of this, essentially random, sample available to this study would fall into this group, while 97% of the test groups would fall within a COV of 0.30, which approximately corresponds to a factor of safety of 4.0. Therefore, while actual manufacturer's data should be used to establish a factor of safety where the design capacity is derived from tests, a factor of safety of 4.0 could safely be applied to the manufacturer's data where the average tested strength is provided, but statistical indices were not. As can be seen from the COVs reported throughout this paper from individual limit states, the proposed strength prediction models yield COV in most cases well under 0.20. Table 3 summarizes the resistance and safety factors for all limit states considered in the paper.

From the standpoint of reliability and statistical performance, the authors believe that statistical indices presented herein show that PAFs represent a viable alternative to screws for the attachments of mechanical and architectural components to steel members even in regions with higher Seismic Design Categories. The viability of this alternative would be consistent with the current and past use of PAFs for attachment of cold-formed steel deck diaphragms and shear walls for resisting seismic forces. Furthermore, recent research on seismic behavior of fastenings in diaphragms (Essa et al. 2002) found energy-dissipation properties of PAF connections vastly superior to those of welded or screw connections.

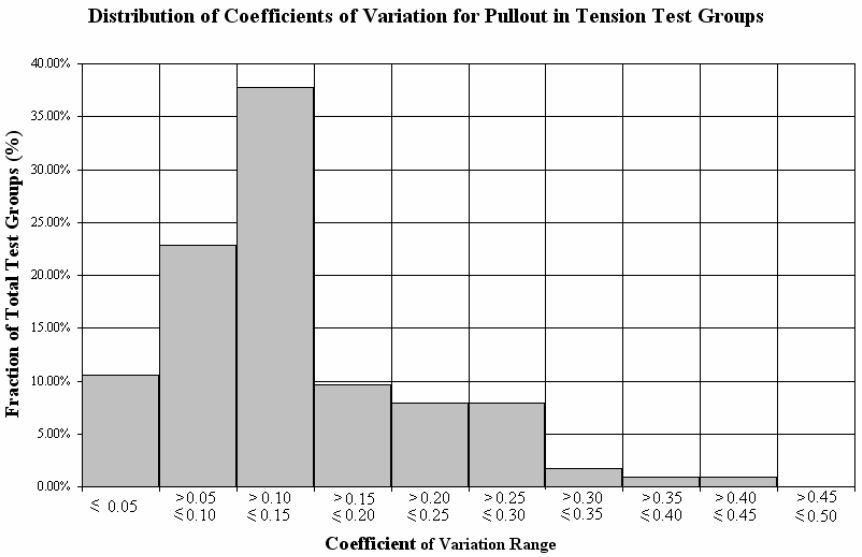

Figure 12 Distribution of COV from 114 Test Groups

Table 3 Resistance & Safety Factors for Power Actuated Fasteners

LIMIT STATE	ϕ	Ω	ϕ_{LSD}
Tension Fracture*	0.60	2.65	0.50
Tension Pullout Table 1 Strengths Tested Strengths	0.55 Calculated per AISI S100-2007 Ch. F or 0.40	3.00 Calculated per AISI S100-2007 Ch. F or 4.00	0.45 Calculated per AISI S100-2007 Ch. F or 0.30
Tension Pull-Over	0.60	2.70	0.50
Shear Fracture	0.60	2.65	0.50
Shear Pull-Out	0.65	2.55	0.50
Bearing & Tilting	0.80	2.05	0.65

*Established based on shear fracture tests due to insufficient tensile fracture test sample size. This is conservative, as shear fractures are typically associated with more statistical scatter than tension fractures.

6 SUMMARY AND CONCLUSIONS

The goal of this study was to generate a strength prediction model for power actuated fasteners embedded in steel members, and loaded in shear and tension. The study presents such a model based on an analysis of test reports of four major manufacturers of power actuated fasteners in North America (HILTI, ITW Buildex, Powers Fasteners, and Simpson). The generated strength prediction model is presented in format conducive to its adoption in a North American Code such as AISI S100. The analysis indicates that power actuated fasteners represent a viable alternative to screws within the scope of applications covered by this analysis. This study does not address the effect of fastener groupings or combined shear-tension loadings.

The authors suggest a future comprehensive research effort that would address combined loading checks, investigate the effect of fastener grouping, extend the applicability of the model proposed herein to a wider range of variables and assess the PAF attachments of steel members to other materials.

7 ACKNOWLEDGMENTS

The authors extend their sincerest gratitude to HILTI, ITW Buildex, Powers Fasteners and Simpson for graciously supplying the test reports on which this study was based. The authors also wish to thank AISI and its Technical Manager Dr. Helen Chen for their tireless efforts in coordinating and assisting with this study.

8 REFERENCES

AISC (2005) "Specification for Structural Steel Buildings," American Institute of Steel Construction, Chicago, IL.

AISI (2007) "S100-2007 North American Specification for the Design of Cold-Formed Steel Structural Members" American Iron and Steel Institute, Washington, DC.

ASTM (2008a) "Standard Specification for Steel Bars, Carbon and Alloy, Hot-Wrought, general Requirements for," ASTM Standards in Building Codes, Volume 4, 45th Edition, pp. 64-79.

ASTM (2008b) "E 1190-95 (Reapproved 2007) - Standard Test Methods for Strength of Power-Actuated Fasteners Installed in Structural Members," ASTM Standards in Building Codes, Volume 4, 45th Edition, pp. 615-620.

ASTM (2009) "A 370-09 Standard Test Methods and Definitions for Mechanical Testing of Steel Products," ASTM Standards in Building Codes, Volume 1, 45th Edition.

Beck, H. and Engelhardt, M.D. (2002) "Net Section Efficiency of Steel Coupons with Power Actuated Fasteners," ASCE Journal of Structural Engineering, Vol. 128, Number 1, pp. 12-21.

Beck, H., Engelhardt, M. and Glaser, N. (2003) "Static Pullout Strength of Power Actuated Fasteners in Steel: State-of-the-Art Review," AISC Engineering Journal, 2nd Quarter, pp. 99-110.

Beck, H. and Reuter, M. (2005) "Powder-actuated fasteners in steel construction," 2005 Steel Construction Calendar, Berlin, Germany.

BSI (1967) "BS 860:1967 Tables for comparisons of hardness scales," BSI, London, UK.

DIBt (2004) "Common Understanding of Assessment procedure (CUAP) - Cartridge fired pin for connections for thin gauge steel members and sheeting" Deutsches Institute für Bautechnik, Berlin, Germany.

ECS (2006) "Eurocode 3 – Design of steel structures - Part 1-3: General Rules – Supplementary rules for cold-formed members and sheeting (EN 1993-1-3)," ECS, Brussels, Belgium.

Essa, H.S., Tremblay, R., and Rogers, C. (2002) "Inelastic Seismic Response of metal Roof Deck Diaphragms for Steel Building Structures, Proceedings of 12th European Conference on Earthquake Engineering, European Association for Earthquake Engineering, Elsevier, Oxford, UK.

Galambos T.V. & Ravindra, M.K. (1978) "Properties of Steels for use in LRFD," Journal of Structural Division, ASCE, Vol. 104, No. ST9, pp. 1459 – 1468.

HILTI (2008) "North American Product Technical Guide – A guide to specification and installation," Tulsa, OK.

HILTI (2009) Electronically submitted test data for power-actuated fasteners to AISI (Not For Distribution), HILTI, Tulsa, OK.

HILTI (2010) Electronically submitted test data for power-actuated fasteners to AISI (Not For Distribution), HILTI, Tulsa, OK.

ICC-ES (2010) "Acceptance Criteria for Fasteners Power-Driven into Concrete, Steel, and Masonry Elements (AC70)" International Code Council Evaluation Service, Inc., Whittier, CA.

ITW Ramset (2009) Electronically submitted test data for power-actuated fasteners to AISI (Not For Distribution), ITW Ramset, Glendale Heights, IL.

ITW Ramset (2007) "Ramset Performance/Submittal Information" ITW Ramset, Glendale Heights, IL.

Mujagic, J.R.U., Easterling, W.S., Murray, T.M. (2007) "Drilled Standoff Screws for Shear Connection in Light Composite Trusses," Journal of Constructional Steel Research, Vol. 63, Issue 10, pp. 1404-1414.

Powers Fasteners (2009) Electronically submitted test data for power-actuated fasteners to AISI (Not For Distribution), Powers Fasteners, Brewsters, NY.

Sealtite (2006) "Sealtite Building Fasteners – Technical Data: Performance Data Charts, Laboratory Test Reports & Laboratory Test Methods," Sealtite Building Fasteners, Tyler TX.

Simpson Fasteners (2009) Electronically submitted test data for power-actuated fasteners to AISI (Not For Distribution), Simpsons Fasteners, Pleasanton, CA.

Twentieth International Specialty Conference on Cold-Formed Steel Structures
St. Louis, Missouri, U.S.A., November 3 & 4, 2010

Cold Formed Steel Tension Members with Two and Three Staggered Bolts

D.M. Fox[1] and R.M. Schuster[2]

Abstract

The second edition of the North American Specification for the Design of Cold Formed Steel Structural Members was published in October of 2007 for use in Canada, Mexico, and the United States. This Specification contains two country specific appendices, namely Appendix A (ANSI/AISI S100-07) for use in the US and Mexico and Appendix B (CSA S136-07) for use in Canada. Both Appendix A and B require that a bolt stagger reduction factor of 0.90 be used when calculating the tearing failure strength [resistance] of a cold formed steel member in tension with staggered bolts. This 10% reduction was based on limited testing that was carried out by Dr. Roger LaBoube of the University of Missouri-Rolla, which has now changed its name to the "Missouri University of Science & Technology".

The objective of this study was to establish if this bolt stagger reduction factor is indeed necessary since the stagger term of [$s^2/4g$] has been used in the steel industry for many years without such a reduction. Experimental testing of two and three staggered bolt tension members was carried out in the Structures Laboratory of the Department of Civil Engineering at the University of Waterloo. Based on the test results of the 1.6 mm, 2.1 mm, 2.9 mm, 4 mm, 5 mm, and 6 mm thick steel sheet, it can be concluded that the 0.90 bolt stagger reduction factor is not necessary for the steel plate thicknesses tested.

[1] Engineering Manager, iSPAN Systems, Richmond Hill, Ontario, Canada
[2] Professor Emeritus of Structural Engineering and Director of the Canadian Cold Formed Steel Research Group, Department of Civil Engineering, University of Waterloo, Waterloo, Canada

Introduction

The North American Specification for the Design of Cold Formed Steel Structural Members [1] (herein referred to as the NAS) applies for use in Canada, Mexico, and the United States. This Specification contains two country-specific appendices, namely Appendix A for use in the US and Mexico and Appendix B for use in Canada. Both Appendix A and B require that a bolt stagger reduction factor of 0.9 be used when calculating the nominal tensile resistance at the net section. This 10% reduction factor was based on limited testing that was carried out by Dr. Roger LaBoube at the University of Missouri-Rolla.

The validity of this reduction factor was first brought into question by a Canadian structural engineer who was designing cold formed steel tension members that had the same thickness as hot rolled steel tension members. In the Canadian hot rolled steel standard *"Design of Steel Structures"* (CAN/CSA-S16-09) [2] the procedure for determining the tensile resistance of staggered bolted tension members does not contain a reduction factor, regardless of thickness of the steel plate material. To investigate this difference in design methods, a study was initially carried out at the University of Waterloo by Toutounchian et al [3] using two bolts with two different stagger patterns and six different steel plate thicknesses. A follow-up study was carried out by Farashah [4] to complete the testing of the two-bolt study by Toutounchian et al [3] and to also include three-bolt staggered tension members.

The objective of this work was to analyse the two-bolt and three-bolt staggered test results to establish if the 0.90 reduction factor is required when designing tension member connections with staggered bolt patterns.

Current Design Approaches

Appendix A Method

The method in Appendix A of NAS-07 [1], which applies to the US and Mexico, for calculating the nominal tensile strength of a member for failure due to rupture of the net section involving stagger is:

$$P_n = A_n F_t \qquad \textit{Eq. E3.2-6}$$

$$A_n = C_r [A_g - n_b d_h t + (\sum s'^2/4g)t] \qquad \textit{Eq. E3.2-7}$$

Where,

F_t = Nominal tensile stress in flat sheet; in accordance with Eqs. E3.2-2 to E3.2-5 of the NAS [1]

C_r = Bolt stagger reduction factor = 0.90
s = Sheet width divided by number of bolt holes in cross section being analyzed
F_u = Tensile stress of material
d = Nominal bolt diameter
A_n = Net area of the connected part
A_g = Gross area of member
t = Material thickness
s' = Longitudinal center-to-center spacing of any two consecutive holes
g = Transverse center-to-center spacing between fastener gauge lines
n_b = Number of bolt holes in cross section being analyzed
d_h = Diameter of a standard hole
h = Bolt hole diameter (mm), (bolt diameter + 1/16 in. (1.59 mm))

Appendix B Method

The method in Appendix B of NAS-07 [1], which applies to Canada, for calculating the nominal tensile resistance of a member for failure due to rupture of the net section involving stagger is:

$$T_n = A_n F_u \qquad \textit{Eq. C2.2-1}$$

$$A_n = L_c t \qquad \textit{Eq. C2.2-2}$$

$$L_c = C_r L_s \qquad \textit{Eq. C2.2-4}$$

Where,
A_n = Critical *net area* of connected part (mm^2)
F_u = Tensile strength of steel (MPa)
L_c = Summation of critical path lengths of each segment along a potential failure path of minimum strength (mm)
t = Material thickness (mm)
C_r = Bolt stagger reduction factor = 0.90
L_s = Net failure path length inclined to force [including (s^2/4g) allowance for staggered holes] (mm)
s = Pitch, fastener spacing parallel to force (mm)
g = Gauge, fastener spacing perpendicular to force (mm)
w = Specimen width (mm)
h = Bolt hole diameter (mm), (bolt diameter + 1 mm (0.0394 in.)

Test Program

Shown in Table 1 and Table 2 are the thicknesses and dimensions of the steel sheets that were provided by ArcelorMittal. Six steel sheet thicknesses were chosen for the two-bolt plates and five thicknesses were chosen for the three-bolt plates; steel sheet thicknesses ranged from approximately 1.6 mm [0.06in] to 6 mm [0.25in]. All specimens were prepared by Baumeier Corporation in Waterloo, Ontario. Specimens were laser cut resulting in consistent workmanship with precise plate dimensions and hole patterns. All specimen dimensions were selected in order to ensure that fracture of the net section was the governing failure mode and that other modes, such as bearing failure, would not occur.

The test specimens were fabricated as rectangular plates with a constant length of 200 mm for the two-bolt plates and a constant length of 240 mm for the three-bolt plates. Single shear and double shear connections were tested. For double shear connections where specimens were designated as having the outside sheets controlling, the inside sheet thickness was selected in order to ensure failure in the outside sheets. Where specimens were designated as having the inside sheet controlling, the outside sheets of the double shear connection were selected in order to ensure failure in the inside sheet.

Shown in Figure 1 and Figure 2 are schematic diagrams of the two-bolt and three-bolt specimens, respectively. For the case of three-bolt connections, two different bolt stagger orientations were tested as shown in Figure 2(a) and Figure 2(b). The ultimate tensile stress, F_u, of the specimens were obtained from coupon tests that were carried out at the University of Waterloo; results of the coupon tests can be found in Table 1 and Table 2.

All tests were carried out in the Structures Laboratory of the Department of Civil Engineering at the University of Waterloo, the results of which are summarized in Table 3 through Table 7. Shown in Figure 3 is a photograph of the test frame that was used with all specimens which were loaded quasi-statically until failure. Typical failure in both two-bolt and three-bolt specimens occurred as fracture of the net section along the bolt holes as shown in Figure 4. The failure load was recorded for each specimen, a summary of which is included in Table 3 through Table 7.

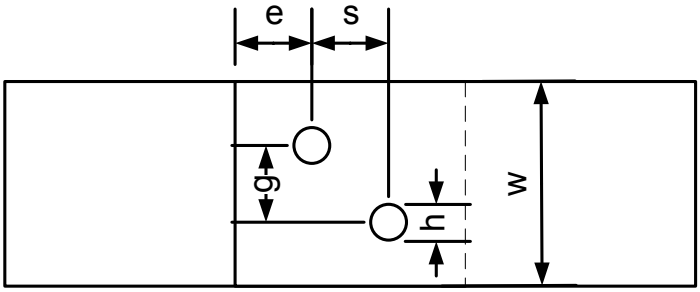

Figure 1 Schematic Diagram of Two-Bolt Specimens

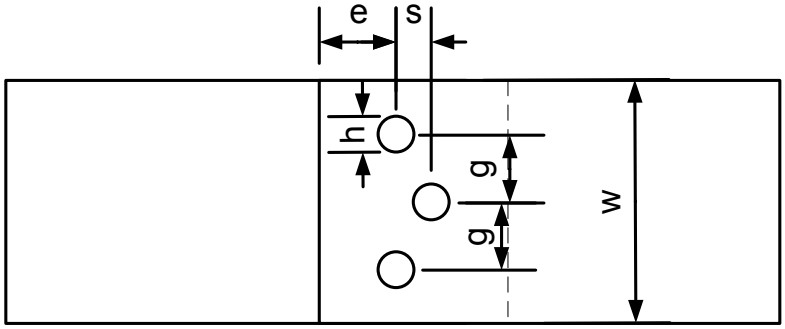

(a) With Stagger Pattern 1

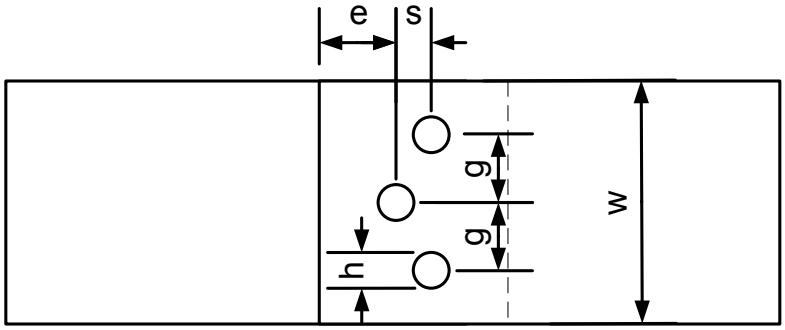

(b) With Stagger Pattern 2

Figure 2 Schematic Diagram of Three-Bolt Specimens

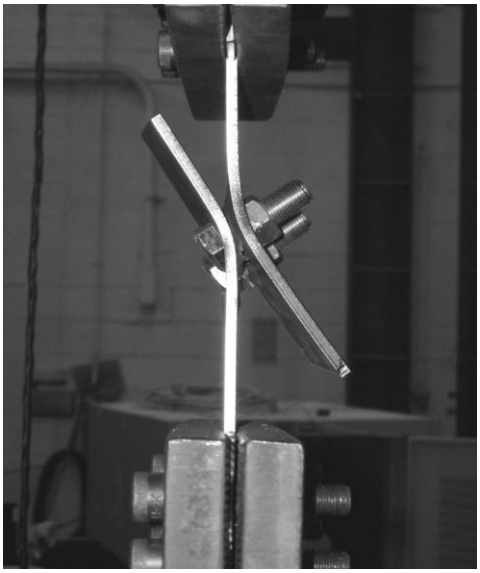

Figure 3 Photograph of Test Specimen in Tensile Test Machine

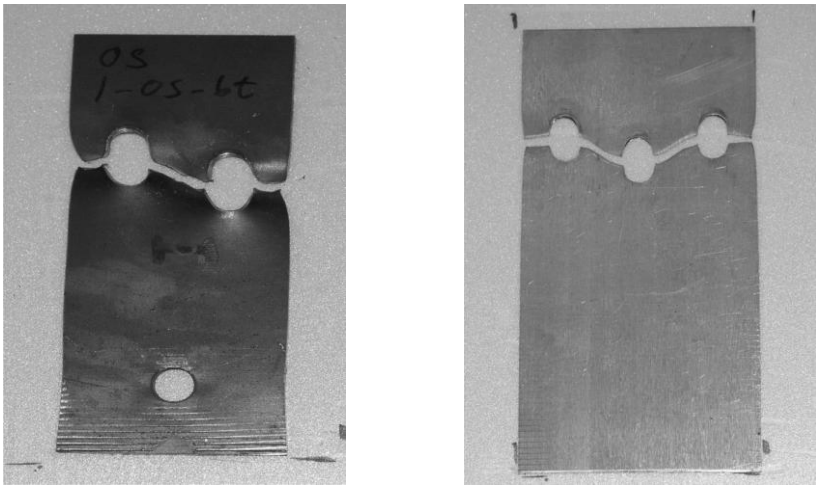

(a) Two-bolt Specimen Failure (b) Three-bolt Specimen Failure

Figure 4 Photograph of Typical Observed Failure Modes

Analysis of Test Results

In order to ascertain whether a reduction factor is required for staggered bolts, the predicted nominal strength [resistance] was calculated without the reduction factor as follows:

$$T_{n,\,NR} = A_n F_u \qquad \textit{Eq. 1}$$

$$A_{n,\,NR} = L_c\, t \qquad \textit{Eq. 2}$$

$$L_{c,\,NR} = L_s \qquad \textit{Eq. 3}$$

Where,

$A_{n,\,NR}$ = Critical *net area* of connected part without a reduction factor for staggered bolts (mm^2)

F_u = Tensile strength of steel (MPa)

$L_{c,\,NR}$ = Summation of critical path lengths of each segment along a potential failure path of minimum strength without a reduction factor for staggered bolts (mm)

L_s = Net failure path length inclined to force [including ($s^2/4g$) allowance for staggered holes] (mm)

s = Pitch, fastener spacing parallel to force (mm)

g = Gauge, fastener spacing perpendicular to force (mm)

Since the specimens were fabricated such that fracture of the net section was the controlling failure mode, only fracture of the net section was considered in the calculations with the allowance for staggered holes. The results of the calculations for each test specimen are included in Table 3 through Table 7. Also included is the ratio of tested strength [resistance] to predicted nominal strength [resistance] for each test specimen.

A reduction factor would be required if, on average, specimens tended to have the ratio of tested strength to predicted nominal strength below 1.0. As shown in Table 3 through Table 7, the average ratio ranged from 1.09 to 1.11. Further, the standard deviation ranged from 0.03 to 0.11, meaning that the most of the test specimens' predicted nominal strength [resistance], calculated by Eq. 1 without a hole stagger reduction factor, proved to be accurate or conservative. This can also be observed from Figure 5 and Figure 6. Since the large majority of the test to calculated strength [resistance] ratios are above the ideal line of 1.0, it can be stated that a reduction factor is not required in order to accurately predict the nominal strength [resistance] of tension members with staggered bolt holes for the steel thicknesses tested.

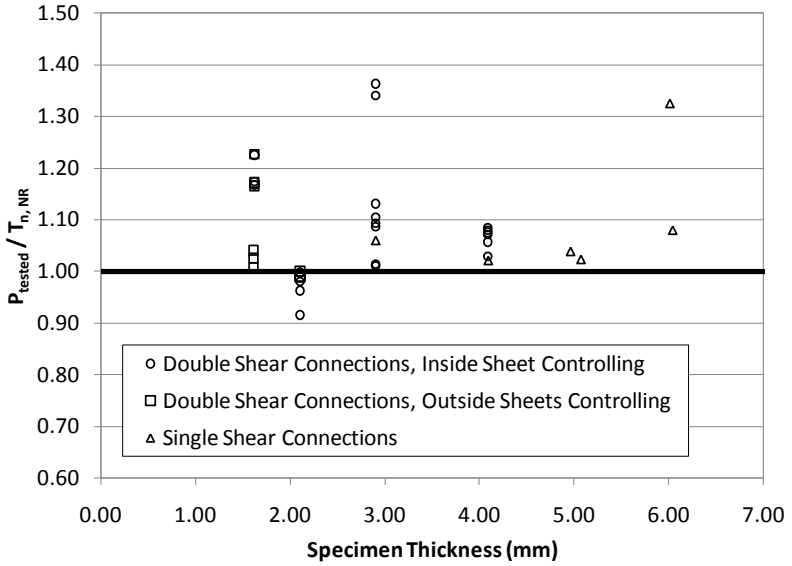

Figure 5 Tested strength to predicted nominal strength of two-bolt specimens

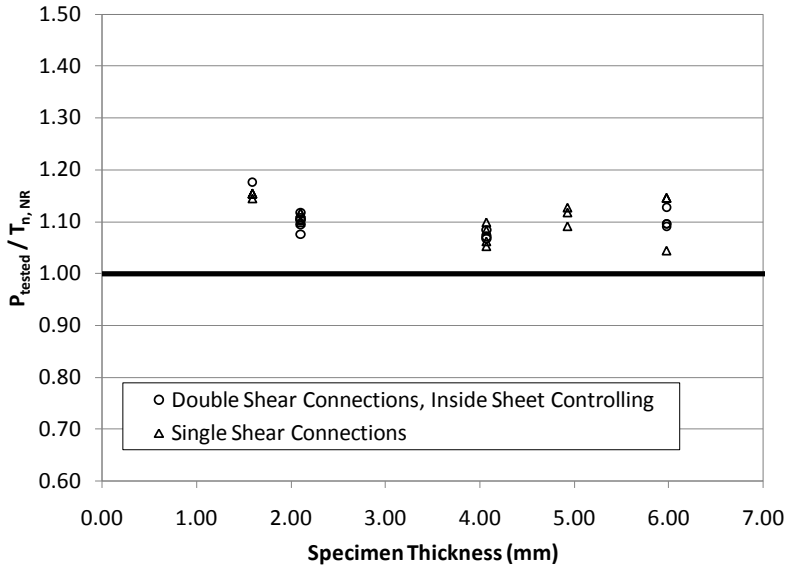

Figure 6 Tested strength to predicted nominal strength of three-bolt specimens

Summary

Presented in this paper is a study conducted at the University of Waterloo in order to ascertain the need for a reduction factor currently included in the NAS [1] for staggered bolted connections. An experimental test program was conducted to collect data to either substantiate the need for or the possible elimination of the reduction factor.

Based on the test results, it was shown that the majority of the tested connection strengths are conservatively predicted using the current NAS [1] equations without the staggered bolt hole reduction factor for the steel thicknesses tested. As such, it is recommended that consideration be given to remove the reduction factor from both Appendix A and Appendix B of the NAS [1], which would bring tension members in line with provisions contained in other current steel design standards.

References

[1] AISI (2007). North American Specification for the Design of Cold-Formed Steel Structural Members. American Iron and Steel Institute: Washington, D.C.

[2] CSA (2009). CAN/CSA-S16-09: Design of Steel Structures. Canadian Standards Association: Toronto, ON

[3] Toutounchian, A., Canete, D., Mazhar, S., and Guermon, T. (2007). Cold Formed Steel Tension Member Connections with Staggered Bolts. 4th Year Civil Engineering Project, Department of Civil Engineering, University of Waterloo: Waterloo, ON

[4] Farashah, M. (2009). Cold Formed Steel Tension Member Connections with Two and Three Staggered Bolts. Co-operative Education Report, Department of Civil Engineering, University of Waterloo: Waterloo, ON

Table 1 Mechanical Properties of Sheet Steel used in 2 Bolt Specimens

Material ID	t (mm)	F_y (MPa)	F_u (MPa)	% Elong
2B-1.6	1.62	n/a	372	41%
2B-1.6-S1-O	1.61	n/a	427	33%
2B-2.1	2.10	n/a	462	33%
2B-2.1-S1-O	2.11	n/a	469	31%
2B-2.9	2.90	n/a	347	45%
2B-4.0	4.09	n/a	555	31%
2B-5.0-S0.5	4.96	n/a	649	28%
2B-5.0-S0/S1	5.07	n/a	624	28%
2B-6.0-S0/S0.5	6.01	n/a	322	46%
2B-6.0-S1	6.04	n/a	373	47%

Table 2 Mechanical Properties of Sheet Steel used in 3 Bolt Specimens

Material ID	t (mm)	F_y (MPa)	F_u (MPa)	% Elong
3B-1.6	1.59	378	422	34%
3B-2.1	2.10	376	447	32%
3B-4	4.07	602	675	25%
3B-5	4.93	512	609	20%
3B-6	5.98	287	375	41%

Table 3 Summary of Test Results, 2 Bolt Tests, Single Shear Connections

Specimen ID	t (mm)	F_u (MPa)	d (mm)	w (mm)	s (mm)	g (mm)	h (mm)	P_{tested} (kN)	$T_{n, NR}$ (kN)	$\frac{P_{tested}}{T_{n, NR}}$
O-2.9t-0.5S-1	2.90	347	12.7	75.0	12.7	35.0	13.7	52.0	49.1	1.06
O-4t-0.5S-1	4.09	555	12.7	75.0	12.7	35.0	13.7	113	111	1.02
O-5t-0.5S-1	4.96	649	12.7	75.0	12.7	35.0	13.7	163	157	1.04
O-5t-1.0S-1	5.07	624	12.7	75.0	25.4	35.0	13.7	169	165	1.02
O-6t-0.5S-1	6.01	322	12.7	75.0	12.7	35.0	13.7	125	94	1.32
O-6t-1.0S-1	6.04	373	12.7	75.0	25.4	35.0	13.7	127	118	1.08
								Average		1.10
								Standard Deviation		0.11

Table 4 Summary of Test Results, 2 Bolt Tests, Double Shear Connections, Outside Sheets Controlling

Specimen ID	t (mm)	F_u (MPa)	d (mm)	w (mm)	s (mm)	g (mm)	h (mm)	P_{tested} (kN)	$T_{n, NR}$ (kN)	$\frac{P_{tested}}{T_{n, NR}}$
O - 1.6 t - 0.5 S - 1	1.62	372	12.7	75.0	12.7	35.0	13.7	72.1	58.8	1.23
O - 1.6 t - 0.5 S - 2	1.62	372	12.7	75.0	12.7	35.0	13.7	68.9	58.8	1.17
O - 1.6 t - 0.5 S - 3	1.62	372	12.7	75.0	12.7	35.0	13.7	68.5	58.8	1.17
O - 1.6 t - 1 S - 1	1.61	427	12.7	75.0	25.5	35.0	13.7	74.8	71.8	1.04
O - 1.6 t - 1 S - 2	1.61	427	12.7	75.0	25.5	35.0	13.7	72.4	71.8	1.01
O - 1.6 t - 1 S - 3	1.61	427	12.7	75.0	25.5	35.0	13.7	73.7	71.8	1.03
O - 2.1 t - 0.5 S - 1	2.10	462	12.7	75.0	12.7	35.0	13.7	93.5	94.6	0.99
O - 2.1 t - 0.5 S - 2	2.10	462	12.7	75.0	12.7	35.0	13.7	93.7	94.6	0.99
O - 2.1 t - 0.5 S - 3	2.10	462	12.7	75.0	12.7	35.0	13.7	94.7	94.6	1.00
								Average		1.09
								Standard Deviation		0.11

Table 5 Summary of Test Results, 2 Bolt Tests, Double Shear Connections, Inside Sheet Controlling

Specimen ID	t (mm)	F_u (MPa)	d (mm)	w (mm)	s (mm)	g (mm)	h (mm)	P_{tested} (kN)	$T_{n, NR}$ (kN)	$\frac{P_{tested}}{T_{n, NR}}$
I - 1.6 t - 0.5 S - 1	1.62	372	12.7	75.0	12.7	35.0	13.7	36.0	29.4	1.23
I - 1.6 t - 0.5 S - 2	1.62	372	12.7	75.0	12.7	35.0	13.7	34.5	29.4	1.17
I - 1.6 t - 0.5 S - 3	1.62	372	12.7	75.0	12.7	35.0	13.7	34.3	29.4	1.17
I - 2.1 t - 0.5 S - 2	2.10	462	12.7	75.0	12.7	35.0	13.7	43.3	47.3	0.92
I - 2.1 t - 0.5 S - 3	2.10	462	12.7	75.0	12.7	35.0	13.7	47.2	47.3	1.00
I - 2.1 t - 1 S - 2	2.10	462	12.7	75.0	25.5	35.0	13.7	48.8	50.7	0.96
I - 2.1 t - 1 S - 3	2.10	462	12.7	75.0	25.5	35.0	13.7	49.7	50.7	0.98
I - 2.9 t - 0.5 S - 1	2.90	347	12.7	75.0	12.7	35.0	13.7	49.6	49.1	1.01
I - 2.9 t - 0.5 S - 2	2.90	347	12.7	75.0	12.7	35.0	13.7	55.5	49.1	1.13
I - 2.9 t - 0.5 S - 3	2.90	347	12.7	75.0	12.7	35.0	13.7	66.9	49.1	1.36
I - 2.9 t - 1 S - 1	2.90	347	12.7	75.0	25.5	35.0	13.7	53.3	52.6	1.01
I - 2.9 t - 1 S - 2	2.90	347	12.7	75.0	25.5	35.0	13.7	57.5	52.6	1.09
I - 2.9 t - 1 S - 3	2.90	347	12.7	75.0	25.5	35.0	13.7	70.5	52.6	1.34
I-2.9t-0.5S-1	2.90	347	12.7	75.0	12.7	35.0	13.7	53.3	49.1	1.09
I-2.9t-0.5S-2	2.90	347	12.7	75.0	12.7	35.0	13.7	54.2	49.1	1.10
I-4t-0.5S-1	4.09	555	12.7	75.0	12.7	35.0	13.7	117	110.7	1.06
I-4t-0.5S-2	4.09	555	12.7	75.0	12.7	35.0	13.7	119	110.7	1.08
I-4t-0.5S-3	4.09	555	12.7	75.0	12.7	35.0	13.7	120	110.7	1.08
I-4t-1.0S-1	4.09	555	12.7	75.0	25.4	35.0	13.7	128	118.5	1.08
I-4t-1.0S-2	4.09	555	12.7	75.0	25.4	35.0	13.7	122	118.5	1.03
I-4t-1.0S-3	4.09	555	12.7	75.0	25.4	35.0	13.7	127	118.5	1.07
									Average	1.10
									Standard Deviation	0.10

Table 6 Summary of Test Results, 3 Bolt Tests, Single Shear Connections

Specimen ID	t (mm)	F_u (MPa)	d (mm)	w (mm)	s (mm)	g (mm)	h (mm)	P_{tested} (kN)	$T_{n, NR}$ (kN)	$\frac{P_{tested}}{T_{n, NR}}$
O-1.6t-0.5S-1	1.59	422	12.7	110	12.7	35.0	13.7	54.7	47.8	1.14
O-1.6t-1.0S-1	1.59	422	12.7	110	25.4	35.0	13.7	60.5	52	1.15
O-1.6t-1.0S-2	1.59	422	12.7	110	25.4	35.0	13.7	60.5	52	1.15
O-2.1t-0.5S-1	2.10	447	12.7	110	12.7	35.0	13.7	74.7	67	1.12
O-2.1t-0.5S-2	2.10	447	12.7	110	12.7	35.0	13.7	73.7	67	1.10
O-2.1t-1.0S-1	2.10	447	12.7	110	25.4	35.0	13.7	81.9	73	1.12
O-2.1t-1.0S-1	2.10	447	12.7	110	25.4	35.0	13.7	80.6	73	1.10
O-4t-0.5S-1	4.07	675	12.7	110	12.7	35.0	13.7	212	196	1.08
O-4t-0.5S-2	4.07	675	12.7	110	12.7	35.0	13.7	215	196	1.10
O-4t-1.0S-1	4.07	675	12.7	110	25.4	35.0	13.7	226	215	1.05
O-4t-1.0S-2	4.07	675	12.7	110	25.4	35.0	13.7	228	215	1.06
O-5t-0.5S-1	4.93	609	12.7	110	12.7	35.0	13.7	239	214	1.12
O-5t-0.5S-2	4.93	609	12.7	110	12.7	35.0	13.7	241	214	1.13
O-5t-1.0S-1	4.93	609	12.7	110	25.4	35.0	13.7	256	235	1.09
O-6t-0.5S-1	5.98	375	12.7	110	12.7	35.0	13.7	183	160	1.15
O-6t-0.5S-2	5.98	375	12.7	110	12.7	35.0	13.7	183	160	1.15
O-6t-1.0S-1	5.98	375	12.7	110	25.4	35.0	13.7	183	175	1.04
									Average	1.11
									Standard Deviation	0.04

Table 7 Summary of Test Results, 3 Bolt Tests, Double Shear Connections, Inside Sheet Controlling

Specimen ID	t (mm)	F_u (MPa)	d (mm)	w (mm)	s (mm)	g (mm)	h (mm)	P_{tested} (kN)	$T_{n, NR}$ (kN)	$\frac{P_{tested}}{T_{n, NR}}$
I-1.6t-0.5S-1	1.59	422	12.7	110	12.7	35.0	13.7	56.2	47.8	1.18
I-2.1t-0.5S-1	2.10	447	12.7	110	12.7	35.0	13.7	73.2	66.8	1.10
I-2.1t-0.5S-2	2.10	447	12.7	110	12.7	35.0	13.7	74.0	66.8	1.11
I-2.1t-0.5S-3	2.10	447	12.7	110	12.7	35.0	13.7	74.7	66.8	1.12
I-2.1t-1.0S-1	2.10	447	12.7	110	25.4	35.0	13.7	78.9	73.3	1.08
I-2.1t-1.0S-2	2.10	447	12.7	110	25.4	35.0	13.7	80.9	73.3	1.10
I-2.1t-1.0S-3	2.10	447	12.7	110	25.4	35.0	13.7	81.0	73.3	1.10
I-4t-0.5S-1	4.07	675	12.7	110	12.7	35.0	13.7	212	196	1.08
I-4t-0.5S-2	4.07	675	12.7	110	12.7	35.0	13.7	212	196	1.08
I-4t-1.0S-1	4.07	675	12.7	110	25.4	35.0	13.7	230	215	1.07
I-4t-1.0S-2	4.07	675	12.7	110	25.4	35.0	13.7	229	215	1.07
I-6t-0.5S-1	5.98	375	12.7	110	12.7	35.0	13.7	175	160	1.10
I-6t-0.5S-2	5.98	375	12.7	110	12.7	35.0	13.7	180	160	1.13
I-6t-1.0S-1	5.98	375	12.7	110	25.4	35.0	13.7	191	175	1.09
I-6t-1.0S-2	5.98	375	12.7	110	25.4	35.0	13.7	192	175	1.10
									Average	1.10
									Standard Deviation	0.03

Twentieth International Specialty Conference on Cold-Formed Steel Structures
St. Louis, Missouri, U.S.A., November 3 & 4, 2010

STUDY ON THE BEHAVIOUR OF COLD-FORMED STEEL ANGLE TENSION MEMBERS

R.PadmaPriya[1] and Dr.S.Kandasamy [2]

ABSTRACT

Cold-formed steel tension members with bolted end connections are frequently used in a variety of structures such as trusses, transmission towers etc. Among all the shapes, angles are widely used. When angle sections are connected with gusset plates and eccentrically loaded, their ultimate load-carrying capacity is influenced by the effect of shear lag. This paper presents the details of an experimental and numerical investigation with a primary objective of studying the effect of shear lag on cold-formed steel single and double angles subjected to tension. Seventy-two single plain and lipped angles made from thicknesses 2,3 and 4 mm connected to gusset plates at their ends by ordinary black bolts were tested. Forty-eight double angles of 3 and 4 mm thicknesses connected to the opposite side of gusset plate and to the same side of the gusset plate at their ends by black bolts were also tested. All the one hundred and twenty specimens were tested in an Universal Testing machine subjected to eccentric tensile load. From the test results, load vs deflection behaviour and the failure modes were studied. The actual load carried by the specimen was compared with the theoretical load carrying capacity predicted by International codal provisions and with the load carrying capacity predicted by numerical investigation by ANSYS. An empirical equation is proposed to determine the load-carrying capacity of the cold-formed steel angles and the predicted values agree with the experimental results.

INTRODUCTION:

Cold- formed steel structural elements are widely used as structural elements in roofs, decks, wall panels, trailer bodies, agricultural equipments, aircrafts, etc. Angles are the most basic and widely used sections among the various forms of all rolled steel sections available. Practically angles are connected with gusset plates through one leg and due to this there will be non-uniform stress distribution due to eccentrically applied load. **Chesson and**

[1] Lecturer in Civil Engineering , SRM University, Kattankulathur, Chennai.
[2] Dean, Anna University Tiruchirapalli, Ariyalur campus, Ariyalur, India.

Munse carried out the study of shear lag effects on single and double angles made of hot rolled sections. Their study included different cross-sectional configurations, connections, materials and fabrication methods. The theoretical concept of shear lag and its effect on the angle members were based on test results of 218 specimens (among which there were 137 angle specimens) of various configurations. **Chi – Ling Pan** conducted tests on cold formed steel channel sections with different dimensions to investigate the effect of shear lag. The comparisons were made between the test results and predictions computed based on several specifications. To study the stress distribution at the various locations of the cross-section of specimen, the finite element software ANSYS was used. **Epstein and Chamarajnagar** formulated a 20 node quadratic brick element model. The material nonlinear effects were modeled using the Von-Mises yield criterion and the material stress-strain curve was assumed to be elastic perfectly plastic. **La–Boube and Yu** conducted an experimental and analytical study at the University of Missouri–Rolla, to expand the knowledge and understanding of the behaviour of cold-formed steel bolted connections. The first part concentrated on the tensile capacity, bearing capacity and the interaction of tension and bearing capacities of flat sheet cold-formed steel bolted connections. In the second part, the tensile capacity and bearing capacity of bolted connections of flat sheet, angle and channel cold-formed steel members were addressed. **Mohan Gupta and L.M.Gupta** analyzed angles with bolted connections using Finite Element method giving due considerations to associated problems such as the shape of the material, stress-strain curve, the contact between the gusset plate and the angle, the appropriate failure criteria, the effect of punching of holes etc. He also analysed angles under tension in the limit state format giving due considerations to block shear failure and yielding of gross section. The factor of safety obtained as a result indicated adequate representation of design strengths. **Wu and Kulak** conducted an experimental investigation of single and double angle tension members to examine the effect of shear lag on the net section rupture capacity of the cross section. They tested 24 specimens (11 single angle members and 13 double angle members) to compare the ultimate loads with the earlier test results obtained by others. They also conducted finite element investigation to determine the stress distribution of the critical cross section at ultimate load. **Valdier Francisco de paula et al,** presented experimental results of 66 specimens carried out on cold-formed steel angles fastened with bolts under tension. He conducted multiple linear regression analysis and suggested the expression for net section efficiency (U) which depended on the geometrical factors such as connection eccentricity ($\overline{X}$), connection length (L), width of connected leg of the angle (b_c), net width of the angle with connected leg (b_{cn}), width of unconnected leg (b_d), nominal bolt diameter (d) and angle thickness (t).

All the above investigations were made for the hot rolled double angle sections. There were only limited investigations for cold-formed steel members. The present investigation aims to study the behaviour of cold-formed steel angle members.

CODAL PROVISIONS

The existing Indian Standard code of practice for cold-formed steel IS 801-1975 does not elaborately deal with the design of tension members. The following codal provisions are used to predict member capacities of the cold-formed steel angle members.

American Iron and Steel Institute : Appendix A of North American specification, 2007 Edition

The nominal tensile strengthe strength P_n of the member,

$P_n = A_e F_u$

where A_e = UA_n and $U = 1.0 - 1.20\ \bar{x} / L < 0.9$ but shall not be less than 0.4

A_e = effective net area of the section

A_n = net area of the connected part.

$\bar{x}$ = distance from shear plane to centroid of the cross section.

L = length of the end connection i.e. distance between the outermost bolts in the joint along the length direction.

Australian/NewZealand Standards: AS/NZS 4600-2005

The nominal section capacity of a member in tension shall be taken as the lesser of

$N_t = A_g f_y$ and

Nt = $0.85\ K_t A_n f_u$

where A_g = gross cross sectional area of the member

f_y = yield stress of the material

K_t = correction factor for distribution of forces.

for eccentrically connected single angles and double angles connected to opposite side of the gusset plate, the value of $K_t = 0.85$

for double angles connected to the same side of the gusset plate the value of $K_t = 1.0$

A_n = net area of the cross-section, obtained by deducting from the gross area of the cross-section, the sectional area of all penetrations and holes, including fastener holes.

f_u = tensile strength used in the design.

British Standards: BS:5950 (Part 5)-1998

The tensile capacity P_t, of a member

$P_t = A_e * p_y$

Single angles

For single angles connected through one leg only, the effective area A_e is computed as

$A_e = a_1(3a_1+4a_2)/ (3a_1+a_2)$

Double angles

For double angles connected to opposite side of gusset plate, the effective area is determined as

$A_e = a_1(5a_1+6a_2)/ (5a_1+a_2)$

For double angles connected to the same side of gusset plate the effective area can be determined as that of single angles.

A_e = effective area of the section

a_1 = the net sectional area of the connected leg

a_2 = the gross sectional area of the unconnected leg

p_y = the design strength.

EXPERIMENTAL INVESTIGATION

A total of one hundred and twenty experiments using seventy-two single angle specimens with and without lips of 2, 3 and 4mm thickness and twenty-four double angle specimens connected back to back side of the gusset plate of 3mm and 4mm thickness and twenty-four double angle specimens connected to the same side of the gusset plate of 3mm and 4mm thickness with bolted connections were conducted under eccentric tensile loads. The specimens were fabricated from 2mm, 3mm, 4mm thickness cold- formed steel sheets of grade St- 34-1079 by bending and press breaking operations. Standard tension tests were conducted on coupons, stress vs strain curve was plotted as shown in fig 1. The values of yield stress, ultimate stress, modulus of elasticity and elongation obtained for these thicknesses of cold formed steel sheets are presented in the Table 1.

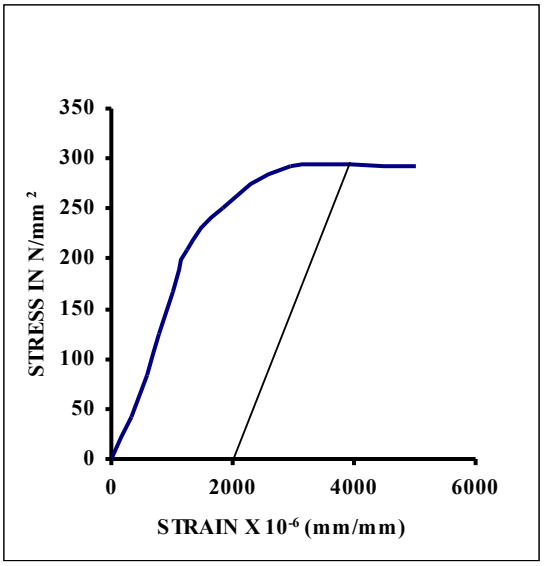

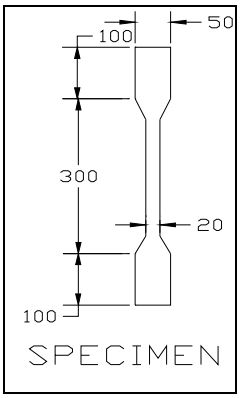

Fig 1 Standard tension test

Table 1. MECHANICAL PROPERTIES OF STEEL SHEET

Thickness of steel sheet in mm	Yield Stress in MPa (f_y)	Ultimate Stress in MPa (f_u)	Modulus of Elasticity in MPa	f_u/f_y	Percentage elongation in 200mm gauge length
2	210	268	2.00×10^5	1.27	10
3	228	292	2.00×10^5	1.28	11
4	235	313	2.03×10^5	1.33	14

The specimens were tested as two different section configurations namely single angles and double angles. The single angle specimens were connected with their larger leg to end gusset plates of mild steel of 6mm thickness. Ordinary black bolts of 12mm diameter are used as connectors for specimens made from 2mm and 4mm thickness sheets. In case of specimens fabricated from 3mm thickness sheet 10mm diameter bolts were used. The double angle specimens were connected with their larger leg with two mild steel gusset plates of 8mm and 12mm thickness using ordinary black bolts of 10mm

and 12mm diameter. The gusset plates were not reused for single angle specimens and were reused for double angle specimens. The required number of bolts are calculated for all specimens and were provided according to the design procedures. All the specimens were fabricated for a length of 500mm. The width of the gusset plate was kept 10mm more than the width of the connected leg. The length of gusset plate was provided according to the requirement of pitch and edge distance as per Indian code of practice. All the members were connected with gusset plate to the larger side by means of bolts.

Fig 2,and 3 present the details of the fabricated single and double angle specimens. The specimens were tested in Universal Testing machine of 400kN and 1000KN capacity. The specimens were fixed vertically by gripping the gusset plates. The load was applied eccentrically through the gusset plates. Demec gauge was used for measuring the elongation for a gauge length of 200mm. The experimental set up is shown in fig 4,5,6. Figure 7 shows the gusset plates used for the connection. The load is gradually applied with suitable increments from control panel and at each increment of loads corresponding elongation was taken. The yield, ultimate and breaking loads were also observed. The distance of separation between gusset plate and test specimens was also recorded. The procedure is repeated till the failure stage is reached in all specimens. The observed yield load and ultimate load of the specimens tested are recorded.

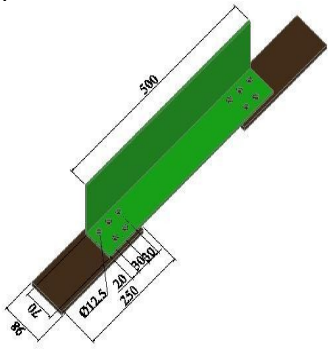

Fig 2 Details of single plain angle specimen provided with bolts in staggered pitch

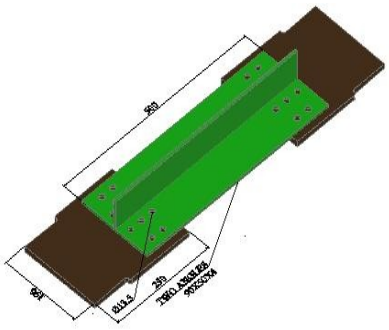

Fig 3 Details of double angle specimens connected to same side provided with bolts in staggered pitch.

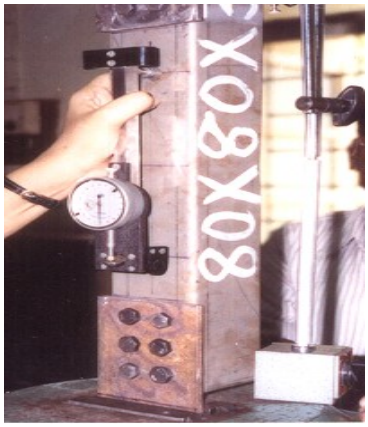

Figure 4 Experimental set up for single angle specimen

Figure 5 Experimental set up for double angles connected to opposite side of gusset plates

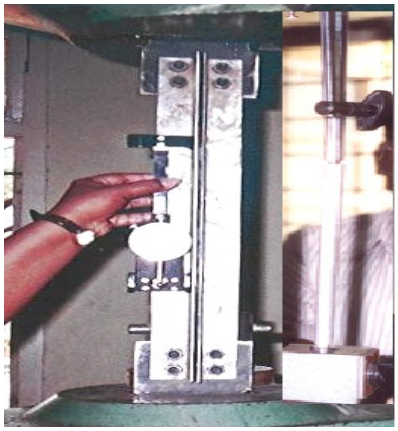

Figure 6 Experimental set up for double angles connected to same side of gusset plates

Figure 7 Gusset plates used for connection.

NUMERICAL INVESTIGATION:

The goal of the finite element analysis is to develop a model that could study the behaviour of bolted cold-formed steel single and double angle tension members. The behaviour observed during the tests was used for preparing a finite element model. All the one hundred and twenty specimens were modeled using the finite element program ANSYS (version 10). The problem was studied as a nonlinear load vs displacement analysis including plasticity and nonlinear effect of geometry. SHELL 63 element type was used to model the single and double angle specimens. It is a 4 noded 3-dimensional quadratic elastic shell element. It has both bending and membrane capabilities. This element has six degrees of freedom at each node: translations in the nodal x,y and z directions and rotations about the nodal x,y and z axes. A typical mesh of the model is shown in fig. 8,9. In the finite element models, the shear deformation of the bolts was ignored. The load was assumed to transfer from gusset plate to the angle fully by the bearing of the bolts.

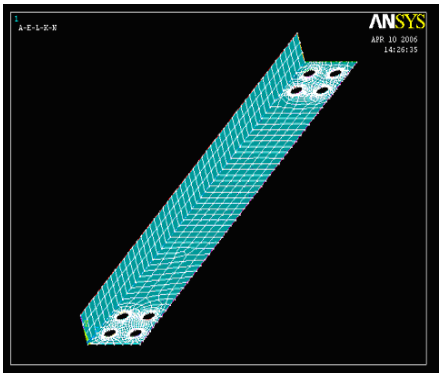

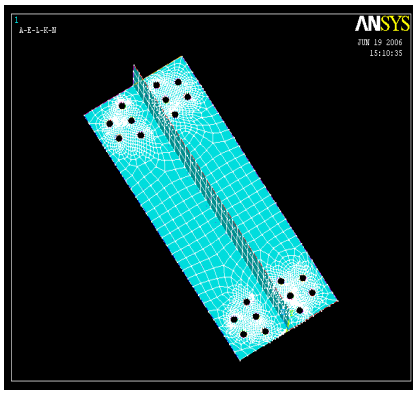

Figure 9 Element mesh for double unequal angle 100x50x3 connected to the same side of gusset plate

RESULTS AND DISCUSSION

The behaviour of cold-formed steel single and double angles when subjected to eccentric tension were studied. The ultimate-load carrying capacities of the specimens were compared with the load carrying capacities predicted using the American, Australian/New Zealand and British standards.

The experimental results were also compared with the numerical results obtained using ANSYS software and with the proposed equation for tensile load carrying capacity obtained using the nonlinear regression analysis.

1) EXPERIMENTAL INVESTIGATION

a) Ultimate Load-Carrying Capacity

The experimental ultimate loads for all the cold-formed steel single angles are presented in Table 2. It is observed that in the case of single equal lipped angles the average increase in ultimate load is 1.2 times greater than that of single equal plain angles. In the case of single unequal lipped angles the average increase in ultimate load is found to be 1.24 times greater than that of single unequal plain angles. The average increase in ultimate load for double equal angles connected to opposite side of the gusset plate is 1.25 times greater than that of double equal angles connected to the same side of the gusset plate. In the case of double unequal angles connected to oppostie side of the gusset plate the average increase in ultimate load is 1.27 times greater than that of double unequal angles connected to the same side of the gusset plate.

Table 2 Ultimate load carrying capacity of the single angles

S. No.	Size of the specimen (mm)	Ultimate load carrying capacity (P_{exp}) in kN		
		t = 2mm	t = 3mm	t = 4mm
1	40×40×t	25	47.5	64
2	50×50×t	33	55	80.5
3	60×60×t	47.5	69	83
4	70×70×t	55	82	92
5	80×80×t	60	96	123
6	40×25×t	19	33	42.5
7	50×25×t	28.5	41.5	59.5
8	60×30×t	36	43.5	62.5
9	60×40×t	39	50.5	68
10	80×30×t	41	68	80
11	90×50×t	51	88	101
12	100×50×t	66	98	125
13	40×40×15×t	34	59	75
14	50×50×15×t	43	63	98

15	60×60×15×t	57.5	71	103
16	70×70×15×t	60	109	135
17	80×80×15×t	72	124	137
18	40×25×15×t	26	57	64.3
19	60×25×15×t	40	60	70
20	60×30×15×t	43	62	75.5
21	60×40×15×t	48	63	83
22	80×30×15×t	56	74	90
23	90×50×15×t	60	86	120
24	100×50×15×t	65	106	125

b) Load vs Deflection

Figures 10 and 11 show the typical load versus deflection behaviour for single angles with and without lips and double angles. From the graphs, it is observed that the ultimate load carrying capacity increases as the cross-sectional area and number of bolts in the connection increases. It is also observed that when the rigidity of the connection increases the stiffness of the member also increases.

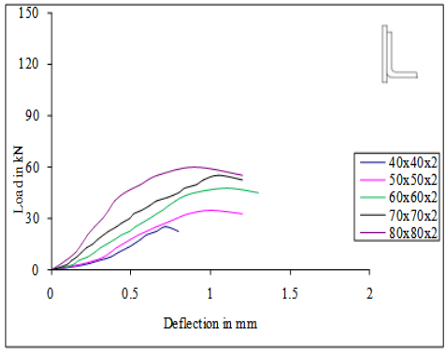

Fig 10 Load Vs Deflection for single equal plain angle thickness 2mm

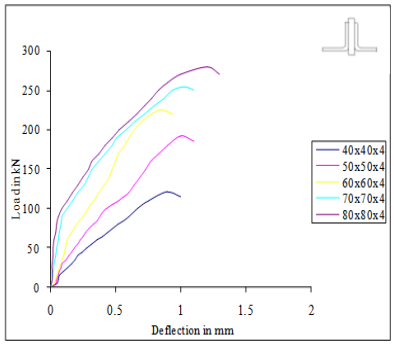

Fig 11 Load vs Deflection for double equal angle (opposite side), thickness 4mm

c) Modes of Failure

The mode of failure of all single and double angle specimens were noticed during testing. Generally tearing failure, block shear failure, net section fracture failure were observed as in fig 12,13, and 14 . The failure modes are

different for single and double angle sections. The mode of failure depends upon the cross section and rigidity of connection.

During the loading process, the gusset plates of double angle members remained straight. However, in the case of single angles the gusset plate and the angles bent during loading. This is due to eccentrically applied load. This kind of bending is referred as global bending. As the load was being applied, the corners of the angle at the two ends gradually separated from the gusset plates for both single and double angle members. Thus, a gap was formed between the corner of the connected leg and the gusset plate. This is referred as local bending. The visible length of gap was usually from the edge of the angle to the innermost bolt. The width of the gap varied from one specimen to another, with a maximum observed value of 10mm. Generally larger gaps were associated with the cases of greater eccentricity of the cross-section, smaller angle thicknesses and shorter connection lengths.

There was no major slip of the connections during the tests. All the specimens failed at the critical cross-section (inner most bolt hole) as the ultimate load was reached. After necking, the critical cross-section was torn out from the edge of the connected leg to the hole then to the corner of the angle. The specimens carried some amount of load beyond the ultimate load and until failure. It was noted that all the bolts were still tight after completion of the tests. This indicates that the bolts were not highly stressed during the tests. The outstanding leg which is subjected to compression experiences local buckling nearer to the supports.

Fig 12 Tearing failure of lipped angle 60×25×15×3

Fig 13 Block shear failure of single plain angle 40x25x3

Fig 14 Net section fracture failure of plain angle 90×50×3

2) COMPARISON OF EXPERIMENTAL AND PREDICTED ULTIMATE LOADS

A comparative study between the experimentally observed ultimate loads of the specimen tested with the tensile load carrying capacity of equations of the following codes North American Specification-2007, AS/NZS:4600-2005, BS:5950 (Part 5)-1998 is made to review the the procedures recommended.

The comparison of predicted ultimate loads by the three various codes for single and double angles tested are shown in Figures 15 and 16. The tensile capacity equations of the international codes take it into account the effect of shear lag and incorporates the capacity reduction factor in addition to net effective area of the section. In case of single angles the values predicted by AISI and AS/NZS are nearly 11% lower than the ultimate loads irrespective of whether the angle is equal or unequal and provided with or without lip. BS code underestimates the values by 29% with respect to experimental ultimate loads. Provision of lip increases the load carrying capacity of the angles by 22%.

In case of double angles the ultimate loads predicted by the AISI and AS/NZS are nearly 20% lower than the experimental ultimate loads. BS code underestimates the values for double angles by 21%. It is also observed that the load carrying capacity for double angles connected to opposite side of the gusset plate is 26% more than that of double angles connected to the same side.

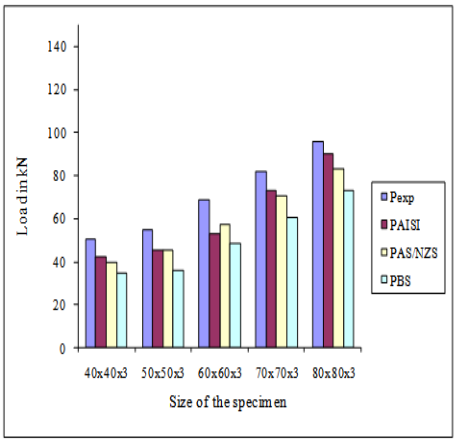

Fig 15 Comparison of ultimate loads with loads based on codal provisions for single equal plain angles

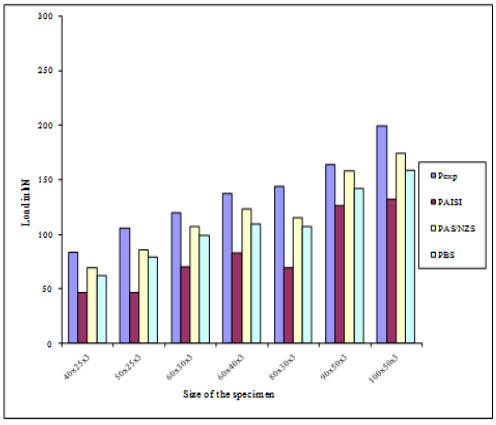

Fig 16 Comparison of ultimate loads with loads based on codal provisions for double unequal angles connected to opposite side of the gusset plate

3) NUMERICAL INVESTIGATION

To perform the non-linear analysis, the angle specimens are modeled based on the experimental set up incorporating geometric imperfections. The geometric imperfections included the thickness of the section, width of the connected leg, width of unconnected leg in case of single plain angles and it includes width of lip in case of lipped angles. As the nonlinear problem is path dependant, the solution process requires a step by step load incremental analysis. In the analysis, the solution usually converged very slowly after yielding, and the increment for each load step had to be made very small. Yielding is determined using von-Mises yield criteria. At the completion of each incremental solution, the program adjusts the stiffness matrix to reflect the nonlinear changes in structural stiffness before proceeding to the next load increment. ANSYS employs Newton-Raphson equilibrium iterations. The general post processor in ANSYS is used to review results at each load increments. Fig 17 and 18 shows the stress distribution.

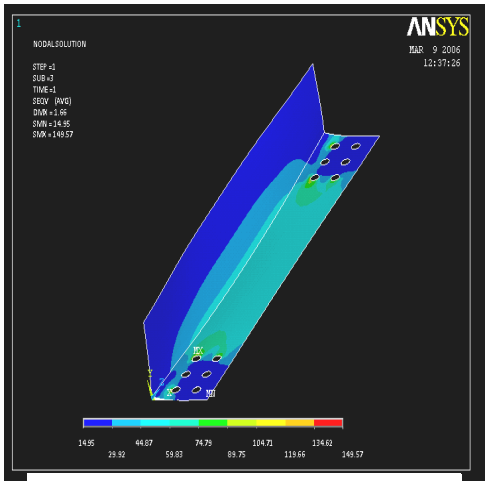

Fig 17 Stress distribution for single plain equal angle 80×80×3

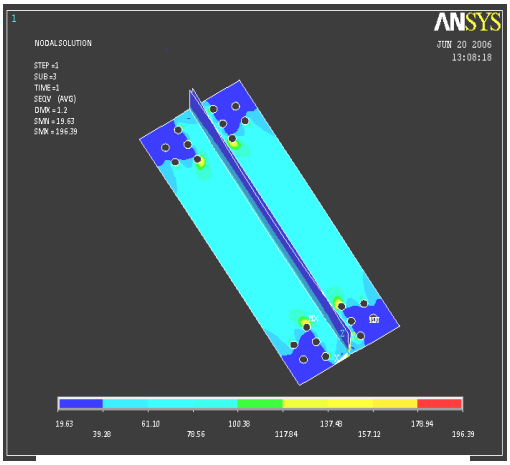

Fig 18 Stress distribution for double angle 100×50×4 connected to the same side of the gusset plate

4) PROPOSED EQUATION FOR PREDICTING STRENGTH DUE TO NET SECTION FRACTURE FAILURE.

The tensile strength of the angle sections can be evaluated in terms of the ratio of its average stress at ultimate load (P_{exp}/A_n) to the ultimate tensile strength (f_u) of the material. The ratio is called as the net section efficiency

which represents reduction in load carrying capacity. The comparisons between the test results and the predicted values computed according to codal provisions have been discussed in the previous sections. Based on the above comparisons, geometrical factors such as connection eccentricity ($\overline{x}$), connection length (L), width of connected leg of the angle (a_c), net width of connected leg of the angle (a_{cn}), width of unconnected leg (a_d), nominal bolt diameter (d) and angle thickness (t) have effect on net section efficiency. Therefore, new net section efficiency (U) equation is developed for both single and double angles incorporating the above geometrical factors. In order to establish the form of the equation, regression analysis including linear and non-linear regression analysis have been performed using commercially available statistical software Sigmaplot 10. The net section efficiency equation is

$$U=1.024-0.301(\overline{x}/L)-\left(0.12a_{cn}+0.22a_d-0.761d-1.5t\right)/a_c$$

Based on the net section efficiency equation, it is recommended that for cold-formed steel angle members, the nominal tensile strength (P_{un}) of angle sections can be calculated as

$P_{un} = UA_nf_u$

where A_n = Net area of cross section

U = net section efficiency

CONCLUSIONS

Based on the experimental, theoretical and numerical investigations the following conclusions are made.

1) The ultimate load carrying capacity increases as the cross – sectional area increases. Provision of more number of bolts improves the connection rigidity which also contributes to increase in load carrying capacity.
2) The presence of lip increases the load carrying capacity of single angles by 22%. The load carrying capacity increases by 26% for double angles connected to the opposite side of the gusset than the connected to same side of gusset plate.
3) Cold-formed steel angles with larger outstanding legs experiences local buckling under eccentric tensile loading.
4) In case of single angles the values predicted by the international codes AISI and AS/NZS are nearly 11% lower than the experimental ultimate loads irrespective of whether the angle is equal or unequal and provided with or without lip.BS code underestimates the values for single angles by 29% with respect to experimental ultimate loads.

5) In case of double angles the ultimate loads predicted by the AISI and AS/NZS are nearly 20% lower than the experimental ultimate loads. BS code underestimates the values for double angle members by 21% with respect to experimental ultimate loads.
6) The stress contours obtained in the finite element analysis indicates that maximum stresses occur in the innermost bolt holes from which the experimental failures were initiated.
7) The proposed equation for net section efficiency is applicable only when longer leg of the angle is connected.

REFERENCES:

1. AISI commentary (2007), 'Design of Cold-formed Steel Structural Members ", North American Specification.
2. AS/NZS: 4600 (2005), 'Cold-formed Steel Structures', Australia / New Zealand Standard.
3. BS:5950-Part 5 (1998), 'Structural Use of Steelwork in Building-Code of practice for design of cold-formed thin gauge sections', British Standards Institution.
4. Chesson EFjr. and Munse W.H "Riveted and bolted joints truss type tensile connections", J.Struct Div., ASCE, Vol 89(1) 1963, pp 67 – 106.
5. Chi – Ling pan "Prediction of the strength of bolted cold – formed channel sections in tension", Thin walled structures , Vol 42 (2004), pp 1177 – 1198.
6. Epstein, H.I and Chamarajanagar, R., "Finite element studies for correlation with block shear tests, "Computers and Structures", Vol.61, No.5, 1996 pp 967-974.
7. Eric Yue Wu and Geoffrey L.Kulak (1997), "Shear lag in bolted angle tension members", Journal of Structural Engineering, Vol.123, No:9 pp 1144-1152.
8. Gupta L.M and Mohan Gupta (2004), "Evaluation of stress distribution in bolted steel angles under tension", Electronic Journal of Structural Engineering.
9. Gupta L.M and Mohan Gupta (2005), "Limit state design of bolted steel angles under tension", Journal of Structural Engineering, Vol.31, No.4, pp265-274.
10. LaBoube R.A. and Yu W.W. (1995), 'Tensile and bearing capacities of bolted connections', Final summary Report, Civil Engineering study 95-6, University of Missouri-Rolla.

11. Valdier Francisco de Paula, Luciano Mendes Bezerra and William Taylor Matias (2008), 'Efficiency reduction due to shear lag on bolted cold-formed steel angles', Journal of Constructional Steel Research, Vol.64, pp.571-583.

Twentieth International Specialty Conference on Cold-Formed Steel Structures
St. Louis, Missouri, U.S.A., November 3 & 4, 2010

Angle Cleat Base Connections

M. Dundu[1] and S. Maphosa[2]

Abstract

Tests, performed on base connections fabricated from cold-formed channels and hot-rolled angle cleats, are presented in this paper. This research is part of an on-going research to develop portal frames made out of cold-formed steel. The base connections are subjected to an axial load and moment. Hot-rolled angle cleats are used to prevent premature failing of the base connections. Several loading configurations are considered and these are dependent on the eccentricity of the load. In all the tests the cold-formed channels failed by local buckling. A significant amount of bearing distortion was observed in the heavily loaded flange. The use of bolted angle cleats allows for a simple connection to be developed, which can result in significant cost savings within the steel construction industry.

[1] Senior Lecturer, University of Johannesburg, Dept. of Civil Engineering, P. O. Box 524, Auckland Park, 2006, South Africa.
[2] Student, University of Johannesburg, Dept. of Civil Engineering, P. O. Box 524, Auckland Park, 2006, South Africa.

Introduction

The weight of a steel structure including all other loads (live loads or dead loads) to which it may be subjected are borne by its column base which transmit these loads to the foundation. The successful transfer of these loads to the foundations requires that the base connections be properly designed and installed, because this is critical for the effective and efficient performance of the structure. A key factor in erecting a building is the simplicity in which the base connections can be produced. The design and detailing of the connections in a building has a significant effect on costs.

Welded base plate connections are commonly used within the construction industry to connect the column to the base plate. This type of connection can create assembly problems and uncertainties, in terms of workmanship and economy. A viable alternative to this connection, especially for portal frames spanning from 5 to 16m, are angle cleats base connections. The main advantage of angle cleat connections is that no welding is required, thus they can fabricated and assembled with minimum skill. The aim of this investigation is to determine the feasibility of using angle cleat connections as column base connections. The results obtained from the experiments are then compared with the ones determined from the theoretical analysis to evaluate whether the connection is sufficient in resisting these loads.

Structural form of the connections

In previous work, portal frames were developed from cold-formed lipped channels, connected back-to-back at the eaves and apex connections (Dundu and Kemp 2006). Current investigations are focused on the base connections of these frames. Three base connections are investigated in these tests; 1) Base connections with cold-formed angle cleats, connected to the flanges only, 2) Base connections with hot-rolled angle cleats, connected to the flange only and 3) Base connections with hot-rolled angle cleats connected on both the flanges and web. In base connections 1 and 2, angle cleats are connected to the flanges by two bolts and a single bolt secures them to the foundation as shown in Figure 1(a). Since the connection configuration in this figure is such that loads are transferred from the entire column section through the flanges only to the angle cleats, in order to increase the capacity of the connection it was decided to incorporate another angle cleat in the web to form base connection 3. The plan of this

connection is shown in Figure 1(b). In both base connections the angle cleats are of the same size and the column is short in order to prevent premature failure caused by overall flexural buckling. The angle cleats are connected to the column such that no end bearing at the bottom of the column takes place; instead the load is fully transferred to the foundation through angle cleats. As shown in the figure, the longer leg of the cleats is connected to the flange of the column. The angle cleats were chosen so that they can accommodate two bolts.

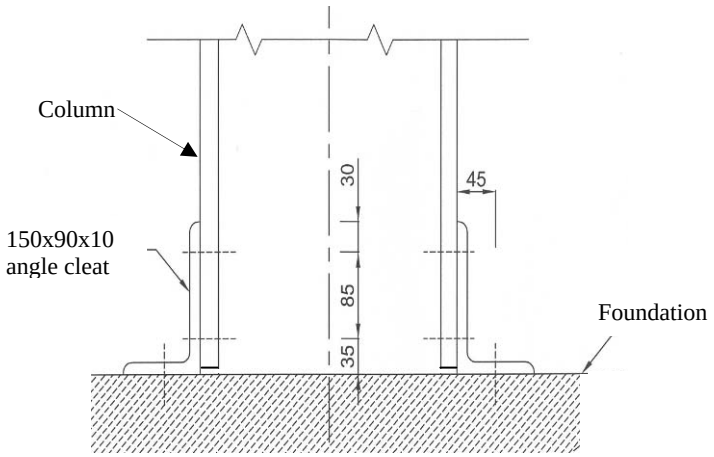

(a) Base connection 1 and 2

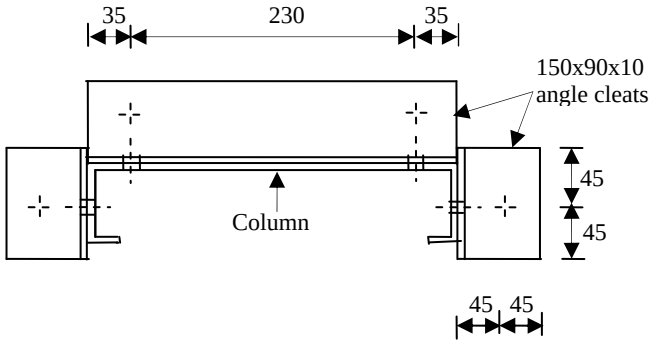

Figure (b) Plan of base connection 3

Figure 1 Base connections

Test procedure of base connections

Prior to testing the base connections, material properties had to be determined. Coupon tests were prepared to establish the yield stress, ultimate stress and the elastic modulus of the channel sections. The yield stress and the elastic modulus are used to calculate the effective area of the channels and the squash load of the channels, whilst the ultimate stress is used to calculate the bearing resistance of the connections (see Tables 2). No material tests were carried out for the bolts and the hot-rolled angle cleat since their strength was found to be less critical than the strength of the channels. Grade 8.8 bolts have a minimum tensile stress of f_u = 800MPa (SASCH, 2005). Standard washers were placed under the head of the M20 bolts and under the nuts to guard against rotation of the bolt and deformation of the thin material adjacent to the bolt. The diameter of all bolt-holes was made 1mm greater than the nominal diameter of the bolt to reduce slip in the connections. All bolts were fully threaded.

The bases were loaded using a 500kN Instron Testing Machine. A total of 24 column bases were tested. For each base connection, two tests were performed with the load applied at centroid of the column section (Load case 1) as shown in Figure 2(a), one third of the depth of the section (Load case 2), edge of the column section (Load case 3) and through a beam (Load case 4) as shown in Figure 2(b). A beam was introduced in Load case 4 in order to generate a large moment into the connection. Variables in the tests include the size of the column sections, number and type of angle cleats, material properties, and location of loading. A list of these variables and the corresponding bases are given in Table 1. High strength structural bolts, size M20, of Grade 8.8 steel are used for the base connections.

(a) Load cases 1-3

(b) Load case 4

Figure 2 Base connections with angle cleats connected to the flange only

Table 1 Variables in the test set-up

Angle cleats	Load Cases	Column Section	f_y (MPa)	f_u (MPa)
Cold-formed angle cleats connected to the flange only				
150x75x3	Load Case 1	300x50x20x3	262.43	345.80
150x75x3	Load Case 2	300x50x20x3	262.43	345.80
150x75x3	Load Case 3	300x50x20x3	262.43	345.80
*150x75x3	Load Case 4	300x65x20x3	256.00	315.00
Hot-rolled angle cleats connected to the flange only				
150x90x10	Load Case 1	300x65x20x3	346.05	473.90
150x90x10	Load Case 2	300x65x20x3	346.05	473.90
150x90x10	Load Case 3	300x65x20x3	346.05	473.90
*150x90x10	Load Case 4	300x65x20x3	256.00	315.00
Hot-rolled angle cleats connected to the flange and web				
150x90x10	Load Case 1	300x75x20x3	264.72	365.88
150x90x10	Load Case 2	300x75x20x3	264.72	365.88
150x90x10	Load Case 3	300x75x20x3	264.72	365.88
150x90x10	Load Case 4	300x75x20x3	264.72	365.88

* Note the change in material properties

All tests are arranged in such a way that the column does not bear on its bottom face, but is suspended entirely by M20 bolts. Since these tests were performed in

the laboratory the angle cleats were bolted to a plate instead of the concrete foundation. A compressive loading was applied along the minor axis of the channel sections through specially designed plates with circular grooves at the centre to accommodate a steel ball. The steel ball ensured that the applied load is a point load and the bottom plate prevented the top of the stub column from localized damage. The applied load and shortening were recorded at pre-determined intervals using an automatic data acquisition system as the experiments were carried out. The load was applied at a gradual rate of 2mm/min to allow the structure to deform in a ductile manner. In Load Case 4, the load was applied at the shear centre of the column section to prevent it from twisting.

Modes of failure

Cold-formed angle cleat connected to the flanges only

In all tests where cold-formed angle cleats were used the base connection failed prematurely by the deformation of the angle cleats. When the load was gradually applied at the centroid of the column section, the first sign of deformation was observed at the bottom of the web as it curved into a parabolic shape (Figure 3(a)). This was followed by the deformation of the angle cleats. The deformation of the angle cleats became excessive as the load was increased, consequently causing the set-up to fail. Significant cross bending occurred in the channel (Figure 3(b)) when the load was applied at the edge of the column section (Load case 3). This was immediately followed by the deformation of the angle cleat, directly below the load. The set-up ultimately failed due to excessive deformation of this angle cleat. No deformation was experienced in the other angle cleat, implying that little or no load was carried by this angle cleat. In the case where the load was applied through a beam the moment uplifted one angle cleat and a compressed the other. The base connection failed by the opening up of the angle cleat on the tension side and the closing of the angle cleat on the compression side. No bearing distortions were experienced in the bolt holes of all tests in this group.

(a) Deformation of web and angle cleats

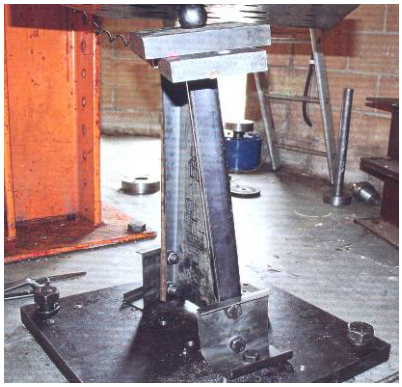

(b) Cross-bending of channels

Figure 3 Failure of cold-formed angle cleats connected to the flange only

Hot-rolled angle cleats connected to the flanges only

Distortional buckling of the stub column was experienced in all the tests conducted. In Load Case 1, where the compressive load was applied at the centre, distortional buckling resulted in equal outward movement of the column flanges as shown in Figure 4 (a). Large deformations occurred in both flanges of the column just above the angle cleat. In the other two cases distortional buckling was more pronounced in the flange subjected to a larger force. The final mode of failure in all tests where rigid cleats were used was local buckling in the flange (see Figure 4(b)). Local buckling occurred after considerable rotation of the flange above the angle cleat. After local buckling, the applied load dropped slowly.

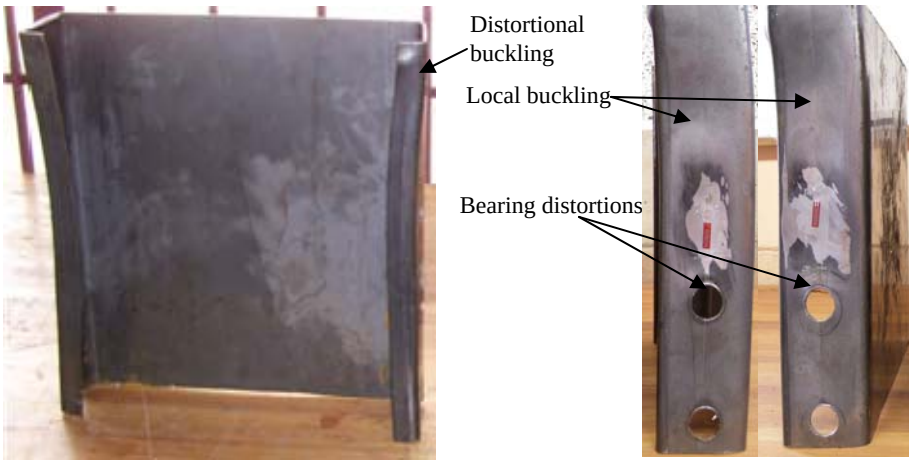

(a) Distortional buckling (b) Buckling and bearing failure

Figiure 4 Filure of hot-rplled angle cleats connected to the flange only

After testing, it was observed that both channels experienced significant bolt-bearing deformations around the bolt-holes. These bearing deformations or distortions were found to be of equal magnitude in the first series of tests, where the compressive load was applied at the centre. In the other two cases, where the load was applied eccentrically from the centre, no bearing deformation was observed in the lightly loaded flange. Bearing distortions were more pronounced in the flange that transferred more load to the angle cleat (Figure 4(b)). Bearing distortion of steel around bolt-holes is a ductile mode of failure and provides the ductility required for moment redistribution.

Hot-rolled angle cleats connected to the flanges and web

As in hot-rolled angle cleats connected to the flange only, three modes of failure were identified in these base connections, that is, distortional buckling, local buckling of the channel section and bearing failure around the bolt-holes. Distortional buckling was observed in load cases 1-3. Local buckling of the channel section was the final mode of failure in all load cases. Deformation began in the flange as a result of distortional buckling and progressed into the web. Unlike base connections of hot-rolled angle cleats connected in the flange only, where local buckling occurred just above the cleats, in this case local buckling was experienced at the beam-column connection. This mode of failure did not

occur close to angle cleats because the base was significantly stiffened. Bearing distortion was more visible in specimens where the load was applied away from the column centre (load case 2, 3 and 4). .

(a) Local buckling due to Load case 1 (b) Local bucking due to Load Case 4

Figure 5 Failure of hot-rolled angle cleats connected to the flange and web

Test Results

A summary of the average maximum load and moment, applied on the base connections and the calculated unfactored resistances are given in Table 2. In this table, N_{max} and M_{max} are the maximum vertical force and moment applied to the base, respectively, N_y is the squash load ($A_{ef}f_y$) of the column and V_{rj} is the resistance of two bolts. The area (A_{ef}) is calculated based on the effective properties of the sections. The joint resistance V_{rj} is evaluated based on the bearing resistance of the plate, which in all cases is much less than the shearing resistance of the bolts. Based on the design recommendation of Kemp (2001), a coefficient C of 1.8 for a standard washer under the nut and bolt head is used in the bearing resistance calculations. This factor depends on the ratio of bolt diameter to member thickness. Bearing resistance or capacity (B_r) of the connections is established from the following equation.

$$B_r = atf_u \leq Cdtf_u \quad (1)$$

where, t is the thickness of channel, d is the diameter of bolt, f_u is the minimum tensile strength of the channel, a is the distance from centre of hole to the edge towards which the force is directed and C is the bearing coefficient. It is assumed that the force applied to the bolts in the flanges is shared equally between the two bolts. These resistance values are determined using the South African code, SANS 10162-2-2005. This code is based on the Canadian structural steel code, CAN-S16.1-M89.

Table 2 Comparison of calculated and tests results

Load Cases	Column Section	N_{max} (kN)	M (kNm)	Load on Angle Cleats (kN)		N_y (kN)	Vrj (kN)
				LHAC	RHAC		
Cold-formed angle cleats connected to the flange only							
1	300x50x20x3	79.06	0	39.53	39.53	213.27	74.69
2	300x50x20x3	57.79	2.89	19.26	38.53	213.27	74.69
3	300x50x20x3	37.63	5.64	0	37.63	213.27	74.69
4	300x75x20x3	16.00	8.00	0	16.00	247.60	68.04
Hot-rolled angle cleats connected to the flange only							
1	300x65x20x3	200.00	0	100.00	100.00	282.73	102.36
2	300x65x20x3	150.00	7.50	50.00	100.00	282.73	102.36
3	300x65x20x3	110.00	16.50	0	110.00	282.73	102.36
4	300x75x20x3	43.67	22.33	0	43.67	247.60	68.04
Hot-rolled angle cleats connected to the flange and web							
1	300x75x20x3	201.23	0	100.62	100.62	254.41	79.03
2	300x75x20x3	159.76	8.00	53.25	106.51	254.41	79.03
3	300x75x20x3	85.28	12.79	0	85.28	254.41	79.03
3	300x75x20x3	36.98	21.27	0	36.98	254.41	79.03

A comparison of the test results and calculated unfactored yield resistance shows the applied load for each case to be smaller than the unfactored yield resistance (N_y). The maximum vertical force of Load Cases 1, 2, 3 and 4 for the base connection with cold-formed angle cleats connected in the flange only, achieved 37%, 27%, 18% and 6% of the squash load, respectively. These low forces were caused by the premature failure of the cold-formed angle cleats. Significant

increases in load is realised when hot-rolled angle cleats are used, instead of the cold-formed angle cleats. However, the yield resistance of the channel is not attained due to local buckling failure. Load Cases 1, 2, 3 and 4 achieved 71%, 53, 39% and 18% of the yield resistance when the hot-rolled angle cleats are connected to the flange only. Local buckling was initiated in the flanges followed by the buckling of the web. In order to make the base connection stiffer than the one with hot-rolled angle cleats in the flange only, another angle cleat was connected to the web in the last configuration. As indicated in Table 2, this configuration did not achieve the desired results. There is little or no increase in base connection resistance, compared to the base connection with hot-rolled angle cleats connected to the flange only. This can be explained by the fact the base connection did not fail, instead the base resistance is determined by the strength of the column section.

In the base configurations with the angle cleats connected to the flanges only and the load is applied at the centre, the stress from the column to the bolts is transferred at approximately 45°. Half of this load is resisted by the Right Hand Angle Cleat (RHAC) and the other half is resisted by the Left Hand Angle Cleat (LHAC). In Load Case 2 of the same base configuration, the load is applied at one third of the depth of the channel. Consequently, there is a proportional distribution of the force from the column, with two-thirds of the force carried by the Right Hand Angle Cleat and the other one-third carried by the Left Hand Angle Cleat. Obviously this means that one column flange is more stressed than the other. In Load case 3, where the load is applied at the edge of the channel, the stresses are mainly concentrated in the corresponding angle cleat connection. The other base connection carries very little or no force at all. All load cases failed when the heavier loaded flange achieved a force of about 38kN for the cold-formed angle cleats and 100kN for the hot-rolled angle cleats. The bolts connecting the column to the angle cleat did not fail. Bolt-bearing distortions around bolt-holes (not complete failure) were only observed around holes. This means that the capacity of the bolts in shear and bearing was not reached despite the fact that partial bearing failure occurred in the connection.

Load-displacement graphs

The behaviour of the three base connections are shown by load-deformation curves in Figures 6, 7 and 8. These load-displacement curves represent the average curve for the tests in each load case. The load-deflection curves for Load Case 4 are deliberately excluded from these graphs because the base connections

experienced relatively large deflections and low loads in comparison with other load cases. The load-deflection curves show the initial stages to be linear followed by a non-linear range. The non-linear response and decreasing connection stiffness exhibited late in the loading sequence is attributed, primarily, to local buckling in the flange. The non-linear response exhibited by the structures occurs at approximately 85% of the ultimate load. After this point large deformations take place and result in the collapse of the base. Both graphs show decrease in load carrying capacity of the base connections as the eccentricity of the applied load was increased.

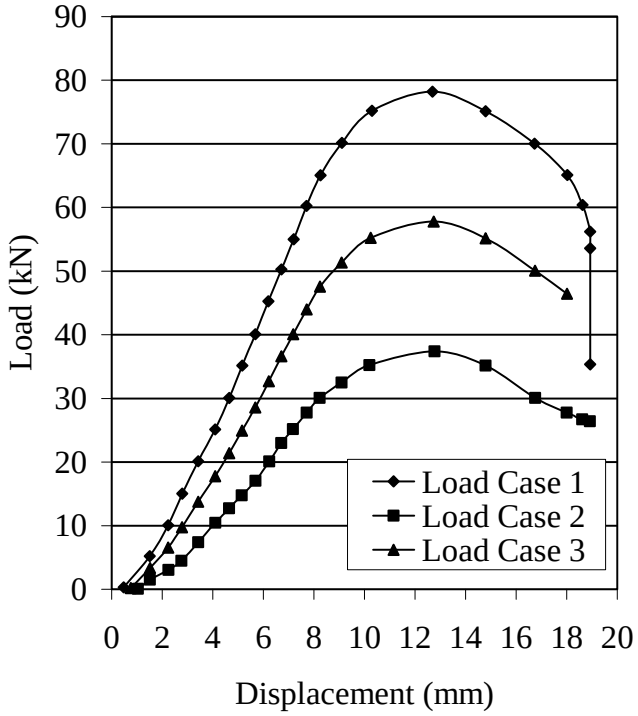

Figure 6 Cold-formed angle cleats, connected to the flanges

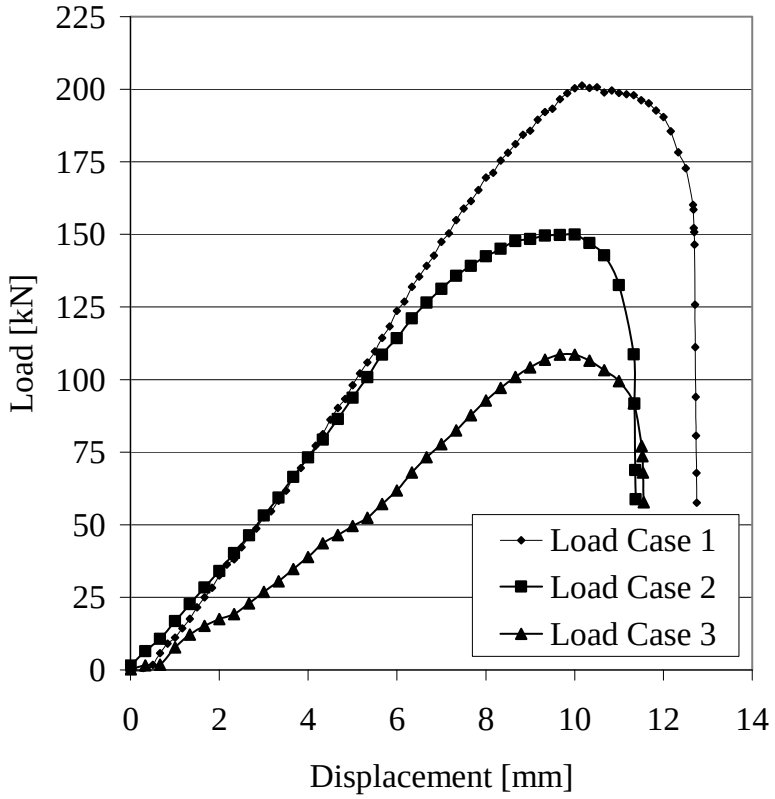

Figure 7 Hot-rolled angle cleats, connected to the flange only

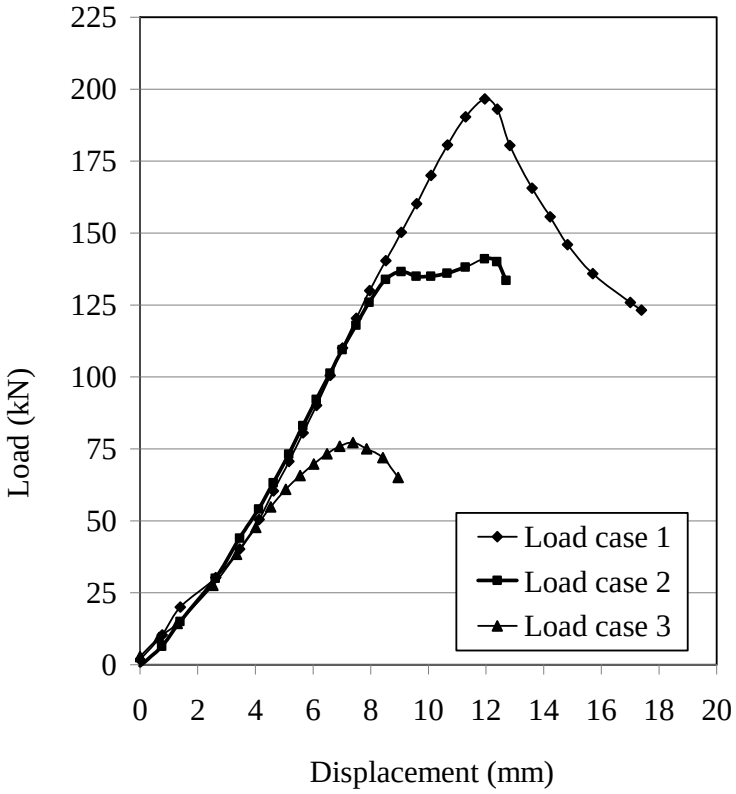

Figiure 8 Hot-rolled angle cleats connected on both the flanges and web

Conclusions

This paper shows that angle cleat base connections can be a viable alternative to welded base connections, especially for cold-formed portal frames spanning from 5 to 16m. Observed modes of failure include premature deformation of the angle cleats, distortional and local buckling of the channel section and bearing distortion in the bolts. Premature deformation of the angle cleats was experienced in all tests where cold-formed angle cleats were used, whilst distortional buckling, local buckling and bearing failure were experienced in connections with hot-rolled angle cleats. The final mode of failure of base connections with hot-rolled angle cleats was local buckling of the flange followed by the web. Local

buckling was made more critical by stress concentrations in the bolted flange. The non-linear load-shortening response exhibited late in the loading sequence of all the load cases is attributed, primarily, to ductile bolt-bearing deformation and local yielding of the flange below the inside bolt. Bearing distortion of bolt-holes is important in that it provides the ductility required for moment redistribution.

Acknowledgements

The authors wish to thank University of Johannesburg Research Committee (URC) for sponsoring this research.

References

CAN – S16.1 – M89, “Steel Structures for Buildings – Limit States Design”, Canadian Standards Association, Rexdale, Ontario, Canada, 1989.

Dundu, M. and Kemp, A.R., “Strength requirements of single cold-formed channels connected back-to-back”, Journal of Construction Steel Research 2006, 62, 250-261.

Dundu, M. and Kemp, A.R., “Plastic and flexural behaviour of single cold-formed channels connected back-to-back”, Journal of Structural Engineering, ASCE 2006, 132(8), 1223-1233.

Kemp, A.R., “Bearing capacities and modes of failure in single-bolt lap joints”, Journal of the South African Institution of Civil Engineering, 2001, 43(1), 13-18.

SANS 10162-2, “South Africa Standard Code of Practice for the Structural use of Steel, Part 2 - Limit States Design of Cold-formed Steelwork”, South African Bureau of Standards, Pretoria, 2005.

Twentieth International Specialty Conference on Cold-Formed Steel Structures
St. Louis, Missouri, U.S.A., November 3 & 4, 2010

SOME ASPECTS ON SEISMIC DESIGN OF FRAMES DESIGNED WITH COLD FORMED STEEL SHAPES.

By Eng. Gabriel Valencia.[1]

ABSTRACT.

The response of cold-formed steel structures to seismic excitations is not the same as that of structures designed with rolled shapes, in fact, the seismic design codes require that the shapes, meet minimum width/thickness ratios, which virtually no commercial cold formed steel shapes meet, so the design of structures with these elements is excluded from those codes. Different types of beam-to-column connections, made using cold-formed steel shapes have been tested, in order to establish their response to cyclic loads of increasing magnitude. The analysis of these connections using theoretical models with Finite Element Analysis (FEA), and through monotonic and cyclic laboratory tests specimens is presented. Finally, based on the analysis of the hysteretic behavior, as well as the FEA, some recommendations for the design and use of moment frames designed with cold-formed steel shapes in seismic areas are presented.

1. INTRODUCTION.

In several codes and design specifications, for steel structures, it is established that when the seismic response modification coefficient, R, used to determine the seismic design forces, is equal to or less than 3, the structure is not required to satisfy seismic provisions, ie, AISC (AISC, 2005), Sec.1; FEMA 450, Sec. 8.2.1 and Table 4.3-1; ASCE7, Sec. 14.1.2, on the condition that these structures are used in Seismic Categories B, C or D, and in certain cases in Categories D or E. For the specific case of design of structures constructed with light-framed shapes, ASCE7 (ASCE, 2005) in Sec. 14.1.2, says: "An R factor as set forth in Table

[1] *Professor of the National University of Colombia, Bogotá, Colombia*

12.2-1 is permitted where the structure is designed and detailed in accordance with AISI Lateral, for light-framed cold-formed steel construction … Systems not detailed in accordance with AISI-Lateral shall use the R factor designated for Structural steel systems not specifically detailed for seismic resistance", that means, R = 3. It is worth noting that AISI-Lateral (AISI, 2004), contains only design requirements for shear walls, diagonal strap bracing and diaphragms, but not for moment frames (MFs).

In summary, when designing MFs constructed with cold-formed steel shapes, according to the mentioned codes, a seismic response modification coefficient, R, of 3 can be used, at least if the structure will be localized in categories B, C or D (and in some cases E or F). Nevertheless, the author considers that designing with values of R greater than 1.0 (eventually 1.5), can lead to unsafe and unreliable designs, and for that reason, has considered it necessary to study the behavior of the beam-to-column connections of light-framed members, loaded by seismic actions (cyclic actions), as a first approach to the study of the behavior of MFs constructed with cold-formed steel shapes in seismic areas.

2. CONNECTIONS PROGRAM.

Within the connection qualification program under process at the National University of Colombia under direction of the author, 28 beam-to-column connections constructed with cold-formed steel shapes have been studied analytically and experimentally. Beams, as well as columns, have been designed with double C shapes, arranged in a box-type section or an I-section, varying characteristics such as sections combinations, width-thickness ratios and type of reinforcement (stiffeners, continuity plates, etc.). Among the studied connections, there are very simple ones such as that of a box-type beam weld connected to a box-type column, without any special reinforcement, or others with I-section beams, some with stiffeners, continuity plates, seat plates, shear plates, lateral plates, and combinations of reinforcements such as those mentioned. It must be noted that in all cases the feasibility of construction of the connection has been taken into account. The theoretical behavior of the connections was evaluated considering, among others, two very important aspects from the point of view of seismic response in the building in which they are intended to be used: 1) theoretical resistance of the members, according to the principle of strong-column/weak-beam, and 2) resistance of the elements of the connection such as plates, welds, stiffeners, etc, calculated assuring that they remain in the elastic range even if the connected members reach plastic deformation. In Table 1 and Figure 1 the different types of studied connections are shown.

Table 1. Analytical and experimental models.

Ref	Beam	Column	Connection elements and stiffeners
C-1	Box-type	Box-type	A seat plate
C-2	Box-type	Box-type	As C-1 plus stiffeners at the column (as continuity plates)
C-3	I-Section	Box-type	A seat plate, a top plate and a shear plate
C-4	I-Section	Box-type	As C-3 plus stiffeners at the column (as continuity plates)
C-5	Box-type	Box-type	Lateral plates
C-6	Box-type	Box-type	Extended continuity plates

Notes: (1) In all cases, members were formed by 2 C shapes.
(2) For each type of assembly, different width-thickness ratios were tested

3. ASPECTS OF CONNECTIONS BEHAVIOR.

The theoretical behavior of the connections was evaluated with finite element analysis, FEA, with both elastic and inelastic models. The theoretical resistance of the chosen sections was determined according to the AISI specifications (AISI, 2004), considering the post-buckling resistance. Given that various width-thickness ratios were used, in some cases, the expected resistance to bending came well below the flexural plastic resistance, M_p, evaluated with the theoretical yield strength (as if it were a compact section), due to the appearance of the local instability phenomena, developed even in the elastic range. AISI considers this phenomenon specifying the use of an effective section, which's properties: area, inertia and modulus of the section, are less than those of the real section. AISI accepts that the design resistance be "based on inelastic reserve capacity, when some special conditions are met: 1) the member is not subject to twisting or to lateral, torsional, or torsional-flexural buckling, 2) the effect of cold work of forming is not included in determining the yield point, F_y, 3) the ratio of the depth of the compressed portion of the web to its thickness does not exceed λ_1, 4) the shear force does not exceed $0.6F_y\,ht$ for LRFD, 5) the angle between any web and the vertical does not exceed 30 degrees" (AISI, p61). In any case, the nominal resistance, M_n, shall not exceed $1.25\,S_eF_y$.

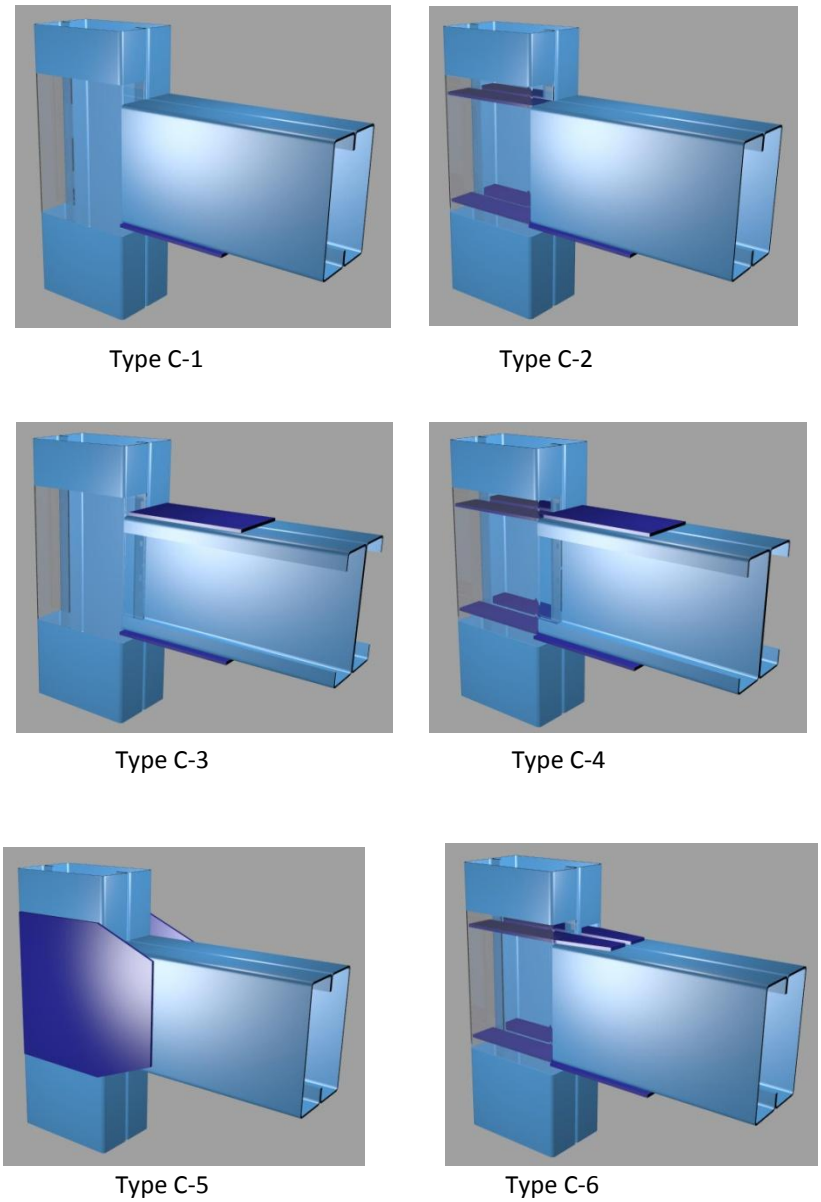

Figure 1 – Sketches of the analytically and experimentally analyzed models.

On the other hand, the design of the elements of the connections, that is, stiffeners, continuity plates, seat plates, shear plates, lateral plates as well as welded joints, was performed considering that the stresses acting on them for maximum expected actions, do not exceed the theoretical yield strength, F_y, of the steel used in their fabrication, this in order to assure that the inelastic rotations of the connection are nor influenced by an inelastic behavior of such elements. Finally, the connections were analyzed using FEA within the theoretical studies, with the use of two analytical programs, one of normal use in design offices (SAP), and one that allows more detailed modeling (ANSYS). Both elastic and inelastic analyses were conducted, with and without formulation of local buckling. For the later, bilineal stress-strain curves were defined with $E_{inel} = E/30$.

These FEA analyses were carried out searching for possible correspondences with the behavior determined in the tests, so as to recommend theoretical analysis procedures that are less demanding and costly than experimental ones, for design of connections equal or similar to those used in these researches. In Figure 2 various aspects of analysis were observed for one of the type C-5 connections (Ref. Table 1 and Fig. 1) performed on ANSYS.

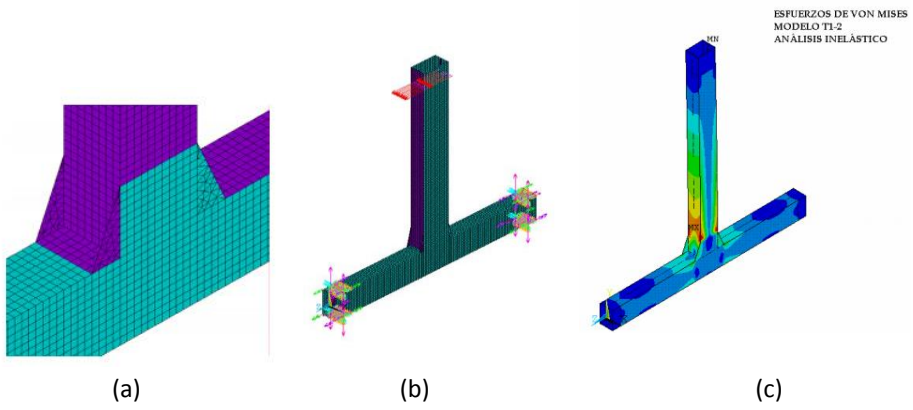

Figure 2. With reference to connection C-5 (Fig. 1), (a) meshed for FEA analysis, (b) constraints and loads, (c) Von Misses stress diagrams obtained through an inelastic analysis

4. EXPERIMENTAL PHASE.

The trend of actual codes, with respect to the study of connections, is to establish that the behavior of these should be verified by realistic scale cyclic testing, "because the initiation and propagation of fracture cannot reliably predicted by analytical means alone" (AISC, 2005b). Such tests must consider the loading history, for which loading protocols are specified. For the analysis of connections in the present research, the protocol established by AISC in appendix S for connections with standard hot-rolled shapes, was used in the initial tests.

Nevertheless, the results of these first tests demonstrated that it is not convenient to use this protocol, as it did not allow visualizing of the behavior of the connection in the elastic range, which for the case of light-framed shapes holds great importance, due to the development of local buckling with stress less than the yield strength. For this reason, the protocol presented in Table 2 was adopted, in which deformation refers to the displacement of the loaded end of the beam, as a function of δ_y which is the correspondent to the appearance of the theoretical M_y of the beam. The load application rate used was 0.1 mm/s, so that the stresses increments at beam flanges were within the range of 0.9-4 ksi/s (6-30 MPa/s), which is used in simple tension tests. The typical test sample is shown in Figure 3. The test variables were controlled through a system of automatic data collection and a numeric dynamic control actuator for the application of loads.

In Figure 4 the behavior of one of the C-5 connections during loading process can be seen. According to the forecast obtained through an inelastic FEA with ANSYS, Figure 4(a), in the corners of the box section of the beam, high stress concentrations should be present. This phenomenon was widely confirmed during the tests, as can be seen in Figure 4(b) and (c).

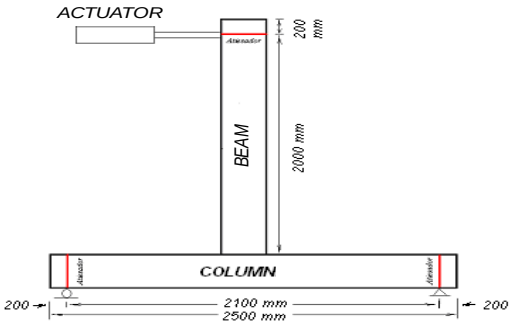

Figure 3. Prototype of the tested connection.

(a) (b) (c)

Figure 4. With reference to connection C-5 (Ref Fig 1), (a) Von Misses stress distribution, (b) sample at an intermediate load phase, (c) sample at the end of the test [11].

Table 2. Loading protocol.

Load Step	Cycles Qty	Displacement
1	6	0.25 δ_y
2	6	0.50 δ_y
3	6	0.75 δ_y
4	4	1.00 δ_y
5	4	1.25 δ_y
6	4	1.50 δ_y
7	2	1.75 δ_y
8	2	2.00 δ_y
9	2	2.25 δ_y
10	2	2.50 δ_y
11	2	2.75 δ_y
12	2	3.00 δ_y

5. RESULTS

5.1 Moment-rotation curves – Monotonic load.

The curve presented in Figure 5(a) shows the variation of the displacements measured at the end of the beam with respect to the load increments, corresponding to one of the tests with monotonic load, in this case, for the connection in which lateral plates were installed (C-5 type connection, Fig. 1). The figure includes the theoretical inelastic curves found with the two analysis software programs (SAP and ANSYS). These curves were plotted for all tests, and in general their aspect coincides with that of Figure 4(a), except for connections without any reinforcement.

5.2 Load History Curves. All connections were also tested with incremental cyclic loads. The results were represented with hysteretic curves. In Figure 5(b) the corresponding curve for one of the C-5 type connections is presented. The great resistance degradation is evident at few cycles from the beginning of the loading process due to the local buckling phenomena. As can be seen in Figure 5(c), in the initial loading phase (i.e. until maximum resistance is attained), the curve with monotonic load represents with good accuracy, the behavior of the connection, nevertheless, in the inelastic range, the observed behavior in the hysteretic curve shows a degradation of resistance, significantly greater than what is predicted by the monotonic curve.

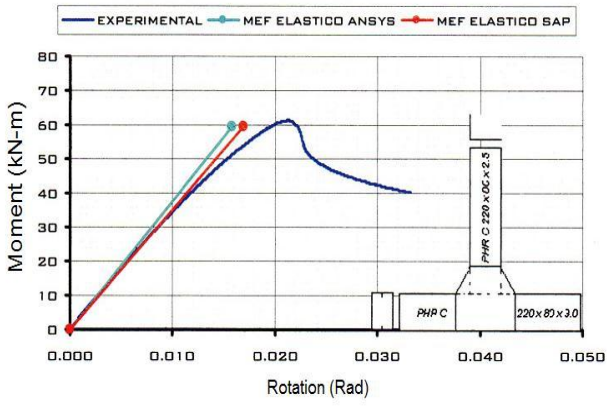

Figure 5(a). Moment-rotation curve, including the theoretical curves determined with SAP and ANSYS for connection C-5 (see Fig 1).

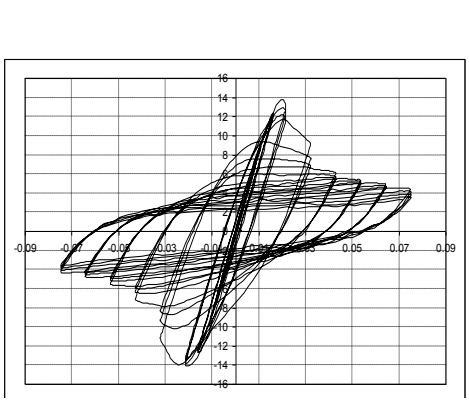

(b)

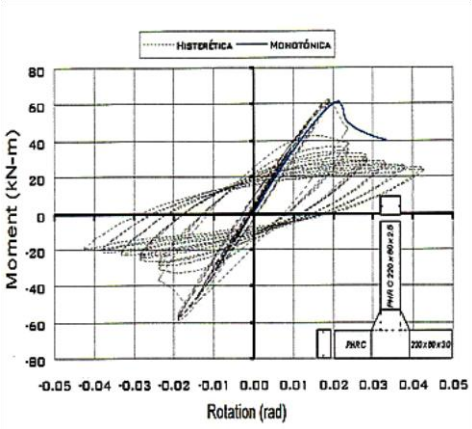

(c)

Figure 5 (Cont.) With reference to connection C-5 (See Fig. 1), (b) hysteretic curve for the same connection, (c) correlation of the monotonic and cyclic curves. Both are tests result curves.

In general, M-θ curves estimated through the inelastic models kept good correlation with the real curves. Although estimated curves loose correlation approximately up to 12%, they basically keep the same trend to degrade in resistance. This can be related to the fact that theoretical curves do not contemplate the phenomenon of local buckling, even though they do consider the inelastic range of the steel (Villar-Valencia, 2007).

5.3. Failure Types. A summary of the failures detected in the tests, are:

- Great deformations at the panel zone, Fig. 6a.
- Local buckling of the flanges in compression with stresses below yield strength, Fig. 4b.
- Tear of the walls in the column when the beam is an I section, Fig. 6c.
- Tear in the flanges in zones of high stress concentrations, at the points where reinforcements used in the different connections end, Fig. 4c and 6b.
- Tear in the flanges in the zones of high stress concentrations at the beam to column joint when there are no reinforcements, Fig. 6d.
- Local buckling of the flanges between welds (when intermittent welds are used) in zones of greater moment.
- Initiation of local buckling of the web at a distance d/2 from the connection, Fig. 6e.
- Local buckling of the flange near the reinforcements end, Fig. 4c and 6f.

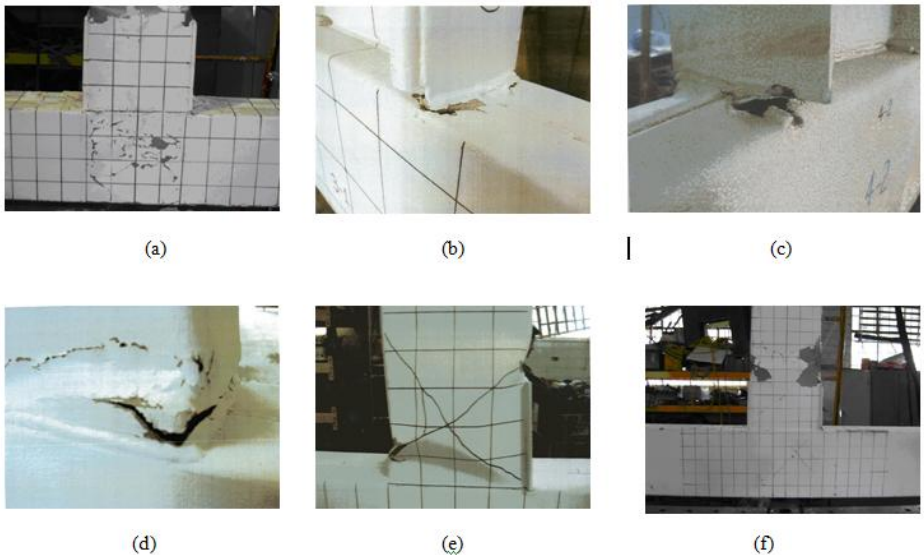

Figure. 6 Some of the failures detected in the tests. Pictures (a) and (f) from Valencia-López, 2005, others from Valencia, Salinas, 2007.

5.4 Response modification coefficient, R estimation.

For estimating the response modification coefficient, R, the capacity spectrum method, and the Newmark and Hall (Newmark, 1982) method were used. Some MFs frames were analyzed. Their characteristics were, 20' (6.0 m) of span and three floors with height between floors of 8.2' (2.5 m), with connections modeled with M-θ curves based on the results of the theoretical analyses and laboratory tests, as studied previously.

Considering the resistance and rigidity degradation, the conclusion that the value of R lays between 1.5 and 1.8 is drawn. The fact is that rigidity degradation limits greatly the response of the structure in the inelastic range, due to the appearance of the phenomena described in 5.3, showing in the capacity curve as a loss of resistance and lateral rigidity, where for small load increments, deformations increase considerably.

6. CONCLUSIONS.

1. Given the low energy dissipation capacity in the inelastic range, as a consequence of local instability shown by the elements, the use of cold-formed steel shapes in structures that require especial or moderate energy dissipation must be made carefully. Actually, according to AISC (AISC, 2005b) criteria, frames resistant to especial or intermediate moments shall not be designed with these types of elements. The resistance degradation as a result of the action of dynamic loads is very strong, and that fact limits its seismic behavior.

2. It is not convenient to use beam-column connections made with cold-formed steel shapes without using internal reinforcements as continuity plates at the column, as well as external reinforcements. The most satisfactory behaviors have been obtained for C-4, C-5 and C-6 connections. Connections with no reinforcements (internal and/or external) have a poor performance, and their resistance is below the bending resistance of the beams.

3. The weld detailing is very important. Some of the tested samples showed local failures at the ends of welds applied between C shapes of the beam, just away from the interface with the column, because these welds were not so long.

4. Beams made with I sections composed by two back-to-back C shapes, connected to a box-section type column, show non-recommendable behaviors. Not only deformations of connections are very significant, but there are also tears of the columns, torsion phenomena of the beams, buckling of compression flange (despite the lips), and other local phenomena which diminish capacity sensibly.

5. FEA models with ANSYS, shows a good correlation with the experimental results and predict with an approximation no farther than 10% the basic parameters, such as deflections, moments and generally the connection behavior with monotonic loads (López-Valencia, 2005). Nevertheless, the degradation of the resistance in cycles after the initial ones is not detected with FEA.

6. For the design of MFs, “as long as no further researches are conducted, it is recommended to use a value of R for seismic design between 1.2 and 1.5, for structures built with cold-formed shapes, with width-thickness ratios of

around 100 to 200 for webs and of 30 to 40 for flanges, as long as continuity plates in the interior of the column are used" (López-Valencia, 2005).

7. The degradation of the moment capacity that is found in tests with cyclic load is considerably greater than that with monotonic load. For this reason it is not recommended to determine the behavior of this type of shapes based on monotonic tests results.

8. Up to the point where this research has come, no models of columns with axial loads have been tested yet. It is intended to be done in further phases, but it is estimated that their influence will not be significant, given that the main instability phenomena are presented in the beams and in the connection itself

ACKNOWLEDGMENTS

The results of this ongoing research have been obtained thanks to the outstanding work of engineers Enrique López (López-Valencia, 2005) and Sergio Villar (Villar-Valencia, 2007), students of the Master's program in Structures at the National University de Colombia in Bogotá.

Appendix – Notation.

E = Modulus of elasticity of steel = 29,000 ksi (200000MPa).
F_y = Specified minimum yield stress of the compression flange
h = Distance between the flanges less the inside corner radius on each side,
t = Thickness of element
M_n = Nominal flexural strength
M_y = Yield moment about the axis of bending
S_e = Effective section modulus
λ_1 = With-thickness limit ratio equal to $\frac{1.11}{\sqrt{F_y/E}}$
δ_y = Displacement of the loaded end of a beam which correspond to the appearance of M_y.
θ = Rotation angle of a connection.

REFERENCES.

AISC, American Institute of Steel Construction, 2005, Specification for Structural Steel Buildings, Chicago, Il.

------, Seismic Provisions for Structural Steel Buildings, 2005, AISC 341-05, Chicago, Il.

AISI, American Iron and Steel Institute, 2001, North American Specification for the Design of Cold-Formed Steel Structural Members, Washington, DC.

-------, 2004, Standard for the Design of Cold Formed Steel Framing, Lateral Design, Washington, DC,.

ASCE, American Society of Civil Engineers, 2006, Minimum Design Loads for Buildings and Other Structures - ASCE7-05, Reston, Vg.

Jong-Kook H., Atsushi S., Chia-Ming U. & Ken W., Cyclic Testing of Cold-Formed Steel Special Bolted Moment Frame Connections, bssconline.org/08ProposalPDFs/ASCE.

López-Guerrero, E. & Valencia-Clement, G, 2005. Precalificación de Conexiones para Pórticos de Lámina Delgada, Bogotá, Universidad Nacional de Colombia.

NEHRP, National Earthquake Hazards Reduction Program, 2003, Recommended Provisions for Seismic Regulations for New Buildings and other Structures, FEMA 450, Federal Emergency Management Agency.

Newmark, N.M. & Hall W.J., 1982, Earthquake Spectra and Design. California, EERI Monograph Series, EERI, Oakland.

Valencia, G. 2002, Estructuras de Acero. Bogotá, Colombia Escuela Colombiana de Ingeniería.

Villar-Salinas, S. & Valencia-Clement, G., 2007, Calificación de Conexiones para Pórticos de Lámina Delgada – 2ª Parte, Bogotá, Colombia, Universidad Nacional de Colombia.

Yu, Wei-Wen, 1991, Cold-Formed Steel Design. New York, USA. Second Edition.

Twentieth International Specialty Conference on Cold-Formed Steel Structures
St. Louis, Missouri, U.S.A., November 3 & 4, 2010

Screw Connections Subject to Tension Pull-Out and Shear Forces

R. M. Francka[1] and R. A. LaBoube[2]

Abstract

Currently, the behavior of screw connections subject to combined tension pull-out and shear forces is not well understood. An experimental study was conducted at Missouri University of Science and Technology to better understand the relationship or interaction between these forces. The test program evaluated four parameters that may influence the behavior of pure tension and pure shear in screw connections: the thickness of the sheet not in contact with the screw head, the ultimate strength of the steel, the ductility of the steel, and the screw diameter. Based on the behavior observed and analysis of the test data, this work formulated new design recommendations for use in calculating the design capacity of screw connections subject to this potential limit state.

INTRODUCTION

Screws are a practical and economical means to connect cold-formed steel structural members. They provide a rapid and effective way of connecting members subject to tension, shear, or combined tension and shear forces. For example, common construction methods often use clip angles to connect bracing members or joists to supporting rim joists (Figure 1). These clip angles may be subject to simultaneous tension and shear forces.

In 1946, the American Iron and Steel Institute (AISI) began leading the building industry with the release of its first edition of the *Specification for the Design of Light Gage Steel Structural Members* (AISI, 1946). The most recent edition, the *North American Specification for the Design of Cold-Formed Steel Structural Members* (AISI S100*)*, was released in 2007.

[1] Former graduate student, Missouri S&T, Rolla, MO
[2] Curators Distinguished Teaching Professor, Missouri S&T, Rolla, MO

Currently, the specification includes provisions that assess the design strength of a screw connection subject to pure tension, pure shear, and combined tension pull-over and shear forces. Additional guidance is required to determine the design capacity when screw connections are subject to both combined tension pull-out and shear forces.

Figure 1 Screw Connections Potentially Subject to Pull-out and Shear Forces

LITERATURE REVIEW

Several research studies provide the foundation for this research study (Pekoz, 1990; Zwick and LaBoube, 2006). Pekoz investigated screw connections subject to pure tension pull-out and pure shear forces alone. Zwick and LaBoube studied the consequence of combined pull-over and shear loading on screw connections. Additional information pertaining to these studies and the behavior of screw connections is given by Yu and LaBoube (2010).

These research studies form the basis for the design provisions of the *North American Specification for the Design of Cold-Formed Steel Structural Members* (AISI S100, 2007). The AISI S100 nominal strength, P_n, are as follows:

For shear alone the nominal shear strength shall be calculated as follows:

If $t_2/t_1 \leq 1.0$, P_{ns} shall be taken as the smaller of

$$P_{ns} = 4.2(t_2^3 d)^{1/2} F_{u2} \quad (1)$$

$$P_{ns} = 2.7 t_1 d F_{u1} \quad (2)$$

$$P_{ns} = 2.7 t_2 d F_{u2} \quad (3)$$

If $t_2/t_1 \geq 2.5$, P_{ns} shall be taken as the smaller of

$$P_{ns} = 2.7 t_1 d F_{u1} \quad (4)$$

$$P_{ns} = 2.7 t_2 d F_{u2} \quad (5)$$

If $1.0 < t_2/t_1 < 2.5$, P_{ns} shall be calculated by linear interpolation between the above two cases.

Where d = nominal screw diameter, P_{ns} = nominal shear strength per screw, t_1 = thickness of member in contact with screw head or washer, t_2 = thickness of member not in contact with screw head or washer, F_{u1} = tensile strength of member in contact with screw head or washer, F_{u2} = tensile strength of member not in contact with screw head or washer.

For tension alone the nominal pull-out strength, P_{not}, shall be calculated as follows:

$$P_{not} = 0.85 t_c d F_{u2} \quad (6)$$

Where d = nominal screw diameter, t_c = lesser of the depth of penetration and thickness t_2, P_{not} = nominal pull-out strength per screw, F_{u2} = tensile strength of member not in contact with screw head or washer.

For tension alone the nominal pull-over strength P_{nov}, shall be calculated as follows:

$$P_{nov} = 1.5 t_1 d_w' F_{u1} \quad (7)$$

Where t_1 = thickness of member in contact with screw head or washer, F_{u1} = tensile strength of member in contact with screw head or washer, d_w' = effective pull-over diameter determined in accordance with (a), (b), or (c) as follows:

(a) for a round head, a hex head, or hex washer head screw with an independent and solid steel washer beneath the screw head
$d_w' = d_h + 2t_w + t_1 \leq d_w$
where
d_h = screw head diameter or hex washer integral washer diameter
t_w = steel washer thickness
d_w = steel washer diameter

(b) for a round head, a hex head, or hex washer head screw without an independent washer beneath the screw head:
$d_w' = d_h$ but not larger than ½ in.

(c) for a domed (non-solid and independent) washer beneath the screw head, it is permissible to use d_w' as calculated in (a), with d_h as the washer diameter, t_w as the thickness of the material of the washer, and t_1 as previously defined. d_w' cannot exceed 5/8 in. Alternatively, pull-over design values for domed washers, shall be permitted to be determined by test in accordance with Chapter F of AISI S100.

For screw connections subject to combined shear and tension pull-out the following nominal strength relationship applies

$$\frac{Q}{P_{ns}} + 0.71\frac{T}{P_{nov}} \leq \frac{1.10}{\Omega} \tag{8}$$

Where Q = required allowable shear strength of connection, T = required allowable tension strength of connection, P_{ns} = nominal shear strength per screw = 2.7 $t_1 d F_{u1}$, P_{nov} = nominal pull-over strength of connection = 1.5 $t_1 d_w F_{u1}$, d_w = larger of screw head diameter or washer diameter.

Equation 8 is valid for connections that meet the following limits: 0.0285 in. $\leq t_1 \leq$ 0.0455 in., No. 12 and No. 14 self-drilling screws with or without washers, $d_w \leq$ 0.75 in., $F_{u1} \leq$ 70 ksi, and $t_2/t_1 \geq$2.5.

EXPERIMENTAL INVESTIGATION

Parameters evaluated in this study were the thickness of the sheet not in contact with the screw head or washer, the tensile strength of the material, the ductility of the material, and the screw diameter.

The mechanical properties of the sheet steel used in this investigation were determined by performing tensile coupon tests in accordance with ASTM A 370 (2007). Table 1 summarizes the results of the coupon tests and lists these properties: uncoated sheet thickness, yield stress, tensile strength and percent elongation. The notations N and L indicate the normal- and low-ductility steels, respectively.

Table 1 Material Properties

Specimen	Uncoated Thickness	Yield Stress	Tensile Strength	F_u/F_y	Elongation
	t (in)	F_y (ksi)	F_u (ksi)		%
20N	0.0297	41.41	48.295	1.166	42.58
18N	0.0394	29.25	47.315	1.618	38.38
16N	0.0521	62.205	75.49	1.214	29.69
14N	0.0724	68.39	74.32	1.087	34.38
20L	0.0327	102.75	105.99	1.032	2.34
18L	0.0375	91.175	91.18	1.000	1.17
16L	0.0508	84.25	89.645	1.064	3.91
14L	0.0675	117	120.565	1.030	2.73

Test Fixture. The test fixture consisted of a welded T-section and a rotating arm. This test fixture was essentially the same fixture as previously used by Stirnemann and LaBoube (2008). Welded T-sections were fabricated at 15°, 30°, 60°, and 75°. These variations in the angle of orientation induced different combinations of tension and shear forces, thus providing a range of data to define the interaction of tension pull-out and shear forces. The majority of the tests used three angles; fifteen degrees, thirty degrees, and sixty degrees, but a few tests were also completed at seventy-five degrees (Figure 2).

(a) 15° (b) 30° (c) 60° (d) 75°

Figure 2. Angles of Rotation

Test Specimen. Each test specimen consisted of a 12 in. x 12 in. deck section screwed to a 6 in. x 2 in. or 3 in. flat sheet (Figures 3 and 4). Details pertaining to the test specimen parameters and fabrication can be found in Francka and LaBoube (2009).

Figure 3 Typical Test Specimen Configuration

Figure 4 Illustration of Flat Sheet Attached to Test Fixture Plate

Test Procedure. Each prepared test specimen was mounted in an MTS 880 Material Test System (Figure 2). A computer data acquisition system recorded the load and displacement during each test. Load and displacement were recorded for each test at eight intervals per second to ensure that the maximum load was recorded.

During the initial testing, distortion of the flat sheet was observed thus the stiffness of flat sheet in the test specimen was further evaluated. Normal-ductility test specimens were stiffened using a brake press. Each of the long sides was bent to form ½ in. edge stiffeners (Figure 5).

Figure 5 Flat Sheet with Edge Stiffeners

Table 2 summarizes the tests performed to assess the contribution of the stiffer sheet on the connection strength.

Table 2 Comparison of Stiffened versus Unstiffened Specimens

		Ultimate Strength (lbf)					
		Unstiffened Specimen		**Average**	**Stiffened Specimen**		**Average**
Angle of Rotation	**15°**	468.8	494.3	481.6	374.3	452.4	413.4
	30°	352.7	353.6	353.2	321.1	365.3	343.2
	60°	320.9	337.6	329.3	317.7	323.5	320.6

Tilting of the screw and tearing were the failure modes observed in both stiffened and unstiffened specimens (Figure 6). Based on Table 2 and a comparison of the load versus deflection curves (Figure 7), the stiffness of the test specimens did not affect the ultimate strength of connections subject to combined tension pull-out and shear.

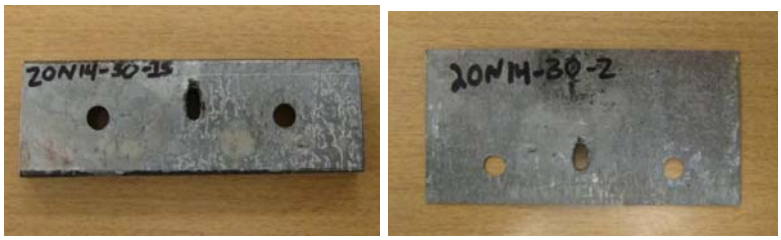

Figure 6 Comparison of Stiffened versus Unstiffened Failure Modes

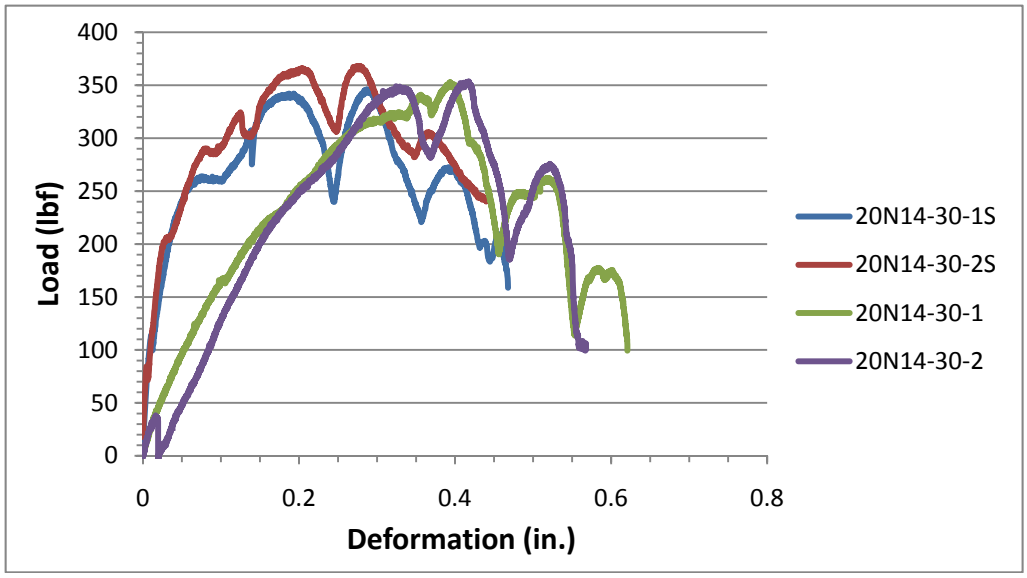

Figure 7 Load versus Deflection of 30° Test Specimens

TEST RESULTS

A total of eighty-four tests were performed. Thirty-nine were normal-ductility test specimens, and thirty-six were low-ductility test specimens.

Each test specimen was tested until failure. If the screw failed, the test was classified as inconclusive for purposes of this study and removed from the results. Screw failures occurred only in angles introduced to larger shear components, specifically 15° and 30°.

A typical load versus displacement curve is shown in Figure 8. The peaks of the curve represent the points at which the threads of the screw were pulled through the hole. As each layer of threads caught the sheet, the connection gained strength until it reached the peak strength of those threads and so on and so forth. The ultimate strength of the connection, P_u, was defined as the highest load carried during loading, regardless of deformation.

The typical failure mode observed in all tests was a combination of screw pull-out (tension failure), tilting of the screw (shear failure), and bearing of the sheet (shear failure). However, the normal- and low-ductility specimens did perform differently with respect to deformation and strength.

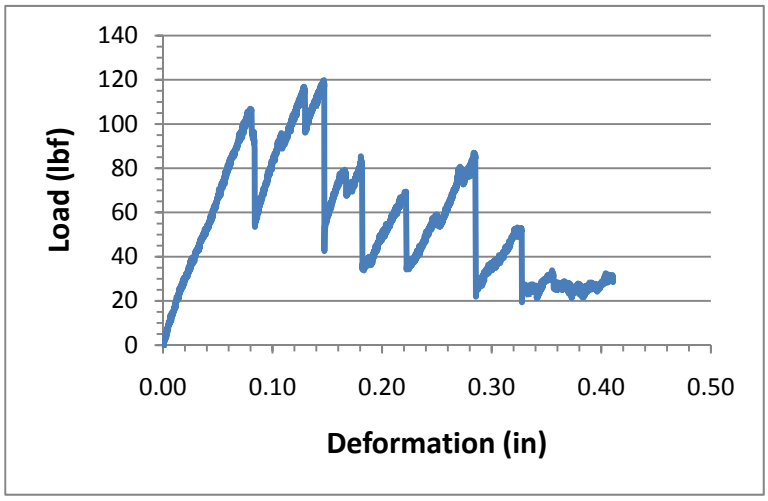

Figure 8 Example Load versus Deformation Curve

Normal-Ductility Specimens. All normal-ductility specimens experienced plastic deformation. Figure 9 shows a typical normal-ductility specimen after testing. Given the same sheet thickness and screw diameter, the normal-ductility steel deformed more than the low-ductility steel, and tearing of the sheet was more prominent. Figure 10 shows a normal-ductility specimen (18N) and a low-ductility specimen (18L). The distortion of the sheet was typical of all normal-ductility and low-ductility specimens. The distortion was not an effect of eccentricity, but rather of the combination of the tension pull-out and shears forces.

The ultimate strength, $P_{u,}$ was determined from the recorded data. Based on the angle of the test, the ultimate tension and ultimate shear forces P_{ut} and P_{uv}, respectively, were calculated using basic trigonometry. Table A.1 of Francka and LaBoube (2009) provides all of the test data.

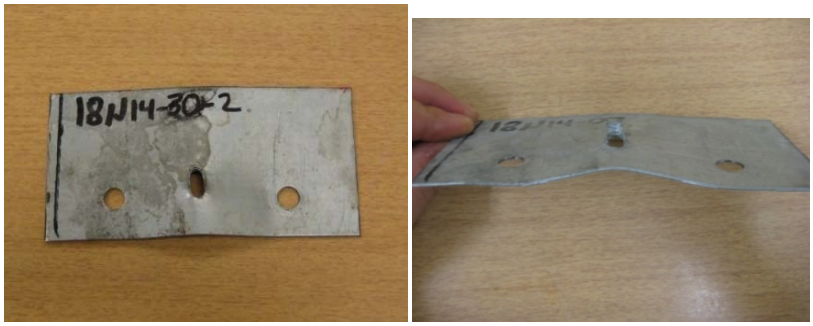

Figure 9 Typical Normal-Ductility Flat Sheet after Testing

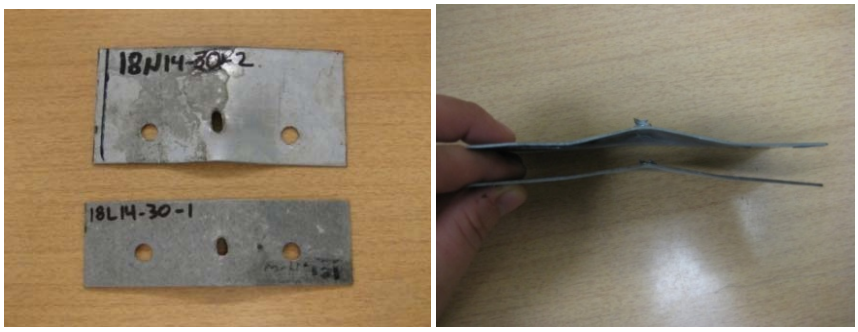

Figure 10 Comparison of Normal- and Low-Ductility Flat Sheets

Low-Ductility Specimens. Low-ductility specimens typically experienced less plastic deformation than the normal-ductility specimens. Figure 10 shows a low-ductility specimen (18L) and a normal-ductility specimen (18N). The low-ductility specimens had less deformation, and tilting of the screw was more prominent due to the resistance of the steel to allow tearing to occur (Figures 10 11). The same distortion effects observed in the normal-ductility specimens were apparent in the low-ductility tests, but they were typically less prominent. Many low-ductility specimens never reached inelasticity, and deformation was not permanent.

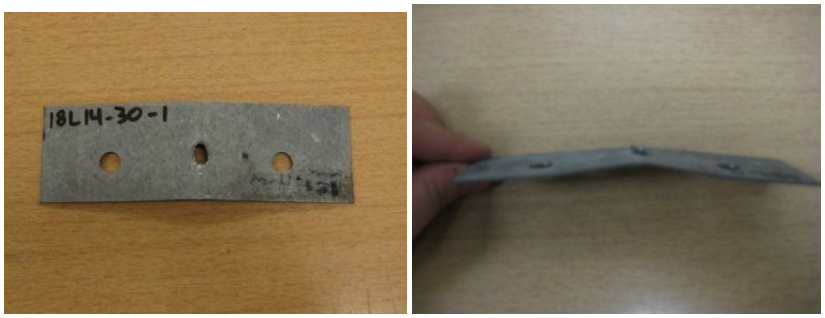

Figure 11 Typical Low-Ductility Flat Sheet after Testing

The ultimate strength, $P_{u,}$ was determined as for normal-ductility. The tension and shear components were also determined. Table A.2 of Francka and LaBoube (2009) contains the complete test data information.

DATA ANALYSIS USING AISI EQUATIONS

Using design Equations 1 through 6, the nominal strengths were calculated for tension pull-out, P_{not}, and shear, P_{ns}. The ultimate load applied to each test specimen was evaluated for its tension and shear components, P_{ut} and P_{uv}, respectively. These ultimate strength components were then normalized using the nominal strength equations to form the ratios P_{ut}/P_{not} and P_{uv}/P_{ns}. Francka and LaBoube (2009) presents complete details pertaining to the analysis results for the normal- and low-ductility test data, respectively.

Evaluation of Screw Diameter. Influence of the screw diameter was investigated to assess its' impact on the connection capacity. All of the tests performed for the 30° angle configuration used a broad range of screw sizes (No. 8, 10, 12, and 14). Figures 12 and 13 show a graph of the normalized shear strength, P_{uv}/P_{ns}, versus the normalized tension pull-out strength, P_{ut}/P_{not}.

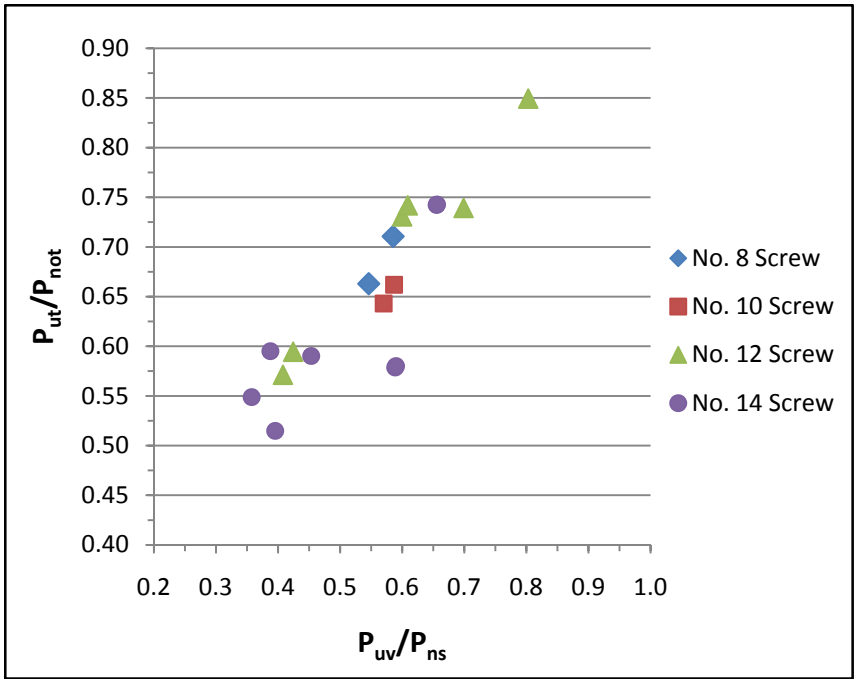

Figure 12 Evaluation of Screw Size - Normal Ductility

Based on the distribution of the data for all screw diameters at 30° although screw diameter affected the overall strength of the connection, it did not influence the interaction of the combined loading. These conclusions justified a reduction in the number of tests required for this study. The other test angle configurations were tested using only one screw size. At 60° No. 10 screws were used. At 15°, however, No. 14 screws were used due to the large shear loads being induced. For tests performed at 75° degrees used No. 8 and No. 10 screws were used.

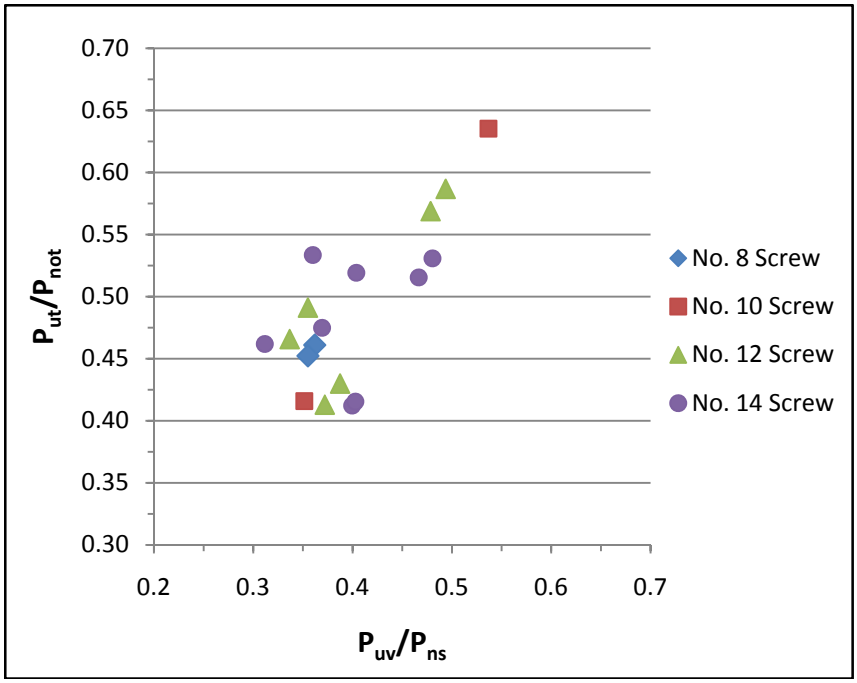

Figure 13 Evaluation of Screw Size – Low Ductility

Shear versus Tension Pull-out. To illustrate the interaction between tension pull-out and shear forces within a screw connection, Figure 14 provides the ratios of ultimate strength to nominal strength, P_{uv}/P_{ns} versus P_{ut}/P_{not}. As illustrated, a relationship is apparent between the normalized tension pull-out and shear forces. Clearly the normal-ductility test specimens performed at a higher normalized capacity than did the low-ductility test specimens.

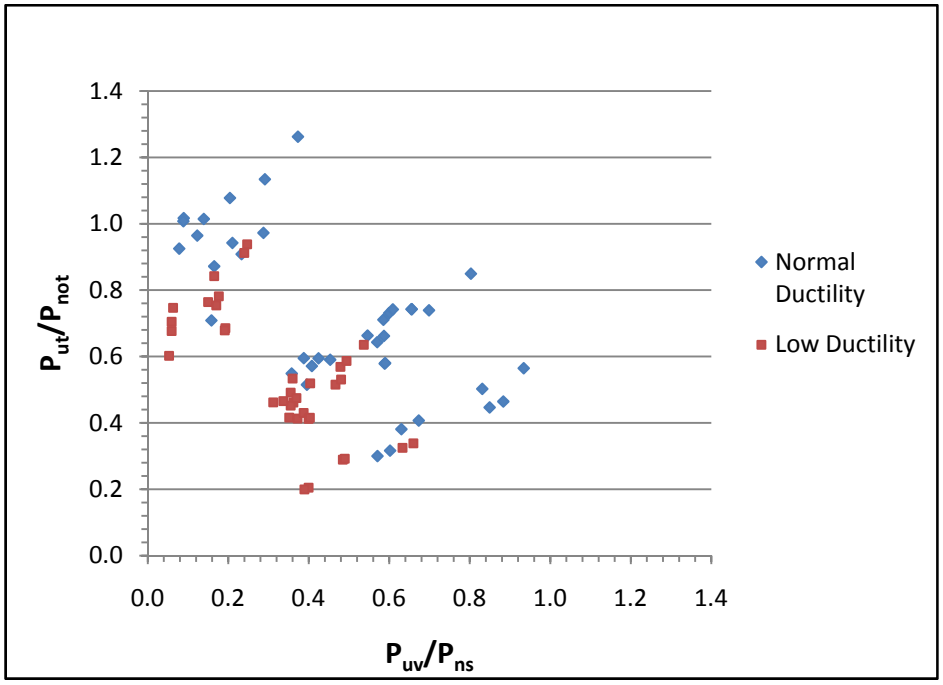

Figure 14 Pull-out and Shear Interaction using AISI Equations

DEVELOPMENT OF INTERACTION EQUATION

Figures 15 and 16 summarize the test data and the normalized relationships between the shear force and the tension pull-out force. Several nonlinear and linear interaction equations were investigated to achieve a desirable mean, standard deviation, and coefficient of variation. An adjustment factor, L, was implemented to reflect the behavior of the low-ductility steel test specimens. The following presents the best-fit cases for a tri-linear and nonlinear interaction equation.

Tri-Linear Interaction Equation. The proposed tri-linear interaction equation, Equation 9, was derived using the data shown in Figure 14. The complete data summary can be found in Tables B.1 and B.2 of Francka and LaBoube (2009). The mean value and coefficient of variation used to determine appropriate resistance and safety factors (ϕ for LRFD and LSD, and Ω for ASD) are also presented in Tables B.1 and B.2. Figure 15 illustrates the correlation between the test data and Equation 9, for both with the normal- and low-ductility test data. Based on Figure 15,

when: $P_{uv}/P_{ns} \geq 0.15$ and $P_{ut}/P_{not} \geq 0.15$

$$\frac{P_{uv}}{LP_{ns}} + \frac{P_{ut}}{LP_{not}} \leq 1.15 \tag{9}$$

Where L = 1.0, for $F_u/F_y \geq 1.087$, L = 0.75, for $F_u/F_y \leq 1.064$,

$P_{ns} = 4.2(t_2^3 d)^{1/2} F_{u2}$ nominal shear strength of connection, Eq. 1

$P_{not} = 0.85 t_c d F_{u2}$ nominal pull-out strength of connection, Eq. 6

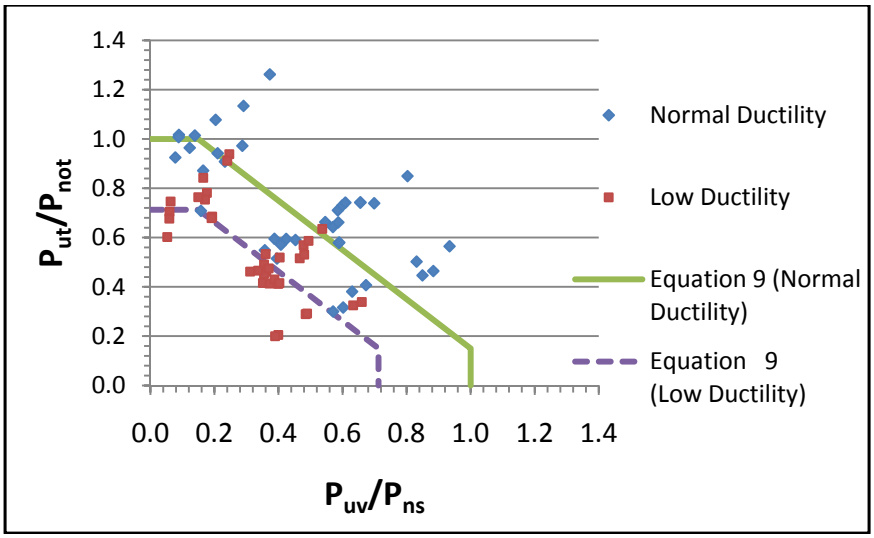

Figure 15 Tri-Linear Equation Interaction Relationship

Nonlinear Interaction Equation. The proposed nonlinear interaction equation is Equation 10 and is shown on Figure 16. It was derived using the data shown on Figure 14 and data from Tables B.1 and B.2 of Francka and LaBoube (2009). The mean value and coefficient of variation were used to determine appropriate resistance and safety factors. This evaluation can be found in Tables D.1 and D.2 of Francka and LaBoube (2009).

$$\left(\frac{P_{uv}}{LP_{ns}}\right)^{1.15}+\left(\frac{P_{ut}}{LP_{not}}\right)^{1.15}\le 1.0 \qquad (10)$$

where:

$L = 1.0$, for $F_u/F_y \ge 1.087$,
$L = 0.80$, for $F_u/F_y \le 1.064$,
$P_{ns} = 4.2(t_2^3 d)^{1/2} F_{u2}$ nominal shear strength of connection, Eq. 1
$P_{not} = 0.85 t_c d F_{u2}$ nominal pull-out strength of connection, Eq. 6

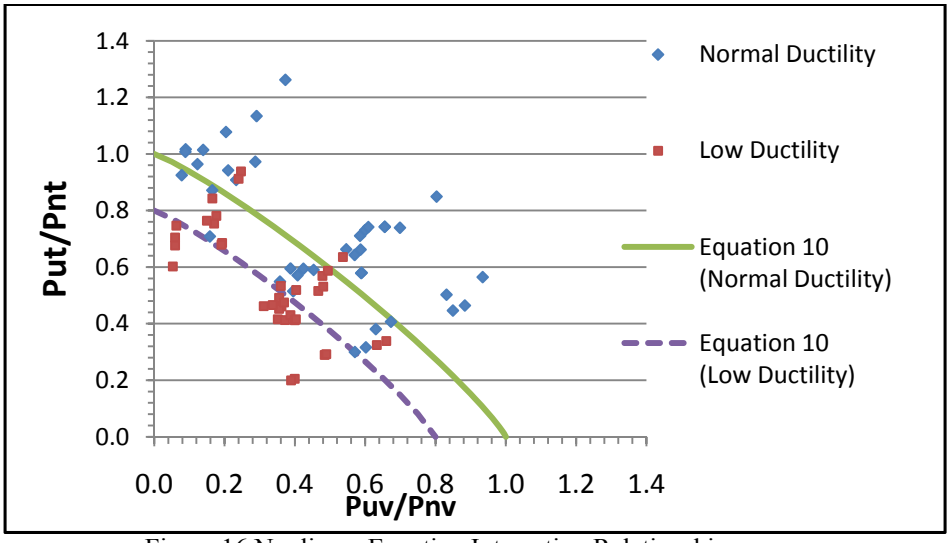

Figure 16 Nonlinear Equation Interaction Relationship

CONCLUSIONS

This study assessed the interaction relationship between tension pull-out and shear forces in screw connections of cold-formed structural steel structural members. A total of eighty-four tests were performed. Based the evaluation of the test data interaction equations were proposed for use in designing screw connections subject to this limit state.

BIBLIOGRAPHY

American Iron and Steel Institute. (1946). *Specification for the Design of Light Gage Steel Structural Members* (1946 ed.). New York, NY: AISI.

North American Specification for the Design of Cold-Formed Steel Structural Members, AISI S100-2007, American Iron and Steel Institute, Washington D.C.

ASTM International. (2007), "*A370-071 Standard Test Methods and Definitions for Mechanical Testing of Steel Products*,": ASTM International, West Conshohocken, PA.

Francka, R.M. and LaBoube, R.A. (2009), "Screw Connections Subject to Tension Pull-Out and Shear Forces," Final Report, Wei-Wen Yu Center for Cold-Formed Steel Structures, Rolla, MO.

Pekoz, T. (1990), "Design of Cold-Formed Steel Screw Connections" Proceedings of the Tenth Specialty Conference on Cold-Formed Steel Structures", Wei-Wen Yu Center for Cold-Formed Steel Structures, Rolla, MO.

Stirnemann, L.K. and LaBoube, R.A. (2008), "Behavior of Arc Spot Weld Connections Subjected to Combined Shear and Tension Forces," Proceedings of the 19th International Specialty Conference on Cold-Formed Steel Structures, Wei-Wen Yu Center for Cold-Formed Steel Structures, Rolla, MO.

Yu, W.W. and LaBoube, R.A. (2010). *Cold-Formed Steel Design* (4th ed.), John Wiley and Sons Inc., New York, NY

Zwick, K., & LaBoube, R. A. (2006), "Self-Drilling Screw Connections Subjected to Combined Shear and Tension", Final Report, Wei-Wen Yu Center for Cold-Formed Steel Structures, University of Missouri-Rolla, Civil, Architectural, and Environmental Engineering, Rolla, MO

Twentieth International Specialty Conference on Cold-Formed Steel Structures
St. Louis, Missouri, U.S.A., November 3 & 4, 2010

CFSEI: Educating North American Practitioners in Principles of CFS Framing Design

W. D. Allen[1]

Abstract

Educating North American structural engineers in the principles of cold-formed steel (CFS) design in general, and about CFS framing in particular, has a unique set of challenges. The undergraduate curricula virtually ignore the subjects, and only a handful of graduate programs address the issue. Several industry associations have existed for engineers, but none specialize in CFS framing. Several organizations existed in the cold-formed steel framing marketplace, but none were set up to accommodate engineers. This paper will review the formation, development, growth, and maturation of one such education- and engineer-focused organization within the framework of the USA design and construction marketplace, and discuss the practicality and potential for this as a use of industry resources for market growth and development.

Introduction

In 1994, representatives from the steel company USS-Posco set up a meeting with key steel framing industry stakeholders in California, USA. They knew they had an excellent product in cold-formed steel (CFS) framing, and saw a huge need for housing and other steel-framed structures in the growing cities and communities across North America. However, they had run into several barriers for acceptance of their products. At this meeting and other gatherings, they had chipped away at each of these barriers with potential solutions. They had developed strategies for educating carpenters, converting wood framers, setting up product distribution, and development of cost-effective tools and systems. But they did not have a solution for the design professionals and building officials: how to educate them on the proper design and inspection of CFS framing. One of several ideas put forth that day was an association

[1] Technical Director, Steel Framing Alliance; Technical Director, Steel Stud Manufacturers Association; Technical Director, Cold-Formed Steel Engineers Institute (CFSEI).

especially for engineers: a way to produce design resources for the most common CFS design challenges, and a way to develop educational programs and presentations to go along with those resources. The firm handling advertising and public relations for USS-Posco drew up a plan for underwriting and financing such an organization, and within a few weeks, the Light Gauge Steel Engineers Association (LGSEA) was born.

In several ways, the LGSEA has fulfilled its mission to provide education and training to North American designers. However, along the way there were some difficulties and missteps, and lessons learned. The new organization that has emerged from a refocus of the LGSEA is now the CFSEI: the Cold-Formed Steel Engineers Institute. This paper supports the argument that specialty associations for educating and enabling practicing structural engineers CAN succeed, given the proper guidance, personnel, and resources. The LGSEA / CFSEI will be presented as a model for such and association, with examples given of successes and failures in meeting their mission. The conclusion presents the vision for the future of CFSEI, and how the current framework and association is meeting that vision in a down construction market and difficult financial times.

Funding

Whenever a group is formed or technical resources are developed, the cost of developing these resources is always an issue. The initial capital outlay for getting the LGSEA started was provided by USS-Posco. They paid the individual who was the part-time staff of the organization, helped draw up the initial incorporation papers, and provided cash for the initial operating budget. They even paid the first members to come to meetings, and set up the first seminars. Knowing that a funding model was not sustainable, they worked with the initial members and volunteers to develop a long-term funding strategy. At that time, the vision was for a large association, consisting of thousands of engineers as well as industry partners. The plan was to set up a dues structure that could be self-sustaining: by charging enough dues to members, they could pay for staff, projects and programs. This would be supplemented by the sale of publications and the registration fees for educational programs. Membership would be encouraged by member discounts on publications and programs: a principle that has been successful and is still in place today.

The initial budget projections required a fairly large membership and growth to pay for the programs needed to saturate the engineering community with the educational material they needed. Since membership had to grow over time, dues revenue would have to be supplemented. Also, even with a full,

sustainable membership, it was unrealistic to believe that a full-time paid staff could be hired with the specific technical knowledge needed to develop and produce all of the resources needed. Therefore, a key to the initial and ongoing strategy was to develop a cadre of working volunteers to assist and supplement the paid staff. This will be covered in more detail in the Manpower section of this paper.

Another important initial funding strategy was underwriting by industry partners. Organizations such as manufacturers of CFS framing products and accessories, fasteners, software, and other industry associations were targeted as potential supporters of the LGSEA. On one level, this funding strategy has been successful, but it has simultaneously led to tension and conflict within the industry. The source of the conflict was the competition between industry associations for the same limited dollars. Shortly after the formation of the LGSEA, other groups were either in existence or being formed with goals that included the growing the market for CFS framing. Although not necessarily focused on the education of engineers and design professionals, these groups would go to the same sources – manufacturers within the industry – to obtain funding for projects and programs. These manufacturers who also had limited budgets for industry funding, started to feel that their monies were being spent on programs and staff that were in some cases duplicative and redundant. LGSEA, as well as the other industry associations, were politely asked to work together to develop a funding scheme that would eliminate overlapping efforts. This was one of the main reasons that the LGSEA eventually came under the umbrella of the North American Steel Framing Alliance.

Both in the early days of the LGSEA and in the present strategy of the CFSEI, the organization found other ways to leverage industry support. Representatives of manufacturing organizations served as volunteers within the leadership structure. They provided meeting spaces for chapters, committees, and task groups. They provided venues and materials for educational seminars. Their volunteers helped write and review technical documents. And eventually, a dues structure was set up to allow an annual payment that was commensurate with both the size of the company and the potential benefits received from existence of and participation in the association. The current structure of the CFSEI reflects this evolution.

In the intermediate years, however, there were funding problems. As the initial funding from USS-Posco expired, there was not enough dues revenue to cover costs. The single paid staff member would sometimes go for a two or more months without pay, as dues payments trickled in or if underwriting checks were delayed. Payments for presentations, programs, printing, and other projects

were delayed during slow income periods. And once membership had reached about 500 engineers, the rate of growth declined, so dues revenue was an issue. The Board considered raising dues on members. Reviewing the cost/benefits to practicing engineers, and what other associations were charging, it was difficult to justify fees greater than $100 per person per year. It was discovered that many individuals would sign up for one year, get the binder and mailed tech notes, and then let their membership lapse. In addition, large firms would have only one individual sign up for membership, and then share the resources amongst all members at that firm.

These funding problems, as well as some other issues with manpower and leadership, led to two fundamental changes within the LGSEA. The first was the alignment of the organization with the Steel Framing Alliance (SFA), and the second was the development of a membership-category based dues structure.

Alignment with SFA was a difficult issue: especially for the engineering leadership that comprised the board of directors at the time. There was a major concern that what had started out as an engineering association led by engineers but funded by commercial interests would become merely a vehicle to promote commercial products to the CFS engineering community. In addition, there was a concern about compromising the technical integrity of published documents. Overriding these concerns was the financial reality that the association could not continue to exist with its current rate of spending and income. As a part of the alignment, safeguards were put in place through the CFSEI Operating Procedures that would ensure leadership of the association by practicing professional engineers. The funding program was set up so that members of CFSEI first had to be members of the Steel Framing Alliance, and they were able to opt-in to CFSEI membership. Dues revenues would go into the SFA account, but from this account the CFSEI budget would be formulated, which allowed for a more stable cash flow over the course of a fiscal year.

Through this SFA membership alignment, the membership category based dues structure was another strategy that helped solve the funding issues of LGSEA and CFSEI. Because most major framing manufacturers were already members of the Steel Stud Manufacturers Association (SSMA), the LGSEA worked out an agreement with SSMA so that membership levels in LGSEA would mirror those within SSMA. SSMA had already developed an assessment structure that forced members with higher sales volume to pay higher fees, while at the same time allowed them greater say in the budgeting process. LGSEA was able to use the existing member category structure at SSMA to set dues levels that aligned with sales volumes. For framing manufacturers that were not SSMA members, they would be asked to pay dues at the highest SSMA member category. This

was not to discourage these manufacturers from participating in the engineers association, but to encourage them to participate in their manufacturers association. Although a similar structure was not available for manufacturers of non-framing products, such as tools, fasteners, and connectors, the SSMA model was used for allowing membership and funding by those manufacturer members. Also, larger companies were permitted more members, which allowed them to receive CFSEI and LGSEA documents at multiple branch locations.

The success of this program eventually led to a program of multiple member discounts at a single firm. As noted above, typically a single member would join CFSEI/LGSEA from a single firm. Under CFSEI, the association began more aggressively marketing the value of the 25% discount on programs and publications, as well as reduced member rates for additional members at the same firm. During this membership campaign, additional members from the same companies increased by over 500% for CFSEI.

During 2008, CFSEI membership peaked at just under 800 members. Membership has been down since then, attributed primarily to the current USA recession and decreased construction across North America. However, although staff has been reduced, CFSEI remains a vibrant and viable organization, and although 2009 – 2011 budgets have been reduced, the association is not in danger of collapse due to financial issues.

Personnel and Manpower

To meet the educational mission of the LGSEA and CFSEI, the founders and stakeholders realized that volunteers would be needed: for both the development and delivery of the technical and educational resources, and for leadership of the association. Because of funding issues, it was clear that no more than one or two paid staff would be able to work full-time for the association, without drastic changes in the funding program. The partnership with the Steel Framing Alliance (SFA) helped, in that some of the SFA staff resources could be used for CFSEI programs. Because the early LGSEA staff had no technical background, it was quickly clear that volunteers and contract labor would be needed to develop many of the documents and programs the association envisioned for educating engineers.

With a limited number of structural designers well versed in CFS framing initially, there was a fairly small pool of talent to draw from with respect to Technical Note authors and seminar presenters. The initial authors were a mix of paid contractors and volunteers, many of whom saw the economic benefits to

their own companies and practices in developing these products for the LGSEA. The volunteer model continues today in CFSEI, since in the current budget little funding is available for contract authorship. The addition of technical staff has helped, since initial review, layout, and graphics/detailing can be completed or reviewed by staff, before and during the volunteer technical review process.

Under the current Operating Procedures, the elected officers and voting members of the board of directors consist entirely of unpaid volunteers. There are term limits, to prevent stagnation in the board membership, and local chapters provide training and development of a younger generation of board members who may eventually choose to graduate to the national board. Two face-to-face meetings are held during the year, with the balance of board and staff meetings being held via conference call. All chapter presidents have a standing invitation to all board meetings and may participate in all debate, although only elected national board members have voting rights. So far, this model has worked well, even though budget cutbacks reduced the number of full-time staff at the beginning of 2010. The existence of the educational programs and materials of LGSEA and CFSEI have allowed more engineers to be better qualified in CFS design, thus creating a larger cadre of potential volunteers from which future authors, presenters, and officers may be selected.

Guidance

With an initial mission of educating engineers and design professionals, the LGSEA found that early strategy was fairly straightforward: find out what structural engineers needed to know to safely and accurately design CFS framing, and then create resources and educational materials to fill those needs. Initially, the single paid staff member of LGSEA managed volunteers and contracted with writers to develop and publish these documents. The primary vehicle for this technology transfer was the Technical Note (figure 1). Each note took a specific design principal or strategy, and developed it through text and design examples. Other products developed at the time included newsletters and live seminars. The newsletters, in addition to information about the association and upcoming programs, had a specific section entitled “Technical Exchange.” The Technical Exchange provided a forum for members and others to submit articles and information about design, that did not merit a full technical note, but was still useful for CFS framing designers. In addition, technical articles on recent research, building codes, and structural news were included, as well as announcements of upcoming technical presentations.

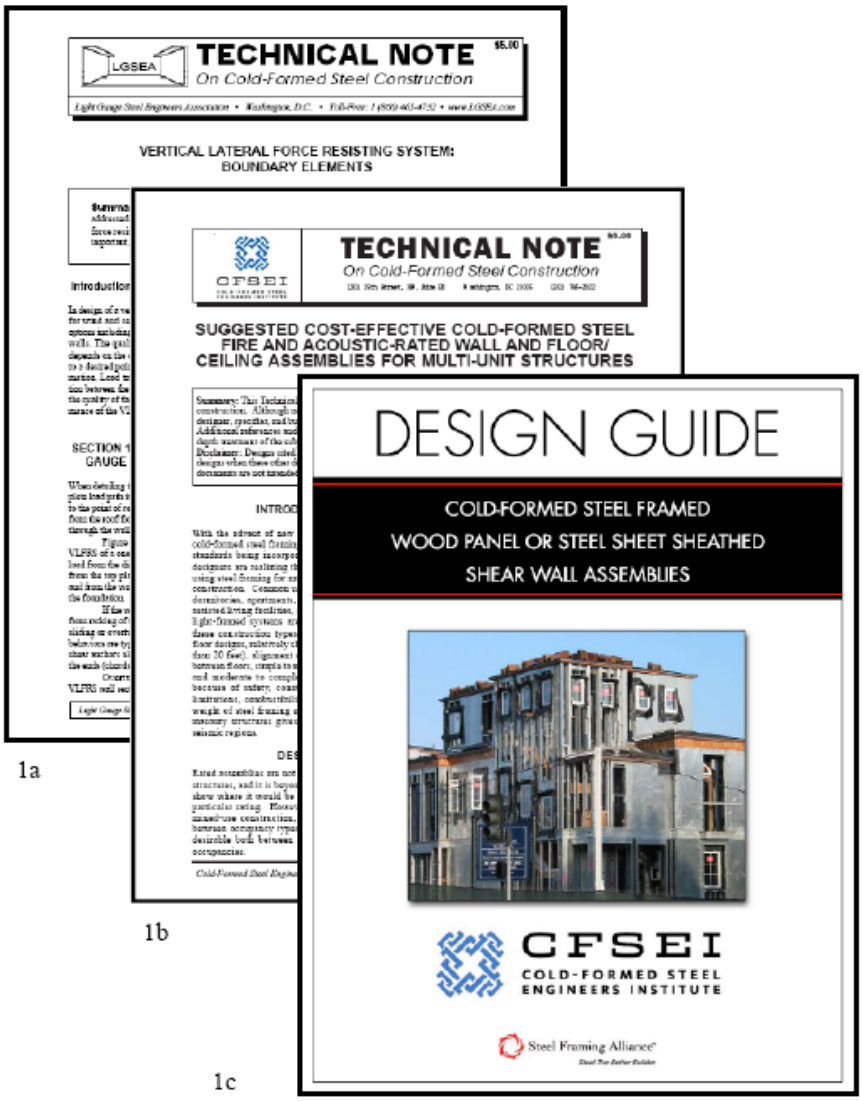

Figure 1: Technical Documents from CFSEI:
1a: LGSEA Technical Note
1b: CFSEI Technical Note
1c: CFSEI Design Guide

This model worked well for the first few years. As more notes were developed, new members were issued a binder with a full compliment of CFSEI print documents and newsletters. Quarterly newsletters were mailed to all members, and Technical Notes that had been developed since the last newsletter were included with the mailing.

The Local Chapter Model

As the membership grew, the leadership saw there was a need for a broader strategy. An association headquartered in California had difficulty developing growth in other areas of the country, and grass-roots efforts were needed to recruit members and attendees at local programs. These local programs were needed to not only provide the education to engineers in a face-to-face setting, but also to develop membership and networking at a local level. thus the chapter model was developed.

Local chapters provided an organization and platform for local events and activities, and were better able to address local engineering priorities such as high-seismic and high-wind issues. The first LGSEA chapter was organized in Hawaii, where termite restrictions had provided a unique opportunity for CFS framing construction. Because of the requirement of pressure-treated lumber, CFS framing enjoyed a moderate cost advantage in Hawaii. There was an urgent need for the training of the local engineering community, and the existing LGSEA structure and technical documents provided a good starting point. The framing community had already formed the Hawaii Pacific Steel Framing Alliance (HPSFA), and several engineers were members. The local structural engineering association also had a strong presence, and most engineers were already familiar with one another's work and practice. Working with active members of the local engineering community, the national staff developed a framework for chapter activities that included local leadership in a board of directors, annual election of officers, a set of chapter by-laws, and a framework for implementing local educational programs tied to the needs of the engineering community. Dr. Reynaud Serrette of Santa Clara University was brought in as the keynote speaker at the first event, where he discussed recent testing of CFS shearwalls. The meeting was well attended, and soon, the LGSEA Hawaii chapter was hosting quarterly events and networking seminars, and became an integral part of the Hawaii engineering community.

Since then, chapters have been established in Atlanta, California, and Florida, and in 2011 the CFSEI Texas Chapter will begin operations. Each chapter has experimented with different types of programs and procedures, but all have

found that addressing local issues and leveraging programs based on national publications and resources works best.

Strategic Planning

In 2006, the LGSEA saw membership growth becoming stagnant. They had successfully partnered with the Steel Framing Alliance, and did not have as much of a concern about funding, but they wanted to ensure the leadership and activities of the association adhered to high moral and ethical engineering and management principals, and that their mission was still appropriate for educating engineers in the 21st century. To meet these ends, the staff and leadership of SFA and LGSEA set up a two-day strategic planning session in Baltimore, Maryland, on the campus of Johns Hopkins University (CFSEI, 2006) Facilitated by Liza Bolles of Newport Partners, LLC, the volunteers not only developed an updated mission and vision for the association, but eight prioritized "key strategies" for implementation of the mission (Figure 2). In addition, to better reflect the new mission and the move of the North American steel industry away from the term "gauge," the name of the association was debated and changed. For a very brief period, the association's name was the "Steel Framing Engineers Council," or SFEC. Upon reflection over dinner and drinks after the second day of planning ended, the name was quickly changed to CFSEI: the Cold-Formed Steel Engineers Institute (CFSEI, 2006)

Under this new framework, local chapters were given more input into national decisions, with assignment of a board-level chapter liaison. An implementation plan was set up for technical document development, and new staff was hired to specifically focus on technical products and programs. In addition, an annual meeting was incorporated into the national organization activities, to provide a "State of the Institute" address to members and stakeholders, and to facilitate networking on a national level. The 2010 CFSEI annual meeting, hosted by the CFSEI Atlanta/Southeast chapter, succeeded in attracting over 100 CFSEI members, guests, and sponsors, and not losing money in the process.

CFSEI Mission

To enable and aid engineers in the efficient structural design of safe and cost effective cold-formed steel (CFS) framed structures.

Vision

CFSEI is recognized as the preeminent worldwide technical resource for cold-formed steel framing design.

Key Strategies

The eight key strategies, in order of highest to lowest priority, identified as most important to the current success of CFSEI are:

1. Produce technical documents that enable and aid engineers
2. Create and promote the CFSEI brand
3. Increase relevance to chapter activities and local membership needs
4. Provide timely and competent response to technical inquiries on CFS
5. Provide forums for exchange of information and ideas related to CFS
6. Partner with aligned organizations
7. Help focus research spending on the needs of engineers
8. Develop awareness of CFS through the formal education system

Figure 2: CFSEI Mission, Vision, and Key Strategies.

Implementation and the Future of the Institute

With the funding, guidance, and personnel in place, the leadership and volunteers must still implement the plan for moving the association forward. To this end, the key strategies help prioritization, and development of technical documents is at the top of the list. In addition to the Technical Notes mentioned throughout this paper, CFSEI is working on more comprehensive documents called Design Guides. The first design guide published under the CFSEI name

was the *Design Guide for Cold-Formed Steel Framed Wood Panel or Steel Sheet Sheathed Shear Wall Assemblies*, by primary author Jeff Ellis of Simpson Strong-Tie, released in 2009. (CFSEI, 2009). This 57-page document included detailed examples of shear wall design in a 2-story structure, and showcased application of the latest code provisions. Data from this document has been used in CFSEI-developed presentations, including the latest to be presented in October 2010. Ellis has developed live versions of this presentation, and has given it at all of the active CFSEI chapter locations.

Another delivery option that had been used initially in 2004 was web-based seminars. These web-seminars, or webinars, enable CFSEI to reach a broader audience, and reduce the costs of speaker travel and room/lodging expenses for both presenters and participants. Feedback from the first two CFSEI webinars in 2010 has been positive. A third webinar is planned for December 2010, with quarterly webinars presented thereafter. Topics mirror those used in chapter presentations, and coincide with release of applicable technical documents.

With all of this information being developed and disseminated as a part of CFSEI programs and publications, it is very important for the technical credibility of the association that all technical material receive a critical technical review by engineers and specialists knowledgeable in the appropriate subject matter. That is why the CFSEI Operating Procedures include a requirement for review by a Technical Review Committee (TRC), composed of industry experts and specialists. Currently chaired by Rob Madsen of Devco Engineering, the committee has a standing membership, which is augmented by technical reviewers and experts on specific topics, which may sometimes be beyond the scope of typical structural engineering practice. Fore example, with the publication of Technical Note T001-09, *Suggested Cost-Effective Cold-Formed Steel Fire and Acoustic-Rated Wall and Floor/Ceiling Assemblies for Multi-Unit Structures*, acoustical experts were brought in for both the development and review of the document (CFSEI, 2009.)

Conclusions

Based on the findings of this review of the actions and activities of the CFSEI / LGSEA, it is clear that specialty associations for educating and enabling practicing structural engineers can succeed, given the proper guidance, personnel, and resources. Key factors of this success include a strategic plan that considers the existing construction market and allied organizations. It also includes a long-term plan for funding, that incorporates a tiered membership level based dues structure, and underwriting by other industry associations. It must also address both paid staff and volunteer manpower issues, and find

creative ways to leverage both manpower and funds to serve the goals of the association, as well as the needs of the larger engineering community. It must do this in a context of ethical behavior, both in engineering design and business management.

References

Cold-Formed Steel Engineers Institute (CFSEI). (2006). *Operating Procedures for the Cold-Formed Steel Engineers Institute.*

Cold-Formed Steel Engineers Institute (CFSEI). (2009). *Design Guide for Cold-Formed Steel Framed Wood Panel or Steel Sheet Sheathed Shear Wall Assemblies.*

Cold-Formed Steel Engineers Institute (CFSEI). (2009). Technical Note T001-09, *Suggested Cost-Effective Cold-Formed Steel Fire and Acoustic-Rated Wall and Floor/Ceiling Assemblies for Multi-Unit Structures*.

Appendix: Organizations Referenced

AISI	American Iron and Steel Institute
CFSEI	Cold-Formed Steel Engineers Institute
HPSFA	Hawaii Pacific Steel Framing Alliance
LGSEA	Light Gauge Steel Engineers Association (now the Cold-Formed Steel Engineers Institute)
NASFA*	North American Steel Framing Alliance (now the Steel Framing Alliance)
SFA	Steel Framing Alliance
SFEC	Steel Framing Engineers Council – the name briefly considered for the CFSEI
SSMA	Steel Stud Manufacturers Association

*Abbreviation not used in this document, but organization is referenced.